

—

~

.

.



— —

.

—

•  
•  
•

# Design and Synthesis of Bifunctional Molecules for Directing Phosphorylation

**Charles Scott Fuller Robertson**

Medicinal Chemistry, Cancer Research UK Cancer Therapeutics Unit

The Institute of Cancer Research

University of London

This thesis is submitted in partial fulfilment of the requirements for the degree of Doctor of Philosophy

September 2022



## **Signed Declaration**

I, Charles Robertson, confirm that the work presented in this thesis is my own. Where work has been performed by others, and where information has been derived from other sources, I confirm that this has been indicated in the thesis.

Charlie Robertson

September 2022

## **Acknowledgements**

Firstly, I would like to thank Ben and Swen for the opportunity to carry out my PhD at The Institute of Cancer Research. I have learnt a huge amount from each of you in Chemistry, Drug Discovery and of course in how to write a thesis. I would also like to thank my industrial supervisor, Jason Kettle and AstraZeneca for sponsoring my PhD.

A huge thank you to all those at the ICR who helped me throughout this project. From the HDSD Team Harry Saville, Yvette Newbatt and Caroline Ewens for their help in teaching me how to use the equipment and how to set up assays and Daniel Miller for teaching me about cell culture and how Western Blots are not the same as a TLC. I would also like to thank Theo Roumeliotis, Laura Ramos Garcia and Tencho Tenev for their help with different chapters of my work.

A huge thank you to the collaborators from different institutions of James Murphy and Cheree Fitzgibbon of the Walter and Eliza Hall Institute of Medical Research for their helpful advice on MLKL and expressing the recombinant protein, and to Jon Elkins of the University of Oxford and Benedict-Tilman Berger of the Goethe University Frankfurt for their help around the expression and testing of STK10.

I would like to thank everyone in Med Chem Team 4 who has supported me over the course of my PhD; Owen, Matt, Jack, Rosemary, Alfie, Will, Alice, Pasquale, Nick, Katie and Dani – a huge thank you to all of you for advice, guidance and positive attitude.

I would also like to thank my parents and friends for their support over the past four years; I hope you look forward to trying to read this.

Finally, I would like to thank my fiancée, Flo for her unending support over 4 years and especially near the end, I couldn't have done this without you.



## **Abstract**

The field of bifunctional molecules such as PROTAC, DUBTAC and PhoRC has demonstrated that inducing proximity between two protein complexes is sufficient to redirect post-translational modifications (PTMs), and effect cellular function. As phosphorylation plays a key role in many cellular functions such as cell growth, signalling and death, the ability to selectively and dose dependently direct phosphorylation of a target protein would be a novel and powerful chemical tool, complementary to kinase inhibitors.

Our hypothesis is that rationally designed bifunctional molecules could redirect AMPK to phosphorylate neo-substrates by inducing proximity between a kinase and a target protein. The aim of this work is to show increased levels of phosphorylation of a target protein.

Here we show the development of bifunctional molecules, capable of binding AMP-activated protein kinase (AMPK) and target proteins. We used structural information to identify suitable solvent exposed sites on published AMPK small molecule activators, then designed and synthesised relevant compounds to test their activity. Likewise, a suitable ligand for target proteins was selected and a solvent exposed site identified and validated, and a library of bifunctional compounds synthesised using click chemistry. Testing these compounds in global unbiased phosphoproteomics has shown selective increase in phosphorylation at specific sites, which we sought to confirm with multiple techniques.

We anticipate these bifunctional compounds act through ternary complex formation and demonstrate selectivity based on the overall structure of the target protein. Furthermore, we hope that this work may provide a basis for this emerging method of directing phosphorylation.

## **Abbreviations**

A-loop:	Activation loop
AMP:	Adenosine monophosphate
ADP:	Adenosine diphosphate
ATP:	Adenosine triphosphate
AMPK:	5'- Adenosine Monophosphate Kinase
CIP:	Chemical Inducers of Proximity
CRISPR:	Clustered Regularly Interspaced Short Palindromic Repeats
CuAAC:	Copper(I)-catalysed Azide-Alkyne Cycloaddition
DCM:	Dichloromethane
TR- FRET:	Time Resolved Fluorescence resonance energy transfer
HEPES:	(4-(2-hydroxyethyl)-1-piperazineethanesulfonic acid)
IC <sub>50</sub> :	half maximal inhibitory concentration
K <sub>d</sub> :	Dissociation constant
LC-MS:	Liquid Chromatography Mass Spectrometry
MLKL:	Mixed Lineage Kinase Domain-Like
MOE:	Molecular operating environment
PDB:	Protein data bank
PHICs:	Phosphorylation-Inducing Chimeric Small Molecules
PhoRC:	Phosphatase recruiting chimeras
PROTAC:	Proteolysis Targeting Chimeric small molecules
RIPK3:	Receptor-interacting serine/threonine-protein kinase 3
r.t.:	room temperature
ret. time:	retention time

SEM:	2-(Trimethylsilyl)ethoxymethyl
SMKI:	Small molecule Kinase Inhibitors
S <sub>N</sub> Ar:	Nucleophilic aromatic substitution
SPR:	Surface Plasmon Resonance
STK10:	Serine/Threonine Kinase 10
TFA:	Trifluoroacetic acid

## **Table of Contents**

<b>Abstract of Thesis</b> .....	2
Chapter 1 Introduction .....	16
1.1 Role of Protein Phosphorylation and Kinase Recognition .....	16
1.2 Tools and methods for investigating the biological role of phosphorylation 18	
1.3 Bifunctional molecules .....	20
1.4 Proteolysis Targeting Chimeric small molecules .....	23
1.5 Deubiquitinase-Targeting Chimera (DUBTAC) .....	27
1.6 Bifunctional molecules for acetylation.....	28
1.7 Bifunctional molecules for phosphorylation .....	29
1.8 Designing bifunctional compounds .....	31
1.9 Adenosine Monophosphate kinase (AMPK) .....	34
1.10 Mixed Lineage Kinase Domain-Like Protein .....	36
1.10.1 Cellular role and Therapeutic relevance .....	38
1.11 Introduction to Phosphoproteomics .....	40
1.12 Click chemistry.....	42
1.13 Biochemical assays for measuring ternary complex formation .....	44
1.14 Aim and Hypotheses.....	47
Chapter 2 Single ligands .....	49
2.1 5'Adenosine Monophosphate kinase.....	49
2.2 Binding of 991 and solvent exposed sites .....	50
2.3 AMPK activator synthesis .....	53
2.4 Design rationale.....	55
2.4.1 Acid replacement on 991 .....	55
2.4.2 2-Position on 991 .....	57
2.4.3 Back pocket of 991 .....	59
2.4.4 991 inactive control .....	63
2.5 Binding of 577 and design rational.....	64
2.6 AMPK Activator testing .....	66
2.7 ADP Glo Assay results .....	68

2.7.1	Confirming literature compounds.....	68
2.7.2	Testing back pocket 991/CCT390619 analogues .....	69
2.7.3	577 results.....	71
2.8	Summary and discussion .....	71
2.9	Mixed Lineage Kinase Domain-Like Protein (MLKL).....	73
2.9.1	Synthesis of the amide bioisostere of 1.....	74
2.10	Synthesis of dummy linker analogues.....	80
2.10.1	Para-phenyl .....	80
2.10.2	Meta-phenyl replacement .....	81
2.10.3	5-pyrazine position.....	82
2.10.4	Alkyne based linkers.....	84
2.11	Summary.....	88
2.12	Crizotinib dummy linkers.....	88
2.13	Testing Crizotinib and AMPK activators against AMPK.....	91
2.14	Developing a MLKL LanthaScreen Assay .....	92
2.15	IC <sub>50</sub> Experiments.....	96
2.16	Summary.....	100
2.17	Bifunctional compound design.....	100
2.17.1	Functionalising AMPK activator 991 .....	100
2.17.2	Functionalising AMPK activator 577 .....	103
2.17.3	Functionalising Crizotinib.....	104
2.17.4	Click chemistry optimisation .....	105
2.18	Testing for neo-phosphorylation.....	109
2.18.1	Measuring ADP produced .....	109
2.18.2	Cellular testing .....	111
2.19	Summary.....	113
2.20	Conclusion and future plans.....	114
Chapter 3	Utilising Phosphoproteomics for identifying neo-substrates.....	116
3.1	Serine/Threonine Kinase 10 (STK10) Introduction.....	125

3.2	Phosphoproteomics repeat with controls.....	128
3.3	NanoBRET .....	130
3.4	AlphaScreen development for STK10.....	134
3.5	STK10 Complex Immunoprecipitation (Co-IP).....	146
3.6	Measuring Phosphorylation of STK10 in cells .....	147
3.7	Measuring STK10 phosphorylation biochemically .....	149
3.7.1	Using Western Blots.....	149
3.7.2	Recombinant Mass Spectrometry assay .....	153
3.7.3	Following up on the Mass Spectrometry assay .....	157
3.8	Conclusions.....	165
Chapter 4 RIPK1 introduction .....		168
4.1	RIPK1 Function in cells.....	169
4.2	Role of Phosphorylation in RIPK1 function .....	170
4.3	RIPK1 inhibitors .....	171
4.4	Synthesis of bifunctional compounds .....	174
4.5	Cellular testing.....	177
4.5.1	Measuring RIPK1 Phosphorylation.....	177
4.5.2	RIPK1 phenotypic assay.....	178
4.5.3	Co-Immunoprecipitation.....	182
4.6	Conclusion .....	184
Chapter 5 Conclusions and Future Directions .....		185
Chapter 6 Experimental.....		190
6.1	AMPK activity assay .....	190
6.2	MLKL LanthaScreen Binding Assay .....	190
6.3	AlphaScreen Assay.....	191
6.4	Western Blotting .....	191
6.5	Phosphoproteomic analysis .....	193
6.6	Sample preparation for phosphoproteomic analysis.....	193
6.7	High-pH Reversed-Phase peptide fractionation and phosphopeptide enrichment .....	194
6.8	LC-MS analysis .....	195

6.9	Database search and quantification.....	195
6.10	Cloning and transfection FLAG-STK10.....	196
6.11	FLAG Pull down.....	197
6.12	ATP-Cell titre Glo .....	197
6.13	STK10 Expression.....	198
6.14	Measuring phosphorylation in vitro.....	198
6.15	Recombinant Mass spectrometry assay.....	198
6.16	In silico .....	199
6.17	Chemistry.....	199
6.17.1	General Experimental .....	199
6.18	General procedures .....	201
6.18.1	General Method for Amide coupling .....	201
6.18.2	General method for Ester hydrolysis .....	201
6.18.3	General method for a nitro reduction .....	201
6.18.4	General Method for making NHS-esters.....	202
6.18.5	General conditions for Swern oxidation .....	202
6.18.6	General conditions for reductive aminations .....	202
6.18.7	General method for click couplings .....	203
Chapter 7	References .....	292

## Chapter 1 Introduction

### 1.1 Role of Protein Phosphorylation and Kinase Recognition

Phosphorylation is the attachment of a phosphate group to a biological substrate and is the most frequently observed post-translational modification of proteins. Phosphorylation can alter the activity of substrate and is responsible for plethora of downstream signalling and effects that govern cell growth, division and death.<sup>1, 3</sup>

In the cell, proteins can become phosphorylated via auto-phosphorylation or through phosphorylation by an upstream kinase.<sup>4</sup> Both these phosphate groups typically come from the terminal phosphate of ATP and mostly occur on the amino acids Serine, Threonine and Tyrosine.

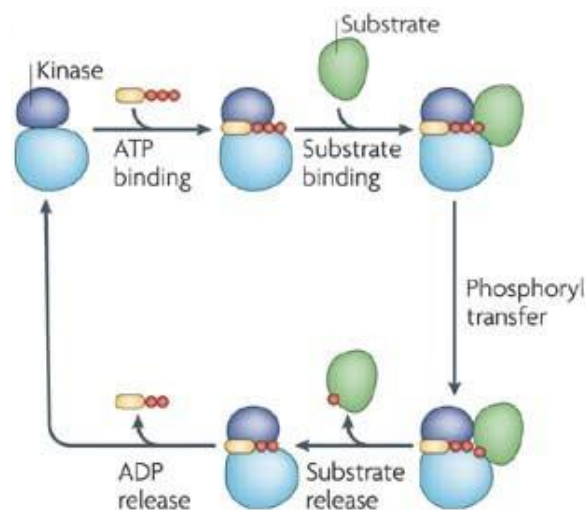


Figure 1.1 - Mechanism of phosphorylation induced by a kinase<sup>1</sup>

Over 57,000 have been putatively observed, and if every serine, threonine or tyrosine is considered as a potential phosphosite, then there are an estimated  $\approx 700,000$  phosphosites or P-sites in a cell.<sup>1, 5</sup> As such kinases have a number of mechanisms for selectively recognising and phosphorylating substrates.

Firstly, the primary structure of amino acids immediately before or after the P-site, known as the Consensus motif, drastically affect the recognition of a peptide as a substrate. Single amino acids are not good substrates for a kinase with local interactions between the kinase active site and the substrate sequence through H



bonding, charge and hydrophobicity required for a kinase to bind a substrate. Analysis of consensus motifs for some kinases has been done as shown in Table 1.1.

Table 1.1 - Kinases and their favoured substrate consensus motifs. X is any peptide,  $\Phi$  is a hydrophobic residue

CDK2	<b>S/T-P-X-K/R</b>
PKA	<b>R-R-X-S/T-<math>\Phi</math></b>
AMPK	<b>R-X-X-S</b>

These consensus motifs do not fully represent the structural requirements of a substrate protein and as such algorithms have been developed to better model the exact weighting of amino acids before and after the P-site.<sup>6</sup>

Kinases and substrates also maintain selectivity through interactions of their tertiary structure, with protein-protein interactions far from the kinase active site and the P-site helping to orientate both proteins appropriately for phosphoryl transfer. An example is shown below in the published crystal structure of murine RIPK3 and MLKL, with both kinase lobes interacting with an opposing structure.

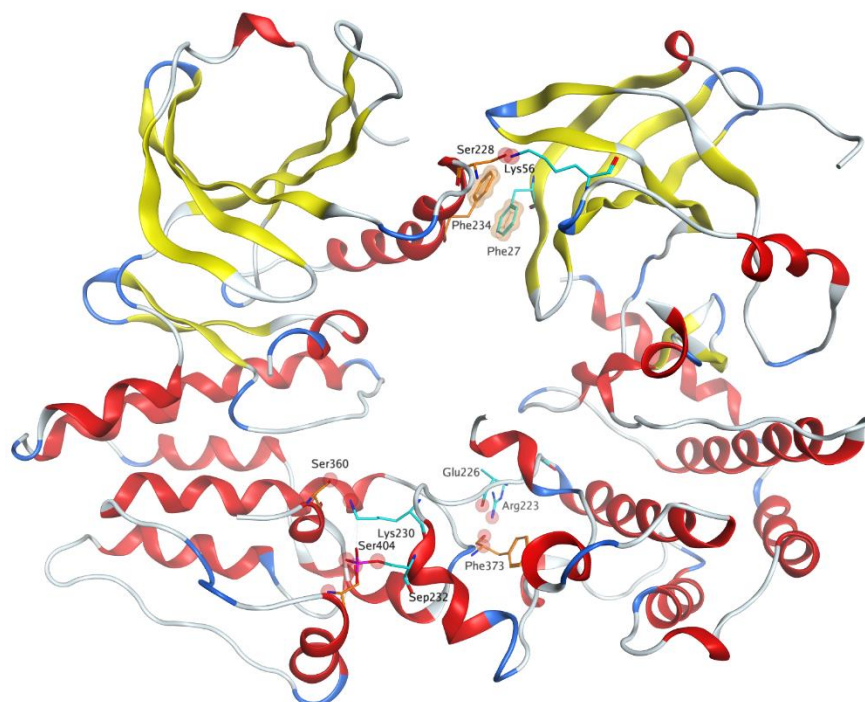


Figure 1.2 - RIPK3 is on the right. MLKL is on the left. PDB: 4M69

Although some kinases are reported to have key distal interactions with substrates, for the most part they are poorly understood.<sup>1</sup>

## **1.2 Tools and methods for investigating the biological role of phosphorylation**

Considering the frequency and importance of phosphorylation in protein function, it is no surprise that extensive efforts have been made to develop chemical and biological tools that can be used to interrogate the function of kinases.

Kinases have been the target of numerous discovery campaigns, which has provided a number of chemical tools and therapeutic drugs, with 72 small molecule kinase inhibitors (SMKIs) having FDA approval as of January 2022.<sup>7,8,9</sup> Kinase inhibitors have generally been designed that bind to the highly conserved ATP binding site and targeting differences between kinase active sites to drive selectivity.<sup>10</sup> As the kinase active site and structure have become increasingly well characterised, the field of kinase inhibitors has grown. Designing kinase inhibitors with sufficient potency and selectivity to block particular signalling pathways is a challenging but well-established field. From a target validation standpoint, the wide range of chemical tools available to block the function of a kinase is key in elucidating their role in a cell.

Most small molecules work by inhibiting kinases giving a loss of function. But it is also possible to discover small molecules which enhance the activity of kinases resulting in a gain of function. This approach allows the function of the protein in its off and on state to be understood. However, kinase activators are generally harder to discover and optimise than inhibitors of the same kinase.<sup>11</sup> Firstly, kinase agonists cannot bind the ATP binding site and identifying functional allosteric sites from crystal structures is challenging. As allosteric sites are not conserved between kinases, there are no common kinase agonist pharmacophores requiring diverse screening libraries which then tend to have low hit rates. However, as kinase agonists are structurally distinct, they typically exhibit very high selectivity.<sup>11-13 12, 14</sup>

An additional difficulty is that the screening for activating compounds requires a functional assay, rather than a more straightforward competition binding assay with an ATP binding site tracer that can be used for inhibitors.<sup>12, 14</sup> An additional

factor that makes agonists harder to discover and develop is that proteins are typically already well optimised for their function, and increasing the stability or activity of an efficient system is much more difficult than binding a site of inhibiting it. These difficulties can be shown in a recent AMPK activator screening of  $\approx 25\ 000$  small molecules which only produced three hits, well below the average hit rate of 1% for antagonists.<sup>15</sup> As such, most enzymes have no known small molecules that will activate them.

Kinase PROTACs have been developed which demonstrate all the advantages of protein degradation that would be expected and are useful chemical tools for investigating kinase function.

An alternative small molecule approach to increasing the activity of a kinase would be to prevent deactivation through inhibition of the phosphatase that dephosphorylates it. Phosphatases are a class of enzymes that remove phosphate groups from proteins and deactivate or 'turn off' the signal. However, the phosphatase family tend to have highly conserved active sites which hampers developing selective phosphatase inhibitors.<sup>16, 17</sup>

Outside of small molecules, directly suppressing or overexpressing a protein can indicate its cellular role and is a commonly employed strategy in target validation. CRISPR and other gene editing techniques can be used to suppress or overexpress certain proteins but as proteins typically have more than one role, it is difficult to determine the direct mechanism behind a resulting phenotype. A huge advantage of chemical tools is that they can be tested in a time and dose dependence, which is not possible with molecular biology methods.

CRISPR has been used to introduce point mutations to act as phosphomimetics.<sup>18</sup> Mutagenesis, the process of selectively mutating amino acids to deduce their role in the function of an enzyme can be useful to probe the role of phosphorylation in cells. Phosphorylation commonly occurs on serine, threonine and tyrosine and these sites can be mutated to an alanine switching 'off' the protein as no phosphorylation can occur, or to a charged amino acid i.e., aspartic or glutamic acid mimicking the protein constantly being 'on'.<sup>19</sup>

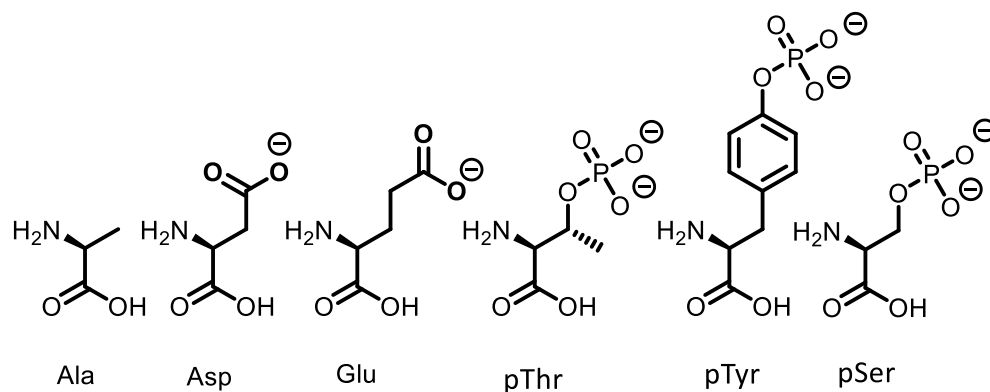


Figure 1.3 - Common amino acids that are phosphorylated or used as phosphomimics.

Whilst point mutations can sometimes act effectively as a phosphomimetic, glutamic and aspartic acid are not always a suitable mutation to copy the phosphorylated protein. In comparison to a phosphate group, they have a -1 charge not -2 charge and differ in geometry and steric size.<sup>18, 20</sup> Being able to directly phosphorylate an amino acid of interest would be useful to understand the exact role of a phosphorylated protein in a cellular pathway.

### 1.3 Bifunctional molecules

Drug design typically focusses on designing a potent selective ligand that non-covalently binds to one protein and blocks the normal function of its target. As the ligand only has an effect when it is bound to the protein this is termed 'occupancy-based pharmacology' and means the drug must be present at high concentrations to maintain its effect - which can be challenging if a high-affinity natural substrate is present.

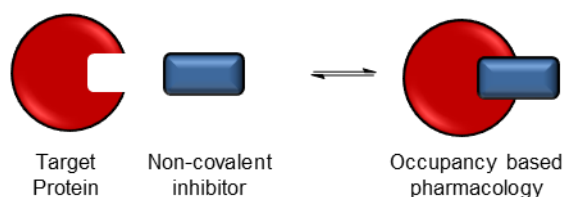


Figure 1.4 - Schematic showing the principle of occupancy-based pharmacology with non-covalent inhibitor

Bifunctional molecules are a more recent development in drug discovery and refer to when two ligands are joined together by a linker with the aim to bind two proteins simultaneously and induce a close proximity. The first reported CIP was FK1012, a homodimer of FK506, which was capable of inducing dimerization of FKBP and starting a signal cascade.<sup>21</sup> However, they are most used for directing post-translational modifications (PTMs) with one ligand binding an effector protein (EP) and the other ligand binding a protein of interest (POI). By binding both biomolecules simultaneously these molecules can force the effector protein to modify the POI with a PTM that alters the function of the target protein (Figure 1.5). This mechanism of action relies on PTMs changing the activity of a protein, and so is termed ‘event-based pharmacology’.

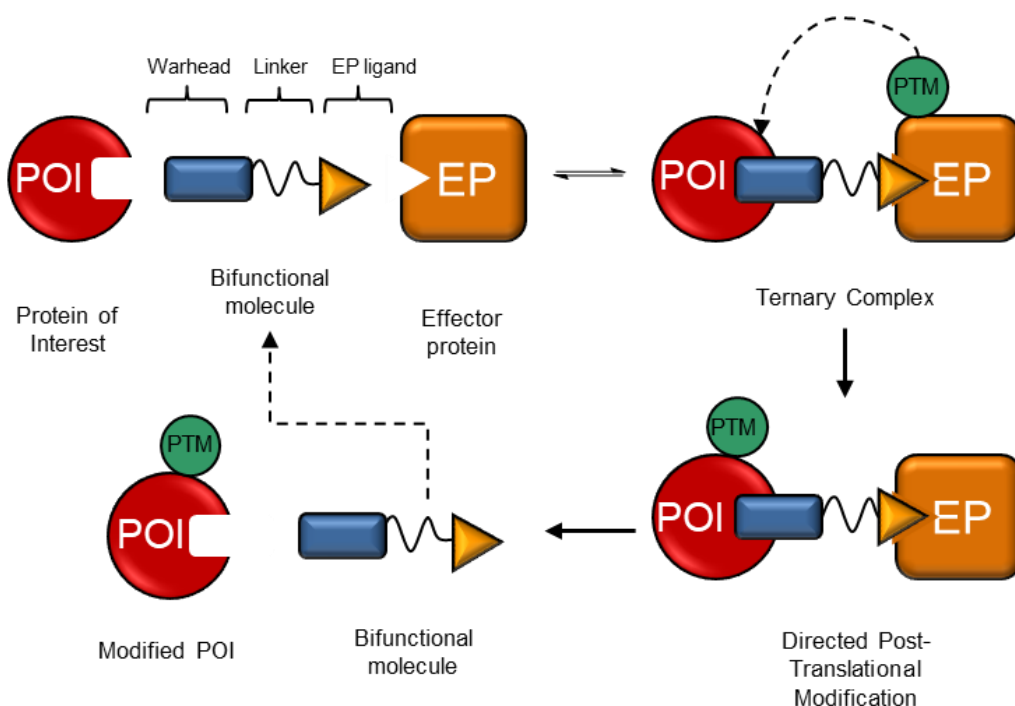


Figure 1.5 - Schematic showing the principle behind event-based pharmacology, and the catalytic cycle of bifunctional compounds

Bifunctional molecules have numerous advantages over a single ligand. As bifunctional molecules work through forming a ternary complex, inducing a PTM and then dissociating, the same bifunctional molecule can be recycled to continually form new ternary complexes and induce the same PTMs on other proteins. This is unlike occupancy-based pharmacology where the pharmacological

effect is dependent on high levels of target engagement with the target protein. The result is that bifunctional molecules can be effective in very low doses. As bifunctional molecules function by inducing a PTM and not by continually binding the POI, it also means lower affinity molecules or ligands that bind a non-functional site on the POI can be used.

The transiently formed ternary complex and event driven pharmacology is also an advantage against proteins that have a high affinity for a natural substrate. As bifunctional molecules only need to form a temporary ternary complex that then dissociates, they do not need to continually outcompete the natural substrate to realise their effect.

The warhead in the bifunctional molecule is primarily what determines which protein is recruited to the ternary complex. Provided a suitable ligand for a different POI exists, it is common and relatively easy to utilise the same EP ligand and simply alter the warhead to target a different protein. This concept has been termed 'plug and play' and means different types of bifunctional molecules can be redirected selectively.

In multiple examples of bifunctional molecules, forming a ternary complex can confer an additional level of selectivity, as some proteins are able to form favourable interactions with each other giving a positive cooperative effect, whilst other proteins form less favourable interactions resulting in negative cooperativity.<sup>22</sup> This selectivity is well reported but only ever deduced from empirical testing with the exact mechanism underlying the favourable and unfavourable interaction unclear.

A key characteristic of bifunctional molecules is the Hook effect, which refers to how the effectiveness drops off at high concentrations of the bifunctional molecule. At low concentrations of bifunctional molecules only small amounts of protein can be recruited into a ternary complex, so relatively small amounts of protein can have a new PTM attached. As bifunctional molecule concentration increases, more ternary complexes can be formed, and this gives a greater response. Past an optimal concentration the bifunctional molecule starts to compete with themselves

for binding sites on the EP and POI, resulting in the formation of binary complexes which do not direct novel PTMs.

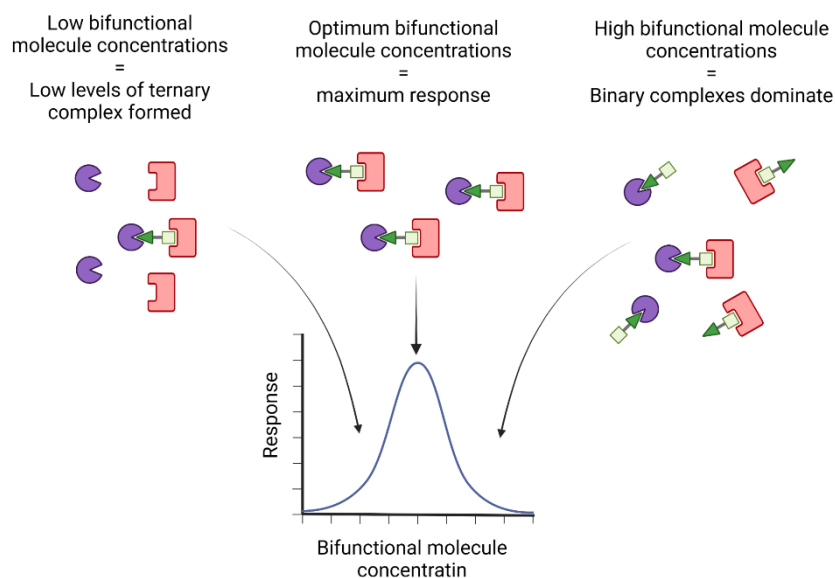


Figure 1.6 - The basis of the Hook effect commonly seen with bifunctional molecules

Due to the crucial role of PTMs in cellular function, bifunctional molecules have been used against a range of targets to direct different types of PTMs.

#### 1.4 Proteolysis Targeting Chimeric small molecules

PROTACs represent the most successful and well used example of bifunctional molecules in a drug discovery setting. PROTACs consist of a E3 ubiquitin ligase binding moiety and ligand for a POI which are covalently joined via a linker. These chimeric compounds form a ternary complex of the E3 ligase and the POI, resulting in the E3 ligase ubiquitinating the POI which leads to its subsequent degradation by the proteasome.

The first PROTAC was successfully published in 2001 degraded the protein methionine aminopeptidase-2 but is now considered a 'bioPROTAC' due to its large peptide structure.<sup>23</sup>

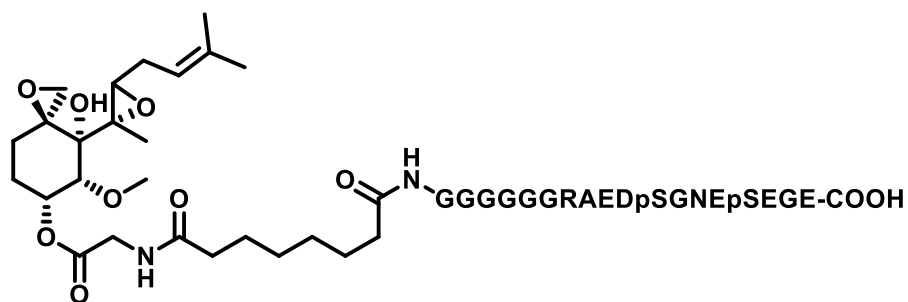


Figure 1.7 - First reported PROTAC molecule

It wasn't until seven years later that a small molecule PROTAC was developed targeting the Androgen receptor and using Nutlin as the ligand for the E3 ligase MDM2.<sup>24</sup>

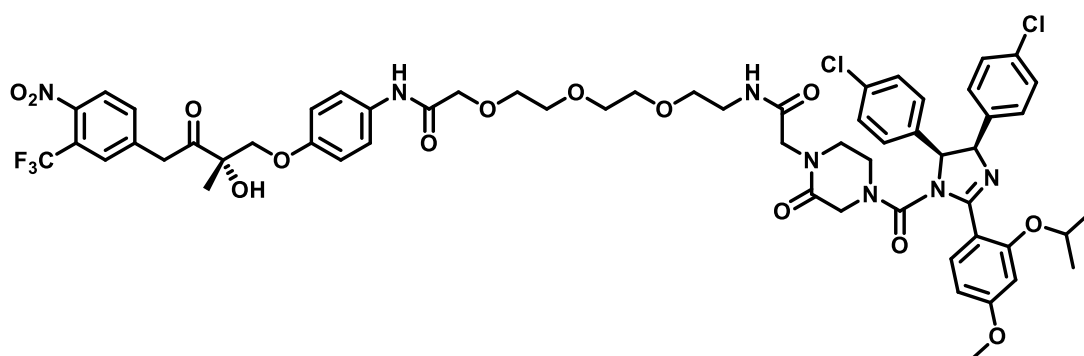


Figure 1.8 - First small molecule PROTAC

A key advantage of this technology is that a successfully designed PROTAC results in degradation of the POI rather than just inhibition.

Many proteins do not have an active site that can be blocked with a small molecule, and proteins often have scaffolding roles that are unaffected even if the active site is blocked with a small molecule. With a PROTAC, non-functional binders of the target protein can be used and as the entire protein is degraded it can no longer carry out either its functional or scaffolding role. This can be useful in target validation, by helping to elucidate the full role of a protein. As PROTACs exhibit a catalytic Mechanism of Action (MoA) they have been shown to give complete degradation at <1nM and can result in pM efficacy in cell lines.<sup>25</sup>



A common side effects of treating a cancer with a small molecule is mutations to reduce binding affinity of the drug to the protein and increased protein. In both these cases PROTACs can offer advantages over a single ligand treatment. In targeting the Androgen receptor, treatment with a small molecule or an optimised PROTAC results in the upregulation of androgens, which can result in a loss of efficacy due to increased competition for the receptor. It was found PROTACs give a smaller drop off in efficacy compared to the single ligand warhead as PROTACs do not need to constantly outcompete the natural substrate, and just need to form the ternary complex.<sup>26</sup>

Due to the extensive work on PROTACs they most easily represent how the correlation of warhead potency, and its resulting cellular effects are as yet poorly understood. For example, in the design of PROTACs targeting TBK1, the binding affinity of the PROTAC for VHL and TBK1 does not completely predict  $DC_{50}$  or  $D_{max}$ . When R = H, the PROTAC has a  $K_d = 725\text{nM}$  against TBK1 with a  $DC_{50} = >1,000\text{ nM}$ , suggesting binding against TBK1 but no successful degradation. However, when R = Me, the PROTAC has a  $K_d = 270\text{ nM}$ , which is a  $\approx 3$ -fold increase in binding affinity, but now degradation is seen with a  $DC_{50} = 92\text{ nM}$  and a  $D_{max} = 89\%$ . As a result, it is clear a potent and effective PROTAC does not require high affinities to the proteins of interest.<sup>27</sup>

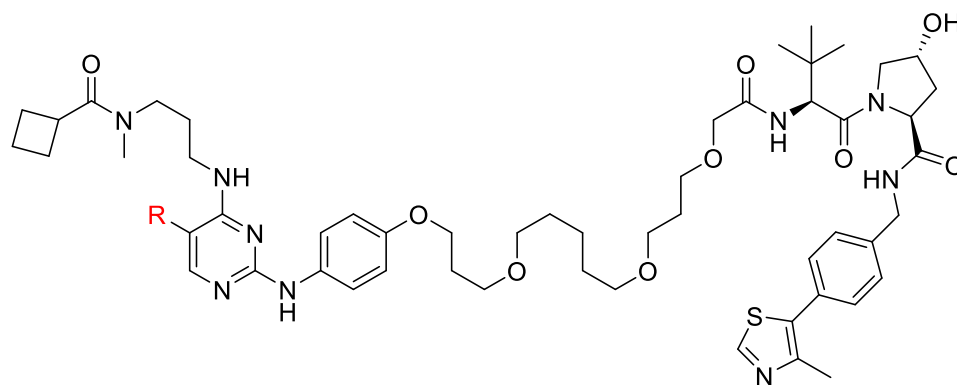


Figure 1.9 - TBK1 PROTAC with the variable group, R, shown in red. Crew 2018

As warhead affinity does not accurately predict degradation, there is no strict cut-off value at which binding affinity is too low to work. However it has been proposed that ligands with an  $K_d < 500$  nM represent a good starting point, with a strong enough affinity to bind the POI strongly enough to induce ternary complex formation.<sup>28</sup>

## 1.5 Deubiquitinase-Targeting Chimera (DUBTAC)

It has been shown that bifunctional molecules can also be used to direct deubiquitinases to neo-substrates and rescue protein degradation. A covalent, non-inhibitory small molecule, EN523, was identified from activity-based protein profiling (ABPP) that bound to OTUB, a DUB. SAR was done to identify a solvent exposed site, on the methyl furan which was then linked to Lumacaftor, a CFTR ligand, with a range of linker lengths and identities.

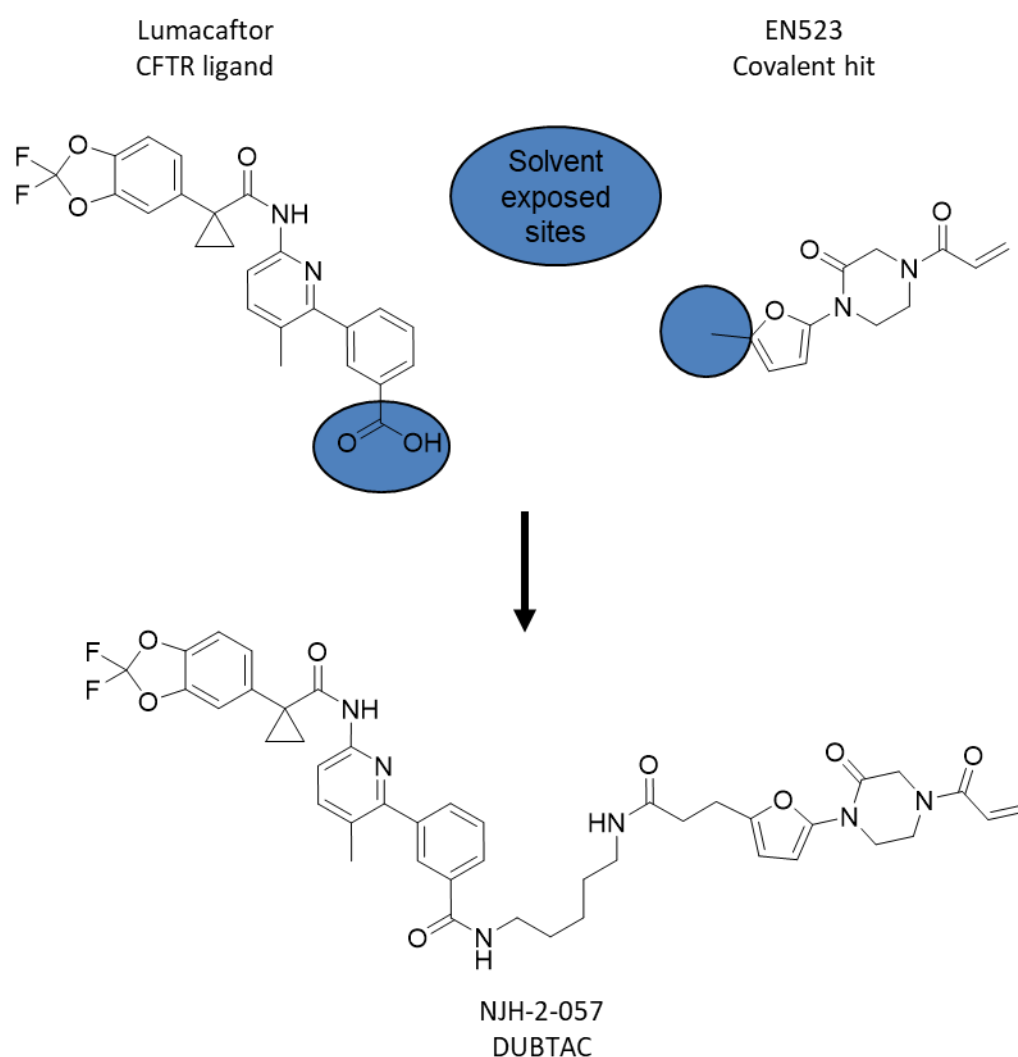


Figure 1.10 - Scheme showing the development of single ligands in a DUBTAC

Testing in cells showed increased levels and stabilisation of CFTR in line with sustained deubiquitination which thus prevents degradation.<sup>29</sup> This method was further developed in the same work by targeting the kinase WEE1 with a WEE1 ligand that had been used in PROTACs suggesting it has potential as a more broadly applicable technology.<sup>29, 30, 31</sup>

## 1.6 Bifunctional molecules for acetylation

A recent development in the field of bifunctional molecules, only published in 2021, is the directed acetylation of proteins, so called AceTAC which stands for acetylation tagging.<sup>32</sup> The authors were able to direct the acyltransferase (KAT) p300/CBP to acetylate histone H3.3, NF- $\kappa$ B and p53. Rather than identify a small molecule warhead, identify solvent exposed sites and then make bifunctional molecules, they instead separately expressed different POIs with a FKBP12<sup>f36V</sup> tag. High affinity ligands with solvent exposed sites for FKBP12<sup>f36V</sup> are known so bifunctional molecules are made that bind the FKBP12<sup>f36V</sup> tag rather than the target protein. As a result, they can use the same AceTAC compound in all target proteins as shown in Figure 1.11

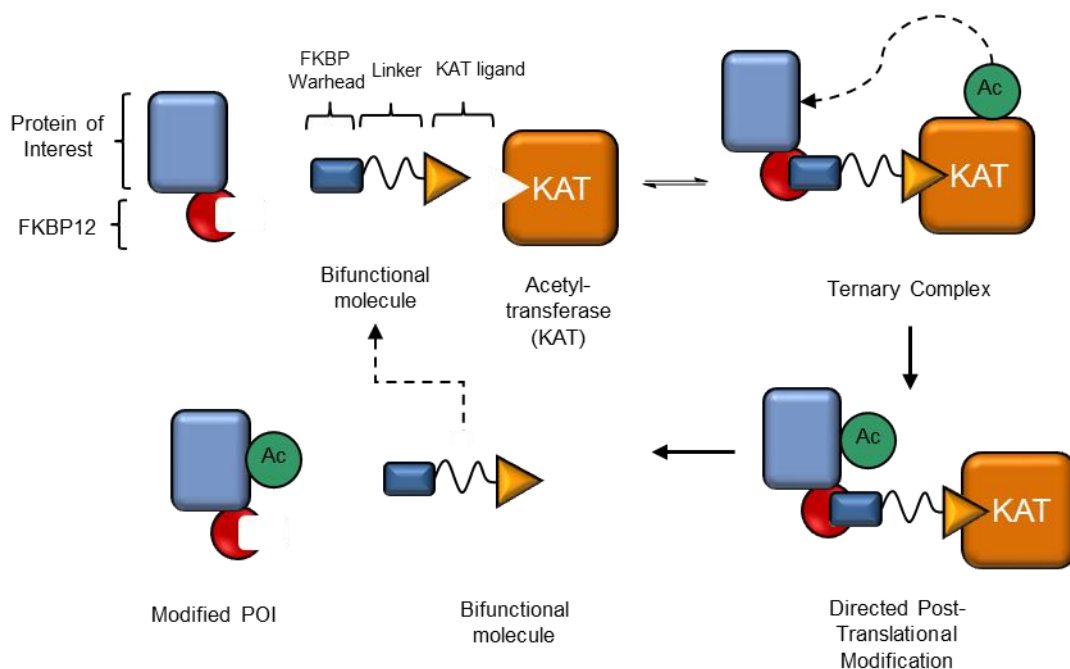


Figure 1.11 - Schematic showing how using an FKBP probe can be used to investigate a POI

Considering the broad range of substrates, they are able to target it suggests this technique may have a broad substrate scope, but as they use a FKBP12 ligand rather than a selective probe this would prevent its use in a native biological system.

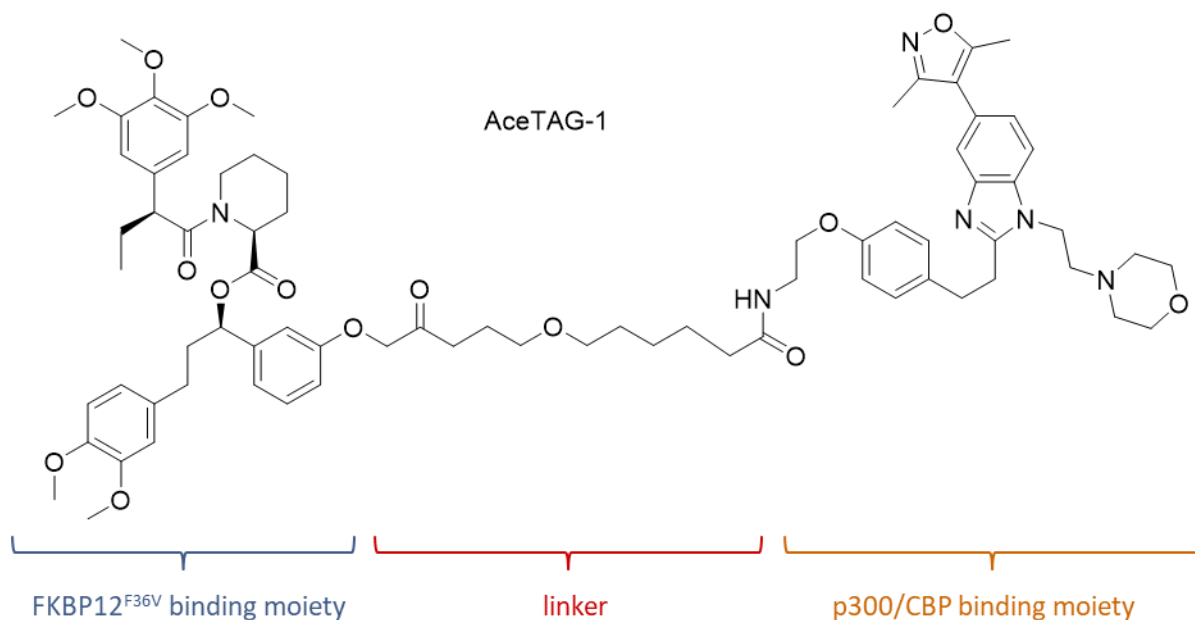


Figure 1.12 - Chemical structure of the AceTAC bifunctional molecule

## 1.7 Bifunctional molecules for phosphorylation

Due to the amenability of PROTACs and the importance of kinases as a class of protein, kinase PROTACs have been shown well reported.<sup>33,34,35</sup> However, being able to alter the phosphorylation of a kinase or a kinase substrate would be a useful chemical tool to validate the relevance of a phosphosite in a disease state.

The aim of my project was to apply the general principles of bifunctional molecules as described in Section 1.3, and rationally design molecules that could induce neo-phosphorylation of substrate proteins. At the time this work was started, no examples of this had been reported and most of the work has been done from the perspective that this was a proof-of-concept idea. However, since we started work,

examples of bifunctional molecules that can induce phosphorylation and dephosphorylation have been published.<sup>36, 37, 38</sup>

A group in 2020 showed that Protein Phosphatase 1 (PP1) could be directed to dephosphorylate AKT and EGFR through the design and synthesis of a rationally designed bifunctional molecules.<sup>36</sup> This concept was termed phosphatase recruiting chimeras (PhoRC), and despite having been published two years ago there have been no further publications related to dephosphorylation with this technique. Potential issues could be the relatively low levels of dephosphorylation that are seen, and that this may not correspond to the desired threshold for altering the phenotype of a cell. In short, achieving functionally relevant levels of altered phosphorylation may be very challenging

The reverse idea of showing directed phosphorylation from a kinase to a neo-substrate has also been recently shown to be possible, with a group publishing the rational design of phosphorylation inducing chimeric small molecules (PHICS).<sup>37</sup> In this work they identify solvent exposed sites on a reported Adenosine Monophosphate Kinase (AMPK) activator and show successful neo-phosphorylation of bromodomain-containing protein 4 (BRD-4) and Bruton Tyrosine Kinase (BTK), using the bifunctional molecules shown below (Figure 1.13). In both cases the ligands for the POI were already successfully used in PROTAC so a solvent exposed site has already been validated.<sup>22,39</sup> In this work they also do not comment on whether cells show an altered phenotype which again suggests that functionally relevant levels of phosphorylation is more difficult to achieve than functionally relevant levels of degradation. This could be as the phosphosites are not physiologically relevant or phosphatases prevent high levels of phosphorylated protein accumulating.

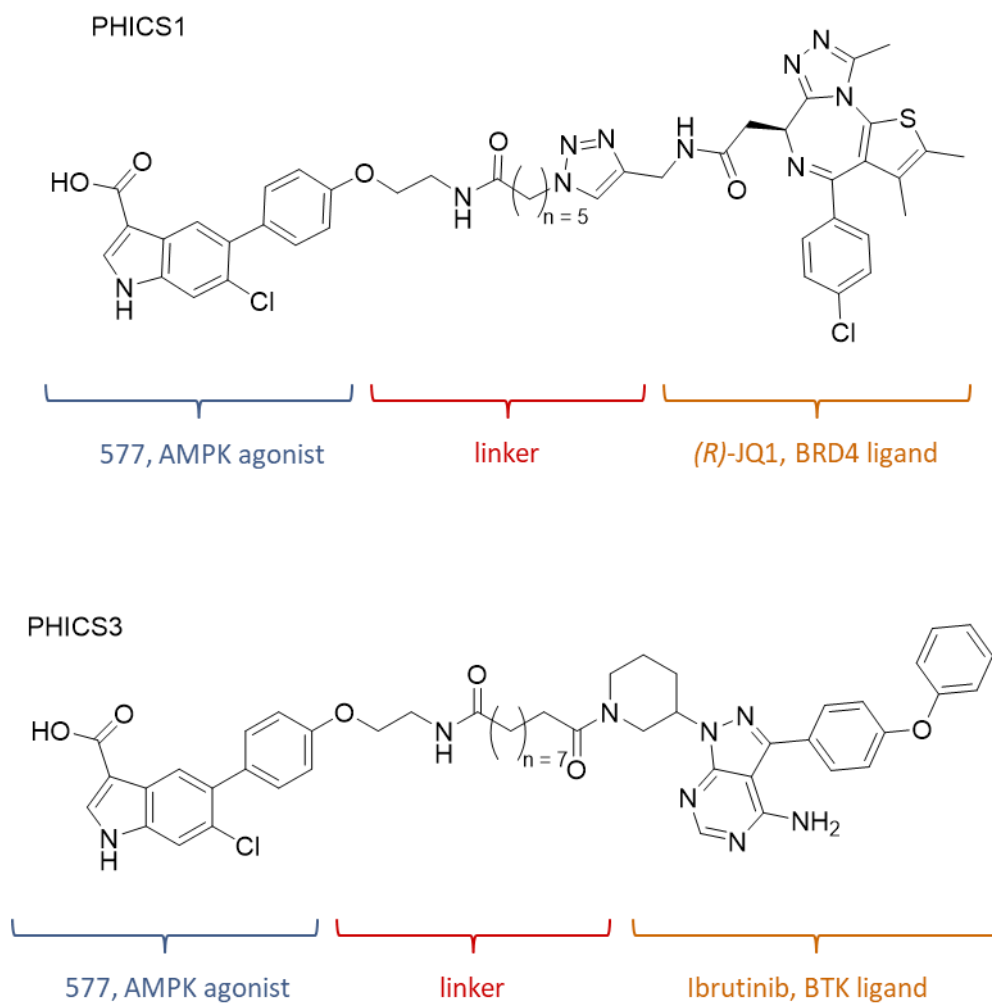


Figure 1.13 - Reported Phosphorylation Inducing Chimeric Small Molecules (PHICS)

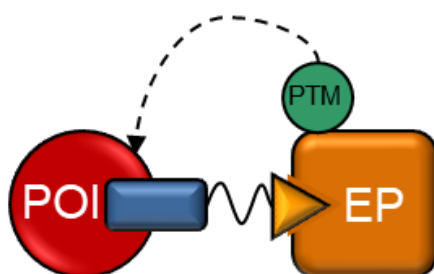
This work has also been developed by the same group redirecting the kinase PKC to phosphorylate neo-substrates.<sup>38</sup>

Unlike PROTAC, where success can be measured by quantifying protein levels, PhoRC and PHICs require individual phosphosites to be identified and their levels monitored, as different phosphosites will have different effects on the protein's function. Existing techniques for examining phosphorylation include using phosphospecific antibodies and phosphoproteomics.

### 1.8 Designing bifunctional compounds

Successfully designed bifunctional compounds should form a ternary complex between a Protein of Interest and an effector protein, of the correct orientation to allow a PTM to be transferred onto the POI. Bifunctional molecule design requires

identifying ligands that can bind to desired proteins, then identifying and validating sites to attach a linker. Once linker attachment sites have been confirmed then bifunctional ligands of a range of linker lengths must be synthesised.



Ternary Complex

Figure 1.14 Diagram of desired ternary complex and subsequent PTM

The first step to successfully designing bifunctional molecules is first identifying the proteins to target, and a key influence is if suitable ligands already exist. Developing single ligands into bifunctional molecules is first done by using structural information to identify solvent exposed sites. Having solvent exposed sites is crucial as the key as the two ligand moieties for the EP and POI will be joined together by a linker, so linking from the ligands must not stop them binding to their proteins.<sup>40,41</sup> These solvent exposed sites are explored by incorporating small flexible group such as an alkyl or glycol chain at the desired position that tests if a linker is tolerated sterically and electronically and doesn't prevent the ligand binding. With certain PROTACs it has been shown different linker sites can result in different levels of degradation, so PHICs with different solvent exposed sites could alter any induced neo-phosphorylation. Another feature from PROTAC is that desirable single ligand potency is 1-500 nM, so wanted to stay within that range.<sup>28</sup>

Additionally for this project we wanted the effector protein to have an allosteric binder that binds the kinase nearby and on the same face as the ATP binding site. The ATP binding site would have on the same face that the POI will be brought close to, so that a phosphate group can be transferred. As we want to redirect the



kinase phosphorylation, not stop it, we could not use a kinase inhibitor and instead needed an allosteric binder or allosteric agonist.

For the POI we wanted to identify a ligand that binds near a functionally relevant phosphosite. As phosphorylation is sometimes non-functional, we ideally wanted to direct phosphorylation to a functionally relevant site so that we could follow up techniques in phenotypic assays. Another technique used to confirm changes in phosphorylation is using phosphospecific antibodies, which are generally only available for the functionally relevant phosphosites, as such by targeting a key phosphosite we would be able to confirm it more easily. Finally, for validating phosphorylation we would like to target a site which has low levels of phosphorylation and is unable to auto phosphorylate, so that neo-phosphorylation is a greater change from the background.

Once solvent exposed sites are validated, the linker between the two binding groups must be designed. Linker length and identity has been shown to be key to activity.<sup>42</sup> Too short a linker results in a bifunctional compound able to bind each half of the protein separately but unable to form a ternary complex and thus no successful directed PTM. Too long a linker is considered better than being too short, but now may result in an entropic penalty from a long flexible linker having its conformation restricted. The general strategy is to synthesis bifunctional compounds with a range of linker lengths and find the optimum length from experimental testing. As such synthetic accessibility is key, as a range of bifunctional compounds have to be made to empirically determine the levels of the PTM of interest.

Most bifunctional compounds contain a long linear linker chain consisting of just alkyl or glycol based groups with the ratio between carbon and oxygen used to alter the lipophilicity.<sup>43</sup> A highly flexible chain allows the two proteins to adopt stable and favourable interactions to form a cooperative and productive complex. The first molecules in each type of -TAC technology has used a simple linear chain, but more recently linker rigidification with alkynes, piperazine and aromatic rings have been used to develop PROTACs with improved degradation profiles.<sup>25,44</sup>

However, even if potent warheads are joined together and the bifunctional molecule can bind each protein separately, this does not mean a stable ternary complex will form. As will be mentioned later in section 1.13, some proteins exhibit negative cooperativity, and this will prevent induction of a PTM.

## 1.9 Adenosine Monophosphate kinase (AMPK)

On the basis of the reasons described in the previous section we selected AMPK as the effector protein for this project, that we would redirect to phosphorylate neo-substrates.

5'- Adenosine Monophosphate Kinase (AMPK) is a heterotrimeric serine threonine kinase composed of three subunits each with different isoforms, catalytic:  $\alpha$ 1 or  $\alpha$ 2, scaffold:  $\beta$ 1 or  $\beta$ 2 and regulatory:  $\gamma$ 1,  $\gamma$ 2 or  $\gamma$ 3. In humans, all subunit combinations are possible, giving 12 possible AMPK isoforms, with different localisations of isoforms throughout the body.

AMPK plays a key role in energy homeostasis as its activity is controlled by energy stress; the levels of ATP and AMP present in the local environment. High AMP levels activate AMPK to switch on catabolic pathways to produce more ATP such as glucose uptake and glycolysis, whilst switching off anabolic pathways that consume ATP such as biomolecule synthesis.<sup>45</sup> AMPK's prominent role means that it is a target for diabetes, with inhibitors and activators of AMPK having been developed. AMPK activators are reported to work by stabilising the active form of AMPK which can catalyse phosphoryl transfer to a substrate and protect AMPK against dephosphorylation which deactivates it.

The first optimised small molecule allosteric activator of AMPK is A-769662, discovered by Abbott.<sup>46</sup> Other groups have developed distinct AMPK activators such as **991**, developed by Merck, and **557**, developed by Pfizer. These two compounds show structural similarity, sharing a similar chloro-substituted 5, 6 fused heterocycle core (Figure 1.15).<sup>15, 47</sup>

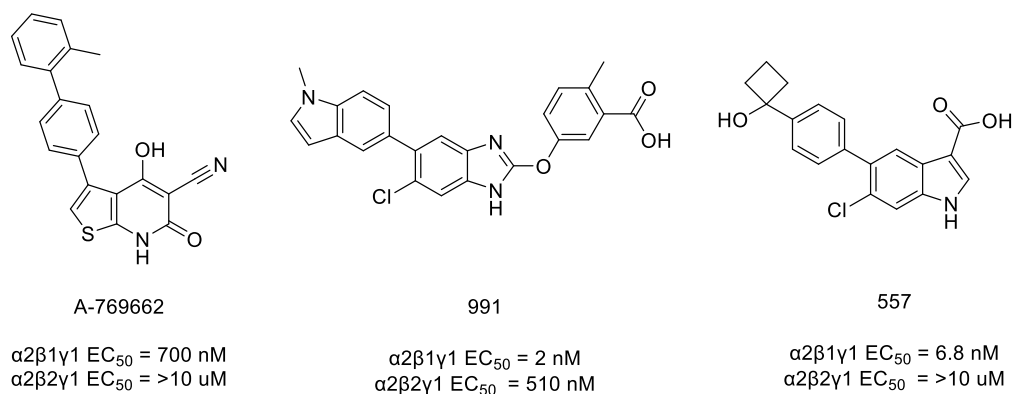


Figure 1.15- Reported AMPK activators

All these small molecule activators bind to an allosteric site between the Carbohydrate Binding Motif (CBM) which is part of the scaffold domain, and the kinase domain. The published crystal structure of **991** bound to full length  $\alpha 2\beta 1\gamma 1$  AMPK shows that **991** binds nearby and on the same face as the active site in an allosteric pocket between the catalytic and CBM (Figure 1.16). The binding location means that if this face of the kinase is brought into proximity with a target protein, then the ATP binding site of AMPK will also be brought into proximity with the target protein. Although a non-functional binder of AMPK could have been used in this project, we hoped that by using an agonist we could use AMPKs increased activity and direct it to neo-substrates.

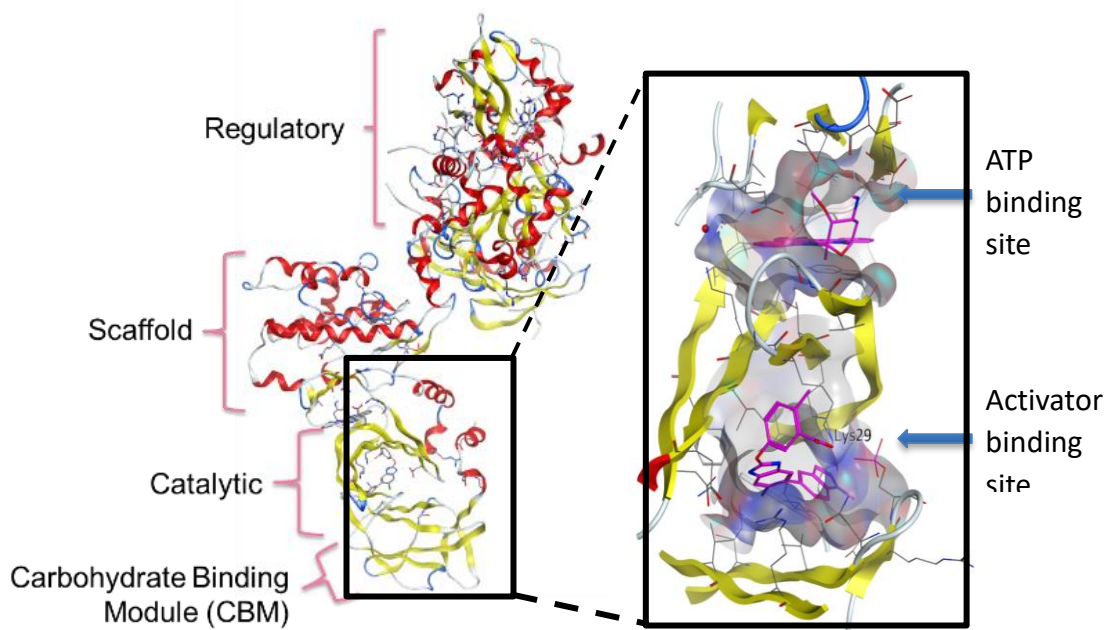


Figure 1.16 - left: Full length AMPK. Right: receptor surfaces of activator and ATP binding sites.

Additionally, as **991** has a low nano-molar  $EC_{50}$  against multiple AMPK isoforms, it placed us well within the desired potency range of <500nM.

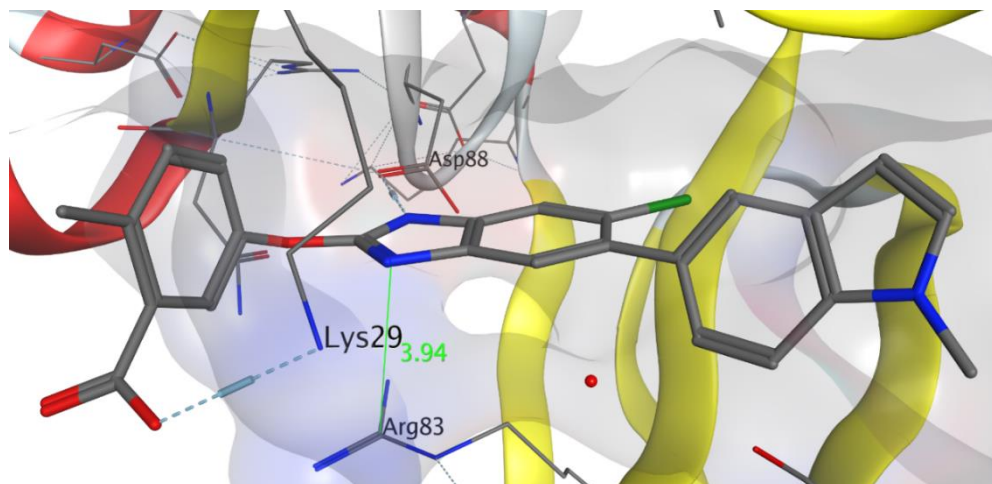


Figure 1.17 - 991 bound to AMPK (PDB: 4CFE)

### 1.10 Mixed Lineage Kinase Domain-Like Protein

For the reasons mentioned in section 1.8, MLKL was chosen as the substrate protein for this project.

Mixed Lineage Kinase Domain-Like (MLKL) is 471 amino acid found in the cytoplasm and nucleus of cells. It consists of a C-terminal pseudokinase domain and an N-terminal 4 Helix-Bundle (4HB) effector domain, attached by two helices called the brace domain. Of the key structural features that define a kinase, MLKL lacks the glycine rich loop, and the HRD and DFG motifs are instead HGK and GFE respectively, but the VAIK motif is conserved. As such, MLKL is unable to catalyse ATP hydrolysis with wild type hMLKL binding ATP with  $K_d = 36 \pm 4 \mu\text{M}$ .<sup>48</sup> It has also been reported that MLKL can not autophosphorylate which made it an ideal substrate protein as any detected phosphorylation in biochemical assay is likely a result of neo-phosphorylation by a kinase.<sup>49</sup>

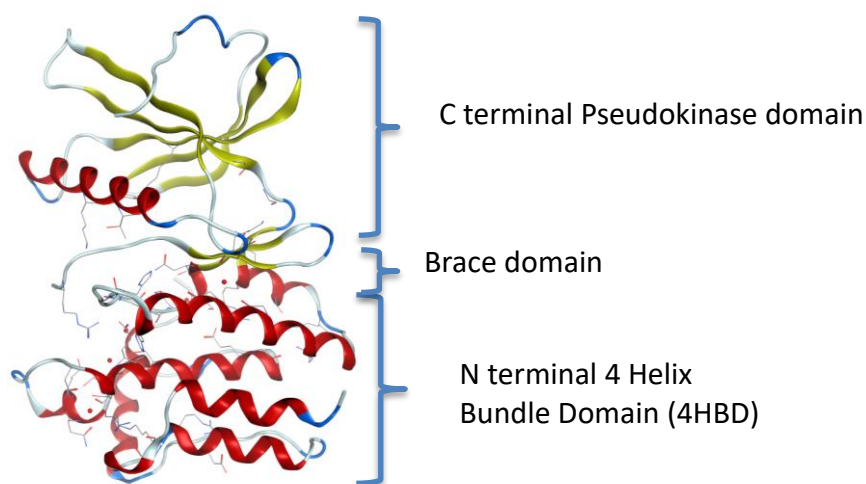


Figure 1.18 - Structure of MLKL. PDB: 5KO1

Pseudokinases have been a typically overlooked drug target as they don't hydrolyse ATP so have not been considered very functionally relevant. Ma et al used a commercial assay testing service to screen 5,000 compounds which bind the ATP site of MLKL which were not further optimised.<sup>2</sup> As such, there are only three reported hit compounds that bind MLKL reversibly with a  $K_D < 1 \mu\text{M}$ , shown below in Figure 1.19:

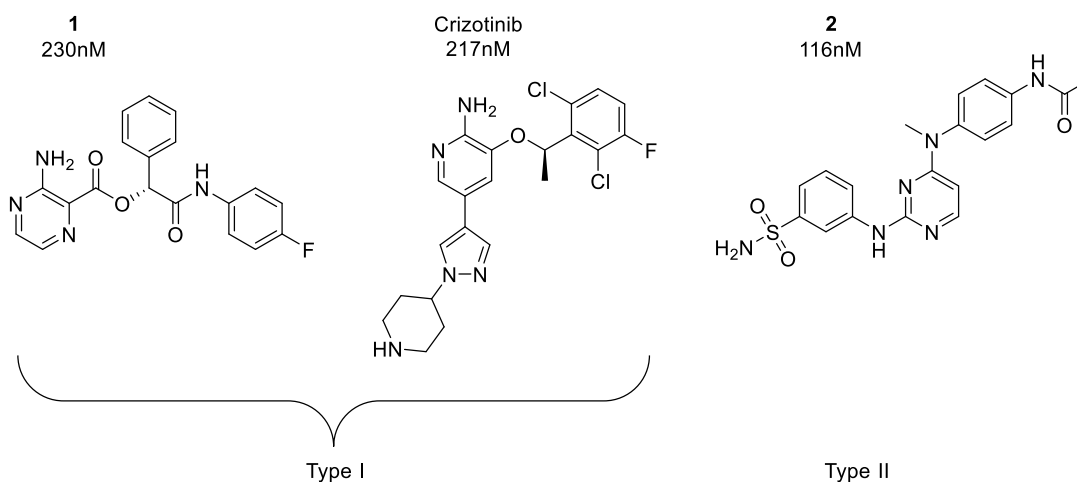
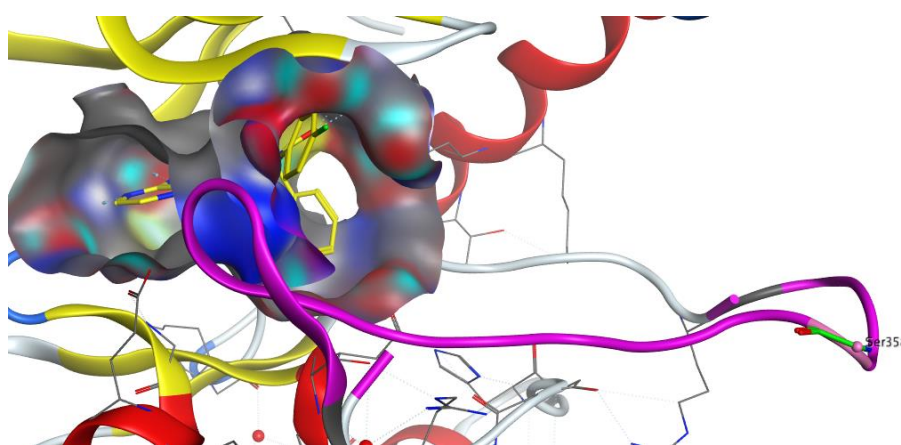


Figure 1.19 – Selected non-covalent binders of MLKL

Compound **1** has been crystallised in the active site of MLKL which allows solvent exposed sites to be identified and shows binding near the activation loop of MLKL. Upon phosphorylation of Ser358 with the activation loop, MLKL becomes activated

and is triggered to cause cell death which would provide an easy read out. As pSer358 is a site of therapeutic interest phosphospecific antibodies are commercially available which would be useful for investigating altered phosphorylation.

It has been proposed that the type II inhibitor **1** increases the solvent exposure and availability of MLKL's activation loop<sup>2, 50</sup>, whereas a type I inhibitor, **2**, binds in a way that reduce the availability of the activation loop.<sup>2</sup> This has however been disputed with similar experiments showing that neither **1** or **2** have a significant impact on pMLKL levels and were unable to rescue cells from necroptosis<sup>2</sup>. As such, the ability of small molecules to inhibit necroptosis is not yet clear, and chemical tools that alter its phosphorylation could be highly useful.<sup>2, 51</sup>



*Figure 1.20 - Crystal structure of **1**, bound to MLKL. The activation loop is modelled and Ser358 is labelled. PDB: 5K01*

### **1.10.1 Cellular role and Therapeutic relevance**

In MLKL's inactive and unphosphorylated form, protein-protein interactions hold the pseudokinase and the 4HB domain together but following phosphorylation of Ser-358 by the upstream kinase RIPK3, conformational changes occur that result in the 4HB domain dissociating from the pseudokinase domain unleashing the 'executioner' function of the protein. In this new conformation MLKL translocates to the cell membrane and forms oligomers which cause permeabilization of the membrane, leading to cell death in the form of necroptosis.<sup>48, 52</sup>

Knock out studies in mice have shown that a lack of MLKL had no effect on health or fertility but were resistant to induced necroptosis.<sup>49</sup> When MLKL expression was restored, sensitivity was restored this suggesting that MLKL only acts as the effector of necroptosis. This one specific function means that if MLKL phosphorylation could be induced with a bifunctional molecule, the only function of MLKL would be to induce necroptosis. To date no other protein kinases are known to phosphorylate MLKL other than RIPK3.

RIPK3 expression is suppressed in certain cancers such as Acute Myeloid Leukaemia (AML), breast and colon, and it has been proposed this, protects the cell against necroptotic cell death.<sup>53, 54, 55</sup> This is exemplified in the figure below showing how the levels of mRNA for RIPK3 are lower in Tumour (T) tissues compared to the surrounding Normal (N) tissue in patient samples, whereas MLKL shows no obvious trend<sup>24</sup>. As such, a chemical tool that could directly phosphorylate and thus activate MLKL in the absence of RIPK1 could be a novel therapeutic approach.

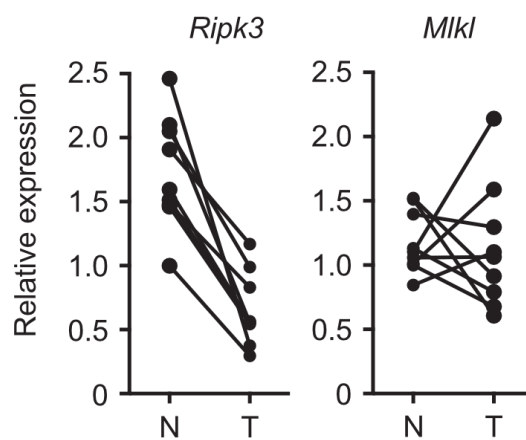


Figure 1.21 - Patient samples showing the mRNA expression levels in surrounding Non-cancerous tissue (N) and in the Tumour (T)

Resisting cell death is a hallmark of cancer and certain cancers are able to become resistant to apoptosis inducing drugs, thus preventing cell death.<sup>56</sup> As apoptosis and necroptosis function via different pathways triggering necroptosis with a bifunctional molecule could provide an approach to killing apoptosis-resistant cancers.<sup>57, 53</sup>

### 1.11 Introduction to Phosphoproteomics

Proteomics refers to the large-scale analysis of proteins in a given system. Analysing the levels of proteins in a cell is a key goal in understanding cellular phenotypes and answering key biological questions, such as the components in a signalling cascade or change in protein levels in response to a drug treatment.

Proteomics uses mass spectrometry to identify peptides from their mass, as the mass is measured it is possible to detect PTMs on proteins. Identifying and characterising phosphosites can provide information on the mechanism behind protein function and this approach, known as phosphoproteomics allows a global picture of signalling events to be quantified with unambiguous assignment of phosphosites.<sup>58</sup>

The proteomic workflow starts with treating cells with a compound at a set concentration and time. The time point needs to be for compounds for permeate cells, engage the target and exert an effect, but too long an exposure can result in multiple downstream effects, making interpretation more complex. After treatment the cells are washed, pelleted then lysed and the cell lysates are digested with Trypsin. This digestion cleaves next to lysine and arginine residues. This means that every possible peptide sequence and mass is already known, and that each peptide formed contains a positively ionisable site thus aiding its detection by mass spectrometry.

If every sample of interest was to be run individually then not only would the instrument time required be incredibly high, but crucially due to the intrinsic systematic errors of mass spectrometry then it would not be possible to compare the levels of protein between samples. To circumvent this issue, each digested cell lysate is treated with a different mass tag to allow sample multiplexing.

A common strategy for sample multiplexing is using Tandem Mass Tags (TMT) which contain three parts: An amine reactive NHS ester, a mass normalisation group and a reporter ion group (Figure 1.22). The NHS-ester reacts with the N-terminal amine of each peptide and ensures all the digested peptides are tagged. The overall structure and total mass of each tag is identical but vary in the number



of heavy isotopes contained in the reporter ion group with up to eight heavy atoms,  $^{13}\text{C}$  and  $^{15}\text{N}$ , able to be incorporated. To keep the mass consistent between tags, for every heavy atom included in the reporter ion group, a heavy atom is removed from the mass normalisation group.<sup>59,60</sup>

Sample multiplexing gives the proteins in each treatment a unique mass response when analysed in MS/MS, allowing multiple sets of cell lysates to be tested simultaneously. At the time of utilising TMT tags in this project the most advanced TMT tags were 16-plex (Figure 1.22).

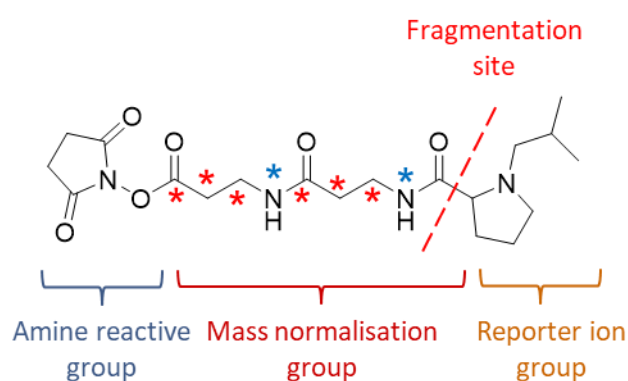


Figure 1.22 - 16-plex TMT isobaric label structures. Red and blue show available sites for heavy atoms in the mass normalisation group

After TMT labelling the samples are then pooled together. For phosphoproteomics an enrichment step is then done. The enrichment step is needed as the phosphorylated peptide is a fraction of the abundance of the non-phosphorylated peptide, and without removing the non-phosphorylated peptides they would be the highest intensity peaks and swamp out the lower abundance phospho-peptide peaks. Peptides are treated with a metal (Fe or Ni) bound to a resin, which coordinates to phosphate groups and allow non-phosphorylated peptides to be washed off. Even with this enrichment, the levels of phospho-peptides are low which typically results in low number of phosphopeptides being identified. This poor coverage means phosphoproteomic samples must be collected in triplicate.<sup>58,</sup>

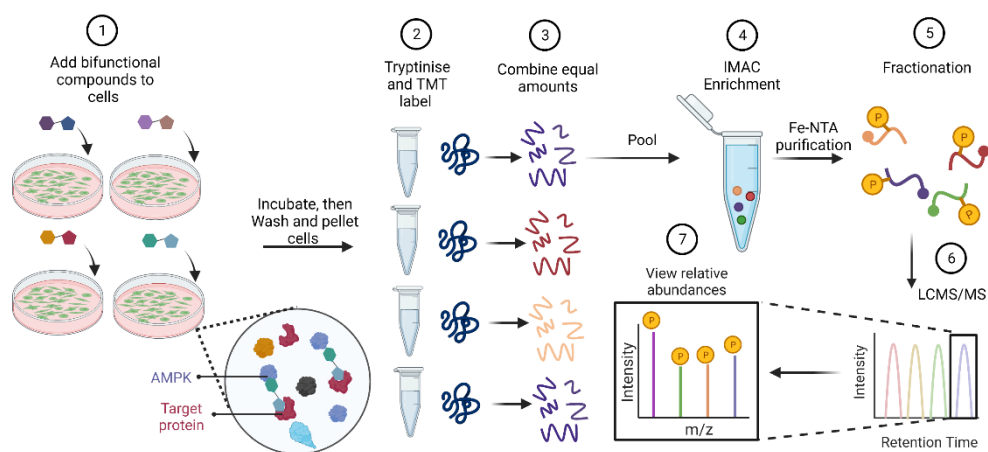


Figure 1.23 - Scheme showing the workflow for phosphoproteomics

Once enriched there are some highly abundant peptide peaks that would limit the detection of lower abundance peptides. To counteract this the enriched samples are subjected to HPLC fractionation which separates peptides based on lipophilicity, to give fractions which are then individually analysed by LCMS/MS. This approach allows lower abundance phosphopeptides to be analysed, with the more fractions collected and analysed, the deeper the coverage of the proteome,

If looking for protein degradation, provided you can confidently identify one peptide for a target protein you can determine the whole protein level and measure degradation. However, in phosphorylation identifying one peptide for a protein will only give information about that exact peptide and give no information on other sites on the protein.

Although phosphoproteomics provides is a useful technique for examining the phosphorylation state of proteins in a cell, it requires confirmation by orthogonal methods such as phosphospecific antibodies.

### 1.12 Click chemistry

Bifunctional compound activity has been shown to be is highly dependent on linker length, with the optimal linker length only found from experimental testing. As a

result, we needed to synthesise a library of bifunctional compounds with varying linker lengths that we could test. To rapidly synthesise a library, we decide to utilise the Copper(I)-catalysed Azide-Alkyne Cycloaddition (CuAAC) as this is a high yielding, quick and stereospecific reaction, which tolerates of a wide range of functional groups and generally proceeds in neutral conditions.

Classic CuAAC conditions use water as a solvent with copper sulphate as the catalyst and sodium ascorbate to reduce the Cu(II) to the active species Cu(I), although as long as Cu(I) is available the reaction can proceed, as shown in Figure 1.24. Whilst stabilising ligands such as TBTA have been reported to increase yields in click chemistry they can interfere with purification, and many high yielding reactions are commonly employed without them.

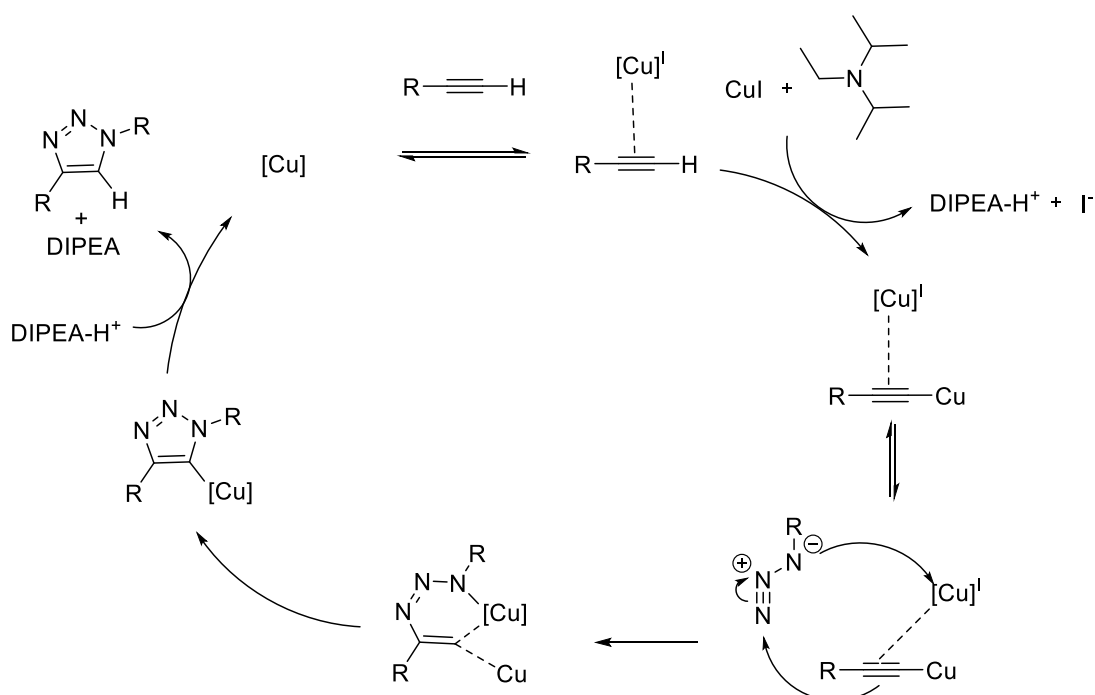


Figure 1.24 - Mechanism of a Copper-Catalysed Azide-Alkyne Cycloaddition

The azide and alkyne precursors can be easily accessed and are relatively stable, meaning that sets of reagents can be prepared and combined in a combinatorial manner to make a large set of products from common intermediates. This convergent approach means that if a new target protein with a ligand and solvent exposed site is identified, then a new library of bifunctional ligands can rapidly be made.

### 1.13 Biochemical assays for measuring ternary complex formation

Although there are many well established assays available for testing the binding of molecules against a single protein, there are relatively few assays for examining ternary complexes. Even with the surge of interest in PROTAC bifunctional molecules, high throughput biochemical assays having seemingly lagged behind the cellular testing, with few PROTAC papers demonstrating or quantifying a ternary complex. This is typically due to protein-protein interaction assays being difficult to optimise and develop. The most commonly used biochemical methods for characterising ternary complexes are Surface Plasmon Resonance (SPR), Time-Resolved Fluorescent Resonance Energy Transfer (TR-FRET) and Amplified Luminescent Proximity Homogeneous Assay AlphaScreen/AlphaLisa.<sup>62,63</sup>

SPR is an established biophysical assay technique that works by immobilising the protein on a surface, then continually flowing over varied concentrations of a small molecule. Increase in the mass of the bound analyte alters the angle of reflected light which is used to infer a rate of binding. This technique has been applied to bifunctional molecules by immobilising one of the target proteins, Protein A, and first adding the bifunctional molecule of interest to get a  $K_D$  of the molecule for the protein. Then the second protein, protein B, is the flowed over, and any association can be measured to give a  $K_D$  for ternary complex formation. By measuring binary and ternary binding affinities, it can be detected to what extent the occupancy of one protein changes binding affinity for the second site, an effect known as cooperativity ( $\alpha$ ) and given by the equation:

$$\alpha = \frac{K_D^{Binary}}{K_D^{Ternary}}$$

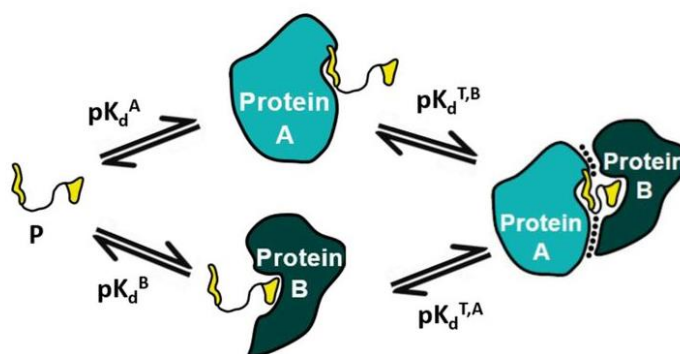


Figure 1.25 - Schematic of SPR for measuring ternary complex formation. Taken from Hughes 2017

When  $\alpha > 1$  this is referred to as 'positive cooperativity' and indicate ternary complex binding is stronger than binary complex binding and indicate a stable complex thus an increased chance of inducing a PTM. Likewise, a  $\alpha < 1$  is referred to as 'negative cooperativity' and indicates an unstable ternary complex is formed, with a decreased chance of directing PTMs.<sup>64</sup>

Although highly useful for the amount of kinetic data that is gained from this assay format, it is fairly low throughput requiring lots of optimisations.

TR-FRET assays are a high throughput assay format in comparison to SPR, as its amenable to miniaturisation and relatively easy to test libraries of compounds simultaneously. The two proteins of interest, with orthogonal affinity tags, are mixed together in the presence of a small molecule. Two antibodies are also added, a donor antibody containing Europium or Terbium, and an acceptor antibody conjugated to a fluorophore, and they bind their respective proteins by recognising the affinity tags. After an incubation period the donor antibody is excited and if the acceptor antibody is in close enough proximity, then the fluorophore can be excited and then release energy which can be read. The closer the proteins, the greater the signal.

However, the energy crossing is very distance dependent with  $E \propto r^{-6}$ , so using this assay technique is heavily dependent on having suitably orientated tags withing 10nm.

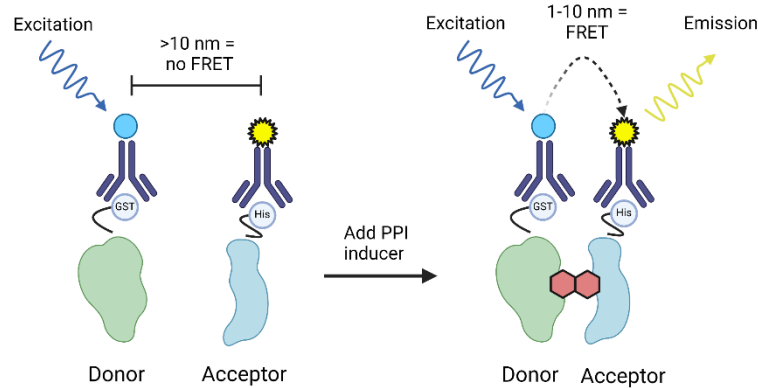


Figure 1.26 - Schematic representation of TR-FRET as a proximity-based assay

Another homogenous, high-through-put assay is the Amplified Luminescent Proximity Homogeneous Assay Screen (AlphaScreen) or AlphaLisa. This technology, like TR-FRET, also works by having orthogonally tagged proteins with complementary antibodies, but the antibodies are immobilised on donor and acceptor beads. The beads are covered in a hydrogel so do not self-aggregate and are small enough not to interfere with pipetting. After an incubation period the donor antibody is stimulated with a laser to releases singlet oxygen that can diffuse for 200nm. If this singlet oxygen reaches an acceptor bead, then the bead emits energy at 615nm which can be measured and used to quantify the association of the 2 proteins.

The large advantage that AlphaScreen has over a TR-FRET assay is the 20-fold increase increased distance between donor and acceptor, thus making the location of the tags less crucial in this assay format

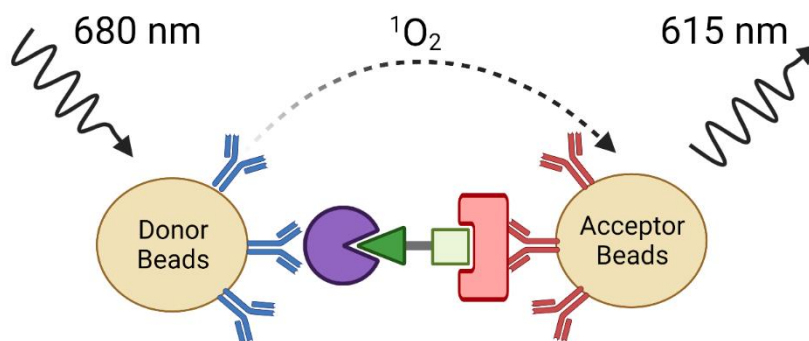


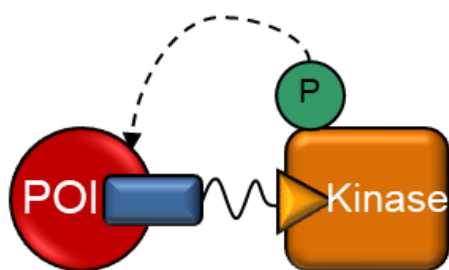
Figure 1.27 - Schematic showing AlphaScreen setup as a proximity based assay. AlphaScreen assay emits at 520-620 nm, whereas AlphaLisa emits at 615 nm

### 1.14 Aim and Hypotheses

The use of bifunctional molecules as PROTACs to direct ubiquitination and drive degradation has been well established in recent years. Using this method, multiple groups have shown various protein classes can be target with therapeutic relevance. However, outside ubiquitination the concept of directing other PTMs is still in its infancy, and the broader utility as a chemical tool is yet to be realised. Phosphorylation is critical in cell functioning, governing cell death, growth and signalling. Based on the number of clinically approved kinase inhibitors, it is clear that altering the phosphorylation of a protein can have therapeutic relevance. As such a tool to direct and increase the phosphorylation of a protein would be novel and interesting.

The aim of this project was to use a kinase to phosphorylate a neo-substrate using a rationally designed bifunctional molecule.

We hypothesised that a rationally designed bifunctional molecule would be able to bind a kinase and substrate protein simultaneously inducing a high local concentration as a ternary complex. This newly formed ternary complex could force the kinase to phosphorylate a substrate protein for which it previously had no affinity, thus leading to altered cell function.



Ternary Complex

*Figure 1.28 - Diagram of a ternary complex and subsequent PTM*

To achieve this, we first identified AMPK and MLKL as the kinase and substrate protein to investigate. To investigate the neo-phosphorylation of MLKL by AMPK we first had to design and synthesise ligands that would show which solvent exposed sites were optimal for bifunctional compounds and test them in an assay. Linker length has a substantial impact on the activity of PROTACs so we would need to synthesise a library of bifunctional compounds and test them to find an optimal linker range for neo-phosphorylation.

Our secondary aim was to investigate how effective a pan-selective warhead is at phosphorylating a broad range of protein targets.

By using unbiased phosphoproteomics, we were able to investigate neo-phosphorylation against a substantial range of targets. This approach would enable the identification of patterns governing neo-phosphorylation, and we hypothesised that certain sequences or structural features would be more susceptible to neo-phosphorylation. Determining the selectivity of phosphorylation through a ternary complex is a crucial step in evaluating its applicability as a therapeutic strategy.



## Chapter 2 Single ligands

### 2.1 5'Adenosine Monophosphate kinase

As mentioned in the introduction AMPK is a heterotrimeric serine threonine protein kinase and was chosen as the effector protein for this project.

AMPK has a key role in energy homeostasis as its activity is increased by AMP binding to the regulatory domain. As a result, when under energy stress with high levels of AMP, AMPK is activated and this drives ATP producing pathways to be switched on. As a result, AMPK has been the target of numerous drug discovery campaigns, and several AMPK activators have been reported (Figure 2.1).

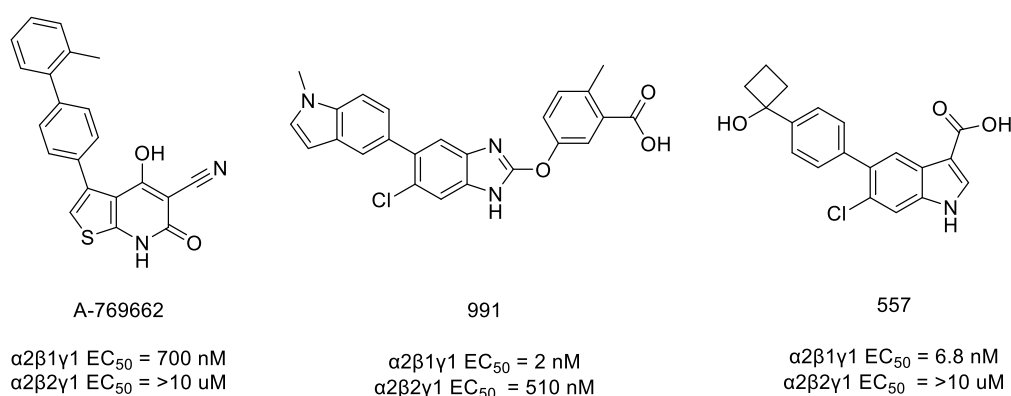


Figure 2.1 - Reported AMPK activators

For this project to work, ATP-competitive inhibitors of the effector protein obviously cannot be used as this would stop AMPK from phosphorylating native and neo substrates. Although a non-functional allosteric binder for AMPK would have been suitable, non-functional binders of proteins are rarely detected and reported. Additionally, we hypothesised that using AMPK activators would increase the levels of neo-phosphorylation of a substrate  $EC_{50}$  as AMPK will be more activated towards phosphorylating substrates.

The location of the binding site of the AMPK activators was also key. We needed small molecules that would bring the ATP binding site of AMPK into close proximity with neo-substrates. We hypothesised that as even if a stable ternary complex with

neo-substrates could form, if no possible phosphosites sites brought close to the ATP binding site on AMPK, then no neo-phosphorylation would occur.

As can be seen from Figure 2.2, activators bind approximately 15Å from the ATP binding site and on the same face of the protein. This suggests that if the activator site is brought close to a substrate, so will the ATP binding site, so AMPK may phosphorylate a neo-substrate.

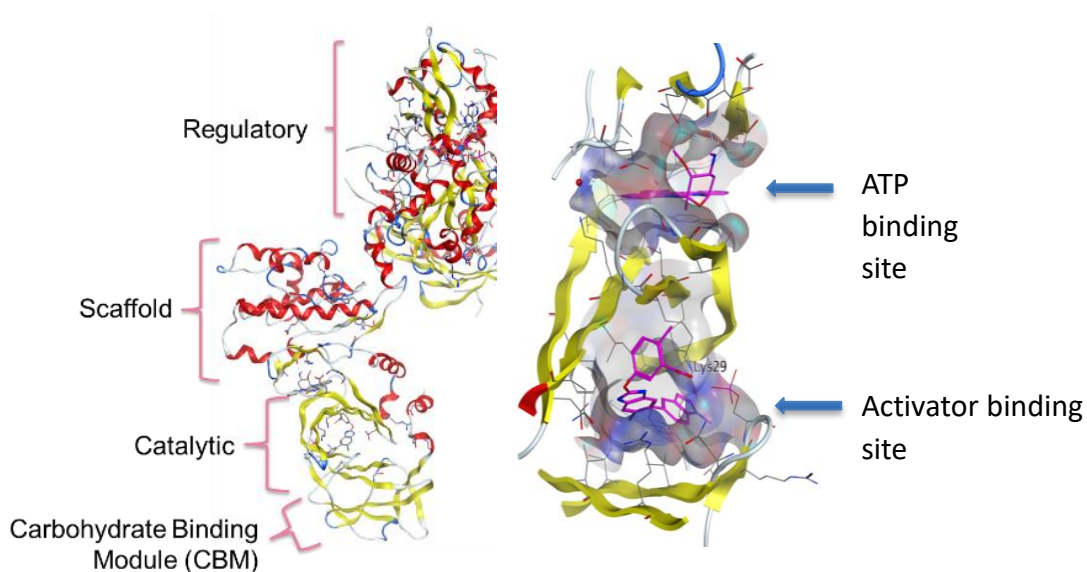


Figure 2.2 - left: Full length AMPK. Right: receptor surfaces of activator and ATP binding sites. PDB : 4CFE

## 2.2 Binding of 991 and solvent exposed sites

We decided to initially focus work on **991** as it is a potent AMPK agonist across multiple AMPK isoforms so was likely to maintain binding below the desired limit of <500nM, and there is a published crystal structure that gave structural information on its binding mode and solvent exposed sites (Figure 2.3).<sup>65,66</sup>

**991** binds to AMPK as shown in Figure 2.3, with the benzimidazole core  $\pi$  stacking with Arg-83 and a salt bridge between the benzimidazole N-H to Asp-88. The methyl benzoic acid points directly out into solvent with another salt bridge formed between the solvent exposed carboxylic acid and Lys-29. Having this structural information on how 991 binds is key, as the first step in making bifunctional

molecules is identifying solvent exposed sites on the small molecule that could potentially tolerate a linker. Once solvent exposed regions of the molecule are identified, small molecules with dummy linkers can be synthesised and tested, to confirm that the addition of linkers will abrogate binding.

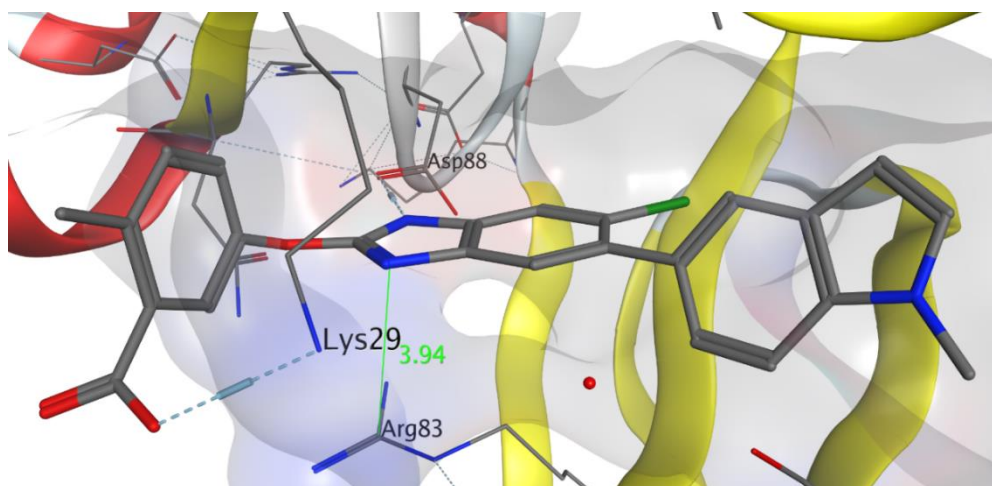


Figure 2.3 - 991 bound to AMPK. PDB: 4CFE

From the crystal structure we identified three solvent exposed sites on **991**; the carboxylic acid group, the 2-position, and the back pocket, as shown in Figure 2.4

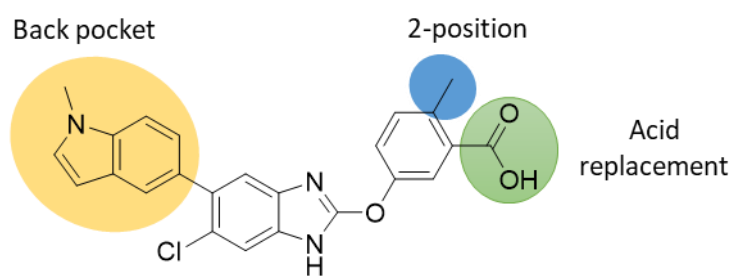


Figure 2.4 - 2D representation of the solvent exposed functional sites on 991

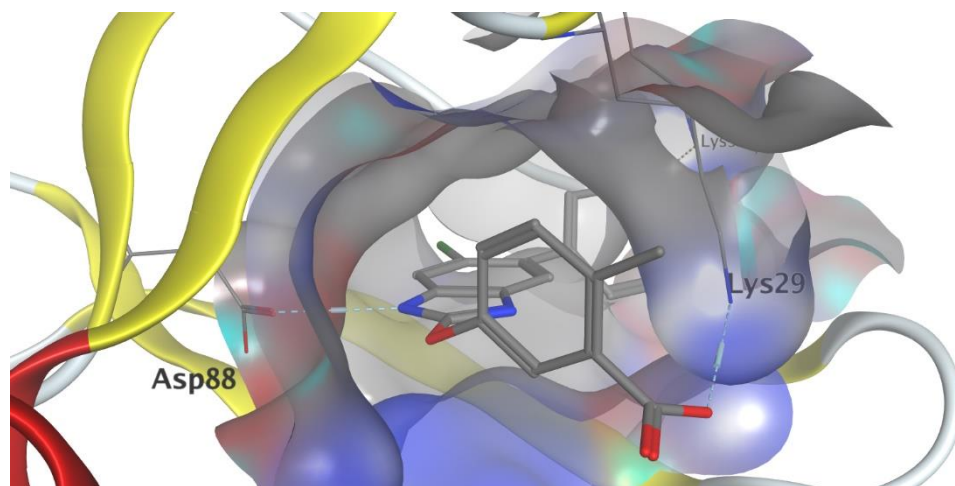


Figure 2.5 - crystal structure showing the methyl benzoic acid pointing out to solvent. PDB: 4CFE

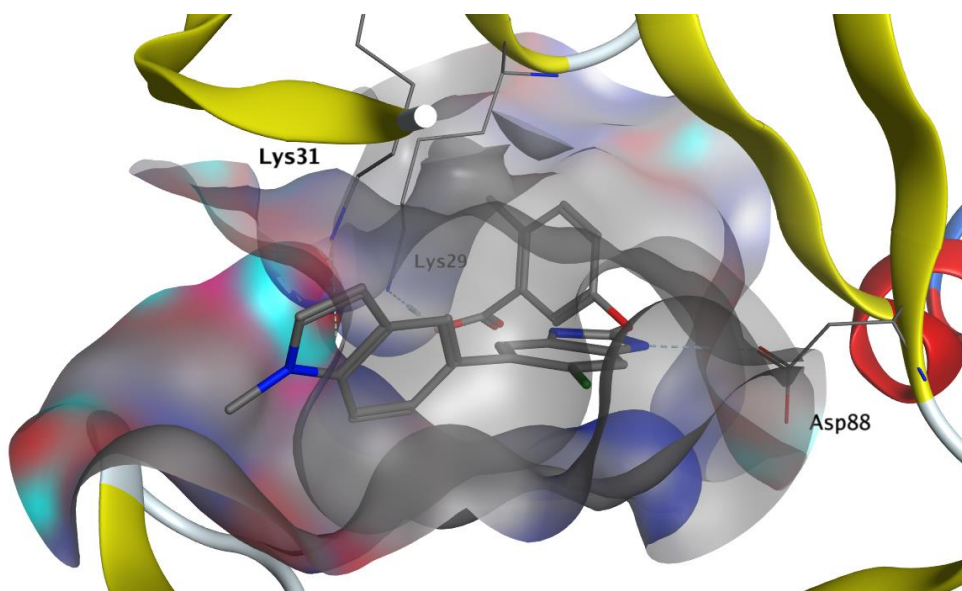


Figure 2.6 - Crystal structure showing the methyl indole exposed to solvent the 'back pocket'. PDB: 4CFE

### 2.3 AMPK activator synthesis

To enable preparation of 991 analogues, we wanted to scale up the synthesis of the benzimidazole core. The benzimidazole core, **8**, was made as reported in literature.<sup>15</sup> The starting material was 5-chloro-2-nitroaniline, **3**, which was subjected to iodination conditions then a nitro reduction using iron to give the dianiline in a high overall yield. The di-aniline **5** was then cyclised with carbon disulphide, methylated and oxidised to give the methyl sulfone **8** in a set of high yielding reactions

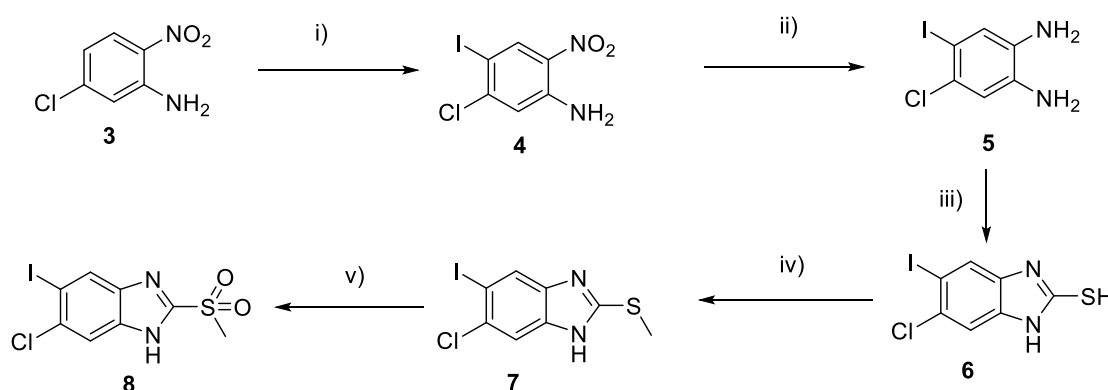


Figure 2.7 - Reaction scheme for the synthesis of the activator core. i) *N*-Iodosuccinimide, AcOH, 50°C, 16h, 90% ii) Fe powder, NH<sub>4</sub>Cl, EtOH, H<sub>2</sub>O, 50°C, 16h, 89% iii) CS<sub>2</sub>, KOH, EtOH, H<sub>2</sub>O, 80°C, 16h, 96% iv) MeI, K<sub>2</sub>CO<sub>3</sub>, Acetone, 0°C → rt, 92% v) mCPBA, DCM 0°C → rt, 1h, 85%

Intermediate **8** was subjected to a Suzuki coupling reaction followed by a SEM protection to give **10**. An S<sub>N</sub>Ar with a phenol followed by SEM deprotection and ester hydrolysis gave **991** in a low yield.

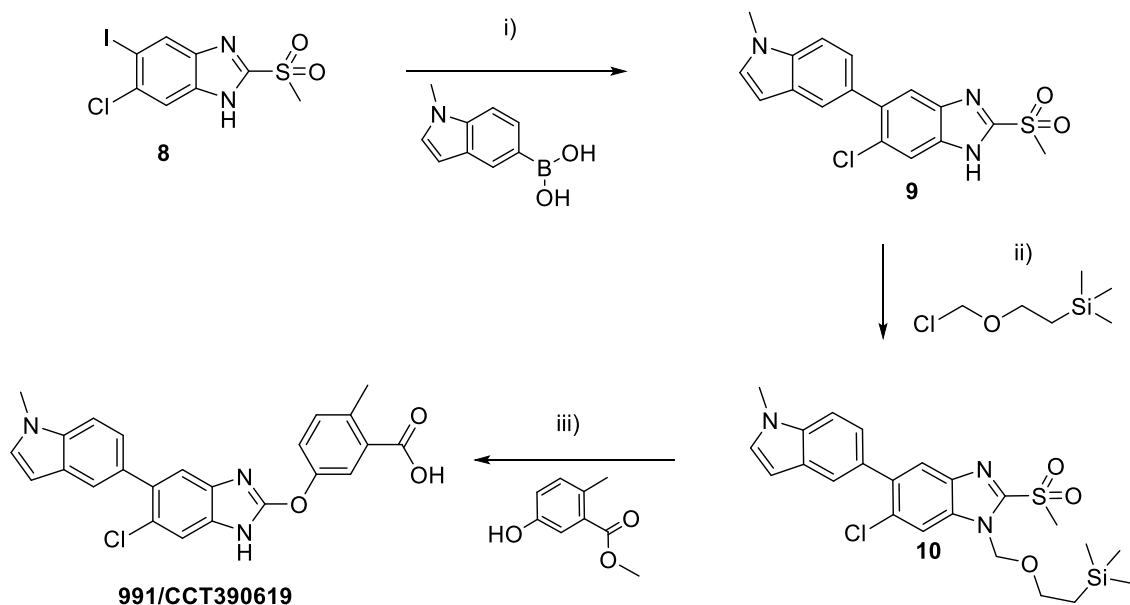


Figure 2.8 - Literature route to synthesis 991. Although the SEM protection here and in following figures as being on only one imidazole N, there was a 1:1 ratio between SEM on either nitrogen. i) 1-methyl-5-indolyboronic acid, Pd(dppf)Cl<sub>2</sub>, K<sub>2</sub>CO<sub>3</sub>, 1,4-Dioxane, H<sub>2</sub>O, 100°C, 6h, 46% ii) 2-(trimethylsilyloxy)ethoxymethylchloride, NEt<sub>3</sub>, THF, rt, 2h, 71% . iii) 5-hydroxy-3-methyl benzoic acid methyl ester, K<sub>2</sub>CO<sub>3</sub>, rt, 3h then TBAF (1M in THF), 80°C, 6h then LiOH, H<sub>2</sub>O, 40°C, 16h. 39%

In order to validate the AMPK activity assay we planned to set up, we wanted to test another literature reported AMPK activator as an additional positive control.<sup>15</sup> We chose a compound that has the same chloro-benzimidazole core as 991 so that we could start from a later stage intermediate. Starting from sulfone **8**, we SEM protected the benzimidazole core and then performed the Suzuki cross coupling with biphenyl boronic acid to give **12**. A S<sub>N</sub>Ar reaction with the phenol and subsequent SEM deprotection and ester hydrolysis gave **CCT390621** in a low yield.

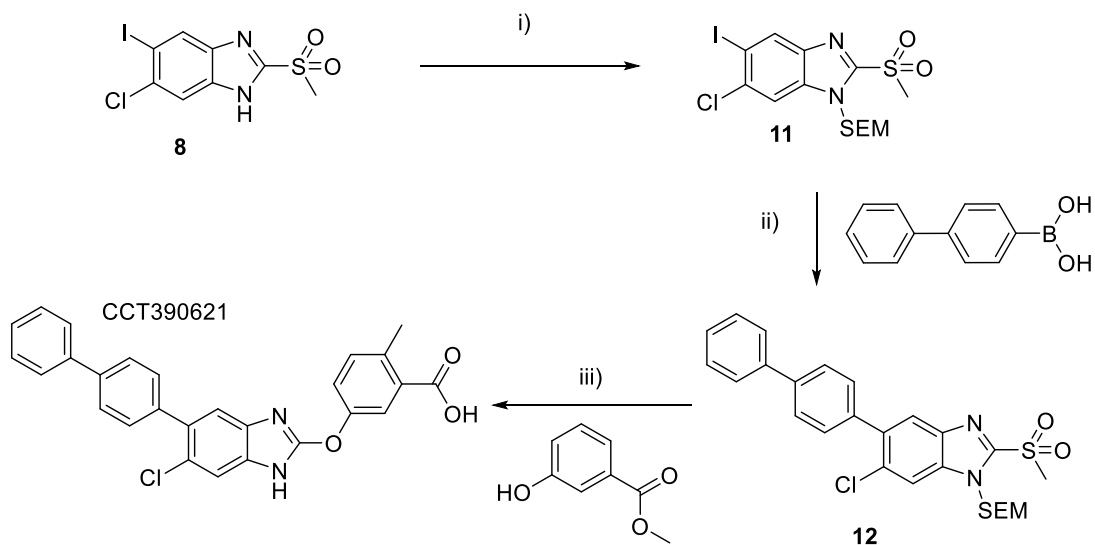


Figure 2.9 - Synthesis of another published AMPK activator, CCT390621.

i) 2-(chloromethoxy)ethyl-trimethyl-silane,  $NEt_3$ , THF, rt, 16h, 76% ii) 4-Biphenylboronic acid,  $Pd(dppf)Cl_2$ ,  $K_2CO_3$ , 1,4-Dioxane,  $H_2O$ , 100°C, 4h. Quant iii) methyl 3-hydroxybenzoate,  $K_2CO_3$ , DMF, 50°C, 16h then TBAF (1M in THF) 50°C, 16h then LiOH, THF,  $H_2O$ , 2h, rt, 19%

## 2.4 Design rationale

Having synthesised two control compounds, **CCT390619** and **CCT390621**, we next wanted to test if substitution at the proposed solvent exposed sites was tolerated. As mentioned in the introduction, dummy linkers are used to confirm that substitution is tolerated at the proposed site, before committing to the lengthy process of making a library of bifunctional compounds. A wide variety of linkers have been used in bifunctional molecules but typically they are alkyl chains containing nitrogen or oxygen to improve physicochemical properties.<sup>43</sup> On this basis we incorporated carbon and heteroatom based dummy linkers to test the solvent exposed sites.

### 2.4.1 Acid replacement on 991

The acid group on 991 represents an easily modifiable handle to make bifunctional compounds through amide couplings, to give acid replacement linkers. The published SAR leading to **991** always maintained this acid functionality suggesting it

may be key to activity, but as the acid is solvent exposed, we predicted the ionic interaction may be weaker than expected and could be lost whilst still maintaining reasonable binding and activation.<sup>15</sup>

We wanted to make a secondary amide which contained an alkyl-heteroatom chain as a dummy linker. Modelling it showed that a secondary amide would point into bulk solvent and the phenyl ring may form a weak interaction with Lys29, which may help compensate for loss of the salt bridge.

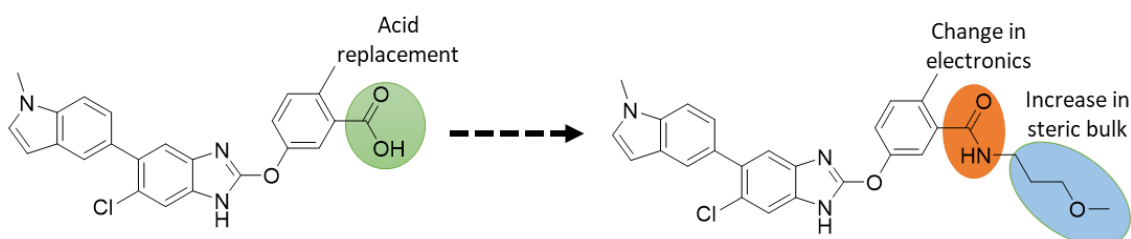


Figure 2.10 - Structure of the acid replacement dummy linker

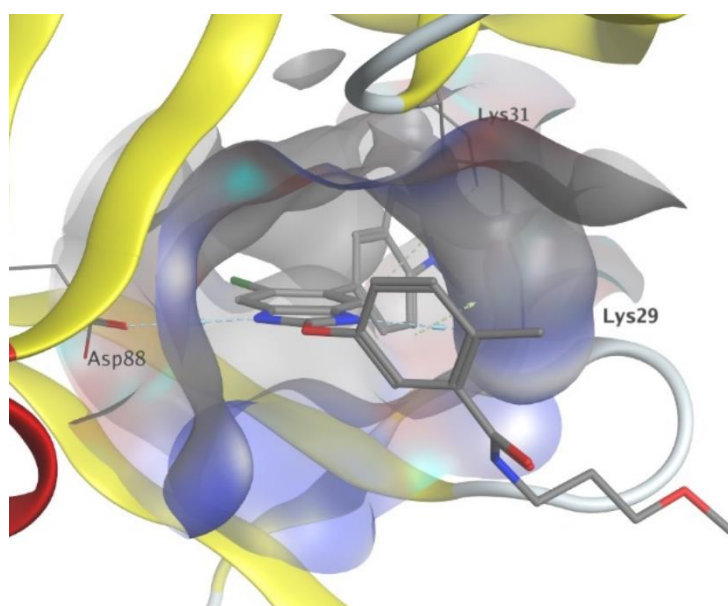


Figure 2.11 - acid replacement dummy linker minimised into the crystal structure of 991 bound to AMPK, PDB:4CFE

This amide analogue was made from coupling the carboxylic acid **13** with 3-methoxypropan-1-amide, to give **14** which was then combined with **10** using a  $S_NAr$  reaction. Subsequent deprotections gave the final compound **CCT390620**, in a reasonable yield



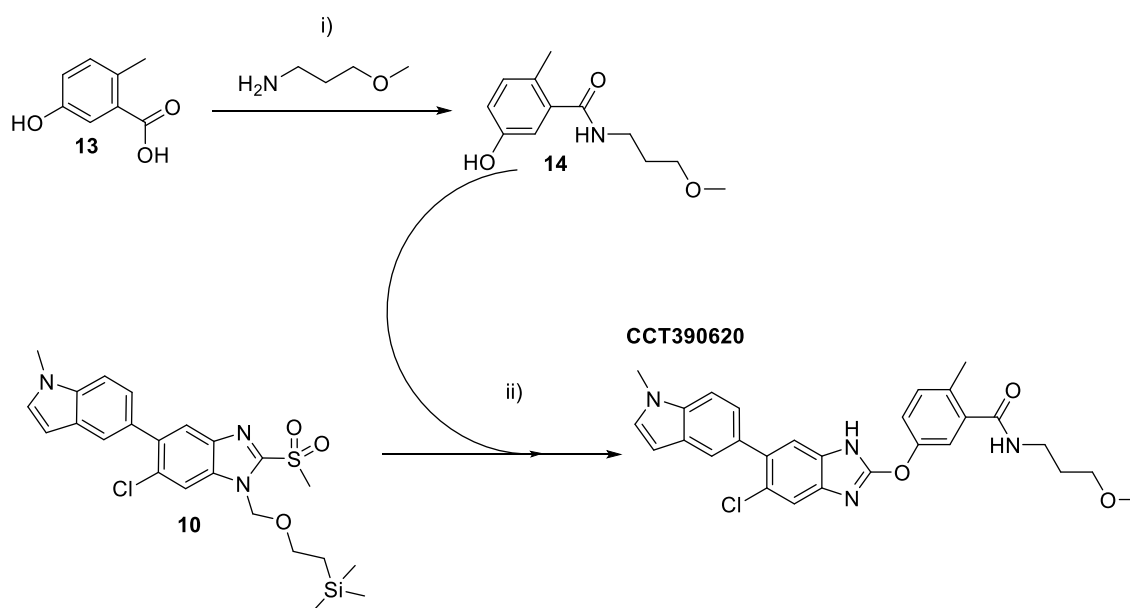


Figure 2.12 - Synthesis of an activator containing a dummy linker i) HATU, DIPEA, DMF, 2h, rt, 84% ii)  $K_2CO_3$ , DMF, 50°C, 16h then TBAF (1M in THF) 80°C, 6h 49% overall

#### 2.4.2 2-Position on 991

The methyl group ortho to the acid is also solvent exposed and keeps the acid group orthogonal to the phenyl ring maximising the acids interaction with Lys-29. As this group does not interact with AMPK itself, we hypothesised extending from the 2-position into solvent would maintain the salt bridge interaction, and thus give a smaller drop-off in binding and activation compared to **991**.

In designing a dummy linker, we wanted to maintain as much flexibility as possible so focussed on saturated linkers. Directly extending from the methyl group in the 2-position in an alkyl chain was not easily synthetically accessible, and as we wanted to keep the acid group free to interact with Lys-29 we didn't want a hydrogen bond donor, such as N-H, in the alpha position as this could form an intramolecular interaction. As such we settled on using oxygen as the first atom to install a dummy linker.

For linker composition we wanted to include heteroatoms, as this is common in linkers to tune physicochemical properties, and we wanted to synthesise this dummy linker in a way that could then be applied to making bifunctional molecules. As a result, we incorporated an amide bond at the end of the group which is a

convenient functional handle. The amine was capped with an acetyl group just to mimic the electronics of an amide.

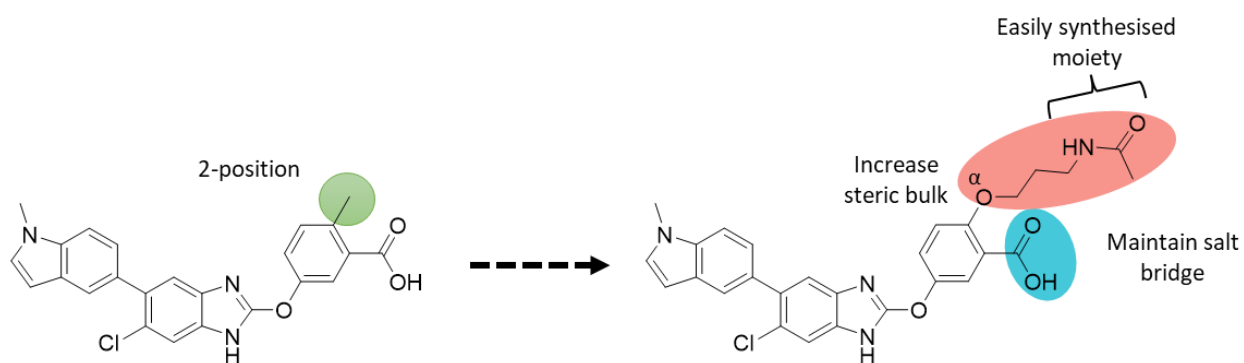


Figure 2.13 - Structure of the 2-position dummy linker

Modelling showed that the dummy linker was not expected to form an intramolecular bond and the acid group maintained a salt bridge interaction, so fulfilled the criteria we wanted.

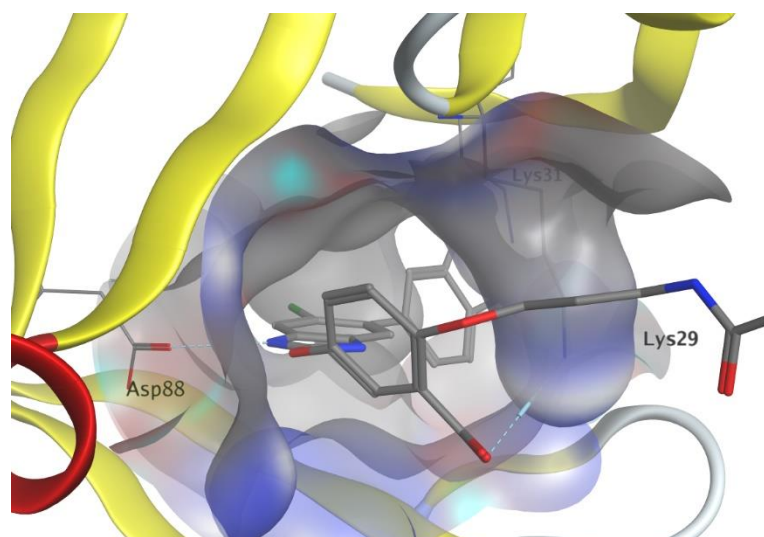


Figure 2.14 - 2-position dummy linker minimised into the crystal structure of 991 bound to AMPK, PDB:4CFE

Exploring the 2-position on the benzoic acid was synthetically challenging. We started from the dihydroxy, **15**, of which we could selectively protect the least hindered position with TBSCl, which then left the 2-hydroxy free for a Mitsunobu reaction to give **17**. The TBSCl group was easily removed, then a  $S_NAr$  with **10** gave intermediate **19**. Deprotection of the Boc group left the amine free to be capped with an acetyl group using Acetyl chloride giving **20**. Deprotection of the SEM group and ester hydrolysis gave the final product, **CCT394076**.

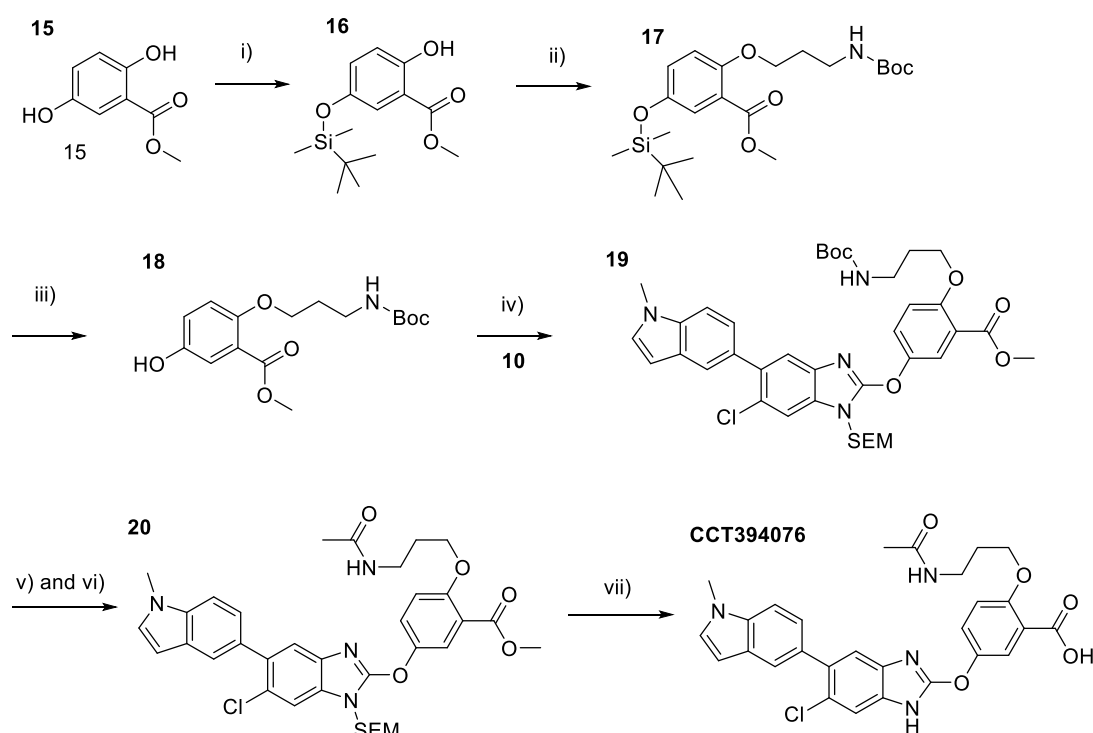


Figure 2.15 - Synthesis of methyl dummy linkers. i) *t*-butyldimethylsilyl chloride, Imidazole, DCM, rt, 16h 62-71% ii) *tert*-butyl-*N*-(3-hydroxypropyl)carbamate, DEAD,  $PPh_3$ , THF, 70C, 24h, 78% iii) TBAF (1M in THF), THF, 0C, 30 mins, 53-77% iv)  $K_2CO_3$ , DMF, rt, 24h, 81% v) TFA, DCM, rt, 16h, 78% vi) AcCl, DIPEA, DCM, 0C, 1h, 65% vii) TBAF (1M in THF), THF, 80C, 16h then LiOH, H<sub>2</sub>O, 16%

### 2.4.3 Back pocket of 991

The hydrophobic space in the back pocket of AMPK is filled by the methyl indole in 991 and has a solvent exposed vector nearby. The SAR around 991 shows that fused and bicyclic ring systems only containing sp<sup>2</sup> atoms are well tolerated, suggesting some flexibility in the pocket, but as no saturated systems were tested it suggests a clear preference for constrained aromatic groups.

Modelling showed that substituting dummy linkers on the methyl indole would clash with the binding pocket, and likely reduce affinity. As such we wanted to establish if more flexible groups with alternative vectors could replace the methyl indole, which would allow a suitable solvent exposed site to be found.

We designed an analogue with a phenoxy-phenyl that maintained two aromatic rings but with a spacer atom between the two rings which docking suggested would allow solvent to be reached (Figure 2.17).

We also hypothesised that a second aromatic ring may be difficult to link from, and AMPK activation may be maintained with only one aromatic ring, in which case a more flexible linear alkoxy linker may allow solvent to be accessed more easily (Figure 2.18)

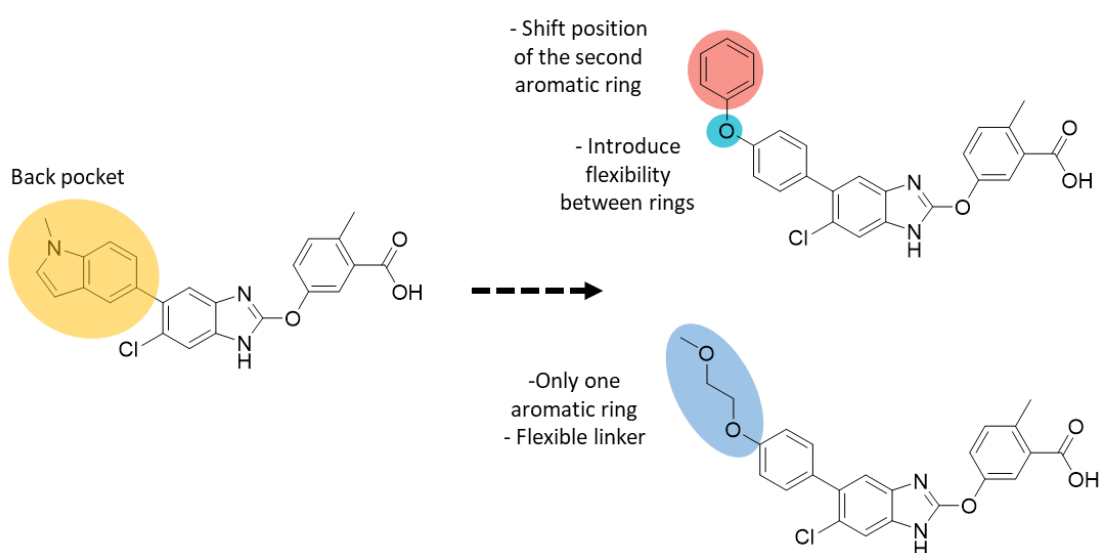
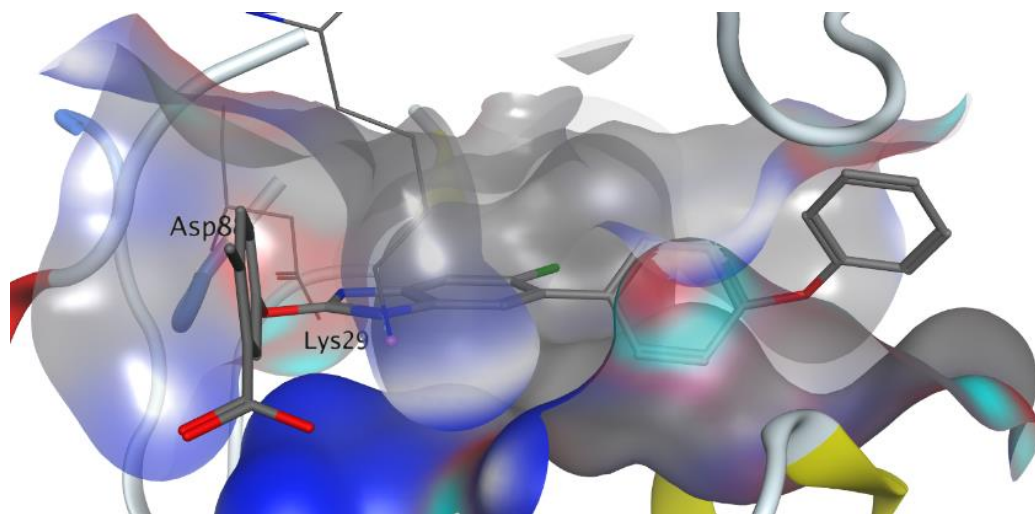
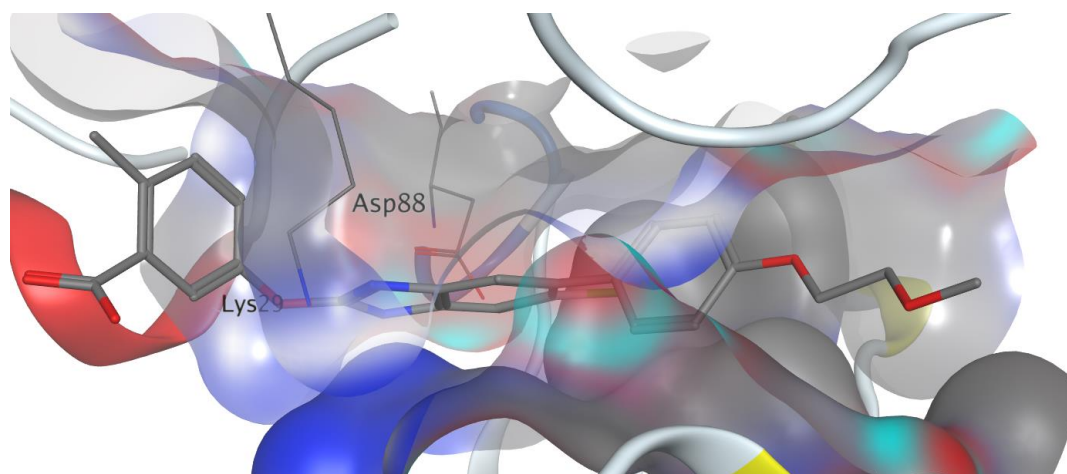


Figure 2.16 - 2D representation of compounds to test the solvent exposed back pocket on 991



*Figure 2.17 - Back pocket dummy linker containing phenoxy-phenyl minimised into the AMPK active pocket. (PDB: 4CFE)*



*Figure 2.18 - Back pocket dummy linker containing an alkoxy-phenyl group minimised into the AMPK active pocket. (PDB: 4CFE)*

To synthesise the desired compounds we used **14** as a substrate for an  $S_NAr$  reaction with phenol **13**, and subsequent SEM and ester deprotection gave **22**. Using this intermediate, **22**, we could perform Suzuki couplings as the final step to synthesise CCT394074 and CCT394075.

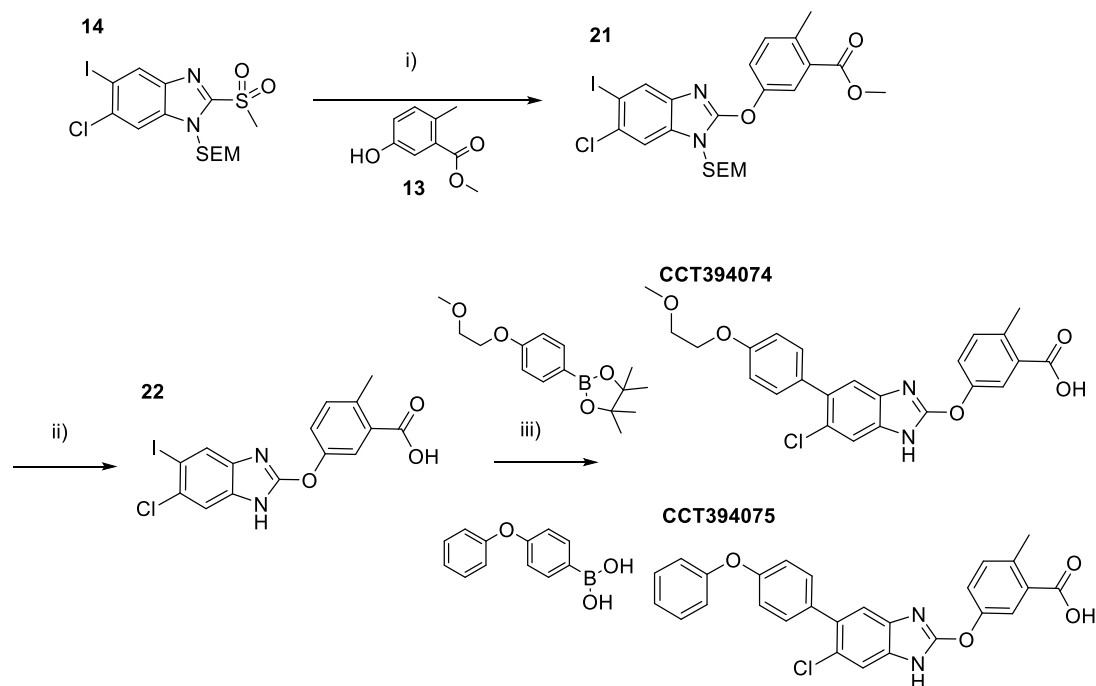


Figure 2.19 - Synthesis to back pocket analogues. CCT394074 i) Boronic ester/acid, Pd(dppf)Cl<sub>2</sub>, K<sub>2</sub>CO<sub>3</sub>, 1,4-Dioxane, H<sub>2</sub>O. 80°C, 16h. 28-32%

The Suzuki cross couplings in Figure 2.19 have poorer yields than previously seen, potentially due to the free carboxylic acid and the benzimidazole now being deprotected which may be able to coordinate to the Palladium and interfere with the cross coupling.

#### 2.4.4 991 inactive control

We anticipated that neo-phosphorylation would proceed via a ternary complex of AMPK and a substrate protein, but also had to consider that the bifunctional compound may only bind one protein in a binary complex and alter the phosphorylation of the substrate protein. As such, we may see altered phosphorylation, but it would not be occurring from a ternary complex. To confirm that it is through a ternary complex we wanted to synthesise an inactive control of 991, which could be used to make bifunctional compounds that would not be able to bind AMPK. In much the same way many PROTACs have their mechanism of action confirmed by using inactive E3 warheads.<sup>26, 65</sup>

From the crystal structure of AMPK bound to 991 (Figure 2.3), the N-H in the benzimidazole was reported to have a key interaction with Asp68. We hypothesised that loss of this interaction would drastically reduce binding and subsequent AMPK activation. To test this we synthesised a methylated control of 991, CCT393901 (Figure 2.20), from methylating **2** and then following the same method as shown in Figure 2.8

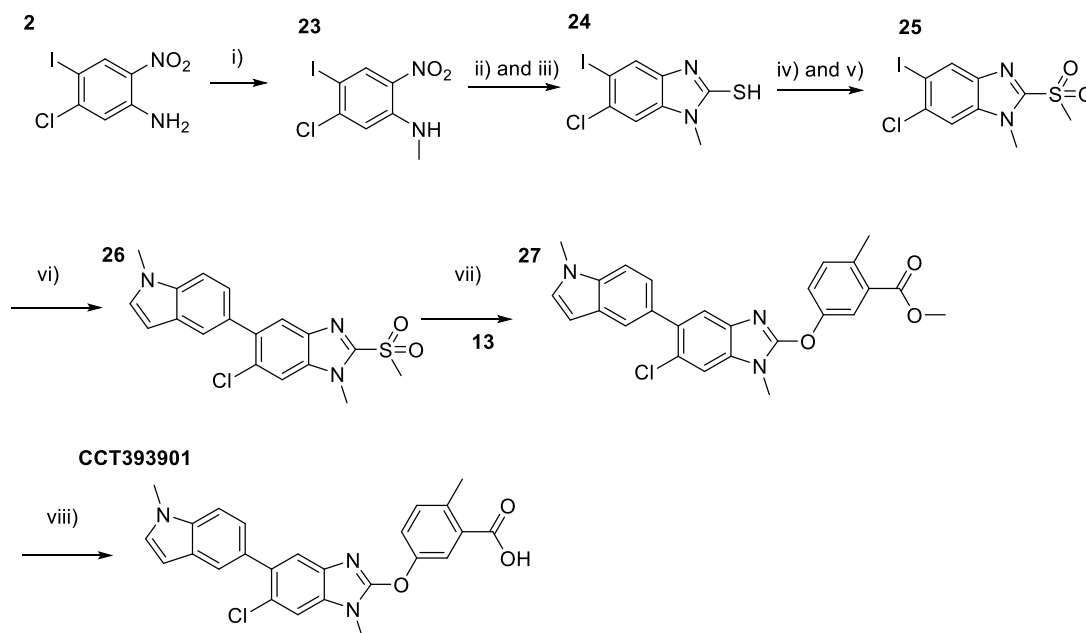


Figure 2.20 - Synthesis of inactive control. i) NaH, MeI, THF, 0°C, 1h, 68% ii) Fe, NH<sub>4</sub>Cl, EtOH, H<sub>2</sub>O, 50°C, 3h, 90% iii) CS<sub>2</sub>, KOH, EtOH, H<sub>2</sub>O, 80°C, 16h, 96% iv) MeI, K<sub>2</sub>CO<sub>3</sub>, Acetone, 0°C → rt, 3h, Quant v) mCPBA, DCM 0°C → rt, 16h, 64% vi) 1-methyl-5-indolylboronic acid, Pd(dppf)Cl<sub>2</sub>, K<sub>2</sub>CO<sub>3</sub>, 1,4-Dioxane, H<sub>2</sub>O, 80°C, 2h, 85% vii) 5-hydroxy-3-methyl benzoic acid methyl ester, K<sub>2</sub>CO<sub>3</sub>, DMF, 60°C, 48h, Quant viii) LiOH, THF, H<sub>2</sub>O, 30°C, 16h

## 2.5 Binding of 577 and design rational

**577** binds in a very similar orientation to **991** with the N-H indole acting as a hydrogen bond donor to Asp-88 and the phenyl group filling hydrophobic space towards the back pocket (Figure 2.21). The acid group has a salt bridge with Lys-29 and the hydroxy cyclobutyl group forms a hydrogen bond with Lys-31.

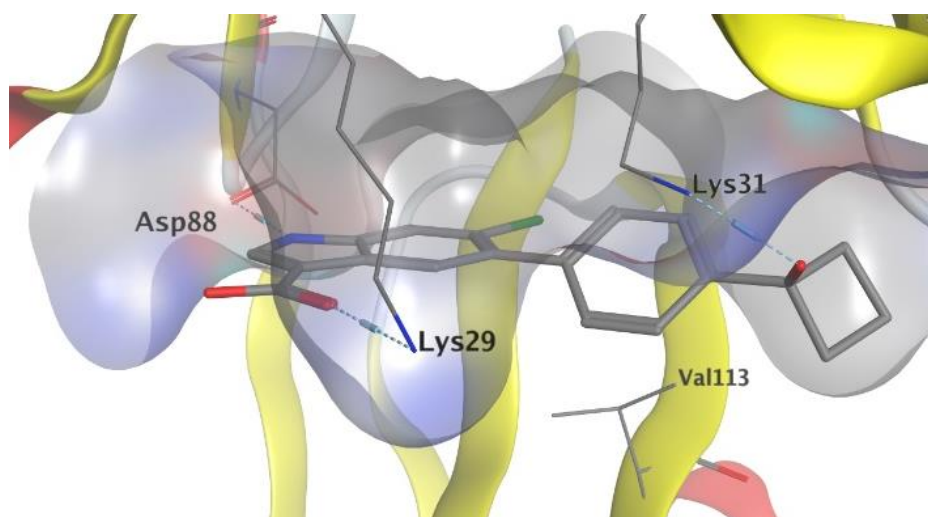


Figure 2.21 - AMPK activator 577 bound to AMPK. PDB: 5KQ5

Based on literature precedent we knew that this activator could tolerate a linker in the back pocket replacing the hydroxy-cyclobutyl.<sup>37</sup>

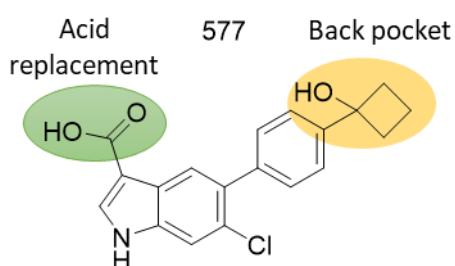


Figure 2.22 - 2D representation of the solvent exposed functional sites on 577

We synthesised CCT390622 which is a previously reported analogue of 577 via the literature route, so that we could confirm its activity in activating AMPK.<sup>37</sup> S<sub>E</sub>Ar was used to substitute **29** with a trifluoroacetyl group at the 3 position which was then



hydrolysed to the acid, then esterified to give the methyl ester **31**. A Suzuki cross coupling with **34**, installed a 4-alkoxy phenyl group to give CCT390617. Although in the literature reported route **CCT390617** is just an intermediate we decided to test this as we felt it was a good compound for testing how key the acid group was in the activation of AMPK.

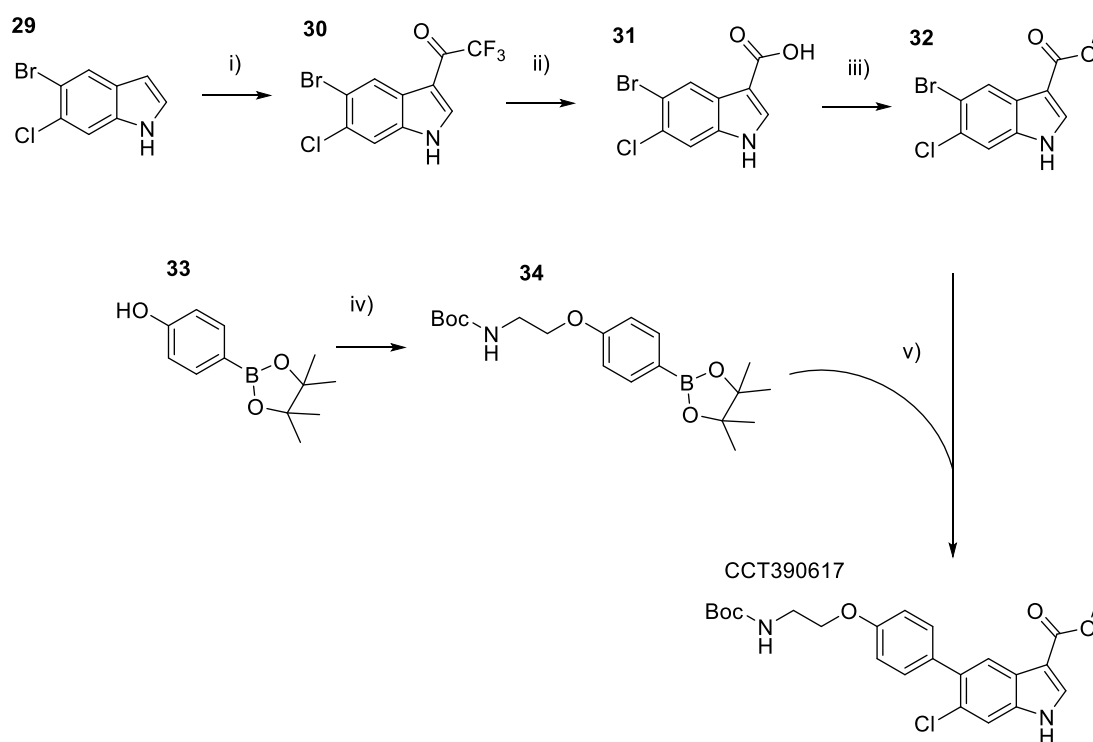


Figure 2.23 - Synthesis towards 577 analogues. i) TFAA, DMF, 0C, 1h, 90% ii) NaOH, H<sub>2</sub>O, 100C, 4h, 93% iii) MeOH, H<sub>2</sub>SO<sub>4</sub>, 90C, 16h, 91% iv) K<sub>2</sub>CO<sub>3</sub>, DMF, 70C, 16h, 98% v) tert-butyl N-[2-[4-(4,4,5,5-tetramethyl-1,3,2-dioxaborolan-2-yl)phenoxy]ethyl]carbamate, Pd(dppf)Cl<sub>2</sub>, K<sub>2</sub>CO<sub>3</sub>, Toluene, H<sub>2</sub>O, 120C, 24h, 63% vi) NaOH, THF, H<sub>2</sub>O, 100C, 6h then TFA, DCM, 0C -> rt, 2h, Quant

Deprotection of Boc and ester group gave **35**. The amine was then functionalised with the Acetyl NHS ester, **36**, to give **CCT390622**.

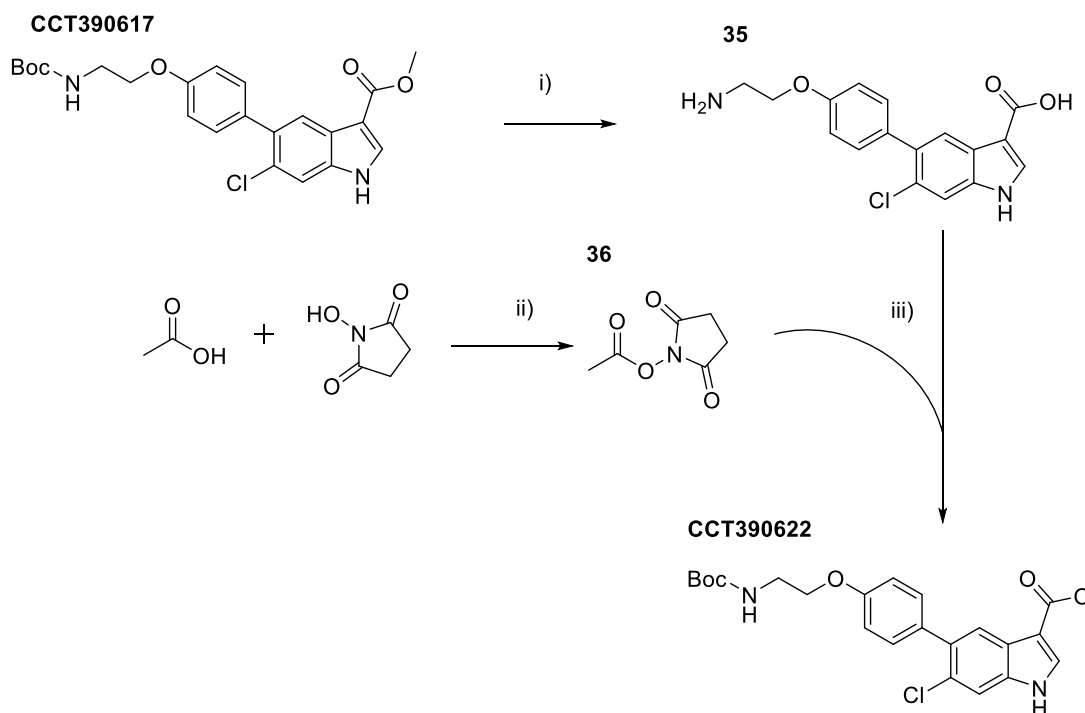


Figure 2.24 - i) NaOH, THF, H<sub>2</sub>O, 100C, 6h then TFA, DCM, 0C -> rt, 2h, Quant ii) EDCI HCl, DCM, rt, 16h, 29% iii) DIPEA, DMF, rt, 2h, 53%,

## 2.6 AMPK Activator testing

In order to test the synthesised activators we needed a robust assay. As these activators bind an allosteric site, the usual ATP-competitive assays such as Fluorescence Resonance Energy Transfer (FRET) or Fluorescence Polarization (FP) that can use commercially available ATP tracers are not applicable here.

AMPK activators have instead been developed and characterised using activity based assays which measure the phosphorylation of a substrate peptide or ADP generated over a given time.<sup>15, 67</sup>

The ADP Glo assay is an activity assay that measures the turnover of ATP to ADP and thus measures the activity of a kinase. The assay works by incubating the kinase with ATP, a synthetic peptide and a small molecule. Agonists increase the activity of the kinase, so result in increased phosphorylation of the substrate peptide and increased turnover of ATP to ADP. After incubation the remaining ATP is then quenched, the ADP is converted back to ATP and a luciferase is added, which generates a luminescent signal directly proportional to the amount of ADP.

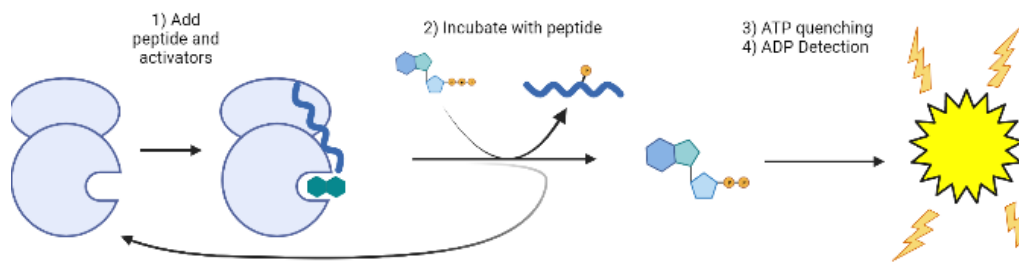


Figure 2.25 - ADP Glo assay scheme

We first performed an enzyme titration and time course to find the required minimum amount of AMPK and incubation period needed to test small molecules, using AMP as an agonist.

The results showed that 6.25 ng per well of AMPK with a 30 minute incubation gave a suitably strong signal compared to the control with no protein to be used for testing small molecules. Higher levels of proteins could have been used but were not

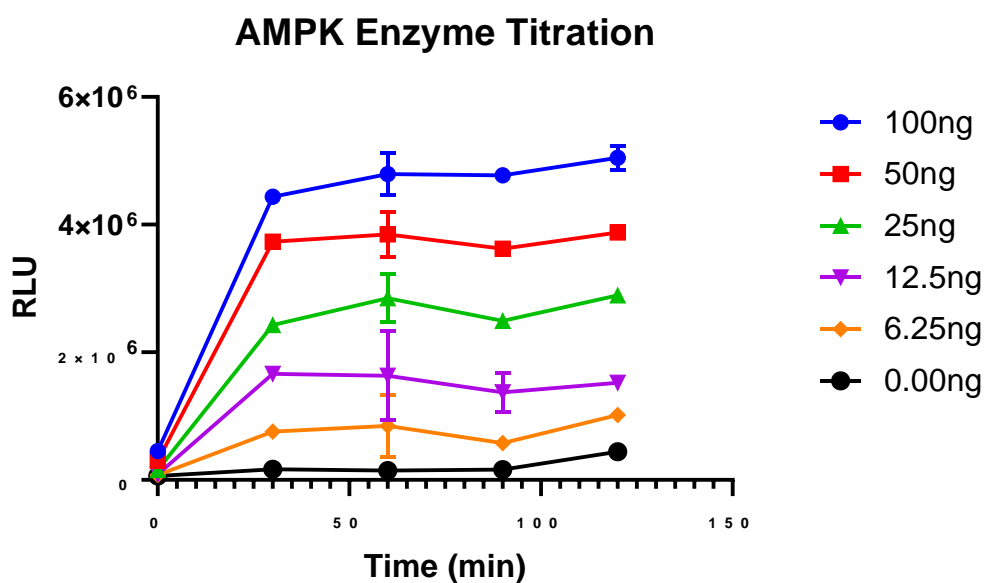


Figure 2.26 - Time and AMPK concentration dependence experiment. AMPK  $\alpha 2\beta 1\gamma 1$

necessary, and we wanted to minimise the protein per well to save costs.

## 2.7 ADP Glo Assay results

### 2.7.1 Confirming literature compounds

We first wanted to test the reported control compounds in the ADP Glo assay to confirm the assay matches literature values.<sup>15</sup>

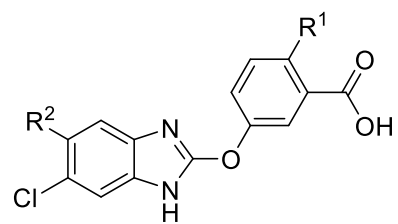


Table 2.1 - ADP Glo assay results for control compounds

CCT Number	Compounds		EC <sub>50</sub> / nM		Activation vs AMP / %	
	R <sup>1</sup>	R <sup>2</sup>	Reported	ADP-Glo	Reported	ADP-Glo
CCT390619	CH <sub>3</sub>		2	2.8	340	315
CCT390621	H		61	35	260	265

These results from Table 2.1, show that the ADP Glo assay is an accurate way of measuring AMPK activation, and gives results consistent with reported values for **CCT390619** and **CCT390621**, thus validating our assay setup.<sup>15</sup> Additionally, testing of the methylated inactive control CCT393901 and saw no AMPK activation, confirming it could be used as in inactive control in future work.

## 2.7.2 Testing back pocket 991/CCT390619 analogues

Having shown the ADP Glo assay is a valid way of measuring AMPK activators we wanted to confirm our designed compounds still activated AMPK and which linker sites on 991 were optimal.

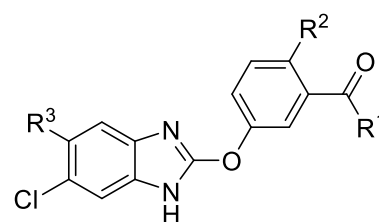


Table 2.2 - ADP Glo assay results dummy linker containing compounds

	Compounds			EC <sub>50</sub> / nM	Activation vs AMP / %
CCT Number	R <sup>1</sup>	R <sup>2</sup>	R <sup>3</sup>		ADP-Glo
CCT390620		CH <sub>3</sub>		160	178
CCT394076	OH			82	185
CCT394074	OH	CH <sub>3</sub>		131	243
CCT394075	OH	CH <sub>3</sub>		659	98

All the tested analogues led to a fairly large drop off in EC<sub>50</sub>, but still stay below the target of <500nM that is reported in literature as a useable range for warheads in bifunctional molecules.<sup>28</sup> All the dummy linker containing compounds activated AMPK to a similar level or more than AMP, suggesting that in a bifunctional compound they would retain activation of AMPK and if able to bring a substrate protein into close and suitable proximity they would be able to increase the rate of

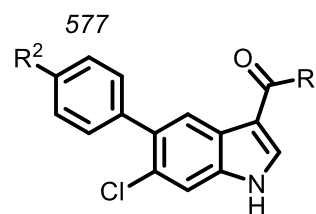
neo-phosphorylation to a substrate protein, in comparison to an allosterin non-activating compound.

The acid replacement, **CCT390620**, shows an  $\approx 60$  fold drop off in  $EC_{50}$  but only a 2 fold drop off in maximum activation, compared to **991** which suggests the salt bridge to Lys-29 contributes but is not critical for binding, and therefore that this is a suitable site for linkers. The 2-position linker, **CCT394076**, retains more activity, losing 30-fold compared to 991 with similar activation vs AMP to **CCT390620**. The loss in  $EC_{50}$  compared to CCT390619 could be due to the electron donating group alkoxy in the ortho position to the acid, altering the pKa of the acid, or the linker may alter the preferred position of the benzoic acid to increase the distance between the carboxylic acid group and Lys29.

Of the back pocket analogues CCT394074 showed that one phenyl ring was able to maintain binding, and that by attaching a flexible glycol group the binding affinity and activation was well maintained. In comparison CCT394075 showed a large decrease in  $EC_{50}$  suggesting that keeping two aromatic groups with flexibility in between them would not be optimal for attaching dummy linkers and reaching solvent. This could be that to fit into the pocket the two aromatic rings adopt an unfavourable torsion angle, which reduces binding.

### 2.7.3 577 results

We also wanted to test the two **577** analogues with dummy linkers and examine the differences in AMPK activation of linking from the carboxylic acid which breaks a salt bridge, compared to dummy linkers at the back pocket position



Compounds	Compounds		EC <sub>50</sub> / nM	Activation vs AMP / %
	R <sup>1</sup>	R <sup>2</sup>		
CCT390622	OH		199	105
CCT390617	OMe		11,270	58

Table 2.3 - Results of testing 577 analogues in the ADP Glo assay

CCT390617 showed that the acid group was key for activity with a very large 55-fold drop off EC<sub>50</sub> with the methyl ester compared to CCT390622. This suggested that bifunctional compounds using 577 should be synthesised from linking at the back pocket.

## 2.8 Summary and discussion

We identified AMPK activators from literature and used structural information to identify solvent exposed sites which we tested through the synthesis of dummy linker containing compounds. We validated an AMPK assay and used this to show that for all sites tested on the **991** core that the dummy linkers were well tolerated, with a summary of results shown below.

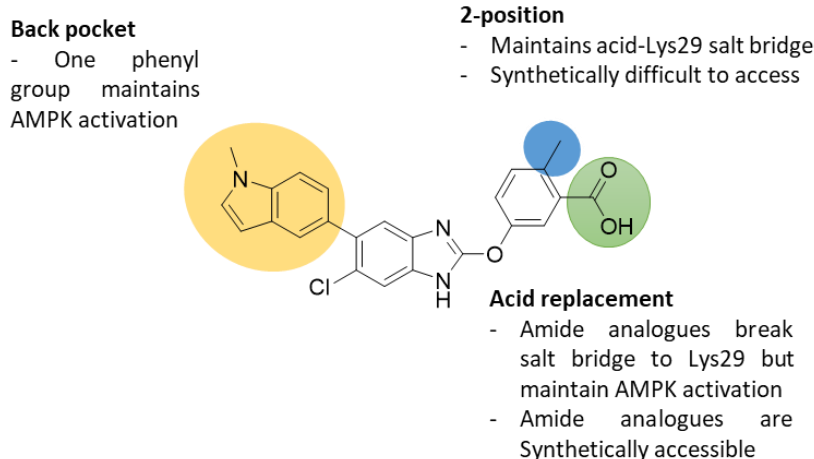


Figure 2.27 - Summary of SAR around the 991 AMPK activator

We tested two 577 analogues which showed the acid group was key for activity so would not be a suitable site for attaching linkers from. However, the back pocket appeared to tolerate a linker well, as was seen in the 991 series with CCT394074.

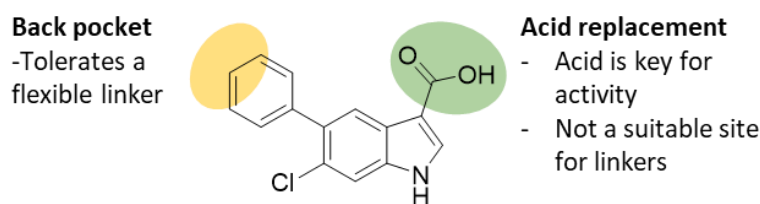


Figure 2.28 - Summary of SAR around the 577 AMPK activator

From the results here we decided to progress with making bifunctional compounds that linked from the acid replacement site on 991 as these were synthetically easiest to make and still activated and bound AMPK <500nM. We also decided to progress with making bifunctional compounds from the back pocket of 577 based on the clear preference for this site.

In PROTAC literature it has been shown that altering the attachment site on the ligands of the target protein and E3 ligase can change the degradation profile. We hypothesised that different attachment sites on an AMPK activator may also induce different levels of neo-phosphorylation or different sites on a substrate protein and that different substrate proteins may be phosphorylated differently. By choosing to link from either side of the binding site in making bifunctional molecules we hoped to investigate if this is observed.



## 2.9 Mixed Lineage Kinase Domain-Like Protein (MLKL)

There are only three reported compounds that bind MLKL reversibly with a  $K_D < 1 \mu\text{M}$ , shown in Figure 2.29.<sup>2, 68, 69</sup>

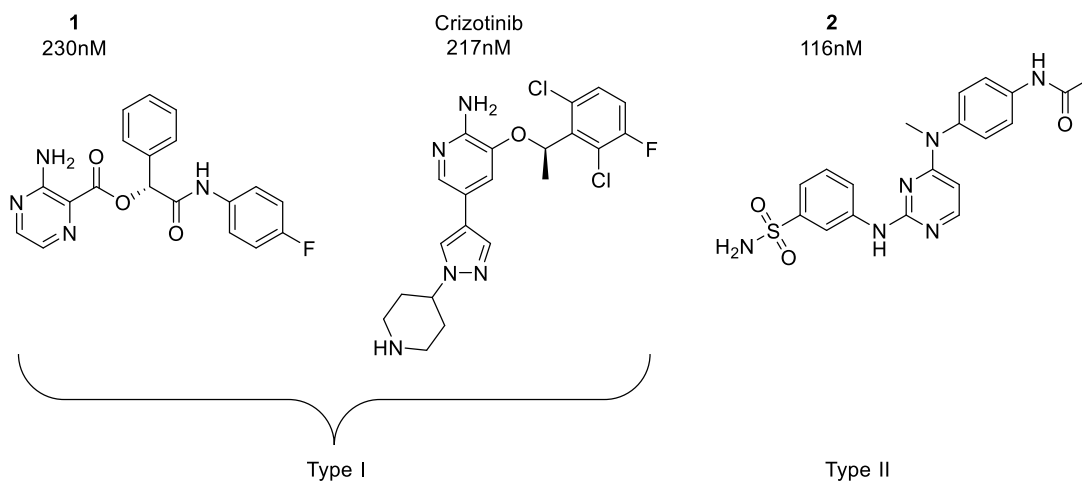


Figure 2.29 - Reported MLKL hits. Information is the cLogP, binding affinity against MLKL and molecular weight.

We firstly ruled out making bifunctional molecules using the Type II inhibitor, on the basis that Type II inhibitors bind proteins in a DFG-out, kinase inactive conformation which limits the availability of the activation loop. As the target amino acid Ser358, is on the activation loop of MLKL, we hypothesised a Type II inhibitor would prevent neo-phosphorylation. Also Type II inhibitors typically display low affinity for active phosphorylated kinases, which could limit their binding in a cellular environment, as they can only bind a fraction of the total protein.<sup>70</sup> Finally, as bifunctional molecules typically have very high molecular weights which leads to poor permeability, we wanted to start with a compound with as low a molecular weight and cLogP as possible, which also disfavoured the Type II inhibitor.

Both Type I inhibitors have similar  $K_D$  values against MLKL, however **1** has a very high selectivity and only inhibits MLKL in a panel of 403 kinases at  $1\mu\text{M}$ , whereas Crizotinib binds numerous kinases.<sup>2</sup> In the context of this project where we wanted to induce neo-phosphorylation, a MLKL selective compound would selectively give

MLKL neo-phosphorylation in a cell, whereas bifunctional molecules with a crizotinib warhead may induce phosphorylation of MLKL but could also induce phosphorylation of multiple other kinases. This would mean any resulting phenotype could not solely be attributed to neo-phosphorylation of MLKL because other proteins may be neo-phosphorylated. However, this would enable us to explore the broader utility of this approach and identify which protein targets of Crizotinib can be neo-phosphorylated.

Due to the high selectivity and the desire to investigate MLKL neo-phosphorylation, we decided to initially work with **1**, and work with crizotinib is described later.

### 2.9.1 Synthesis of the amide bioisostere of **1**

Compound **1** contains an ester group, which presents a potential issue for chemical stability to hydrolysis in synthesis, assays and in cells.<sup>2</sup> To try and avoid stability issues whilst maintaining activity the amide analogue was made. An amide is typically a good bioisostere for an ester as it provides the same heteroatom arrangement, in a similar geometry and maintains the carbonyl for H bonding. There is a central water molecule held by the existing amide, the 5-nitrogen in the pyrazine, and from the crystal structure it appeared that the amide would still be able to coordinate as a Hydrogen bond donor, see Figure 2.34.

To validate the in house MLKL assay we planned to set up, we synthesised compound **1** as a positive control, by coupling intermediate **37** with 4-fluoroaniline, **38**, and then coupling the required pyrazine gave **CCT374741**. The amide analogue, **CCT374740**, was made using the Fmoc protected phenylglycine, **40**, which was coupled to 4-fluoroaniline and deprotected with piperidine giving **42**. The final HATU mediated amide coupling gave **CCT374740**.

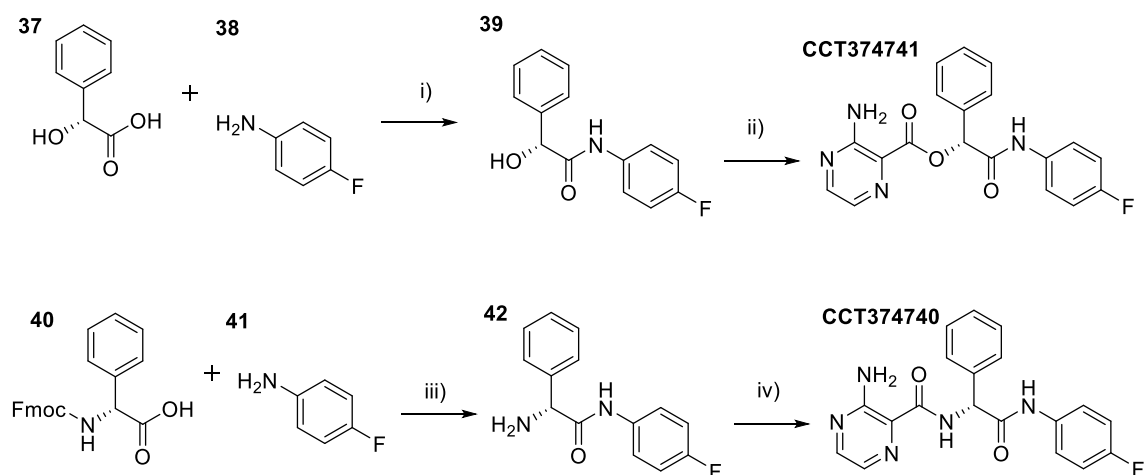


Figure 2.30 - Reaction scheme for the synthesis of compound CCT374741 and CCT374740. i) 4-fluoroaniline, HATU, DIPEA, DMF, rt, 16h, 90% ii) 3-aminopyrazine-2-carboxylic acid, HATU, DIPEA, DMF, rt, 4h, 24% iii) 4-fluoroaniline, HATU, DIPEA, DMF, rt, 1h then piperidine (20%) in DMF, rt, 2h, Quant iv) 3-aminopyrazine-2-carboxylic acid, HATU, DIPEA, DMF, rt, 1h, 2%

To quickly establish if an amide was a suitable bioisostere, **CCT374741** and **CCT374740** were sent for testing at DiscoverX. In this assay format, a known ligand for the target protein is immobilised onto a bead and incubated with a protein that is labelled with a DNA tag. The compounds are then added and compete with the immobilised ligand for the binding site. The more strongly binding the compounds, the more protein that is competed off the beads. The beads are washed to remove unbound protein, and then PCR is used to measure the remaining protein on the beads which is used to generate a  $K_d$ .<sup>71</sup> The results are shown below in

Table 2.4

Table 2.4 - Binding affinity values of **CCT374741** and **CCT374740** from the DiscoverX binding assay

Compound	$K_d$ / nM	Previously reported $K_d$ / nM <sup>2</sup>
<b>CCT374741 (48)</b>	160	230
<b>CCT374740</b>	8800	-

From the results, the affinity of **CCT374741** is confirmed, but the amide analogue **CCT374740** gives a  $\approx$  40-fold drop in affinity. This drop can be rationalised from using the published crystal structure of the ester and replacing the ester group with an amide.<sup>2</sup> Although the 'new' amide is predicted to act as a H bond donor to a centrally held water, in doing so it clashes with the other N-H binding to the water molecule and results in an intramolecular repulsion between the two N-H's.

In the binding site of MLKL this likely means that to maintain binding to the hinge region with the amino pyrazine, the existing amide flips into a new conformation, as shown in Figure 2.33.

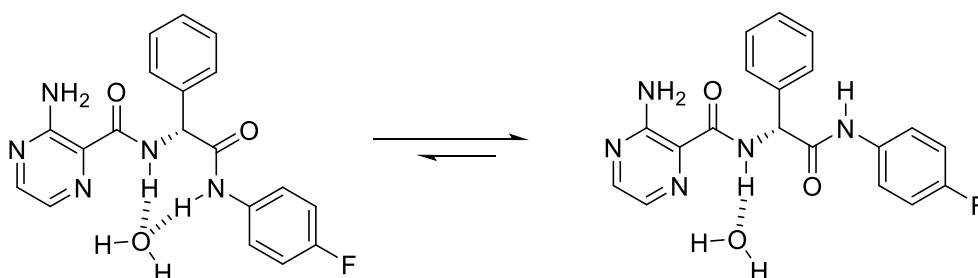


Figure 2.31 - 2D representation of the favoured conformation of CCT374740

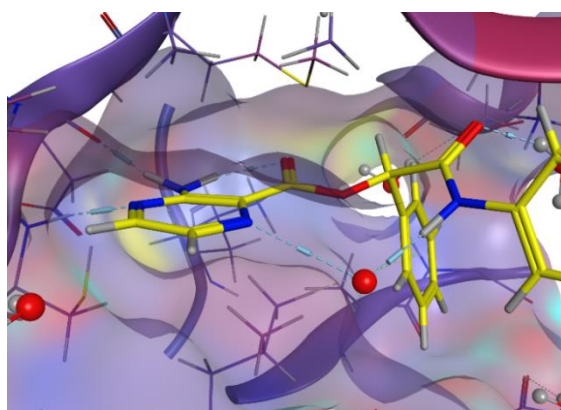


Figure 2.32 - Reported crystal structure of 15 bound to MLKL.<sup>2</sup> PDB: 5KO1

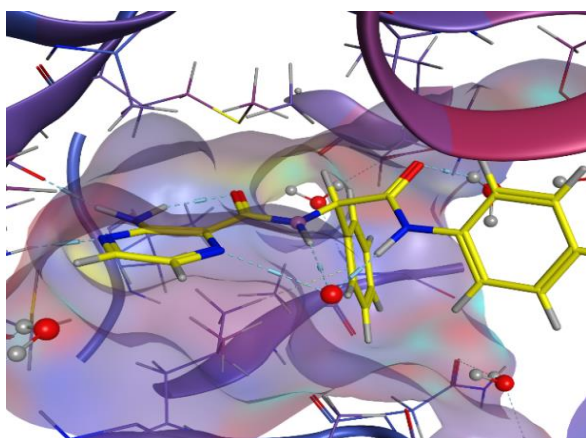


Figure 2.34 - Direct replacement of the ester for the amide

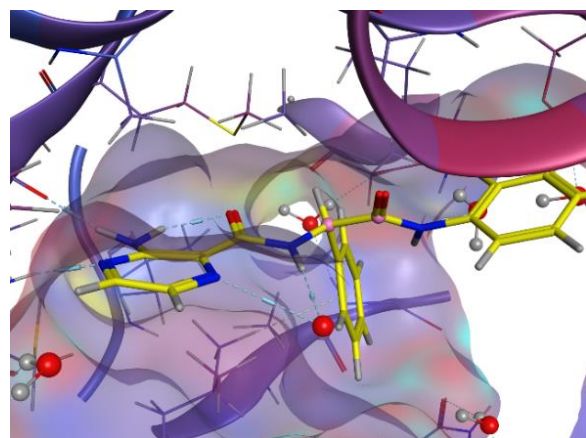


Figure 2.33 - Lowering intramolecular clash flips the existing amide

This drop in potency meant that we did not think the amide analogues would bind MLKL strongly enough to induce a ternary complex. As such, we decided to test the stability of the ester compound and see if it would be stable enough to synthesise bifunctional molecules and in cellular testing.

As the ester group is suitable to hydrolysis, we tested stability of an ester containing compound, **43**, in DMSO and water to ensure the conditions we would get an accurate idea of stability under hydrolytic conditions. We decided to test stability in acidic, neutral and basic conditions to see if analogues were going to be unstable at certain pH values. For acidic conditions we used HCl to acidify the solution to pH = 3, and for basic conditions used 20 equivalents of triethylamine, as it represented a commonly used organic base. We then monitored the conditions by LCMS as shown in Figure 2.35

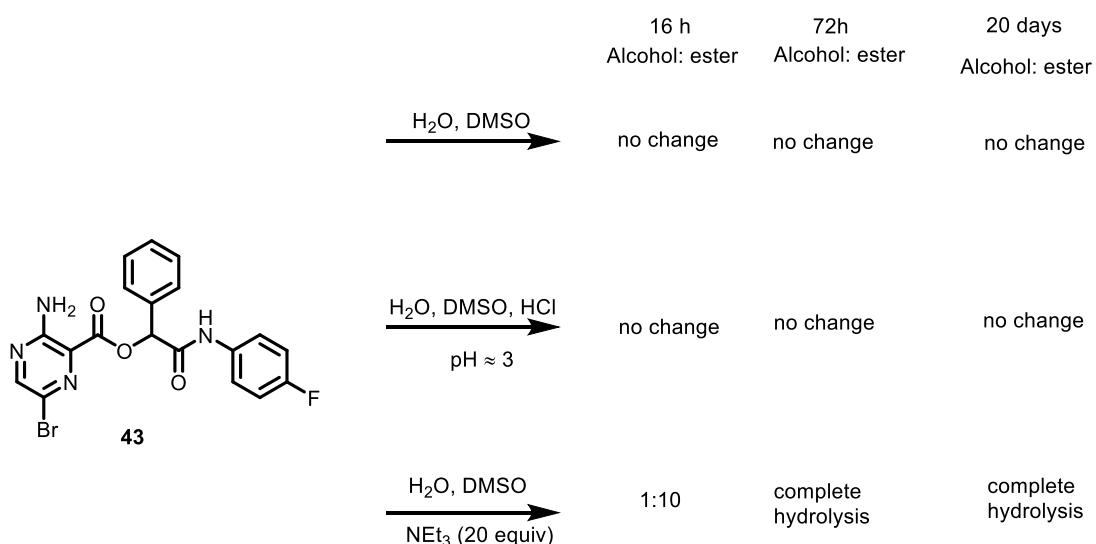


Figure 2.35 - Stability testing of compound 43

We observed a slow rate of hydrolysis in basic conditions but high stability in neutral and acidic conditions. Although ideally, we would see no hydrolysis in any conditions, the rate of hydrolysis in basic conditions was slow enough that we predicted the ester would be stable enough to take forward in making dummy linker containing compounds and bifunctional molecules.

### **3.2.5 Identifying solvent exposed sites and linker attachments**

As with AMPK, the first step to making bifunctional compounds targeting MLKL is to use structural information to identify solvent exposed sites on a small molecule and synthesise compounds with dummy linkers at the solvent exposed site to see if substitution is tolerated.

From a published crystal structure of **1** in the active site of MLKL (Figure 3.20) the key interactions can be visualised.<sup>2</sup> Two hydrogen bonds are formed between the 2-aminopyrazine to the hinge amino acids, Glu284 and Cys286, and the non-substituted phenyl has a Sutor CH bond to Ser335. The 4-Nitrogen of the pyrazine and the amide NH both coordinate a centrally held water and the 4-fluorophenyl stacks with Arg210.

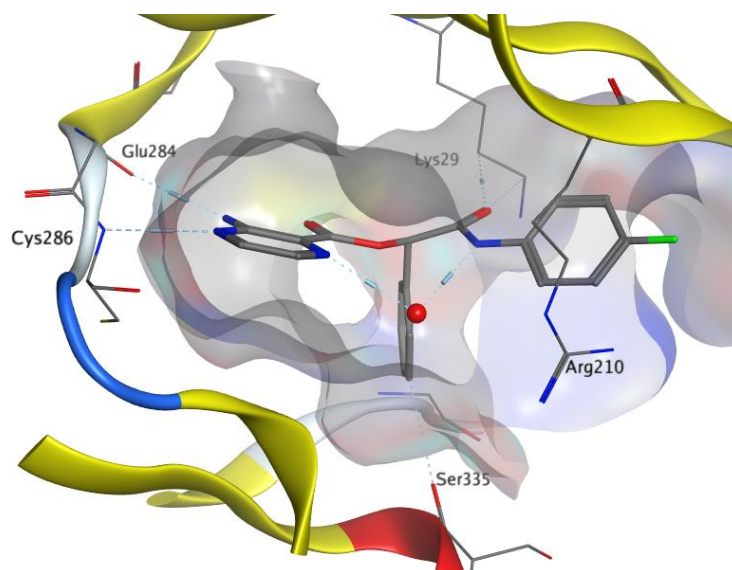


Figure 2.36 – 1 in complex with MLKL. PDB: 5KO1

We identified three solvent exposed sites: the 5-pyrazine position, the para position on the phenyl ring replacing the fluoro and the meta position on the phenyl ring ortho to the fluorine.

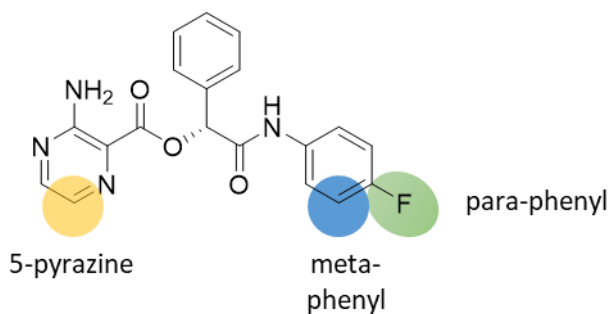


Figure 2.37 - 2D representation of the solvent exposed sites of 1

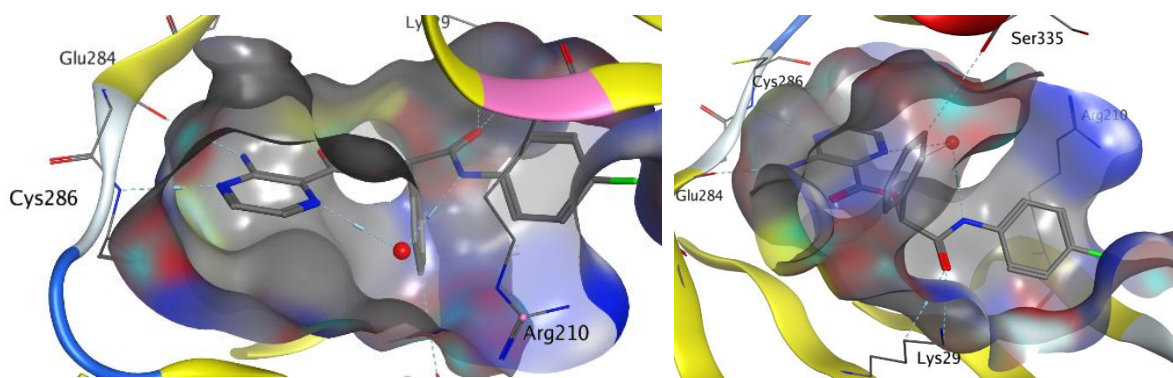


Figure 2.38 - solvent exposed sites of 48. PDB 5KO1

As with dummy linkers on AMPK, we wanted to incorporate a chain with carbon and oxygen and have a dummy linker of sufficient length to test if a full-sized linker could be tolerated.

## 2.10 Synthesis of dummy linker analogues of **1**

### 2.10.1 Para-phenyl

The phenyl ring in **1** is reported to stack with Arg 210 with the fluoro group on the phenyl ring pointing to solvent, so this could be a suitable site for attaching a linker. From modelling as shown in Figure 2.39, it appeared that substituting the fluorine for a glycol linker would maintain the overall binding pose and would be well tolerated. However, the Arg210 has a high B factor in comparison to the rest of the active site, suggesting that it is a flexible group which makes it difficult to interpret exactly how a linker would affect binding.

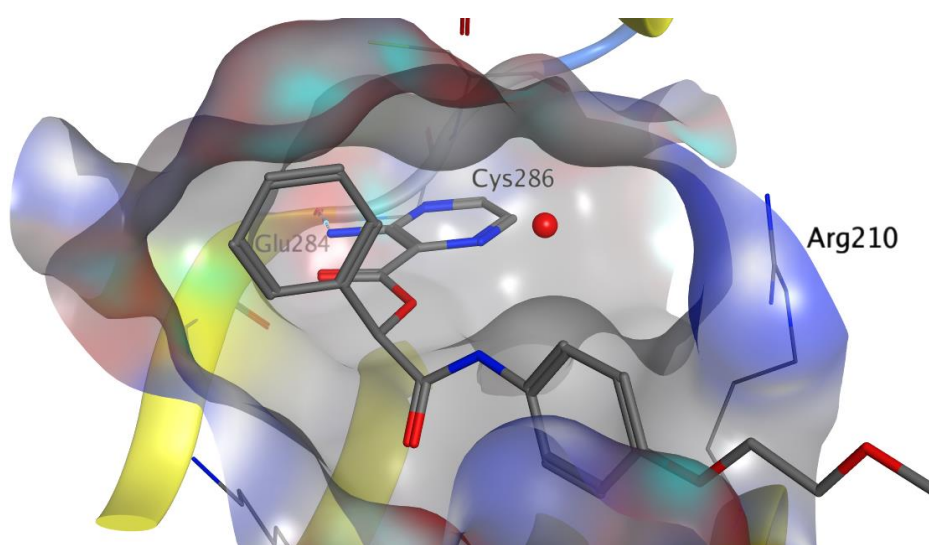


Figure 2.39 - **1** with the fluorine replaced by a glycol dummy linker (PDB:5KO1).

Introducing a dummy linker at the para position on the phenyl side used an  $S_NAr$  reaction between fluoro-4-nitrobenzene, **44**, with 2-methoxyethanol to give intermediate, **45**, that was then reduced with iron and ammonium chloride to the aniline, **45**. This was then coupled to **39**, to give CCT375223 in a low yield.



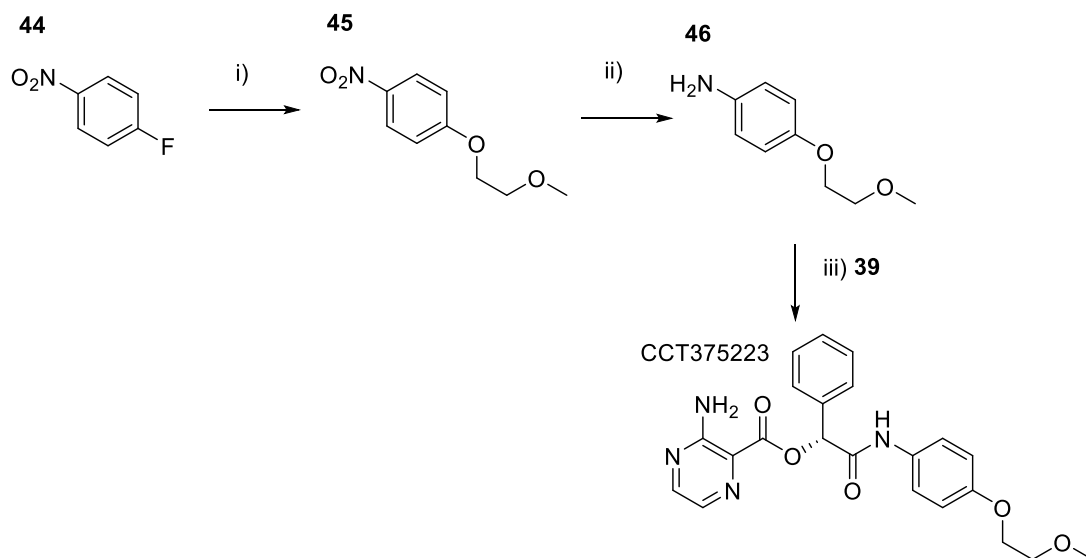


Figure 2.40 -- Reaction scheme for the functionalisation of the PARA-PHENYL replacement dummy linker. i)  $K_2CO_3$ , ACN, 80C, 16h, 88% ii) Fe,  $NH_4Cl$ , EtOH,  $H_2O$ , 70C, 3h, 71% iii) (2R)-2-hydroxy-2-phenyl-acetic acid, HATU, DIPEA, DMF, rt, 2h, then 3-aminopyrazine

### 2.10.2 Meta-phenyl replacement

As the meta position is also solvent exposed, we modelled a dummy linker at this position which lowed well tolerated (Figure 2.41).

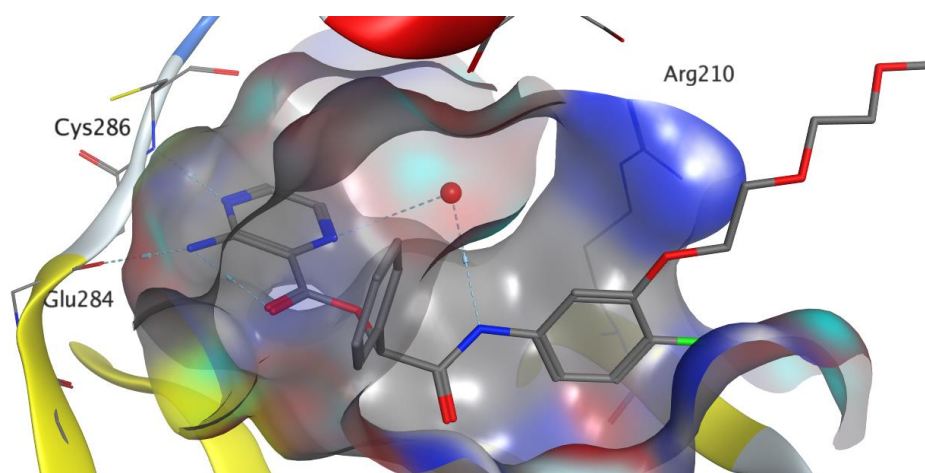


Figure 2.41 - Minimised structure of **1** with a glycol group in the ortho fluorine position. (PDB:5KO1).

Introducing a PEG dummy linker at the meta position was carried out starting from the phenol, **47**, and used a bromo alkyl halide to give **48** in a high yield. Again, a reduction with iron and ammonium chloride gave the aniline **49** in a moderate yield, which was coupled to **39** to give CCT375224 in a low yield

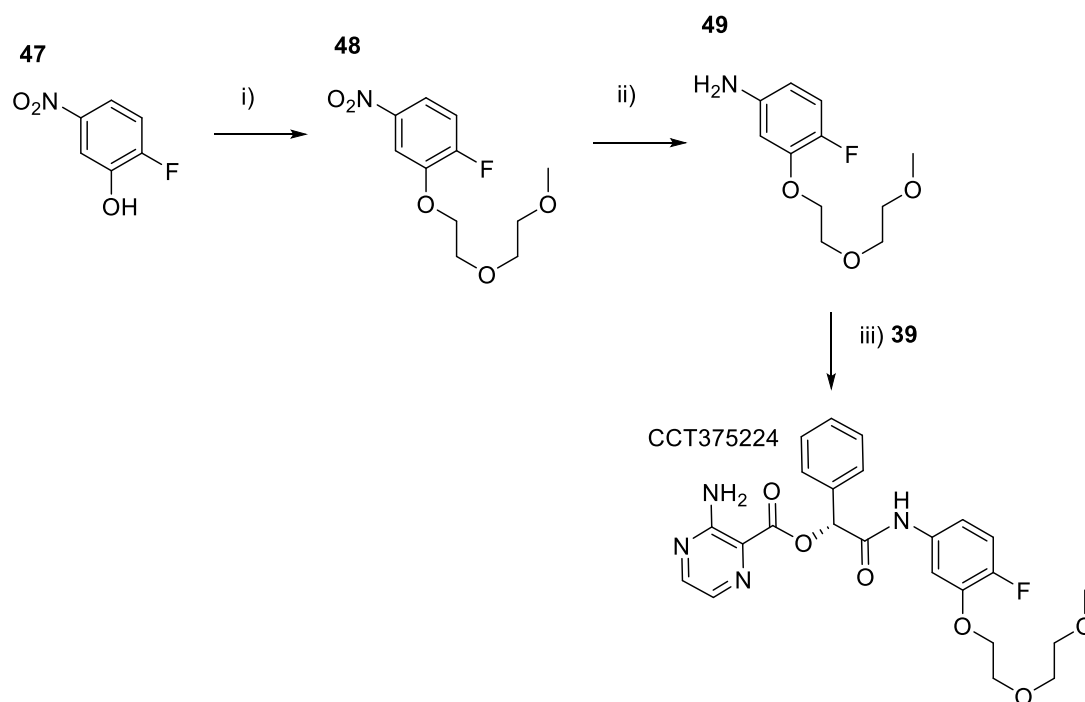


Figure 2.42 - Reaction scheme for the functionalisation at the *m*-phenyl position. i)  $K_2CO_3$ , ACN, 50C, 16h, 93% ii) Fe,  $NH_4Cl$ , EtOH,  $H_2O$ , 80C, 4h, 71% iii) (2R)-2-hydroxy-2-phenyl-acetic acid, HATU, DIPEA, DMF, rt, 2h, then 3-aminopyrazine

### 2.10.3 5-pyrazine position

The 5-pyrazine position is not directly solvent exposed but is pointing towards bulk solvent. As such we wanted to test if we could first extend towards bulk solvent, and if this was tolerated then we could further extend into bulk solvent with dummy linkers.

As there was no published SAR around **1**, we decided to functionalise at this position with an unsubstituted phenyl group as we were focussed on extending to solvent not picking up new interactions to increase binding affinity.

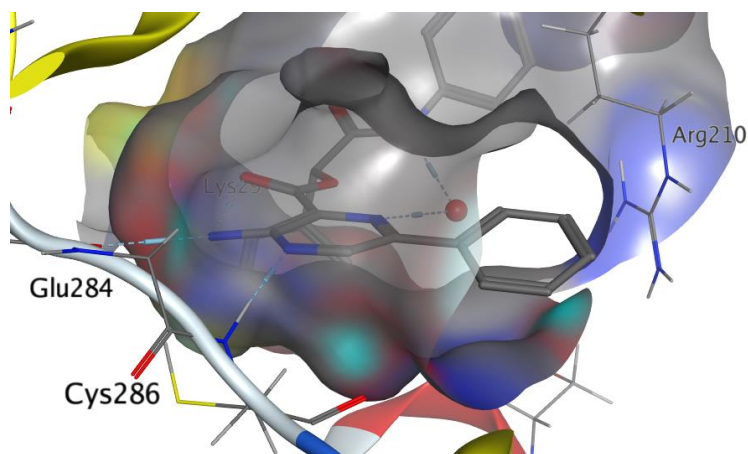


Figure 2.43 - 1 with a phenyl ring in the 5-pyrazine position shows the phenyl ring extends towards bulk solvent. (PDB:5KO1).

A Suzuki coupling of **50** with phenyl boronic acid gave intermediate **51**, in a moderate yield, which was hydrolysed to the acid, **52**. This was then coupled to the secondary alcohol **36**, to give **53** in a low yield.

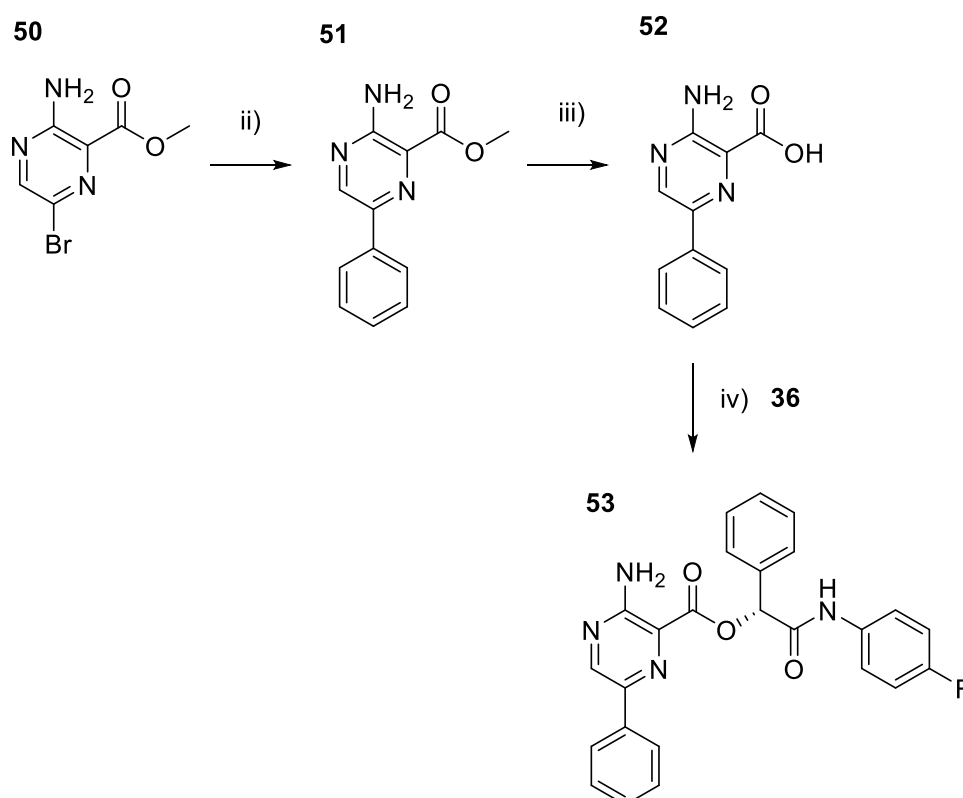
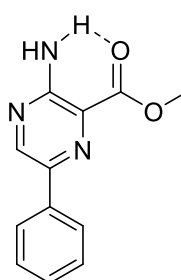


Figure 2.44 -Synthesis of aromatic containing compounds i) HATU, DPIEA, DMF, 90% ii) Pd(dppf)Cl<sub>2</sub>, phenylboronic acid, K<sub>3</sub>PO<sub>4</sub>, 1,4-Dioxane, H<sub>2</sub>O, 85°C, 3h, 70% iii) LiOH, THF, H<sub>2</sub>O, 60°C, 2h, 87%

Both intermediate **51** and **52** proved to be highly insoluble which may be due to the amino and ester carbonyl having an intramolecular H bond, as shown in Figure 2.45. In this adopted conformation, the molecule is very planar which can lead to stacking of molecules together which leads to poor solubility. We hoped that elaboration to **53** could improve solubility as it incorporated a sp<sup>3</sup> atom which reduces the planarity of the molecule, so may reduce intermolecular stacking between molecules thus improving solubility. However, **53** was also highly insoluble and aromatic group derivatives in the 5-pyrazine position were not taken any further.



*Figure 2.45 - Structure of 53, showing the possible intramolecular H bonding responsible for poor solubility*

#### 2.10.4 Alkyne based linkers

Aromatic rings typically reduce solubility of a compound due to a high LogP and their flat structure which allows  $\pi$ -stacking resulting in a high lattice energy.<sup>72</sup> To maintain this desired exit vector at the 5-pyrazine position and address these issues, we decided to use an alkyne as this leads to smaller increases in LogP. To further lower log D and hence improve solubility, we considered incorporating polar and ionisable groups to the molecule. As such we designed and modelled an alkyne containing a morpholine group at the 5-pyrazine position

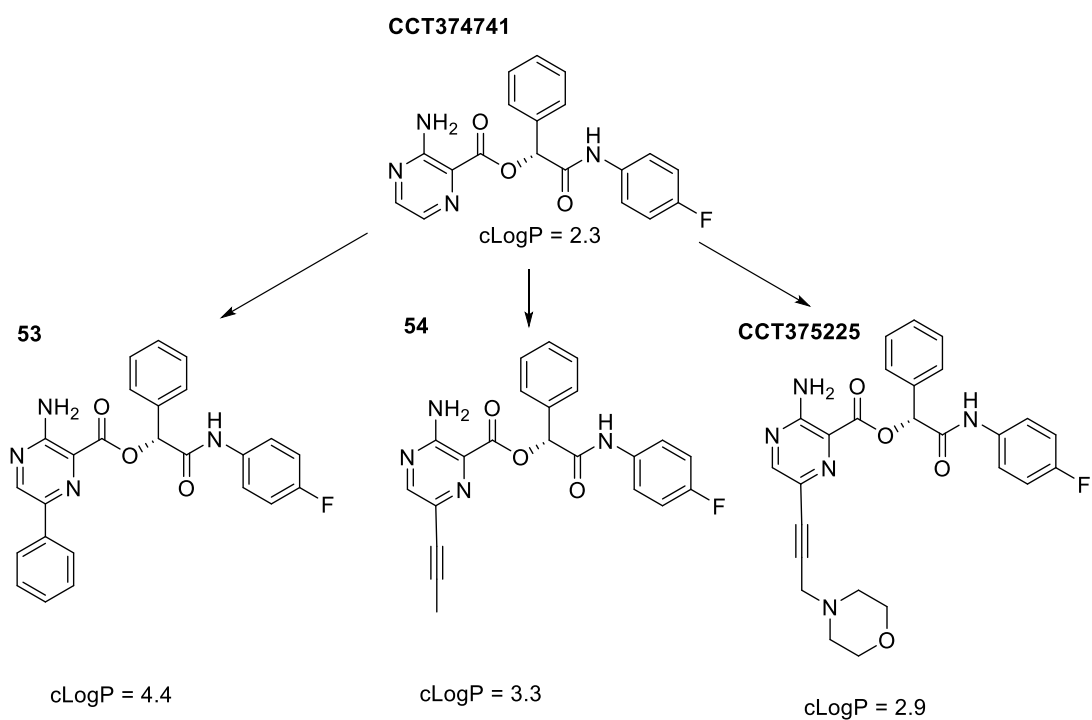


Figure 2.46 - cLogP values for 5-pyrazine dummy linkers. values calculated using MoKa 3

Modelling of CCT375225 suggests the morpholine would be in bulk solvent and not clash with the MLKL binding pocket (Figure 2.47)

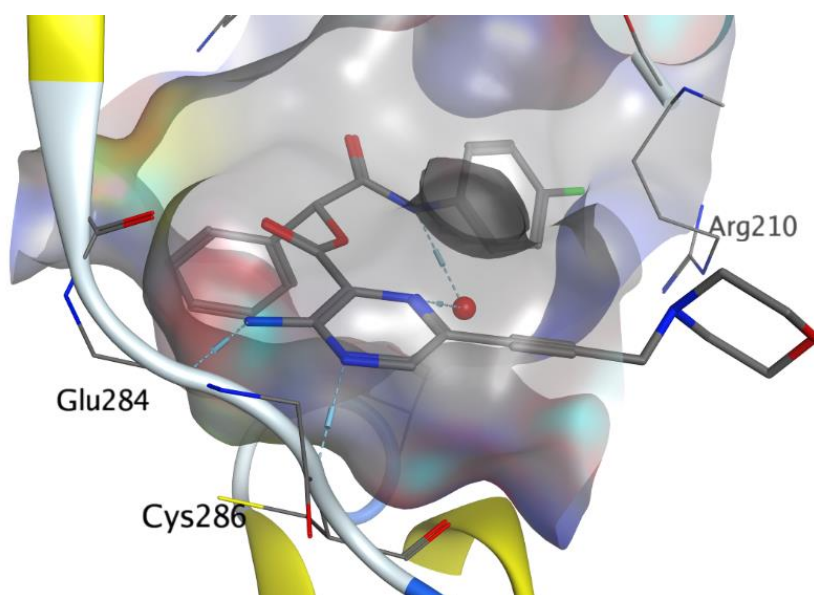


Figure 2.47 - alkyne-morpholine in the 5-pyrazine position

As in Figure 2.44, we started with **50** and used classic Sonogashira conditions to give **55**, which was hydrolysed to **56**, then coupled to the alcohol of **36** to give CCT375225.

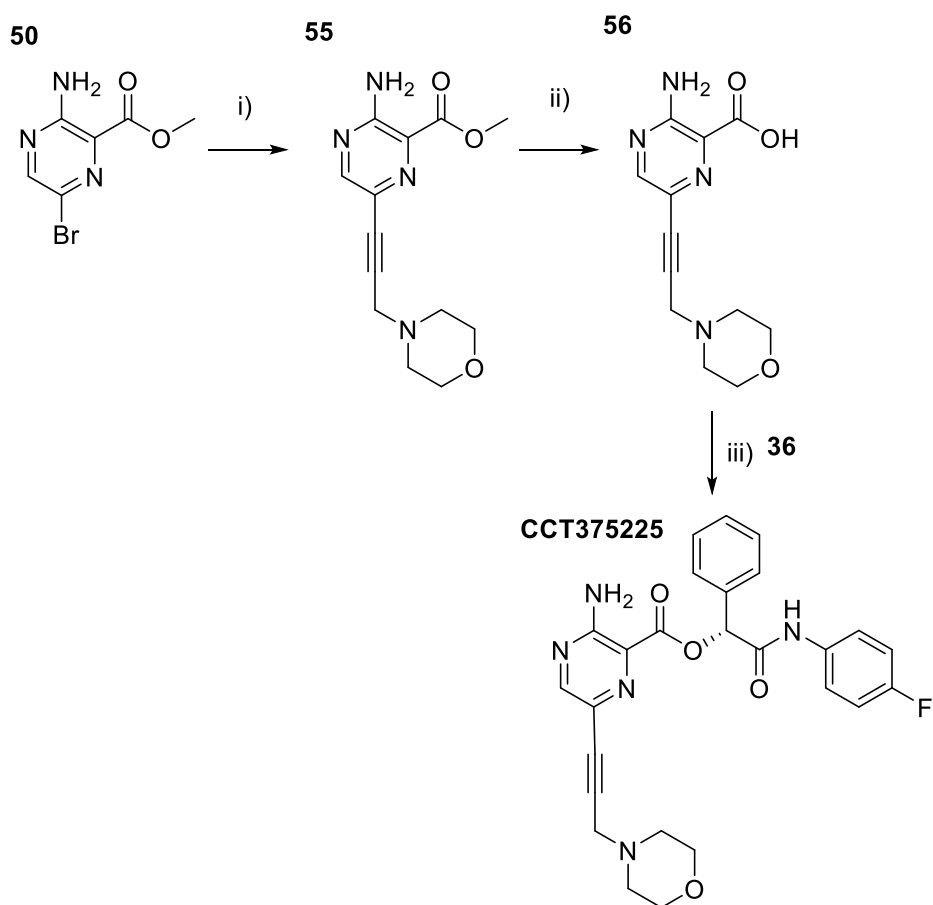


Figure 2.48 - Scheme for the synthesis of an alkyne at the 5-pyrazine position. i) Pd(PPh<sub>3</sub>)<sub>2</sub>Cl<sub>2</sub>, CuI, 70°C, 1.5h, 44% ii) LiOH, THF, H<sub>2</sub>O, Quant iii) HATU, DMF, 16%

Compounds **CCT375225**, **CCT375223** and **CCT375224** were sent to DiscoverX for testing, with results shown in Table 2.5. Each compound tested a different solvent exposed site so we could quickly find the best site(s) to functionalise on.

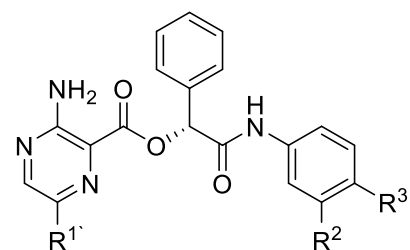
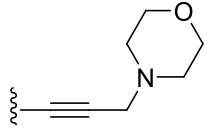
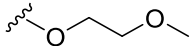
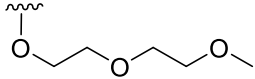


Table 2.5 - Biochemical assay results of dummy linker containing compounds

CCT Number	R <sup>1</sup>	R <sup>2</sup>	R <sup>3</sup>	Kd / nM
CCT374741	H	H	F	160
CCT375225		H	F	900
CCT375223	H		F	>10 000
CCT375224	H	H		4 300

The results show the fluorophenyl was very sensitive to changes with CCT375224 showing a  $\approx$  25-fold drop in affinity and CCT375223 showing no detectable binding. The fluorophenyl ring  $\pi$  stacks with Arg210, but due to poor resolution of Arg210 it is not clear what orientation of the phenyl ring is necessary to maintain binding. We hypothesise that adding an electron donating groups may interfere with the electronics of this interaction or a that a dummy linker alters the orientation of the phenyl ring, and this results in loss of the  $\pi$  stacking hence the loss in binding affinity.

The results show that functionalising on the pyrazine ring resulted in the smallest drop in binding affinity, with a  $\approx$  4-fold drop in binding affinity. This suggests that the 5-pyrazine position is solvent exposed and would represent the best position for linking from **1**.

## 2.11 Summary

We identified the MLKL binder, **1**, from literature and used structural information to design and synthesis analogues containing dummy linker which we predicted may extend into solvent and be possible sites for attaching linkers. Three analogues were synthesised and tested for their  $K_d$  against MLKL and showed dummy linker attachment reduced binding affinity at least four-fold. From PROTAC literature the desired potency of the warhead for the target protein is generally in the  $K_d = 1\text{-}500$  nM range, as this is strong enough to form the ternary complex required for inducing a post-translational modification.<sup>28</sup> Whilst **1** had a  $K_d$  in this range, attaching a dummy linker took us substantially out of this range, and we hypothesised bifunctional molecules would not have been able to bind MLKL strongly enough to form the ternary complex key for inducing neo-phosphorylation. Although earlier work had suggested ester containing compounds would be stable under a range of chemical conditions, in synthesising bifunctional molecules based on **1**, ester hydrolysis was commonly seen especially under basic conditions. As the ester seemed key for retaining activity against MLKL and the goal of this project was to induce neo-phosphorylation not to develop the SAR around **1** we decided to stop synthesise of analogues of **1** and focus on functionalising and making bifunctional molecules using Crizotinib as a warhead.

## 2.12 Crizotinib dummy linkers

As mentioned in 2.9: Mixed Lineage Kinase Domain-Like Protein (MLKL), Crizotinib is a reported binder of MLKL with a  $K_d = 217\text{nM}$ . Crizotinib is a pan-selective kinase inhibitor so binds many other kinases than MLKL, which would mean that if these compounds were tested in cells and showed a phenotype then it would not be possible to directly attribute it to MLKL phosphorylation. However, as this was a proof-of-concept project initially we wanted to show neo-phosphorylation and if necessary, then work on designing more selective probes.

Crizotinib is an optimised compound and approved drug so was likely to have greater stability and solubility compared to compound **1**. To identify solvent exposed sites Crizotinib was docked into the crystal structure of compound one



bound to MLKL. As the hinge binding of kinases is typically key for activity, we generated a pharmacophore for the H bond donor and acceptor from the 2-amino pyrazine in compound **1** and docked Crizotinib. The best ranked hit showed that the 2-amino pyridine in Crizotinib maintained this hinge interaction to Cys286 and Glu284 (Figure 2.49)

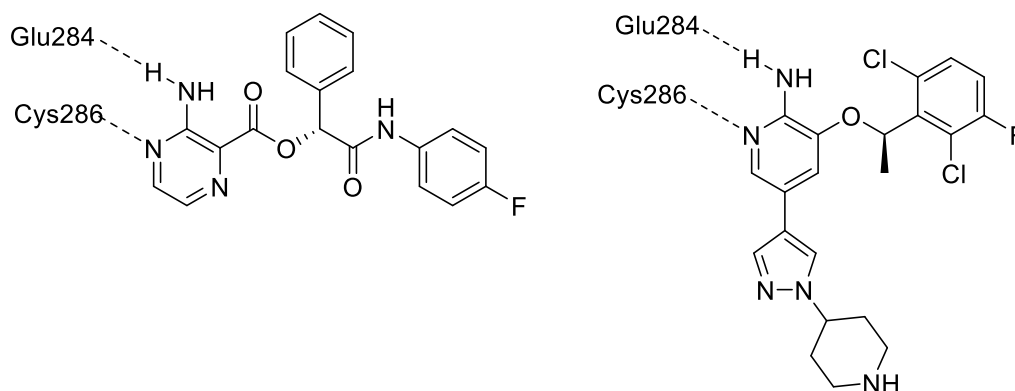


Figure 2.49 - 2D representation of compound **1** binding MLKL and the predicted docked structure of Crizotinib binding MLKL through the hinge

This predicted binding mode showed the pyrazole and piperidine on Crizotinib were already solvent exposed and the piperidine was not interacting with MLKL so could tolerate a linker without affecting binding (Figure 2.50)

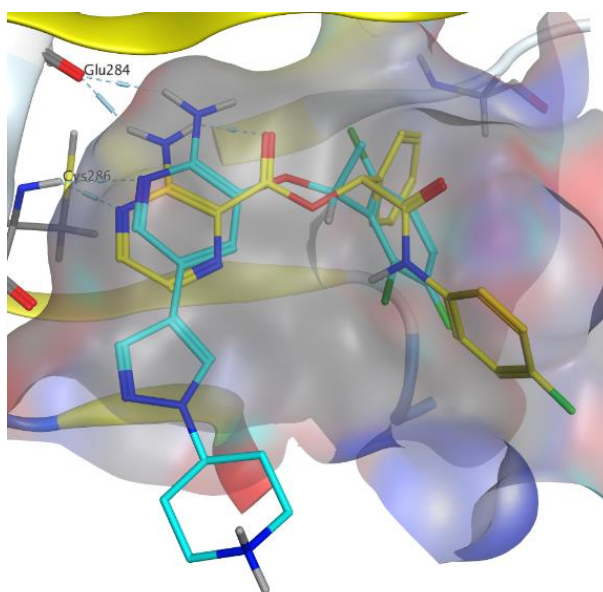


Figure 2.50 - Crizotinib (cyan) docked into the MLKL nucleotide binding site (PDB: 5K01)

To confirm the piperidine NH was not key for binding and that it was solvent exposed we needed to synthesise dummy linker containing compounds that linked from this position. As the piperidine nitrogen is the most reactive nitrogen in Crizotinib we were able to use commercially brought Crizotinib and functionalise the piperidine through an amide coupling or reductive amination. We chose these two reactions as they are generally moderate to high yielding steps and for substrates used a glycol acid to give CCT389351 or an aldehyde to give CCT390196. The composition of these groups was again chosen to reflect the composition of standard linkers found in bifunctional molecules and was mainly to test whether substituting on the piperidine nitrogen was tolerated.

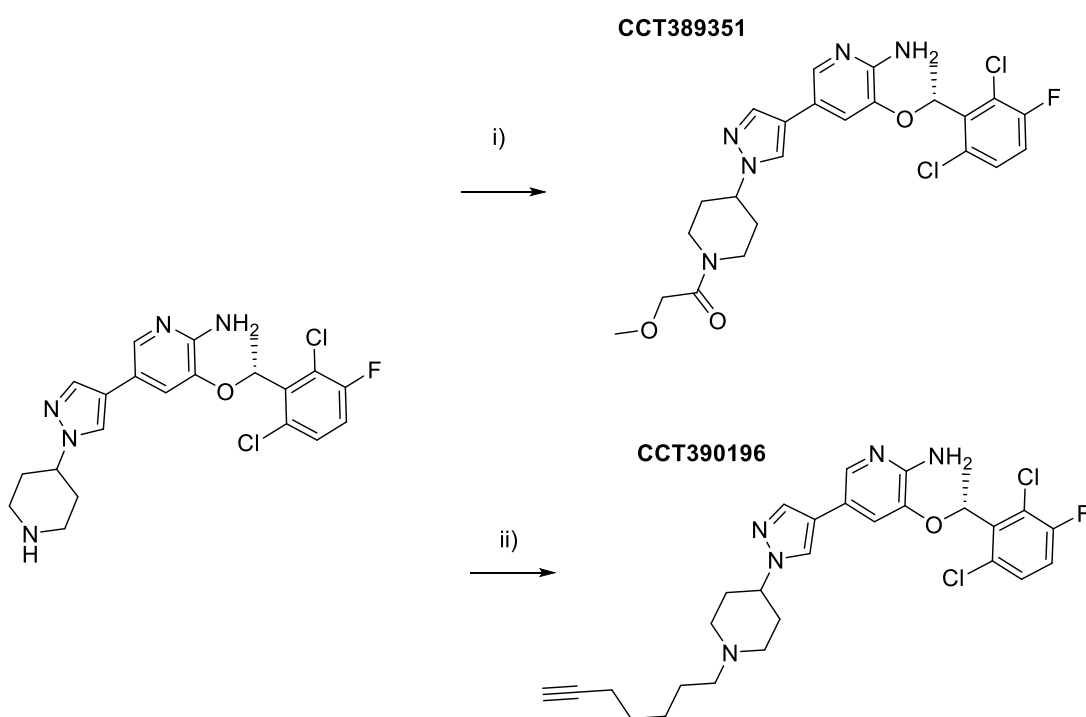


Figure 2.51 - Synthesis of substituted piperidines starting from crizotinib. i) 2-Methoxyacetic acid, HATU, DIPEA, DCM, rt, 2h, 78% ii) hept-6-ynal, sodium triacetoxyborohydride, DCM, rt, 24h, 58%

### 2.13 Testing Crizotinib and AMPK activators against AMPK

In a bifunctional molecule, each part of the bifunctional molecule either binds the effector protein or protein of interest. However, Crizotinib is reported to be a weak inhibitor of AMPK with a  $K_d = 2.4 \mu\text{M}$ , and we wanted to ensure that bifunctional compounds consisting of Crizotinib joined to an AMPK activator would not just inhibit AMPK as this would prevent AMPK from binding ATP and inducing neo-phosphorylation of neo-substrates. As the AMPK activators have much lower  $EC_{50}$  values than the  $IC_{50}$  of crizotinib for AMPK we hypothesised there would be a reasonable concentration range where the proposed bifunctional compounds would still be able to activate AMPK.

To test this hypothesis, we did a dose response of Crizotinib and the two different AMPK activators, CCT390622 and CCT390619 to see if the activation of AMPK would outweigh the inhibition (Figure 2.52).

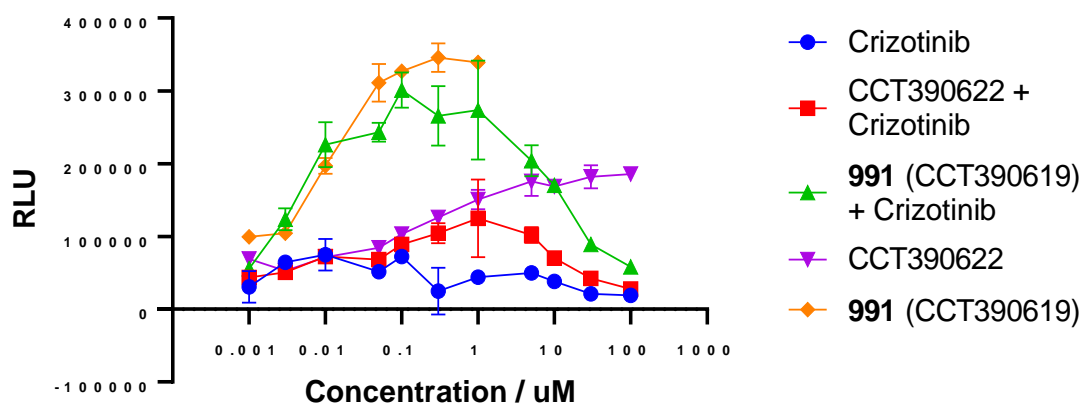


Figure 2.52 - ADP Glo results of AMPK activation vs inhibition in the presence of Crizotinib and AMPK activators

The results show that for both activators, as expected, at low concentration of activator and Crizotinib, the Crizotinib has no inhibitory effect, as the activator outweighs the inhibition from Crizotinib, and the curves are like those for the activator only. However, at increasing concentrations, inhibition from crizotinib leads to a decrease in AMPK activation. However, even at high concentrations past Crizotinib's  $K_d$  for AMPK, the levels of ADP are higher than crizotinib on its own, so the overall effect is still AMPK activation. This supported the use of Crizotinib as a warhead in bifunctional molecules to direct neo-phosphorylation.

#### **2.14 Developing a MLKL LanthaScreen Assay**

Previous hits against MLKL reported in literature were identified by thermal shift, or outsourcing to DiscoverX.<sup>2</sup> However, MLKL was a difficult protein to source commercially so performing thermal shift experiments would have been very expensive, and do not necessarily reflect the binding affinity of a small molecule to a protein. Outsourcing to DiscoverX is expensive so we felt developing an in-house assay would be advantageous. However no high through method of testing MLKL binders was reported at this time so we needed to develop a suitable assay.

The LanthaScreen assay is a Time-Resolved Fluorescence Resonance Energy Transfer (TR-FRET) that measures displacement of an ATP-competitive probe from the binding site. The assay is set up using three components; a tagged protein, a Europium labelled anti-tag antibody and a 'tracer' molecule. The Tracer is an ATP competitive warhead linked to an Alexa Fluor<sup>TM</sup> fluorophore. In the absence of a competitor, the Europium is excited with a laser and when it relaxes it releases energy at 615nm. If the Europium and the tracer are close enough, then an energy transfer can occur that results in the tracer being excited and then emitting energy at 665 nm.

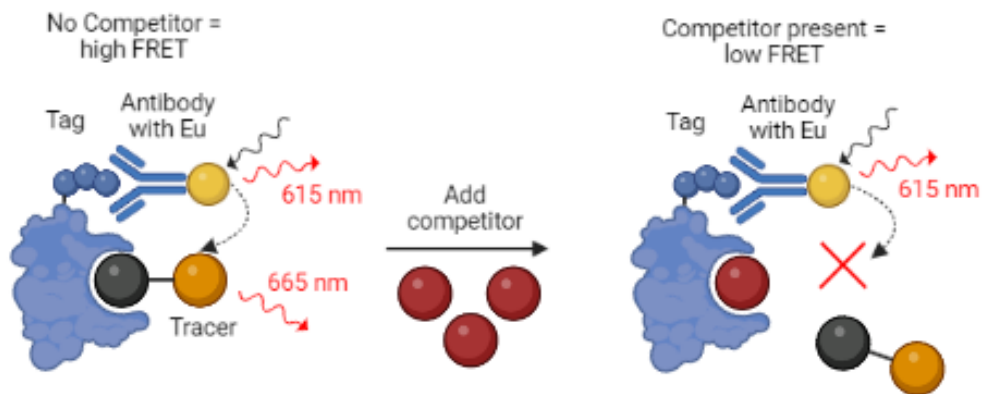
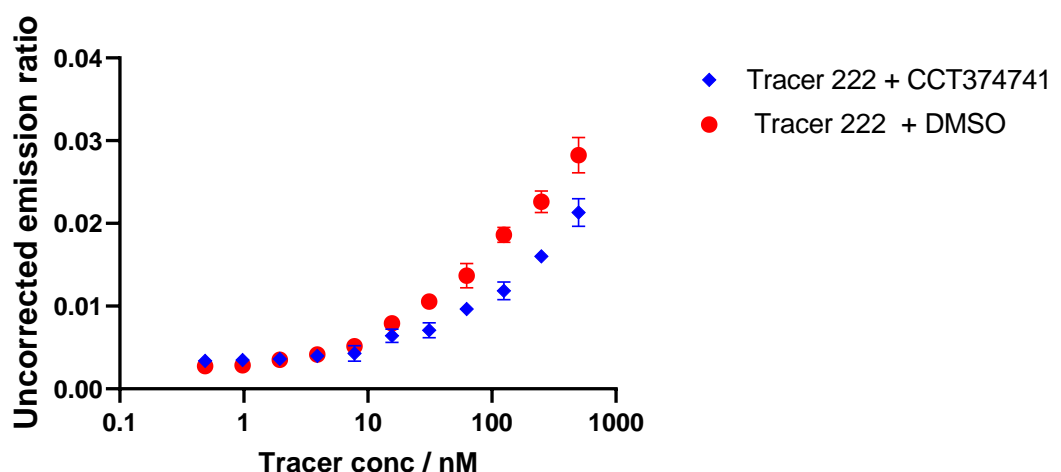


Figure 2.53 - Scheme showing the principle behind the LanthaScreen assay

Both these wavelengths can be measured to find the ratio of 665nm to 615nm to give an emission ratio. If a competitor is present then the tracer is outcompeted from the ATP binding site, resulting in no energy transfer to the tracer, and reduced emission at 665nm, giving a reduced FRET.

To optimise the assay, we used CCT374741 as the competitor molecule at 10 $\mu$ M and performed a tracer titration. As we knew CCT374741 bound to the active site of MLKL, an observed shift in FRET with a tracer is likely due to competition for that site.

### Uncorrected emission ratio 222 1h incubation



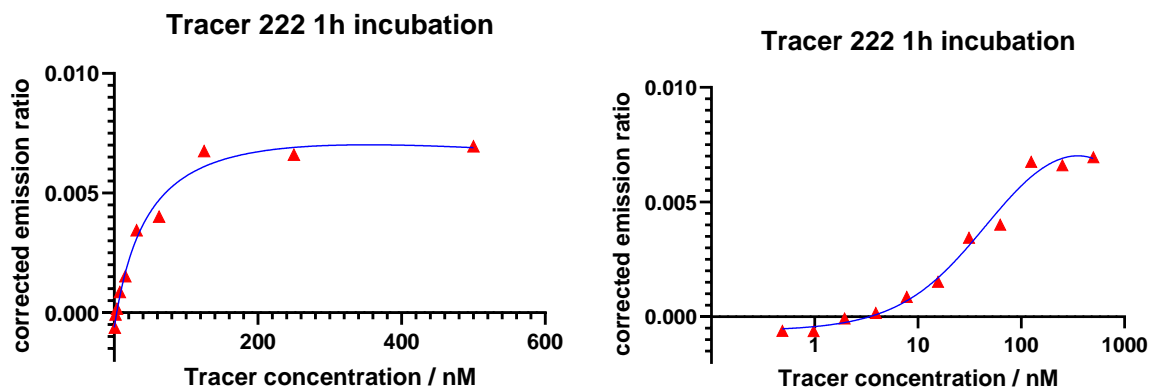


Figure 2.54 – Tracer titration of Tracer 222 against CCT374741.

After an incubation of 1h at rt, the emission at 665 and 615 nm was read. All commercially available tracers from ThermoFisher™ were tested (tracers 178, 199, 222, 236, 314, 1710), which are all based on pan-selective kinase inhibitors. However only tracer 222 gave the desired change in emission ratio, see Figure 2.54.

Tracer 222 gave a  $K_d = 50$  nM, which was suitable. However, from analysing the signal to background  $\left(\frac{\text{value without competitor}}{\text{value with competitor}}\right)$  of the uncorrected emission the highest value was only 1.4 at 62.5nM. A signal to background value of  $>2$  is recommended to make sure the values from a competitor are significantly different to without a competitor and so binders of MLKL can be identified. We also noted the values of the corrected emission ratios are 100-fold smaller than the corrected emission ratios typically seen in these assays. As CCT374741 was sparingly soluble we thought solubility may be an issue. To confirm this was a genuine signal we repeated the titration with CCT374741 and tested Crizotinib as a control compound at 10 $\mu$ M. As both these compounds bind the active site with similar  $K_d$  values, we expected them to give similar emission ratios.

## Uncorrected emission ratio with Tracer 222

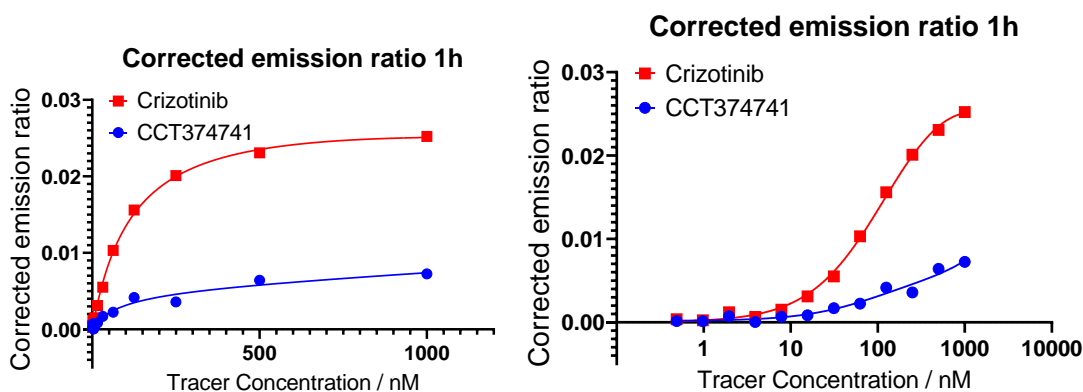
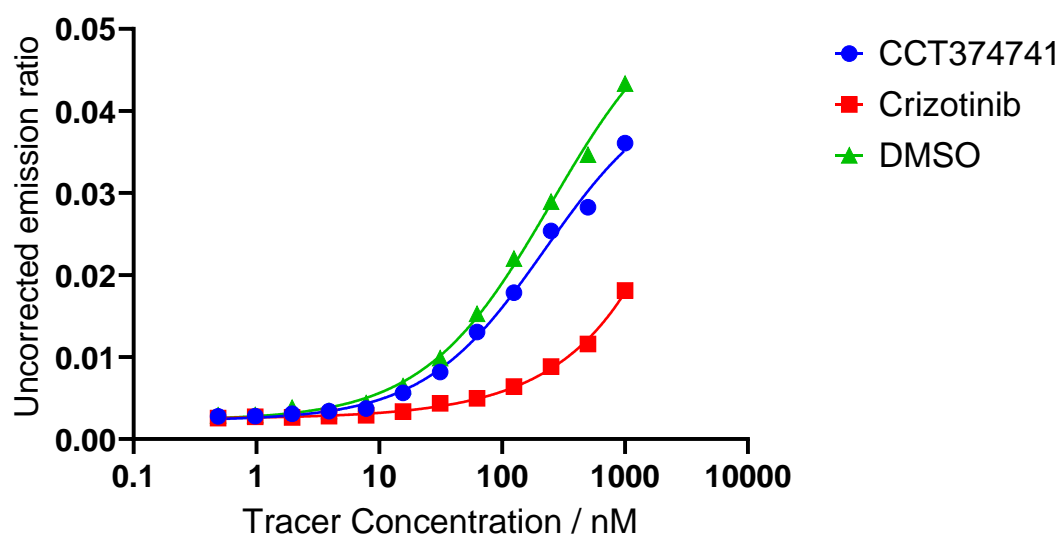


Figure 2.55 – Repeat of Tracer 222 titration against CCT374741 and Crizotinib.

The titration confirmed the shift seen with CCT374741 and Tracer 222 again gave a similar  $K_d$  value to that seen in the previous experiment with a  $K_d = 89$  nM suggesting good reproducibility. Crizotinib gave a slightly higher  $K_d = 125$  nM but much larger shifts in emission ratios compared to CCT374741 and gives much higher corrected emission ratios. As a result, crizotinib gave a much larger assay window of 3.1, compared to 1.7 for CCT374741 at 62.5 nM of tracer 222. We hypothesize this is due to poor solubility of CCT374741 resulting in a lower concentration than 10  $\mu$ M being in solution in the assay. This means there is less of the competitor present to compete with the tracer, so less of a shift in values than compared with Crizotinib.

As Tracer 236 is more commonly used in LanthaScreen assays we repeated the experiment testing Crizotinib with tracer 236, to see if we could see an effect. We also wanted to confirm the shift seen with tracer 222 (Figure 2.56).

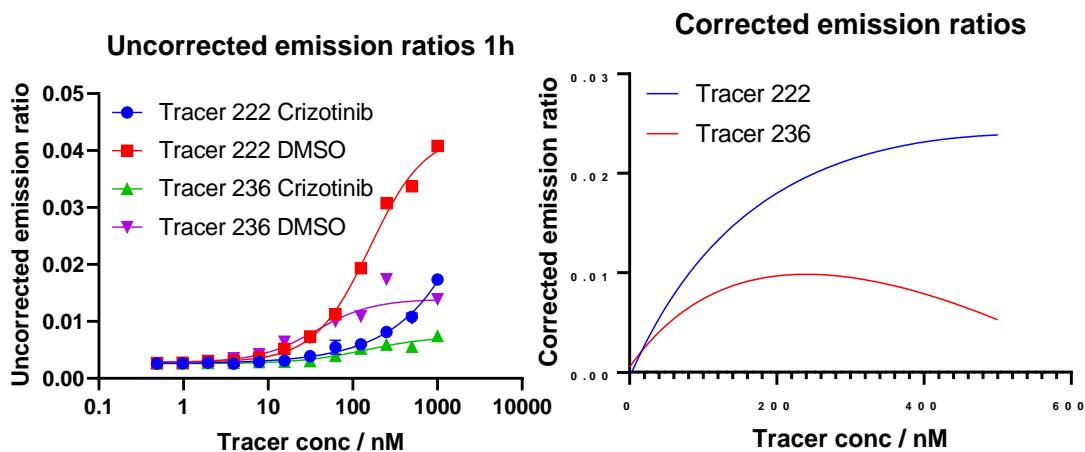


Figure 2.56 - Left: Uncorrected emission ratios found by dividing emission 665 nm by emission at 615 nm. Right) corrected emission ratio found by subtracting the uncorrected emission ratio from the DMSO control

Although Tracer 236 is the most used tracer for kinases, it was tracer 222 which showed the highest uncorrected and corrected emission ratio, Figure 2.56. As MLKL is a pseudokinase, it's reasonable that the most common tracers for kinases is not the most suitable one in this case. Tracer 222 was found to have a  $K_d = 298\text{nM}$ , and at a Tracer concentration of 125 nM the assay window was 3.2. This suggested good reproducibility and that with small molecules we could see a large enough shift in emission compared to the background to determine  $IC_{50}$  values.

### 2.15 $IC_{50}$ Experiments

Having identified a suitable tracer and its  $K_d$ , we wanted to validate the assay by measuring  $IC_{50}$  values and see if they correlated with the testing at DiscoverX

CCT374741 was tested against tracer 222 concentration with the tracer at a concentration of 62.5 nM as that gave the best assay window.



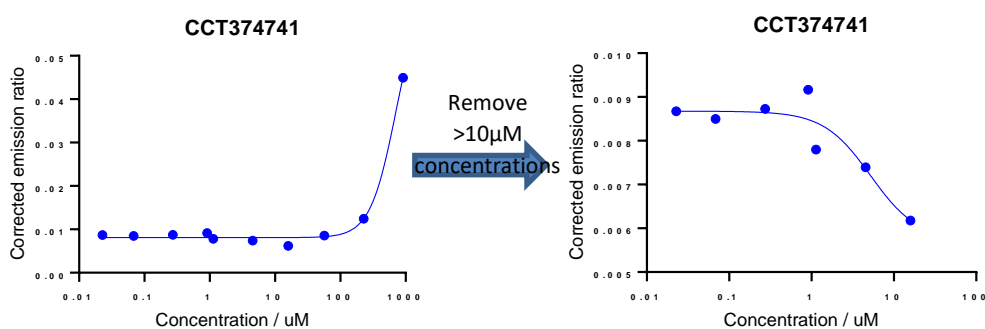


Figure 2.57 - Testing CCT374741 against MLKL in a LanthaScreen assay. Tracer 222 is at 62.5 nM

In the IC<sub>50</sub> experiment at high concentrations of CCT374741 there a large increase in signal and even if these values are excluded the IC<sub>50</sub> = 5.2 μM, which is much higher than expected (Figure 2.57). To understand if this was a general effect or specific to this compound we tested four kinase inhibitors (Crizotinib, Lestaurtinib, Dasatinib, Axitinib) that had been tested at DiscoverX and found to have a wide range of IC<sub>50</sub> values, to see if the LanthaScreen could accurately match an established technique (Table 2.6).

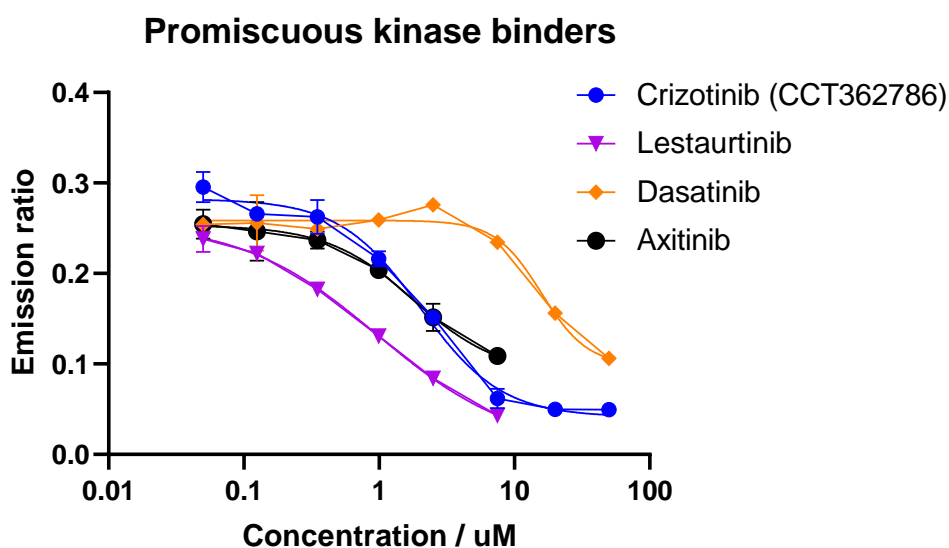


Figure 2.58 - IC<sub>50</sub> curves for promiscuous kinase inhibitors

Table 2.6 - Figure of known binders of MLKL, Literature value refers to testing done at DiscoverX. Outsourced testing refers to compounds sent to DiscoverX. LanthaScreen refers to in house experiments done

Compound	Literature value Kd / nM	Outsourced Testing Kd / nM	LanthaScreen IC <sub>50</sub> / nM
Crizotinib	217	1 300	2 015
Lestaurtinib	-	6 500	975
Dasatinib/Sprycel	-	8 200	15 820
Axitinib	-	120	1 791

The results show that the LanthaScreen assay correlates reasonably well with the results from DiscoverX testing for Crizotinib and Dasatinib. In the LanthaScreen assay graph, Figure 2.58, the last two points at the highest compound concentration for axitinib and lestaurtinib had to be removed as they show an increase in emission ratio, hence why their IC<sub>50</sub> values are far from DiscoverX values. This is likely to be solubility related with Axitinib (4.2uM at pH 7.4) and Lestaurtinib have reported solubility <10 uM,<sup>73</sup> whereas crizotinib and Dasatinib have reported solubility >10µM.<sup>74</sup> This increase in emission ratio is also what was observed in Figure 2.57, with CCT374741 which was poorly soluble.

Knowing that Crizotinib LanthaScreen assay gave full curves with no outliers, we then tested the two dummy linker containing compounds where crizotinib had been functionalised on the piperidine NH to test if linkers were tolerated at the expected site.

## MLKL binders - IC<sub>50</sub>

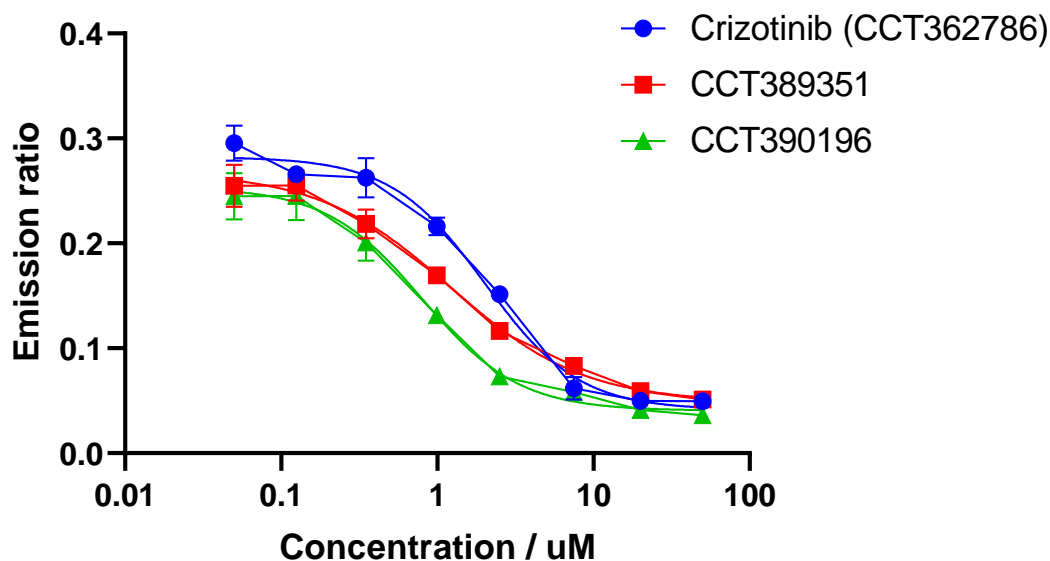


Figure 2.59 - IC<sub>50</sub> curves for Crizotinib with and without a dummy linker

In the LanthaScreen assay both CCT389351 and CCT390196 have activities similar to Crizotinib itself, suggesting the piperidine nitrogen in is solvent exposed and not key for binding to MLKL. If these dummy linker containing compounds had given a large increase or decrease in binding affinity then it would have suggested the docking was incorrect.

Table 2.7 - Data from LanthaScreen testing of compounds CCT389351 and CCT390196

Compound	Literature value K <sub>d</sub> / nM	Outsourced testing K <sub>d</sub> / nM	LanthaScreen IC <sub>50</sub> / nM
Crizotinib	217	1 300	2 015
CCT389351	-	-	1 216
CCT390196	-	-	800

## 2.16 Summary

Docking of Crizotinib against MLKL was performed and suggested an easily modifiable piperidine nitrogen would allow linkers to be attached without interfering with binding.

To test this, we synthesised two dummy linker compounds which we tested in a newly developed MLKL LanthaScreen and showed that Crizotinib could be functionalised with dummy linkers whilst retaining MLKL binding. Having identified a suitable warhead ligand for targeting MLKL we then moved on to synthesising bifunctional molecules

## 2.17 Bifunctional compound design

As explained in the introduction, linker length is a key factor in the activity of bifunctional molecules, with short linkers unable to bind both protein simultaneously and long linkers giving reduced PTM compared to an optimum linker length. To find the optimum linker length a library of bifunctional compounds with a range of different linker lengths must be synthesised and tested.

We chose to use click chemistry as the final step of joining the AMPK activator moiety with the Crizotinib warhead moiety as these reactions are typically quick and clean with few by-products. Additionally, like with PROTAC we envisioned a 'plug and play' system where different proteins could be targeted by attaching differing warheads. By using click chemistry if we had AMPK activators containing azides it would mean that a new protein could be targeted easily by attaching a simple terminal alkyne contain linker to a new warhead.

### 2.17.1 Functionalising AMPK activator 991

As azides are generally more reactive and harder to synthesise than an alkyne, we chose to functionalise the AMPK activators with the azides and Crizotinib with the alkyne. To maximise the range of linker lengths that could be made with the fewest number of bifunctional compounds we designed a 'long' and a 'short' AMPK azide and then a range of crizotinib based alkynes

To synthesise the required azides, an amide coupling with **991** was employed to give **57** in a reasonable yield.

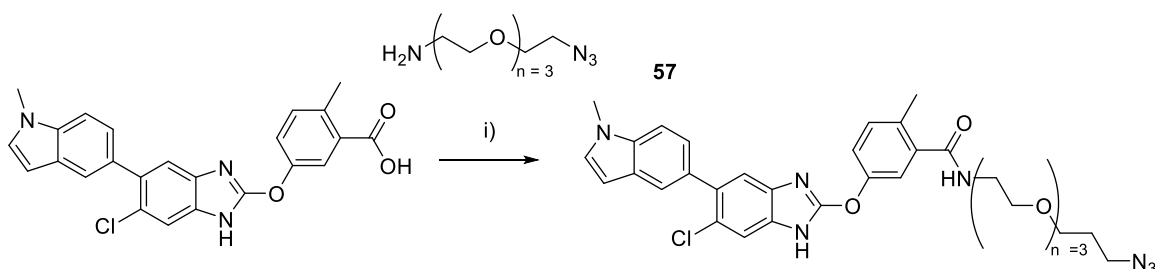


Figure 2.60 - Functionalisation of 991 to contain a long azide linker i) HATU, DIPEA, DMF, rt, 2h, Quant

Making a shorter chain azide was more synthetically challenging. As azides have a high nitrogen to oxygen and carbon ratio, they can be unstable and explosive, with the following equation giving an idea of the stability of azide containing compounds:<sup>75</sup>

$$\frac{(N_{Carbon} + N_{oxygen})}{N_{Nitrogen}}$$

Values  $\geq 3$  being needed for a substance to be considered stable enough to be isolated and stored. To try and keep the above ratio as high a value as possible and install a linker with an ethylene gap between the 991 scaffold and the azide, we planned a synthetic route using 2-Bromoethylamine, and then a subsequent  $S_N2$  reaction to give the azide (Figure 2.61)

The initial amide coupling worked well to give the ethylbromide, however the following  $S_N2$  resulted in no azide containing material, **51**, being detected by LCMS. Instead, a  $m/z$  corresponding to the elimination product to the alkene, **52**, was seen. Previous work in the group showed that using ethylbromide in a  $S_NAr$  at high temperature followed by a  $S_N2$  with sodium azide worked well, so we suspected that the 4,5-dihydrooxazole, **52**, shown in Figure 2.61 may be forming

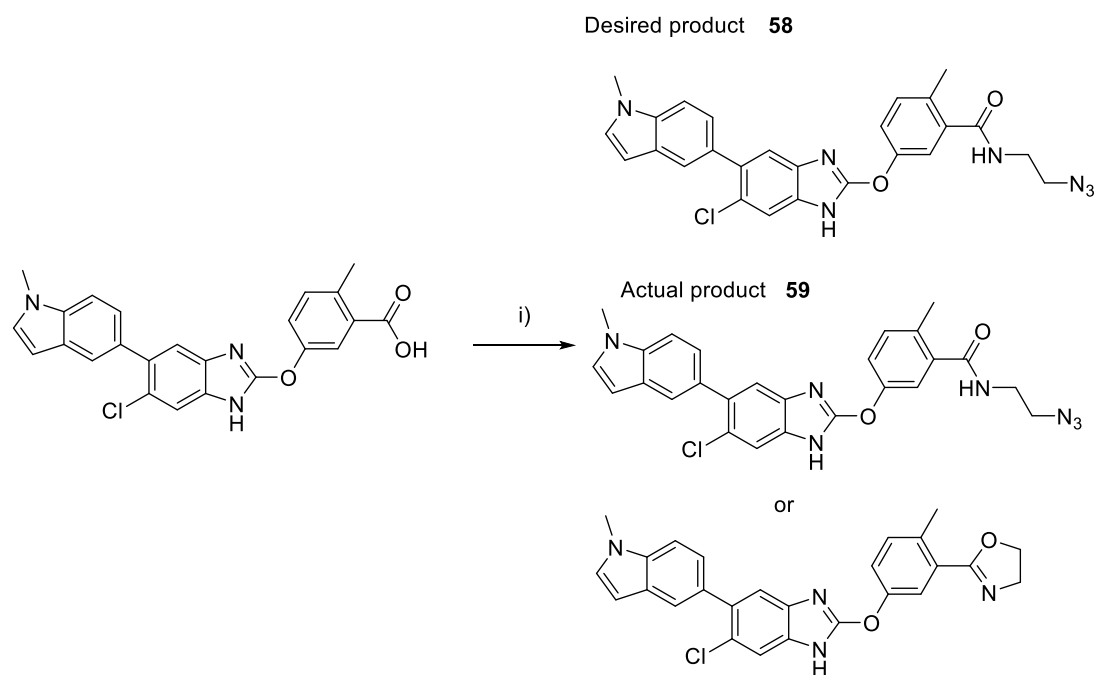


Figure 2.61 -Functionalisation of 991 to ethylene linkers. i) 2-Bromoethylamine hydrobromide, HATU, DIPEA, DMF, 0C, 1h then work up, then DMF, NaN<sub>3</sub>

We proposed that if we extended the chain by an extra methylene then any cyclisation product would now have to form a six membered ring not a five membered ring. Whilst six membered rings are more thermodynamically stable than five membered rings, they are kinetically slower to form so may not form under these conditions

The amide coupling with 3-Bromopropylamine was successful, and subsequent treatment with sodium azide to **60** was successful on a small scale.

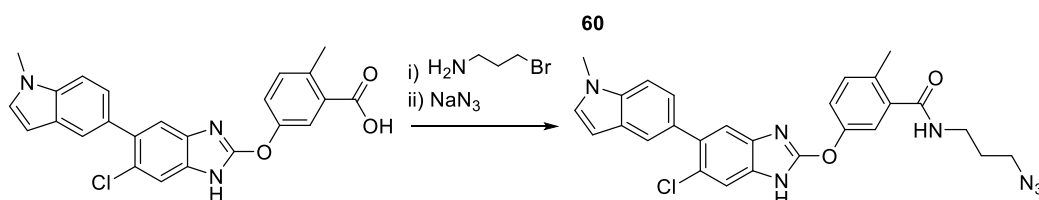


Figure 2.62 - Functionalisation of 991 to make short azide linkers. i) 3-Bromopropylamine hydrobromide, HATU, DIPEA, DMF, 0C, 1h ii) NaN<sub>3</sub>, DMF, 2h, rt, Quant

However, on scale up difficulties with purification and the safety risks of sodium azide led us to switch to using 3-azidopropylamine from a commercial supplier and using an amide coupling to produce the desired short chain azide, **60**.

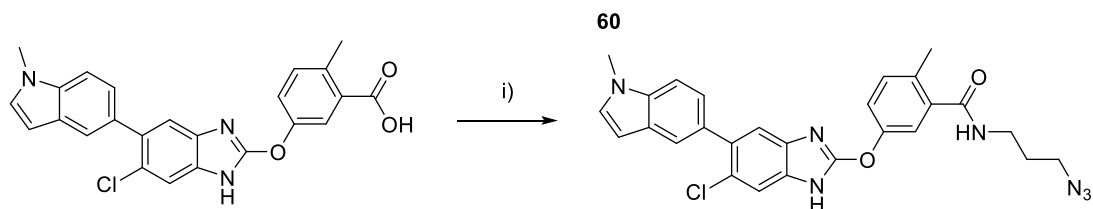


Figure 2.63 - Functionalisation of 991 to make short azide linkers

### 2.17.2 Functionalising AMPK activator 577

We also wanted to functionalise the **577** activator with a long and short azide linker to maximise the number of bifunctional molecules that could be made from the smallest number of azides. As **35** contains an acid and an amine, if we had used standard amide coupling conditions we likely would have seen dimers forming. To get around this we made the NHS-esters of the azides and then reacted with **35**.

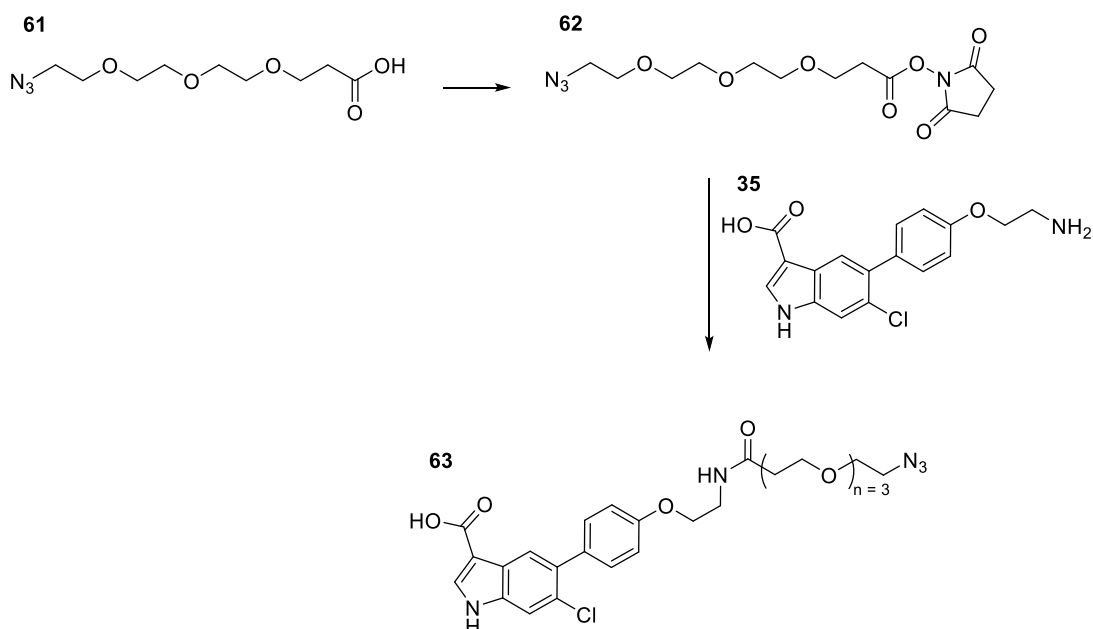


Figure 2.64 - Functionalisation of 577 to make the long azide linker.

Having had issues synthesising the short azide for the 991 AMPK activator we decided to buy the azide-alkyl acid **64** from a commercial supplier and make the NHS ester

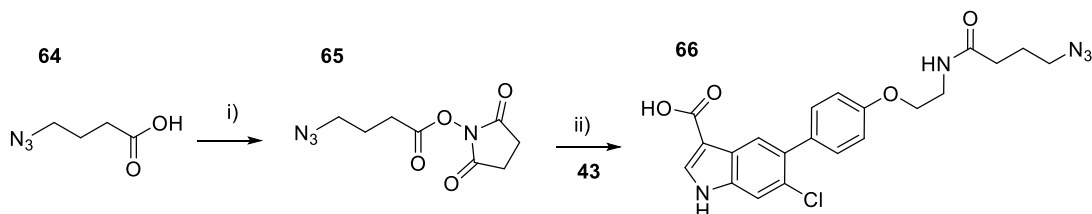


Figure 2.65 - Functionalisation of 577 to make a short azide linker. i) EDCI, DCM, rt, 5h, 83% ii) EDCI, DCM, rt, 16h, 97% iii) DIPEA, DMF, rt-70C, 1h-2 days, 52-79% iv) DIPEA, DMF, rt, 4h, 59%

### 2.17.3 Functionalising Crizotinib

Having shown crizotinib could be functionalised on the piperidine and maintain binding, we needed to functionalise Crizotinib on the piperidine nitrogen with linkers containing a terminal alkyne, so that they could be coupled to the azide containing AMPK activators.

As shown in Table 2.7 the piperidine nitrogen could be converted to an amine or amide and maintain similar levels of binding. Bifunctional molecules usually consist of a long linear chain so have a high degree of flexibility, thus allowing the two proteins in a ternary complex to adopt favourable conformation for a PTM to be induced. To give maximum flexibility of the linker we decided that having the piperidine as a tertiary amine would be better than an amide. We also predicted that the amine would give higher solubility than the amide as it can protonate at physiological pH. Bifunctional molecules usually have poor solubility so we anticipated the ionisable group may help alleviate poor solubility to an extent



To functionalise the piperidine nitrogen with terminal alkyne groups we oxidised alcohol-alkyl-alkynes to aldehydes, **88-90**, using Swern oxidations and then used reductive aminations to alkylate on the piperidine N-H.

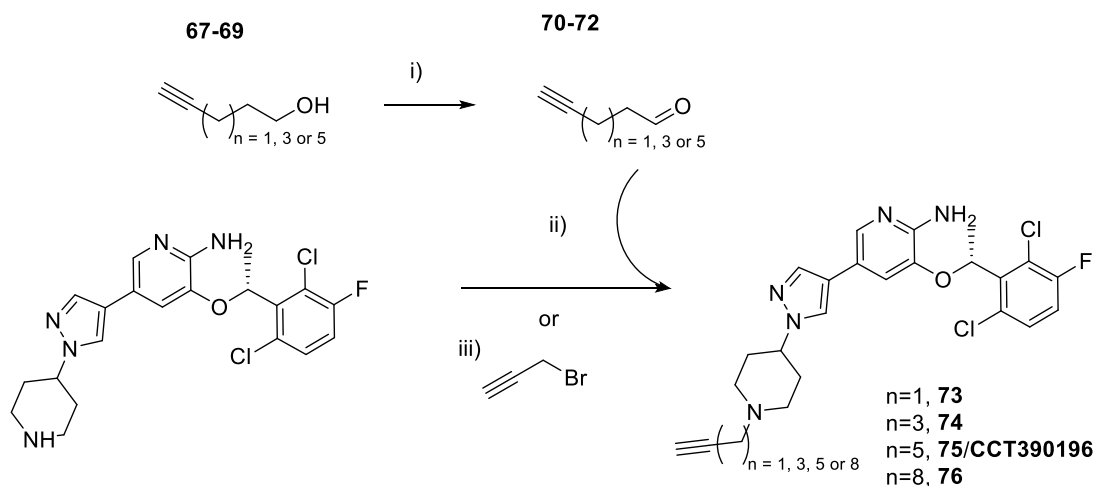


Figure 2.66 – i) DMSO, Oxayly chlorinde,  $\text{Net}_3$ ,  $-78\text{C} \rightarrow \text{rt}$  ii) STAB, DCM, iii)  $\text{K}_2\text{CO}_3$ , ACN, 16h

#### 2.17.4 Click chemistry optimisation

'Classic' click conditions use water as a solvent with copper sulphate as the catalyst and sodium ascorbate to reduce the  $\text{Cu}(\text{II})$  to the active species  $\text{Cu}(\text{I})$ . However, initial reactions using **991** azides and crizotinib alkynes failed to work due to the poor aqueous solubility of **991** analogues. As a result, we switched to using DMF as a solvent, with  $\text{CuI}$  as the catalyst and DIPEA as a base.<sup>76</sup> The short and long azide linkers of **991** were coupled with the crizotinib alkynes giving eight bifunctional compounds in total (Figure 2.68 and Figure 2.67).

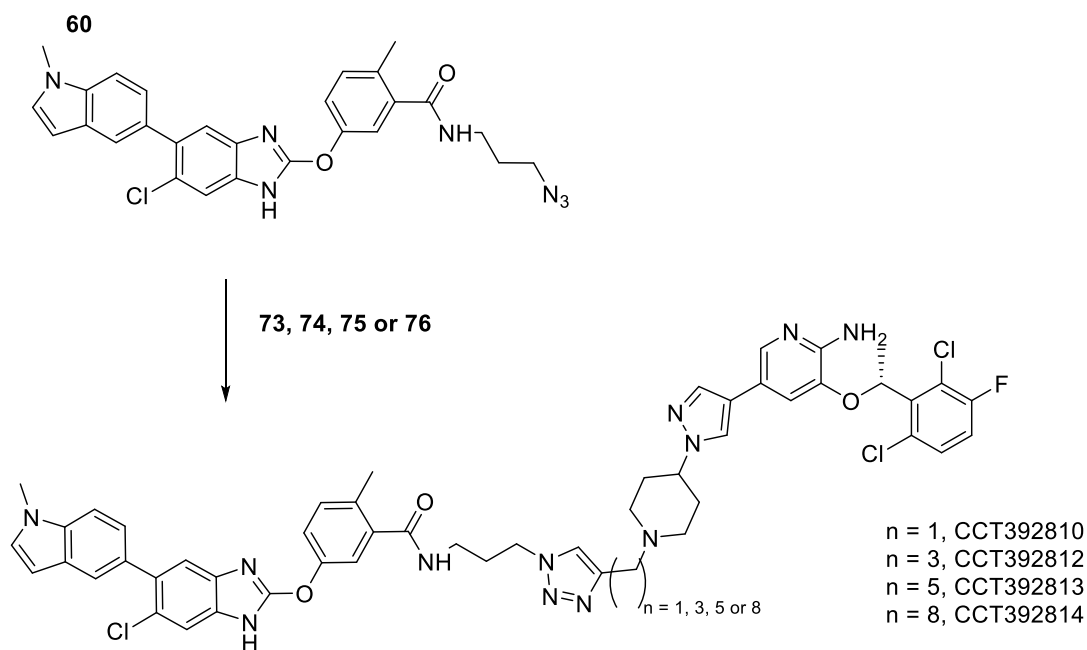


Figure 2.68 - Click conditions for clicking short azide linkers of 991 analogues to crizotinib alkynes.  
 DMF, CuI (0.2 equiv), DIPEA (1.5 equiv), rt, 2h

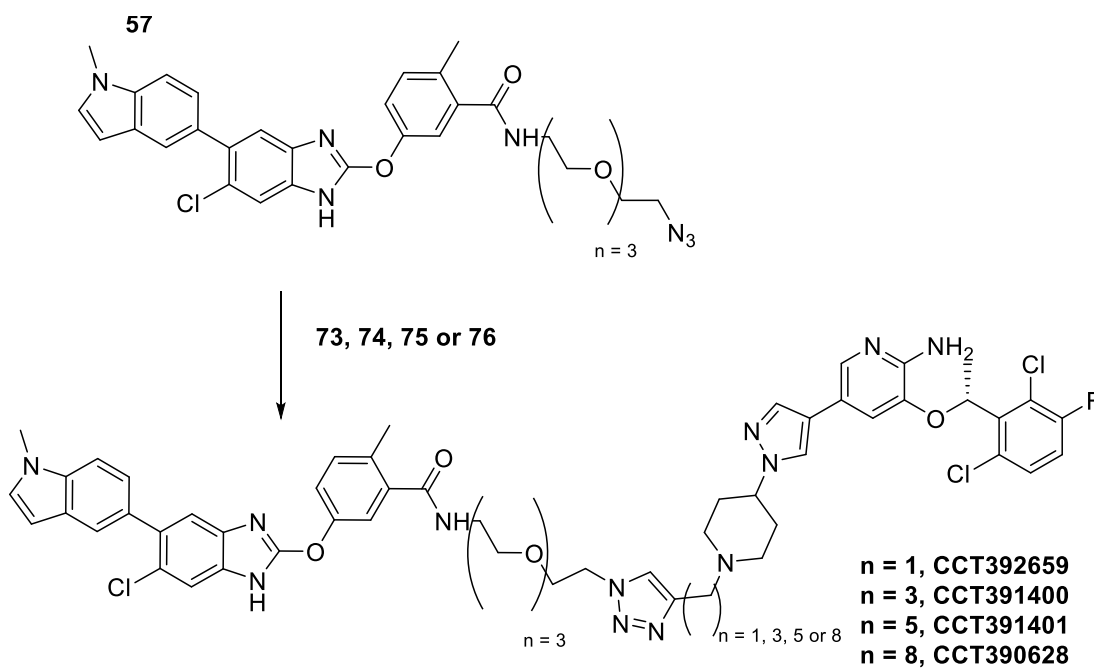


Figure 2.67 - Click conditions for clicking long azide linkers of 991 analogues to crizotinib alkynes.  
 DMF, CuI (0.2 equiv), DIPEA (1.5 equiv), rt, 2h

Through using click chemistry we had been able to synthesise a range of linker lengths. If you count linker length from the methylene next to the amide nitrogen on 991 to the first methylene on the piperidine nitrogen (Figure 2.69) then we had linker lengths from 7 to 22 atoms, which we hypothesised was a good range of bifunctional compounds for finding the optimal linker length.

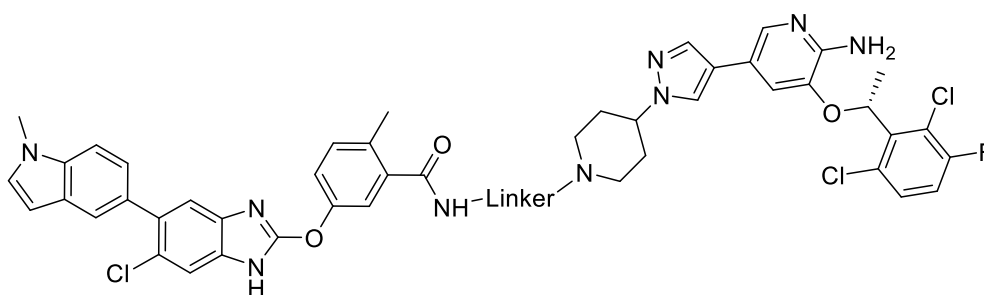


Figure 2.69 - Schematic of a 991 bifunctional compound showing where linker lengths are counted from

Table 2.8 - Table showing the number of atoms in a given linker

AMPK MLKL	60	57
<b>73</b>	7 atoms CCT392810	15 atoms CCT392659
<b>74</b>	9 atoms CCT392812	17 atoms CCT391400
<b>75</b>	11 atoms CCT392813	19 atoms CCT391401
<b>76</b>	14 atoms CCT392814	22 atoms CCT390628

The **577** azides were then coupled with the Crizotinib alkyne containing compounds to give eight bifunctional compounds

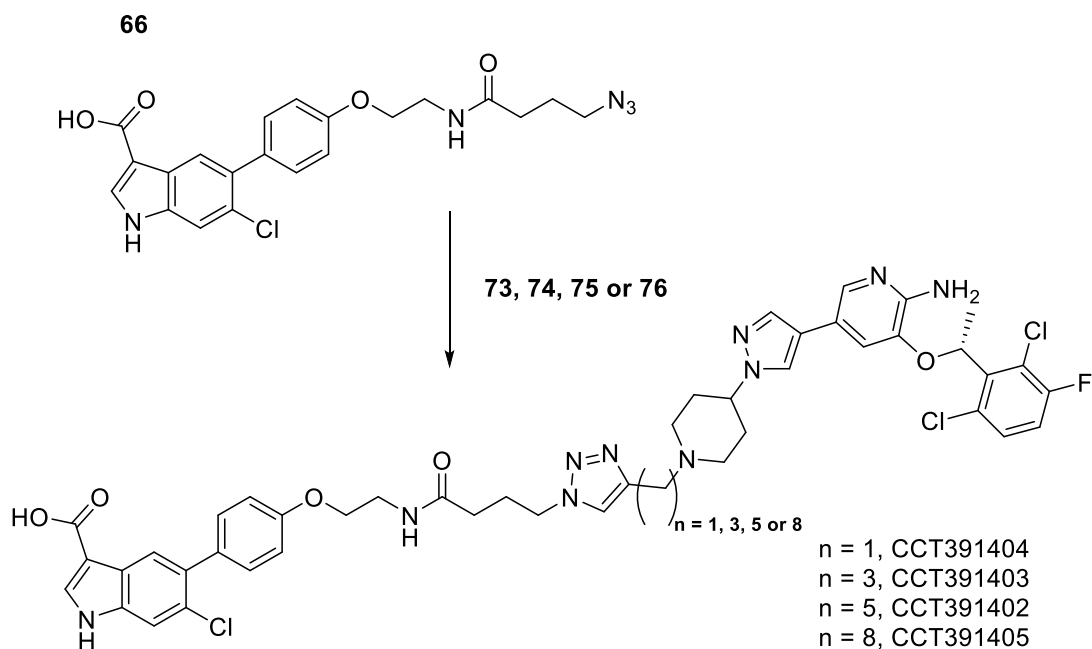


Figure 2.70 - Click conditions for clicking 577 short azide analogues to crizotinib alkynes. DMF, CuI (0.2 equiv), DIPEA (2.5 equiv), rt, 2h

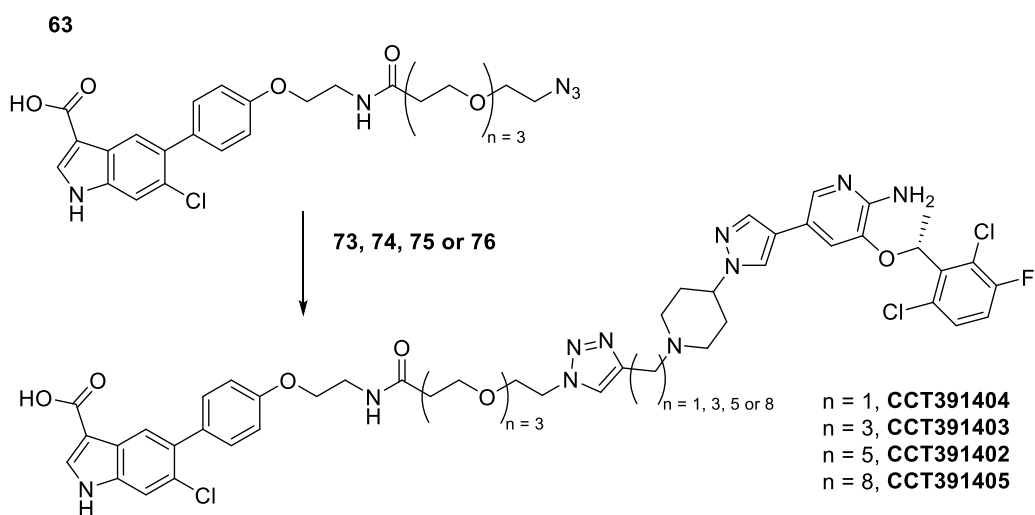


Figure 2.71 - Click conditions for clicking 577 long azide analogues to crizotinib alkynes. DMF, CuI (0.2 equiv), DIPEA (2.5 equiv), rt, 2h

## 2.18 Testing for neo-phosphorylation

### 2.18.1 Measuring ADP produced

We wanted to test these compounds for their ability to induce neo-phosphorylation of MLKL by AMPK. Ideally, we wanted an *in vitro* method that could be used to show if neo-phosphorylation was occurring across multiple compounds and concentrations.

Directing examining phosphorylation of a substrate protein such as MLKL is very challenging. Having utilised an ADP-Glo assay we hypothesised that we could incubate AMPK, MLKL with ATP and a bifunctional compound and that as phosphorylation of MLKL would be ATP dependent, we could measure the resulting ADP produced and use this as an indication as to whether neo-phosphorylation was occurring. Literature had suggested this was a feasible approach, so we kept the assay concentrations of AMPK and ATP the same as in previous ADP Glo assays and used MLKL at 200nM with a 2h incubation based on literature precedent.<sup>37</sup>

We had found commercial MLKL to be of variable quality, and typically expressed in *E. Coli*. In this expression system Ser358 is phosphorylated and therefore unsuitable for our work. As a result, the MLKL we had been using was from the Murphy Lab and was expressed in insect cells as in this expression system Ser358 remains unphosphorylated. To conserve this limited supply of MLKL, we tested only selected compounds and at a range of three bifunctional compound concentrations, as hopefully this would allow us to see an effect at least one concentration. The compounds were selected on linker length, and came from the bifunctional compounds synthesised from 'short azide linkers' as from literature linkers of 11 to 13 atoms had shown to be able to induce phosphorylation of a neo-substrate

In this experiment we ran a DMSO control of AMPK, MLKL and ATP with no compound present to measure the background changes in ADP levels. The highest and lowest levels of these DMSO controls is plotted below as horizontal dotted lines in Figure 2.72

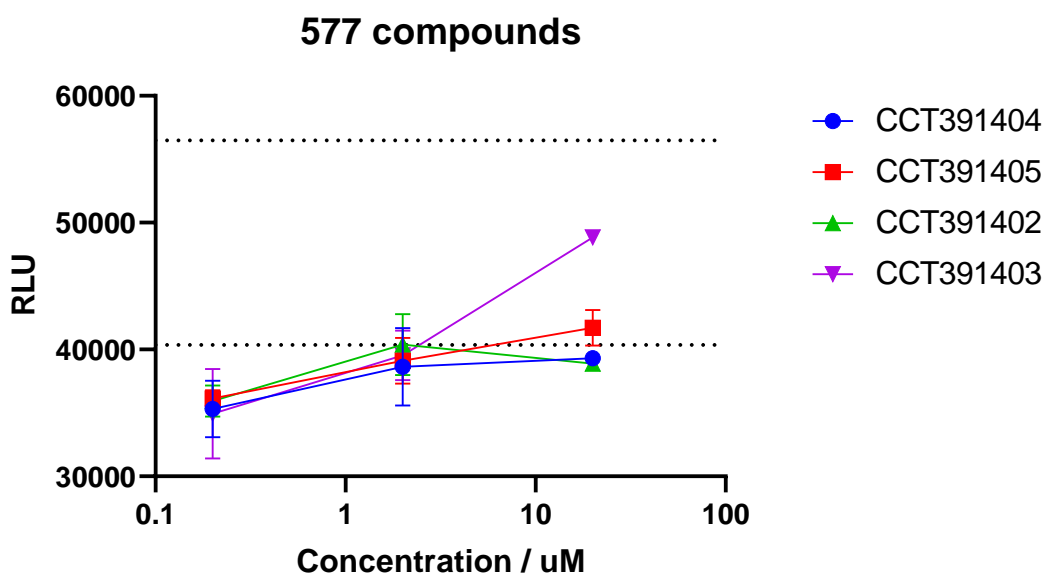
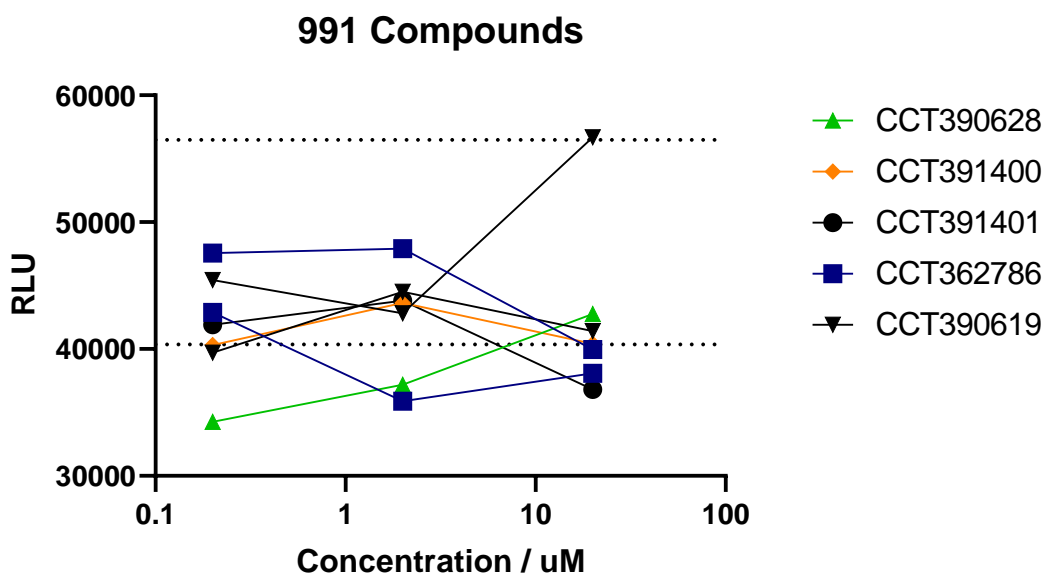


Figure 2.72 - ADP Glo assay results from incubating 991 and 577 bifunctional molecules with AMPK, MLKL and ATP.

The ADP- Glo results show that none of the bifunctional compounds result in an increase in signal outside the controls, suggesting no neo-phosphorylation occurs under these conditions.

A potential reason for this negative result is that there is not enough substrate present to give a large enough increase in ADP compared to the DMSO control. We then performed a titration of the synthetic substrate peptide of AMPK, SAMStide to see what concentration of substrate is needed to show ADP production over the background

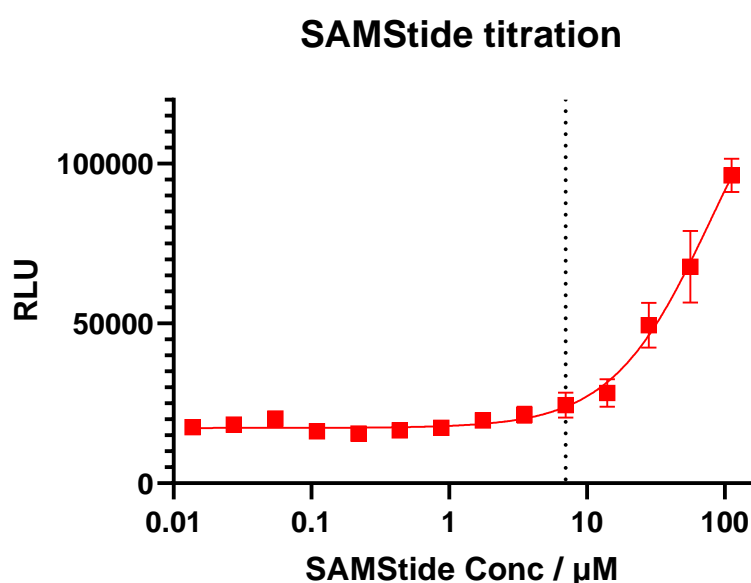


Figure 2.73 - Titration of SAMStide in the presence of AMPK A2B1G1 for 2h.

The experiment showed that  $7\mu\text{M}$  of SAMStide is needed to show a change from the baseline, which is well above the levels of MLKL that had been used, in the previous experiment. Also, SAMStide is an optimised synthetic substrate of AMPK so is likely to be phosphorylated at a much faster rate than a large protein, so would suggest that concentrations of  $>7\mu\text{M}$  of MLKL would be needed to observe a signal. Due to the limited availability of MLKL it meant that testing for phosphorylation of MLKL in this assay format would not be possible. As such, we concluded the ADP-Glo assay was not a suitable method to measure MLKL phosphorylation by AMPK.

### 2.18.2 Cellular testing

From testing the Crizotinib and AMPK activators with dummy linker we were confident that the bifunctional compounds were able to bind AMPK and MLKL

separately but unable to design a suitable biochemical assay we decided to move to testing these compounds in cells and then measure phosphorylation through using phosphospecific antibodies. Thus, removing the issue of the limited supply of MLKL recombinant protein.

We tested all the bifunctional compounds in HEK293T cells for 4h at 5 $\mu$ M. However, Western blots showed no increase when imaged with the phosphospecific antibody for pSer356. This could be because there is no phosphorylation occurring or that phosphorylation is occurring but it's too low to be detected. We also considered that other sites on MLKL for which there is no-phosphospecific antibodies may be neo-phosphorylated.

On the basis that phosphorylation of Ser358 will only drive cell death via necroptosis we tested these compounds in an ATP-Cell titre Glo assay (Figure 2.74). This assay measures ATP present in cells and thus is used to interpret cell death. However, we also felt using a phenotypic assay would also provide insight into if other physiologically relevant sites of MLKL were phosphorylated, or if a ternary complex between MLKL and AMPK was forming, as feasibly both these effects could affect cell viability.

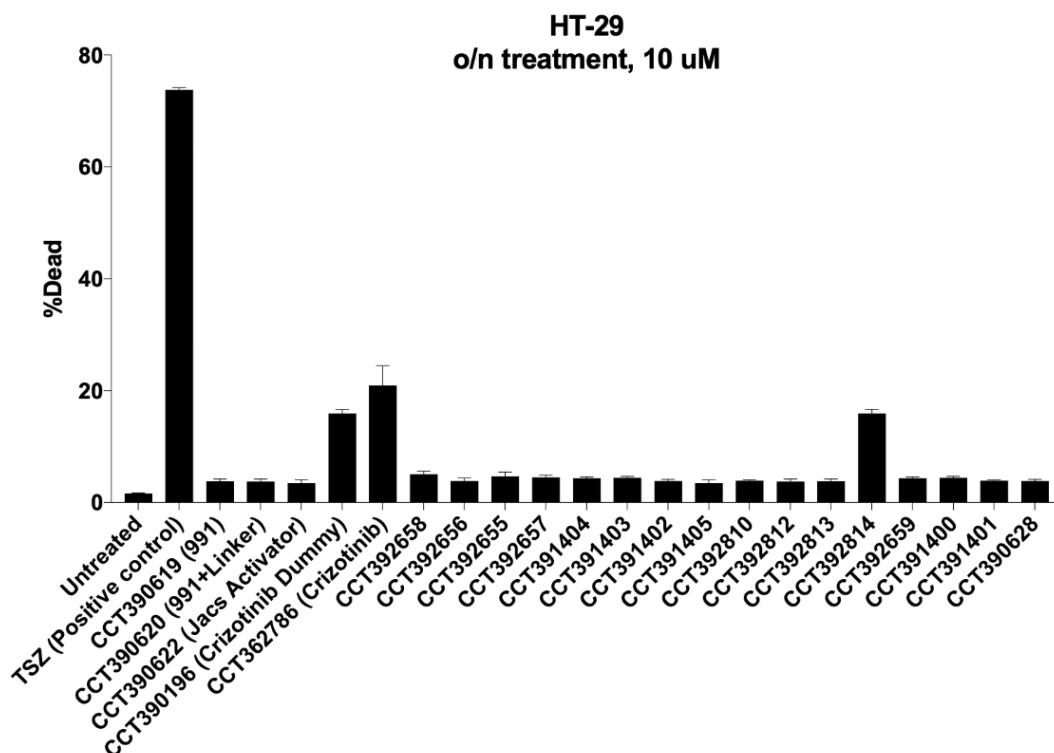


Figure 2.74 - Bifunctional compounds Cell Viability results. Performed by Laura Ramos Garcia.



A 16h treatment showed that none of the AMPK controls showed an increase in cell death. Crizotinib and Crizotinib with a dummy linker showed an increase in cell death, however as Crizotinib hits multiple kinases, there are many possible off-targets at the 10 $\mu$ M concentration used that could cause this effect. Most of the other bifunctional compounds do not replicate this cell death despite containing a Crizotinib substructure. This may suggest that the bifunctional compounds have poorer permeability so insufficient compound concentrations are present to mediate the increase in cell death. Of the bifunctional compounds tested, only CCT392814 showed an increase in cell death like that seen for the Crizotinib compounds. For forming a ternary complex and inducing phosphorylation, we expected there to be an optimum linker length, but also that linkers of similar length would exert a similar effect, which was clearly not seen in Figure 2.74

To confirm if this was a genuine result the AMPK activator (CCT390620), crizotinib with a dummy linker (CCT394628) and the bifunctional compound CCT392814 were retested in the same cell death assay format. However, none of the treatments showed a significant change in cell survival from the DMSO control

As a result, we concluded it was likely that MLKL activity and phosphorylation was not being significantly altered by these bifunctional compounds.

## **2.19 Summary**

A library of bifunctional compounds was synthesised with two different AMPK activator and a Crizotinib warhead, of varying linker length using click chemistry.

Selected compounds were tested in an ADP-Glo assay but did not show an increase in ADP-Glo outside the controls. A SAMStide titration showed that peptide substrates would have to be present at >7 $\mu$ M, which was not possible for investigating MLKL. As such we decided to use phenotypic screens to investigate if the function of MLKL was altered on compound treatment.

## 2.20 Conclusion and future plans

Based on structural information solvent exposed sites on two AMPK activators were identified and investigated through the synthesis of dummy linker containing compounds. An ADP-Glo assay was set up and used to measure activation and EC<sub>50</sub> of novel analogues.

In targeting MLKL a highly selective, low molecular weight hit compound was identified from literature, and from a published crystal structure three solvent exposed sites were identified and dummy linker analogues synthesised. Testing was done through DiscoverX and showed a clear preference for the 5-pyrazine position, however due to reduced binding affinity, poor solubility and stability issues, bifunctional compounds with this warhead were not made. Instead, we decided to functionalise crizotinib to make bifunctional compounds, as this had a similar binding affinity towards MLKL and would allow us to target other proteins. We also developed a LanthaScreen assay for MLKL to allow in-house testing of compounds, which showed good correlation with testing by DiscoverX.

A library of bifunctional compounds has been made using click chemistry and a select number were tested with MLKL, AMPK and ATP in an ADP-Glo assay, however we saw no increased turnover of ATP. Treatment of HEK293 cells with bifunctional compounds showed no pSer358 MLKL, and a cell viability assay showed no sustained increase in cell death. As a result, we decided to stop work on targeting and phosphorylating MLKL.

Additionally, reasons from switching away from targeting MLKL are that although Crizotinib had been reported to bind MLKL with K<sub>d</sub> = 217nM, retesting at DiscoverX and testing newly developed LanthaScreen suggested binding affinity may be >1μM. Although it was and is, still not clear what binding affinity is required for driving ternary complex formation and subsequent neo-phosphorylation, we had been aiming for <500nM and felt the weak affinity may limit MLKL phosphorylation. Additionally, it was possible that MLKL will not form a cooperative ternary complex with AMPK, and it may take the remaining time of the project to realise this conclusion. Although assays for examining ternary complex formation could have

been developed there was potential that lots of effort would be put into finding the MLL+KL and AMPK do not form a cooperative ternary complex.

With a small library of bifunctional compounds based around a Crizotinib warhead in hand we focussed on how we could use our library to identify neo-substrates of AMPK and build our understanding of the scope of this approach. This work is described in Chapter 3.

## Chapter 3 Utilising Phosphoproteomics for identifying neo-substrates

---

PROTACs have demonstrated that certain proteins are more amenable to degradation than others, and we suspected this would also be true for inducing neo-phosphorylation; with certain proteins being more readily recruited to AMPK and phosphorylated. However, it is not yet possible to predict what determines successful recruitment and post translational modification with bifunctional molecules. This must be determined empirically with experimental methods.

A recent publication showed that AMPK could be redirected to neo-substrates and induce phosphorylation of BRD-4 and BTK with selective ligands or the substrate protein.<sup>37</sup>

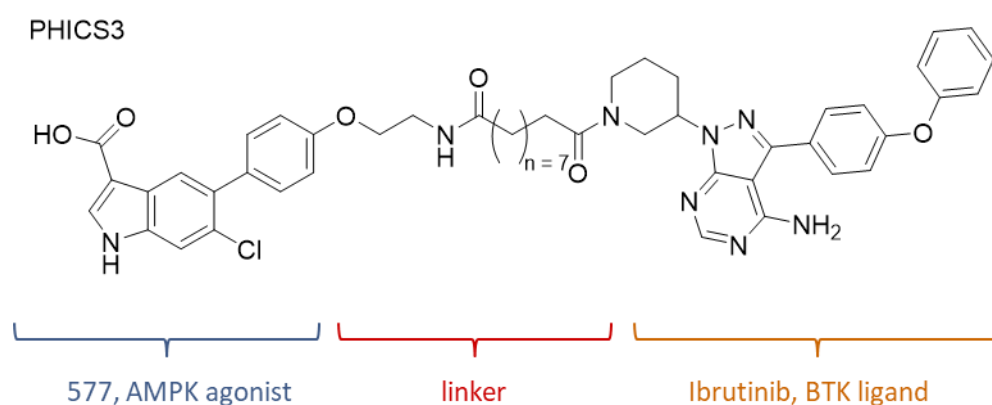


Figure 3.1 - Reported PHICS

Whilst the concept had been shown to work, we wanted to investigate how broadly applicable PHICS and neo-phosphorylation would be towards substrate proteins, and if selectivity towards certain sequences or structural features of proteins could be elucidated.

When synthesising bifunctional molecules to target MLKL we made molecules with the pan-selective Type-I kinase inhibitor, Crizotinib, as a warhead. A promiscuous warhead was intentionally used as it meant we could look for neo-phosphorylation of other kinase targets of Crizotinib and avoid the long process of identifying a suitable ligand, attaching dummy linkers, measuring affinity and then synthesising new bifunctional molecules. In PROTAC literature, a ligand with a  $K_d \leq 500$  nM is generally considered a sufficient binding affinity to form a ternary complex and achieve degradation.<sup>28</sup> Crizotinib binds 67 kinases with a  $K_d \leq 500$  nM giving a large range of kinase targets binding within the target potency range.<sup>77</sup> Additionally using a Type I inhibitor we would bind targets in an active conformation which we predicted would increase the susceptibility of proteins to neo-phosphorylation.

We selected kinases as a substrate protein due to the importance of phosphorylation on kinase function, and hypothesised the likelihood of identifying a physiologically relevant phosphosite was increased by investigating kinases instead of a different protein family such as bromodomains or GPCRs.

The availability of pan-selective kinase inhibitors meant we could use a ligand with a very high number of protein targets. Thus, giving us the broadest possible substrate scope in which to identify neo-phosphorylation.

We were inspired by the Crew and Fisher groups who used non-selective kinase warheads, attached them to E3 ligands to make non-selective PROTAC molecules and used proteomics to map protein degradation.<sup>65, 33</sup> The results showed that high warhead binding affinity does not equate to high degradation as the ternary complexes are not always cooperative. This again suggests that making bifunctional molecules and measuring the effects on each protein individually would have been a time consuming and potentially fruitless method.

They showed that micromolar ligands were able to give degradation, and as Crizotinib binds 173 kinases with a  $K_d < 10 \mu\text{M}$ , this increases the potential number of targets to interrogate.

We felt that global unbiased phosphoproteomics with our bifunctional molecules could be used to achieve the same effect to measure neo-phosphorylation. We hypothesise that the Crizotinib warhead from the bifunctional molecule would be able to engage many kinases, of which some could then form stable ternary complex with AMPK. Then in a ternary complex, a smaller number of proteins would then be able to adopt a suitable orientation for phosphoryl transfer giving selective phosphorylation which could then be identified and quantified via phosphoproteomics.

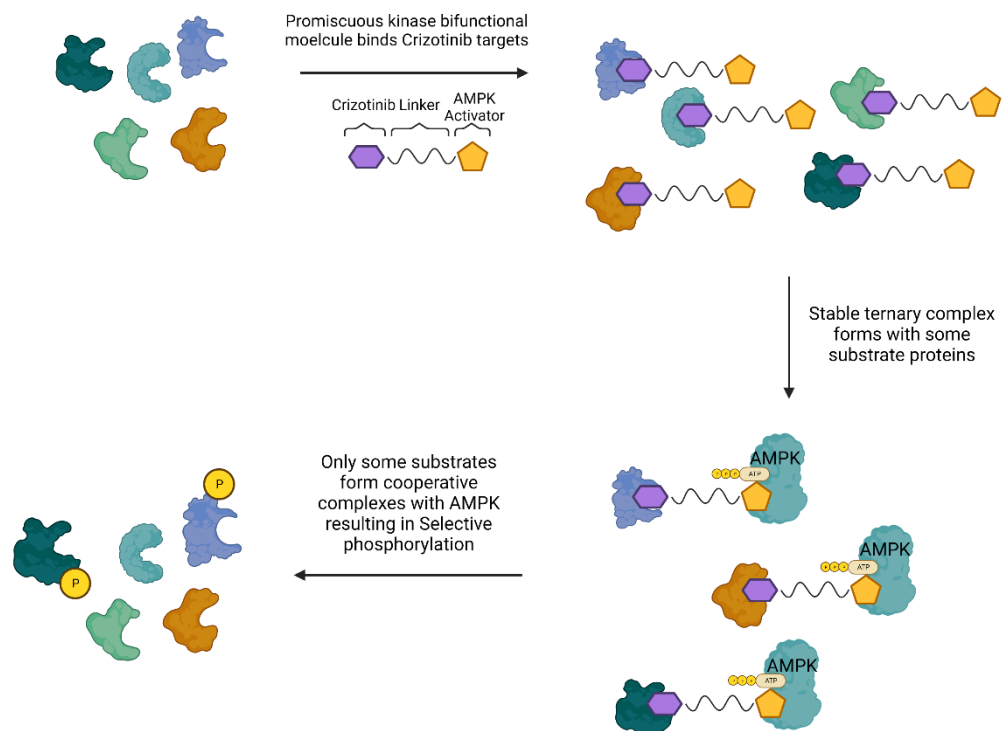


Figure 3.2 - Schematic showing how phosphoproteomics can be used to find substrate proteins

When tested in a kinome wide panel of 442 kinases, Crizotinib binds 67 kinases with a  $K_d \leq 500 \text{ nM}$  and 173 kinases with a  $K_d < 10 \mu\text{M}$ , which represented a large number of targets that may have altered phosphorylation.<sup>77</sup>

However, not all proteins can be detected in phosphoproteomics; either because the peptides don't give a good mass response or that the protein has too low an

expression. 51 of the 173 kinases that Crizotinib binds to are actually detected in phosphoproteomic datasets, Table 3.1, which still gave a substantial number of targets to detect changes of phosphorylation.

*Table 3.1 - Known substrates of crizotinib that are detected in phosphoproteomic datasets*

SRC (560 nM)	ROCK1 (3 700 nM)	EPHB4 (570 nM)	TAOK1 (1 200 nM)	ABL (78 nM)	ULK1 (6 700 nM)
EPHA1 (140 nM)	FYN (1 300 nM)	NEK9 (790 nM)	CAMKK2 (1 500 nM)	MAP3K1 (1 100 nM)	LOK/STK10 (44 nM)
EPHA2 (100 nM)	SRPK1 (1 800 nM)	MAP4K5 (79 nM)	DCLK1 (330 nM)	ABL2 (460nM)	MINK (4,400 nM)
CDK7 (330 nM)	SIK2 (200 nM)	RIPK1 (1 600 nM)	TAOK2 (900 nM)	NEK7 (5 700nM)	M3K2 (72 nM)
AAK1 (2 300 nM)	PIP5K1A (3 200 nM)	SLK (18 nM)	TBK1 (690 nM)	MAP3K3 (110 nM)	PRKR (1,100 nM)
RIOK1 (6 100 nM)	MET (2.1 nM)	LYN (940 nM)	FER (270 nM)	RIPK4 (2 100 nM)	BIKE (740 nM)
YES (770 nM)	ROCK2 (3 300 nM)	RIPK2 (900 nM)	TYK2 (210 + 2 000 nM)	DYRK2 (4 000 nM)	CDC2L1 (760 nM)
SNARK (120 nM)	DAPK1 (74%)	ERK5 (510 nM)	IKKB (5,500 nM)	DCAMKL2 (370 nM)	FGFR3 (2,700 nM)
BMPR2 (61%)	MST2 (990 nM)	MST1 (580 nM)	-	-	-

In phospho-proteomics each compound treatment must be run in triplicate, and 16plex TMT were available at the time meaning four compounds could be tested, with a DMSO control.

The bifunctional molecules are unlikely to bind the kinase and target protein in the exact same instant, with a ternary complex more likely to be formed by one binding moiety binding to one protein forming a binary complex, and then binding and recruiting the other protein to form the ternary complex. As such, a mixture of ternary and binary complexes will exist. Formation of a binary complex with AMPK may lead to increased AMPK activation and increased phosphorylation of AMPK substrates, and formation of a binary complex with a target protein may increase or decrease phosphorylation.

Therefore, the contributions of the bivalent complexes must be controlled for in this experiment. One approach would have been to test an AMPK activator and Crizotinib separately to account for how a bifunctional molecule may change phosphorylation in a binary complex, but this would have meant that only two bifunctional compounds could be tested per phosphoproteomic run.

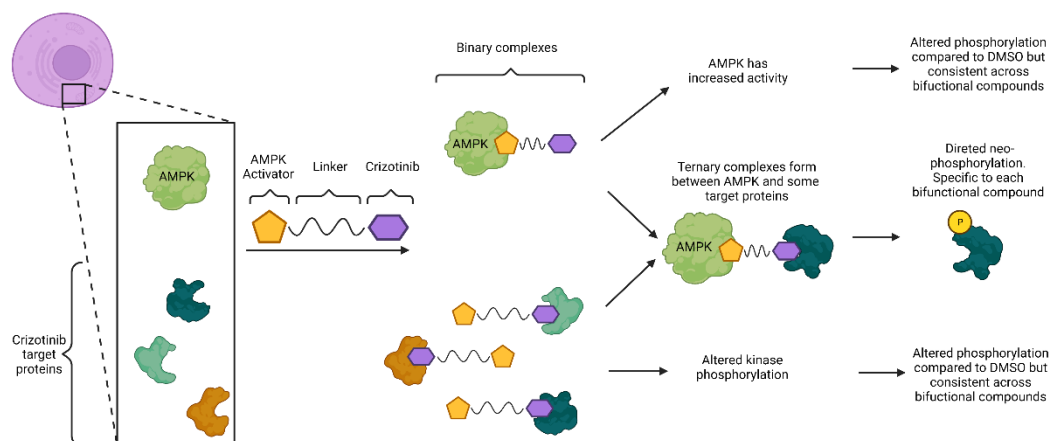


Figure 3.3 - Schematic showing how bifunctional molecules may form binary complexes and alter phosphorylation

This being a proof-of-concept idea, we wanted to test as many bifunctional compounds as possible to increase the chances of seeing neo-phosphorylation.



In order to maximise coverage whilst controlling for binary complex effects, we tested four bifunctional compounds keeping the same exit vectors and maintaining similar linker identities. In this approach any effects of AMPK activation or Crizotinib binding would occur similarly between all compound treatments and any phosphopeptides showing increased abundance across all four compound treatments could be discarded in the analysis. If any changes of phosphosite abundance were observed in three sets or fewer, we predicted this would be due to changes in linker length and identity, and could be further profiled in conditions where crizotinib and an AMPK activator were present as single ligand controls

We selected four bifunctional compounds that were based on the **577** AMPK activator instead of the 991 AMPK activator.<sup>37</sup> Although **577** is selective for  $\beta 2$  isoforms of AMPK and so has the potential to recruit fewer isoforms of AMPK than **991**, bifunctional molecules containing the **577** AMPK warhead had been shown to work biochemically and in cells.<sup>37</sup>

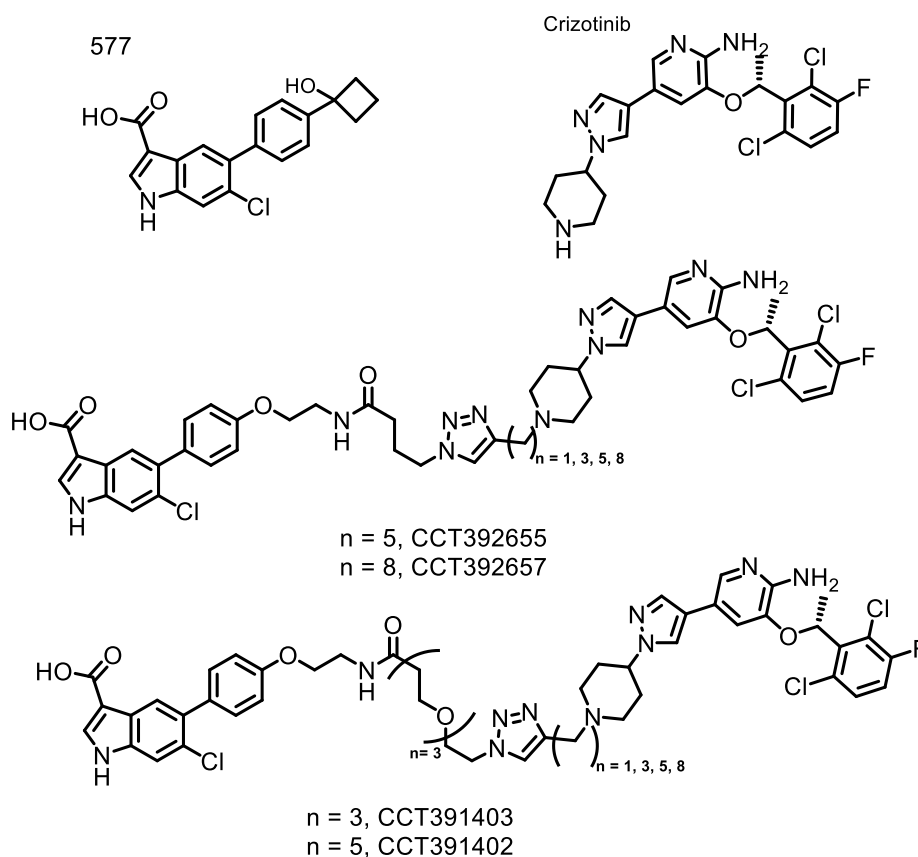


Figure 3.4 - Structures of bifunctional compounds tested in phosphoproteomics and single ligand molecules

We used HEK293 cells as these are commonly used and easy to propagate and treated cells with compounds at 5µM for 4h. This concentration was chosen as Crizotinib inhibits AMPK-α1 with a  $K_d = 2.4 \mu\text{M}$  and AMPK-α2 with a  $K_d = >10 \mu\text{M}$ , so anticipate little or no inhibitory effect of these bifunctional compounds in cells at 5µM.<sup>77</sup>

Also, knowing that solubility was less than 10 µM didn't want the compounds to precipitate and when treating the cells, I saw no compound crashing out. A relatively short time point of 4h was chosen as we wanted to capture the results of neo-phosphorylation directly resulting from AMPK interacting with a neo-substrate, rather than secondary or tertiary effects. The compounds were treated, pelleted then frozen and sent to the Proteomic Core facility at the ICR for analysis.

The phosphoproteomics gave good coverage with >23,000 phosphosites being identified from 5,353 different proteins. Results are shown in Figure 3.5, with the volcano plots showing significance vs abundance compared to the DMSO control. For cut-offs, any proteins that showed upregulation across the DMSO control and all bifunctional compound treatments were discarded, as this was likely a result of DMSO treatment. Additionally, where all four compounds showed increase in abundance for a phosphopeptide it was discarded, as this was likely due to the bifunctional molecule acting as a single ligand and altering the phosphorylation of a protein, as described above. The p value and fold change values cut off values were fairly stringent compared to literature, with significance cut offs of p value <0.01 (horizontal dotted line in, Figure 3.5). For changes in abundance, the ratio between compound treatment and DMSO was found:  $\log_2 \left( \frac{\text{abundance from compound treatment}}{\text{average of DMSO abundance}} \right)$ . Values which are greater than a 80% change away from the DMSO, i.e., more than 180%, are commonly accepted as a large enough change to be true (vertical lines in Figure 3.5 and Figure 3.7).<sup>33, 78</sup>

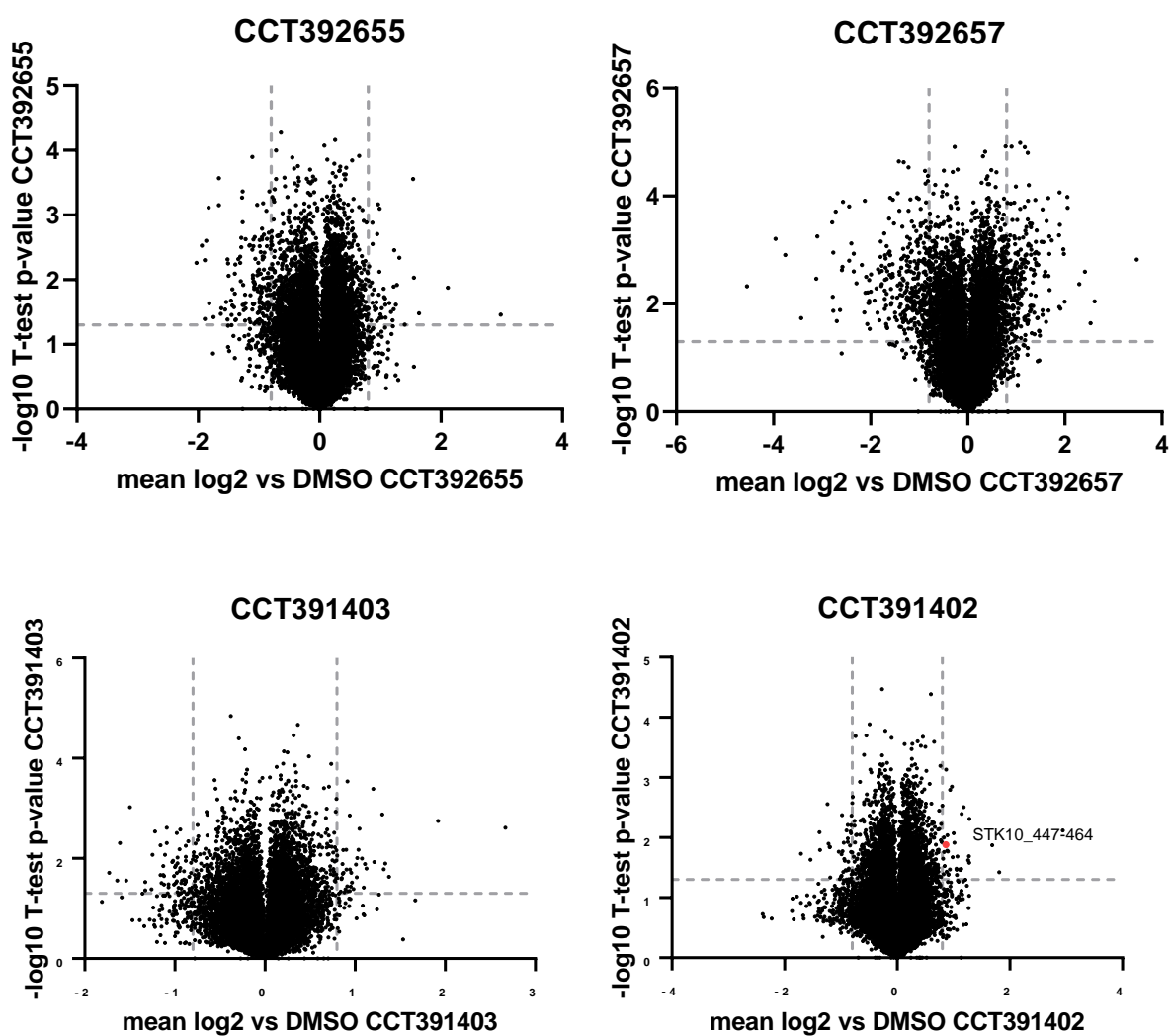


Figure 3.5 – Phosphoproteomic volcano plots.  $\log_2$ (Fold change of abundance with compound/DMSO control).

Applying these cut-offs resulted in eight phosphosites of increased abundance with compound treatment, which is a hit rate of 0.035% of all phosphopeptides identified and a hit rate of 0.02% compared to the 5,353 proteins identified.

Table 3.2 -  $\log_2(\text{ratio of abundance of compound treatment/DMSO})$ . Orange values show an increase of 80% (>0.85). Blue values show 50% increase (>0.58)

	Log <sub>2</sub> (abundance/DMSO)			
	CCT391402	CCT391403	CCT392655	CCT392657
TPR	0.42	0.16	1.32	-0.23
LARP4B	0.31	0.51	1.06	0.021
IVNS1ABP	0.69	0.94	0.79	0.38
KIAA1522	0.36	0.47	0.81	0.36
SPICE1	0.45	0.10	0.87	1.35
CUL4B	0.33	0.28	0.24	0.88
STK10	0.86	0.43	0.30	-0.0031
RGCC	1.28	0.71	0.35	0.24

The only known target of Crizotinib that passed the cut-offs was Serine/Threonine Kinase 10, STK10. The increased abundance of the other phosphopeptides could be false positives or secondary effects from compound treatment. It is also possible the other proteins in do bind Crizotinib but as they are not kinases there are no reports of their affinity for Crizotinib. Although peptide sequences of other targets of crizotinib were found, they showed no increase in phosphorylation with any of the bifunctional compounds. We can't discount that novel phosphorylation did occur on other proteins and we couldn't detect it,

As a known target of Crizotinib, STK10 had the highest likelihood of being a genuine hit. The difference in neo-phosphorylation between compounds of different linker lengths, gave us confidence that STK10 was neo-phosphorylated by forming a ternary complex with AMPK, rather than an effect from binding AMPK or STK10 as a binary complex (Figure 3.7 and Figure 3.6).

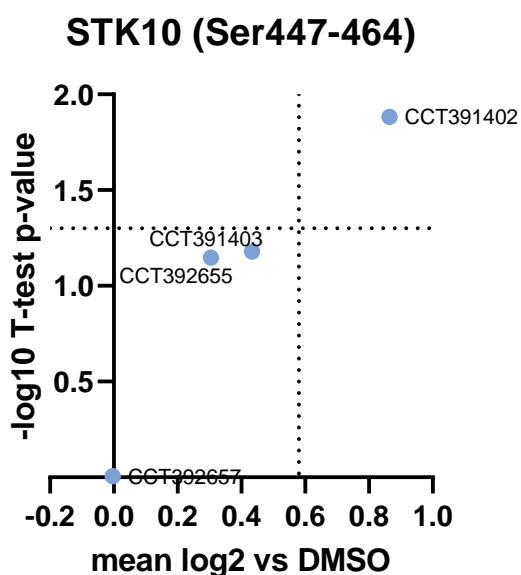


Figure 3.7 - Volcano plot showing the abundance and significance of the phosphopeptide 447-464 of STK10

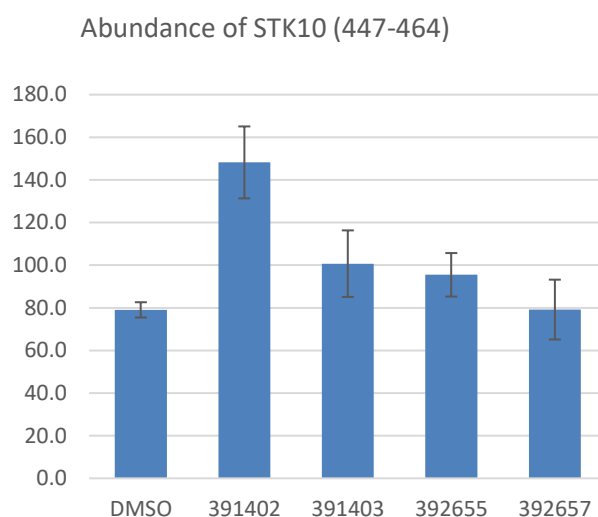


Figure 3.6 - Graph showing the abundance of phosphopeptide 447-464 of STK10 on compound treatments.

Based on the high level of change in phosphorylation, the statistical significance and the high affinity of Crizotinib for STK10 we wanted to confirm this result and use orthogonal techniques to show neo-phosphorylation was robustly observed and the result of a ternary complex.

### 3.1 Serine/Threonine Kinase 10 (STK10) Introduction

STK10 is a 968 amino acid, 112kDa kinase with an N terminal kinase domain and a C-terminal domain. It associates and phosphorylates PLK1 which has a key role in cell cycle regulation and STK10 inactive mutants show altered cell cycles.<sup>79</sup> STK10 knockdown reduced growth through inducing apoptosis in Ewing's sarcoma and can limit cell proliferation through loss of activation of p38 MAPK, so has been proposed as an oncology target.<sup>80, 81</sup> STK10 is able to auto-phosphorylate, whereby

a protein phosphorylates itself, and trans-phosphorylate, where the proteins dimerise and phosphorylate each other.<sup>4</sup> To date there are no reported selective inhibitors of STK10 (defined as having 10-fold selectivity for STK10 over another protein), with STK10 predominantly being identified as an off-target. From analysis of non-selective kinase inhibitors against panels of kinases, STK10 typically has a high selectivity score, indicating poor selectivity.<sup>77, 82, 83</sup> It has been proposed this is due to a very flexible binding site with molecules mainly interacting through hydrophobic interactions.<sup>83</sup>

The first question to address is whether this was a believable result. As shown in Figure 3.8, crizotinib is reported to bind STK10 with a  $K_d = 44$  nM and so has a low binding affinity that would suggest it be recruited to form ternary complexes.<sup>77</sup> Docking experiments of Crizotinib into a crystal structure of STK10, suggested the 2-amino pyrimidine group on Crizotinib binds to the hinge, and that the piperidine is solvent exposed (Figure 3.8). This is consistent with docking of Crizotinib in MLKL, and overall suggested that it is likely that these bifunctional compounds can bind STK10.<sup>84</sup>

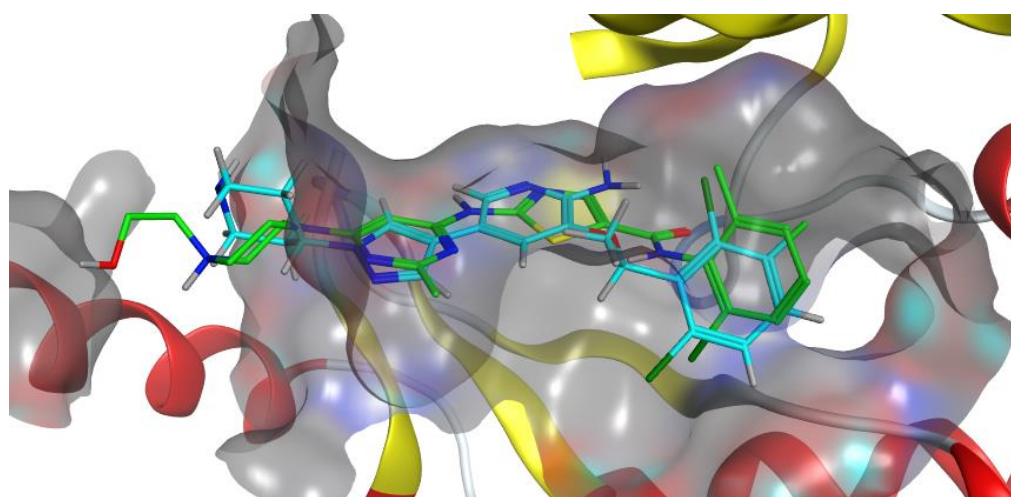


Figure 3.8 - Crizotinib docked into human STK10. Original file shows STK10 bound to dasatinib (PDB: 5OWR)

The next question is whether the actual sequence and site of increased STK10 phosphorylation was logical. As previously mentioned, AMPK naturally prefers to phosphorylate serine's in the consensus motif of RXXS.<sup>6</sup> The STK10 peptide sequence of increased abundance is ASQSRPNSSALETLGGEK which does contain multiple serine's and a threonine residue, but also contains an RXXS motif with Ser454 coming 2 amino acids after an Arginine. Knowing the propensity of AMPK for the RXXS motif and having a neo-substrate containing that sequence added confidence that the results from phosphoproteomics were genuine.

For the site of phosphorylation, we anticipated the optimal site would be solvent exposed and flexible, as this could then adopt a suitable conformation to interact with AMPK. Although there are no crystal structures that show structural information about the location of the sequence, we used AlphaFold and saw that the residue is on a long flexible loop in reasonable proximity to the active site, suggesting that it could be suitably orientated for phosphorylation.

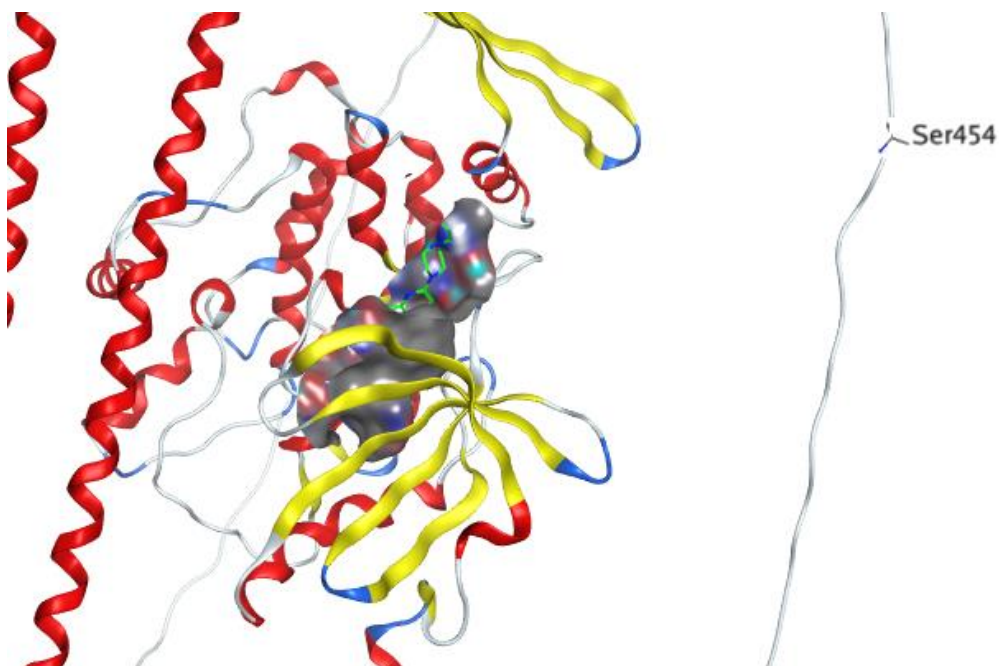


Figure 3.9 - AlphaFold predicted structure showing orientation between binding site and Ser454

### 3.2 Phosphoproteomics repeat with controls

Global phosphoproteomics is a useful technique for mapping the phosphorylation of proteins in a cell but due to the high numbers of sites identified in a single run it is possible to achieve false positives and we wanted to confirm STK10 phosphorylation.

In order to confirm STK10 phosphorylation and build confidence in the result, we repeated the phosphoproteomics of CCT391402 incorporating single ligand controls. To this end we used CCT390196 and CCT390622, as single ligand controls for Crizotinib and 577, which would confirm that STK10 phosphorylation was a result of an AMPK-STK10 ternary complex and not one binding moiety altering a proteins phosphorylation.

In addition to testing CCT391402 at the original concentration of 5 $\mu$ M, we also tested at a 5-fold lower concentration of 1 $\mu$ M to see if there was a dose-dependent effect on STK10 phosphorylation. Due to the hook effect from forming a ternary complex, bifunctional compounds can have decreased activity at higher concentrations, so we wanted to see if we saw higher levels of STK10 phosphorylation at lower concentrations. By testing at a five-fold difference in concentration, we considered it a significant enough change to see genuine changes in phosphorylation.

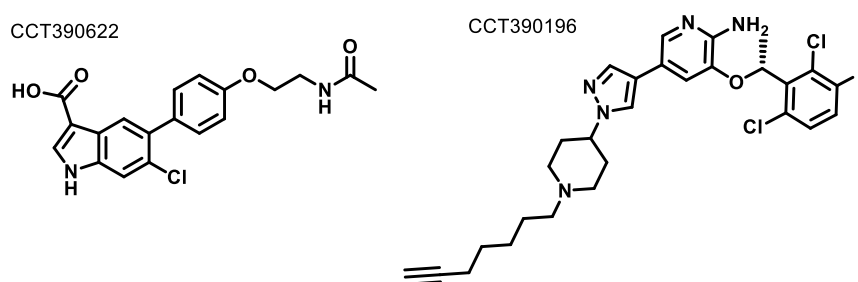


Figure 3.10 - structures of single ligand control for phosphoproteomics

Having identified four sets of conditions, we treated HEK293 cells with 5 $\mu$ M of compound for 4h, then pelleted and sent for analysis at the Proteomics Core



facility. In this run the coverage was much less than the initial phosphoproteomics run with only  $\approx 13,000$  phosphosites observed from 4,785 proteins. This lower number of identified phosphosites was due to technical issues of the enrichment beads. However, the STK10 447-464 sequence was detected with medium confidence with results shown in Figure 3.11.

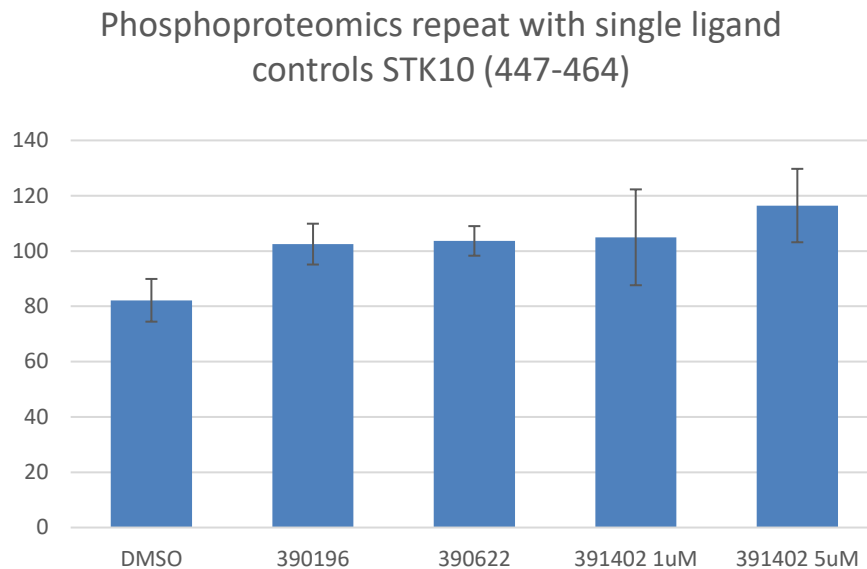


Figure 3.11 - Graph showing the abundance of the STK10 phospho-peptide 447-464. Single ligands are tested at 5 $\mu$ M.

The repeat shows that the CCT391402 5 $\mu$ M treatment has a statistically significant increased abundance of the STK10 447-464 phosphopeptide in comparison to the DMSO control, which is what was observed in the first run. However, neither of the CCT391402 treatments showed a statistically significant increase over the single ligand controls.

Because of the high  $\log_2(\text{FoldChange})$  and high statistical significance observed in the first phosphoproteomic run for the STK10 447-464 sequence, and the issues in this run with the peptide enrichment resin, we wanted to conduct a further repeat of the experiment to confirm the significant changes we had observed and thoroughly investigate the changes compared to single ligand controls.

We repeated this experiment with the same cell lysates but with a new phospho-enrichment resin. However, with this new resin we did not detect any peptides of

STK10. One issue can be is that in unbiased phosphoproteomics, the MS/MS equipment detects the highest intensity mass signals and may miss lower intensity signals, and STK10 may be a low abundance protein that is not being detected. As we knew the exact peptide sequence of interest, we then ran a targeted method where the machine only detects a specific mass, and so even if it's low intensity it's more likely to be detected. However, this also failed to detect the target STK10 peptide.

At this point the cell lysates were now unusable after multiple freeze thaw cycles. Performing proteomics is a labour-intensive technique requiring cells to be cultured, treated with compounds, then pelleted frozen and sent to the Proteomics facility. From here sample preparation is also labour intensive and the time taken from growing the cells to having the data analysed was approximately two months, with no guarantee that a clear result will be achieved. As such we decided not to repeat phosphoproteomics and following advice from the Proteomics Core team, focus on orthogonal approaches to show the target engagement and neo-phosphorylation of STK10.

### **3.3 NanoBRET**

As bifunctional molecules contain two ligands linked together, they generally have a high molecular weight and a high number of Hydrogen Bond donors and acceptors which leads to poor physicochemical properties such as low permeability. To build confidence in our finding from phosphoproteomics, we wanted to confirm that our bifunctional molecules could engage STK10 in cells.

The results of STK10 phosphorylation in phosphoproteomics suggested some SAR around linker length with only CCT391402 showing a significant increase (Figure 3.6 and Figure 3.7). One reason could be that CCT391402 has an optimal linker length and so is the only compound that can form a productive ternary complex with STK10 and AMPK. However, it could also be that the other bifunctional compounds are less permeable so have a lower concentration inside the cell, and this low permeability rather than linker length is responsible for lower phosphorylation.

To test this hypothesis, we were fortunately able to have our compounds tested by Stefan Knapp and Benedict-Tilman Berger, at the Goethe University Frankfurt, in a NanoBRET STK10 assay in HEK293 cells.<sup>85</sup> NanoBRET assays measure the displacement of a fluorescent tracer from STK10 that is fused to a Nanoluciferase. Displacement stops the transfer of energy from luciferase tag to tracer, and if used to quantify the displacement of the tracer.<sup>86</sup>

We tested single ligand controls to confirm Crizotinib with and without a linker could engage STK10 in cells and tested AMPK activators to ensure that this part of the bifunctional molecule was not binding to STK10 at the tested concentration.

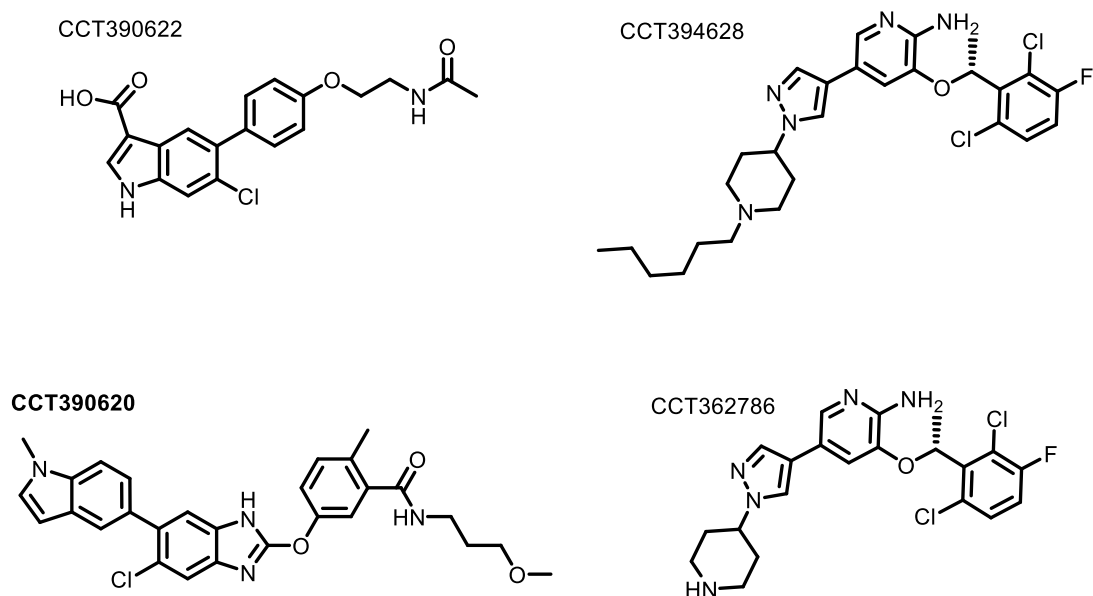


Figure 3.12 - Single ligands tested in NanoBRET assay against STK10

We also sent six bifunctional compounds from the 577 series including the compounds tested in phosphoproteomics, Figure 3.13.

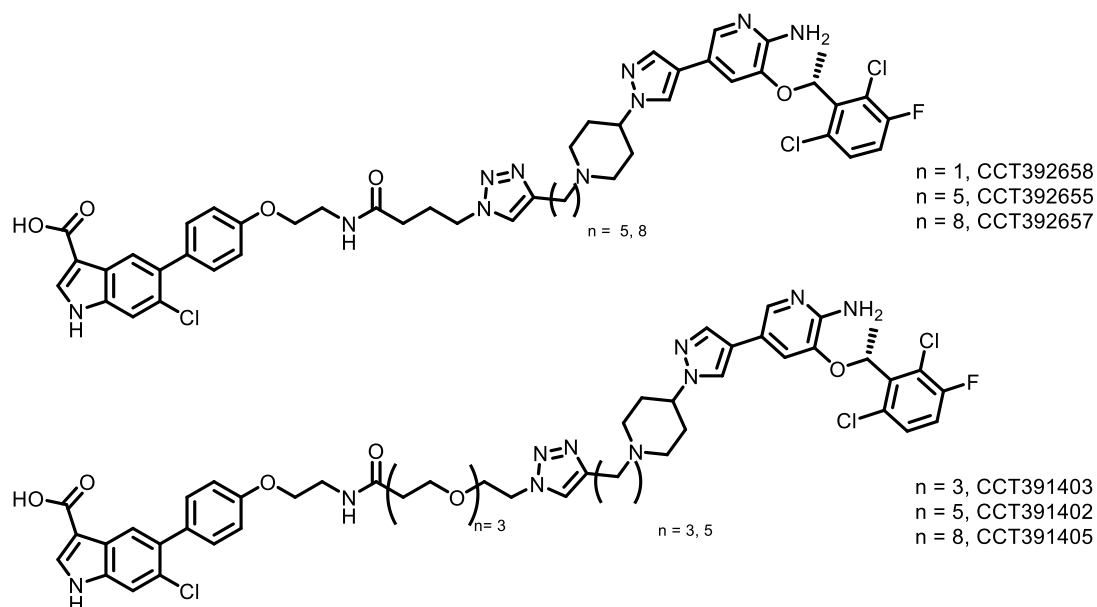


Figure 3.13 – Structures of the 577 bifunctional compounds tested in NanoBRET assay against STK10

Although we hadn't tested any of the 991 series of bifunctional compounds in proteomics, we wanted to confirm if they could engage STK10 in cells as we aimed to use these compounds in follow up experiments, to determine the SAR around neo-phosphorylation. Structures of the compounds tested are shown below in Figure 3.14.

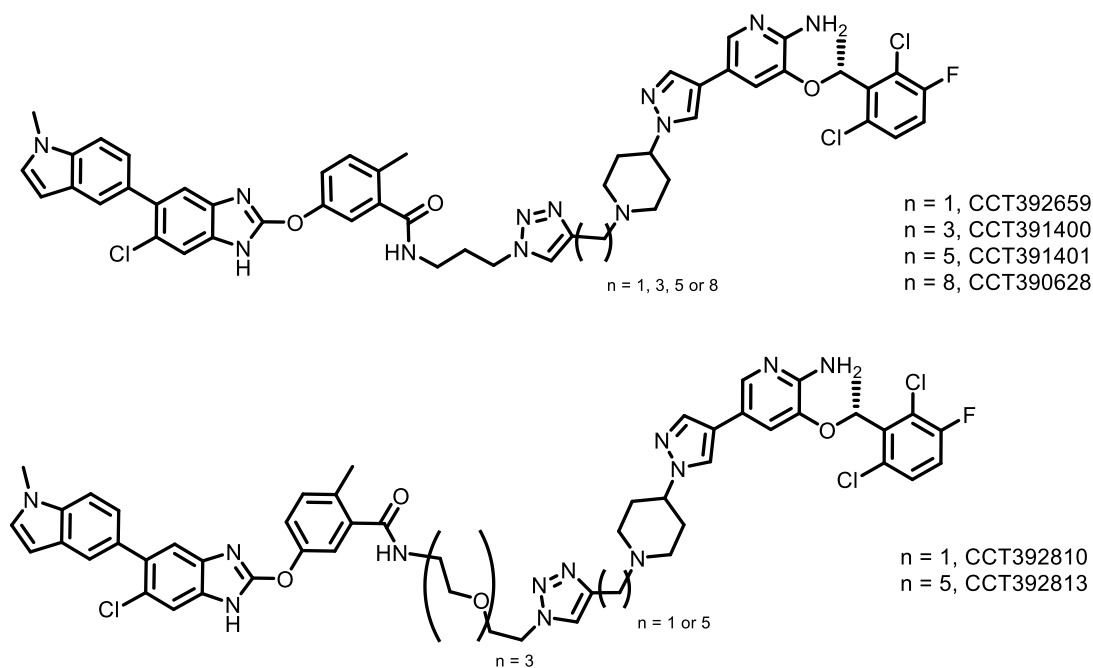


Figure 3.14 -- Structures of the 991 bifunctional compounds tested in NanoBRET assay against STK10

The results from the NanoBRET are shown below in Table 3.3.

Table 3.3 - NanoBRET results for STK10 engagement. Compounds tested in phosphoproteomics are in bold and underlined

Compound	EC <sub>50</sub> / $\mu$ M
CCT390622	No binding
CCT390620	16.6
CCT394628	0.324
Crizotinib/ CCT362786	0.160
CCT392658	4.03
<u>CCT392655</u>	<b><u>6.05</u></b>
<u>CCT392657</u>	<b><u>10.00</u></b>
<u>CCT391403</u>	<b><u>3.45</u></b>
<u>CCT391402</u>	<b><u>3.61</u></b>
CCT391405	18.90
CCT392810	7.98
CCT392813	9.38
CCT392659	8.91
CCT391400	7.14
CCT391401	12.30
CCT390628	17.80

All bifunctional compounds show lower EC<sub>50</sub> values than Crizotinib/CCT362786, and crizotinib with a dummy linker, CCT394628, which is likely due to poorer permeability from bifunctional molecules having a much higher molecular weight

and increased number of hydrogen bond donors and acceptors. Many pan-selective kinase inhibitors exhibit a 100-1000 fold drop off in NanoBRET vs biochemical testing against STK10.<sup>83</sup> With a biochemical  $IC_{50} = 44\text{nM}$  of Crizotinib against STK10, a four-fold drop off into cellular potency to  $EC_{50} = 160\text{nM}$  is good translation to cellular efficacy and the dummy linker analogue exhibits only a 2-fold drop off showing a linker does not abrogate the binding of Crizotinib.<sup>84</sup>

The NanoBRET data showed that CCT391402 has an  $EC_{50} = 3.61\ \mu\text{M}$  which confirms that it can engage the target at the concentration used in phosphoproteomics. Additionally, CCT391403 shows similar engagement to CCT391402 in NanoBRET but as shown in Figure 3.6 and Figure 3.6, shows significantly less phosphorylation than CCT391402, suggesting the induced phosphorylation is linker length dependent.

There is no clear trend in what drives the different  $EC_{50}$  values amongst the tested bifunctional compounds. However, bifunctional molecules are well known for having idiosyncratic permeability with molecules able to form intramolecular bonds that can mask certain structural features that aids permeability, thus increasing target engagement.<sup>87</sup>

Having confirmed engagement of STK10 in cells at the concentration tested in phosphoproteomics, we wanted to move forward and show that these bifunctional compounds were forming a ternary complex between AMPK and STK10.

### **3.4 AlphaScreen development for STK10**

We expected neo-phosphorylation to be driven through a ternary complex of AMPK, STK10 and bifunctional molecule, and wanted to set up a high throughput, robust biochemical assay that would show this.

Based on literature precedent for measuring proteins interacting with AMPK we decided to develop an AlphaScreen assay which is a proximity-based assay. As discussed in the introduction, AlphaScreen is a high through homogenous format which has been previously used to show ternary complex formation by bifunctional molecules.<sup>37</sup> Additionally, there was in-house experience of running it, so anticipated it could be developed rapidly.

An AlphaScreen requires the two proteins of interest to have orthogonal affinity tags, e.g. His or GST, which are then captured onto donor and acceptor beads. The mixture is then incubated allowing the proteins to associate and interact with each other, which then brings the beads into close proximity. After a set period of time, the donor bead is excited, stimulating the release of singlet oxygen which can diffuse to the donor bead triggering emission at 615 nm which can then be detected, as shown in Figure 3.15.

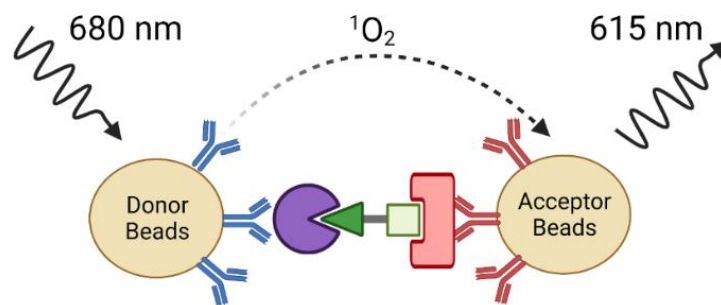


*Figure 3.15 - Illustration showing an optimised AlphaScreen assay*

AlphaScreen assays typically exhibit a hook effect (Figure 3.16) with protein concentrations; as at low protein concentrations, not enough protein is available to bind to the beads so very little proximity is induced, hence a low signal. Then at high protein concentrations the beads are saturated with protein, but now the complexes form between bound protein and unbound protein, rather than both proteins being bound, resulting in a low signal. As a result, setting up an AlphaScreen assay requires an enzyme titration to find the protein concentration that gives the optimal signal.

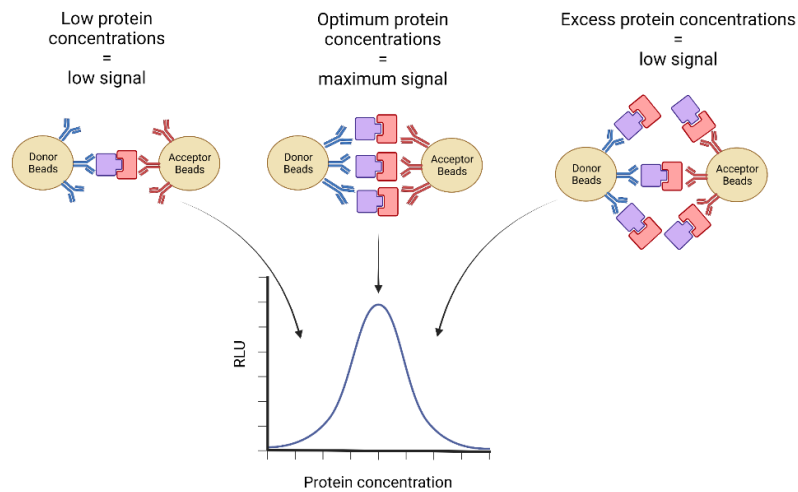


Figure 3.16 - How protein concentration affects an AlphaScreen readout

The enzyme titration relies on the two proteins having an affinity for each other, so that the signal changes with protein concentration. Typically, in a drug discovery format small molecules are usually being tested for disrupting the interaction between two proteins with a natural affinity for each other, whereas we had to try and optimise an assay with two proteins with no intrinsic affinity for one another. Like with protein concentrations, these bifunctional molecules will also have a hook effect in a dose response, as at low concentrations a relatively small amount of the ternary complex is formed so gives a low signal. Then at high concentrations of bifunctional compound, binary complexes of protein and bifunctional compound predominate again giving a low signal. This is shown below in Figure 3.17.

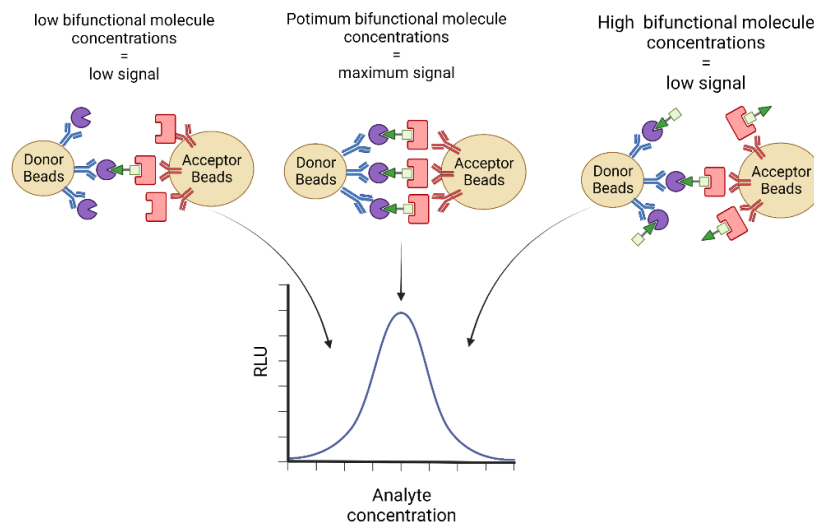



Figure 3.17 - How bifunctional molecule concentration affects an AlphaScreen readout




In order to account for both possible hook effects, from protein and compound concentration, we decided to perform three protein titrations at three concentrations of CCT391402 at 200nM, 1µM, and 5µM, and a DMSO control. The protein concentrations that were used are shown in Table 3.4 and although we had many bifunctional compounds, CCT391402 was used as it was the hit from phosphoproteomics and so was considered to be the most likely to show a positive effect.

In phosphoproteomics a concentration of 5µM was used, however binding in cells is usually weaker than in biochemical assay so wanted to test at lower concentrations. By testing three concentrations with 5-fold difference we hoped that at least one concentration would be in the optimum signal range, which we could then focus on.

*Table 3.4 - Protein concentrations used for the protein titration experiment*



STK10 \ AMPK		1	2	3	4	5	6	7
		100nM	30nM	10nM	3nM	1nM	0.3nM	0nM
A	100 nM							
B	30 nM							
C	10 nM							
D	3 nM							
E	1 nM							
F	0.3 nM							
G	0 nM							



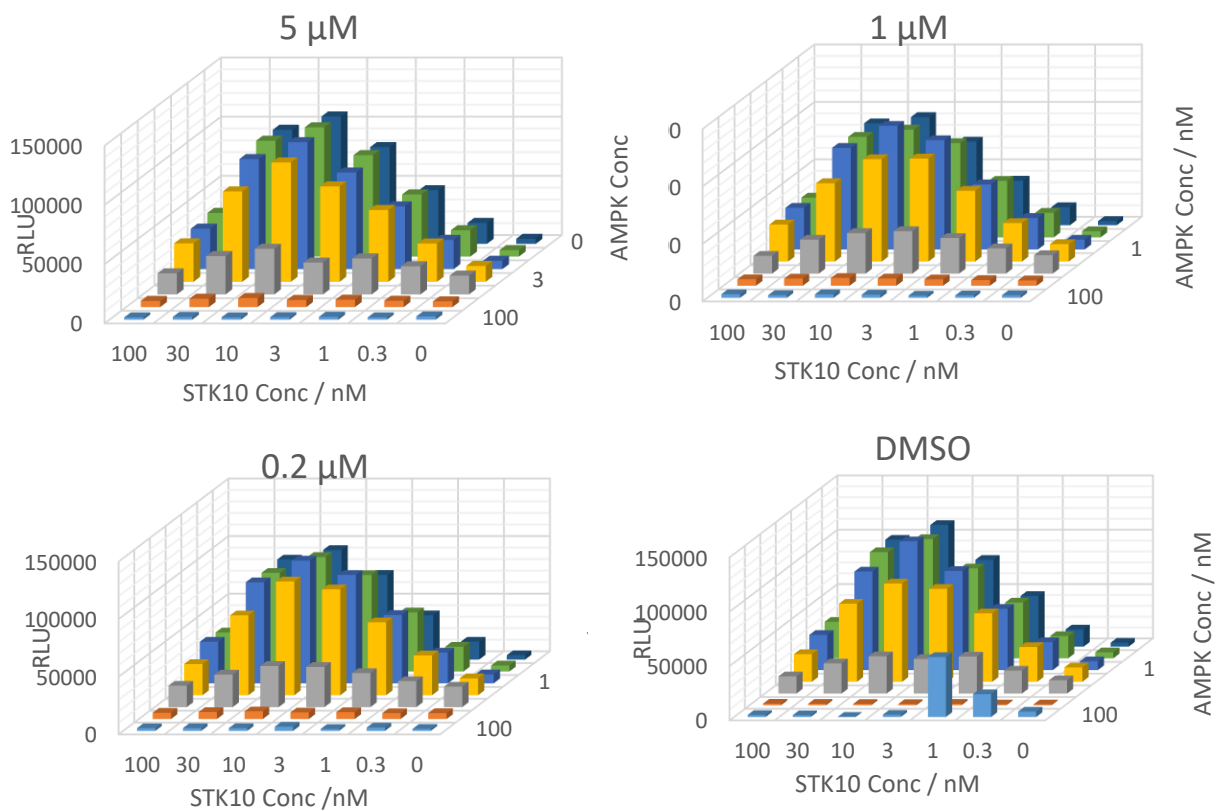


Figure 3.18 – AlphaScreen results for the compound protein titration experiment.

The assay was set up and read multiple times up. A 24h incubation time was required to achieve good levels of luminescence and see the expected bell-shaped curves with protein concentration.

The DMSO control is run to show the natural affinity between the 2 proteins, and any induced proximity from the bifunctional compound is found from subtracting the DMSO Relative Luminescence Units (RLU) values at the same protein concentrations. However, when this is done, the resulting corrected values are predominantly negative suggesting no increased association between AMPK and STK10 (see Figure 3.19). The typical issue causing high background signal is non-specific interactions, however increasing Tween-20, a detergent, concentrations did not help improve the signal.

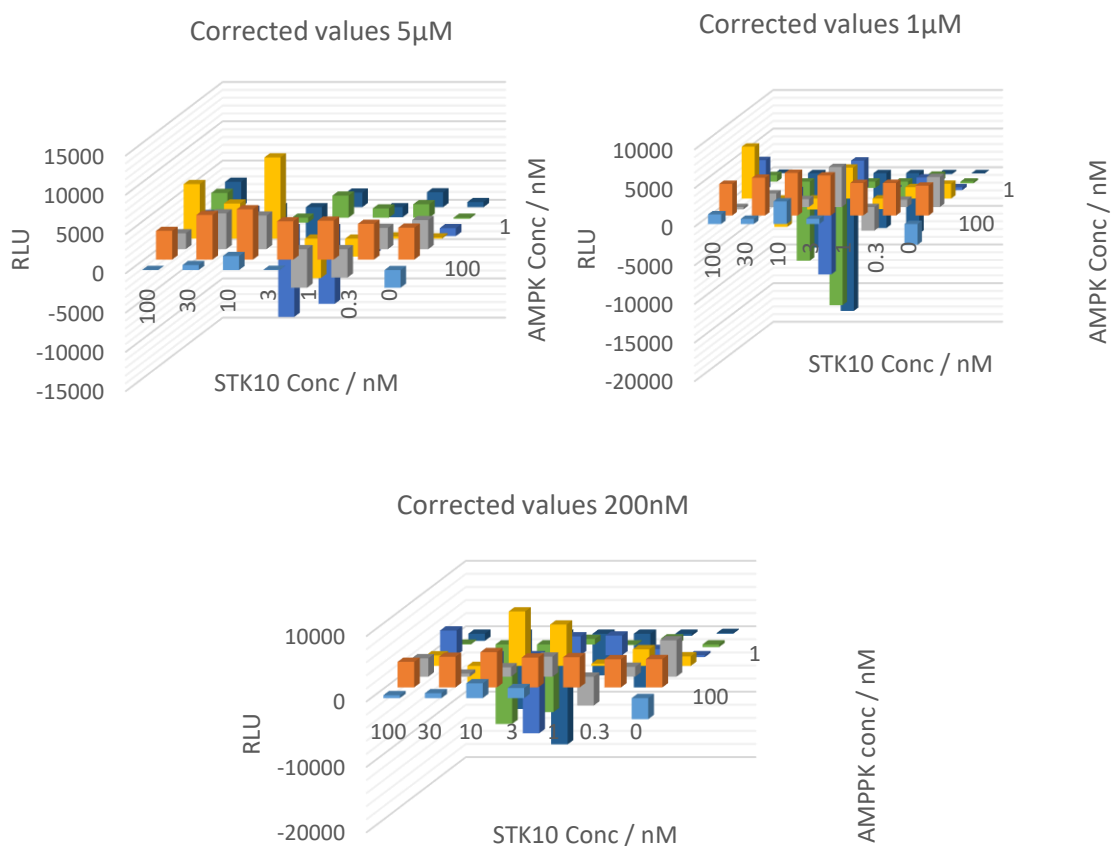


Figure 3.19 – Corrected emissions for enzyme titrations in the presence of CCT391402. 24h read

From these adjusted results the vast majority of protein concentrations looked unusable however it was noted that at 30nM AMPK (orange bars in Figure 3.19) all concentrations of STK10 gave a positive value, and as it seemed to follow the expected Hook effect with low values observed when at the high and low end of

STK10 concentrations suggested it may be a narrow but usable set of conditions for testing for ternary complex formation.

We therefore repeated the experiment at 30nM AMPK, 1 $\mu$ M CCT391402 and varying STK10 concentration, but this unfortunately showed no effect. As mentioned before there are two hook effects to account for in a AlphaScreen assay: one from native protein-protein interactions and the other from bifunctional molecules. Our current experiments had so far mainly focussed on the assumption that three different concentrations would provide a suitable concentration range to find a set of protein concentrations, but we also had to consider that we might be missing the compound concentrations that would give the highest levels of ternary complex formation and would give the highest readout.

To investigate this, we decide to do an eight-point dose response in duplicate of CCT391402 with 30nM AMPK and 10nM STK10. The concentrations of STK10 and AMPK were chosen as these concentrations gave the highest value as shown in Figure 3.19, and the results from this dose response are shown below in Figure 3.20.

### 30 nM AMPK, 10 nM STK10 and dose response of CCT391402

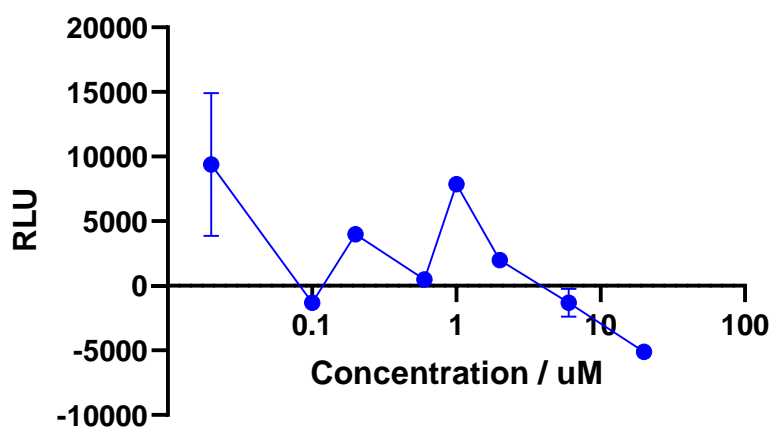


Figure 3.20 - 30 nM AMPK, 10 nM STK10 and varying concentrations of CCT391402. Values have been corrected by subtracting DMSO control.

The compound dose response looked like it was displaying the hook effect which would be consistent with forming a ternary complex and suggested CCT391402 was

able to bind AMPK and STK10 simultaneously to form a ternary complex. However, the RLU values were an order of magnitude lower than what AlphaScreen assays usually have, and there are clearly some concentrations of CCT391402 that have values out of line with a bell-shaped curve.<sup>88</sup> As a result, we wanted to confirm this result with as much confidence as possible and so performed a ten-point dose response in triplicate (Figure 3.21).

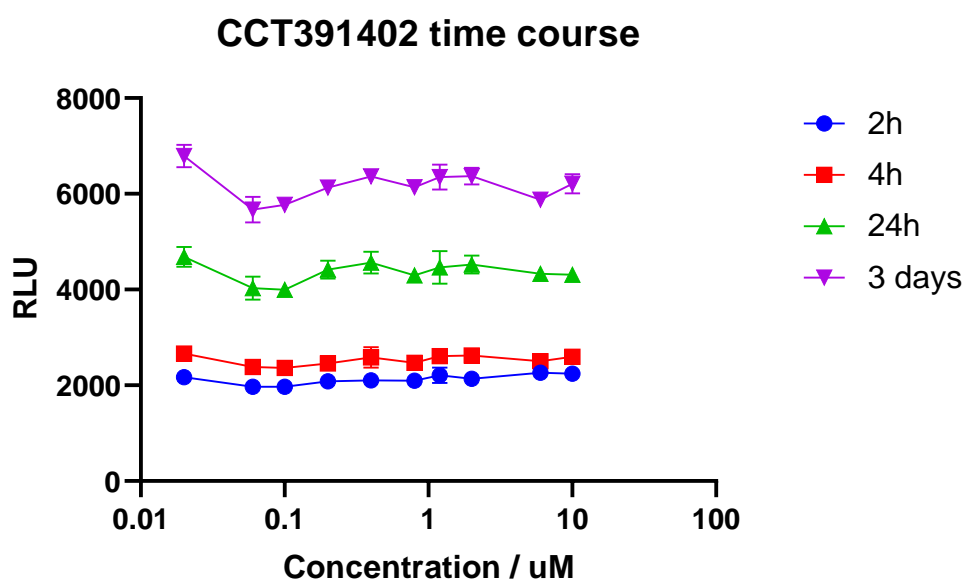


Figure 3.21 - Repeat experiment for 30 nM AMPK and 10 nM STK10 and dose dependence of CCT391402. These are raw values and not corrected for DMSO controls

The repeat failed to show a bell-shaped curve and so indicated no ternary complex or induced proximity between STK10 and AMPK. Over time the readout value increases but at no point shows a Hook effect, or any dependence on compound concentration, suggesting no ternary complex is being formed. Additionally, AlphaScreen assays should be quick assays, and be readable within 2 hours, with values typically being between 40,000-100,000 after 2h which is much higher than our observed signal.<sup>88</sup> Although the absolute signal is not what determines if an assay is suitable, it hinted towards poor association of the protein and that it would be difficult to optimise.

We had been using CCT391402 as it is the hit from phosphoproteomics, so felt it had the best chance of showing ternary complex formation. However, we thought the lack of induced proximity might be compound specific and decided to profile other bifunctional compounds.

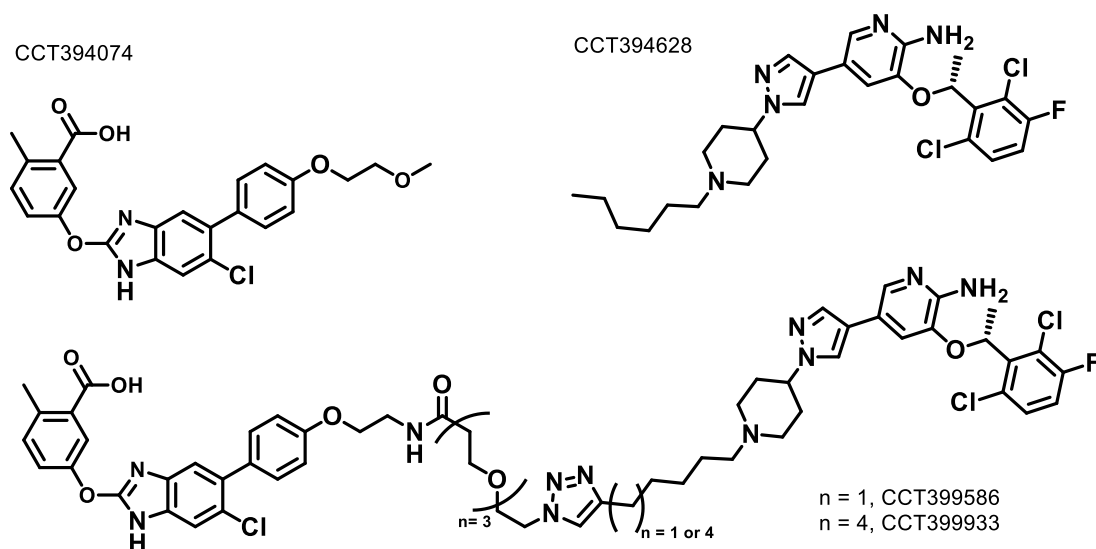


Figure 3.22 - Structure of 991 analogues tested in the AlphaScreen

We decided to test the longest bifunctional compounds as a longer length is more likely to be able to bind the two proteins simultaneously. Structures for the compounds tested are shown in Figure 3.22 and Figure 3.24. Having seen inconsistent results between assays we wanted to test compounds of similar structure in order to establish if there was any SAR. Compound structures are shown in Figure 3.22

None of the 991 analogues showed an increase in proximity.

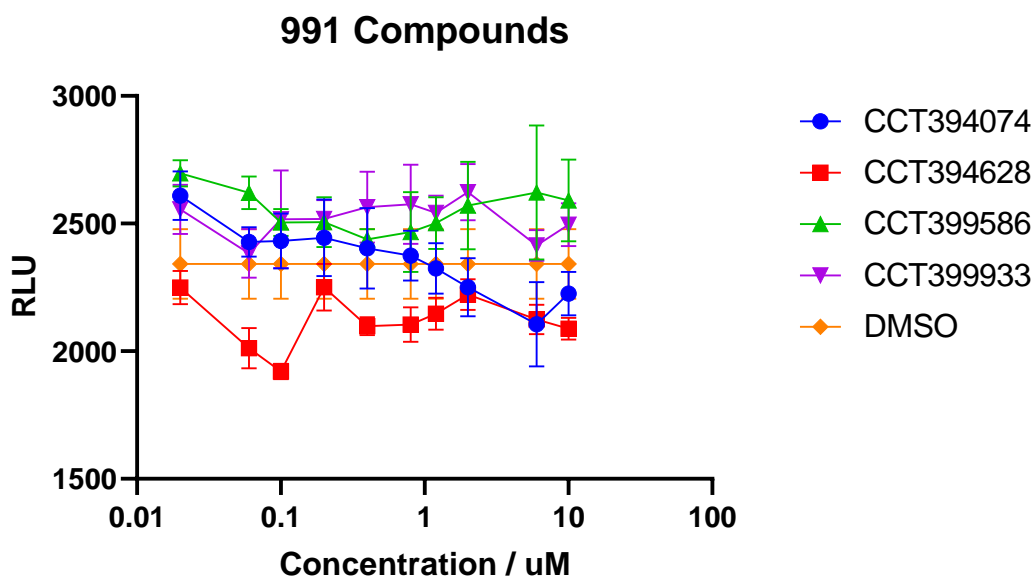


Figure 3.23 - Dose dependence of 991 based bifunctional molecules with 30 nM AMPK and 10 nM STK10

We also tested CCT391402 and a longer linker length analogue, but again saw no increased proximity between AMPK and STK10.

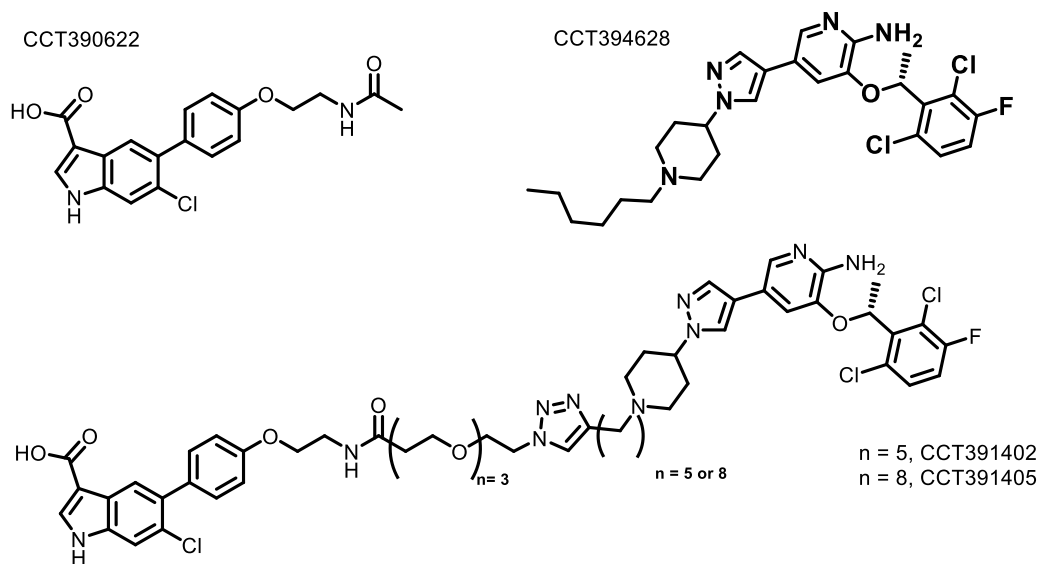


Figure 3.24 - Structure of 577 analogues tested in the AlphaScreen

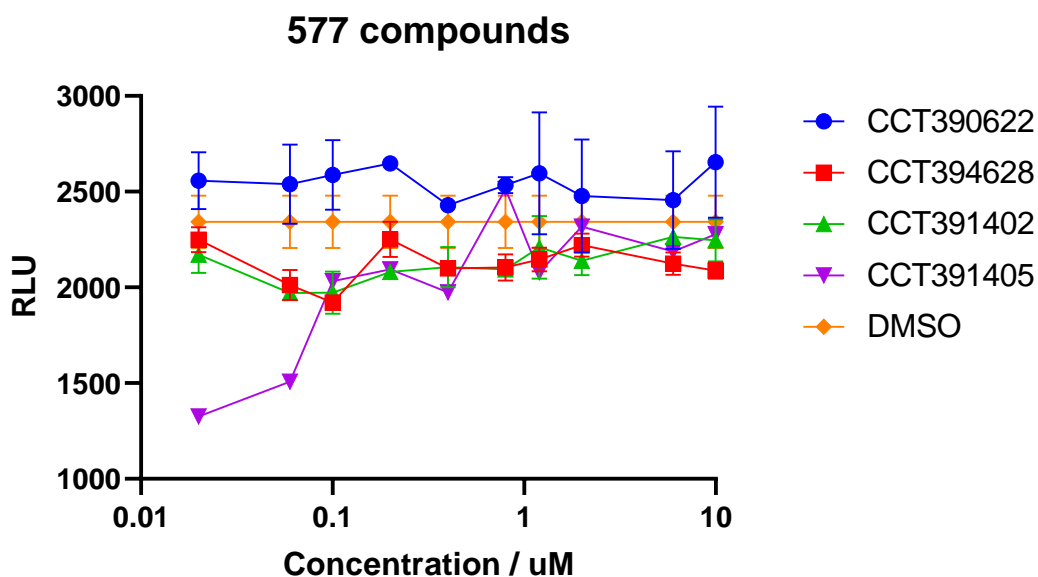


Figure 3.25 - Dose dependence of bifunctional molecules with 30 nM AMPK and 10 nM STK10

The results show no compound exhibited a hook effect or a large change from the DMSO background, which suggested no induced proximity and so no ternary complex formation.

This could be that no ternary complex is formed or that the assay is not appropriately engineered to detect it. A common reason for this assay format not working is low protein binding to the beads, as this results in low proximity between the donor and acceptor beads even if the proteins are in a ternary complex. This issue would give a low readout which is what is observed in our assay work. However, we felt confident that this wasn't the issue as we had used beads that are reported to work with all components of the buffer and protein formulations. For the His-AMPK we used it directly in line with literature reported conditions. Additionally, we made sure that there were no assay components that would quench the singlet oxygen and prevent an assay readout.

Another reason for no readout could be that the distance between the beads may be too far for the singlet oxygen to travel. As the protein tags bind the beads, this issue is due to the tags being inappropriately placed for the assay set up. Although the distance between tags in a AlphaScreen assay is greater than other methods for



measuring proximity, it still requires a distance <200 nm, which we can't confirm. Although the conditions replicate how the His-AMPK has been used in AlphaScreen buffers, so suggests it has an appropriately placed tag, there is no information as to whether this is a suitable assay format for STK10. Typically, STK10 has been tested in activity assays which don't require a tag.

As we do see a bell-shaped curve in the enzyme titrations (Figure 3.18) we had to consider that the proteins may be interacting either through stable protein-protein interactions or non-specifically, and the bifunctional molecules cannot increase on what is already a strong protein-protein complex. However, if the proteins were interacting then we anticipated that compounds that bind one or more of the proteins would disrupt this interaction and we would see a decrease, which we do not observe. Additionally, neither of the AMPK activators or crizotinib with a dummy linker appear to give a significant drop in ternary complex formation. The lack of change suggests AMPK and STK10 are not interacting partners.

In summary, we were not able to see ternary complex formation in the AlphaScreen assay and decided that it was not a suitable assay format for this project. We still wanted to show a ternary complex formation and having seen potential neophosphorylation in cells decided to try alternative experiments to investigate ternary complex formation.

### 3.5 STK10 Complex Immunoprecipitation (Co-IP)

A quick and easy way to investigate protein-protein interactions can be to perform a complex immunoprecipitation (IP), which is a technique that uses an antibody to pull down a specific protein. Proteins which are associated strongly with that target protein are pulled down with it and can then be detected by Western blotting.

As we were targeting STK10 based on the phosphoproteomics data, which we hypothesised was a result of an AMPK-bifunctional compound-STK10 ternary complex, it seemed logical to repeat these exact conditions and look for a STK10 and AMPK ternary complex in a cellular context.

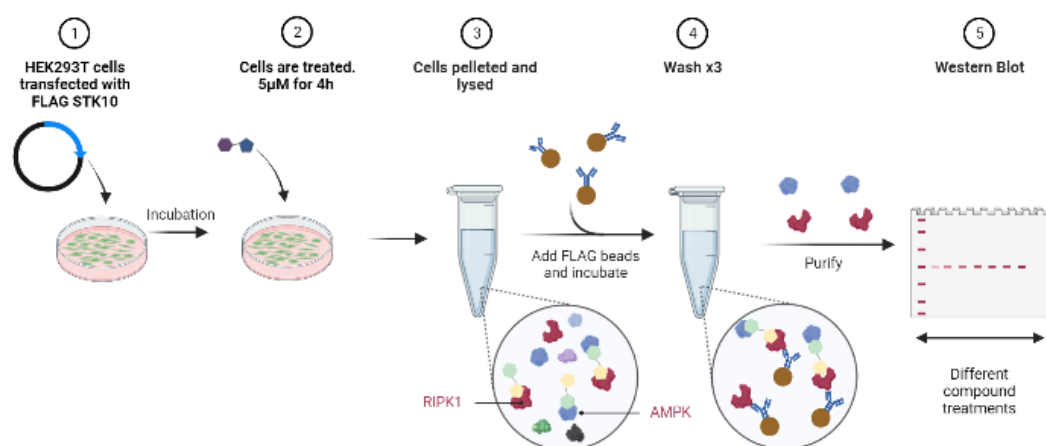


Figure 3.26 - Schematic depicting the stages of performing an IP experiment

Briefly, HEK293T cells were transfected with a plasmid containing STK10 with a FLAG tag, which causes over-expression of STK10 with a FLAG tag on the end. The cells are then treated with the compounds at 5 μM for 4h, the same time and concentration used in phosphoproteomics. Cells are then lysed and incubated with anti-FLAG magnetic beads which pull down the STK10 and any associated proteins. The lysate mixture is washed to remove non-specific binding, then denatured and run on a Western Blot, with the results being shown in Figure 3.27.

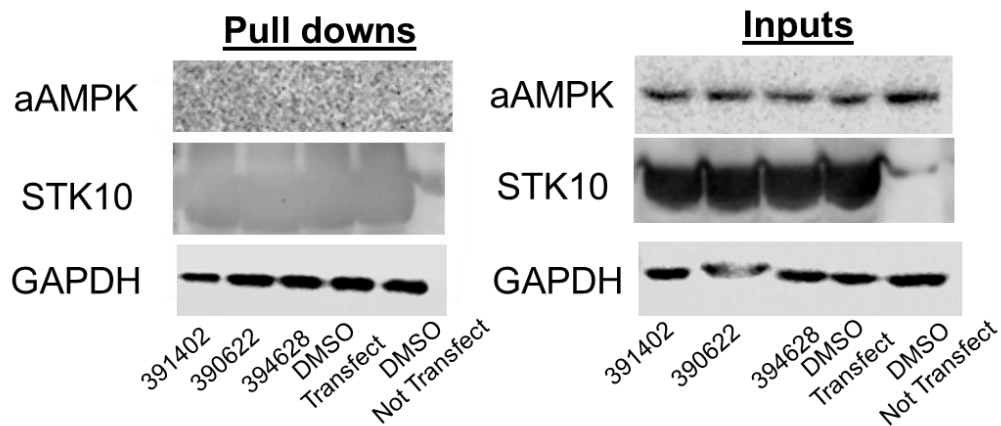


Figure 3.27 - IP experiment looking for AMPK and STK10 association

The input results show STK10 is highly expressed, as expected from the transfection, and they show AMPK is present in the lysate. The pull-down western blots have the STK10 signal saturating the reader so indicate the STK10-Flag can bind to the anti-Flag beads but show no AMPK. The lack of AMPK shows it hasn't been pulled down with the STK10 and suggests that either no ternary complex is formed or that the interaction between AMPK and STK10 in cells is very transient with weak affinity, and the washing steps are too harsh so AMPK and STK10 can't maintain their association. Additionally, the FLAG beads may bind STK10 in an orientation that breaks its association with AMPK, so any STK10 pulled down has no AMPK and any STK10 interacting with AMPK can't be pulled down.

### 3.6 Measuring Phosphorylation of STK10 in cells

Although the pull-down experiment suggested either no or a weakly interacting ternary complex, it was still possible that CCT391402 is able to bind AMPK and STK10, but only forming a weak and unstable ternary complex but one that is long lived enough for neo-phosphorylation. As such we designed a set of experiments to try and validate the neo-phosphorylation of STK10 observed in phosphoproteomics.

As the 447-464 STK10 sequence had been detected to have increased phosphorylation we would ideally have antibodies for each potential phosphosite in the STK10 'ASQSRPNSSALETLGGEK' sequence, which would allow us to selectively

investigate phosphorylation of each site. However, no STK10 phospho-specific antibodies are commercially available.

We proposed AMPK was phosphorylating the RXXS sequence based on its established consensus motif, and this was consistent with phosphoproteomics, so decided to use a Phospho-AMPK Substrate Motif antibody that binds to RXXpS/pT motifs in proteins. As this antibody recognises and binds all available RXXpS/pT motifs in proteins, we expected a base level of normal STK10 phosphorylation, but were optimistic that we would see a significant change on treatment with a bifunctional compound. We repeated the same co-IP procedure as above using transfected STK10-Flag and imaged with the Phospho-AMPK Substrate Motif antibody with results shown below in Figure 3.28.



*Figure 3.28 - Western blots of FLAG-STK10 using RXXpS antibody*

Figure 3.28 shows that STK10 has a high level of endogenous RXXpS/pT phosphorylation, with no increase in the presence of a bifunctional molecule. We saw a slight decrease in signal with the treatment of CCT394628, the crizotinib and a dummy linker, perhaps suggesting crizotinib inhibits STK10 phosphorylation.

In summary, analysis of cell lysates with a phospho-antibody suggested high levels of phosphorylated STK10 which made it impossible to detect neo-phosphorylation from treatment with a bifunctional compound.

This suggested that if we wanted to examine neo-phosphorylation of STK10 then we would have to use a more controlled system to examine phosphorylation.

### **3.7 Measuring STK10 phosphorylation biochemically**

#### **3.7.1 Using Western Blots**

In the cell, phosphorylation is frequently performed on a protein by an upstream kinase and as seen in Figure 3.28, STK10 is heavily phosphorylated, which means any neo-phosphorylation may be swamped. To try and see if changes in phosphorylation could be detected in a more controlled biochemical environment, we combined recombinant AMPK, STK10, ATP and CCT391402 directly, and then monitored phosphorylation through western blots using the phospho-AMPK substrate motif antibody to image.

To perform these experiments, it's crucial that the STK10 being used is unphosphorylated, as phosphorylated this would give a high background and give the same issues as shown in Figure 3.28. As commercial vendors supply STK10 which is highly phosphorylated, we decided to express STK10 in-house using a STK10-His plasmid, gifted from Dr Jonathan M. Elkins of the Structural Genomics Consortium. We transfected insect, Sf9 cells then cell lysates were purified through Talon, which was then treated with a His tagged phosphatase and a His tagged TEV protease. This cleaved the His tag from STK10 and dephosphorylated any available phosphosites on STK10. This mix was then purified by Size Exclusion Chromatography and then Talon to give 12 mg of STK10.

To confirm the phosphorylation state and confirm STK10 was successfully produced, we western blotted the protein and used a STK10 antibody or the RXXpS antibody. Additionally, we treated the STK10 with a commercially available lambda phosphatase (LPP) to see if there was any change in signal (Figure 3.29).

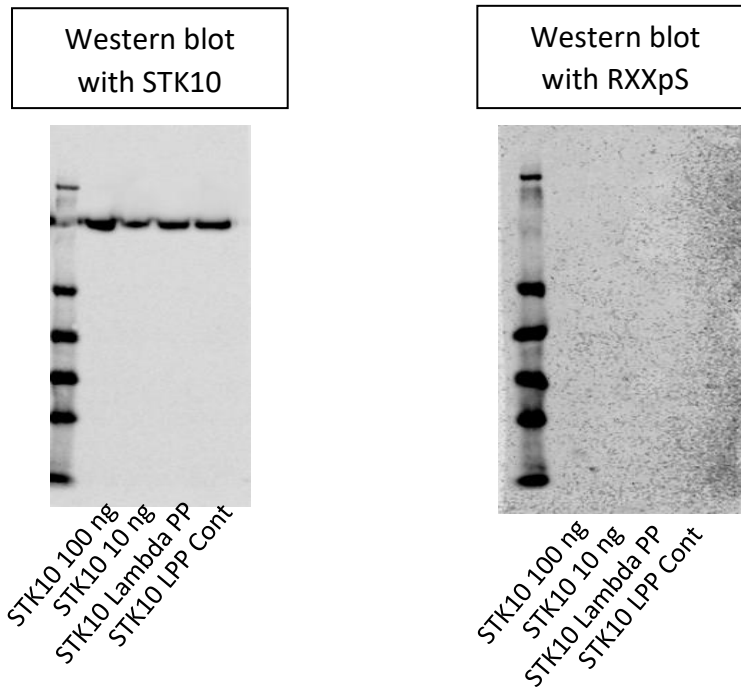


Figure 3.29 - Western blots of Sf9 expressed STK10. STK10 100ng and 10 ng is protein straight from expression. Lambda phosphatase treatment is STK10 treated with a commercial phosphatase. LPP Cont. is the control for LPP treatment

In Figure 3.29 the western with the STK10 antibody confirms the expressed protein is STK10 and shows no other protein are being detected. On the right, the RXXpS clearly shows no phosphorylation is detected, which suggests the phosphatase treatment was successful.

On this basis we set up a set of experiments to investigate phosphorylation induced by bifunctional compounds. For experimental controls we incubated STK10 with and without ATP, to examine background auto- or trans-phosphorylation. We also incubated STK10 with AMPK, again with and without ATP to examine if AMPK would alter the phosphorylation of STK10. Although we had a library of bifunctional compounds, we decided to focus on just one bifunctional compound: CCT391402, the compound that gave increased phosphorylation of STK10 in phosphoproteomics.

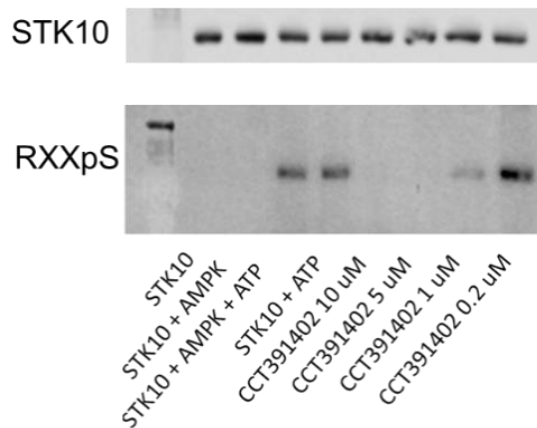


Figure 3.30 - Western blots of STK10 phosphorylation experiments. CCT391402 treatments all contain 20 nM AMPK, 700 nM STK10, 150  $\mu$ M ATP.

From the first experiment we can see that STK10 + ATP already shows phosphorylation, as described earlier, STK10 has been shown to autophosphorylate trans-autophosphorylate. Addition of AMPK does not increase phosphorylation on STK10 confirming that STK10 is not an AMPK substrate.

The compound treatment of CCT391402 showed no phosphorylation of STK10 at 10 $\mu$ M and 5 $\mu$ M, a small amount of phosphorylation at 1 $\mu$ M but interestingly showed an increased signal at 200nM. This set of responses could be because at concentrations >200 nM, only binary complexes of CCT391402 with STK10 or AMPK form and this prevents ternary complex forming and subsequent neo-phosphorylation.

However, it is also possible that the crizotinib warhead binds STK10 and is just preventing autophosphorylation at high concentrations, although in this experiment there appears to be more phosphorylation in the presence of CCT391402 than with ATP alone.

As Western blots are a difficult technique to quantify, we repeated the experiment placing the CCT391402 200nM treatment directly next to the controls to allow for easy comparison.

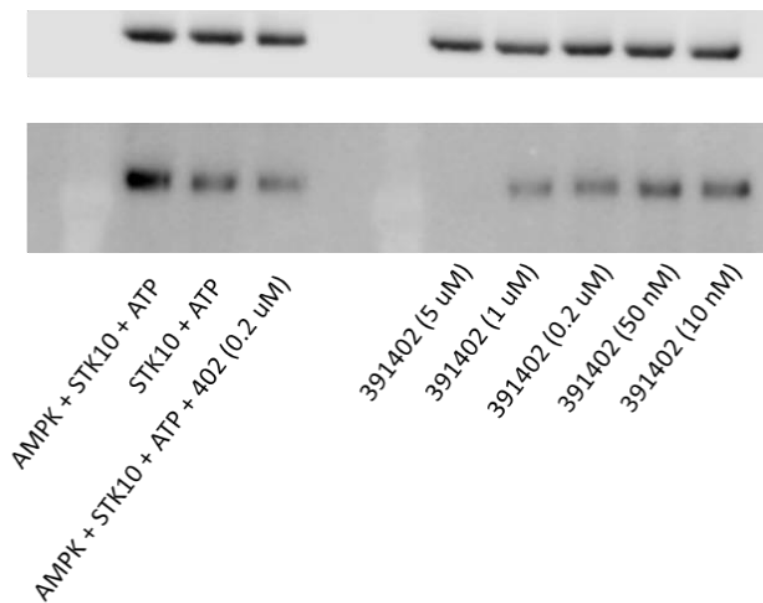


*Figure 3.31 - Western blots of STK10 phosphorylation experiments. CCT391402 treatments all contain 20 nM AMPK, 700 nM STK10, 150 μM ATP.*

Disappointingly in this case we didn't see increased phosphorylation with CCT391402 at 200nM. The dose dependent decrease in phosphorylation with CCT391402 as shown in Figure 3.31 suggests that reduced inhibition of autophosphorylation is the likely cause of the increase in phosphorylation observed in Figure 3.30.

From the data above we do not observe an increase in phosphorylation of RXXpS sites in STK10. However, there were multiple possible sites in the sequence from phosphoproteomics so we could not rule out a neo-phosphorylation is occurring on a different site. Literature suggested that induced proximity of a kinase and substrate protein, can overrule the preferred consensus motif of kinases, and that multiple sites on a substrate protein are phosphorylated with the same bifunctional compound. We therefore wanted an alternative method that could confirm the exact site(s) of phosphorylation taking place.

As such we felt it unlikely that the full extent of phosphorylation cannot be reliably determined using western blots, and we needed a more to design a more quantitative and thorough methodology



### 3.7.2 Recombinant Mass Spectrometry assay

To assign and quantify the phosphosites we decided that a mass spectrometry technique would be the best method, as this could potentially detect multiple sites, as well as determining the relative abundance of each phosphorylated site. As this method is resource intensive, we initially focussed on a small set of tests to see what phosphosites could be detected and if we were likely to see a change.

We identified four sets of conditions which we felt would answer key questions. After expressing STK10 we had used a His-tagged phosphatase to remove existing phosphorylation. To investigate the extent of dephosphorylation, we treated a sample with DMSO, and the resulting values in Table 3.5 and

Table 3.6 are relative to this treatment.

To confirm that dephosphorylation was complete we also treated STK10 with a commercial Lambda phosphatase (LPP) and tested this in parallel. In previous experiments (Figure 3.30 and Figure 3.31) we observed STK10 autophosphorylation, so we incubated STK10 with ATP to measure this. Finally, we wanted to look for neo-phosphorylation with a bifunctional compound, so tested STK10 with ATP, CCT391402 and AMPK.

Samples were made up with a concentration of 700nM STK10 and where applicable 150µM ATP and 20nM AMPK, then snap frozen and sent for analysis at the Proteomics Core facility, where the samples were digested, TMT labelled then enriched and analysed by LC-MS.

In the first run we identified 53 phosphopeptides. We first looked at the phosphosites in the 447-464 sequence, as from phosphoproteomics this was the peptide sequence of interest, with results shown in Table 3.5. The results are the  $\text{Log}_2(\text{FoldChange})$  of the abundance from the treatment divided by the DMSO control.

Table 3.5 – Phospho-peptides in the 447-464 STK10 sequence. STK10 + LPP: STK10 incubated with a commercial lambda phosphatase.

Sequence	Log2(abundance/DMSO)		
	STK10 + ATP	STK10 + LPP	STK10 + ATP + AMPK + CCT391402
[K].ASQSRPNSSALETLGGEK.[L] S448, T459	94.98046	2.324138	39.33793
[K].ASQSRPNSSALETLGGEK.[L] T459	159.9552	0.626437	55.96897
[K].ASQSRPNSSALETLGGEK.[L] S450	490.7747	4.277011	147.6368
[R].SQKASQSRPNSSALETLGGEK.[L] T459	10.82184	0.467816	0.902299

The values for the STK10 + ATP show every site in the sequence of interest has increased with ATP, suggesting STK10 readily auto-phosphorylates at multiple sites. This also suggests the His-tagged phosphatase used in expressing the protein was successful in dephosphorylating phosphosites, as they clearly have a propensity to phosphorylate readily.

The STK10 + LPP phosphatase treatment unexpectedly showed an increase in phosphorylation compared to the DMSO control, which suggests the lambda phosphatase was increasing phosphorylation of STK10. As no ATP is included in this STK10+LPP treatment, we concluded that these increases are an experimental or equipment error. As such, to prevent false positives results from mass spectrometry, a Log2(FC) change would have to be >5 from background to be considered relevant.

Treatment of STK10 with AMPK, ATP and CCT391402 showed no increases in phosphorylation of any sites in the 447-464 sequence of STK10 compared to the STK10 + ATP treatment. This suggests that increases relative to DMSO are likely due to auto-phosphorylation and not from a ternary complex forming.

As mentioned, 53 peptides of different phosphorylation were identified and although most phosphosites showed highest levels of phosphorylation with just STK10 and ATP, there were some phosphosites that showed higher levels of phosphorylation of STK10 with AMPK, ATP and CCT391402 (

Table 3.6) and discussed further below.

*Table 3.6 - Sites of increased STK10 phosphorylation in the presence of CCT391402, AMPK and ATP*

Sequence	Log2(abundance/DMSO)		
	STK10 + ATP	STK10 + LPP	STK10 + ATP + AMPK + CCT391402
[K].IISEDEK.[K] S549	4.7	0.7	17.8
[K].NPETRPSAAQLLEHPFVSSITSNK.[A] [T/S] 278-301	0.8	0.1	1.8
[K].NPETRPSAAQLLEHPFVSSITSNK.[A] [T/S], 278-301, Deamidated	1.4	0.2	2.3
[K].QVAEQGGDLSPAANR.[S] S438, Deamidated	1.0	0.2	1.8
[K].QVAEQGGDLSPAANR.[S] S438	1.8	0.6	3.2
[K].SDPPTLLTPSKWSVEFR.[D] S261	2.8	0.3	4.7
[R].DSFIGTPYWMAPEVVMCETMK.[D] S191, Carbamidomethyl	7.6	0.2	9.6
[K].RDSFIGTPYWMAPEVVMCETMK.[D] S191, Carbamidomethyl, Oxidation	72.0	2.6	95.4
[K].RDSFIGTPYWMAPEVVMCETMK.[D] S191, Carbamidomethyl	23.1	0.7	28.1

[R].DSFIGTPYWMAPEVVMCETMK.[D] S191, Carbamidomethyl, Oxidation	28.2	13.9	36.6
[K].RDSFIGTPYWMAPEVVMCETMK.[D] S191	1.5	0.03	1.8

Although most peptides had a low level of change in the STK10 + LPP compared to the DMSO control, the value of  $\log_2(\text{FC}) = 13.9$  observed for the oxidised S191 peptide in

Table 3.6, suggested that the error of the technique may make it difficult to confirm genuine phosphorylation. Many phosphosites in the STK10+ ATP+ AMPK + CCT391402 treatment show approximately a two-fold increase to the STK10+ATP control; given the errors noted it is difficult to claim these are significant. However, from examining these phosphosites with the AlphaFold structure of STK10, they are all surface exposed and near the STK10 active site, which perhaps suggest they are at least feasible candidate sites for neo-phosphorylation.

As new phosphosites of interest tended to be detected multiple times but with different modifications e.g. S191 and S438, it increased confidence that a real change in phosphorylation was occurring, but further work would be needed to confirm this.

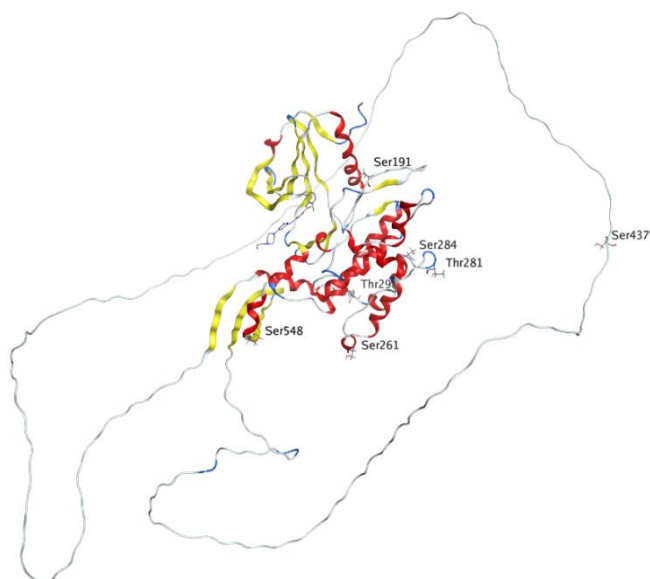


Figure 3.32 - AlphaFold structure of STK10 showing the phosphosites from Table 8.2

Of the peptides in

Table 3.6, we noticed that none contained an RXXS motif, indicating that using the Phospho-AMPK Substrate Motif antibody that recognises RXXpS/pT motifs would not be able to detect phosphorylation on these sites as we had previously tried (Figure 3.30 and Figure 3.31) thus supporting the decision to move to a mass spectrometry technique to identify phosphosites.

Given the potential for error in this technique we looked to repeat these experiments in triplicate with single ligand controls (Figure 3.33).

### **3.7.3 Following up on the Mass Spectrometry assay**

For follow up experiments we could use 18-plex experiments, which meant six different conditions could be analysed per run. All experiments were done with 700 nM STK10, and if required 20nM AMPK and 150 $\mu$ M ATP for 2h at room temperature. We needed to test STK10 with ATP as a background for autophosphorylation in every run, so that we could get a Log<sub>2</sub>(FoldChange) for the different treatments. We also wanted to test CCT391402 with STK10 and ATP without AMPK, to see if the bifunctional molecule was binding in such a way that it increased or altered the autophosphorylation of STK10

Table 3.6. We also wanted to examine if AMPK was able to alter the phosphorylation of STK10 so also tested STK10 + AMPK + ATP.

To investigate if AMPK could induce neo-phosphorylation, we tested CCT391402, and compared this to single-ligand controls CCT390622 and CCT394628 at 200nM.

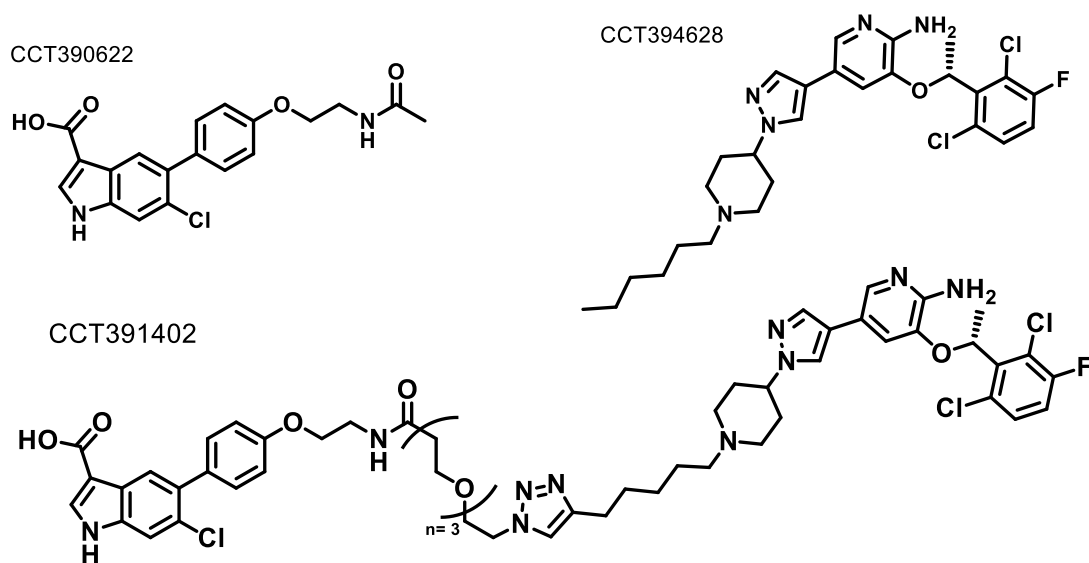


Figure 3.33 - Structures of compounds for testing in the mass spectrometry assay

In these experiments we were able to identify 71 phosphopeptides with data shown in Figure 3.34 and Figure 3.36. The previous results from Table 3.5 and Table 3.6 suggested a large  $\text{Log}_2(\text{FC})$  is needed to build confidence in seeing neophosphorylation, so in the following analysis we applied a cut off and only examined peptides with a  $\text{Log}_2(\text{FC}) > 5$  in order to minimise false positives. The data shown in Figure 3.34 and Figure 3.36 uses the same order of peptide IDs.

Table 3.7 - Sequences and amino acid position of STK10 that had a Log2(FC) >5 in mass spectrometry in at least one condition. Conditions with Log2(FC) >5 are highlighted in orange

Peptide ID	Sequence	Log2(abundance/DMSO)				
		STK10 + ATP + AMPK + CCT3914 02	STK10 + ATP + CCT3914 02	STK10 + ATP + AMPK + CCT3906 22	STK10 + ATP + AMPK + CCT3906 28	STK10 + ATP + AMPK + DMSO
1	[R].DSDCSSLCTSESMDYGTNL STDLSLNK.[E] S507	4.3	0.9	-11.0	8.6	-0.2
17	[K].RDSFIGTPYWMapeVVM CETMK.[D] S191	14.3	-8.4	1.1	2.4	-0.4
18	[K].LANGSLEPPAQAAPGPSK. [R] S469	2.9	-7.4	11.9	-10.3	1.7
32	[K].AGNVLMTLEGDIR.[L] T166	-10.9	-5.2	-0.7	-2.6	9.6
38	[K].IKQFSQQEEK.[R] S844	0.7	-0.1	-2.5	6.3	-0.1
42	[K].QFSQQEEK.[R] S844	0.1	1.5	-1.8	6.4	-0.8
44	[R].DSFIGTPYWMapeVVMC ETMK.[D] S191	23.3	-10.0	-3.2	10.0	2.2
46	[K].SRPVSMdar.[I] S413, S417	-9.9	11.3	-12.2	17.3	-2.0
48	[R].SLQTTSPVvAPGNENGL AVPVPLR.[K] S387, T390	50.4	20.0	-31.4	31.7	-4.0
49	[R].NQTQLSNKHELQLEQMH K.[R] S584	1.1	-1.5	-8.2	19.4	-6.2
54	[K].AGNVLMTLEGDIR.[L] T166	1.6	9.2	-4.4	2.4	0.8
67	[K].RLTTDNR.[R] T714	-3.0	9.0	-17.3	8.4	6.5

CCT391402 with AMPK, graph A in Figure 3.34, shows increased Ser191 on peptide 17 and Ser191 on peptide 44. Ser191 is also an increased phosphosite from

Table 3.6 so it built confidence this could be a site of neo-phosphorylation. Also increased is peptide 48 corresponding to 2 phosphorylation's on Ser387 and Thr390 in the same peptide.

In the absence of AMPK, graph B in Figure 3.34, the phosphorylation events on peptides 17 and 44 were not observed, suggesting that these could be genuine, ternary complex mediated neo-phosphorylation. Bis-phosphorylation of peptide 48 (p-Ser387 and p-Thr390) is still observed in the absence of AMPK suggesting some level of background autophosphorylation. In addition, we observe three new phosphorylation events: 2 phosphorylation's on Ser413 and Ser417 on peptide 46, Thr166 on peptide 54, and Thr714 on peptide 67. We do not have a clear explanation for why there would be more phosphorylation events in the absence of AMPK. One possibility could be that the ternary complex formation with AMPK blocks some phosphorylation sites on STK10 or this could also be random error in the experiment.

When CCT390622, the AMPK activator (graph C in Figure 3.34), is tested only one site at Ser469 on peptide 18 has increased phosphorylation. We hypothesise that an AMPK agonist binding may change AMPK's protein surface and alter its specificity towards substrates, however if this was true, we would expect to see other unique phosphopeptides in this treatment.

As shown in graph D in Figure 3.34, when CCT394628 (Crizotinib with a dummy linker), is tested peptide 46, peptide 48 and peptide 67 are all increased, as was observed in treatment with CCT391402, and peptides 44 and 48 are increased, as observed in treatment with AMPK and CCT391402. This suggests that Crizotinib binding may alter STK10 autophosphorylation. As Crizotinib binding would outcompete ATP, if this result is genuine, it suggests trans-autophosphorylation is occurring with altered specificity for substrates sites upon binding Crizotinib. We also see increased phosphorylation of Ser507 on peptides 1, Ser844 on peptide 38,



Ser844 on peptide 42 and Ser584 on peptide 49, which again suggests Crizotinib binding may alter STK10 autophosphorylation.

Examining graph E in Figure 3.34, shows that in the presence of AMPK with no bifunctional compound present, only two peptides, 67 and 32 are increased suggesting AMPK does not naturally phosphorylate STK10. As these both have relatively small  $\text{Log}_2(\text{FC})$  values this may be due to, may be due to experimental error.

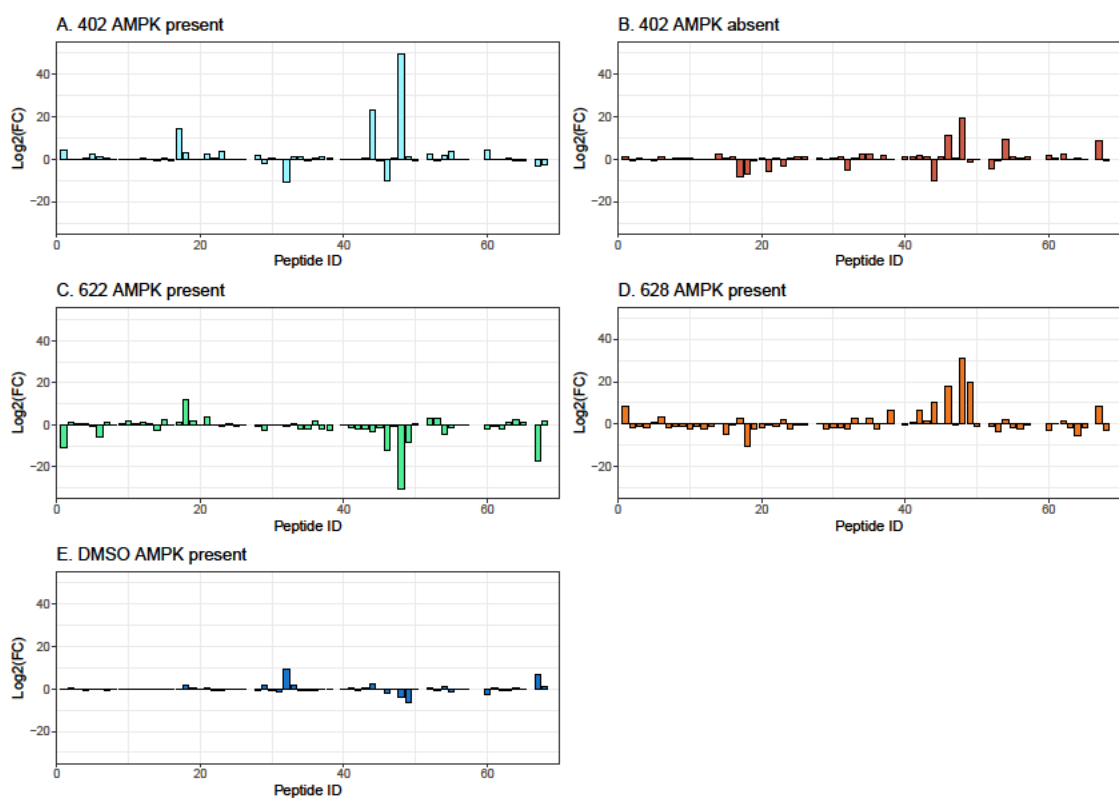


Figure 3.34 - Mass spectrometry data of STK10 phosphopeptides. x axis is assigned peptide ID. Y axis is  $\text{Log}_2(\text{FoldChange})$  relative to a STK10 and AMPK sample

To further investigate whether the sites of increased phosphorylation seen with CCT391402 were real, we performed a series of experiments of varying concentrations of CCT391402 to examine if a Hook effect or dose dependence was observed. A hook effect would be evidence that supports the formation of a ternary complex.



Table 3.8 - Sequences and amino acid position of STK10 that had a Log<sub>2</sub>(FC) >5 in mass spectrometry in at least one condition. Conditions with Log<sub>2</sub>(FC) >5 are highlighted in orange

Peptide ID	Sequence	Log <sub>2</sub> (abundance/DMSO)				
		CCT391 402 40nM	CCT391 402 200nM	CCT391 402 1,000n M	CCT391 402 5,000n M	CCT399 586 200nM
1	[R].DSDCSSLCTSESMDYGT NLSTDLSLNK.[E] S507	12.0	8.8	1.8	-26.9	10.2
11	[R].SLQTTSPVAPGNEN GLAVPVPLR.[K] T391	-19.1	-0.3	4.8	60.4	-47.7
24	[K].EMGSLSIKDPK.[L] S514, S516	5.6	0.3	-2.1	-15.3	4.9
25	[K].RDSFIGTPYWMapeVV MCETMK.[D] S191, T208	2.0	-4.1	-0.1	-0.8	5.4
47	[K].RSDCSSLCTSESMDYGT TNLSTDLSLNK.[E] S485, S488	2.4	1.5	1.5	-8.2	5.3
48	[R].SLQTTSPVAPGNEN GLAVPVPLR.[K] S387, T390	-9.7	-0.1	0.6	-6.7	19.4
54	[K].AGNVLMTLEGDIR.[L] T166	3.5	11.6	-1.9	12.6	-9.5
70	[K].LANGSLEPPAQAAPGP SKR.[D] S481	-0.1	-1.7	-2.2	-8.5	13.2

Testing at 40nM shows a large increase in peptide 1 abundance which corresponds to Ser507 and increased Ser514 and Ser516 on peptide 24. The next concentration of 200 nM also shows a high level of Ser507 on peptide 1, in addition to increased levels of Thr166, peptide 54, however these increases were not observed in Figure 3.34 under the same conditions suggesting these findings are not robust. Disappointingly, the increased levels of Ser191 observed in the previous experiments (Table 3.7 and Table 3.8) did not confirm here suggesting these findings are not robust.

We noted that in this run the Log<sub>2</sub>(FC) values are generally much smaller in comparison to those in Figure 3.34, which also suggests high variability between runs.

The 1000nM treatment of CCT391402 shows no changes >5. However, Thr391 (peptide 11) did have log<sub>2</sub>(FC) = 4.7, which then increased to log<sub>2</sub>(FC) = 60 at 5,000nM concentration. Peptide 54 also had increased abundance like as seen in the 200 nM treatment but not at 1,000nM so it is unlikely that this is a neo-phosphosite.

We tested CCT399586 at 200nM and expected similar if not more increased peptides compared to CCT391402 at 200nM, as the 991 warhead binds AMPK more strongly than the 577 warhead. However, the only peptide that CCT399586 and any CCT391402 treatment have in common is peptide 1, with Ser507. CCT399586 also phosphorylates peptide 25 at Ser191 and Thr208 and peptide 48 on Ser387 and Thr390 which are sequences of increases abundance in the previous run of CCT391402 at 200 nM with AMPK suggesting some overlap. CCT399586 also phosphorylates peptide 47 at Ser485 and Ser488 and finally peptide 70 at Ser481, which are not increased in any other treatments

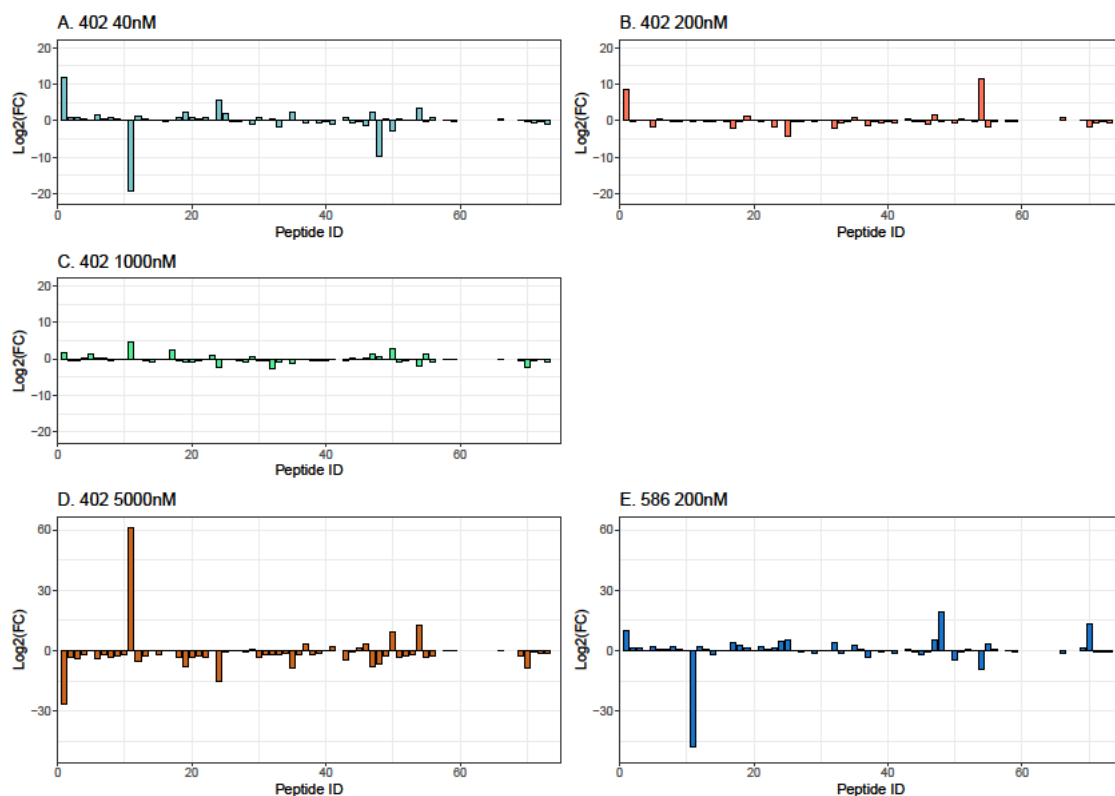


Figure 3.36 -Mass spectrometry data of STK10 phosphopeptides. x axis is assigned peptide ID. Note the different y axis scale of A-C vs D-E

In summary, the results from mass spectrometry are quite variable which prevents a clear conclusion being drawn. Some sites appear repeatedly and may warrant further investigation; however, this technique seems highly variable thus limiting the ability to find genuine phosphosites from background autophosphorylation

### 3.8 Conclusions

We aimed to map the increases in phosphorylation of known Crizotinib substrate proteins utilising global unbiased phosphoproteomics to understand the rules around induced phosphorylation and find novel substrate proteins. Using this technique, we were able to identify STK10 as a hit with an increased phosphosite that contained the AMPK phospho motif of RXXS. Structural analysis suggested this was a rational hit, and we attempted to confirm this with multiple orthogonal techniques.

An AlphaScreen was utilised by performing multiple enzyme titrations in the presence of CCT391402 but failed to show any induced proximity. To circumvent the potential issues from that assay format such as unsuitable tag placement, we then focussed on confirming STK10 as a neo-substrate in cellular conditions. To do this we mirrored the phosphoproteomic conditions and used co-IP or western blots to investigate ternary complex formation or phosphorylation. Due to the poor resolution of these techniques, we expressed STK10 and tried to track changes in phosphorylation with Western blots, but we were unable to accurately replicate results, likely due to intrinsic error associated this technique.

To quantitatively monitor phosphorylation a set of mass spectrometry conditions were designed and tested with initial results showing that some sites of STK10 are selectively phosphorylated when treated with CCT391402. None of the phosphoproteomic sites showed increased phosphorylation suggesting the phosphoproteomic result was a false positive or may be a downstream effect from compound treatment and not a result of AMPK directly phosphorylating STK10.

We chose to target kinases with a pan-selective warhead because kinase activity is heavily regulated by phosphorylation, so hypothesised that we had an increased chances of identifying a therapeutically relevant phosphosite. However, follow up experiments examining STK10 phosphorylation was hampered by the high levels of autophosphorylation STK10 displays, even in recombinant mass spectrometry assays.

Our conclusion from phosphoproteomics was that we found far fewer hits than we expected to find, having only found a single protein showing increases phosphorylation on compound treatment. Although there are no reports of mapping the degradation profile of Crizotinib based PROTACs, work using the promiscuous kinase inhibitor Foretinib has been done, and in a proteomics screen where 7,826 proteins were identified a VH298 based PROTAC gave significant degradation of 36 proteins and a Thalidomide based PROTAC resulted in degradation of 62 proteins. This corresponds to 0.46% and 0.0.79% respectively of all proteins detected being degraded. By contrast this work identifies only one

possible hit out of 5,353 proteins which is 0.02% of all proteins detected, a much lower hit rate, even if STK10 phosphorylation could have been confirmed.

The higher pan-selectivity of Foretinib compared to Crizotinib does not completely explain this difference. Testing of Crizotinib and Foretinib in a kinome wide panel of 442 kinases shows Crizotinib binds 67 kinases with a  $K_d \leq 500$  nM and 173 kinases with a  $K_d < 10$   $\mu$ M, and Foretinib binds 163 kinases with a  $K_d \leq 500$  nM and 236 kinases with a  $K_d < 10$   $\mu$ M. Although Foretinib binds more targets more potently, this still doesn't scale to only one hit for Crizotinib and suggests phosphorylation may be more difficult to induce and detect than degradation. We aimed to show how generally applicable PHICS would be to inducing neo-phosphorylation and this work suggests this is not such an easily applicable approach as PROTAC.

It might be that the substrate specificity of AMPK for substrate is much higher than it is for E3 ligases to ubiquitinate neo-substrates. Although PROTACs have an E3 binding moiety, PROTACs actually recruit a large multiprotein complex to induce ubiquitination, and this large complex may confer a level of flexibility that allows ubiquitination more readily in comparison to phosphorylation, whereas perhaps the complex of AMPK and a substrate protein is too small to allow easy phosphate transfer.

In future if using phosphoproteomics to examine neo-phosphorylation, we would enrich cell lysates for kinases to try and identify a greater number of Crizotinib target proteins. This would give an increased number of targets and increase the robustness of the data as abundance would likely be higher and multiple phosphosites for the same protein may be identified increasing confidence that it is a neo-substrate. Enrichment methods could use Kinobeads which contain immobilised kinase ligands that can pull down kinase in washing steps, or test compounds in a cell line with tagged AMPK and then pull down AMPK and analyse associated proteins.

## Chapter 4 RIPK1 introduction

---

Receptor Interacting Kinase I (RIPK1) is a cytoplasmic 76kDa serine/threonine kinase consisting of an N terminal kinase domain, an intermediate linker, then a RIP homotypic interaction motif (RHIM) and Death Domain (DD) domain at the C-terminus. The RHIM and DD domains are instrumental in the scaffolding role of the protein in forming protein complexes.

RIPK1 is a key regulator of the immune response through its downstream roles in cellular stress caused by the pro-inflammatory cytokine Tumour Necroptosis Factor (TNF), and subsequent innate receptors like TNFR1, TLR3 and TLR4. RIPK1 is a key regulatory protein in balancing cell survival, inflammation and cell death.<sup>89</sup> Due to these key roles in cell function RIPK1 is associated with numerous diseases including psoriasis, ulcerative colitis, rheumatoid arthritis and cancer.<sup>90</sup>

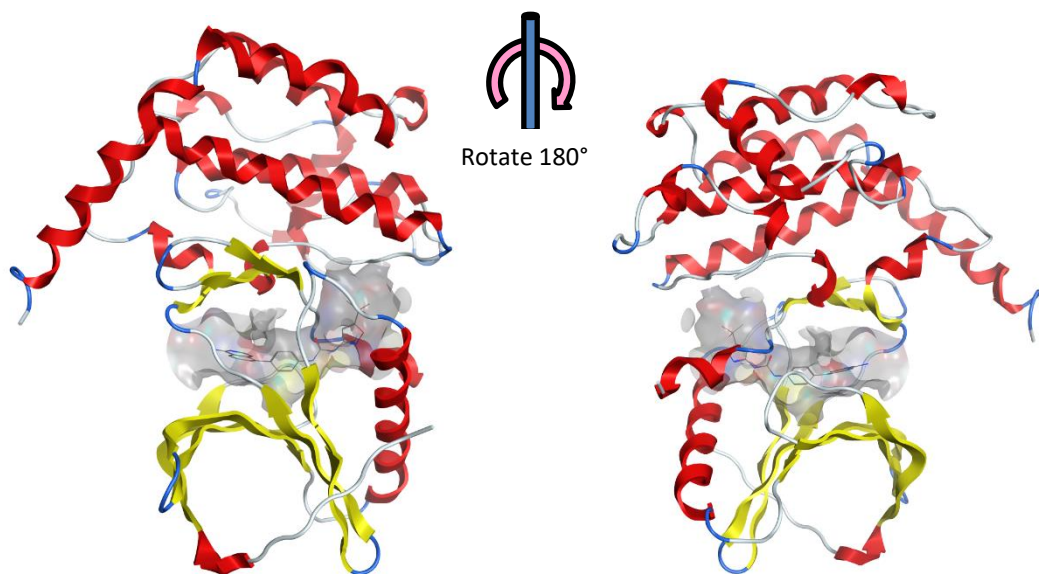


Figure 4.1 - Crystal structure of RIPK1. PDB: 4NEU



#### 4.1 RIPK1 Function in cells

Under normal conditions the binding of TNF to TNFR1 leads to the formation of a multiprotein complex at the cell membrane known as Complex I. The primary role of this complex is to signal through NF- $\kappa$ B which drives cell survival. In this complex RIPK1 is ubiquitinated and phosphorylated at Ser320, which marks it for degradation by Cellular Inhibitors of Apoptosis (cIAPs) and prevents RIPK1 activation respectively. Under these conditions RIPK1 has a scaffolding function, no kinase activity and the cell survives. However, RIPK1 is a positive and negative regulator of cell death and if this signalling is compromised, for example through the loss or inhibition of cIAPs, then Complex II can be formed. Exactly what determines RIPK1 moving from Complex I to II is unclear, but it is hypothesised that reduced ubiquitination or de-ubiquitination of RIPK1 unleashes its potential cell death function.<sup>91</sup> Complex II formation can also be driven through treatment with a cIAP inhibitor such as Tolinapant (ASTX660) or a Second Mitochondria-derived Activator (SMAC) mimetic, which stops RIPK1 degradation.

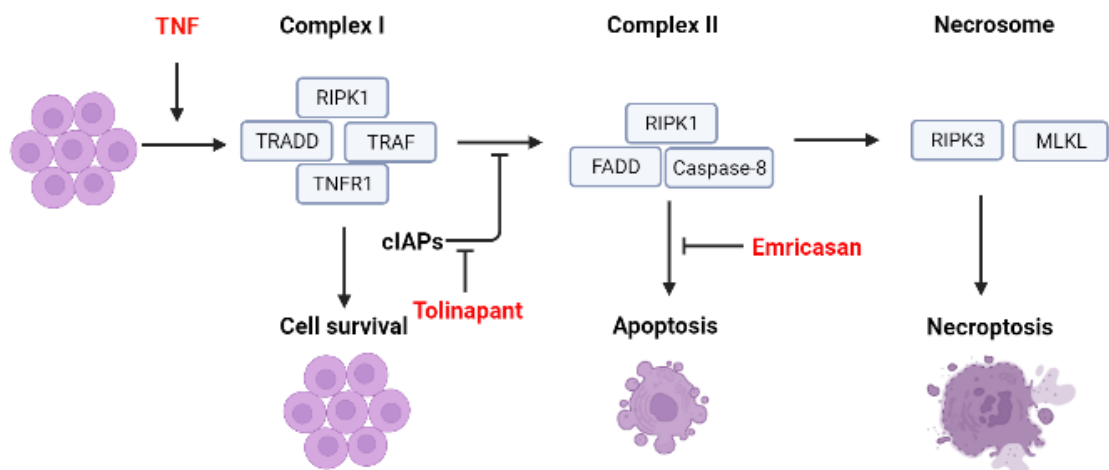


Figure 4.2 - Simplified scheme showing the pathway of RIPK1 in cell survival and cell death

In Complex II, RIPK1 binds to FADD and Caspase-8 which can drive apoptotic cell death. If caspase-8 is absent or inhibited with a small molecule such as Emricasan, then levels of RIPK1 accumulate and this drives the formation of another cytosolic complex, the Necrosome. This complex is a heterodimer between RIPK1 and RIPK3 interacting through their RHIM domains, and this drives RIPK3 activation through auto-phosphorylation. This newly activated RIPK3 then interacts with and drives

MLKL phosphorylation, which then forms oligomers, causing membrane pores and triggering necroptosis, a highly pro-inflammatory form of cell death. Cells rarely undergo necroptosis naturally, and it most typically a response seen after viral infection when cells need to die and be destroyed in an immunogenic way to prevent further infection.<sup>92</sup>

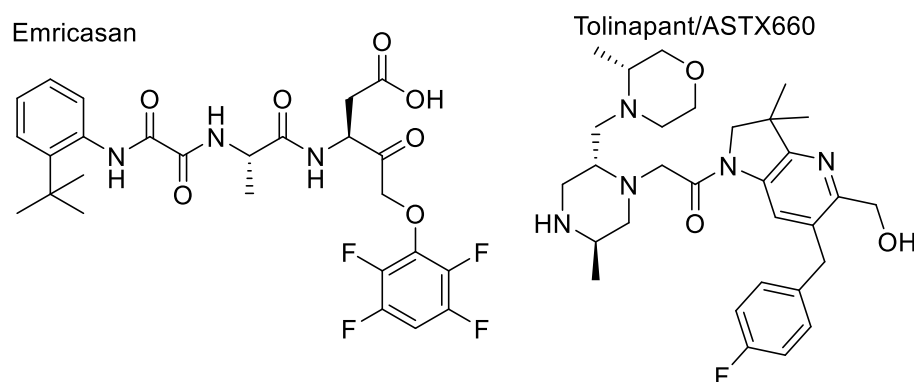


Figure 4.3- Structures of current tools used to alter cell death pathways

In summary, RIPK1 is a regulator of tissue homeostasis controlling cell death pathways downstream of TNFR1 and other innate immune receptors. If signalling is not compromised then RIPK1 promotes cell survival, and contrary a failure of the pathway can lead to RIPK1 driven cell death.<sup>93</sup>

#### 4.2 Role of Phosphorylation in RIPK1 function

Phosphorylation of RIPK1 significantly affects its activity and function in a cell. When driving cell survival, RIPK1 is phosphorylated by Mitogen-activated protein kinase (MK2) at Ser320 and Ser335, which inactivates RIPK1s kinase function and prevents its association with RIPK3. Whereas the auto-phosphorylation at Ser161 and Ser166 are widely reported to increase RIPK1 activity with mutagenesis studies showing a S161A on RIPK1 reduces activity by 20% and the S166A mutation reduces activity by 70%.<sup>94</sup> Additionally, RIPK1 has many sites that are phosphorylated (Figure 4.4) but it is unknown how phosphorylation of many of these sites affect RIPK1s function. As such, chemical tools that could modulate phosphorylation of RIPK1 would be novel and useful.

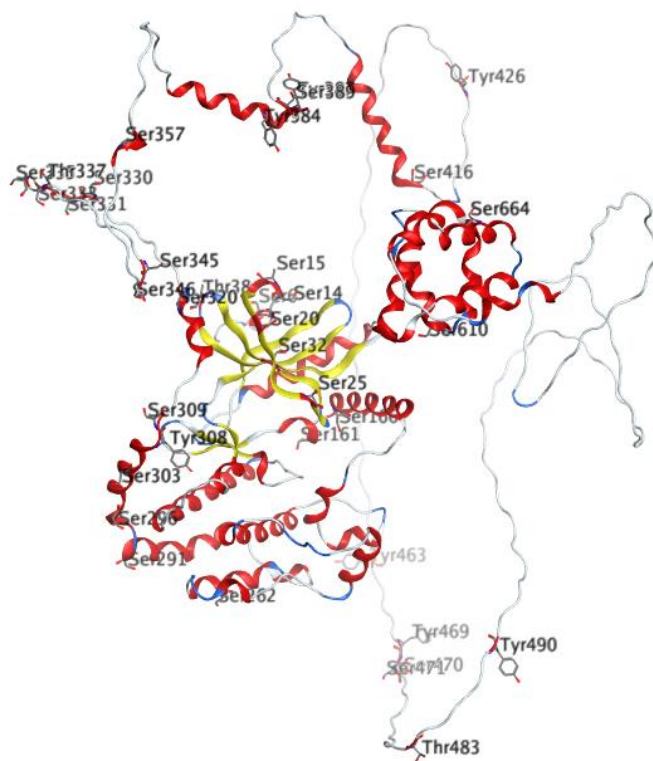


Figure 4.4 - All reported phosphosites of RIPK1. Structure from AlphaFold and sites from phosphosite.com

Additionally, in the context of this project where we want to use bifunctional molecules to induce phosphorylation of a substrate by AMPK, AMPK displays specificity for phosphorylating substrate peptides with the sequences of RXXS, which RIPK1 has for Ser320 (VKRMQSLQLD). As Ser320 is a physiologically relevant phosphosite it represents an attractive target that would modify RIPK1's activity.<sup>6</sup>

### 4.3 RIPK1 inhibitors

Due to RIPK1's role in cell death and inflammation, selective and potent inhibitors have been developed. The first class of compounds were Necrostatins, identified from phenotypic screens that prevented necroptosis.<sup>95</sup> These compounds were found to be Type III kinases, which bind an allosteric pocket, which has been further targeted most notably by GSK to give GSK547 and GSK3145095. The latter has been progressed to clinical trials for pancreatic cancer.<sup>96, 97</sup> Active site inhibitors have also

been discovered, with PK68 representing a very potent and selective Type II inhibitor selective also identified from a phenotypic screen.<sup>96, 98, 99</sup>

When considering what warhead to use in making bifunctional molecules, we needed to consider that most groups, including the Meier group who were performing the biological testing of compounds, frequently use human and murine models. As a result, the bifunctional molecules we made would need to be capable of interacting with hRIPK1 and mRIPK1. For this reason, the most recent RIPK1 clinical candidate GSK'095 with an  $EC_{50} = 10\text{nM}$  in a human cell line, U937, was discounted due to low cellular efficacy in a murine cell line, L929 with an  $EC_{50} = 1.3\mu\text{M}$ , which has prevented its use in rodent oncology models.

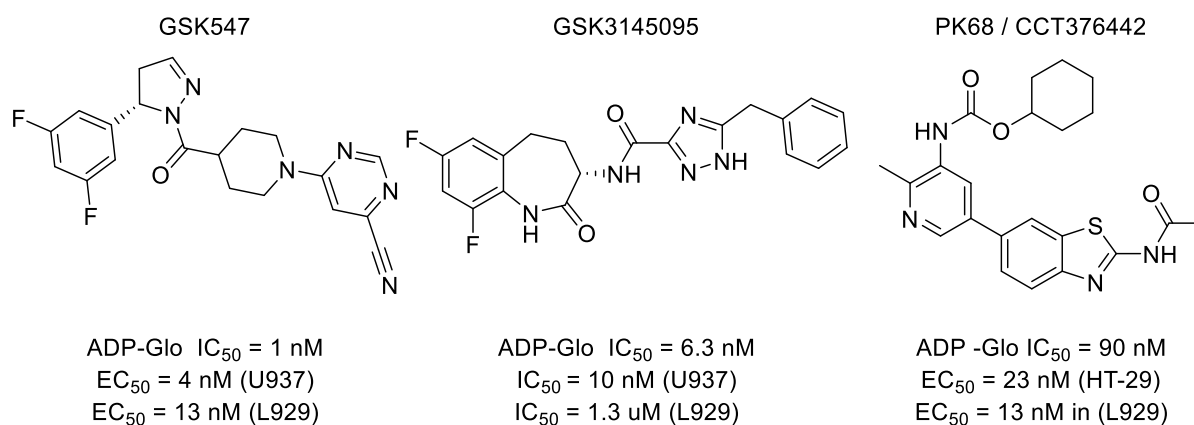
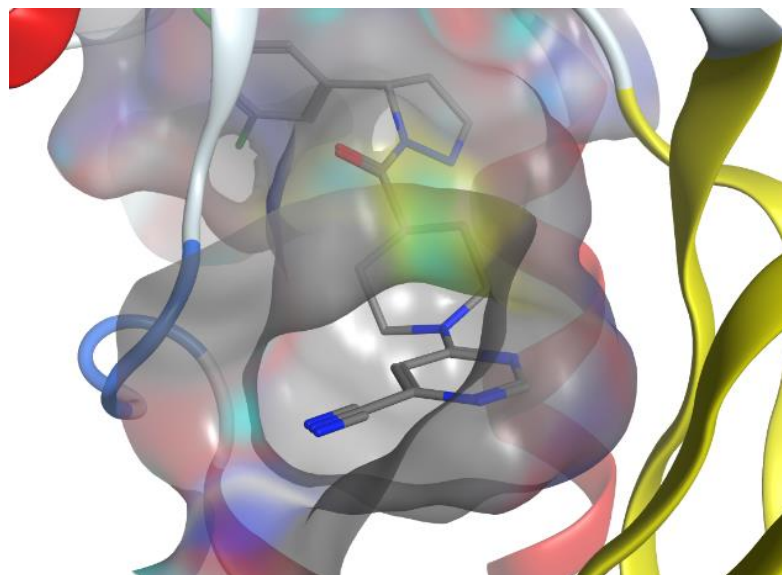


Figure 4.5 - Lead RIPK1 inhibitors and associated biochemical and cellular potencies

When tested in cell viability assays in HT29 cells, a human cell line, PK68 demonstrates an  $EC_{50} = 23\text{nM}$ . GSK547 is also potent in human cell lines,  $EC_{50} = 4\text{nM}$  in U937 cells. In the L929 cell line PK68  $EC_{50} = 13\text{nM}$  and for GSK'547  $EC_{50} = 32\text{nM}$ , so both compounds show good cellular efficacy in human and mouse cell lines. However, the published crystal structure of GSK'547 indicated that the most solvent exposed part of the molecule is the cyano group on the pyrimidine ring (Figure 4.6). However, this nitrile group lies in a fairly tight channel suggesting that linkers would have to be fairly rigid to avoid disrupting binding and that GSK547 may be difficult to link from whilst maintaining binding affinity. Additionally, the partially saturated dihydropyrazole ring was a cause for concern as if oxidised to an

aromatic pyrazole there is complete loss of binding to RIPK1, and the stereochemistry could be difficult requiring chiral separation.



*Figure 4.6 - Published crystal structure of RIP1 kinase in complex with GSK547 (PDB: 6HHO)*

Although there is no published crystal structure of PK68 bound to RIPK1, docking suggests the acetamide on the amino-benzothiazole core of PK68 was solvent exposed as shown in Figure 4.7. Based off this, work in Medicinal Chemistry Team 4 and the Meier group has functionalised from this position to successfully make RIPK1 PROTACs, so it was known this position would tolerate a linker. A key issue in warhead choice is selectivity, as like with a small molecule inhibitor, fewer off targets is generally considered advantageous as it allows a greater understanding of the exact function of the target protein. Although the GSK537 core is reported to have very high selectivity, PK68 is still fairly selective showing binding at >50% inhibition for only five other kinases (TRKA, TRKB, TRKC, TNIK, and LIMK2), when screened in a panel of 369 kinases at 1 $\mu$ M.<sup>96, 98</sup>

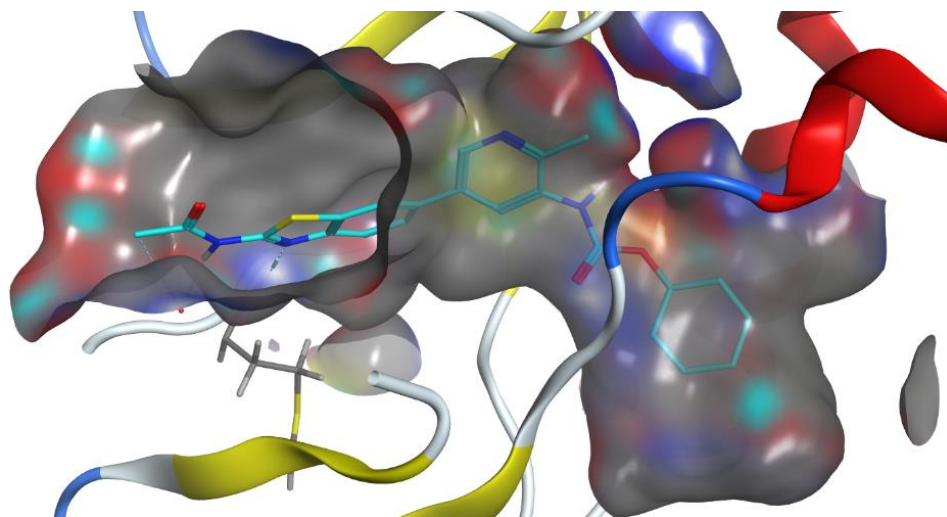


Figure 4.7 - PK68 docked into a crystal structure of RIPK1 using MOE (PDB: 4NEU)

Additionally, one of the issues that we felt was key to driving neo-phosphorylation was using a warhead which is potent enough to form a stable ternary complex. It has been suggested that as an approximate guideline for successfully designing bifunctional molecules, the single ligands should have a <500nM binding affinity to the POI.<sup>28</sup> As PK68 has a <100nM IC<sub>50</sub> in a biochemical assay and cellular assays it put us well below the threshold and represented a solid starting point. Based on work in Medicinal Chemistry 4 targeting RIPK1 with PROTACs, and the collaboration with the Meier group I decided to work on using the PK68 warhead to make bifunctional compounds.

#### 4.4 Synthesis of bifunctional compounds

As mentioned in Chapter 2, the AMPK activators were functionalised with azides so that new target proteins could be investigated by attaching simple alkyne groups to a warhead. Knowing a solvent exposed site on PK68, a route to a series of RIPK1 bifunctional molecules of varying linker lengths was designed that built on the developed click chemistry. As the azide moiety had already been functionalised on AMPK activators, PK68 needed to be functionalised with alkynes, which was done through amide couplings on the 2-amino-benzothiazole, as shown below in Figure 4.8. Due to the poor reactivity of the 2-amino group and poor solubility of PK68,

HATU and DMF were used with long reaction times to achieve moderate to high yields of functionalised alkynes.

PK68

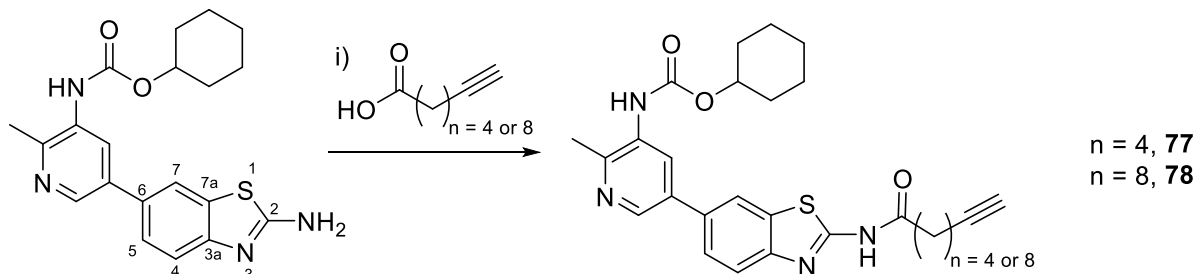


Figure 4.8 - Functionalisation of the 2-amino group to contain alkynes ;) HATU, DMF, 3 days

The alkynes were then used in the optimised click chemistry conditions, keeping DMF as the solvent for solubility. They were reacted with the previously synthesised azide containing AMPK activators based on 991, to give the four 991 based RIPK1 bifunctional molecules.

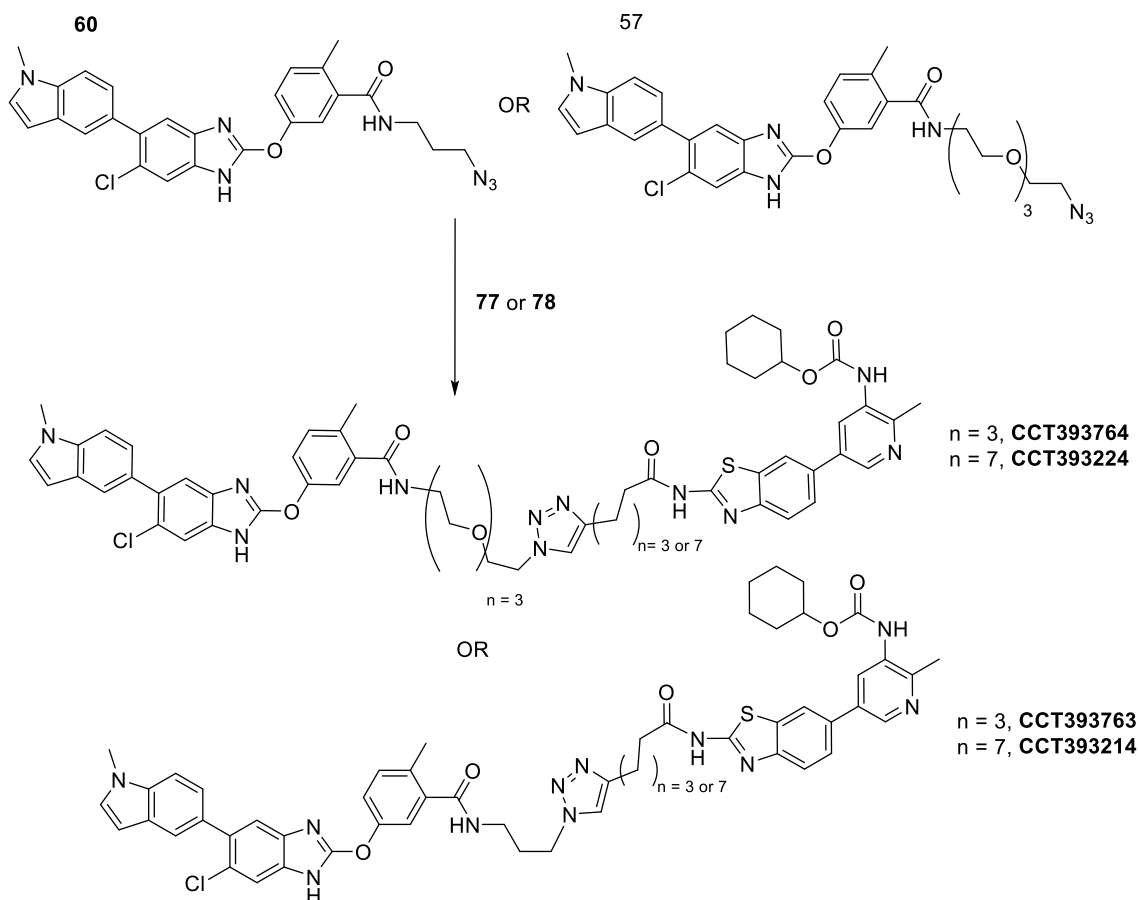


Figure 4.9 - Scheme showing the route to 991 based bifunctional compounds

The same click coupling was done with the 577 AMPK activator analogues, overall giving eight bifunctional compounds with linker lengths from 11 to 23 atoms.

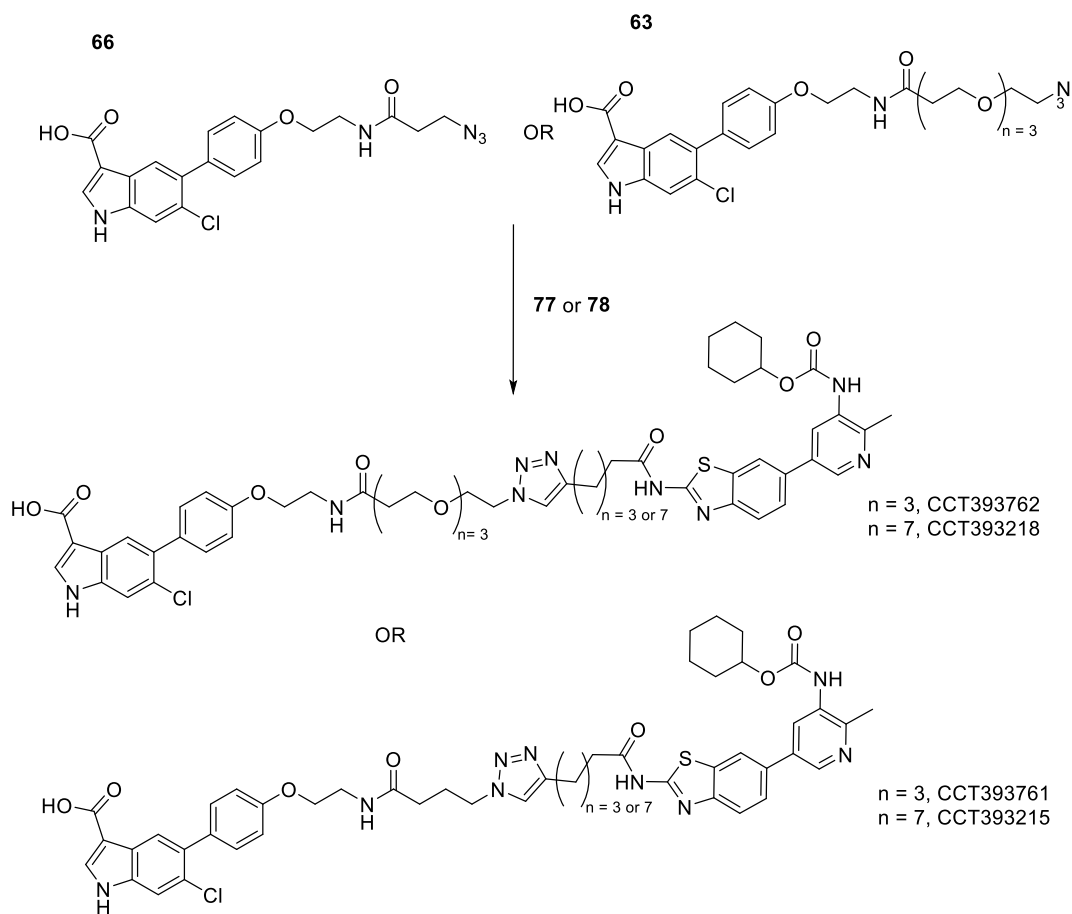


Figure 4.10 - Scheme showing the synthesis of 577 based bifunctional compounds



## 4.5 Cellular testing

### 4.5.1 Measuring RIPK1 Phosphorylation

Having made a small library of bifunctional compounds we needed to test them for inducing neo-phosphorylation. Having struggled with other proteins to obtain unphosphorylated protein in large enough amounts for experimental work we decide to go straight to cellular testing in HT-29 cells. These are a human colon cancer cell line, that are used extremely frequently in studying necroptosis and are known to express RIPK1.

Based on literature precedent of inducing neo-phosphorylation with bifunctional molecules, ternary complex and subsequent phosphorylation has been shown after a 4h treatment with PHICS at a concentration of 5 $\mu$ M. Based on the novelty of this work we decided to replicate the same condition and tested the series of bifunctional compounds at 5 $\mu$ M for 4h in HT-29 cells. Western blots were developed using two phospho-specific antibodies, Ser166 and Ser320. As mentioned Ser320 is a deactivating phosphosite and Ser166 is an activating phosphosite.

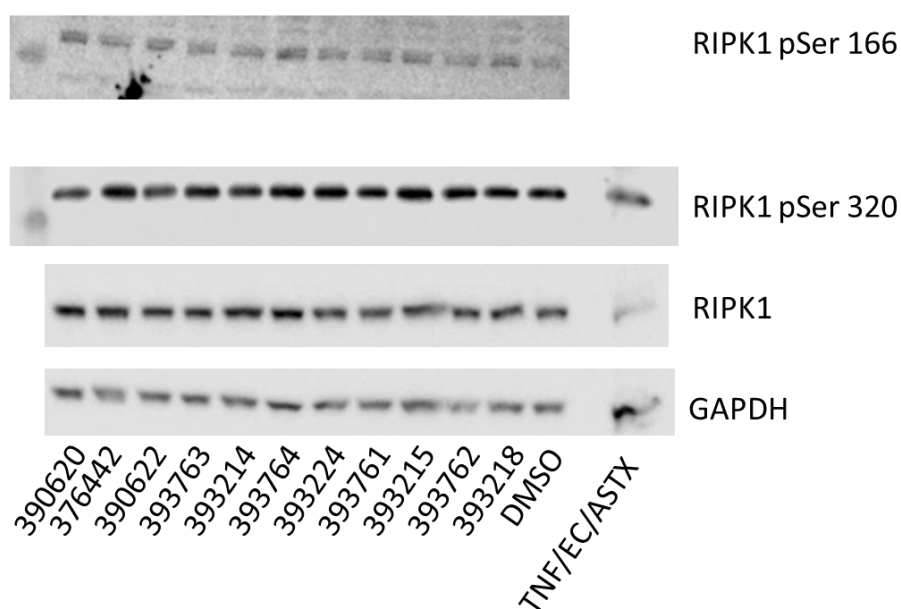


Figure 4.11 - Western blots of HT-29 cells. Treated at 5 $\mu$ M for 4h.

The results in Figure 4.11 show that Ser320, which is in the RXXS AMPK substrate motif, is already phosphorylated at very high levels which shows RIPK1 is still mainly in an inactivated form. Additionally, Ser166 does not have increased phosphorylation after any compound treatment compared to the DMSO control. The positive control of TNF/EC/ASTX gives such a strong signal at Ser166, that it's not been possible to image it on the same western as the compound treatments. It's been reported that at certain sites in certain conditions the RIPK1 band can shift depending on its phosphorylation, but in this case the blots seem to come at a similar level, so suggests no altered phosphorylation.<sup>100</sup>

In summary, none of the bifunctional compounds showed altered phosphorylation of Ser320 or Ser166 on RIPK1 when tested at 5 $\mu$ M for 4h in HT-29 cells. As PK63/CCT376442, showed no change in phosphorylation it is possible that the compounds can bind RIPK1 and AMPK separately in a cell, but do not induce ternary complexes. It was also possible that phosphorylation on other sites on RIPK1 is occurring and we can't detect it, or that RIPK1 is forming a complex with AMPK but the complex is not suitably orientated for phosphorylation to be induced at Ser320 or Ser166.

#### **4.5.2 RIPK1 phenotypic assay**

Given the literature precedent for finding tool compounds targeting RIPK1 in phenotypic screens, we hypothesised that a cell-based viability assay may be more informative as to RIPK1s function and activity in a cell. To test this, the Meier group tested these compounds in an ATP Cell Titre Glo assay, which measures the amount of ATP present in cells, which is used to interpret the number of viable cells so indicates cell survival under different conditions.

As in the previous cell testing, we tested the bifunctional compounds at 5 $\mu$ M for 4h in HT-29 cells which are labelled as 'CCT' in the cell survival graphs, Figure 4.12 to Figure 4.14. Due to the high number of phosphosites on RIPK1 which alter RIPK1 function, we did not know how RIPK1 function would be affected. The bifunctional molecules may phosphorylate and activate RIPK1, phosphorylate and deactivate RIPK1 or just interact with AMPK and RIPK1. To test these multiple hypotheses we

tested compounds on their own, or in one of two combinations. One combination was with Tumour Necrosis Factor (TNF) at 10ng/ml and Emricasan (EC) a caspase inhibitor at 5 $\mu$ M, or TNF (10ng/ml)/ EC (5 $\mu$ M) and Tolinapant (ASTX), a cIAP inhibitor, at 1 $\mu$ M (see Figure 4.3 for chemical structures).

To test if the bifunctional compounds were phosphorylating and activating RIPK1 we used the TNF/EC treatment, which triggers the NF- $\kappa$ B pathway and drives Complex I formation, but as cIAPs still function this leads to cell survival. In fact, activation of NF- $\kappa$ B increases cell survival and so in this treatment cell survival can be >100%. However, we speculated that if bifunctional compounds could activate RIPK1 past a threshold in the TNF/EC treatment then we would see necroptotic cell death. If there was enough activated RIPK1 or it was recruited and protected from ubiquitination then it could form Complex II, and because caspase activity is reduced that would lead to cell death, which would be measured. Simply it removed the checkpoint between Complex II and forming the Necrosome, meaning that activated RIPK1 causes necroptosis.

However, we could not discount that phosphorylation may be occurring in a place that would reduce RIPK1 activation or form a ternary complex that would protect RIPK1 from recruitment into different complexes, and this could reduce cell death. To test this, cells were also treated with TNF/EC/ASTX, with Tolinapant preventing the ubiquitination and subsequent degradation of RIPK1. This triple combination drives high levels of necroptosis, and gives very low cell survival, so any increases in survival would suggest RIPK1 recruitment or deactivation.

As shown in Figure 4.12 and as expected, the single ligand AMPK activators show no different effects to the DMSO control as they are unable to alter RIPK1 activity. Additionally, the RIPK1 inhibitor PK68/CCT376442, shows the expected results with an increase in cell survival on TNF/EC treatment as the kinase function of RIPK1 is blocked and the scaffolding ability remains. The kinase function of RIPK1 is key to driving necroptosis and as PK68 blocks it, in the TNF/EC/ASTX treatment, the cell survival also stays high.

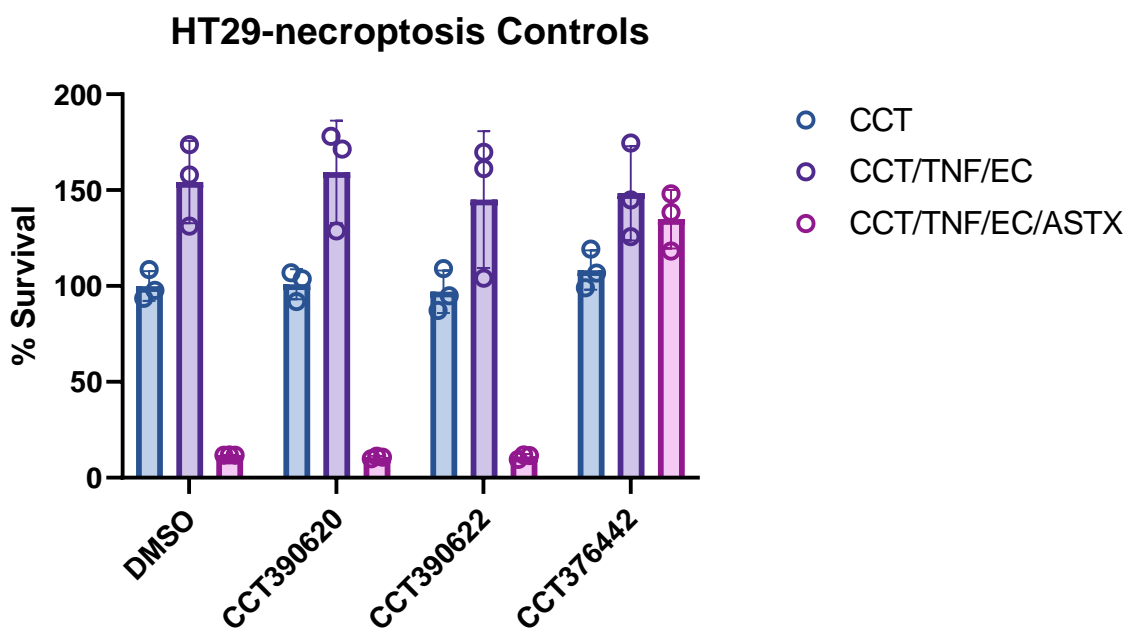
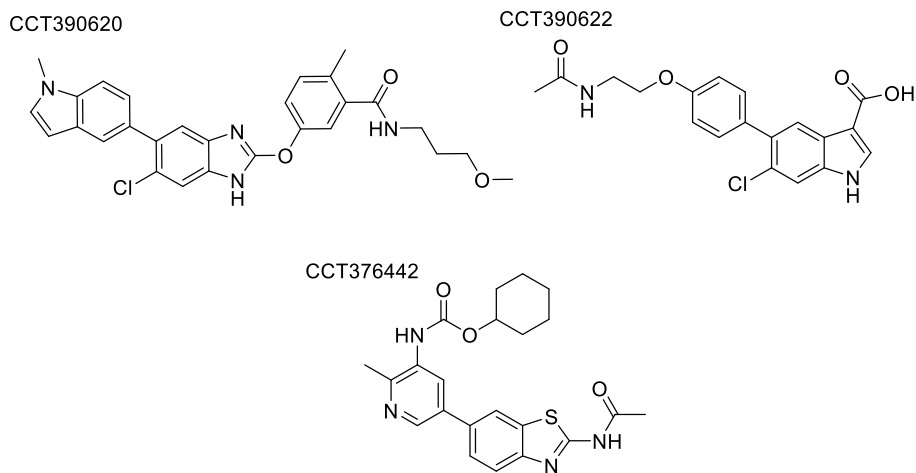


Figure 4.12 - Cell viability graph for the single ligand control molecules and chemical structures

Testing of the “577-series” of bifunctional compounds, shown in Figure 4.13, showed no decrease in cell survival with the TNF/EC treatments compared to DMSO control, suggesting they are not activating RIPK1. In the combination treatment of TNF/EC/ASTX, the bifunctional molecules protect against cell death, as the PK68 warhead maintaining binding to RIPK1, stopping its kinase activity and preventing necroptosis. Whilst disappointing not to see any increased cell death, it at least suggested that the compounds are able to enter cells and engage the target.

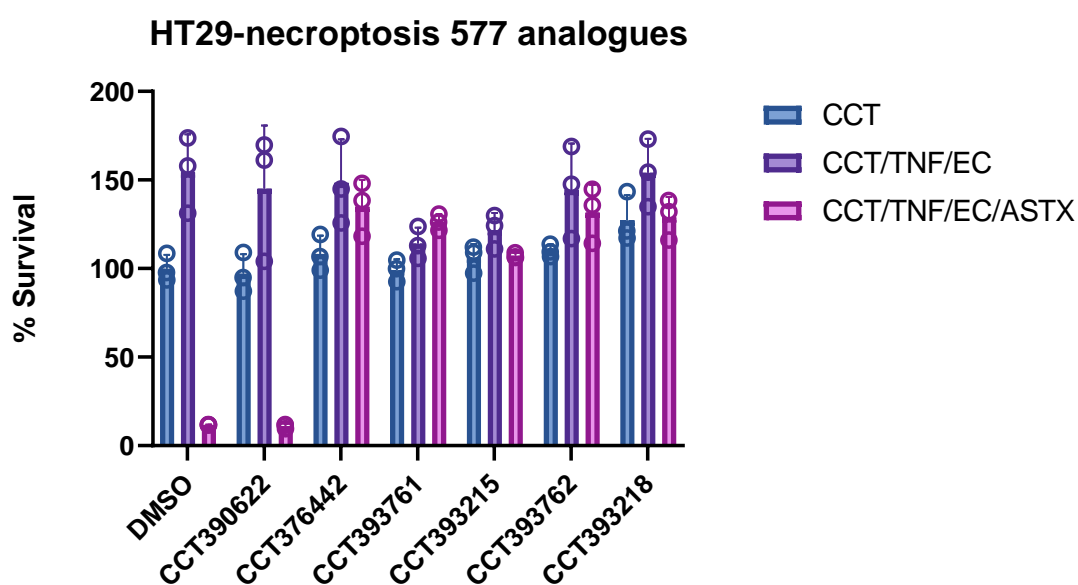


Figure 4.13 - Cell survival graph for the “577-series” of bifunctional

The “991-series” were tested, see Figure 4.14, and again we see no decrease in cell survival in the TNF/EC treatment suggesting RIPK1 is not being activated to drive necroptosis. Having observed the “577-series” protect against necroptosis in the TNF/EC/ASTX treatment a similar trend was expected here. However, in the CCT/TNF/EC/ASTX combination the cell survival is generally quite low suggesting these compounds do not engage RIPK1 so do not stop induced necroptosis. This is likely due to the higher molecular weight of the 991 AMPK warhead over the 577 AMPK warhead which lowers permeability.

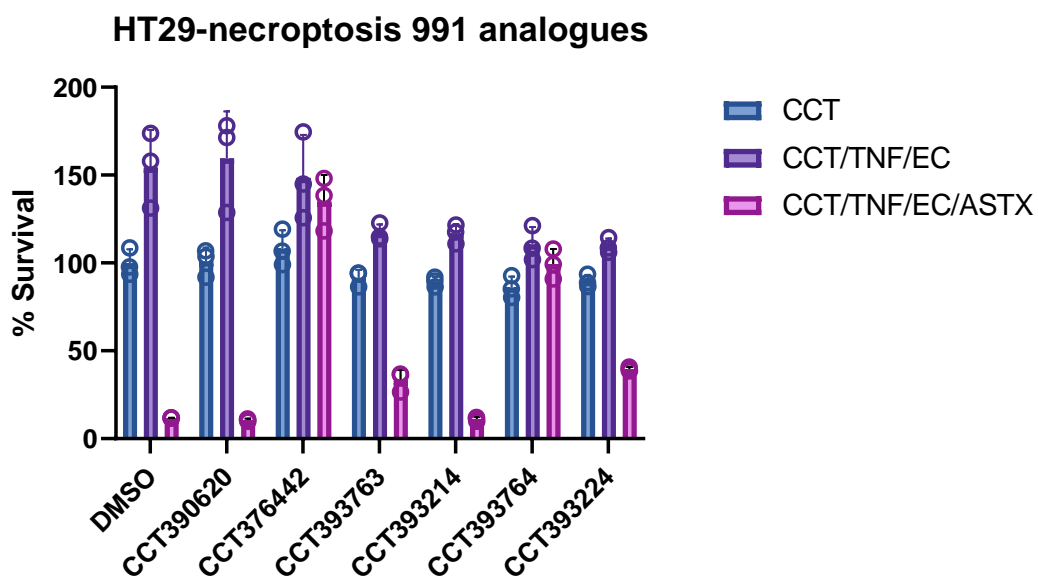


Figure 4.14 - Cell survival graph for the "991-series" of bifunctional compounds

### 4.5.3 Co-Immunoprecipitation

As the aforementioned results are showed no effect we wanted to determine if there was interaction between AMPK and RIPK1. Co-immunoprecipitations (Co-IPs) are a fairly quick and easy way of examining the binding partners of a protein in a cellular environment. Briefly, cells are treated with a compound for a specified time, then lysed. A RIPK1 antibody is added and incubated allowing the protein-antibody complex to form. Beads are added which bind to the RIPK1 antibody, and the RIPK1 is now immobilised on the beads. The beads are washed to remove any non-specific binding proteins then the resulting complexes are denatured and run in a western blot, which can then be probed to show which proteins have been bound to RIPK1

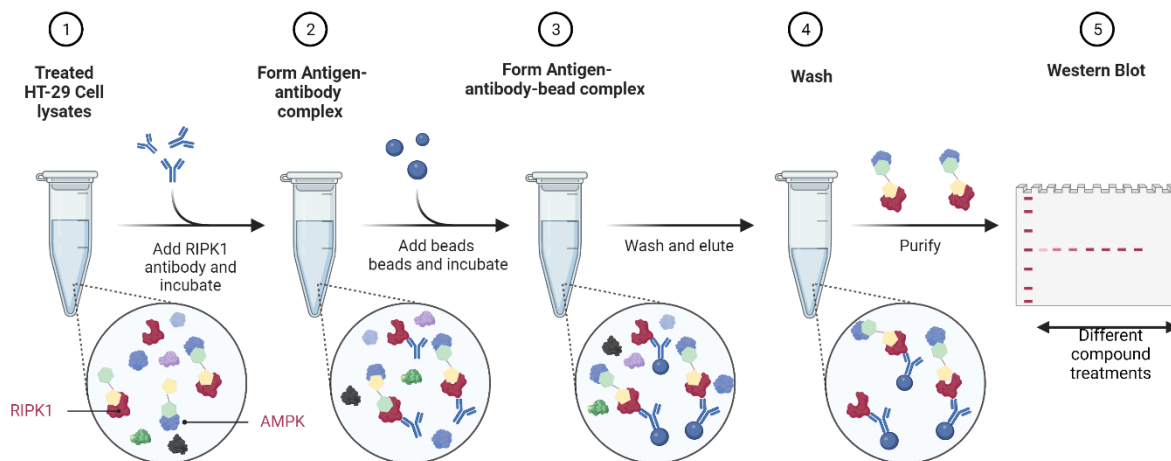


Figure 4.15 - Scheme showing the procedure for a co-Immunoprecipitation

To examine for any ternary complex formation between AMPK and RIPK1 in cells, HT-29 cells were treated with all the synthesised bifunctional compounds and single ligand controls for 4h at 5 $\mu$ M, before being lysed and a co-IP being performed. However, the co-IP of RIPK1, did not show any AMPK being pulled down with RIPK1 (Figure 4.16). As the Meier group frequently perform this co-Immunoprecipitation experiments with RIPK1 to look for associated proteins, the experimental set up is valid and it is more likely that both AMPK and RIPK1 do not associate or that any association is transient and/or has weak affinity.

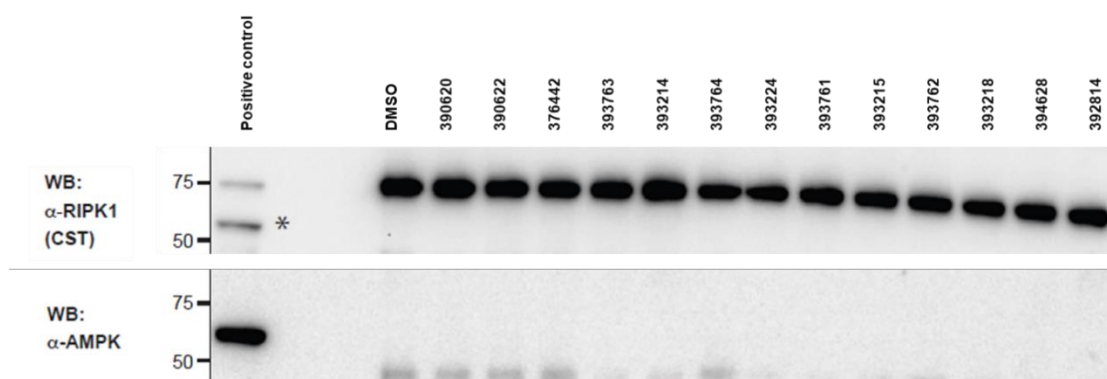


Figure 4.16 - Western blot for the Co-IP experiment

In previous examples of performing co-IP experiments to interrogate the effect of bifunctional molecules, the protein of interest is over-expressed suggesting that it is difficult to show an interaction at endogenous protein expression levels.<sup>36, 37</sup> As such, to further explore if a ternary complex was forming between RIPK1 and AMPK

one of the proteins could be overexpressed, however due to limited time this was not done.

#### **4.6 Conclusion**

From the protection against cell death observed in the cell viability assay it suggests the bifunctional compounds are able to engage with RIPK1 and likely also AMPK in cells, so testing at 4h at 5 $\mu$ M was a good set of conditions to use. However, we saw no increase in phosphorylation of Ser320 or Ser166 in HT-29 cells when examined by western blotting, and no changes in necroptosis when these bifunctional compounds were combined with the necroptotic stimuli TNF/EC or TNF/EC/ASTX, which suggests that the compounds are not forming a ternary complex.

We were not able to show any ternary complex formation through a co-immunoprecipitation technique. This may be because RIPK1 and AMPK have a weak association and the washing conditions are too harsh and the buffer disrupts AMPK and RIPK1 interacting, or possibly that AMPK and RIPK1 do not form a ternary complex in cells.

Both the AMPK and RIPK1 ligand used are fairly potent and below the 500nM cut off for binding affinity so it is unlikely that binding affinity of the bifunctional compounds is too high. Although many chemical tools for investigating necroptosis have been discovered through cellular assays, the disadvantage of this assay format is that it is difficult to interpret why an effect may not be occurring. To investigate this, further work could include a biochemical assay to measure proximity between RIPK1 and AMPK such as SPR or AlphaScreen as described in section 1.13 Biochemical assays for measuring ternary complex formation, as this would measure if the proteins are able to form a ternary complex.



## Chapter 5 Conclusions and Future Directions

---

The aim of this project was to design and synthesise bifunctional molecules that could drive neo-phosphorylation of a substrate protein by inducing a ternary complex with a kinase. A kinase activator and a warhead ligand were identified from literature, with structural information used to identify solvent exposed sites, from which a library of PHICS were made.

The starting point for the project was identifying the AMPK activator **991**, from literature and using structural information to identify solvent exposed sites. Dummy linker containing compounds were synthesised to confirm suitable sites for making bifunctional compounds through testing in an ADP Glo assay. Results are summarised below in Figure 5.1.

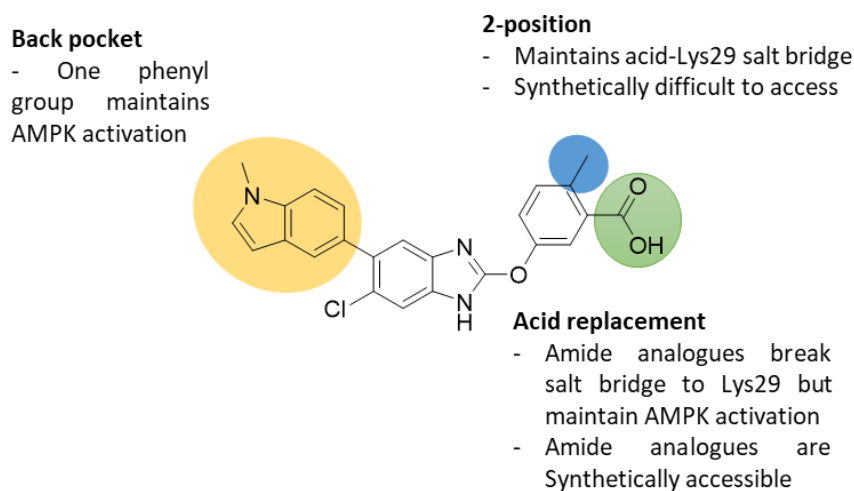


Figure 5.1 - SAR for attaching dummy linkers to 991

The main area of focus for synthesising bifunctional molecules was on the acid replacement group, as the acid was an easy substrate for amide couplings to append linker moieties and maintain AMPK activation.

The first substrate protein we investigated was MLKL with a highly selective and relatively potent ligand sourced from literature. A published crystal structure was used to identify solvent exposed sites, and synthesis of dummy linker containing compounds showed clear preference for linkers at the 5-pyrazine position. This work showed the ester group was key for activity and initially appeared relatively

stable. However, in synthesising bifunctional molecules ester hydrolysis was observed and analogues were poorly soluble. As such we decided to work on another reported hit against MLKL, which was Crizotinib. As an optimised compound with no labile functional groups, Crizotinib removed stability issues and minimised issues with solubility. Additionally docking showed the pyrazole-piperidine of Crizotinib occupied the same solvent exposed vector as the dummy linker at the 5-pyrazine on **1** suggesting the ligand was already solvent exposed. A newly developed LanthaScreen assay showed Crizotinib analogues with dummy linkers on the piperidine were equipotent with Crizotinib.

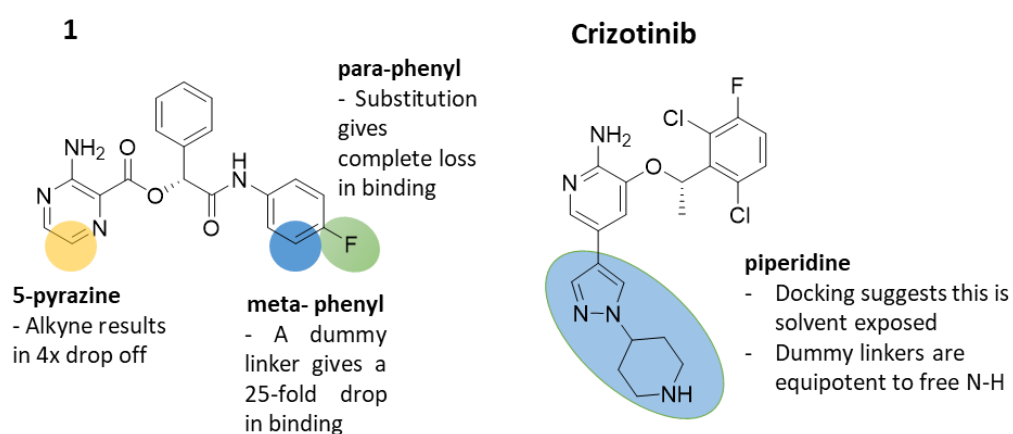


Figure 5.2 - Summarised SAR of compound **1** and crizotinib against MLKL

A library of bifunctional compounds was synthesised but testing *in vitro* and in cells but failed to show any neo-phosphorylation of MLKL. We targeted MLKL as it is a poorly investigated protein as chemical tools altering its function would be novel and the necroptosis pathway has an interesting role cancer. However, the lack of an established assay and poor commercial availability of recombinant MLKL made investigating phosphorylation very challenging. We were able to develop a high throughput assay and contribute to understanding the SAR around MLKL. These insights will be followed up in subsequent project within the team on optimising MLKL binders.

Using the pan selective kinase inhibitor Crizotinib was a deliberate choice to allow us to investigate phosphorylation of other proteins and investigate how generally

applicable PHICS are. As phosphorylation is key in determining kinase activity, we hypothesised targeting kinases would increase the chances of identifying a physiologically relevant phosphosite. We were inspired by the Crews and Fisher groups who used proteomics to map the degradation of PROTACs with promiscuous warheads and so applied a similar approach to this work. Four bifunctional compounds with a Crizotinib warhead were tested in global unbiased phosphoproteomics to look for neo-phosphorylation, from which STK10 was identified as a protein with increased phosphorylation in the presence of CCT391402. Follow up techniques to confirm this effect included an AlphaScreen assay, co-IP and western blots using an AMPK phospho-antibody to identify and quantify phosphosites. However, we were not able to confirm a ternary complex of STK10 and AMPK or show neo-phosphorylation. Follow up biochemical mass spectrometry experiments did suggest increases in phosphorylation of sequences on STK10, suggesting that AMPK and STK10 may form a weakly associated transient complex but this requires further work to fully confirm the mechanism.

It is clear that rationally designed bifunctional molecules have multiple advantages over occupancy-based molecules, with their catalytic function and 'plug and play' methodology making them a versatile tool. Based on the increasing number of PTMs that are able to be directed, the utility of bifunctional compounds as chemical probes and therapeutic agents is only likely to increase.

PROTACs have been proven to work for over a decade and this has resulted in well validated E3 ligands such as thalidomide and VHL298 with well-established solvent exposed sites. Due to the number of PROTACs reported in the literature, the principles around linker design and length are well known and the rapid proliferation in publications around PROTACs demonstrates that this method can be generally applied. Although initial work on PHICS has shown AMPK can be directed to induce phosphorylation of neo substrates, this work suggests the generality of using bifunctional molecules to direct AMPK to induce neo-phosphorylation may be limited. However, with reported PHICS the field is likely to grow rapidly.

A further contrast between PROTAC and PHICS is the relative simplicity of examining protein degradation compared to phosphorylation. In PROTAC methodology the site of ubiquitination is rarely explored, as it is degradation that is of interest not the specific site being modified. It is worth noting that most PROTAC papers do not examine where or what type of ubiquitination has been induced, even though this may play a role in effective degradation. Any resulting degradation can be shown fairly easily with western blots, which whilst semi-quantitative is a robust technique requiring little optimisation, and as antibodies for many proteins are commercially available this technique is broadly applicable. However, when directing neo-phosphorylation, identifying and quantifying the exact phosphosite is of crucial importance, as phosphorylation of different sites can have opposing functions but there very few techniques for showing neo-phosphorylation. In the context of examining STK10 phosphorylation, it may be that phosphorylation is induced but we currently lack the tools to robustly show it. Phospho-specific antibodies are rarely commercially available and often specific for an exact phosphosite.

This issue of needing to identify the exact site that is being phosphorylated is also a limitation in phosphoproteomics as the exact same peptide sequence needs to be detected in all treatments to establish if neo-phosphorylation is occurring. The information on the phosphorylation of one site does not give any information on the phosphorylation of surrounding sites. Whereas in PROTAC when proteomics has been used to look for degradation, if a peptide sequence has reduced abundance, then the entire protein has been degraded. Another advantage of proteomics is that as multiple sequences for a protein are used to confirm degradation the data is more robust and reduces the likelihood of false positives. Many of the current limitations of directing neo-phosphorylation are currently due to limited experimental techniques available to measure phosphorylation. However, with continued work focussed on induced phosphorylation these issues will be resolved in time.

A final question that has yet to be answered in PHICS is what level of neo-phosphorylation is required to achieve a phenotypic effect. As the levels of a

phosphorylated protein are a fraction of total protein level achieving therapeutically relevant levels of phosphorylation may be more difficult than achieving therapeutically relevant levels of degradation. Considering how difficult it is to predict positive or negative cooperativity in PROTAC and modelling ternary complexes, it is unlikely that future work directing phosphorylation will be able to predict and target specific phosphosites from in silico work only. Although there are currently huge advances being made in predicting protein and protein complex structures so this may change, I expect that PHICS with different attachment sites and linker lengths will phosphorylate different sites, and this will have to be determined experimentally.

The field of bifunctional molecules is only likely to expand with the types of PTMs that can be induced, with methylation and glycosylation representing common and therapeutically relevant PTMs yet to be directed by bifunctional molecules. Additionally, the numbers and types of substrates class of bifunctional molecule will increase as more work is published in the field.

Overall, this project identified and characterised the binding of an AMPK activator and identified solvent exposed sites for making PHICS. Work against MLKL resulted in the development of an assay and SAR which will be used in developing small molecule binders of MLKL in future work. A library of bifunctional molecule has been synthesised using an AMPK activator and a Crizotinib warhead and could be used against more established oncology targets such as ALK. Using phosphoproteomics with bifunctional molecules was used to identify STK10 as a hit protein. A variety of biological techniques were used to try and show proximity but were ultimately unsuccessful. Utilising mass spectrometry to monitor phosphorylation of STK10, showed neo-phosphorylation may be induced but requires future work to fully confirm this effect.

## Chapter 6 Experimental

---

### 6.1 AMPK activity assay

The assay was performed in ProxiPlate-384 Plus (PerkinElmer, 6008280), Plating used the Echo ECHO®550 acoustic dispenser to dispense a range of volumes from 10mM, 0.10mM and 1nM stock solutions (100% DMSO). The wells were backfilled with DMSO to 100nL Control wells of 100nL DMSO were made for 1% (v/v) of DMSO in all wells. A control dose response using AMPK (A2/G1/B1, V4014, Promega) was performed. AMPK was diluted in assay buffer of 40 mM Tris pH 7.5, 20 mM MgCl<sub>2</sub>, 0.1 BSA and 50 μM DTT. 1μL of SAMStide (HMRSAMSGHLVKKRR, 1mg/mL) was added. Then ultra-pure ATP (V915, Promega) was added to achieve an assay concentration of 150μM.

The plate was incubated for 30 mins at room temperature, then 5μL ADP-Glo reagent (V912B) was added, centrifuged (1 min, 1000 rpm), then incubated for 40 mins. In the dark 10μL Kinase Detection Reagent (V9102) was added, and the plate sealed with a top seal, centrifuged (1 min, 1000 rpm) and incubated at room temperature in the dark. After 40 mins Luminescence was measured on Envision multilabel plate reader using Protocol: US Luminescence 384. EC<sub>50</sub> values and activation values were calculated using GraphPad Prism 8.1.0 using non-linear fit, variable slope of log(agonist) vs. response.

### 6.2 MLKL LanthaScreen Binding Assay

MLKL was provided by the Murphy group, N-terminal GST - Streptavidin binding peptide - hMLKL, 200mM NaCl, 20mM HEPES pH 7.5, 5% v/v glycerol. Expressed in Sf21 insect cells.

The assay was performed in ProxiPlate-384 Plus (PerkinElmer, 6008280), containing MLKL (5nM), LanthaScreen™ Eu-anti-GST Antibody (2nM, PV5595, Thermo Fisher Scientific and Kinase Tracer 222 (62.5 nM, PV6121 Thermo Fisher Scientific), components were added in the order listed and between each addition the plate was spun at 1000 rpm for 1 min. Assay buffer (50 mM HEPES pH 7.5, 10 mM MgCl<sub>2</sub>,

1 mM EGTA, 1 mM DTT and 0.01% (w/v) Brij-35) and all wells contain 2% (v/v) DMSO.

The plate was incubated for 1h at room temperature then read on Envision multilabel plate reader using a LanthaScreen aperture to record the acceptor/tracer emission (665 nM) and the antibody/donor emission (615 nM). IC<sub>50</sub> values were determined using a non-linear regression fit of the log(inhibitor concentration) versus emission ratio with variable slope equation.

### **6.3 AlphaScreen Assay**

The Echo was used to plate out compounds with 1% (v/v) into a ProxiPlate-384 Plus (PerkinElmer, 6008280). AMPK (V4014, Promega) was diluted to 120nM in reaction buffer (50 mM HEPES pH 7.5, 100mM NaCl, 10mM MgCl<sub>2</sub>, 0.01% BSA and 1% Tween-20 (v/v)). STK10 (SignalChem S29-11G-10) was diluted to 40nM in reaction buffer. Ni Chelate Donor beads (Perkin Elmer, 5mg/mL, AS101D) and the Anti-GST AlphaLISA Acceptor beads (Perkin Elmer, 5mg/mL, AL110C), were diluted separately to 80µg/µL for an assay concentration of 20µg/µL.

3µL of each component was added with the plate spun (1 min, 1000 rpm) between each addition. The was sealed and incubated at room temperature in the dark. The plate was then read after 2h, 4h and other times as specified, using the Envision multilabel plate reader with the AlphaScreen HTS method with the 384-A1 aperture.

### **6.4 Western Blotting**

All Westerns blots used HEK293T, or HT-29 cells that were incubated at 37 °C with 5% CO<sub>2</sub> in Dulbecco's Modified Eagle's medium. 250,000 cells were plated in each well of a 6 well plate in 2 ml DME media and treated with the indicated compound and doses for the specified time. Media was then aspirated, and cells were washed with ice cold PBS then lysed using 150µL of D0.4 lysis buffer (20 mM HEPES pH 7.5, 10% Glycerol, 0.4 M KCl, 0.4% Triton X-100, 15 mM EDTA) containing 1X protease inhibitor (cOmplete™, Mini, EDTA-free Protease Inhibitor Cocktail, Sigma,

4693159001, diluted from 30x stock made up in water) + 1X phosphatase inhibitors (PhosSTOP, Sigma, 4906845001, diluted from 30x stock made up in water). Cells were centrifuged at maximum speed for 5 minutes at 4°C, then the supernatant was transferred to a fresh ice-cold Eppendorf. A stock solution of BSA in water was made up at 10 mg/ml. 5 1:1 dilutions were made up from this (5, 2.5, 1.25, 0.625, 0.3125 mg/ml). 1ul of each stock solution starting at 5mg/ml, and 1l of each supernatant sample, were plated out into a 96 well plate, in duplicate. 200ul 1x Protein Assay Dye Reagent Concentrate (Bio-Rad, #5000006) was added to each well, plus duplicate blank samples. Absorbance at 590nm was measured, a line of best fit calculated, and the concentration of protein in each sample determined. NuPAGE LDS Sample buffer (Thermo, NP0008) and NuPAGE Sample Reducing Agent (Thermofisher, NP0009) were added at 1x final concentration and samples heated for 5 mins at 90°C. NuPAGE 4-12% Bis-Tris gels, 1.5mm (15 wells) were used for all Western blots. Gels were clipped into XCell SureLock™ Mini-Cell Electrophoresis System tanks and 1X NuPAGE MOPS running buffer was added. Sample was added to relevant lanes, with 10µl of SeeBlue™ Plus2 Pre-stained Protein Standard (Thermofisher, LC5925) as a marker. Equal protein levels were added to all wells then run at 150V for 90 mins. Gel was taken out, and top and bottom cut off. A square of Immobilon-P PVDF Membrane (Millipore, IPVH00010) was equilibrated in MeOH. Stack was assembled by equilibrating all components in 1X NuPAGE Transfer Buffer (Thermofisher, NP00061). Each stack consists of one sponge, two squares of Whatman paper, membrane, gel, two squares of Whatman paper and a sponge. Protein was transferred in Mini Trans-Blot® Cell (Bio-Rad, 1703930) at 100V for 90 mins. Membrane was blocked for at least 30 mins in 5% BSA/TBS/0.05% TWEEN 20 (TBST). Antibody was added at desired concentration in either 5% BSA/TBST, and incubated overnight at 4°C. Antibodies used are: RIPK1 (Cell Signalling technology, D94C12, 1:1000 dilution), Phospho-RIPK1 (Ser166, CST, D813A, 1:1000 dilution), Phospho-RIPK1 (Ser320, E2R3N, 1:1000 dilution), AMPKα (D63G4, 1:1000 Dilution), STK10 (Abcam, ab70484, 1:1000 Dilution), GAPDH (CST, D4C6R, 1:5000), Phospho-MLKL (Ser345, CST ,D6E3G, 1:1000), AMPK Substrate Motif [LXRX(pS/pT) antibody (CST, 5759, 1:1000 dilution) in 5% BSA/TBST.



Blots were then washed 3 x 5 mins in TBST. A secondary antibody was added at 1:5000 in 5% milk/TBST and incubated on a rocker for 1h at room temperature. Secondary antibodies were Bio-Rad Goat Anti-Rabbit IgG (H+L)-HRP Conjugate #1706515 or Bio-Rad Goat Anti-Mouse IgG (H+L)-HRP Conjugate #1706516. Blots were then washed 3 x 5 mins in TBST and developed using Pierce™ ECL Western Blotting Substrate (ThermoFisher, 32106) or Immobilon Western Chemiluminescent HRP Substrate (Millipore), with the latter being high sensitivity. Blots were exposed and imaged using the LI-COR.

## **6.5 Phosphoproteomic analysis**

Phosphoproteomics used HEK293T cells of which 1,500,000 cells were plated into Nunc™ EasYDish™ Dishes (ThermoFisher, 150468) and incubated at 37 °C with 5% CO<sub>2</sub> in Dulbecco's Modified Eagle's medium for 48 hours. Cells were then treated with compounds at the specified concentration for the started time period. After which the media was aspirated, and cells were washed with ice cold PBS then scraped with 200µL ice cold PBS, and transferred to an ice cold Eppendorf. Cell suspensions were then centrifuged at maximum speed for 5 minutes at 4°C. Supernatant was then aspirated and the cell pellets snap frozen and sent to the ICR Proteomics core Facility for cell lysis and analysis.

Following work was carried out by Dr Theo Roumeliotis

## **6.6 Sample preparation for phosphoproteomic analysis**

Cell pellets were lysed in 150 µL lysis buffer containing 100 mM triethylammonium bicarbonate (TEAB), 1% sodium deoxycholate (SDC), 10% isopropanol, 50 mM NaCl and Halt protease and phosphatase inhibitor cocktail (100X) (Thermo, #78442) on ice, with 15 sec of pulsed probe sonication followed by heating at 90 °C for 5 min and sonication for another 5 sec. Protein concentration was measured with the Quick Start Bradford protein assay (Bio-Rad) according to manufacturer's instructions. Protein aliquots of 60 µg were reduced with 5 mM tris-2-carboxyethyl phosphine (TCEP) for 1 h at 60 °C and alkylated with 10 mM iodoacetamide (IAA) for 30 min in the dark. Proteins were digested overnight with trypsin at a final

concentration of 75 ng/ $\mu$ L (Pierce). Peptides were labelled with the TMTpro-16plex reagents (Thermo) according to manufacturer's instructions. The pooled sample was acidified with 1% formic acid, the precipitated SDC was removed by centrifugation and the supernatant was SpeedVac dried. Samples with recombinant proteins were adjusted to 100 mM TEAB, reduced, alkylated, trypsin digested and TMTpro-18plex labelled as above.

### **6.7 High-pH Reversed-Phase peptide fractionation and phosphopeptide enrichment**

For the total phosphoproteome analysis, high-pH Reversed-Phase (RP) chromatography was performed using the XBridge C18 column (2.1 x 150 mm, 3.5  $\mu$ m, Waters) on a Dionex UltiMate 3000 HPLC system. Mobile phase A was 0.1% (v/v) ammonium hydroxide and mobile phase B was acetonitrile, 0.1% (v/v) ammonium hydroxide. The TMTpro labelled peptides were fractionated at 0.2 mL/min with the following gradient: 5 minutes at 5% B, up to 12% B in 3 min, for 32 min gradient to 35% B, gradient to 80% B in 5 min, isocratic for 5 minutes and re-equilibration to 5% B. Fractions were collected every 42 sec, combined into 30 fractions and SpeedVac dried.

Phosphopeptide enrichment was performed in the first 20 peptide fractions with the High-Select Fe-NTA Phosphopeptide Enrichment Kit (Thermo) using a modified protocol in a well plate tip-array format. A volume of 50  $\mu$ L resin/buffer was transferred on top of 10  $\mu$ L filter tips that were fitted on a 96-well plate using a tip rack. The resin was washed three times with 40  $\mu$ L wash/binding solution and centrifugation at 500 g for 1 min. Peptides were reconstituted in 30  $\mu$ L wash/binding solution and loaded onto the tip-columns with the resin. After 30 min, the resin was washed three times with wash/binding solution and the flow-throughs were collected in a clean 96-well plate with centrifugation at 500 g for 1 min each time. Phosphopeptides were eluted twice with 40  $\mu$ L elution buffer in a clean 96-well plate with centrifugation at 500 g for 1 min, transferred in glass vials (Waters, P/N 186005669CV) and SpeedVac dried. Phosphopeptide enrichment for the digested and TMTpro labelled recombinant protein samples was performed

with the High-Select Fe-NTA Phosphopeptide Enrichment Kit (Thermo) following the manufacturer's instructions.

## **6.8 LC-MS analysis**

LC-MS analysis was performed on a Dionex UltiMate 3000 UHPLC system coupled with the Orbitrap Lumos Mass Spectrometer (Thermo Scientific). Peptides were loaded onto the Acclaim PepMap 100, 100  $\mu\text{m} \times 2 \text{ cm}$  C18, 5  $\mu\text{m}$ , trapping column at flow rate 10  $\mu\text{L}/\text{min}$  and analysed with an Acclaim PepMap (75  $\mu\text{m} \times 50 \text{ cm}$ , 2  $\mu\text{m}$ , 100  $\text{\AA}$ ) C18 capillary column. Mobile phase A was 0.1% formic acid and mobile phase B was 80% acetonitrile, 0.1% formic acid. For the phosphopeptide analysis, the separation method was: for 60 min gradient 5%-38% B, for 10 min up to 95% B, for 5 min isocratic at 95% B, re-equilibration to 5% B in 5 min, for 10 min isocratic at 5% B at flow rate 300 nL/min. MS scans were acquired in the range of 375-1,500 m/z with mass resolution of 120,000, AGC  $4 \times 10^5$  and max IT 50 ms. Precursors were selected with the top speed mode in 3 sec cycles and isolated for HCD fragmentation with quadrupole isolation width 0.7 or 0.9 Th. Collision energy was 36% with AGC  $1 \times 10^5$  and max IT 100 ms at 50K resolution. Targeted precursors were dynamically excluded for further fragmentation for 30 seconds with 7 ppm mass tolerance. For the flow-through analysis from the recombinant protein samples, a 95 min gradient 5%-38% B was used, HCD spectra were acquired at 30K resolution with 45 sec dynamic exclusion.

## **6.9 Database search and quantification**

The mass spectra were analysed in Proteome Discoverer 2.4 (Thermo Scientific) with the SequestHT search engine for peptide identification and quantification. The precursor and fragment ion mass tolerances were 20 ppm and 0.02 Da respectively. Spectra were searched for fully tryptic peptides with maximum 2 missed-cleavages. TMTpro at N-terminus/K and Carbamidomethyl at C were selected as static modifications. Oxidation of M, Deamidation of N/Q and Phosphorylation of S/T/Y were selected as dynamic modifications. Spectra were searched against reviewed UniProt Homo Sapiens protein entries, peptide confidence was estimated with the

Percolator node and peptides were filtered at q-value<0.01 based on decoy database search. The reporter ion quantifier node included a TMTpro quantification method with an integration window tolerance of 15 ppm. Only peptides with average reporter signal-to-noise>3 were used and phosphorylation localization probabilities were estimated with the IMP-ptmRS node.

## 6.10 Cloning and transfection FLAG-STK10

Plasmid was supplied by Jon Elkins, University of Oxford. Cloning procedure was performed by Dr Daniel Miller as follows:

STK10 was PCR amplified from a STK10 expression plasmid using the following primers and Phusion High-Fidelity DNA Polymerase (NEB), following manufacturer's instructions. Primers were designed to add an N-terminal NheI restriction site and

NheI-FLAG-STK10 F	ATATGCTAGCATGGACTACAAGGACGACGATGACAAGgcttttgccaatttccg ccg
STK10-NotI R	ATATGCGGCCGCttaagaagcatccgcagaac

FLAG tag, and a C-terminal NotI site.

PCR product was gel purified, and then digested with NheI-HF (NEB) and NotI-HF (NEB) in CutSmart Buffer (NEB) for 2h at 37°C, before purification using Qiagen PCR Purification kit. pcDNA3.1-Hygro(+) was digested with NheI-HF (NEB) and NotI-HF (NEB) in CutSmart Buffer (NEB) for 2h at 37°C, with CIP (NEB) added for the final hour, before gel purification. Digested PCR product was ligated into digested plasmid at a 3:1 molar ratio using T4 DNA ligase (NEB) and following manufacturer's instructions. Ligated plasmid was transformed into NEB 5-alpha competent bacteria and selected with Ampicillin. Successful cloning of FLAG-STK10 was confirmed by Sanger sequencing.

Transfection was performed by myself or Dr Daniel Miller:

1,500,000 cells were plated into Nunc™ EasYDish™ Dishes (Thermofisher, 150468) and incubated at 37 °C with 5% CO<sub>2</sub> in Dulbecco's Modified Eagle's medium for 24 hours. To each plate was added 4µg of STK10-FLAG plasmid, 800µL DMEM and 20µL Lipofectamine™ 2000 Transfection Reagent (Thermofisher, 11668500). As a control 800µL DMEM and 20µL Lipofectamine™ 2000 Transfection Reagent (Thermofisher, 11668500) was added to one cell plate, which was treated with DMSO when the other plates were treated with compounds. Compounds were added for the specified time and concentration, the media aspirated and the cells washed with 1 x 2mL ice cold PBS, then lysed with 600µL lysis buffer and analysed via Western blotting as described in 6.4.

### **6.11 FLAG Pull down**

Anti-FLAG M2 Magnetic Beads (Millipore M8823) were used in the Immunoprecipitation experiments. 1,500,000 cells were plated into Nunc™ EasYDish™ Dishes (Thermofisher, 150468) and incubated at 37 °C with 5% CO<sub>2</sub> in Dulbecco's Modified Eagle's medium for 48 hours. Compounds were added for the specified time and concentration, the media aspirated and the cells washed with 1 x 2mL ice cold PBS, then lysed with 600µL lysis buffer (50mM Tris HCl, 120mM NaCl, 1mM EDTA and 1% Triton containing 1X protease inhibitor (cOmplete™, Mini, EDTA-free Protease Inhibitor Cocktail, Sigma, 4693159001, diluted from 30x stock made up in water) + 1X phosphatase inhibitors (PhosSTOP, Sigma, 4906845001, diluted from 30x stock made up in water)). An input sample was removed and then remaining amount incubated with equilibrated beads. Beads were equilibrated by taking 260µL of beads and suspending in 1.2 mL TBS and shaken. Beads were then washed 2 x 1.2 mL TBS then taken up in 650uL TBS. Then 100uL was added to each cell lysate. Mixture slowly rocked overnight at 4C. Beads were washed 3 x 1mL ice cold TBS then 20uL of 1X NuPAGE LDS Sample buffer (Thermo, NP0008) was added to each Eppendorf. Each sample was then heated at 90°C for 5 mins, then analysed via Western blots as previously described.

### **6.12 ATP-Cell titre Glo**

Experiments were carried out by Laura Ramos Garcia ot Tencho Tenev as specified.

Assay were carried out as per manufacturer's instructions in a 96-well plate. 10,000 HT-29 cells were plated per well. Compounds were added at the specified concentration and for the specified time before, 20uL CellTitre-Glo reagent (Promega, G7558) was added. After 10 mins Luminescence was recorded and normalised to a DMSO control.

### **6.13 STK10 Expression**

The DNA Plasmid was supplied by Jon Elkins, University of Oxford. Expression was carried out by Craig McAndrew at the Institute of cancer research as reported in literature.<sup>81</sup>

The plasmid was cloned into a baculovirus transfer vector (pFB-Bio5) that which adds a N-terminal TEV protease sequence and a His tag and a promotor region. E Coli were used to prepare the bacmid which was used to transfect insect Sf9 cells. After expression the protein was purified through HiTrap TALON® crude 5mL column. Purified fractions were treated with TEV protease (TEV:Protein 1:50) and 500µL Lambda phosphatase, then purified via Superdex 200, then reverse Talon crude 5mL. Fractions concentrated to give 9.5 mg of STK10 at a concentration of 2.23 mg/mL

### **6.14 Measuring phosphorylation in vitro**

AMPK (A2/G1/B1, V4014, Promega) at 20nM and STK10 (expressed in house) at 700 nM were combined together with ultra-pure ATP (V915, Promega) at 150µM. Compounds were added at the specified concentration and the reaction was incubated at room temperature for the specified time. The reaction was quenched through addition of PAGE LDS Sample buffer (Thermo, NP0008) and NuPAGE Sample Reducing Agent (Thermofisher, NP0009) at 1x final concentration which were analysed via Western blots as described.

### **6.15 Recombinant Mass spectrometry assay**

Assay buffer used was 50 mM HEPES pH 7.5, 100mM NaCl, 10mM MgCl<sub>2</sub> and 0.01% BSA. STK10 (expressed in house) was where applicable combined with AMPK (A2/G1/B1, V4014, Promega) at 20nM.

Where applicable the Lambda Protein Phosphatase (New England BioLabs, P0753L) was utilised as per manufacturers instructions. As applicable compounds were tested at the desired concentration for 2h, or DMSO was added to give 2% DMSO (v/v). Where required ultra-pure ATP (V915, Promega) was added to achieve an assay concentration of 150µM.

Samples were then snap frozen and sent to the Proteomics Core facility, when they were as per the sample preparation for phosphoproteomic analysis and LC-MS as previously described.

## **6.16 In silico**

Docking, modelling and Images were performed using MOE 2020.09

Moka 3 was used for cLogP calculations

## **6.17 Chemistry**

### **6.17.1 General Experimental**

All anhydrous solvents and reagents were obtained from commercial suppliers (Acros, Alfa Aesar, Apollo, Fisher Scientific, Fluorochem, Sigma Aldrich, Thermo Scientific and VWR) and used without further purification.

Analytical thin layer chromatography (TLC) was performed on pre-coated aluminium sheets (60 F<sub>245</sub> nm, Merck) and visualised by short-wave UV light. Semi-automated flash column chromatography was carried out using a Biotage SP4 purification system, using Biotage SNAP KP-Si cartridges. Melting points were determined on a Stanford Research EZ-melt apparatus and are uncorrected. IR analyses were carried out on a Bruker Alpha-P FT-IR spectrometer and absorptions are specified in wavenumbers (cm<sup>-1</sup>).

$^1\text{H}$  NMR spectra were recorded on a Bruker AMX 500 (500 MHz) spectrometer or at 600 MHz on a Bruker Avance NEO 600 (MHz 600) spectrometer equipped with a 5 mm TCI-Cryo probe using an internal deuterium lock. Chemical shifts were measured in parts per million (ppm) relative to tetramethylsilane ( $\delta = 0$ ) using the following residual solvent signals:  $\text{CDCl}_3$  ( $\delta_{\text{H}}$  7.26) and  $\text{CD}_3\text{OD}$  ( $\delta_{\text{H}}$  3.32). Data are presented in the following format: chemical shift (integration, multiplicity, coupling constants ( $J$ ) in Hz, assignment). Coupling constants,  $J$ , are measured to the nearest 0.1 Hz, Atom numbering is arbitrary and does not refer to IUPAC nomenclature.

$^{13}\text{C}$  NMR spectra were recorded at 126 MHz on a Bruker AMX 500 (500 MHz) spectrometer or at 151 MHz on a Bruker Avance NEO 600 (MHz 600) spectrometer equipped with a 5 mm TCI-Cryo probe using an internal deuterium lock. Chemical shifts were measured in parts per million (ppm) relative to tetramethylsilane ( $\delta = 0$ ) using the following residual solvent signals:  $\text{CDCl}_3$  ( $\delta_{\text{C}}$  77.2) and  $\text{CD}_3\text{OD}$  ( $\delta_{\text{C}}$  49.0). Data are presented in the following format: chemical shift (assignment) and for selected signals, multiplicities were assigned. Chemical shifts are quoted to 0.1 ppm. Atom numbering is arbitrary and does not refer to IUPAC nomenclature.

$^{19}\text{F}$  NMR were recorded at 471 MHz on a Bruker AMX 500 (500 MHz) spectrometer using an internal deuterium lock. Chemical shifts were measured in parts per million (ppm) relative to tetramethylsilane ( $\delta = 0$ ). Data are presented in the following format: chemical shift (multiplicity, coupling constants ( $J$ ) in Hz). Coupling constants  $J$  are measured to the nearest 1 Hz.

LCMS analyses and high-resolution mass spectrometry were performed on an Agilent 1200 series HPL and diode array detector coupled to a 6120 time of flight mass spectrometer with dual multimode APCI/ESI source. Samples were supplied at approximately 1 mg/mL solutions in MeOH with 0.5-10  $\mu\text{L}$  injected on a partial loop fill. Analytical separation was carried out at 30  $^{\circ}\text{C}$  on a Merck Purospher STAR column (RP-18e, 30 x4 mm) using a flow rate of 1.5 mL/min in a 4 minute gradient elution; solvents – aqueous (0.1% formic acid) and methanol (0.1% formic acid). UV detection was at 254 nm. Molecular weight scan range was 85 – 950, 160 – 950 or 160 – 1700. HRMS references: caffeine  $[\text{M}+\text{H}]^+$  195.08765; hexakis (2,2-



difluoroethoxy)phosphazene [M+H]<sup>+</sup> 622.02896; and hexakis(1H,1H,3H-tetrafluoropnetoxy)phophazene [M+H]<sup>+</sup> 922.00980.

Semi Preparative method was carried out as follows: 500 µL standard injections (with needle wash) of the sample were made onto a Phenomenex Gemini C18 110A column (250 x 21.2 mm, Phenomenex, Torrence, CA, USA). Chromatographic separation at room temperature was carried out using a 1260 Infinity II Series Preparative HPLC (Agilent, Santa Clara, USA) over a 15 minute gradient elution from 20:80 to 0:100 water:methanol (both modified with 0.1% formic acid) at a flow rate of 20 mL/min.

## **6.18 General procedures**

### **6.18.1 General Method for Amide coupling**

The acid (1 equiv) was stirred in DMF (0.8-0.16 M). 2-(7-Aza-1H-benzotriazole-1-yl)-1,1,3,3-tetramethyluronium hexafluorophosphate (1-1.05 equiv) and DIPEA (3 equiv) were added and the solution stirred at rt for 10-15 mins. The amine (1-1.05 equiv) was added and the solution stirred for 2h-16h. The solution was diluted with 10mL EtOAc and 10 mL water. The org phase was washed 3 x 30 mL water, and 1 x 30 brine, then dried (MgSO<sub>4</sub>), vacuum filtered and vacuum filtered and concentrated *in vacuo* then purified via silica chromatography (Biotage Sfar 10g) 0 - > 100% EtOAc in cyclohexane to afford the title compound.

### **6.18.2 General method for Ester hydrolysis**

The ester was stirred in THF (0.2 M) and water (0.2 M). Lithium hydroxide was added (3 equiv), and the solution stirred at r.t. for 3 – 16h. Reaction mixture concentrated in vacuo to a suspension then cooled to 0°C and acidified to pH = 1-2. The precipitate was vacuum filtered to give the title compound

### **6.18.3 General method for a nitro reduction**

The nitro containing compound was dissolved in a 2:1 EtOH: H<sub>2</sub>O (0.05M). Fe powder (3 equiv) and NH<sub>4</sub>Cl (5 equiv) were added, and the black mixture stirred at

70-80°C for 3-4 h. Filtered through a pad of celite and concentrated in vacuo. Partitioned between DCM and H<sub>2</sub>O, aq phase extracted 3 x DCM. Combined organics were dried over MgSO<sub>4</sub> and vacuum filtered, and concentrated in vacuo and purified via column chromatography.

#### **6.18.4 General Method for making NHS-esters**

The amine was taken up in DCM (0.2M) and EDCI (2 equiv was added) and the solution stirred at rt for 10 mins, then N-hydroxysuccinimide (1.5 equiv) was added. The solution was stirred rt overnight. Solution was partitioned between 10 mL DCM and 20 mL sat NaHCO<sub>3</sub> solution. Organic phase was washed 1 x 10 mL NaHCO<sub>3</sub> and 1 x 10 mL brine. Organic phase was dried over MgSO<sub>4</sub>, vacuum filtered and concentrated in vacuo to give the desired product as a colourless oil

#### **6.18.5 General conditions for Swern oxidation**

20 mL Dry DCM (0.12M) and Oxaly chloride (2 equiv) was cooled to -78C in a 50 mL RBF under N<sub>2</sub>. After 10 mins DMSO (3.5 equiv) in Dry DCM (1mL) was added dropwise and stirred at -78C for 10 mins. Then the relevant alcohol in 2mL Dry DCM was added. The pale-yellow solution was stirred at -78C for 45 mins. Then triethylamine (5 equiv) was added dropwise and the solution left to warm to rt overnight giving a pale yellow solution with a white suspension. The solution was cooled to 0C then 15 mL H<sub>2</sub>O was added and the org phase washed 1 x 15 mL 1M HCl, 1 x 15 mL Sat NaHCO<sub>3</sub> and 1 x 15 mL brine. The org phase was dried over MgSO<sub>4</sub>, and concentrated in vacuo to give the desired aldehyde

#### **6.18.6 General conditions for reductive aminations**

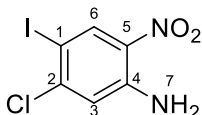
Crizotinib was taken up in Dry DCM ( 5.00 mL, 0.0200 M ). Then the desired aldehyde (1.2 equiv) was added followed by sodium triacetoxyborohydride ( 2 equiv) was added giving a white suspension. Reaction was monitored by LCMS with more aldehyde being added as required

Solution partitioned between 15 mL water and 10 mL DCM added. Aq phase extracted 3 x 10 mL DCM, dried over MgSO<sub>4</sub>, vacuum filtered and concentrated in vacuo to give a yellow oil. Purified via column chromatography (0 - 5 - 15 - 20 % MeOH in DCM) to give the desired product

#### 6.18.7 General method for click couplings

A 2ml microwave vial was charged with the relevant azide (1 equiv) and the relevant alkyne (1.1 equiv) were taken up in dry DMF (0.02M), and purged with N<sub>2</sub>. N,N-Diisopropylethylamine (1.5-2.5 equiv) was then added, followed by Copper Iodide (0.2 equiv). The reaction mixture was stirred at rt under N<sub>2</sub> for 1 - 4 hrs and monitored by LCMS. 1 equiv of metal scavenger (MP-TMT, isonaut technologies, 0.70 mmol/g, Lot No: 03426) was added and stirred at rt for 1 hr. Suspension was filtered and the filtrate concentrated, then dissolved in 1 mL of 1:1 DMSO: ACN and purified via Prep HPLC.

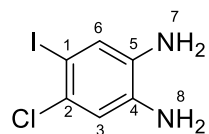
#### 5-chloro-4-iodo-2-nitroaniline, **4**



To a brown suspension of 5-chloro-2-nitro-aniline, **1**, ( 4.36 g, 25.265 mmol) in AcOH ( 43.60 mL) was added N-Iodo succinimide ( 5.68 g, 25.265 mmol) . The resulting yellow mixture was heated to 50°C overnight. Reaction mixture was filtered and washed with 1 x 20 mL AcOH, 1 x 20 mL deionised water, 1 x 20 mL sat NaHCO<sub>3</sub> sol. and 1 x 20 mL water. To afford the title compound (7.49 g, 99%, 25.098 mmol) as an orange solid

Ret. time = 3.01 mins. Observed m/z 298.9057. Calculated Formula [M+H]<sup>+</sup> C<sub>6</sub> H<sub>5</sub> Cl I N<sub>2</sub> O<sub>2</sub>. Target m/z 298.9079. Error (ppm) -7.3. δ<sub>H</sub> (DMSO-d<sub>6</sub>, 500 MHz): 7.24 (s, 1H, H3), 7.59 (s, 2H, H7), 8.33 (s, 1H, H6). δ<sub>C</sub> (DMSO-d<sub>6</sub>, 126 MHz): 79.48 (C1), 118.99 (C3), 130.73 (C5), 136.43 (C6), 144.32 (C4), 146.50 (C2)

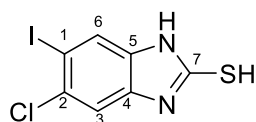
#### 4-chloro-5-iodobenzene-1,2-diamine, **5**



An orange/brown suspension of 5-chloro-4-iodo-2-nitro-aniline, **2** ( 565.00 mg, 1.893 mmol) in Ethanol ( 12.41 mL) and Water ( 2.33 mL) was degassed 3 x Ar, then NH<sub>4</sub>Cl ( 253.97 mg, 4.748 mmol) and Iron ( 583.21 mg, 10.443 mmol) were added. The black slurry was heated to 50°C overnight then filtered through celite, concentrated *in vacuo*, and partitioned between EtOAc (130 mL) and sat NaHCO<sub>3</sub> sol (130 mL). The Aq phase was extracted 3 x 50 mL EtOAc, and the combined organics were dried over MgSO<sub>4</sub>, vacuum filtered, concentrated *in vacuo* to afford the title compound (446 mg, 88%, 1.6612 mmol) as a yellow solid

Ret. time = 1.68 mins. Observed m/z 268.9334. Calculated formula C<sub>6</sub>H<sub>7</sub>ClIN<sub>2</sub>  
Target m/z 268.9337. Error (ppm) -1.07. δ<sub>H</sub> (DMSO-d<sub>6</sub>, 500 MHz): 6.65 (s, 1H, H3), 6.93 (s, 1H, H6). δ<sub>C</sub> (DMSO-d<sub>6</sub>, 126 MHz): 80.63 (C1), 114.06 (C3), 123.55 (C6), 124.31 (C2), 136.37 (C4), 137.49 (C5).

#### 5-chloro-6-iodo-1H-benzo[d]imidazole-2-thiol, **6**

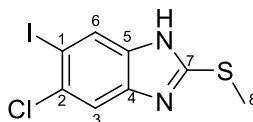


To a black solution of 4-chloro-5-iodo-benzene-1,2-diamine, **3**, ( 446.00 mg, 1.6612 mmol) in EtOH ( 2.52 mL) and Water ( 0.42 mL) , was added KOH ( 112.04 mg, 1.9968 mmol) and carbon disulfide ( 0.12 mL, 1.9968 mmol) and the black solution heated at 80°C overnight. Solvent was removed *in vacuo*. 20 mL water was added giving a slurry and AcOH was added drop wise giving a fine grey precipitate that was vacuum filtered and washed with ice cold to afford the title compound (377 mg, 73%, 1.214 mmol) as a grey solid.

Ret. time = 2.54 mins. Observed m/z 310.8905. Calculated Formula [M+H]<sup>+</sup> C<sub>7</sub> H<sub>5</sub> Cl I N<sub>2</sub> S. Target m/z 310.8901. Error (ppm) 1.07. δ<sub>H</sub> (DMSO-d<sub>6</sub>, 500 MHz): 7.36 (s, 1H,

H6), 7.62 (s, 1H, H3).  $\delta_c$  (DMSO-d6, 126 MHz): 88.99 (C1), 109.82 (C6), 119.46 (C3), 129.85 (C2), 134.01 (C4), 134.87 (C5), 170.33 (C7).

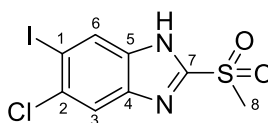
#### 5-chloro-6-iodo-2-(methylthio)-1H-benzo[d]imidazole, 7



6-chloro-5-iodo-1H-benzimidazole-2-thiol, **4**, ( 5.55 g, 17.879 mmol) was stirred in acetone ( 111.05 mL) giving a black suspension. The reaction mixture was cooled to 0°C then K<sub>2</sub>CO<sub>3</sub> ( 1.24 g, 8.9395 mmol) was added, followed by Iodomethane ( 0.56 mL, 8.9395 mmol) and the mixture was left to warm to rt. After 1 hour another portion of K<sub>2</sub>CO<sub>3</sub> ( 1.24 g, 8.9395 mmol) was added followed by Iodomethane ( 0.56 mL, 8.9395 mmol) and the reaction mixture stirred at r.t. for 2 h. 20mL water was added then, then solvent was removed *in vacuo*. The brown residue was partitioned between 100mL EtOAc and 100 mL water, and the aq phase extracted 3 x 50 mL EtOAc. The combined organics were dried over MgSO<sub>4</sub>, vacuum filtered and concentrated *in vacuo* to afford the title compound (5.87 g, 101%, 18.085 mmol) as a black solid.

Ret time = 2.72 mins. Observed m/z 324.9058. Calculated Formula [M+H]<sup>+</sup> C<sub>8</sub> H<sub>7</sub> Cl I N<sub>2</sub> S. Target m/z 324.9058. Error (ppm) 0.14.  $\delta_H$  (DMSO-d6, 500 MHz): 2.70 (s, 3H, H6), 7.71 (s, 1H, H3), 7.98 (s, 1H, H6).  $\delta_c$  (DMSO-d6, 126 MHz): 13.82, (C8), 89.28, (C1), 113.42 – 114.22 (C3), 123.23 – 124.37 (C6), 128.75 – 130.61 (C2), 139.22 (C5), 140.18 (C4), 153.69 – 155.45 (C7).

#### 5-chloro-6-iodo-2-(methylsulfonyl)-1H-benzo[d]imidazole, 8

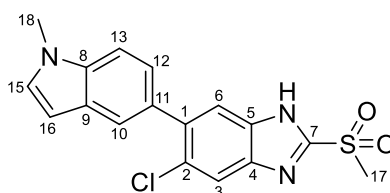


To a brown suspension of 6-chloro-5-iodo-2-methylsulfonyl-1H-benzimidazole, **5**, ( 1.57 g, 4.8279 mmol) in DCM ( 78.38 mL) at r.t., was added 3-Chloroperoxybenzoic

acid ( 2.27 g, 10.139 mmol) portion wise, giving a light brown solution. The solution was stirred at r.t. for 10 minutes. The reaction mixture was cooled to 0°C and quenched with sat. sodium bisulfite solution and 50 mL of 10% sat NaHCO<sub>3</sub> was added. The Aq phase was extracted 3 x 40 mL DCM. Combined org phases were dried over MgSO<sub>4</sub>, vacuum filtered and concentrated *in vacuo*. The orange/brown solid was triturated from 4.5 mL MeOH to afford the title compound (660 mg,35%, 1.6659 mmol) as an off white solid.

Ret. time = 2.7 mins. Observed m/z 356.8957 . Calculated Formula [M+H]<sup>+</sup> C<sub>8</sub> H<sub>7</sub> Cl I N<sub>2</sub> O<sub>2</sub> S. Target m/z 356.8956. Error (ppm) 0.23.  $\delta_{\text{H}}$  (DMSO-d<sub>6</sub>, 500 MHz): 3.52 (s, 3H, H11), 7.98 (s, 1H, H3), 8.29 (s, 1H, H6).  $\delta_{\text{C}}$  (DMSO-d<sub>6</sub>, 126 MHz): 42.34 (C8), 93.40 (C1), 117.14 (C3), 127.61 (C6), 132.51 (C2), 138.23 (C4), 138.79 (C5), 151.03 (C7).

#### 5-chloro-6-(1-methyl-1H-indol-5-yl)-2-(methylsulfonyl)-1H-benzo[d]imidazole, 9

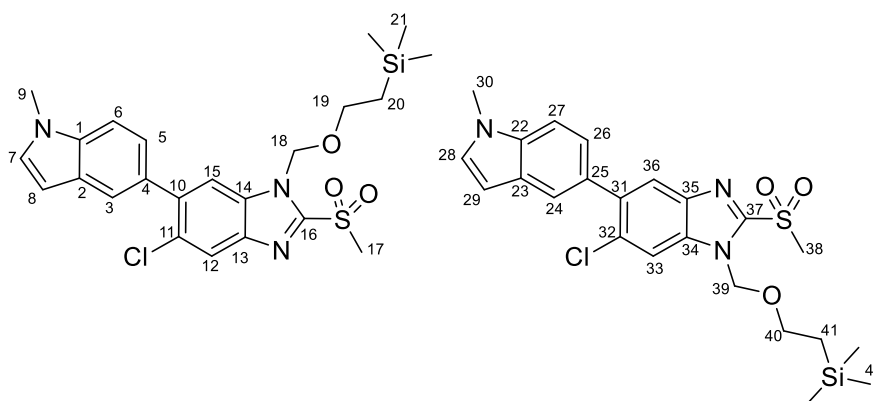


6-chloro-5-iodo-2-methylsulfonyl-1H-benzimidazole, **6**, ( 644.00 mg, 1.8061 mmol) in 1,4-Dioxane ( 12.87 mL) and H<sub>2</sub>O ( 2.70 mL) was degassed with N<sub>2</sub> for 5 mins. 1-methyl-5-indolyboronic acid ( 379.26 mg, 2.1673 mmol) , K<sub>2</sub>CO<sub>3</sub> ( 748.86 mg, 5.4183 mmol) and Pd(dppf)Cl<sub>2</sub> ( 147.49 mg, 0.1806 mmol) were added. The black reaction mixture was then degassed with N<sub>2</sub> for 5 mins, then heated to 100°C for 5.5 hrs then concentrated *in vacuo*, diluted in EtOAc and filtered through celite. The black solution was diluted with 10 mL water and the aq phase extracted 3 x 15 mL EtOAc. The combined organics were dried over MgSO<sub>4</sub>, vacuum filtered and concentrated *in vacuo*. Then purified by reverse-phase chromatography to afford the title compound (300 mg, 46%, 0.8337 mmol) as a black oil

Ret. time = 2.9 mins. Observed m/z 360.0563. Calculated Formula [M+H]<sup>+</sup> C<sub>17</sub> H<sub>15</sub> Cl N<sub>3</sub> O<sub>2</sub> S. Target m/z 360.0568. Error (ppm) -1.48.  $\delta_{\text{H}}$  (DMSO-d<sub>6</sub>, 500 MHz): 3.52 (s, 3H, H17), 3.83 (s, 3H, H18), 6.48 (d, J = 3.1 Hz, 1H, H16), 7.18 – 7.24 (m, 1H, H12),

7.38 (d, J = 3.1 Hz, 1H, H15), 7.50 (d, J = 8.5 Hz, 1H, H13), 7.57 – 7.61 (m, 1H, H14), 7.66 (s, 1H, H6), 7.91 (s, 1H, H3).  $\delta_c$  (DMSO-d<sub>6</sub>, 126 MHz): 32.35 (C18), 42.21 (C17), 100.43 (C16), 109.01 (C13), 117.50 (C3), 118.30 (C6), 121.11 (C10), 122.79 (C12), 127.55 (C9), 128.02 (C2), 129.94 (C1), 130.13 (C15), 135.52 (C8), 137.5 (C4), 137.85 (C11), 138.17 (C5), 150.74 (C7).

**5-chloro-6-(1-methyl-1H-indol-5-yl)-2-(methylsulfonyl)-1-((2-(trimethylsilyl)ethoxy)methyl)-1H-benzo[d]imidazole, 10**

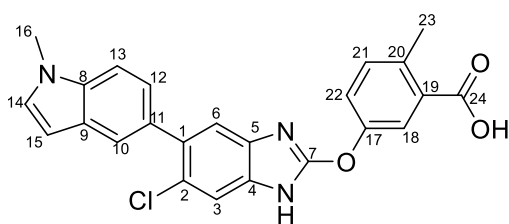


To a brown suspension of 6-chloro-5-(1-methylindol-5-yl)-2-methylsulfonyl-1H-benzimidazole, **7**, (138.00 mg, 0.3835 mmol) in THF (1.02 mL) was added 2-(trimethylsilyl)ethoxymethylchloride (0.09 mL, 0.4986 mmol) and triethylamine (0.11 mL, 0.7670 mmol). The reaction mixture was stirred at r.t. overnight. Another portion of 2-(trimethylsilyl)ethoxymethylchloride (0.01 mL, 0.0767 mmol) and triethylamine (0.02 mL, 0.1534 mmol) were added and the reaction mixture stirred at r.t. for 2 hrs. Solvent removed *in vacuo*, and the solid partitioned between 10 mL EtOAc and 10 mL H<sub>2</sub>O. Aq phase extracted 3 x 10 mL EtOAc, combined orgs were dried over MgSO<sub>4</sub>, vacuum filtered and concentrated *in vacuo* then purified via column chromatography 0 → 15% EtOAc in cyclohexane to afford the title compound (134 mg, 71%, 0.2734 mmol) as a yellow oil

Ret. time = 3.39 mins. Observed m/z 490.1378. Calculated Formula [M+H]<sup>+</sup> C<sub>23</sub> H<sub>29</sub> Cl N<sub>3</sub> O<sub>3</sub> S Si. Target m/z 490.1382. Error (ppm) -0.83.  $\delta_H$  (DMSO-d<sub>6</sub>, 600 MHz): -0.10 (9 H, s, H42), -0.06 (9 H, s, H21), 0.82 – 0.85 (2 H, m, H41), 0.86 – 0.90 (2 H, m, H20), 3.58 – 3.65 (10 H, m, H17, H20, H38, H40), 3.84 (3 H, s, H9), 3.85 (3 H, s, H30), 5.98 (2 H, s, H39), 5.99 (2 H, s, H18), 6.46 – 6.51 (2 H, m, H8, H29), 7.21 (1 H, dd, J

8.4, 1.7, H5), 7.24 (1 H, dd, J 8.4, 1.7, H26), 7.40 (1 H, d, J 3.1, H7), 7.41 (1 H, d, J 3.0, H29), 7.52 (1 H, d, J 8.4, H6), 7.54 (1 H, d, J 8.4, H27), 7.59 (1 H, d, J 1.6, H3), 7.61 (1 H, d, J 1.7, H24), 7.85 (1 H, s, H12), 7.91 (1 H, s, H33), 8.09 (1 H, s, H36), 8.12 (1 H, s, H15).  $\delta_c$  (DMSO-d<sub>6</sub>, 151 MHz): -0.96 (C21, C44) 17.66 (C41), 17.68 (C20), 33.06 (C30), 33.08 (C9), 43.56 (C17, C38), 66.69 (C40), 66.74 (C19), 74.09 (C39), 74.16 (C18), 101.13 (C29), 101.14 (C8), 109.74 (C6), 109.79 (C27), 113.72 (C15), 115.42 (C33), 121.69 (C36), 121.85 (C3, C35), 123.36 (C5), 123.45 (C26), 123.54 (C12), 128.25 (C23), 128.27 (C2), 128.77 (C32), 130.29 (C25), 130.35 (C10), 130.81 (C11), 130.88 (C7), 131.00 (C28), 134.96 (C34), 135.29 (C14), 136.26 (C22), 136.33 (C1), 138.51 (C4), 139.59 (C35), 139.98 (C13), 140.08, (C25), 150.20 (C37), 150.30 (C16).

**5-[[6-chloro-5-(1-methylindol-5-yl)-1H-benzimidazol-2-yl]oxy]-2-methyl-benzoic acid, 991/ CCT390619**



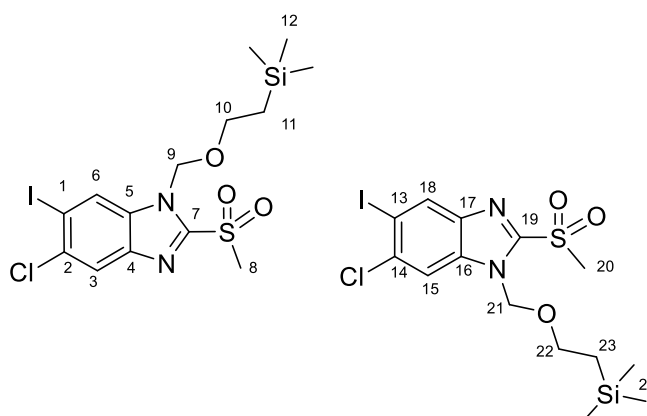
To a pale yellow of 2-[(6-chloro-5-iodo-2-methylsulfonyl-benzimidazol-1-yl)methoxy]ethyl-trimethyl- $\lambda^4$ -sulfane), **8**, ( 347.95 mg, 0.7089 mmol) in DMF ( 4.93 mL) was added 5-hydroxy-3-methyl benzoic acid methyl ester, **11**, ( 120.16 mg, 0.7231 mmol) and K<sub>2</sub>CO<sub>3</sub> ( 195.96 mg, 1.4178 mmol) giving a yellow solution with a slight brown precipitate which was stirred at r.t. for 24 hours, then concentrated *in vacuo*. The residue was dissolved in THF ( 5.00 mL) and tetrabutylammonium fluoride ( 1.25 mL, 1.2497 mmol) 1M in THF was added dropwise, and the pale yellow solution was stirred at r.t. overnight. Another portion of tetrabutylammonium fluoride ( 1.25 mL, 1.2497 mmol) was added and the yellow solution heated to 80°C for 6 hrs, then more tetrabutylammonium fluoride ( 1.25 mL, 1.2497 mmol) was added and the reaction mixture stirred for 1 hr at 80°C then solvent was removed *in vacuo* to a green oil. The oil was partitioned between EtOAc (15mL) and 1:1 water: sat NH<sub>4</sub>Cl sol (15ml). The aq layer was extracted 3 x EtOAc (15mL). Combined org phases were dried (MgSO<sub>4</sub>), vacuum filtered and concentrated *in vacuo* which was taken up in THF ( 4.00 mL)



and Water ( 2.00 mL). Lithium hydroxide ( 4.03 mg, 0.1682 mmol) was added and the mixture was heated to 45°C for 1 hr, then cooled and concentrated *in vacuo* and purified via column chromatography 0-> 15% MeOH in DCM then reverse phase 0-> 100% MeOH to afford the title compound (4 mg, 1%, 0.0093 mmol) as an off white solid

Ret. time = 3.05 mins. Observed m/z 432.1107. Calculated Formula [M+H]<sup>+</sup> C<sub>24</sub> H<sub>19</sub> Cl N<sub>3</sub> O<sub>3</sub>. Target m/z 432.1109. Error (ppm) -0.48. m.p.: 189-191°C.  $\nu_{\max}$  (cm<sup>-1</sup>): 2927 (br, s, COOH), 717 (s, C-Cl).  $\delta_{\text{H}}$  (DMSO-d<sub>6</sub>, 600 MHz): 2.56 (s, 3H, 23), 3.83 (s, 3H, 16), 6.47 (d, J = 3.0 Hz, 1H, 15), 7.19 (dd, J = 8.4, 1.7 Hz, 1H, 12), 7.34 (d, J = 2.0 Hz, 1H, 6), 7.37 (d, J = 3.1 Hz, 1H, 14), 7.42 (d, J = 8.4 Hz, 1H, 21), 7.48 (d, J = 8.4 Hz, 1H, 13), 7.51 – 7.55 (m, 2H, 3, 22), 7.56 (d, J = 1.6 Hz, 1H, 10), 7.80 (d, J = 2.6 Hz, 1H, 18).  $\delta_{\text{C}}$  (DMSO-d<sub>6</sub>, 151 MHz): 20.63 (C23), 32.57 (C16), 100.58 (C15), 109.14 (C13), 114.91 (C3), 115.93 (C6), 121.28 (C10), 121.78 (C18), 123.15 (C12), 123.82 (C22), 124.83 (C2), 127.78 (C9), 130.19 (C14), 130.62 (C19), 130.77 (C1), 131.66 (C20), 132.98 (C21), 134.86 (C4), 135.58 (C8), 136.38 (C7), 136.62 (C5), 136.65 (C11), 151.05 (C17), 167.78 (C8).

**2-[(6-chloro-5-iodo-2-methylsulfonyl-benzimidazol-1-yl)methoxy]ethyl-trimethyl-silane and 2-[(5-chloro-6-iodo-2-methylsulfonyl-benzimidazol-1-yl)methoxy]ethyl-trimethyl-silane, 11**

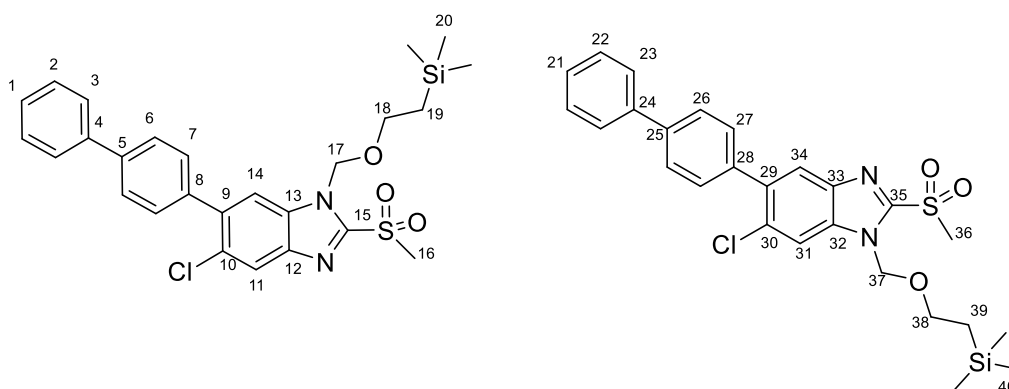


6-chloro-5-iodo-2-methylsulfonyl-1H-benzimidazole, **6**, ( 780.00 mg, 0.4375 mmol), was dissolved in THF ( 15.85 mL) to give a pale yellow solution. 2-

(trimethylsilyl)ethoxymethylchloride ( 0.10 mL, 0.5717 mmol) and triethylamine ( 0.12 mL, 0.8750 mmol) were added to give a white suspension. The mixture was stirred at r.t. overnight. Then another portion of triethylamine ( 0.24 mL, 0.1750 mmol) and 2-(trimethylsilyl)ethoxymethylchloride ( 0.10 mL, 0.5717 mmol) were added and the reaction mixture stirred for 4 hrs at r.t overnight then concentrated *in vacuo*, and partitioned between 20mL Water and 20mL EtOAc. Aq phase extracted 3 x 20 mL EtOAc, then combined organics were washed 1 x 50 mL 2M HCl, 1 x 50 mL brine, then dried over MgSO<sub>4</sub>, vacuum filtered and concentrated *in vacuo*. Purified via column chromatography, 0 -> 8% EtOAc in cyclohexane, to afford the title compound (195 mg, 46%, 0.2003 mmol) as an off white solid.

Ret. time = 3.34 mins. Observed m/z 508.9579. Calculated Formula [M+H]<sup>+</sup> C<sub>14</sub> H<sub>20</sub> Cl I N<sub>2</sub> Na O<sub>3</sub> S Si. Target m/z 508.9589. Error (ppm) -2.06. δ<sub>H</sub> (DMSO-d<sub>6</sub>, 500 MHz): -0.10 (9 H, s, 24), -0.10 (9 H, s, 12), 0.80 – 0.86 (4 H, m, 11, 23, 13, 42), 3.54 – 3.59 (4 H, m, 10, 22), 3.60 (3 H, s, 20), 3.61 (3 H, s, 8), 5.93 (2 H, s, 21), 5.94 (2 H, s, 9), 8.16 (1 H, s, 3), 8.22 (1 H, s, 15), 8.49 (1 H, s, 18), 8.52 (1 H, s, 6). δ<sub>C</sub> (DMSO-d<sub>6</sub>, 126 MHz): -1.47 (C<sub>24</sub>), -1.46 (C<sub>12</sub>), 17.14 (C<sub>23</sub>), 17.16 (C<sub>11</sub>), 42.99 (C<sub>20</sub>), 43.02 (C<sub>8</sub>), 66.26 (C<sub>10</sub>, 22) 73.73 (C<sub>21</sub>), 73.74 (C<sub>9</sub>), 92.98 (C<sub>13</sub>), 95.68 (C<sub>1</sub>), 113.07 (C<sub>15</sub>), 120.87 (C<sub>3</sub>), 123.68 (C<sub>6</sub>), 131.85 (C<sub>18</sub>), 132.58 (C<sub>17</sub>), 134.28 (C<sub>4</sub>), 135.25 (C<sub>16</sub>), 136.05 (C<sub>5</sub>), 140.25 (C<sub>14</sub>), 140.83 (C<sub>2</sub>), 150.09 (C<sub>19</sub>), 150.14 (C<sub>7</sub>).

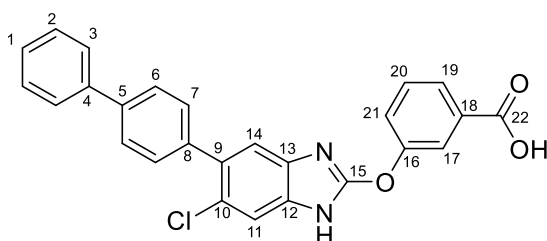
**2-[[5-chloro-2-methylsulfonyl-6-(4-phenylphenyl)benzimidazol-1-yl]methoxy]ethyl-trimethyl-silane and 2-[[6-chloro-2-methylsulfonyl-5-(4-phenylphenyl)benzimidazol-1-yl]methoxy]ethyl-trimethyl-silane, 12**



2-[(5-chloro-6-iodo-2-methylsulfonyl-benzimidazol-1-yl)methoxy]ethyl-trimethyl-silane ( 188.00 mg, 0.2549 mmol) and 2-[(6-chloro-5-iodo-2-methylsulfonyl-benzimidazol-1-yl)methoxy]ethyl-trimethyl-silane ( 188.00 mg, 0.2549 mmol), **9**, in 1,4-Dioxane ( 1.61 mL) and H<sub>2</sub>O ( 0.54 mL) were degassed with N<sub>2</sub> for 5 minutes. 4-Biphenylboronic acid ( 53.00 mg, 0.2676 mmol) and K<sub>2</sub>CO<sub>3</sub> ( 105.68 mg, 0.7646 mmol) were added, followed by Pd(dppf)Cl<sub>2</sub> ( 10.94 mg, 0.0127 mmol) , and the black mixture degassed with N<sub>2</sub> for 2 mins and heated to 100°C for 4 hrs. The mixture was partitioned between 15mL sat NaHCO<sub>3</sub> and 15 mL EtOAc and the aq phase extracted 3 x 10 mL EtOAc. Combined organics were dried over MgSO<sub>4</sub>, vacuum filtered and concentrated *in vacuo* to a black oil. Purified via column chromatography 0 -> 27% EtOAc in cyclohexane to afford the title (138 mg, 106%, 0.2689 mmol) as a yellow oil.

Ret. time = 3.69 mins. Observed m/z 513.1431. Calculated Formula [M+H]<sup>+</sup> C<sub>26</sub> H<sub>30</sub> Cl N<sub>2</sub> O<sub>3</sub> S Si. Target m/z 513.1429. Error (ppm) 0.28.  $\delta_H$  (DMSO-d<sub>6</sub>, 600 MHz): -0.10 (s, 9H, 40), -0.06 (s, 9H, 20), 0.84 (t, J = 8.1 Hz, 2H, 19), 0.88 (t, J = 8.1 Hz, 2H, 39), 3.62 (s, 6H, 16, 36), 3.63 (s, 4H, 18, 38), 5.99 (s, 2H, 17,,), 6.00 (s, 2H, 37), 7.41 (td, J = 7.2, 3.1 Hz, 2H, 1, 21), 7.51 (td, J = 7.8, 2.4 Hz, 4H, 2, 22), 7.56 (d, J = 3.5 Hz, 2H, 27), 7.57 (d, J = 3.4 Hz, 2H, 7) 7.74 (t, J = 2.1 Hz, 1H, 3), 7.75 – 7.76 (m, 1H, 23), 7.79 (d, J = 8.2 Hz, 2H, 6), 7.81 (d, J = 8.1 Hz, 2H, 26), 7.93 (s, 1H, 11), 7.99 (s, 1H, 31), 8.15 (s, 1H, 34), 8.17 (s, 1H, 14).  $\delta_C$  (DMSO-d<sub>6</sub>, 151 MHz): -1.44 (C<sub>20</sub>, C<sub>40</sub>) 17.18 (C<sub>39</sub>), 17.20 (C<sub>19</sub>), 43.08 (C<sub>16</sub>, C<sub>36</sub>), 66.24 (C<sub>38</sub>), 66.27(C<sub>18</sub>), 73.67 (C<sub>17</sub>), 73.74 (C<sub>37</sub>), 113.59 (C<sub>14</sub>), 114.85 (C<sub>31</sub>), 121.52 (C<sub>34</sub>), 122.96 (C<sub>11</sub>), 126.48 (C<sub>26</sub>), 126.51 (C<sub>6</sub>), 126.74 (C<sub>23</sub>), 126.75 (C<sub>3</sub>), 129.03 (C<sub>22</sub>), 129.05 (C<sub>2</sub>), 130.19 (C<sub>27</sub>), 130.27 (C<sub>7</sub>), 134.54 (C<sub>13</sub>), 135.28 (C<sub>32</sub>), 136.13 (C<sub>8</sub>), 139.18 (C<sub>9</sub>), 139.55 (C<sub>4</sub>, C<sub>24</sub>), 139.63 (C<sub>29</sub>), 139.73 (C<sub>12</sub>), 139.98 (C<sub>33</sub>), 149.97 (C<sub>15</sub>), 150.16 (C<sub>36</sub>).

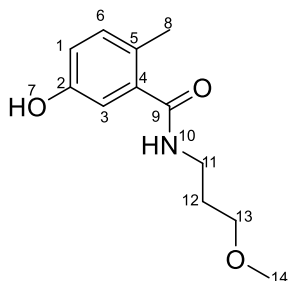
**3-[[6-chloro-5-(4-phenylphenyl)-1H-benzimidazol-2-yl]oxy]benzoic acid, CCT390621**



To a solution of methyl 3-hydroxybenzoate ( 22.04 mg, 0.1448 mmol), **11**, and 2-[[5-chloro-2-methylsulfonyl-6-(4-phenylphenyl)benzimidazol-1-yl]methoxy]ethyl-trimethyl-silane, **10**, ( 64.54 mg, 0.1317 mmol) in DMF ( 0.44 mL) was added K<sub>2</sub>CO<sub>3</sub> ( 70.26 mg, 0.5084 mmol). The yellow solution mixture was stirred at 50°C for 16h. Tetrabutylammonium fluoride ( 0.53 mL, 0.5267 mmol) 1M in THF was added and the yellow suspension heated to 80°C for 4 hrs. Lithium hydroxide ( 9.46 mg, 0.3950 mmol) , THF ( 1.00 mL) and H<sub>2</sub>O ( 0.50 mL) were added and the yellow solution stirred at r.t. for 2 hrs then concentrated *in vacuo* to a brown oil, and purified by reverse-phase chromatography, 0-100% MeOH to afford the title compound (11 mg, 19%, 0.0250 mmol) as an off white solid.

Ret. time = 3.27 mins. Observed m/z 441.0993. Calculated Formula [M+H]<sup>+</sup> C<sub>26</sub>H<sub>18</sub>Cl N<sub>2</sub> O<sub>3</sub>. Target m/z 441.1000. Error (ppm) -1.66.  $\delta_{\text{H}}$  (DMSO-d<sub>6</sub>, 500 MHz): 7.37 – 7.41 (m, 1H, H1), 7.41 (s, 1H, H14), 7.50 (t, J = 7.7 Hz, 2H, H2), 7.52 – 7.55 (m, 2H, H6), 7.59 (s, 1H, H11), 7.63 (t, J = 7.8 Hz, 1H, H20), 7.68 – 7.71 (m, 1H, H21), 7.72 – 7.77 (m, 4H, H3, H7), 7.88 (dt, J = 7.8, 1.4 Hz, 1H, H19), 7.91 – 7.94 (m, 1H, H17).  $\delta_{\text{C}}$  (DMSO-d<sub>6</sub>, 151 MHz): 115.12 (C11), 115.81 (C14), 120.90 (C17), 124.25 (C10), 124.93 (C21), 126.36 (C7), 126.43 (C19), 126.69 (C3), 127.55 (C1), 129.02 (C2), 130.28 (C6, C20), 132.61 (C18), 132.85 (C9), 135.40 (C12), 137.14 (C13), 138.85 (C8), 139.02 (C5), 139.74 (C4), 153.33 (C16), 157.58 (C15), 166.47 (C22).

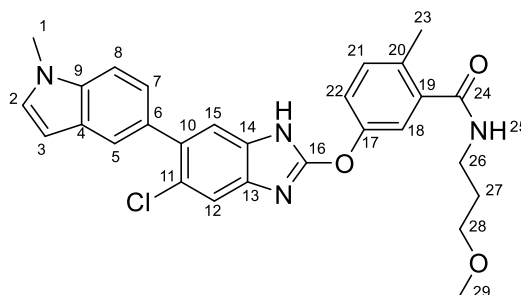
#### 5-hydroxy-N-(3-methoxypropyl)-2-methyl-benzamide, **14**



5-hydroxy-2-methyl-benzoic acid, **11**, (30.00 mg, 0.1972 mmol) was reacted with 3-methoxy propylamine ( 0.02 mL, 0.2070 mmol) as per general method for amide couplings to give the title compound as a colourless oil.

Ret. time = 1.79 mins. Observed m/z 224.1288. Calculated Formula [M+H]<sup>+</sup> C<sub>12</sub> H<sub>18</sub> N O<sub>3</sub>. Target m/z 224.1281. Error (ppm) 3.01.  $\delta_{\text{H}}$  (DMSO-d<sub>6</sub>, 500 MHz): 1.71 (p, J = 6.6 Hz, 2H, H<sub>12</sub>), 2.18 (s, 3H, H<sub>8</sub>), 3.19 – 3.25 (m, 4H, H<sub>11</sub>, H<sub>14</sub>), 3.36 (t, J = 6.6 Hz, 2H, H<sub>13</sub>), 6.69 (d, J = 7.6 Hz, 2H, H<sub>1</sub>, H<sub>3</sub>), 6.99 (d, J = 7.7 Hz, 1H, H<sub>6</sub>), 8.13 (t, J = 5.6 Hz, 1H, N<sub>10</sub>), 9.34 (s, 1H, H<sub>7</sub>).  $\delta_{\text{C}}$  (DMSO-d<sub>6</sub>, 126 MHz): 18.36 (C<sub>8</sub>) 29.26 (C<sub>12</sub>), 36.07 (C<sub>11</sub>), 57.95 (C<sub>14</sub>), 69.69 (C<sub>13</sub>), 113.82 (C<sub>3</sub>), 115.91 (C<sub>1</sub>), 124.74(C<sub>5</sub>), 131.29 (C<sub>4</sub>), 138.21 (C<sub>6</sub>), 154.87 (C<sub>2</sub>), 169.00 (C<sub>9</sub>).

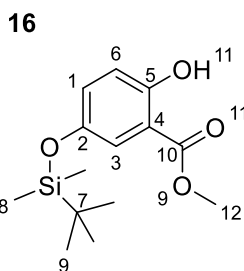
**5-[[5-chloro-6-(1-methylindol-5-yl)-1H-benzimidazol-2-yl]oxy]-N-(3-methoxypropyl)-2-methyl-benzamide, CCT390620**



To a pale yellow solution of 5-hydroxy-N-(3-methoxypropyl)-2-methyl-benzamide, **13**, ( 31.00 mg, 0.1388 mmol) and 2-[[5-chloro-6-(1-methylindol-5-yl)-2-methylsulfonyl-benzimidazol-1-yl]methoxy]ethyl-trimethyl-silane ( 64.54 mg, 0.1317 mmol), **8**, in DMF ( 0.92 mL) was added K<sub>2</sub>CO<sub>3</sub> ( 70.26 mg, 0.5084 mmol) . The yellow suspension were stirred at r.t. for 36 hrs, then heated to 50°C for 6 h. Tetrabutylammonium fluoride ( 0.53 mL, 0.5267 mmol) 1M in THF was added, and the pale yellow solution with a white suspension was heated to 80°C for 6 hrs. 10 mL sat NH<sub>4</sub>Cl and 10 mL EtOAc were added and the aq phase was extracted 3 x 10 mL EtOAc, combined organics were dried over MgSO<sub>4</sub>, vacuum filtered and concentrated *in vacuo*, then purified via reverse phase, 0-100% MeOH, to afford the title compound (31 mg, 47%, 0.0616 mmol) as a white solid.

Ret. time = 3.09 mins. Observed m/z 503.1834. Calculated Formula [M+H]<sup>+</sup> C<sub>28</sub> H<sub>28</sub> Cl N<sub>4</sub> O<sub>3</sub>. Target m/z 503.1844. Error (ppm) -2.11. m.p.: 117-119°C.  $\nu_{\max}$  (cm<sup>-1</sup>): 2928 (br, s, CON-H), 1603 (C=O(CONH)), 14444(s, CH), 721 (s, C-Cl).  $\delta_{\text{H}}$  (DMSO-d<sub>6</sub>, 600 MHz): 1.73 (p, *J* = 6.6 Hz, 2H, H27), 2.35 (s, 3H, H23), 3.22 (s, 3H, H29), 3.26 (q, *J* = 6.8 Hz, 2H, H26), 3.37 (t, *J* = 6.3 Hz, 2H, H28), 3.82 (s, 3H, H1), 6.46 (d, *J* = 3.1 Hz, 1H, H3), 7.18 (dd, *J* = 8.4, 1.7 Hz, 1H, H7), 7.34 (m, 3H, H15, H18, H21), 7.37 (d, *J* = 3.1 Hz, 1H, H2), 7.38 (dd, *J* = 8.4, 2.5 Hz, 1H, H22), 7.47 (d, *J* = 8.4 Hz, 1H, H8), 7.53 (s, 1H, H12), 7.55 (d, *J* = 1.7 Hz, 1H, H5), 8.36 (t, *J* = 5.7 Hz, 1H, H25).  $\delta_{\text{C}}$  (DMSO-d<sub>6</sub>, 151 MHz): 18.78 (C23), 29.15 (C27), 32.56 (C1), 36.25 (C26), 57.93 (C29), 69.67 (C28), 100.58 (C3), 109.14 (C8), 114.89 (C12), 115.87 (C15), 118.88 (C18), 121.16 (C22), 121.27 (C5), 123.14 (C7), 124.82 (C11), 127.78 (C4), 130.20 (C2), 130.74 (C6), 131.76 (C21), 132.50 (C20), 134.80 (C10), 135.58 (C9), 136.46(C14), 136.48 (C13), 138.47 (C19), 142.71 (C16), 150.83 (C17), 167.94 (C24).

#### methyl 5-[tert-butyl(dimethyl)silyl]oxy-2-hydroxy-benzoate, 16

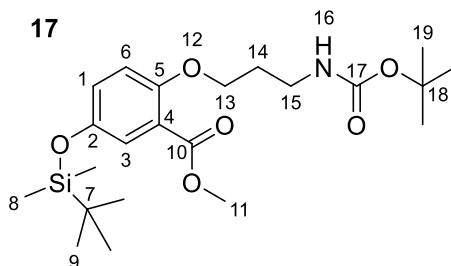


Methyl 2,5-dihydroxybenzoate ( 1.00 g, 5.9471 mmol) and Imidazole ( 607.31 mg, 8.9206 mmol) were taken up DCM ( 39.65 mL, 0.15 M ) and cooled to 0C. t-butyl(dimethyl)silyl chloride ( 1.19 mL, 6.5418 mmol) was added dropwise. The white suspension was stirred at 0C then left to warm to rt overnight. Then diluted with 5 mL DCM and 25 mL water. The org phase was washed with 30 mL 2M HCl and then 30 mL brine. Org phase was dried over MgSO<sub>4</sub>, vacuum filtered and concentrated in vacuo. Purified via column chromatography (Biotage Sfar 5 g 0 - 4 EtOAc in cyclohexane), to afford the title compound (1.07 g, 62%, 3.682 mmol) as a colourless oil.

Formula C<sub>14</sub>H<sub>22</sub>O<sub>4</sub>Si Observed m/z 283.1369539 Calculated m/z 283.1360121 Error (ppm) 3.33 <sup>1</sup>H NMR (600 MHz, Chloroform-d)  $\delta$  0.18 (s, 6H, 8), 0.99 (s, 9H, 9),

3.94 (s, 3H, 12), 6.86 (d,  $J = 8.9$  Hz, 1H, 6), 6.99 (dd,  $J = 8.9, 3.0$  Hz, 1H, 1), 7.27 (s, 1H, 3), 10.36 (s, 1H, 11).  $^{13}\text{C}$  NMR (151 MHz,  $\text{CDCl}_3$ )  $\delta$  -4.39, 8, 18.28, 7, 25.81, 9, 52.45, 12, 112.32, 4, 118.35, 6, 119.57, 3, 128.65, 1, 147.71, 2, 156.37, 5, 170.43, 10.

**methyl 2-[3-(tert-butoxycarbonylamino)propoxy]-5-[tert-butyl(dimethyl)silyl]oxybenzoate, 17**

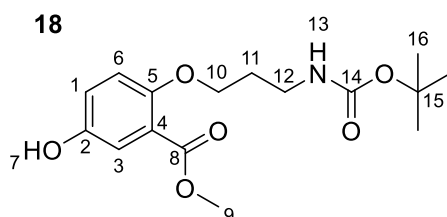


methyl 5-[tert-butyl(dimethyl)silyl]oxy-2-hydroxybenzoate ( 100.00 mg, 0.3541 mmol) was taken up in THF ( 0.89 mL, 0.4 M ), and cooled to 0C. then tert-butyl-N-(3-hydroxypropyl)carbamate ( 121.07  $\mu\text{L}$ , 0.7082 mmol) and Triphenylphosphine ( 185.75 mg, 0.7082 mmol) were added and stirred at 0C for 5 mins. Then Diethyl azodicarboxylate ( 111.51  $\mu\text{L}$ , 0.7082 mmol) was added and the solution stirred at 0C for 5 mins then left to warm to rt and stirred at rt for 1h then 60 C overnight. The solution was cooled to 0C. tert-butyl-N-(3-hydroxypropyl)carbamate ( 121.07  $\mu\text{L}$ , 0.7082 mmol) and Triphenylphosphine ( 185.75 mg, 0.7082 mmol) were added giving a colourless solution. Diethyl azodicarboxylate ( 111.51  $\mu\text{L}$ , 0.7082 mmol) was added dropwise giving a pale yellow solution. Stirred at 0C for 15 mins which gave a white suspension forming. The reaction mixture was heated to 70 C overnight (when the white ppt dissolved giving a pale yellow solution). Then concentrated in vacuo, and partitioned between 1 x 10 mL water and 1 x 10 ml EtOAc. Org phase washed 2 x 10 ml  $\text{NaHCO}_3$  and then 1 x 10 ml brine. Org phase dried over  $\text{MgSO}_4$  then purified via column chromatography (Biotage Sfar Duo 5 g 0 - 10 - 20 EtOAc in cyclohexane). to afford the title compound (121 mg, 78%, 0.2752 mmol) as a colourless oil

Formula  $\text{C}_{22}\text{H}_{37}\text{NO}_6\text{Si}$  Observed  $m/z$  440.2487189 Calculated  $m/z$  440.2462909 Error (ppm) 5.52.  $^1\text{H}$  NMR (600 MHz,  $\text{CDCl}_3$ )  $\delta$  0.17 (s, 6H, 8), 0.97 (s, 9H, 9), 1.44 (s,

11H, 19), 2.00 (p,  $J = 5.6$  Hz, 2H, 14), 3.38 (q,  $J = 5.7$  Hz, 2H, 15), 3.89 (s, 3H, 11), 4.05 (t,  $J = 5.6$  Hz, 2H, 13), 5.85 – 5.93 (m, 1H, 16), 6.82 (d,  $J = 8.9$  Hz, 1H, 6), 6.93 (dd,  $J = 8.9, 3.1$  Hz, 1H, 1), 7.32 (d,  $J = 3.1$  Hz, 1H, 3).  $^{13}\text{C}$  NMR (151 MHz,  $\text{CDCl}_3$ )  $\delta$  -4.38, 8, 18.28, 7, 25.79, 9, 28.60, 19, 29.31, 14, 39.23, 15, 52.20, 11, 68.77, 13, 78.83, 18, 114.27, 6, 120.11, 4, 123.00, 3, 125.31, 1, 148.99, 2, 153.39, 5, 156.52, 17, 166.24, 10.

**methyl 2-[3-(tert-butoxycarbonylamino)propoxy]-5-hydroxy-benzoate, 18**



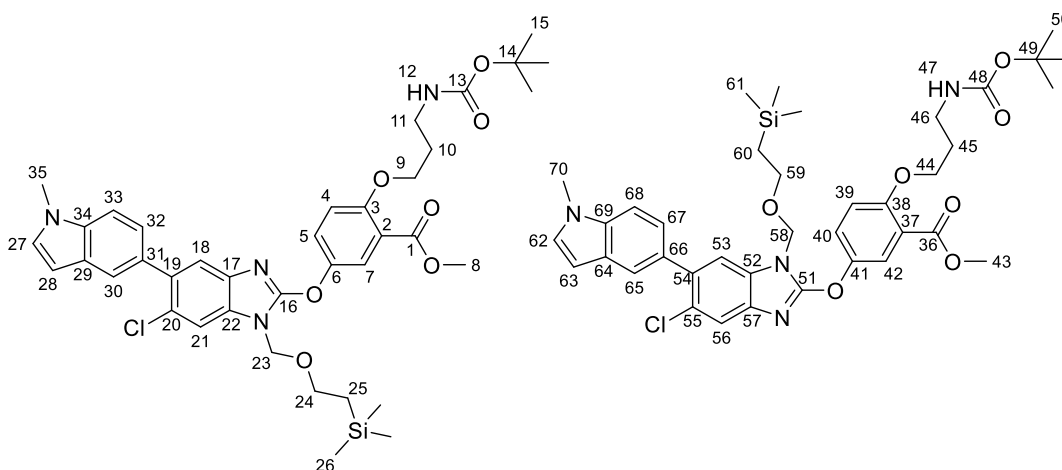
methyl 2-[3-(tert-butoxycarbonylamino)propoxy]-5-[tert-butyl(dimethyl)silyl]oxybenzoate (30.00 mg, 0.0682 mmol) was taken up in Dry THF (0.68 mL, 0.1 M) and the colourless solution cooled to 0°C for 10 mins. Then Tetrabutylammonium fluoride (1M in THF) (0.10 mL, 0.1024 mmol) was added dropwise and the pale yellow solution stirred at 0°C for 15 mins. Then the reaction solution was partitioned between 5 mL EtOAc and 5 mL  $\text{H}_2\text{O}$ . The aq phase was extracted 3 x 5 mL EtOAc and combined organics dried over  $\text{MgSO}_4$ , vacuum filtered and concentrated in vacuo. The resulting oil was dissolved in DMSO (0.8 mL) and directly purified by reverse-phase chromatography (Biotage reverse-phase 12 g Ultra C-18 column; 10-58-67-100% MeOH in  $\text{H}_2\text{O}$  (containing 0.1% formic acid)). Relevant fractions isolated to afford the title compound (17 mg, 77%, 0.0522 mmol) as a white solid

Formula  $\text{C}_{16}\text{H}_{23}\text{NO}_6$  Observed  $m/z$  326.1588957 Calculated  $m/z$  326.1598139 Error (ppm) -2.82.  $^1\text{H}$  NMR (600 MHz,  $\text{CDCl}_3$ )  $\delta$  1.45 (s, 9H, 16), 1.99 (p,  $J = 5.7$  Hz, 3H, 11), 3.38 (q,  $J = 5.8$  Hz, 2H, 12), 3.87 (s, 3H, 9), 4.02 (t,  $J = 5.6$  Hz, 3H, 10), 5.95 (s, 1H, 13), 6.81 (d,  $J = 8.9$  Hz, 1H, 6), 6.98 (dd,  $J = 8.9, 3.2$  Hz, 1H, 1), 7.38 (d,  $J = 3.2$  Hz, 1H, 3).  $^{13}\text{C}$  NMR (151 MHz,  $\text{CDCl}_3$ )  $\delta$  28.61, 16, 29.26, 12, 39.24, 11, 52.21, 9, 68.84, 10, 79.22, 15, 114.81, 6, 118.41, 3, 120.02, 4, 120.98, 1, 149.86, 2, 152.71, 5, 156.80, 14, 166.37, 8.



**methyl 2-[3-(tert-butoxycarbonylamino)propoxy]-5-[6-chloro-5-(1-methylindol-5-yl)-1-(2-trimethylsilylethoxymethyl)benzimidazol-2-yl]oxy-benzoate and methyl 2-[3-(tert-butoxycarbonylamino)propoxy]-5-[5-chloro-6-(1-methylindol-5-yl)-1-(2-trimethylsilylethoxymethyl)benzimidazol-2-yl]oxy-benzoate, 19**

19

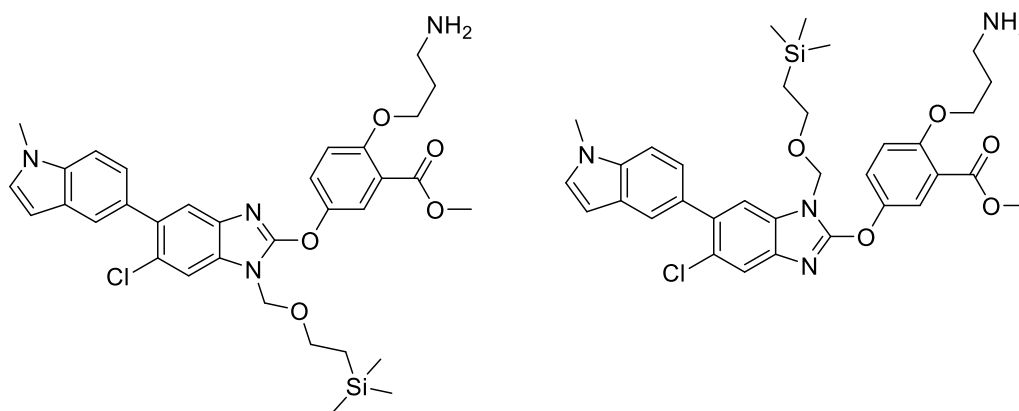


To a pale yellow of 2-[[6-chloro-5-(1-methylindol-5-yl)-2-methylsulfonyl-benzimidazol-1-yl]methoxy]ethyl-trimethyl-silane ( 43.04 mg, 0.0878 mmol) (This is a 1:1 mix of both isomers) in DMF ( 0.92 mL) was added methyl 2-[3-(tert-butoxycarbonylamino)propoxy]-5-hydroxy-benzoate ( 30.00 mg, 0.0922 mmol) giving a yellow solution with a slight brown precipitate. Reaction mixture was stirred at rt for 24 hours then partitioned between 10 ml water and 15 ml EtOAc. Org phase was washed 2 x 10 ml water, then dried over MgSO<sub>4</sub>, vacuum filtered and concentrated in vacuo. The resulting residue was purified by column chromatography 0-30-40% EtOAc in cyclohexane Sfar Duo 10g. Relevant fractions isolated to afford the title compound (52 mg, 81%, 0.0707 mmol) as a white solid.

Formula C<sub>38</sub>H<sub>47</sub>ClN<sub>4</sub>O<sub>7</sub>Si Observed m/z 735.2985 Calculated m/z 735.2981 Error (ppm) 0.5. <sup>1</sup>H NMR (600 MHz, DMSO) δ -0.08 (s, 9H, 61), -0.05 (s, 9H, 26), 0.87 (t, J = 7.9 Hz, 2H, 26), 0.91 (dd, J = 8.5, 7.5 Hz, 2H, 60), 1.37 (s, 16H, 15), 1.38 (s, 10H, 50), 1.78 (p, J = 6.5 Hz, 1H, 10), 1.86 (dp, J = 8.4, 6.5 Hz, 4H, 45), 3.14 (m, 4H, 11, 46), 3.67 (m, 4H, 24, 59), 3.77 (s, 3H, 8), 3.81 (s, 3H, 90), 3.82 (s, 3H, 35), 3.84 (s, 3H, 90),

4.09 (m, 4H, 9, 44), 5.62 (s, 2H, 23), 5.63 (s, 2H, 58), 6.45 (dd,  $J = 3.0, 0.8$  Hz, 1H, 28), 6.47 (dd,  $J = 3.1, 0.8$  Hz, 1H, 63), 7.17 (dd,  $J = 8.4, 1.7$  Hz, 1H, 67), 7.21 (dd,  $J = 8.4, 1.7$  Hz, 1H, 32), 7.26 (dd,  $J = 9.2, 8.1$  Hz, 2H, 4, 39), 7.36 (d,  $J = 3.1$  Hz, 1H, 27), 7.38 (d,  $J = 3.0$  Hz, 1H, 62), 7.40 (s, 1H, 21), 7.47 (d,  $J = 8.5$  Hz, 1H, 33), 7.50 (d,  $J = 8.5$  Hz, 1H, 68), 7.53 (d,  $J = 1.7$  Hz, 1H, 30), 7.57 (d,  $J = 1.7$  Hz, 1H, 65), 7.60 (s, 1H, 18), 7.60 (s, 1H, 56), 7.61 – 7.64 (m, 2H, 5, 40), 7.70 (dd,  $J = 4.9, 3.1$  Hz, 2H, 23, 66), 7.78 (s, 1H, 30).  $^{13}\text{C}$  NMR (151 MHz, DMSO)  $\delta$  -0.92, 15, -0.91, 50, 17.64, 60, 17.65, 25, 28.72, 15, 50, 29.57, 10, 45, 33.01, 35, 33.05, 70, 37.52, 11, 46, 52.54, 8, 52.54, 43, 66.33, 24, 66.37, 59, 67.40, 9, 44, 71.67, 23, 71.71, 58, 77.89, 14, 77.93, 49, 101.02, 28, 101.04, 63, 109.59, 68, 109.64, 33, 111.23, 18, 115.48, 4, 39, 118.72, 53, 120.81, 21, 121.08, 37, 121.09, 1, 121.73, 65, 121.77, 30, 123.13, 7, 123.15, 42, 123.56, 67, 123.57, 32, 125.67, 19, 125.99, 55, 126.21 – 126.29 (m, 56, 40, 5), 128.23, 64, 128.25, 29, 130.67, 27, 130.76, 62, 131.03, 31, 131.06, 66, 133.10, 52, 133.51, 22, 136.05, 69, 136.10, 34, 138.77, 17, 139.36, 57, 146.21, 6, 41, 151.18, 151.20, 155.90 – 156.01 (m, 3, 38), 156.06 – 156.14 (m, 13, 48), 157.18, 16, 157.35, 51, 165.67, 36, 165.69, 1.

**Methyl 2-(3-aminopropoxy)-5-[6-chloro-5-(1-methylindol-5-yl)-1-(2-trimethylsilylethoxymethyl)benzimidazol-2-yl]oxy-benzoate and methyl 2-(3-aminopropoxy)-5-[5-chloro-6-(1-methylindol-5-yl)-1-(2-trimethylsilylethoxymethyl)benzimidazol-2-yl]oxy-benzoate**

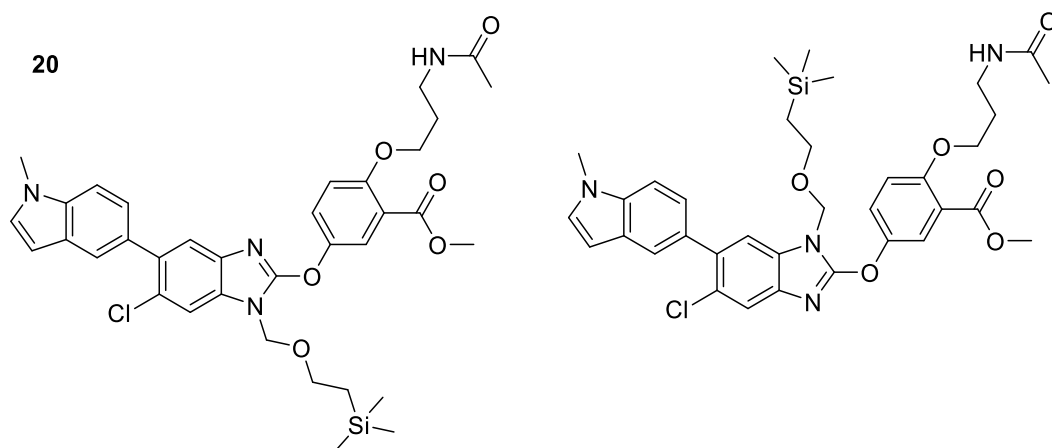


methyl 2-[3-(tert-butoxycarbonylamino)propoxy]-5-[6-chloro-5-(1-methylindol-5-yl)-1-(2-trimethylsilylethoxymethyl)benzimidazol-2-yl]oxy-benzoate ( 17.00 mg,

0.0231 mmol) and methyl 2-[3-(tert-butoxycarbonylamino)propoxy]-5-[5-chloro-6-(1-methylindol-5-yl)-1-(2-trimethylsilylethoxymethyl)benzimidazol-2-yl]oxybenzoate ( 17.00 mg, 0.0231 mmol) were taken up in DCM ( 0.46 mL, 0.1 M ) giving a pale yellow solution. trifluoroacetic acid ( 17.81 uL, 0.2312 mmol) was added giving a light red solution then concentrated in vacuo to afford the title compound (23 mg, 78%, 0.0362 mmol) as a dark red oil (mix of both isomers)

Formula C<sub>33</sub>H<sub>39</sub>ClN<sub>4</sub>O<sub>5</sub>Si Observed m/z 635.2460638 Calculated m/z 635.2451010 Error (ppm) 1.52 Ion Species (M+H)<sup>+</sup>

**methyl 2-(3-acetamidopropoxy)-5-[6-chloro-5-(1-methylindol-5-yl)-1-(2-trimethylsilylethoxymethyl)benzimidazol-2-yl]oxybenzoate and methyl 2-(3-acetamidopropoxy)-5-[5-chloro-6-(1-methylindol-5-yl)-1-(2-trimethylsilylethoxymethyl)benzimidazol-2-yl]oxybenzoate, 20**

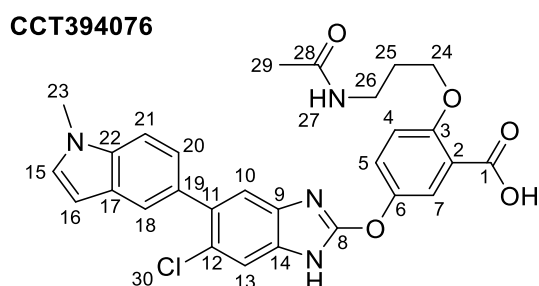


methyl 2-(3-aminopropoxy)-5-[6-chloro-5-(1-methylindol-5-yl)-1-(2-trimethylsilylethoxymethyl)benzimidazol-2-yl]oxybenzoate ( 23.00 mg, 0.0362 mmol) (a 1:1 mix of isomers) were taken up in DCM ( 0.36 mL, 0.1 M ) giving a dark red solution which was cooled to 0C. After 5 mins N,N-Diisopropylethylamine ( 12.68 uL, 0.0724 mmol) was added followed by acetyl chloride ( 1.02 uL, 0.0362 mmol), stirred at 0C for 30. Another acetyl chloride ( 1.02 uL, 0.0362 mmol) was added and left to warm to rt overnight. Another acetyl chloride ( 2.05 uL, 0.0362 mmol) was added. Stirred at 0C for 1h, then partitioned between 10 mL DCM and 10 mL sat NaHCO<sub>3</sub>. The aq phase was extracted 3 x 10mL DCM and concentrated in

vacuo afford the title compound (16 mg, 65%, 0.0236 mmol) as a brown solid (this is a 1:1 mix of isomers).

Formula C<sub>35</sub>H<sub>41</sub>ClN<sub>4</sub>O<sub>6</sub>Si Observed m/z 677.2574484 Calculated m/z 677.2562  
Error (ppm) -1.6 Ion Species (M+H)<sup>+</sup>

**2-(3-acetamidopropoxy)-5-[[6-chloro-5-(1-methylindol-5-yl)-1H-benzimidazol-2-yl]oxy]benzoic acid, CCT394076**



A 0.5-2 mL mw vial was charged with methyl 2-(3-acetamidopropoxy)-5-[6-chloro-5-(1-methylindol-5-yl)-1-(2-trimethylsilylethoxymethyl)benzimidazol-2-yl]oxybenzoate ( 16.00 mg, 0.0236 mmol) (1:1 mix of isomers) in THF ( 0.31 mL, 0.05 M ) giving a pale yellow solution. Tetrabutylammonium fluoride 1M in THF ( 0.12 mL, 0.1181 mmol) was added and the yellow/brown solution capped and heat to 80C for overnight, then concentrated and directly purified by reverse-phase chromatography (Biotage reverse-phase 12 g Ultra C-18 column; 10-65-80-100% MeOH in H<sub>2</sub>O (containing 0.1% formic acid)), relevant fractions were isolated then dissolved in 500ul of 1:1 DMSO:Acetonitrile and purified via Prep HPLC.

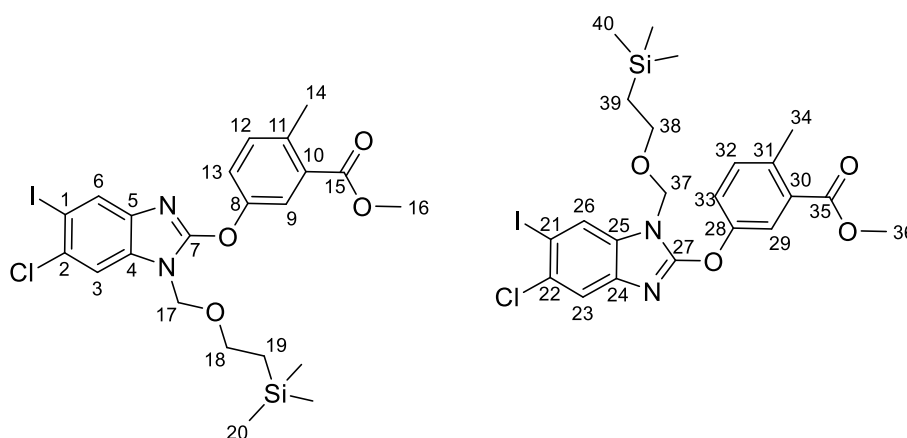
Relevant fractions isolated to afford the title compound (2 mg, 16%, 0.0037 mmol) as a pale red solid

Formula C<sub>28</sub>H<sub>25</sub>ClN<sub>4</sub>O<sub>5</sub> Observed m/z 533.1585258 Calculated m/z 533.1586241  
Error (ppm) -0.18. <sup>1</sup>H NMR (600 MHz, DMSO-*d*<sub>6</sub>) δ 1.82 (s, 3H, 29), 1.87 (p, *J* = 6.3 Hz, 3H, 25), 3.25 (q, *J* = 6.3 Hz, 3H, 26), 3.82 (s, 3H, 23), 4.10 (t, *J* = 6.0 Hz, 3H, 24), 6.46 (d, *J* = 3.0 Hz, 1H, 16), 7.18 (dd, *J* = 8.4, 1.7 Hz, 1H, 20), 7.22 (d, *J* = 9.1 Hz, 1H, 4), 7.33 (s, 1H, 10), 7.37 (d, *J* = 3.0 Hz, 1H, 15), 7.47 (d, *J* = 8.4 Hz, 1H, 21), 7.52 (s, 1H, 13), 7.54 (d, *J* = 1.7 Hz, 1H, 18), 7.57 (dd, *J* = 9.1, 3.1 Hz, 1H, 5), 7.67 (d, *J* = 3.1 Hz, 1H, 7), 7.94 (t, *J* = 5.6 Hz, 1H, 27). <sup>13</sup>C NMR (151 MHz, DMSO-*d*<sub>6</sub>) δ 22.62 , 29,

28.75 , 25, 32.58 , 23, 35.93 , 26, 67.11 , 24, 100.60 , 26, 109.16 , 21, 114.79 , 4, 114.86 , 13, 115.83 , 10, 121.29 , 18, 122.03 , 2, 122.67 , 7, 123.17 , 20, 124.78 , 12, 125.31 , 5, 127.79 , 17, 130.22 , 15, 130.77 , 19, 134.75 , 11, 135.59 , 22, 145.91 , 6, 155.19 , 3, 157.94 , 7, 166.47 , 1, 169.27 , 28.

**methyl 5-[6-chloro-5-iodo-1-(2-trimethylsilylethoxymethyl)benzimidazol-2-yl]oxy-2-methyl-benzoate and methyl 5-[5-chloro-6-iodo-1-(2-trimethylsilylethoxymethyl)benzimidazol-2-yl]oxy-2-methyl-benzoate, 21**

21



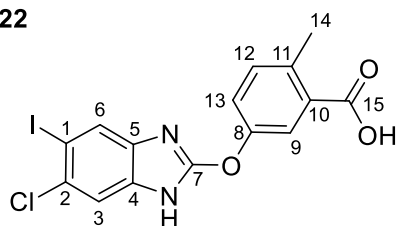
To a pale yellow of 2-[(6-chloro-5-iodo-2-methylsulfonyl-benzimidazol-1-yl)methoxy]ethyl-trimethyl-silane ( 0.99 g, 2.0374 mmol) (1:1 mix of isomers) in DMF ( 20.37 mL) was added 5-hydroxy-3-methyl benzoic acid methyl ester ( 355.49 mg, 2.1393 mmol) and  $K_2CO_3$  ( 281.60 mg, 2.0374 mmol) giving a yellow solution with a white precipitate.

Reaction mixture was stirred at rt for 5 hours then concentrated in vacuo, and partitioned between 25 mL EtOAc and 10 ml water. Aq phase extracted 2 x 10 ml EtOAc. dried over  $MgSO_4$ , vacuum filtered and concentrated in vacuo. then purified via column chromatography (Biotage Sfar Duo 25 g 0 - 15 EtOAc in cyclohexane). Relevant fractions evaporated to afford the title compound (1003 mg, 86%, 1.7507 mmol) as a white solid

Formula C22H26ClIN2O4Si Observed m/z 573.0477 Calculated m/z 573.0473 Error (ppm) 0.7. <sup>1</sup>H NMR (500 MHz, DMSO) δ -0.15 – -0.03 (m, 18H<sub>2</sub>O, 40), 0.87 (tt, *J* = 8.3, 2.0 Hz, 6H, 19, 39), 2.54 (s, 6H, 14, 34), 3.56 – 3.70 (m, 4H, 18, 38), 3.80 – 3.84 (m, 4H, 16, 36), 5.56 – 5.66 (m, 4H, 17, 37), 7.45 (d, *J* = 8.4 Hz, 2H, 12, 32), 7.56 (dd, *J* = 8.5, 2.2 Hz, 2H, 13, 33), 7.69 (q, *J* = 1.5 Hz, 1H, 3), 7.79 – 7.83 (m, 2H, 9, 29), 7.90 (q, *J* = 1.5 Hz, 1H, 6), 7.98 (q, *J* = 1.2 Hz, 1H, 23), 8.16 (d, *J* = 2.0 Hz, 1H, 26). <sup>13</sup>C NMR (126 MHz, DMSO) δ -1.49, 20, 40, 17.12, 19, 39, 20.44, 14, 34, 52.09, 16, 36, 65.91, 38, 65.93, 18, 71.26, 37, 71.27, 17, 88.92, 1, 89.58, 21, 110.71, 6, 118.20, 3, 120.62, 26, 121.78, 9, 121.82, 29, 124.29, 13, 124.34, 33, 128.39, 23, 129.69, 130.27, 130.36, 131.83, 10, 44, 133.08, 12, 32, 133.56, 134.35, 136.97, 31, 136.99, 11, 139.61, 140.43, 150.63, 8, 150.67, 28, 156.55, 156.66, 166.23, 15, 36

### 5-[(6-chloro-5-iodo-1H-benzimidazol-2-yl)oxy]-2-methyl-benzoic acid, **22**

**22**

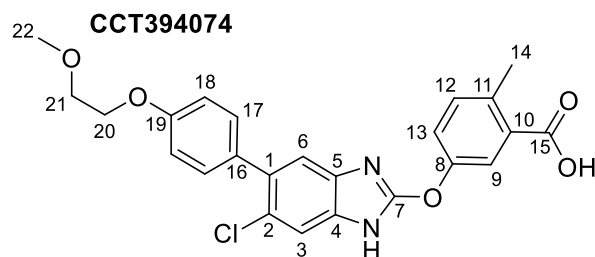


Methyl 5-[6-chloro-5-iodo-1-(2-trimethylsilylethoxymethyl)benzimidazol-2-yl]oxy-2-methyl-benzoate ( 220.00 mg, 0.384 mmol) (1:1 mix of isomers) was taken up in THF ( 6.74 mL, 0.04 M ) giving a pale yellow solution. Tetrabutylammonium fluoride 1M in THF ( 1.92 mL, 1.9201 mmol) was added and the yellow solution capped and heat to 60C for overnight. Then water ( 2.86 mL, 0.04 M ) and lithium hydroxide ( 28.75 mg, 1.152 mmol) were added giving a dark red solution with a white ppt. Heated to 60C overnight then concentrated in vacuo and the reaction mixture was dissolved in DMSO (1 mL) and directly purified by reverse-phase chromatography (Biotage reverse-phase 12 g Ultra C-18 column; 10-65-80-100% MeOH in H<sub>2</sub>O (containing 0.1% formic acid)). relevant fractions were concentrated in vacuo to afford the title compound (91 mg, 55%, 0.2123 mmol) as a white solid

Formula C<sub>15</sub>H<sub>10</sub>ClIN<sub>2</sub>O<sub>3</sub> Observed m/z 428.9511919 Calculated m/z 428.9497394 Error (ppm) 3.39. <sup>1</sup>H NMR (600 MHz, DMSO-*d*<sub>6</sub>) δ 2.54 (s, 3H, 14), 7.40 (d, *J* = 8.4 Hz, 1H, 12), 7.49 (dd, *J* = 8.3, 2.8 Hz, 1H, 13), 7.62 (s, 1H, 6), 7.77 (d, *J* = 2.8 Hz, 1H, 9),

7.89 (s, 1H, 3). <sup>13</sup>C NMR (151 MHz, DMSO-*d*<sub>6</sub>) δ 21.07 , 14, 88.80 , 1, 115.07 , 6, 122.38 , 9, 124.40 , 13, 124.58 , 3, 129.60 , 2, 132.05 , 11, 133.41 , 12, 137.00 , 10, 137.47 , 5, 138.49 , 4, 151.28 , 8, 158.39 , 7, 168.17 , 15.

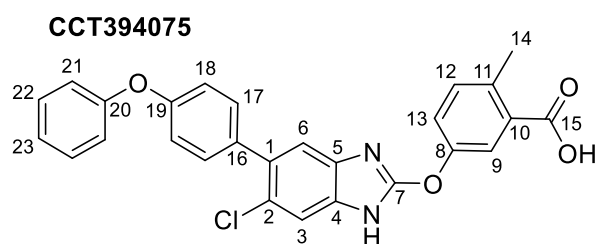
**5-[[6-chloro-5-[4-(2-methoxyethoxy)phenyl]-1H-benzimidazol-2-yl]oxy]-2-methylbenzoic acid, CCT394074**



A 2 ml MW vial was charged with 2-[4-(2-methoxyethoxy)phenyl]-4,4,5,5-tetramethyl-1,3,2-dioxaborolane ( 14.28 mg, 0.0513 mmol ) , 5-[[6-chloro-5-iodo-1H-benzimidazol-2-yl]oxy]-2-methylbenzoic acid ( 20.00 mg, 0.0467 mmol) and K<sub>2</sub>CO<sub>3</sub> ( 19.35 mg, 0.14 mmol) in 1,4-Dioxane ( 0.64 mL, 0.06 M ) and H<sub>2</sub>O ( 0.13 mL, 0.06 M ) , and degassed with N<sub>2</sub> for 5 mins. Then [1,1'-Bis(diphenylphosphino)ferrocene]dichloropalladium(II), complex with dichloromethane ( 2.00 mg, 0.0023 mmol) was added and the mixture degassed then sealed and heated to 80C overnight. Reaction mixture was then concentrated in vacuo, then dissolved in DMSO (1 mL) directly purified via prep HPLC 20:80 to 0:100 water:methanol, to afford the title compound (6 mg, 28%, 0.0131 mmol) as an off white solid

Formula C<sub>24</sub>H<sub>21</sub>ClN<sub>2</sub>O<sub>5</sub> Observed m/z 453.1210060 Calculated m/z 453.1211760 Error (ppm) -0.37. <sup>1</sup>H NMR (600 MHz, DMSO-*d*<sub>6</sub>) δ 2.54 (s, 3H, 14), 3.33 (s, 3H, 22), 3.67 – 3.70 (m, 2H, 21), 4.12 – 4.15 (m, 2H, 20), 6.98 – 7.02 (m, 2H, 18), 7.29 (s, 1H, 6), 7.31 – 7.35 (m, 2H, 17), 7.40 (d, *J* = 8.4 Hz, 1H, 12), 7.49 (dd, *J* = 8.4, 2.7 Hz, 1H, 13), 7.51 – 7.54 (m, 1H, 3), 7.77 (d, *J* = 2.7 Hz, 1H, 9). <sup>13</sup>C NMR (151 MHz, DMSO-*d*<sub>6</sub>) δ 20.61, 14, 58.18 , 22, 66.92 , 20, 70.42 , 21, 112.39 , 6, 113.98 , 18, 121.72 , 9, 123.69 , 13, 124.29 , 2, 127.24 , 3, 130.81 , 17, 131.92 , 10, 132.13 , 16, 132.89 , 12, 136.25 , 11, 151.07 , 8, 157.72 , 1, 157.79 , 19, 167.88 , 15.

**5-[[6-chloro-5-(4-phenoxyphenyl)-1H-benzimidazol-2-yl]oxy]-2-methyl-benzoic acid, CCT394075**

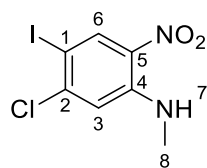


4-phenoxyphenylboronic acid ( 10.99 mg, 0.0513 mmol ) , 5-[[6-chloro-5-iodo-1H-benzimidazol-2-yl]oxy]-2-methyl-benzoic acid ( 20.00 mg, 0.0467 mmol) and Potassium Carbonate ( 19.35 mg, 0.14 mmol) were taken up in 1,4-Dioxane ( 0.64 mL, 0.06 M ) and H<sub>2</sub>O ( 0.13 mL, 0.06 M ) and degassed with N<sub>2</sub> for 5 mins. Then [1,1'-Bis(diphenylphosphino)ferrocene]dichloropalladium(II), complex with dichloromethane ( 2.00 mg, 0.0023 mmol) was added and the reaction mixture degassed for 2 mins, then the tube was capped and heated to 80C for 24 h. Reaction mixture was concentrated in vacuo then dissolved in DMSO (1 mL) directly purified by reverse-phase chromatography (Biotage reverse-phase 12 g Ultra C-18 column; 10-65-80-100% MeOH in H<sub>2</sub>O (containing 0.1% formic acid)). Relevant fractions evaporated to afford the title compound (10 mg, 45%, 0.021 mmol) as an off white solid

Formula C<sub>27</sub>H<sub>19</sub>ClN<sub>2</sub>O<sub>4</sub> Observed m/z 471.1095771 Calculated m/z 471.1106113 Error (ppm) -2.20. <sup>1</sup>H NMR (600 MHz, DMSO-*d*<sub>6</sub>) δ 2.54 (s, 3H, 14), 7.05 (d, *J* = 8.1 Hz, 2H, 18), 7.10 (d, *J* = 8.0 Hz, 2H, 21), 7.18 (t, *J* = 7.3 Hz, 1H, 23), 7.34 (s, 1H, 6), 7.39 – 7.46 (m, 5H, 4, 17, 22), 7.50 (dd, *J* = 8.3, 2.7 Hz, 1H, 13), 7.54 (s, 1H, 3), 7.78 (d, *J* = 2.7 Hz, 1H, 9). <sup>13</sup>C NMR (151 MHz, DMSO-*d*<sub>6</sub>) δ 21.07 , 14, 112.96 , 6, 118.20 , 18, 118.55 , 3, 119.60 , 21, 122.22 , 12, 124.24 , 13, 124.27 , 23, 124.65 , 2, 130.62 , 22, 131.79 , 17, 132.21 , 10, 132.96 , 1, 133.39 , 12, 135.17 , 16, 136.79 , 11, 151.51 , 8, 156.62 , 19, 156.74 , 20, 168.28 , 15.



### **-chloro-4-iodo-N-methyl-2-nitro-aniline, 23**

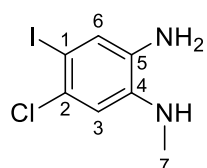


5-chloro-4-iodo-2-nitro-aniline ( 50.00 mg, 0.1675 mmol) was taken up in THF ( 0.84 mL, 0.2 M ) giving a yellow solution which was cooled to 0C for 10 mins. Sodium Hydride ( 8.04 mg, 0.201 mmol) was added giving a dark purple solution which was stirred at 0C for 10 mins. Then Iodomethane ( 10.43  $\mu$ L, 0.1675 mmol) was added and the purple suspension stirred at 0C for 1h. 1ml water was added giving a bright orange solution in a yellow solution, which was concentrated to an orange solid, then purified via column chromatography (Biotage sfar Duo 5g 0-10% EtOAc in cyclohexane).

Relevant fractions isolated to afford the title compound (31 mg, 59%, 0.0992 mmol) as an orange solid.

$^1\text{H}$  NMR (600 MHz, Chloroform-*d*)  $\delta$  3.00 (d,  $J$  = 5.1 Hz, 3H, 11), 6.98 (s, 1H, 3), 7.97 (s, 1H, 7), 8.59 (s, 1H, 6).  $^{13}\text{C}$  NMR (151 MHz, Chloroform-*d*)  $\delta$  30.02 , 8, 78.66 , 1, 113.74 , 3, 131.52 , 5, 137.64 , 6, 146.18, 2, 146.76, 4.

### **4-chloro-5-iodo-N2-methyl-benzene-1,2-diamine, 24**



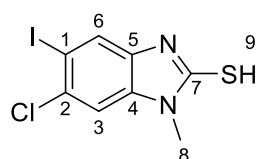
An orange suspension of 5-chloro-4-iodo-N-methyl-2-nitro-aniline ( 689.00 mg, 2.2049 mmol) in Ethanol ( 12.25 mL) and Water ( 2.45 mL) was degassed with N<sub>2</sub> and then ammonium chloride ( 0.30 g, 5.5302 mmol) and then Iron ( 0.68 g, 12.1629 mmol) were added. The slurry was heated to 50C for 3h.

Then filtered through a pad of decelite and washed with EtOH, concentrated in vacuo, then partitioned between EtOAc (10 mL) and water (10 mL). The Aq phase was extracted 3 x 10 mL EtOAc, and the combined organics were dried (MgSO<sub>4</sub>),

vacuum filtered and concentrated in vacuo to a black solid. Used in next step without further purification

Formula C7H8ClIN2 Observed m/z 282.9477227 Calculated m/z 282.9493454 Error (ppm) -5.74. <sup>1</sup>H NMR (600 MHz, CDCl<sub>3</sub>) δ 2.81 (s, 3H, 7), 6.66 (s, 1H, 3), 7.08 (s, 1H, 6). <sup>13</sup>C NMR (151 MHz, CDCl<sub>3</sub>) δ 30.78 , 7, 81.89 , 1, 111.18 , 3, 126.19 , 6, 130.00, 2, 133.86, 5, 140.73 , 4.

#### 6-chloro-5-iodo-1-methyl-benzimidazole-2-thiol, 24

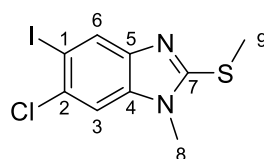


A 50 mL RBF was charged with potassium hydroxide ( 114.40 mg, 2.0389 mmol) in EtOH ( 14.43 mL) and Water ( 2.56 mL) giving a black suspension. 4-chloro-5-iodo-N2-methyl-benzene-1,2-diamine ( 480.00 mg, 1.6991 mmol) and carbon disulfide ( 122.62 uL, 2.0389 mmol) were added and the black solution heated to 80C overnight.

Then the solution was concentrated in vacuo and partitioned between 10 mL water and 10 ml EtOAc. As phase was extracted 3 x 15 mL EtOAc. Combined organics were dried over MgSO<sub>4</sub>, vacuum filtered and concentrated in vacuo giving the title compound (560 mg, 96%, 1.6391 mmol) as a grey solid

Formula C8H6ClIN2S Observed m/z 324.9050450 Calculated m/z 324.9057661 Error (ppm) -2.22. <sup>1</sup>H NMR (600 MHz, DMSO) δ 3.60 (s, 3H, 8), 7.60 (s, 1H, 3), 7.73 (s, 1H, 6), 12.91 (s, 1H, 9). <sup>13</sup>C NMR (151 MHz, DMSO) δ 30.29, 8, 90.36 , 1, 110.15 , 6, 119.35 , 3, 130.58, 2, 131.04, 5, 134.52 , 4, 170.11 , 8.

#### 6-chloro-5-iodo-1-methyl-2-methylsulfanyl-benzimidazole

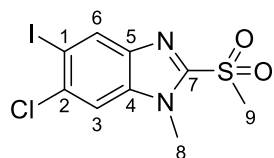


A 50 mL RBF was charged with 6-chloro-5-iodo-1-methyl-benzimidazole-2-thiol ( 500.00 mg, 1.5405 mmol) in acetone ( 15.40 mL) giving a brown suspension which was cooled to 0C. K<sub>2</sub>CO<sub>3</sub> ( 234.20 mg, 1.6945 mmol) was added followed by Iodomethane ( 105.49 uL, 1.6945 mmol) and the reaction mixture stirred at 0C for 30 mins then let to warm to rt and stirred at rt for 3h.

The reaction mixture was concentrated in vacuo and then partitioned between 15 mL EtOAc and 10mL water and 5 ml brine. The aq layer was extracted 3 x 10 mL EtOAc. Combined organic layers dried over MgSO<sub>4</sub>, vacuum filtered and concentrated in vacuo to afford the title compound (493 mg, 95%, 1.456 mmol) as a black solid.

Formula C<sub>9</sub>H<sub>8</sub>ClIN<sub>2</sub>S Observed m/z 338.9206938 Calculated m/z 338.9214162 Error (ppm) -2.13. H NMR (600 MHz, DMSO) δ 2.71 (s, 4H, 9), 3.64 (s, 3H, 8), 7.85 (s, 1H, 3), 8.07 (s, 1H, 6). <sup>13</sup>C NMR (151 MHz, DMSO) δ 14.10 , 9, 30.09 , 8, 88.90 , 1, 110.16 , 3, 127.66 , 6, 129.35, 2, 137.86 , 4, 143.27, 5, 155.55 , 7.

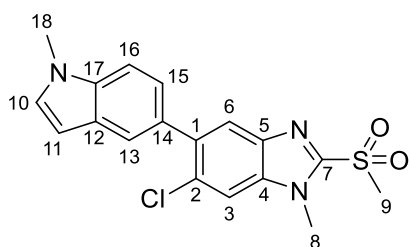
#### 6-chloro-5-iodo-1-methyl-2-methylsulfonyl-benzimidazole, 25



6-chloro-5-iodo-1-methyl-2-methylsulfonyl-benzimidazole ( 705.58 mg, 3.1483 mmol) was taken up in DCM ( 31.48 mL, 0.05 M ) and cooled to 0C. 3-Chloroperoxybenzoic acid (705.58, 3.1 mmol) was added portion wise over 5 mins giving a brown solution. Suspension was stirred at 0C for 1 h then at rt for 2h. Then 3-Chloroperoxybenzoic acid ( 352.79 mg, 1.5741 mmol) was added and stirred overnight. Then 20 mL sodium sulphite solution was added and stirred at rt for 15 mins. The Aq phase was extracted 2 x 10 mL DCM. Combined organics were dried over MgSO<sub>4</sub>, vacuum filtered and concentrated in vacuo to a yellow oil then dissolved in 1mL DMSO (a suspension also formed), and the supernatant was directly purified by reverse-phase chromatography (Biotage reverse-phase 12 g Ultra C-18 column; 10-60-70-100 % MeOH in H<sub>2</sub>O (containing 0.1% formic acid)). Relevant fractions isolated to afford the title compound (316 mg)

Formula C<sub>9</sub>H<sub>8</sub>ClIN<sub>2</sub>O<sub>2</sub>S Observed m/z 370.9112503 Calculated m/z 370.9112454  
Error (ppm) 0.01. <sup>1</sup>H NMR (600 MHz, DMSO-*d*<sub>6</sub>) δ 3.60 (s, 3H, 9), 4.06 (s, 3H, 8), 8.17 – 8.21 (m, 1H, 3), 8.39 – 8.45 (m, 1H, 6). <sup>13</sup>C NMR (151 MHz, DMSO-*d*<sub>6</sub>) δ 32.06 , 8, 42.64 , 9, 92.35 , 1, 112.67 , 3, 131.58 , 6, 133.65, 2, 136.81 , 4, 140.19, 5, 149.84 , 7.

### 6-chloro-1-methyl-5-(1-methylindol-5-yl)-2-methylsulfonyl-benzimidazole, 26



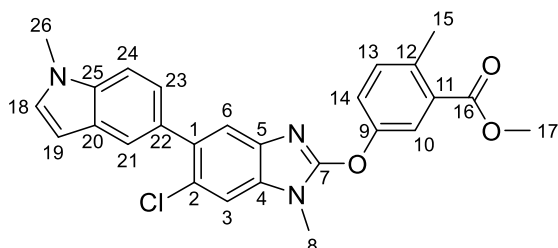
with 6-chloro-5-iodo-1-methyl-2-methylsulfonyl-benzimidazole ( 300.00 mg, 0.8095 mmol) , 1-methyl-5-indolyboronic acid ( 148.74 mg, 0.85 mmol) and Potassium Carbonate ( 335.65 mg, 2.4286 mmol) were taken up in 1,4-Dioxane ( 6.69 mL, 0.1 M ) and H<sub>2</sub>O ( 1.40 mL, 0.1 M ) giving a brown solution, which was purged with Nitrogen. Then [1,1'-Bis(diphenylphosphino)ferrocene]dichloropalladium(II), complex with dichloromethane ( 33.05 mg, 0.0405 mmol) , and the solution purged with Nitrogen, then heated to 90C for 2h under an N<sub>2</sub> atmosphere

The reaction mixture was left to cool to rt then filtered through celite, which was washed with EtOAc, then concentrated in vacuo, then partitioned between 15 mL EtOAc and 15 mL water. Aq phase was extracted 3 x 10 mL EtOAc, combined orgs were dried over MgSO<sub>4</sub>, concentrated in vacuo, Then purified via column chromatography (10g, Biotage Sfar Duo, 0-> 30 -> 100% EtOAc in cyclohexane). Relevant fractions evaporated to give the title compound (258 mg, 85%, 0.6901 mmol) as a yellow solid

Formula C<sub>18</sub>H<sub>16</sub>ClIN<sub>3</sub>O<sub>2</sub>S Observed m/z 374.0726 Calculated m/z 374.0730 Error (ppm) -1.1. <sup>1</sup>H NMR (600 MHz, DMSO-*d*<sub>6</sub>) δ 3.61 (s, 3H, 9), 3.84 (s, 3H, 18), 4.13 (s, 3H, 8), 6.46 – 6.50 (m, 1H, 11), 7.21 (dd, *J* = 8.4, 1.7 Hz, 1H, 15), 7.34 – 7.41 (m, 1H, 10), 7.51 (d, *J* = 8.4 Hz, 1H, 16), 7.58 (d, *J* = 1.7 Hz, 1H, 13), 7.80 (s, 1H, 6), 8.10 (s, 1H, 3). <sup>13</sup>C NMR (151 MHz, DMSO-*d*<sub>6</sub>) δ 32.01 , 8, 32.59 , 18, 42.71 , 9, 100.65 , 11,

109.28 , 16, 112.73 , 3, 121.38 , 13, 122.86 , 6, 123.04 , 15, 127.79 , 12, 129.84 , 2, 129.99 , 14, 130.38 , 10, 135.61 , 4, 135.76 , 10, 137.59 , 1, 139.03 , 5, 149.49 , 7.

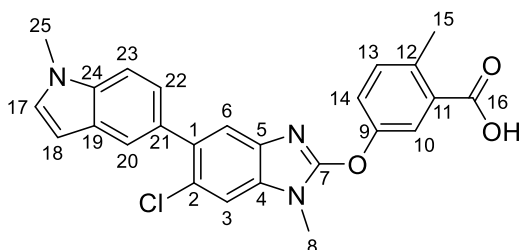
**methyl 5-[6-chloro-1-methyl-5-(1-methylindol-5-yl)benzimidazol-2-yl]oxy-2-methyl-benzoate, 5420-60, 27**



6-chloro-1-methyl-5-(1-methylindol-5-yl)-2-methylsulfonyl-benzimidazole ( 21.00 mg, 0.0562 mmol ) , 5-hydroxy-3-methyl benzoic acid methyl ester ( 14.00 mg, 0.0843 mmol) and Potassium Carbonate ( 11.65 mg, 0.0843 mmol) were taken up in Dry DMF ( 0.22 mL, 0.25 M) giving a brown solution with a white suspension. Stirred rt for 2h, then heated to 60C for 2 days giving a dark brown solution with a white suspension. The reaction mixture was partitioned between 25 mL EtOAc and 10 ml water. Aq phase extracted 2 x 10 ml EtOAc. dried over MgSO<sub>4</sub>, vacuum filtered and concentrated in vacuo. then purified via column chromatography (biotage 10g, 0-30% EtOAc in cyclohexane) to afford the title compound (27 mg, 105%, 0.0587 mmol) as a yellow solid.

Formula C<sub>26</sub>H<sub>22</sub>ClN<sub>3</sub>O<sub>3</sub> Observed m/z 460.1421485 Calculated m/z 460.1422458 Error (ppm) -0.21. <sup>1</sup>H NMR (600 MHz, DMSO-*d*<sub>6</sub>) δ 2.54 (s, 3H, 15), 3.77 (s, 3H, 8), 3.82 (s, 3H, 26), 3.83 (s, 3H, 17), 6.45 (dd, *J* = 3.0, 0.9 Hz, 1H, 19), 7.16 (dd, *J* = 8.4, 1.7 Hz, 1H, 23), 7.36 (d, *J* = 3.1 Hz, 1H, 18), 7.37 (s, 1H, 6), 7.43 – 7.49 (m, 2H, 13, 24), 7.53 (dd, *J* = 1.8, 0.7 Hz, 1H, 21), 7.60 (dd, *J* = 8.4, 2.7 Hz, 1H, 14), 7.72 (s, 1H, 3), 7.86 (d, *J* = 2.7 Hz, 1H, 10). <sup>13</sup>C NMR (151 MHz, DMSO-*d*<sub>6</sub>) δ 20.46 , 15, 28.84 , 8, 32.55 , 26, 52.14 , 17, 100.55 , 19, 109.12 , 24, 110.30 , 3, 120.14 , 6, 121.27 , 21, 121.94 , 10, 123.16 , 23, 124.42 , 14, 124.76 , 2, 127.76 , 20, 130.16 , 18, 130.39, 11, 133.03 , 13, 133.79 , 4, 134.95 , 1, 135.55 , 25, 136.57 , 12, 138.21 , 5, 151.10 , 9, 156.61 , 7, 166.45 , 16.

**5-[6-chloro-1-methyl-5-(1-methylindol-5-yl)benzimidazol-2-yl]oxy-2-methylbenzoic acid, 5420-62, CCT393901**

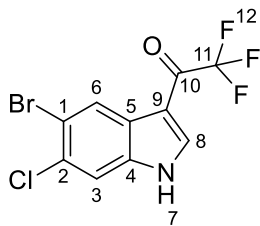


methyl 5-[6-chloro-1-methyl-5-(1-methylindol-5-yl)benzimidazol-2-yl]oxy-2-methylbenzoate ( 27.00 mg, 0.0587 mmol) was taken up in THF ( 0.59 mL, 0.05 M ) and Water ( 0.59 mL, 0.05 M ) giving a yellow suspension. lithium hydroxide ( 7.03 mg, 0.2935 mmol) was added and the suspension stirred at 30C overnight.

Reaction mixture was concentrated in vacuo, then dissolved in DMSO (1 mL) and directly purified by reverse-phase chromatography (Biotage reverse-phase 12 g Ultra C-18 column; 10-65-85-100% MeOH in H<sub>2</sub>O (containing 0.1% formic acid)). Relevant fractions evaporated to afford the title compound (22 mg, 82%, 0.0484 mmol) as an off white solid

Formula C<sub>25</sub>H<sub>20</sub>ClN<sub>3</sub>O<sub>3</sub> Observed m/z 446.1266703 Calculated m/z 446.1265957 Error (ppm) 0.17. <sup>1</sup>H NMR (600 MHz, DMSO) δ 2.54 (s, 3H, 15), 3.76 (s, 3H, 8), 3.81 (s, 3H, 25), 6.45 (dd, *J* = 3.1, 0.9 Hz, 1H, 18), 7.17 (dd, *J* = 8.4, 1.7 Hz, 1H, 22), 7.35 (d, *J* = 3.1 Hz, 1H, 17), 7.37 (s, 1H, 6), 7.39 (d, *J* = 8.4 Hz, 1H, 13), 7.46 (d, *J* = 8.4 Hz, 1H, 13), 7.50 – 7.54 (m, 2H, 5, 20), 7.71 (s, 1H, 3), 7.82 (d, *J* = 2.7 Hz, 1H, 10). <sup>13</sup>C NMR (151 MHz, DMSO) δ 20.63 , 15, 28.86 , 8, 32.57 , 25, 100.59 , 18, 109.14 , 23, 110.30 , 3, 120.14 , 6, 121.30 , 20, 121.88 , 10, 123.20 , 22, 123.60 , 14, 124.76 , 2, 127.79 , 19, 130.18 , 17, 130.84 , 21, 132.32 , 11, 132.79 , 13, 133.80 , 4, 134.95 , 1, 135.58 , 24, 136.24 , 12, 138.27 , 5, 151.09 , 9, 156.67 , 7, 168.00 , 16.

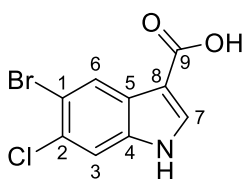
### 1-(5-bromo-6-chloro-1H-indol-3-yl)-2,2,2-trifluoro-ethanone 30



5-Bromo-6-chloro-1H-indole ( 50.00 mg, 0.2169 mmol) was taken up in DMF ( 1.08 mL, 0.2 M ) giving a brown/yellow solution, and cooled to 0C. trifluoric acid anhydride ( 0.12 mL, 0.8677 mmol) was added dropwise, and the solution stirred at 0C for 1h. Sat Na<sub>2</sub>CO<sub>3</sub> solution was added dropwise to the solution at 0C, until bubbling stopped. The tan precipitate was filtered off and washed with ice cold water. Precipitate dried overnight to give the title compound (64 mg, 90%, 0.196 mmol)

Ret. time = 1.669 mins Observed mass 323.9076 Calculated formula [M+H]<sup>+</sup> C<sub>10</sub>H<sub>5</sub>BrClF<sub>3</sub>NO Target m/z 323.9033 Error 13.241. <sup>1</sup>H NMR (600 MHz, Methanol-*d*<sub>4</sub>) δ 7.69 (s, 1H, 3), 8.28 (q, *J* = 1.8 Hz, 1H, 8), 8.50 (s, 1H, 6). <sup>13</sup>C NMR (151 MHz, Methanol-*d*<sub>4</sub>) δ 110.45 , 9, 115.35 , 3, 117.65 , 1, 118.39 (q, *J* = 290.0 Hz, 11), 127.03 , 6, 127.80 , 5, 130.70 , 2, 138.36 , 4, 139.85 (q, *J* = 4.8 Hz, 8), 175.92 (q, *J* = 34.9 Hz, 11). <sup>19</sup>F NMR (471 MHz, Methanol-*d*<sub>4</sub>) δ -74.05 (d, *J* = 1.8 Hz, 12). <sup>19</sup>F NMR (471 MHz, Methanol-*d*<sub>4</sub>) δ -74.05 , 12.

### 5-bromo-6-chloro-1H-indole-3-carboxylic acid, 31

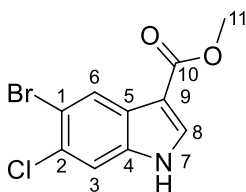


1-(5-bromo-6-chloro-1H-indol-3-yl)-2,2,2-trifluoro-ethanone ( 51.00 mg, 0.1562 mmol) was dissolved in Dry THF ( 1.00 mL, 0.1 M ) and Water ( 0.50 mL, 0.1 M ) giving a brown solution. Sodium Hydroxide ( 1.41 mg, 0.4686 mmol, 3 equiv) was added and the solution heated at 70C overnight then heated to 80C and Sodium Hydroxide ( 3.28 mg, 1.0934 mmol, 7 equiv) NaOH was added. Sodium Hydroxide ( 120.00 mg, 40 mmol) was added and the suspension heated at 100C for 4h.

The solution was cooled to rt, and then 10 mL EtOAc and 5 mL water was added. Acidified to pH 1-2 with 2M HCl, then partitioned and the aq phase extracted 3 x 10 mL EtOAc. Combined organics were dried over MgSO<sub>4</sub>, vacuum filtered and concentrated in vacuo, then dried on the title compound (40 mg, 93%, 0.1457 mmol) as a brown solid

Ret. time = 1.394 mins Observed mass 271.9151 Calculated formula C<sub>9</sub>H<sub>5</sub>BrClNO<sub>2</sub> Target m/z 271.9108 Error 15.707. <sup>1</sup>H NMR (600 MHz, Methanol-*d*<sub>4</sub>) δ 7.63 (s, 1H, 3), 8.00 (s, 1H, 7), 8.32 (s, 1H, 6). <sup>13</sup>C NMR (151 MHz, Methanol-*d*<sub>4</sub>) δ 108.53 , 8, 114.53 , 3, 115.66 , 1, 126.42 , 6, 127.70 , 5, 128.91 , 2, 135.34 , 7, 137.48 , 4, 168.22 , 9.

### **methyl 5-bromo-6-chloro-1H-indole-3-carboxylate, 32**

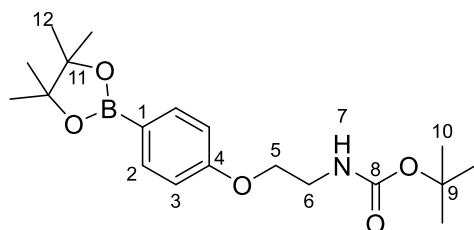


5-bromo-6-chloro-1H-indole-3-carboxylic acid ( 766.00 mg, 2.7905 mmol) was taken up in MeOH ( 56.90 mL, 0.05 M ) giving a brown solution. sulfuric acid (concentrated) ( 0.02 mL, 0.2791 mmol) was added and the solution heated to 60C overnight, then 90C for 24 h. Solution concentrated in vacuo, then partitioned between 20 mL EtOAc and 20 mL (50%sat NaHCO<sub>3</sub> and 50% H<sub>2</sub>O). The aq phase was extracted 3 x 15 mL EtOAc and combined organics dried over MgSO<sub>4</sub>, vacuum filtered and concentrated in vacuo to the title compound (759 mg, 91%, 2.5517 mmol) as a red solid

retention time = 2.750 min Formula C<sub>10</sub>H<sub>7</sub>BrClNO<sub>2</sub> Observed m/z 287.9421377 Calculated m/z 287.9421455 Error (ppm)-0.03. <sup>1</sup>H NMR (600 MHz, DMSO-*d*<sub>6</sub>) δ 3.82 (s, 3H, 11), 7.74 (s, 1H, 3), 8.18 (s, 1H, 8), 8.26 (s, 1H, 6), 12.17 (s, 1H, 7). <sup>13</sup>C NMR (151 MHz, DMSO-*d*<sub>6</sub>) δ 50.99 , 11, 106.05 , 9, 113.92 , 1, 114.03 , 3, 124.67 , 6, 126.00 , 2, 126.50 , 5, 134.75 , 8, 135.84 , 4, 164.13 , 10.



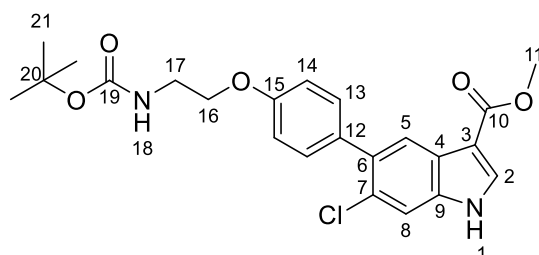
**tert-butyl N-[2-[4-(4,4,5,5-tetramethyl-1,3,2-dioxaborolan-2-yl)phenoxy]ethyl]carbamate, 34**



4-(4,4,5,5-Tetramethyl-1,3,2-dioxaborolan-2-yl)phenol ( 500.00 mg, 2.272 mmol), **29**, was taken up in DMF ( 10.33 mL, 0.2200 M ) giving a black solution. Potassium Carbonate ( 955.75 mg, 6.816 mmol) and 2-(Boc-amino)ethyl bromide ( 509.16 mg, 2.272 mmol) were added and the suspension heated at 60C overnight. More 2-(Boc-amino)ethyl bromide ( 127.29 mg, 0.5680 mmol) was added and the suspension stirred at 60C for 5h. Then the red mixture was partitioned between 15 mL water and 15 mL EtOAc. The aq phase was extracted 3 x 15 mL EtOAc. Combined organics dried over MgSO<sub>4</sub>, vacuum filtered and concentrated in vacuo to a red oil. Purified via column chromatography (0 - 20 % EtOAc in cyclohexane). Relevant fractions evaporated to afford the title compound (816 mg, 79%, 1.7971 mmol) as a colourless oil.

Formula C<sub>19</sub>H<sub>30</sub>BNO<sub>5</sub>. Observed m/z 363.2343260. Calculated m/z 363.2326116. Error (ppm) 4.72. <sup>1</sup>H NMR (600 MHz, Chloroform-*d*) δ 1.32 (s, 12H, 12), 1.44 (s, 9H, 10), 3.53 (q, *J* = 5.5 Hz, 2H, 6), 4.03 (t, *J* = 5.1 Hz, 2H, 5), 5.01 (s, 1H, 7), 6.85 – 6.89 (m, 2H, 3), 7.72 – 7.75 (m, 2H, 2). <sup>13</sup>C NMR (151 MHz, Chloroform-*d*) δ 24.97 , 12, 28.51 , 10, 40.21 , 6, 67.10 , 5, 83.72 , 11, 113.91, 3, 121.19 , 1, 136.69 , 2, 161.25 , 4, 171.30 , 8.

**Methyl 5-[4-[2-(tert-butoxycarbonylamino)ethoxy]phenyl]-6-chloro-1H-indole-3-carboxylate CCT390617**

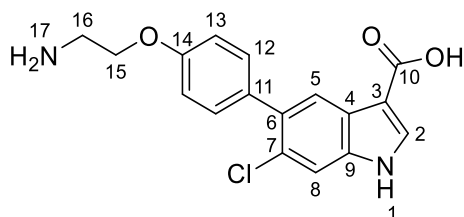


tert-butyl N-[2-[4-(4,4,5,5-tetramethyl-1,3,2-dioxaborolan-2-yl)phenoxy]ethyl]carbamate ( 770.00 mg, 1.6958 mmol) and methyl 5-bromo-6-chloro-1H-indole-3-carboxylate ( 504.41 mg, 1.6958 mmol) were taken up in Toluene ( 35.13 mL, 0.0300 M ) and Water ( 17.30 mL, 0.0300 M ) giving a brown solution. N<sub>2</sub> was bubbled through the solution for 5 mins then Potassium Carbonate ( 1.19 g, 8.4788 mmol) and [1,1'-Bis(diphenylphosphino)ferrocene]dichloropalladium(II), complex with dichloromethane ( 72.82 mg, 0.0848 mmol) were added giving a black mixture and heated to 80°C overnight then 120°C for 24 h

Mixture left to cool to rt, then concentrated *in vacuo* to a black solid which was taken up in 30 mL EtOAc and filtered through celite, and washed with EtOAc. Partitioned with 50 mL water. Aq phase was extracted 2 x 15 mL EtOAc. Combined organics were dried over MgSO<sub>4</sub>, vacuum filtered and concentrated in vacuo. Crude oil was purified via column chromatography (0 - 40 - 45 EtOAc in cyclohexane). Relevant fractions evaporated to give the title compound (511 mg, 62%, 1.0567 mmol) as a white solid

Ret. time = 2.930 mins. Observed mass = 467.1355. Calculated formula [M+Na]<sup>+</sup> C<sub>23</sub>H<sub>25</sub>ClN<sub>2</sub>O<sub>5</sub>Na. Target m/z 467.1344. Error 2.31 ppm. <sup>1</sup>H NMR (600 MHz, Chloroform-*d*) δ 1.47 (s, 9H, 21), 3.52 – 3.62 (m, 2H, 17), 3.90 (s, 3H, 11), 4.08 (t, *J* = 5.1 Hz, 2H, 16), 5.01 – 5.11 (m, 1H, 18), 6.93 – 6.99 (m, 2H, 14), 7.38 – 7.44 (m, 2H, 13), 7.53 (s, 1H, 8), 7.93 (d, *J* = 3.0 Hz, 1H, 2), 8.10 (s, 1H, 5), 8.84 (s, 1H, 1). <sup>13</sup>C NMR (151 MHz, Chloroform-*d*) δ 28.56 , 21, 40.33 , 17, 51.36 , 11, 67.34 , 16, 79.74 , 20, 109.21 , 3, 112.51 , 8, 113.97 , 14, 123.79 , 5, 124.93 , 9, 128.34 , 7, 131.32 , 13, 132.14 , 2, 133.30 , 12, 134.63 , 6, 135.70 , 4, 156.13 , 19, 157.98 , 15, 165.36 , 10.

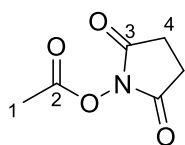
### 5-[4-(2-aminoethoxy)phenyl]-6-chloro-1H-indole-3-carboxylic acid, 35



Methyl 5-[4-[2-(tert-butoxycarbonylamino)ethoxy]phenyl]-6-chloro-1H-indole-3-carboxylate ( 500.00 mg, 1.1238 mmol) was taken up in THF ( 1.00 mL, 0.5600 M) and Water ( 1.00 mL, 0.5600 M) giving a brown suspension. Sodium hydroxide ( 134.86 mg, 3.3715 mmol) was added giving a light green solution which was heated to 100°C for 6h giving a brown suspension in a yellow solution. Concentrated *in vacuo*, then 5 mL water and 10 mL EtOAc was added. Acidified to pH = 3 with 2M HCl. The aq phase was extracted 3 x 10 mL EtOAc and combined organics dried over MgSO<sub>4</sub>, vacuum filtered and concentrated *in vacuo* to a brown oil. Taken up in DCM ( 10.00 mL) giving an off white suspension and cooled to 0°C. Trifluoroacetic acid ( 0.86 mL, 11.238 mmol) was added dropwise giving a brown solution, which was left to warm to rt and stirred for 2h. More trifluoroacetic acid ( 0.43 mL, 5.6191 mmol) was added and the red/brown solution stirred at rt for 1h. The solution was concentrated *in vacuo* to a brown/red oil. Triturated from diethyl ether to afford the title compound (380 mg, 102%, 1.1488 mmol)

<sup>1</sup>H NMR (600 MHz, DMSO-*d*<sub>6</sub>) δ 3.27 (s, 3H, 16), 4.23 (t, *J* = 5.1 Hz, 2H, 15), 7.05 – 7.10 (m, 2H, 13), 7.37 – 7.42 (m, 2H, 12), 7.64 (s, 1H, 8), 7.94 (s, 1H, 5), 8.08 (d, *J* = 2.9 Hz, 1H, 2), 8.13 (s, 1H, 17), 11.93 – 12.17 (m, 1H, 1). <sup>13</sup>C NMR (151 MHz, DMSO-*d*<sub>6</sub>) δ 38.44 , 16, 64.45 , 15, 107.59 , 3, 112.96 , 8, 114.25 , 13, 122.71 , 5, 125.30 , 9, 125.80 , 7, 130.89 , 12, 132.69 , 6, 133.11 , 11, 133.88 , 2, 136.03 , 4, 157.09 , 14, 165.62 , 10.

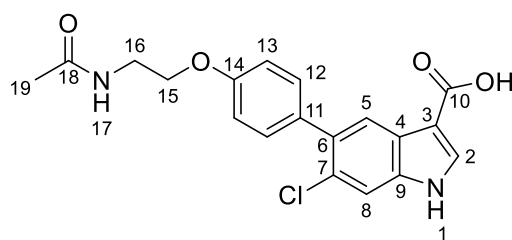
### (2,5-dioxopyrrolidin-1-yl) acetate, 36



A RBF was charged with acetic acid ( 47.62 uL, 0.8326 mmol) in DCM ( 4.16 mL, 0.2000 M ). Then 1-(3-dimethylaminopropyl)-3-ethylcarbodiimide hydrochloride ( 175.58 mg, 0.9159 mmol) was added and the colourless solution stirred at rt for 10 mins then N-hydroxysuccinimide ( 105.41 mg, 0.9159 mmol) was added giving a very small amount of a white solid in a colourless solution. Left to stir at rt overnight. The solution was then diluted with 10 mL DCM and 20 mL sat NaHCO<sub>3</sub> solution was added. The organic phase was washed 2 x 10 mL NaHCO<sub>3</sub> and 1 x 10 mL brine, then dried over MgSO<sub>4</sub>, vacuum filtered and concentrated in vacuo and then on the high vac to afford the title compound (50 mg, 29%, 0.2387 mmol) as a white solid

<sup>1</sup>H NMR (600 MHz, DMSO-d<sub>6</sub>) δ 2.36 (s, 3H, 1), 2.78 – 2.85 (m, 4H, 4). <sup>13</sup>C NMR (151 MHz, DMSO-d<sub>6</sub>) δ 17.23 , 1, 25.42 , 4, 166.30 , 2, 170.23 , 3.

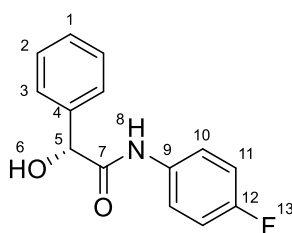
**5-[4-(2-acetamidoethoxy)phenyl]-6-chloro-1H-indole-3-carboxylic acid, CCT390622**



5-[4-(2-aminoethoxy)phenyl]-6-chloro-1H-indole-3-carboxylic acid, **31**, ( 20.00 mg, 0.0605 mmol) was dissolved in DMF ( 0.60 mL, 0.1000 M ) giving a pale red solution. (2,5-dioxopyrrolidin-1-yl) acetate ( 10.45 mg, 0.0665 mmol) was added followed by N,N-Diisopropylethylamine ( 21.17 uL, 0.1209 mmol) and the yellow solution stirred at rt for 2 h. The solution was then concentrated then dissolved in DMSO (0.5 mL) and directly purified by reverse-phase chromatography (Biotage reverse-phase 12 g Ultra C-18 column; 10-30-70-100% MeOH in H<sub>2</sub>O (containing 0.1% formic acid)). Relevant fractions isolated to afford the title compound (12 mg, 53%, 0.0322 mmol) as a white solid

Formula C<sub>19</sub>H<sub>17</sub>ClN<sub>2</sub>O<sub>4</sub>. Observed m/z 373.0957365. Calculated m/z 373.0949612. Error (ppm) 2.08. <sup>1</sup>H NMR (600 MHz, DMSO-*d*<sub>6</sub>) δ 1.84 (s, 3H, 19), 3.44 (q, *J* = 5.7 Hz, 2H, 16), 4.03 (t, *J* = 5.6 Hz, 2H, 15), 6.98 – 7.05 (m, 2H, 16, 13), 7.32 – 7.37 (m, 2H, 12), 7.61 (s, 1H, 8), 7.93 (s, 1H, 5), 8.06 (s, 1H, 2), 8.13 (t, *J* = 5.6 Hz, 1H, 17), 11.94 (s, 1H, 1). <sup>13</sup>C NMR (151 MHz, DMSO-*d*<sub>6</sub>) δ 22.55, 19, 38.30, 16, 66.41, 15, 107.67, 3, 112.84, 8, 114.03, 13, 122.71, 5, 125.29, 4, 125.77, 7, 130.78, 12, 132.52, 11, 132.73, 6, 133.72, 2, 135.92, 9, 157.60, 14, 165.66, 10, 169.50, 18.

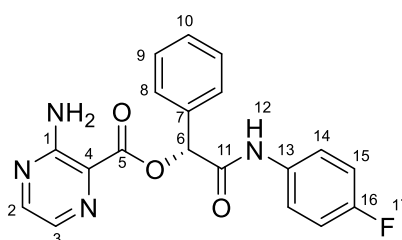
**(2R)-N-(4-fluorophenyl)-2-hydroxy-2-phenyl-acetamide, 39**



(2R)-2-hydroxy-2-phenyl-acetic acid, **17**, (300.00 mg, 1.9717 mmol) was reacted with 4-fluoroaniline (0.20 mL, 2.0703 mmol) as per general method for amide couplings. Purified via column chromatography to give the title compound (437 mg, 90%, 1.7819 mmol) as a yellow solid.

Ret. time = 2.39 mins. Observed m/z 246.0931. Calculated Formula [C<sub>14</sub> H<sub>13</sub> F N O<sub>2</sub>. Target m/z 246.0925. Error (ppm) 2.38. δ<sub>H</sub> (DMSO-*d*<sub>6</sub>, 500 MHz): 5.09 (d, *J* = 4.5 Hz, 1H, H<sub>6</sub>), 6.46 (d, *J* = 4.5 Hz, 1H, H<sub>5</sub>), 7.08 – 7.17 (m, 1H, H<sub>11</sub>), 7.25 – 7.32 (m, 1H, H<sub>1</sub>), 7.32 – 7.39 (m, 1H, H<sub>2</sub>), 7.47 – 7.53 (m, 1H, H<sub>3</sub>), 7.69 – 7.76 (m, 1H, H<sub>10</sub>), 10.01 (s, 1H, N<sub>8</sub>). δ<sub>C</sub> (DMSO-*d*<sub>6</sub>, 126 MHz): 74.02 (C<sub>5</sub>), 115.16 (d, *J* = 22.1 Hz, C<sub>11</sub>), 121.53 (d, *J* = 7.8 Hz, C<sub>10</sub>), 126.60 (C<sub>3</sub>), 127.65 (C<sub>1</sub>), 128.13 (C<sub>2</sub>), 134.98 (d, *J* = 2.6 Hz, C<sub>9</sub>), 140.83 (C<sub>4</sub>), 158.18 (d, *J* = 240.0 Hz, C<sub>12</sub>), 171.16 (C<sub>7</sub>). δ<sub>F</sub> (Chloroform-*d*, 471 MHz): -119.10 (tt, *J* = 9.1, 5.0 Hz, F<sub>13</sub> δ<sub>F</sub> CPD (Chloroform-*d*, 471 MHz): -119.10 (F<sub>13</sub>)

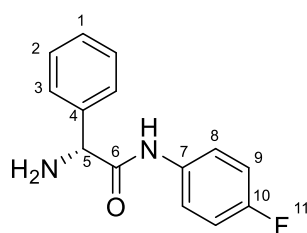
**[(1R)-2-(4-fluoroanilino)-2-oxo-1-phenyl-ethyl] 3-aminopyrazine-2-carboxylate, CCT374741**



(2R)-N-(4-fluorophenyl)-2-hydroxy-2-phenyl-acetamide, **18**, ( 50.00 mg, 0.2039 mmol) was reacted with 3-aminopyrazine-2-carboxylic acid ( 29.78 mg, 0.2141 mmol) as per general for amide couplings. Purified via column chromatography to give the title compound (437 mg, 90%, 1.7819 mmol) as a yellow solid. Purified via Prep HPLC to give afford the title compound(18 mg, 24%, 0.0491 mmol) as a white solid

Ret time = 2.74 mins. Observed m/z 367.1219. Calculated Formula C<sub>19</sub> H<sub>16</sub> F N<sub>4</sub> O<sub>3</sub>. Target m/z 367.1201. Error (ppm) 5.01.  $\delta_H$  (Chloroform-d, 500 MHz): 6.45 (s, 1H, H6), 6.98 – 7.06 (m, 2H, H15), 7.34 – 7.44 (m, 3H, H9, 10), 7.55 – 7.65 (m, 4H, H14, H8), 8.06 (d, J = 2.2 Hz, 1H, H3), 8.29 (d, J = 2.2 Hz, 1H, H2), 9.01 (s, 1H, N12).  $\delta_C$  (Chloroform-d, 151 MHz): 76.40 (C6), 115.81 (d, J = 22.5 Hz, C15), 122.01 (d, J = 7.8 Hz, C14), 123.45 (C4), 127.50 (C8), 129.04 (C9), 129.38 (C10), 133.42 (d, J = 2.8 Hz, C13), 133.94 (C3), 135.36 (C7), 148.62 (C2), 156.37 (C1), 159.76 (d, J = 244.1 Hz, C16), 164.39 , 5, 166.53 (C11).  $\delta_F$  (Chloroform-d, 471 MHz): -117.37 (tt, J = 8.4, 4.6 Hz, F17).  $\delta_F$  CPD (Chloroform-d, 471 MHz): -117.37 (F17).

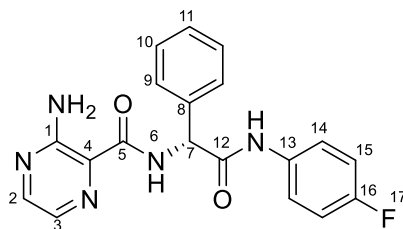
#### (2R)-2-amino-N-(4-fluorophenyl)-2-phenyl-acetamide, **42**



Fmoc-D- $\alpha$ -phenylglycine, **19**, ( 50.00 mg, 0.1339 mmol) was reacted with 4-fluoroaniline ( 0.01 mL, 0.1339 mmol) as per general method for amide couplings, but before dilution was treated with piperidine ( 0.10 mL, 1.0123 mmol) and stirred at rt for 2 hrs. Purified via column chromatography to afford the title compound (34 mg, 104%, 0.1392 mmol) as a white solid.

Ret. time = 1.58 mins. Observed m/z 245.1088. Calculated Formula C<sub>14</sub> H<sub>14</sub> F N<sub>2</sub> O.  
Target m/z 245.1085. Error (ppm) 1.2.  $\delta_{\text{H}}$  (Methanol-d<sub>4</sub>, 500 MHz): 4.62 (s, 1H, H5),  
6.99 – 7.06 (m, 2H, H9), 7.29 – 7.34 (m, 1H, H1), 7.35 – 7.40 (m, 2H, H2), 7.46 – 7.51  
(m, 2H, H3), 7.52 – 7.58 (m, 2H, H8).  $\delta_{\text{C}}$  (Methanol-d<sub>4</sub>, 126 MHz): 60.47 (C5),  
116.26 (d, J = 22.6 Hz, C9), 123.11 (d, J = 7.9 Hz, C8), 128.08 (C4), 129.20 (C1),  
129.85 (C2), 135.64 (d, J = 3.0 Hz, C7), 160.75 (d, J = 242.1 Hz, C10), 173.01 (C8).  $\delta_{\text{F}}$   
(Methanol-d<sub>4</sub>, 471 MHz): -120.26 (tt, J = 9.1, 4.9 Hz, F11).  $\delta_{\text{F}}$  CPD (Methanol-d<sub>4</sub>, 471  
MHz): -120.26 (F11)

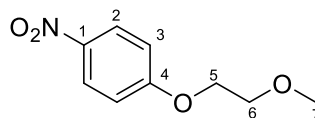
**3-amino-N-[(1R)-2-(4-fluoroanilino)-2-oxo-1-phenyl-ethyl]pyrazine-2-  
carboxamide, CCT374740**



(2R)-2-amino-N-(4-fluorophenyl)-2-phenyl-acetamide, **20**, ( 35.00 mg, 0.1433  
mmol) was reacted with 3-aminopyrazine-2-carboxylic acid ( 20.93 mg, 0.1505  
mmol) as per the general for amide couplings. Purified via Prep HPLC to give the  
title compound (1 mg, 2%, 0.0027 mmol) as a white solid

Ret. time = 2.93 mins. Calculated Mass 366.1366. Observed mass 366.1355.  
Formula C<sub>19</sub>H<sub>17</sub>FN<sub>5</sub>O<sub>2</sub>. Error (ppm) -3.0.  $\delta_{\text{H}}$  (Chloroform-d, 600 MHz): 5.65 (d, J =  
7.0 Hz, 1H, H7), 6.96 – 7.03 (m, 2H, H15), 7.36 – 7.41 (m, 1H, H11), 7.41 – 7.48 (m,  
4H, H14, H10), 7.53 (d, J = 7.2 Hz, 2H, H9), 7.85 (d, J = 2.4 Hz, 1H, H3), 8.16 (d, J = 2.3  
Hz, 1H, H2), 8.97 (d, J = 7.0 Hz, 1H, N6).  $\delta_{\text{C}}$  (Chloroform-d, 151 MHz): 58.32 (C9),  
115.87 (d, J = 22.7 Hz, C15), 121.93 (d, J = 8.1 Hz, C14), 126.03 (C4), 127.79 (C9),  
129.14 (C11), 129.59 (C10), 132.27 (C3), 133.33 (d, J = 2.7 Hz, C13), 137.05 (C8),  
147.27 (C2), 155.13(C1), 159.79 (d, J = 244.2 Hz, C16), 166.13 (C5), 167.86 (C12).  $\delta_{\text{F}}$   
(Chloroform-d, 471 MHz): -117.27 – -117.21 (m. F17).  $\delta_{\text{F}}$  CPD (Chloroform-d, 471  
MHz): -117.24 (d, J = 2.2 Hz, F17).

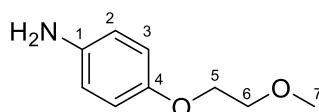
### 1-(2-methoxyethoxy)-4-nitro-benzene, **45**



A microwave vial was charged with 1-fluoro-4-nitrobenzene, **22**, (100.00 mg, 0.7016 mmol) in 2-methoxyethanol (0.11 mL, 1.4033 mmol) giving a colourless solution. Dry Acetonitrile (0.50 mL) and K<sub>2</sub>CO<sub>3</sub> (290.92 mg, 2.1049 mmol) were added and the pale yellow suspension, was stirred at 80°C overnight. Another 2-methoxyethanol (0.11 mL, 1.4033 mmol) was added and the mixture heated to 80°C for 4 hrs. Concentrated *in vacuo*, then partitioned between 15 mL H<sub>2</sub>O and 15 mL DCM. Aq phase extracted 3 x 10 mL DCM. Combined organics dried over MgSO<sub>4</sub>, vacuum filtered and concentrated *in vacuo* to afford the title compound (122 mg, 88%, 0.6187 mmol) as a white solid

Ret. Time = 2.22 mins. Observed m/z 198.0773. Calculated Formula C<sub>9</sub> H<sub>12</sub> N O<sub>4</sub>. Target m/z 198.0761. Error (ppm) 6.15.  $\delta_{\text{H}}$  (Chloroform-d, 500 MHz): 3.45 (s, 3H, H7), 3.73 – 3.83 (m, 2H, H6), 4.17 – 4.26 (m, 2H, H5), 6.89 – 7.08 (m, 2H, H3), 8.08 – 8.25 (m, 2H, H2).  $\delta_{\text{C}}$  (Chloroform-d, 126 MHz): 59.44 (7), 68.19 (C5), 70.73 (C6), 114.68 (C3), 126.01 (C2), 141.77 (C1), 163.94 (C4).

### 4-(2-methoxyethoxy)aniline, **46**



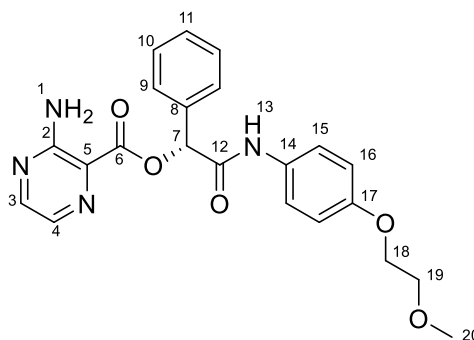
1-(2-methoxyethoxy)-4-nitro-benzene, **23**, (110.00 mg, 0.5578 mmol) was reacted with iron powder (93.47 mg, 1.6735 mmol) as per general method for a nitro reduction. Purified via column chromatography to afford the title compound (66 mg, 71%, 0.3947 mmol) as a brown oil.

Ret. Time = 0.21 mins. Observed m/z 168.1029. Calculated Formula C<sub>9</sub> H<sub>14</sub> N O<sub>2</sub>. Target m/z 168.1019. Error (ppm) 5.85.  $\delta_{\text{H}}$  (Chloroform-d, 500 MHz): 3.42 – 3.44



(m, 3H, H7), 3.68 – 3.73 (m, 2H, H6), 4.04 (ddd,  $J = 4.8, 3.9, 0.9$  Hz, 2H, H5), 6.59 – 6.66 (m, 2H, H2), 6.74 – 6.82 (m, 2H, H3).  $\delta_c$  (Chloroform- $d$ , 126 MHz): 59.27 (C7), 68.06 (C5), 71.32 (C6), 115.95 (C3), 116.43 (C2), 140.32 (C1), 152.01 (C4).

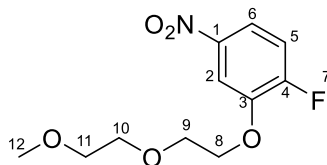
**[(1R)-2-[4-(2-methoxyethoxy)anilino]-2-oxo-1-phenyl-ethyl] 3-aminopyrazine-2-carboxylate, CCT375223**



(2R)-2-hydroxy-2-phenyl-acetic acid (35.03 mg, 0.2302 mmol) was reacted with 4-(2-Methoxyethoxy)aniline ( 0.03 mL, 0.2093 mmol), **24**, as per the general method for an amide coupling but after work up the yellow oil was immediately reacted with 3-aminopyrazine-2-carboxylic acid as per general method for an amide coupling. Purified via Prep HPLC to afford the title compound (10 mg, 11%, 0.0237 mmol) as a white solid

Ret time = 2.42 mins. Observed  $m/z$  302.1417. Calculated Formula  $C_{17}H_{20}NO_4$ . Target  $m/z$  302.1392. Error (ppm) -3.31. (DMSO- $d_6$ , 500 MHz):  $\delta$  3.28 (s, 3H, H20), 3.60 – 3.64 (m, 2H, H19), 4.01 – 4.05 (m, 2H, H18), 6.19 (d,  $J = 2.0$  Hz, 1H, H7), 6.86 – 6.91 (m, 2H, H16), 7.38 (s, 2H, H1), 7.40 – 7.43 (m, 1H, H11), 7.43 – 7.50 (m, 5H, H10, H15), 7.64 (d,  $J = 7.2$  Hz, 2H, H9), 7.95 (d,  $J = 2.2$  Hz, 1H, H4), 8.30 (d,  $J = 2.2$  Hz, 1H, H3), 10.39 (d,  $J = 5.1$  Hz, 1H, H13).  $\delta_c$  (DMSO- $d_6$ , 151 MHz): 58.15 (C20), 67.02 (C18), 70.38 (C19), 75.97 (C7), 114.57 (C16), 120.73 (C15), 122.72 (C5), 127.71 (C9), 128.64 (C10), 128.95 (C11), 131.65 (C14), 132.75 (C4), 135.12 (C8), 148.22 (C3), 154.71 (C17), 156.03 (C2), 165.31 (C6), 166.03 (C12). Mass spec shows hydrolysis of the ester and the alcohol mass is observed.

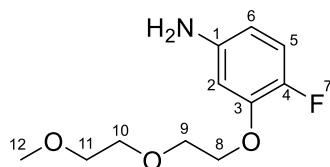
### 1-fluoro-2-[2-(2-methoxyethoxy)ethoxy]-4-nitro-benzene, **47**



An oven dried biotage microwave vial (0.5-2 mL) was charged with 2-fluoro-5-nitrophenol, **25**, (50.00 mg, 0.3183 mmol) in Dry Acetonitrile (0.70 mL) giving a brown solution. Dipotassium carbonate (131.96 mg, 0.9548 mmol) was added giving a suspension, followed by 1-Bromo-2-(2-methoxyethoxy)ethane ( 0.10 mL, 0.6365 mmol) . The dark red mixture was heated to 50°C for 4 hrs. Another portion of 1-Bromo-2-(2-methoxyethoxy)ethane ( 0.10 mL, 0.6365 mmol) and dipotassium carbonate ( 131.96 mg, 0.9548 mmol) were added, and the mixture stirred at 50°C overnight, concentrated *in vacuo*, then partitioned between 15mL of sat Na<sub>2</sub>CO<sub>3</sub> sol and 15 mL DCM. Aq phase was extracted 3 x DCM. Combined organics were dried over MgSO<sub>4</sub>, vacuum filtered and concentrated *in vacuo* to afford the title compound (77 mg, 93%, 0.2970 mmol) as a yellow oil.

Ret time = 2.42 mins. Observed m/z 260.0935. Calculated Formula C<sub>11</sub>H<sub>14</sub>FN<sub>2</sub>O<sub>5</sub>. Target m/z 260.0934. Error (ppm) 0.40.  $\delta_H$  (Chloroform-d, 500 MHz): 3.38 (s, 3H, H12), 3.55 – 3.58 (m, 2H, H11), 3.71 – 3.74 (m, 2H, H10), 3.90 – 3.94 (m, 2H, H9), 4.27 – 4.31 (m, 2H, H8), 7.19 (dd, J = 10.0, 8.9 Hz, 1H, H5), 7.85 (ddd, J = 8.9, 3.9, 2.7 Hz, 1H, H6), 7.91 (dd, J = 7.2, 2.7 Hz, 1H, H2).  $\delta_C$  (Chloroform-d, 126 MHz): 59.21 (C12), 69.53 (C9), 69.63 (C8), 71.07 (C10), 72.06 (C11), 110.55 (d, J = 3.7 Hz, C2), 116.40 (d, J = 20.8 Hz, C5), 117.39 (d, J = 8.3 Hz, C6), 144.38 (d, J = 2.8 Hz, C1), 147.51 (d, J = 12.1 Hz, C3), 156.61 (d, J = 258.6 Hz, C4).  $\delta_F$  (Chloroform-d, 471 MHz): -122.19 (ddd, J = 10.0, 7.2, 3.9 Hz, F7).  $\delta_F$  CPD (Chloroform-d, 471 MHz): -122.19 (F7)

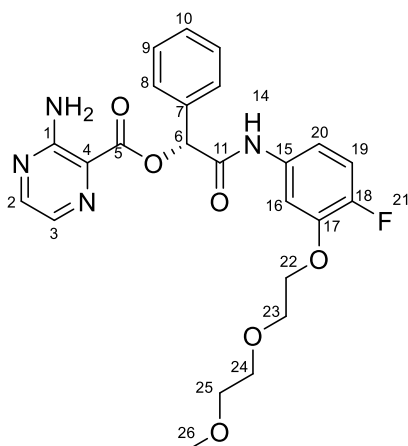
#### 4-fluoro-3-[2-(2-methoxyethoxy)ethoxy]aniline, 48



1-fluoro-2-[2-(2-methoxyethoxy)ethoxy]-4-nitro-benzene, was reacted with iron powder ( 34.26 mg, 0.6134 mmol) as per general method for nitro reduction. Purified via column chromatography to afford the title compound (26 mg, 55%, 0.1134 mmol) as a brown oil.

Ret time = 0.69. Observed  $m/z$  230.1193. Calculated Formula  $[M+H]^+$  230.1193 C<sub>11</sub>H<sub>17</sub>F N O<sub>3</sub>. Target  $m/z$  230.1187. Error (ppm) 2.67.  $\delta_H$  (Chloroform-d, 500 MHz): 3.38 (s, 3H, H<sub>12</sub>), 3.54 – 3.59 (m, 2H, H<sub>11</sub>), 3.69 – 3.74 (m, 2H, H<sub>10</sub>), 3.82 – 3.87 (m, 2H, H<sub>14</sub>), 4.11 – 4.16 (m, 2H, H<sub>8</sub>), 6.17 (ddd,  $J = 8.6, 3.4, 2.7$  Hz, 1H, H<sub>6</sub>), 6.32 (dd,  $J = 7.1, 2.7$  Hz, 1H, H<sub>2</sub>), 6.83 (dd,  $J = 11.2, 8.6$  Hz, 1H, H<sub>5</sub>).  $\delta_C$  (Chloroform-d, 126 MHz): 59.13 (C<sub>12</sub>), 69.08 (C<sub>8</sub>), 69.74 (C<sub>9</sub>), 70.88 (C<sub>10</sub>), 72.04 (C<sub>11</sub>), 103.18 (C<sub>2</sub>), 107.17 (d,  $J = 6.5$  Hz, C<sub>6</sub>), 116.47 (d,  $J = 19.5$  Hz, C<sub>5</sub>), 143.05 (d,  $J = 2.3$  Hz, C<sub>1</sub>), 146.57 (d,  $J = 235.6$  Hz, C<sub>4</sub>), 147.15 (d,  $J = 11.5$  Hz, C<sub>3</sub>).

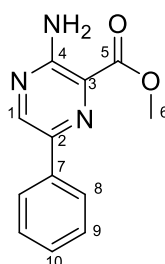
#### [(1R)-2-[4-fluoro-3-[2-(2-methoxyethoxy)ethoxy]anilino]-2-oxo-1-phenyl-ethyl] 3-aminopyrazine-2-carboxylate, CCT375224



(2R)-2-hydroxy-2-phenyl-acetic acid ( 18.98 mg, 0.1248 mmol) was reacted with 4-fluoro-3-[2-(2-methoxyethoxy)ethoxy]aniline, ( 0.05 mL, 0.1134 mmol) as per general method for an amide coupling but after work up the yellow oil was immediately reacted with 3-aminopyrazine-2-carboxylic acid as per the general method for an amide coupling. Purified via Prep HPLC to afford the title compound (4 mg, 7%, 0.0083 mmol) as a white solid.

Ret. time = 2.74 mins. Observed m/z 485.1833. Calculated Formula [M+H]<sup>+</sup> C<sub>24</sub> H<sub>26</sub> F N<sub>4</sub> O<sub>6</sub>. Target m/z 485.1831. Error (ppm) 0.36.  $\delta_{\text{H}}$  (Chloroform-d, 600 MHz): 3.37 (s, 3H, 26), 3.55 – 3.58 (m, 2H, 25), 3.70 – 3.74 (m, 2H, 24), 3.85 – 3.89 (m, 2H, 23), 4.18 – 4.23 (m, 2H, 22), 6.43 (s, 1H, 6), 6.96 – 7.04 (m, 2H, 19,20), 7.34 – 7.45 (m, 3H, 9, 10), 7.56 – 7.66 (m, 3H, 16, 8), 8.06 (d, J = 2.2 Hz, 1H, 3), 8.29 (d, J = 2.2 Hz, 1H, 2), 9.03 (s, 1H, N14).  $\delta_{\text{C}}$  (Chloroform-d, 151 MHz): 59.17 (C26), 69.25 (C22), 69.70 (C23), 70.93 (C24), 72.08 (C25), 76.44 (C6), 108.10 (C16), 112.66 (d, J = 6.6 Hz, C20), 116.15 (d, J = 19.6 Hz, C19), 123.41 (C4), 127.49 (C8), 129.06 (C9), 129.40 (C10), 133.80 (d, J = 3.3 Hz, C15), 133.93 (C3), 135.37 (C7), 146.99 (d, J = 11.8 Hz, C17), 148.67 (C2), 149.77 (d, J = 244.4 Hz, C18), 156.38 (C1), 164.39 (C5), 166.51 (C11). 19F NMR (471 MHz, Chloroform-d)  $\delta$  -137.87 – -137.80 (m, F21). 19F NMR (471 MHz, Chloroform-d)  $\delta$  -137.84 (F21).

### Methyl 3-amino-6-phenyl-pyrazine-2-carboxylate, 51

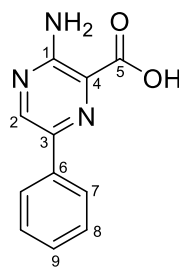


A black solution of Methyl 3-amino-6-bromopyrazine-2-carboxylate, **32**, ( 150.00 mg, 0.6465 mmol) in 1,4-Dioxane ( 3.22 mL) and Water ( 0.80 mL) , was degassed for 5 minutes with N<sub>2</sub>, then phenylboric acid ( 78.82 mg, 0.6465 mmol) and K<sub>3</sub>PO<sub>4</sub> ( 171.53 mg, 0.8081 mmol) were added. The mixture was degassed with N<sub>2</sub> for another 5 minutes. Pd(dppf)Cl<sub>2</sub> ( 27.76 mg, 0.0323 mmol) was added and the

mixture was degassed with N<sub>2</sub> for 5 mins, then heated at 85°C for 3 hours then concentrated *in vacuo*. Partitioned between water (30 mL) and EtOAc (30 mL). The aq phase was extracted 3 x EtOAc (20 mL), and the combined organics were dried over MgSO<sub>4</sub>, vacuum filtered and concentrated *in vacuo*. Purified via column chromatography cyclohexane -> 25% EtOAc to the title compound (104 mg, 70%, 0.4537 mmol) as a black solid.

Ret. time = 1.29 mins. Observed m/z 230.0921. Calculated Formula C<sub>12</sub> H<sub>12</sub> N<sub>3</sub> O<sub>2</sub>. Target m/z 230.0930. Error (ppm) = -3.91.  $\delta_{\text{H}}$  (DMSO-d<sub>6</sub>), 500 MHz):  $\delta$  3.90 (s, 3H, H6), 7.34 – 7.42 (m, 1H, H10), 7.45 – 7.48 (m, 2H, H9), 7.95 – 8.03 (m, 2H, H8), 8.91 (s, 1H, H1).  $\delta_{\text{C}}$  (DMSO-d<sub>6</sub>), 126 MHz): 52.73 (C6), 125.71 (C8), 128.71 (C10), 129.28 (C9), 136.44 (C7), 140.06 (C2), 142.86 (C3), 145.56 (C1), 155.20 (C4), 166.99 (C5).

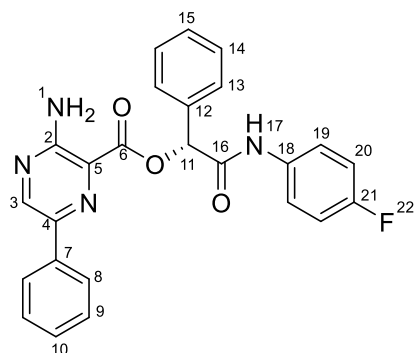
### 3-amino-6-phenyl-pyrazine-2-carboxylic acid, **52**



Methyl 3-amino-6-phenyl-pyrazine-2-carboxylate, **33**, ( 100.00 mg, 0.4362 mmol) was reacted with lithium hydroxide ( 31.34 mg, 1.3087 mmol) as set up as per general method for ester hydrolysis, but heated to 60°C for 2 hrs to give the title compound (82 mg, 87%, 0.3810 mmol) as an off white solid.

Ret. time = 2.22 mins. Observed m/z 216.0775. Calculated Formula [M+H]<sup>+</sup> C<sub>11</sub> H<sub>10</sub> N<sub>3</sub> O<sub>2</sub>. Target m/z 216.0768. Error (ppm) 3.27.  $\delta_{\text{H}}$  (DMSO-d<sub>6</sub>), 500 MHz): 7.33 – 7.38 (m, 1H, H9), 7.40 – 7.50 (m, 2H, H8), 7.93 – 8.07 (m, 2H, H7), 8.76 (s, 1H, H2).  $\delta_{\text{C}}$  (DMSO-d<sub>6</sub>, 126 MHz): 125.91 (C7), 128.37 (C9), 129.15 (C8), 136.88 (C6), 139.49 (C3), 142.85 (C4), 144.09 (C2), 155.46 (C1), 168.53 (8).

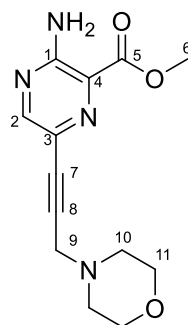
**[(1R)-2-(4-fluoroanilino)-2-oxo-1-phenyl-ethyl] 3-amino-6-phenyl-pyrazine-2-carboxylate, 53**



4-dimethylaminopyridine ( 0.02 mL, 0.1626 mmol) was added to a yellow suspension of 3-amino-6-phenyl-pyrazine-2-carboxylic acid ( 35.00 mg, 0.1626 mmol) and (2R)-N-(4-fluorophenyl)-2-hydroxy-2-phenyl-acetamide, ( 39.82 mg, 0.1623 mmol) in DCM ( 0.91 mL) and the suspension was cooled to 0°C. 1,3-dicyclohexylcarbodiimide ( 35.23 mg, 0.1708 mmol) in DCM ( 0.91 mL) was added and the mixture stirred for 18 hrs at r.t.. 3 mL DMF was added to give a pale yellow solution, and stirred at r.t. for 8 hrs. Another portion of 1,3-dicyclohexylcarbodiimide ( 35.23 mg, 0.1708 mmol) and 4-dimethylaminopyridine ( 0.02 mL, 0.1626 mmol) were added and the reaction mixture stirred overnight then partitioned between 15 mL EtOAc and 15 mL H<sub>2</sub>O were added and the aq phase extracted 3 x 15 mL EtOAc. Combined org phases were dried (MgSO<sub>4</sub>), vacuum filtered and concentrated *in vacuo*. Purified via reverse phase column chromatography, to afford the title compound (9 mg, 12%, 0.0203 mmol).

Ret. time = 3.10 mins. Observed m/z 443.1516. Calculated Formula C<sub>25</sub> H<sub>20</sub> F N<sub>4</sub> O<sub>3</sub>. Target m/z 443.1514. Error (ppm) 0.56.  $\delta_{\text{H}}$  (DMSO-d<sub>6</sub>), 500 MHz): 6.26 (s, 1H, H11), 7.13 – 7.18 (m, 2H, H20), 7.37 – 7.46 (m, 3H, H14, H15), 7.46 – 7.52 (m, 4H, N1, H9, H10), 7.59 – 7.64 (m, 2H, H19), 7.70 – 7.76 (m, 2H, H13), 8.01 – 8.04 (m, 2H, H8), 8.97 (s, 1H, H3), 10.63 (s, 1H, N17).  $\delta_{\text{C}}$  (DMSO-d<sub>6</sub>, 126 MHz): 75.90 (C11), 115.50 (d, J = 22.4 Hz, C20), 121.07 (d, J = 7.9 Hz, C19), 121.35 (C5), 125.15 (C8), 127.35 (C13), 128.36 (C7), 128.50 (C15), 128.74 (C14), 128.89 (C12), 128.97 (C10), 134.83 (d, J = 2.7 Hz, C18), 135.13 (C9), 139.67 (C4), 145.51 (C3), 154.82 (C2), 159.21 (d, J = 240.0 Hz, C21), 165.22 (C8), 166.61 (C16).

### Methyl 3-amino-6-(3-morpholinoprop-1-ynyl)pyrazine-2-carboxylate, 55



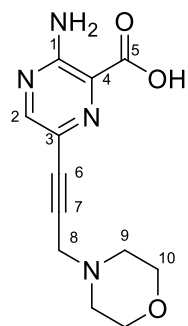
Methyl 3-amino-6-bromopyrazine-2-carboxylate ( 0.05 mL, 0.3448 mmol) was taken up in DMF ( 0.80 mL) giving a black solution. Bis(triphenylphosphine)palladium(II) chloride ( 24.20 mg, 0.0345 mmol) and Copper (I) iodide ( 3.28 mg, 0.0172 mmol) were added and the black mixture degassed with N<sub>2</sub> for 5 mins .

triethylamine ( 0.24 mL, 1.7239 mmol) and 4-(prop-2-yn-1-yl)morpholine ( 0.17 mL, 1.3791 mmol) were added and heated to 70C for 1.5 h. Then the reaction mixture was partitioned between 15 mL DCM and 15 mL sat Na<sub>2</sub>CO<sub>2</sub> sol. Aq phase extracted 3 x 10 mL DCM, Combined organics were dried over MgSO<sub>4</sub>, vacuum filtered and concentrated in vacuo to give a black solid.

The reaction mixture was dissolved in DMSO (0.5 mL) and directly purified by reverse-phase chromatography (Biotage reverse-phase 12 g Ultra C-18 column; 0-10-20-100% MeOH in H<sub>2</sub>O (containing 0.1% formic acid)). Relevant fractions evaporated to give afford the title compound (42 mg, 44%, 0.152 mmol) as a brown solid

Ret. time = 0.45 mins. Observed m/z 277.1289. Calculated Formula [M+H]<sup>+</sup> C<sub>13</sub> H<sub>17</sub> N<sub>4</sub> O<sub>3</sub>. Target m/z 277.1295. Error (ppm) -2.18.  $\delta_{\text{H}}$  (Chloroform-d, 500 MHz): 2.79 (t, J = 4.8 Hz, 4H, H10), 3.64 (s, 2H, H9), 3.80 (t, J = 4.8 Hz, 4H, H11), 3.97 (s, 3H, H6), 8.29 (s, 1H, H2).  $\delta_{\text{C}}$  (Chloroform-d, 126 MHz): 47.43 (C9), 51.71 (C10), 53.13 (C6), 66.14 (C11), 83.35 (C7), 83.89 (C8), 124.07 (C4), 127.43 (C3), 150.54 (C2), 154.35 (C1), 166.27 (C13).

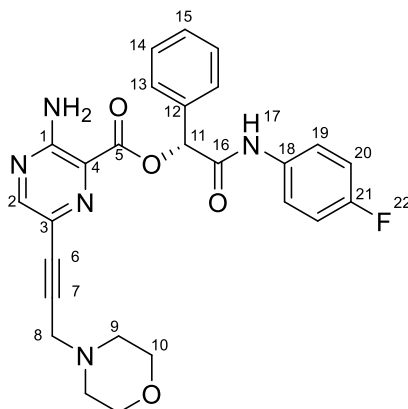
### 3-amino-6-(3-morpholinoprop-1-ynyl)pyrazine-2-carboxylic acid, 56



Methyl 3-amino-6-(3-morpholinoprop-1-ynyl)pyrazine-2-carboxylate, **39**, (1 equiv) was reacted with lithium hydroxide (3 equiv) as per the general method for ester hydrolysis. However instead of precipitating the acid the mixture was directly concentrate and used without further purification in the next step, giving the title compound (quant) as a brown oil.

Ret. time = 0.21 mins. Observed m/z 263.1157. Calculated Formula [M+H]<sup>+</sup> C<sub>12</sub> H<sub>15</sub> N<sub>4</sub> O<sub>3</sub>. Target m/z 263.1139. Error (ppm) 6.85.  $\delta_{\text{H}}$  (DMSO-d<sub>6</sub>, 600 MHz): 2.51 – 2.55 (m, 5H, 9), 3.40 – 3.43 (m, 2H, 8), 3.55 – 3.66 (m, 5H, 10), 8.02 (d, J = 4.7 Hz, 1H, 2).  $\delta_{\text{C}}$  (DMSO-d<sub>6</sub>, 151 MHz): 47.91 (C8), 52.64 (C9), 67.12 (C10), 83.87 (C6), 85.57 (C7), 126.03 (C3), 134.59 (C4), 147.86 (C2), 154.89 (C1), 170.21 (C5).

### [(1R)-2-(4-fluoroanilino)-2-oxo-1-phenyl-ethyl] 3-amino-6-(3-morpholinoprop-1-ynyl)pyrazine-2-carboxylate, CCT375225

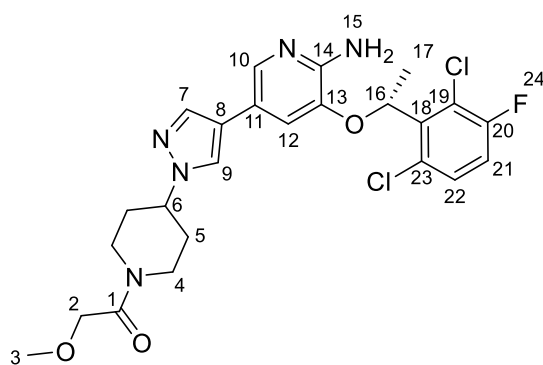




3-amino-6-(3-morpholinoprop-1-ynyl)pyrazine-2-carboxylic acid, **43**, ( 40.00 mg, 0.1525 mmol) was reacted with (2R)-N-(4-fluorophenyl)-2-hydroxy-2-phenylacetamide ( 37.41 mg, 0.1525 mmol) as general method 3. Purified via Prep HPLC to afford the title product (12 mg, 16%, 0.0245 mmol) as an off white solid.

Ret time = 2.41 mins. Observed m/z 490.1891. Calculated Formula [M+H]<sup>+</sup> C<sub>26</sub> H<sub>25</sub> F N<sub>5</sub> O<sub>4</sub>. Target m/z 490.1885. Error (ppm) 1.16.  $\delta_{\text{H}}$  (Chloroform-d, 600 MHz): 2.69 (t, *J* = 4.7 Hz, 4H, 9), 3.59 (s, 2H, 8), 3.78 (t, *J* = 4.7 Hz, 4H, 10), 6.41 (s, 1H, 11), 7.00 – 7.06 (m, 2H, 20), 7.35 – 7.45 (m, 3H, 14, 15), 7.58 – 7.65 (m, 2H, 13), 7.65 – 7.70 (m, 2H, 19), 8.38 (s, 1H, 2), 9.28 (s, 1H, 17).  $\delta_{\text{C}}$  (Chloroform-d, 151 MHz): 48.10 , 8, 52.67 , 9, 66.95 , 10, 76.70 , 11, 82.10 , 6, 86.27 , 7, 115.76 (d, *J* = 22.4 Hz, 20), 121.91 (d, *J* = 7.7 Hz, 19), 122.68 , 4, 127.55 , 13, 128.33 , 3, 129.03 , 14, 129.42 , 15, 133.65 (d, *J* = 2.7 Hz, 18), 135.28 , 12, 151.63 , 2, 154.55 , 1, 159.70 (d, *J* = 244.0 Hz, 21), 163.78 , 5, 166.42 , 16.  $\delta_{\text{F}}$  (Chloroform-d, 471 MHz): -117.98 – -117.05 (s).  $\delta_{\text{F}}$  (Chloroform-d, 471 MHz): -117.98 – -117.05 (m).

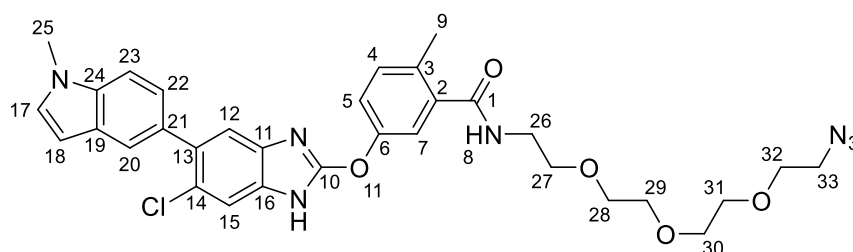
**1-[4-[4-[6-amino-5-[(1R)-1-(2,6-dichloro-3-fluoro-phenyl)ethoxy]-3-pyridyl]pyrazol-1-yl]-1-piperidyl]-2-methoxy-ethanone, CCT389531**



3-[(1R)-1-(2,6-dichloro-3-fluoro-phenyl)ethoxy]-5-[1-(4-piperidyl)pyrazol-4-yl]pyridin-2-amine ( 10.00 mg, 0.0222 mmol) was reacted with 2-Methoxyacetic acid ( 1.87  $\mu$ L, 0.0244 mmol) as per the general conditions for amide couplings. Purified via column chromatography (0 - 15 MeOH% in DCM). to give the title compound (9 mg, 78%, 0.0172 mmol) as a brown oil

Ret. time = 2.08 mins. Observed mass 522.1458. Calculated formula [M+H]<sup>+</sup> C<sub>24</sub>H<sub>27</sub>Cl<sub>2</sub>FN<sub>5</sub>O<sub>3</sub>. Target m/z 522.1475. Error -3.3 ppm. <sup>1</sup>H NMR (600 MHz, Chloroform-d) δ 1.85 (d, J = 6.7 Hz, 3H, 17), 1.90 – 2.04 (m, 2H, 5), 2.16 – 2.27 (m, 2H, 5), 2.81 – 2.88 (m, 2H, 4), 3.14 – 3.24 (m, 1H, 4), 3.45 (s, 3H, 3), 4.01 – 4.09 (m, 1H, 4), 4.09 – 4.22 (m, 2H, 2), 4.33 (tt, J = 11.3, 4.1 Hz, 1H, 6), 4.69 (d, J = 13.8 Hz, 1H, 4), 4.78 (s, 2H, 15), 6.07 (q, J = 6.7 Hz, 1H, 16), 6.86 (d, J = 1.8 Hz, 1H, 12), 7.05 (dd, J = 8.9, 7.8 Hz, 1H, 21), 7.30 (dd, J = 8.9, 4.8 Hz, 1H, 22), 7.47 (d, J = 0.8 Hz, 1H, 9), 7.56 (d, J = 0.8 Hz, 1H, 7), 7.75 (d, J = 1.8 Hz, 1H, 10). <sup>13</sup>C NMR (151 MHz, Chloroform-d) δ 19.04, 17, 33.03, 5, 43.97, 4, 59.05, 6, 59.26, 3, 72.08, 2, 72.58, 16, 115.06, 12, 116.87 (d, J = 23.3 Hz, 21), 119.11, 11, 120.35, 8, 122.19 (d, J = 18.5 Hz, 19), 122.89, 9, 129.08 (d, J = 3.6 Hz, 18), 130.08 (d, J = 8.2 Hz, 22), 135.75, 10, 136.17, 7, 137.08, 23, 139.98, 13, 149.13, 14, 157.70 (d, J = 247.6 Hz, 20), 167.76, 1. <sup>19</sup>F NMR (471 MHz, Chloroform-d) δ -112.05, 24, -73.21 (d, J = 712.5 Hz). <sup>19</sup>F NMR (471 MHz, Chloroform-d) δ -112.04, 24. (Proton decoupled)

**N-[2-[2-[2-(2-azidoethoxy)ethoxy]ethoxy]ethyl]-5-[[6-chloro-5-(1-methylindol-5-yl)-1H-benzimidazol-2-yl]oxy]-2-methyl-benzamide 57**

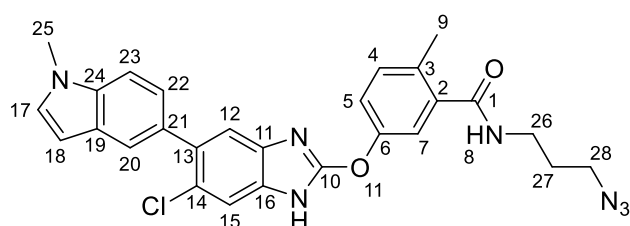


5-[[6-chloro-5-(1-methylindol-5-yl)-1H-benzimidazol-2-yl]oxy]-2-methyl-benzoic acid (200.00 mg, 0.4631 mmol) was reacted with 11-azido-3,6,9-trioxaundecylamine (0.11 mL, 0.5094 mmol) as per general conditions for an amide coupling to afford the title compound (323 mg, 110%, 0.5110 mmol) as a brown solid

Formula C<sub>32</sub>H<sub>34</sub>ClN<sub>7</sub>O<sub>5</sub>. Observed m/z 632.2391413. Calculated m/z 632.2382714. Error (ppm) 1.38. <sup>1</sup>H NMR (600 MHz, DMSO-*d*<sub>6</sub>) δ 2.35 (s, 3H, 9), 3.34 – 3.40 (m, 4H, 26, 33), 3.50 – 3.58 (m, 12H, 27, 28, 29, 30, 31, 32), 3.82 (s, 3H, 25), 6.46 (d, J = 3.0 Hz, 1H, 18), 7.19 (dd, J = 8.4, 1.7 Hz, 1H, 22), 7.30 – 7.34 (m, 3H, 4, 7, 12), 7.35 –

7.38 (m, 2H, 5, 17), 7.47 (d,  $J = 8.4$  Hz, 1H, 23), 7.50 – 7.52 (m, 1H, 15), 7.55 (d,  $J = 1.7$  Hz, 1H, 20), 8.36 (t,  $J = 5.6$  Hz, 1H, 9).  $^{13}\text{C}$  NMR (151 MHz, DMSO- $d_6$ )  $\delta$  18.75 , 9, 32.55 , 25, 38.87 , 26, 49.97 , 33, 68.76, 69.23, 69.54, 69.68, 69.79, 69.81 , (27, 28, 29, 30, 31, 32), 100.56 , 18, 109.10 , 23, 118.85, 121.19, 121.26 , 20, 123.17 , 22, 124.53 , 14, 127.77 , 19, 130.16 , 17, 130.87 , 21, 131.71, 132.36 , 3, 134.48 , 13, 135.55 , 24, 138.22 , 2, 150.98 , 6, 157.90 , 10, 168.11 , 1.

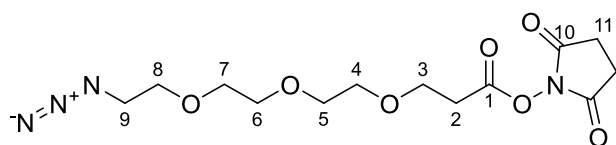
**N-(3-azidopropyl)-5-[[6-chloro-5-(1-methylindol-5-yl)-1H-benzimidazol-2-yl]oxy]-2-methyl-benzamide, 60**



5-[[6-chloro-5-(1-methylindol-5-yl)-1H-benzimidazol-2-yl]oxy]-2-methyl-benzoic acid ( 180.00 mg, 0.2793 mmol) was reacted with 3-azidopropan-1-amine ( 26.04  $\mu\text{L}$ , 0.2653 mmol) as per the general conditions for an amide coupling to give the title compound (63 mg, 44%, 0.1226 mmol) as a white solid.

Formula  $\text{C}_{27}\text{H}_{24}\text{ClN}_7\text{O}_2$ . Observed  $m/z$  514.1742422. Calculated  $m/z$  514.1752772. Error (ppm) -2.01.  $^1\text{H}$  NMR (600 MHz, Chloroform- $d$ )  $\delta$  1.86 (p,  $J = 6.6$  Hz, 2H, 27), 2.36 (s, 3H, 9), 3.40 (t,  $J = 6.6$  Hz, 2H, 28), 3.47 (t,  $J = 6.6$  Hz, 2H, 26), 3.82 (s, 3H, 25), 6.52 (d,  $J = 2.3$  Hz, 1H, 18), 6.75 (t,  $J = 6.0$  Hz, 1H, 8), 7.09 (d,  $J = 2.4$  Hz, 1H, 17), 7.11 – 7.15 (m, 2H, 5, 7), 7.25 (d,  $J = 1.6$  Hz, 1H, 4), 7.27 – 7.31 (m, 1H, 22), 7.33 – 7.38 (m, 1H, 23), 7.64 (s, 1H, 20).  $^{13}\text{C}$  NMR (151 MHz, Chloroform- $d$ )  $\delta$  19.23 , 9, 28.88 , 27, 33.07 , 25, 37.69 , 26, 49.44 , 28, 101.40 , 28, 108.67 , 23, 118.92 , 4, 121.80 , 5, 122.14 , 20, 123.94 , 22, 126.66, 128.32 , 17, 129.54 , 19, 131.59 , 21, 132.46 , 7, 133.19 , 3, 136.02, 136.07 , 24, 137.31 , 2, 137.35 , 10, 151.02 , 6, 170.07 , 1.

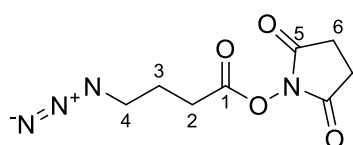
**(2,5-dioxopyrrolidin-1-yl) 3-[2-[2-(2-azidoethoxy)ethoxy]ethoxy]propanoate, 62**



3-(2-(2-(2-azidoethoxy)ethoxy)ethoxy)propanoic acid was combined with N-hydroxy succinimide as per general Method for making NHS-esters, to afford the title compound (97%) as a colourless oil

$^1\text{H}$  NMR (600 MHz, DMSO- $d_6$ )  $\delta$  2.81 (s, 4H, 11), 2.92 (t, J = 6.0 Hz, 2H, 2), 3.39 (t, J = 4.9 Hz, 2H, 8), 3.51 – 3.56 (m, 8H, 4, 5, 6, 7), 3.59 – 3.61 (m, 2H, 9), 3.72 (t, J = 6.0 Hz, 2H, 3).  $^{13}\text{C}$  NMR (151 MHz, DMSO- $d_6$ )  $\delta$  25.44 , 11, 31.61 , 2, 50.00 , 8, 65.22 , 3, 69.25 , 9, 69.68, 69.72, 69.80, 69.82, 167.34 , 1, 170.12 , 10.

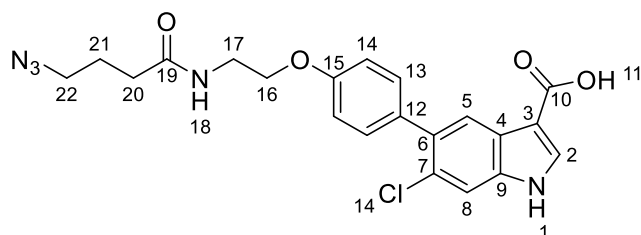
### 33, (2,5-dioxopyrrolidin-1-yl) 4-azidobutanoate, 65



4-azidobutanoic acid was combined with N-hydroxy succinimide as per general Method for making NHS-esters, to afford the title compound (76%) as a colourless oil

$^1\text{H}$  NMR (600 MHz, Chloroform- $d$ )  $\delta$  1.97 – 2.04 (m, 2H, 3), 2.72 (t, J = 7.2 Hz, 2H, 2), 2.84 (s, 4H, 6), 3.44 (t, J = 6.6 Hz, 2H, 4).  $^{13}\text{C}$  NMR (151 MHz, Chloroform- $d$ )  $\delta$  24.24 , 3, 25.70 , 6, 28.21 , 2, 50.10 , 4, 168.07 , 1, 169.20 , 5.

### 5-[4-[2-(4-azidobutanoylamino)ethoxy]phenyl]-6-chloro-1H-indole-3-carboxylic acid, 66

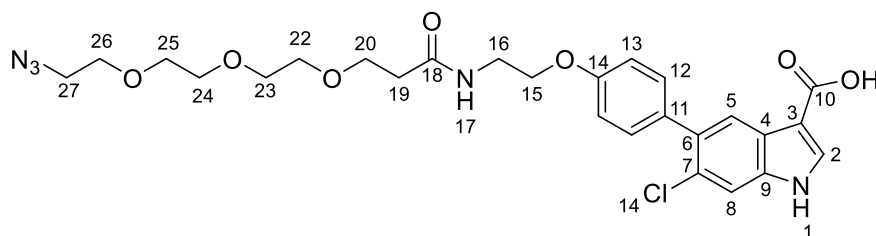


5-[4-(2-aminoethoxy)phenyl]-6-chloro-1H-indole-3-carboxylic acid, **31**, ( 179.38 mg, 0.5423 mmol) was taken up in DMF ( 2.00 mL, 0.2800 M ) giving a dark red solution. (2,5-dioxopyrrolidin-1-yl) 4-azidobutanoate, **35**, ( 140.00 mg, 0.5694 mmol) was added and the red solution stirred at rt for 4h. Solution heated to 70C for 2 days then concentrated in vacuo and dissolved in DMSO (1 mL) and directly

purified by reverse-phase chromatography (20-45-80-100% MeOH in H<sub>2</sub>O (containing 0.1% formic acid)). Relevant fractions concentrated in vacuo to the title compound (102 mg, 41%, 0.2308 mmol) as an orange solid.

Formula C<sub>21</sub>H<sub>20</sub>ClN<sub>5</sub>O<sub>4</sub>. Observed m/z 442.1285235. Calculated m/z 442.1276583. Error (ppm) 1.96. <sup>1</sup>H NMR (600 MHz, DMSO-*d*<sub>6</sub>) δ 1.76 (p, *J* = 7.1 Hz, 2H, 21), 2.20 (t, *J* = 7.1 Hz, 2H, 20), 3.31 – 3.35 (m, 2H, 22), 3.46 (q, *J* = 5.6 Hz, 2H, 17), 4.04 (t, *J* = 5.6 Hz, 2H, 16), 6.99 – 7.05 (m, 2H, 14), 7.32 – 7.37 (m, 2H, 13), 7.62 (d, *J* = 1.0 Hz, 1H, 8), 7.93 (d, *J* = 1.4 Hz, 1H, 5), 8.07 (d, *J* = 1.7 Hz, 1H, 2), 8.16 (t, *J* = 5.6 Hz, 1H, 18), 11.91 – 11.94 (m, 1H, 1), 12.10 (s, 1H, 11). <sup>13</sup>C NMR (151 MHz, DMSO-*d*<sub>6</sub>) δ 24.49, 21, 32.12, 20, 38.27, 17, 50.27, 22, 66.37, 16, 107.59, 3, 112.86, 8, 114.05, 14, 122.70, 5, 125.26, 4, 125.81, 7, 130.78, 13, 132.51, 12, 132.78, 6, 133.79, 2, 135.92, 9, 157.63, 15, 165.60, 10, 171.58, 19.

**5-[4-[2-[3-[2-[2-(2-azidoethoxy)ethoxy]ethoxy]propanoylamino]ethoxy]phenyl]-6-chloro-1H-indole-3-carboxylic acid, **63****

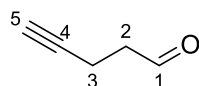


5-[4-(2-aminoethoxy)phenyl]-6-chloro-1H-indole-3-carboxylic acid, **31**, ( 80.00 mg, 0.2419 mmol) was dissolved in DMF ( 1.61 mL, 0.1500 M ) giving a pale red solution.

(2,5-dioxopyrrolidin-1-yl) 3-[2-[2-(2-azidoethoxy)ethoxy]ethoxy]propanoate, **34**, ( 99.93 mg, 0.2902 mmol) was added followed by N,N-Diisopropylethylamine ( 84.68 uL, 0.4837 mmol) and the yellow solution stirred at rt for 2 h. Solution concentrated and then dissolved in DMSO (0.8 mL) and directly purified by reverse-phase chromatography in 2 injections (10-55-75-100% MeOH in H<sub>2</sub>O (containing 0.1% formic acid)). Relevant fractions concentrated to give the title compound (70 mg, 52%, 0.1250 mmol) as a white solid

Formula C<sub>26</sub>H<sub>30</sub>ClN<sub>5</sub>O<sub>7</sub>. Observed m/z 560.1908288. Calculated m/z 560.1906525. Error (ppm) 0.31. <sup>1</sup>H NMR (600 MHz, Chloroform-d) δ 2.53 (t, J = 5.7 Hz, 2H, 19), 3.36 (t, J = 5.0 Hz, 2H, 27), 3.60 – 3.65 (m, 10H, 22, 23, 24, 25, 26), 3.66 – 3.70 (m, 2H, 16), 3.75 (t, J = 5.7 Hz, 2H, 20), 4.07 (t, J = 5.2 Hz, 2H, 15), 6.89 – 6.94 (m, 2H, 13), 6.96 (t, J = 5.8 Hz, 1H, 17), 7.35 – 7.40 (m, 2H, 12), 7.55 (s, 1H, 8), 8.01 (d, J = 2.9 Hz, 1H, 2), 8.12 (s, 1H, 5), 9.11 (s, 1H, 1). <sup>13</sup>C NMR (151 MHz, Chloroform-d) δ 37.06, 19, 39.17, 16, 50.80, 27, 66.93, 15, 67.36, 70.13, 26, 70.47, 20, 70.60, 70.69, 70.82, 108.33, 3, 112.69, 8, 114.02, 13, 123.84, 5, 125.23, 4, 128.34, 7, 131.31, 12, 133.25, 11, 133.37, 2, 134.76, 6, 135.85, 9, 157.99, 14, 168.32, 10, 172.22, 18.

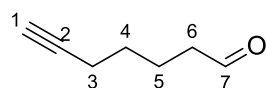
#### pent-4-ynal, 70



pent-4-yn-1-ol was reacted as per the general method for Swern oxidations, to afford the title compound as a pale yellow oil (86%)

<sup>1</sup>H NMR (500 MHz, Chloroform-d) δ 1.95 – 1.99 (m, 1H, 5), 2.45 – 2.52 (m, 2H, 3), 2.65 – 2.71 (m, 2H, 2), 9.76 – 9.79 (m, 1H, 1). <sup>13</sup>C NMR (126 MHz, Chloroform-d) δ 11.71, 3, 42.42, 2, 69.38, 5, 82.39, 4, 200.25, 1.

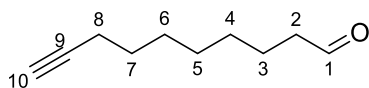
#### hept-6-ynal, 71, 98%



hept-4-yn-1-ol was reacted as per the general method for Swern oxidations, to afford the title compound as a pale yellow oil (98%)

<sup>1</sup>H NMR (600 MHz, Chloroform-d) δ 1.51 – 1.60 (m, 2H, 4), 1.71 – 1.79 (m, 2H, 5), 1.92 – 1.97 (m, 1H, 1), 2.18 – 2.24 (m, 2H, 3), 2.42 – 2.49 (m, 2H, 6), 9.66 – 9.85 (m, 1H, 7). <sup>13</sup>C NMR (151 MHz, Chloroform-d) δ 18.30, 3, 21.20, 5, 27.88, 4, 43.41, 6, 68.87, 1, 83.88, 2, 202.30, 7.

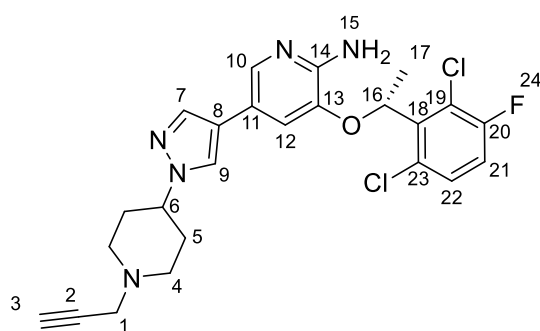
#### dec-9-ynal, 72, 64%



dec-4-yn-1-ol was reacted as per the general method for Swern oxidations, to afford the title compound as a black yellow oil (64%)

<sup>1</sup>H NMR (500 MHz, Chloroform-d)  $\delta$  1.27 – 1.36 (m, 4H, 4), 1.36 – 1.43 (m, 2H, CH<sub>2</sub>), 1.47 – 1.56 (m, 2H, 7), 1.58 – 1.67 (m, 2H, 3), 1.93 (t, J = 2.7 Hz, 1H, 10), 2.17 (td, J = 7.1, 2.6 Hz, 2H, 8), 2.42 (td, J = 7.3, 1.8 Hz, 2H, 2), 9.76 (t, J = 1.8 Hz, 1H, 1). <sup>13</sup>C NMR (126 MHz, Chloroform-d)  $\delta$  18.47, 8, 22.11, 3, 28.47, 7, 28.60, CH<sub>2</sub>, 28.94, 4, 29.12, CH<sub>2</sub>, 43.99, 2, 68.31, 10, 84.73, 9, 202.96, 1.

**3-[(1R)-1-(2,6-dichloro-3-fluoro-phenyl)ethoxy]-5-[1-(1-prop-2-ynyl-4-piperidyl)pyrazol-4-yl]pyridin-2-amine, 73**

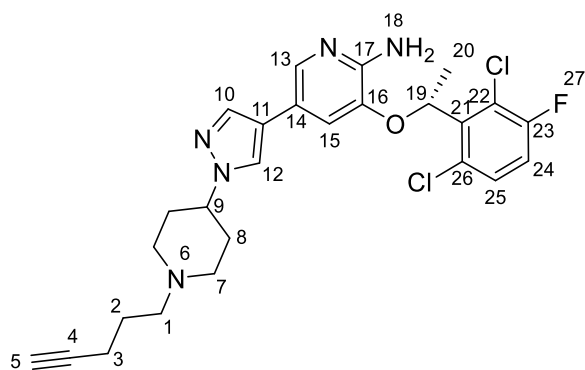


Crizotinib (30.00 mg, 0.0666 mmol) was taken up in Acetonitrile (1.00 mL, 0.0400 M) and DMF (0.50 mL, 0.0400 M) giving a white suspension. Potassium Carbonate (9.67 mg, 0.0699 mmol) was added, then Propargyl bromide in toluene (7.5371  $\mu$ L, 0.0699 mmol) was added giving a brown solution and the suspension stirred at rt for 10 mins, then heated to 30°C overnight. Reaction mixture partitioned between 15 mL DCM and 15 mL H<sub>2</sub>O. The aq phase was extracted 3 x 5 mL DCM and combined organics dried over MgSO<sub>4</sub>, vacuum filtered and concentrated in vacuo to give 3-[(1R)-1-(2,6-dichloro-3-fluoro-phenyl)ethoxy]-5-[1-(1-prop-2-ynyl-4-piperidyl)pyrazol-4-yl]pyridin-2-amine (38 mg, 95%, 0.0635 mmol) as a brown solid.

Ret. time = 1.666 mins. Observed mass 488.1420894. Calculated formula [M+H]<sup>+</sup> C<sub>24</sub>H<sub>24</sub>Cl<sub>2</sub>FN<sub>5</sub>O. Target m/z 488.1414705 <sup>1</sup>H NMR (600 MHz, Chloroform-d)  $\delta$  1.84

(d,  $J = 6.7$  Hz, 3H, 17), 2.02 – 2.11 (m, 2H, 5), 2.16 – 2.22 (m, 2H, 5), 2.28 (t,  $J = 2.4$  Hz, 1H, 3), 2.42 (td,  $J = 11.7, 2.5$  Hz, 2H, 4), 3.01 (dt,  $J = 11.7, 3.1$  Hz, 2H, 4), 3.37 (d,  $J = 2.5$  Hz, 2H, 1), 4.11 (tt,  $J = 11.6, 4.2$  Hz, 1H, 10), 4.76 – 4.87 (m, 2H, 15), 6.06 (q,  $J = 6.7$  Hz, 1H, 16), 6.86 (d,  $J = 1.8$  Hz, 1H, 12), 7.04 (dd,  $J = 8.9, 7.9$  Hz, 1H, 21), 7.29 (dd,  $J = 8.9, 4.8$  Hz, 1H, 22), 7.48 (d,  $J = 0.8$  Hz, 1H, 9), 7.55 (d,  $J = 0.8$  Hz, 1H, 7), 7.74 (d,  $J = 1.8$  Hz, 1H, 10).  $^{13}\text{C}$  NMR (151 MHz, Chloroform-*d*)  $\delta$  19.03, 17, 32.57 (d,  $J = 3.7$  Hz, 5), 46.94, 1, 51.37, 4, 59.20, 12, 72.55, 16, 73.49, 3, 78.71, 2, 115.09, 12, 116.84 (d,  $J = 23.2$  Hz, 21), 119.37, 4, 120.07, 8, 122.18 (d,  $J = 18.7$  Hz, 19), 122.48, 9, 125.72, 19, 129.06 (d,  $J = 3.7$  Hz, 23), 130.07, 22, 135.54, 135.77, 7, 137.06, 25, 139.97, 10, 148.98, 1, 157.67 (d,  $J = 251.6$  Hz, 20).  $^{19}\text{F}$  NMR (471 MHz, Chloroform-*d*)  $\delta$  -112.03, 24  $^{19}\text{F}$  NMR CPD (471 MHz, Chloroform-*d*)  $\delta$  -112.02, 24

**3-[(1R)-1-(2,6-dichloro-3-fluoro-phenyl)ethoxy]-5-[1-(1-pent-4-ynyl-4-piperidyl)pyrazol-4-yl]pyridin-2-amine, 74**



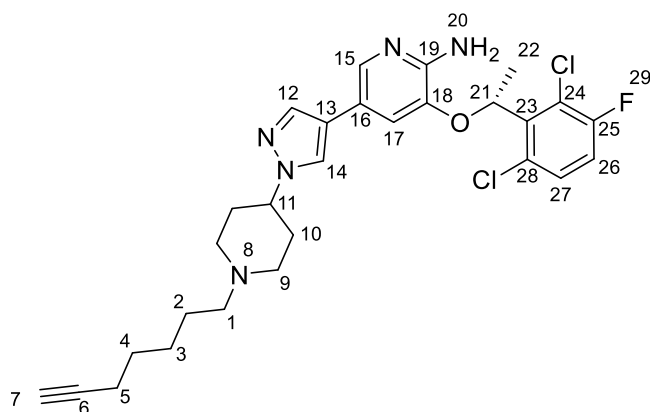
Crizotinib was reacted with pent-4-ynal, as per general method for reductive amination, to afford the title compound (63%)

Formula C<sub>26</sub>H<sub>28</sub>Cl<sub>2</sub>FN<sub>5</sub>O. Observed m/z 516.1739406. Calculated m/z 516.1727706. Error (ppm) 2.27.  $^1\text{H}$  NMR (600 MHz, Chloroform-*d*)  $\delta$  1.75 (p,  $J = 7.1$  Hz, 2H, 2), 1.85 (d,  $J = 6.7$  Hz, 3H, 20), 1.96 (t,  $J = 2.6$  Hz, 1H, 5), 2.00 – 2.06 (m, 2H, 8), 2.14 – 2.22 (m, 5H, 7, 8), 2.26 (td,  $J = 7.1, 2.7$  Hz, 2H, 3), 2.49 – 2.54 (m, 2H, 1), 3.06 (dt,  $J = 12.6, 3.6$  Hz, 2H, 7), 4.12 (tt,  $J = 11.4, 4.1$  Hz, 1H, 9), 5.22 (s, 2H, 18), 6.07 (q,  $J = 6.7$  Hz, 1H, 19), 6.87 (d,  $J = 1.8$  Hz, 1H, 15), 7.05 (dd,  $J = 8.9, 7.8$  Hz, 1H, 24), 7.30 (dd,  $J = 8.9, 4.8$  Hz, 1H, 25), 7.49 (d,  $J = 0.8$  Hz, 1H, 12), 7.55 (d,  $J = 0.8$  Hz,



1H, 10), 7.68 (d,  $J = 1.8$  Hz, 1H, 13).  $^{13}\text{C}$  NMR (151 MHz, Chloroform- $d$ )  $\delta$  16.56 , 3, 19.03 , 20, 25.93 , 2, 32.43 , 8, 52.52 , 7, 57.06 , 1, 59.52 , 9, 68.73, 5, 72.67 , 19, 84.12 , 4, 115.31 , 15, 116.91 (d,  $J = 23.1$  Hz, 24), 119.08 , 14, 119.87 , 11, 129.08 (d,  $J = 3.8$  Hz, 21), 130.13 (d,  $J = 10.4$  Hz, 25), 134.31 , 13, 135.72 , 10, 136.95 , 26, 140.13 , 16, 149.18 , 17, 157.69 (d,  $J = 241.4$  Hz, 23).  $^{19}\text{F}$  NMR (471 MHz, Chloroform- $d$ )  $\delta$  -111.96 , 27.  $^{19}\text{F}$  NMR (471 MHz, Chloroform- $d$ )  $\delta$  -111.97, 27.

**3-[(1R)-1-(2,6-dichloro-3-fluoro-phenyl)ethoxy]-N-hept-6-ynyl-5-[1-(1-hept-6-ynyl-4-piperidyl)pyrazol-4-yl]pyridin-2-amine, 75/CCT390196**



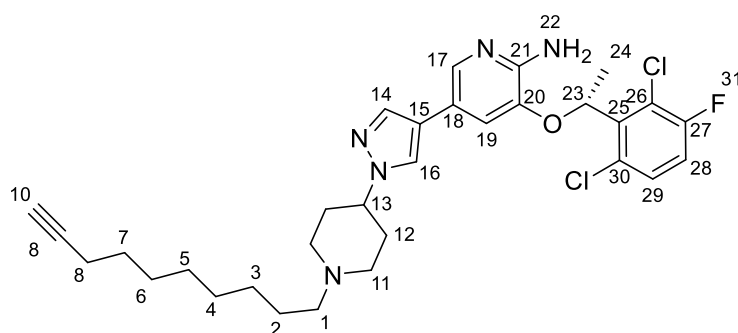
Crizotinib was reacted with hept-6-ynal as per general method for reductive amination to afford the title compound as a brown amorphous solid (58%)

Ret time mins = 1.811. Formula C<sub>28</sub>H<sub>32</sub>Cl<sub>2</sub>FN<sub>5</sub>O. Observed  $m/z$  544.2032775. Calculated  $m/z$  544.2040708. Error (ppm) -1.46.  $^1\text{H}$  NMR (600 MHz, Chloroform- $d$ )  $\delta$  1.39 – 1.46 (m, 2H, 3), 1.52 – 1.59 (m, 4H, 2, 4), 1.84 (d,  $J = 6.7$  Hz, 3H, 22), 1.94 (t,  $J = 2.6$  Hz, 1H, 7), 2.02 – 2.10 (m, 3H, 10), 2.15 – 2.23 (m, 5H, 9, 10, 5), 2.41 – 2.46 (m, 2H, 1), 3.09 (dt,  $J = 12.3, 3.5$  Hz, 2H, 9), 4.13 (tt,  $J = 11.2, 4.1$  Hz, 1H, 11), 5.07 (s, 2H, 20), 6.06 (q,  $J = 6.7$  Hz, 1H, 21), 6.85 (d,  $J = 1.8$  Hz, 1H, 17), 7.04 (dd,  $J = 8.9, 7.9$  Hz, 1H, 28), 7.29 (dd,  $J = 8.9, 4.8$  Hz, 1H, 27), 7.49 (d,  $J = 0.8$  Hz, 1H, 14), 7.54 (d,  $J = 0.8$  Hz, 1H, 12), 7.67 – 7.72 (m, 1H, 15).  $^{13}\text{C}$  NMR (151 MHz, Chloroform- $d$ )  $\delta$  18.45 , 5, 19.00 , 22, 26.37, 3, 28.39 , 2, 32.19 , 10, 52.37 , 9, 58.22 , 1, 59.25 , 11, 68.46 , 7, 72.61 , 21, 84.53 , 6, 115.21 , 17, 116.87 (d,  $J = 23.2$  Hz, 26), 119.11 , 16, 119.95 , 13, 122.17 (d,  $J = 19.3$  Hz, 24), 122.58 , 14, 129.05 (d,  $J = 3.8$  Hz, 23), 130.03

, 27, 134.72 , 15, 135.70 , 12, 136.96 , 23, 140.06 , 18, 149.12 , 19, 157.66 (d,  $J = 249.9$  Hz, 29, 25).  $^{19}\text{F}$  NMR (471 MHz, Chloroform-*d*)  $\delta$  -112.00 , 29.  $^{19}\text{F}$  CPD NMR (471 MHz, Chloroform-*d*)  $\delta$  -112.00, 29

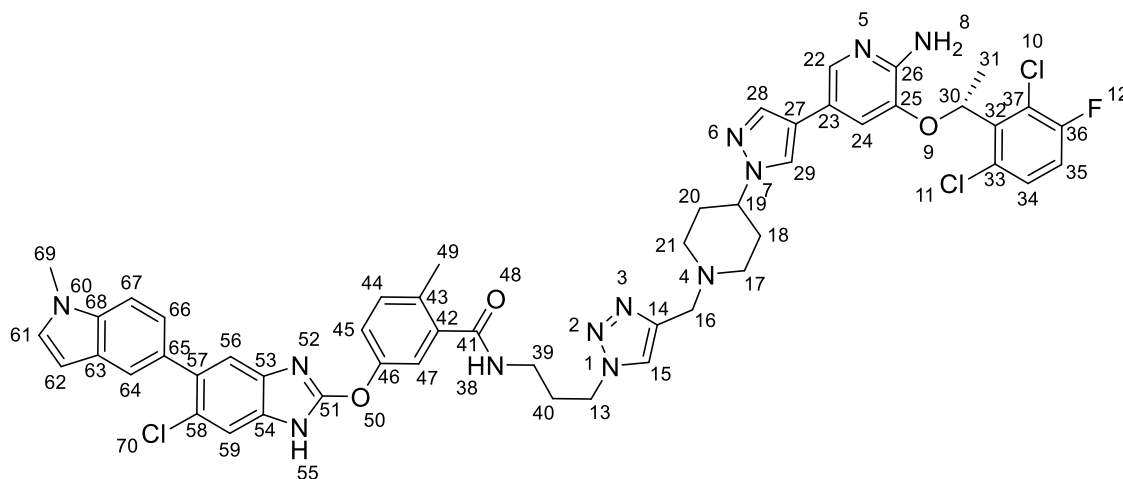
**5-[1-(1-dec-9-ynyl-4-piperidyl)pyrazol-4-yl]-3-[(1R)-1-(2,6-dichloro-3-fluorophenyl)ethoxy]pyridin-2-amine, 76**

Crizotinib was reacted with dec-9-ynal as per general method for reductive amination to afford the title compound as a brown amorphous solid (66%)



Ret time mins = 2.214 mins. Formula C<sub>31</sub>H<sub>39</sub>Cl<sub>2</sub>FN<sub>5</sub>O. Observed  $m/z$  586.2512. Calculated  $m/z$  586.2510. Error (ppm) 0.47.  $^1\text{H}$  NMR (600 MHz, Chloroform-*d*)  $\delta$  1.31 – 1.37 (m, 3H, 3, 4, 5), 1.38 – 1.45 (m, 2H, 6), 1.51 – 1.61 (m, 2H, 7), 1.87 (d,  $J = 6.6$  Hz, 3H, 24), 1.96 (t,  $J = 2.7$  Hz, 1H, 10), 2.09 – 2.16 (m, 2H, 12), 2.17 – 2.34 (m, 4H, 12), 2.44 – 2.51 (m, 2H, 1), 3.15 (dt,  $J = 12.0, 3.8$  Hz, 2H, 11), 4.18 (tt,  $J = 11.1, 4.1$  Hz, 1H, 13), 5.28 (s, 2H, 22), 6.09 (q,  $J = 6.7$  Hz, 1H, 23), 6.89 (d,  $J = 1.7$  Hz, 1H, 19), 7.07 (dd,  $J = 8.9, 7.8$  Hz, 1H, 28), 7.33 (dd,  $J = 8.9, 4.7$  Hz, 1H, 29), 7.51 (s, 1H, 16), 7.56 (s, 1H, 14), 7.70 (s, 1H, 17).  $^{13}\text{C}$  NMR (151 MHz, Chloroform-*d*)  $\delta$  18.51, 8, 19.02 , 24, 26.58, 2, 27.57, 3, 28.57, 7, 28.78, 6, 29.13, 4, 29.44, 5, 31.94, 12, 52.15 , 11, 58.30 , 1, 59.04 , 13, 68.24 , 10, 72.67 , 23, 84.86 , 8, 115.30 , 19, 116.91 (d,  $J = 23.1$  Hz, 28), 118.99 , 18, 119.94 , 15, 122.19 (d,  $J = 18.7$  Hz, 26), 122.60 , 16, 129.07 (d,  $J = 3.8$  Hz, 25), 130.08 , 29, 134.22 , 17, 135.73 , 14, 136.92 , 30, 140.12 , 20, 149.22 , 21, 157.72 (d,  $J = 250.2$  Hz, 27).  $^{19}\text{F}$  NMR (471 MHz, Chloroform-*d*)  $\delta$  -111.96, 31.

**N-[3-[4-[[4-[4-[6-amino-5-[(1R)-1-(2,6-dichloro-3-fluoro-phenyl)ethoxy]-3-pyridyl]pyrazol-1-yl]-1-piperidyl]methyl]triazol-1-yl]propyl]-5-[[6-chloro-5-(1-methylindol-5-yl)-1H-benzimidazol-2-yl]oxy]-2-methyl-benzamide, CCT392810**

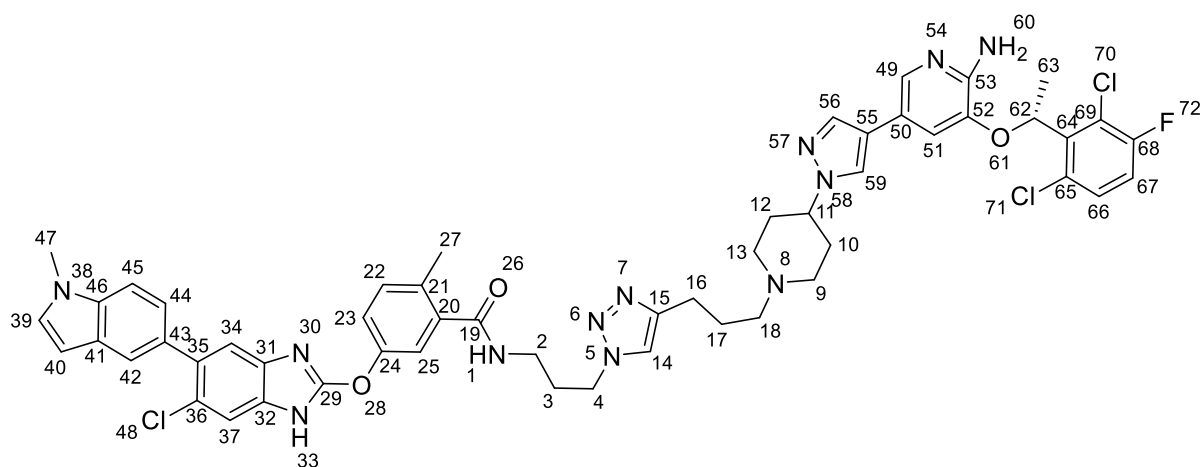


The general procedure for click coupling was carried out with the desired azide (N-(3-azidopropyl)-5-[[6-chloro-5-(1-methylindol-5-yl)-1H-benzimidazol-2-yl]oxy]-2-methyl-benzamide, 60, and alkyne (3-[(1R)-1-(2,6-dichloro-3-fluoro-phenyl)ethoxy]-5-[1-(1-prop-2-ynyl-4-piperidyl)pyrazol-4-yl]pyridin-2-amine, 73) to afford the title compound as an off white solid (59%)

Formula C<sub>51</sub>H<sub>48</sub>Cl<sub>3</sub>FN<sub>12</sub>O<sub>3</sub>. Observed m/z 1001.3080031. Calculated m/z 1001.3094713. Error (ppm) -1.47. <sup>1</sup>H NMR (600 MHz, DMSO-*d*<sub>6</sub>) δ 1.80 (d, *J* = 6.7 Hz, 3H, 31), 1.85 – 2.01 (m, 5H, 18', 18'', 20', 20''), 2.08 (q, *J* = 6.9 Hz, 1H, 40), 2.11 – 2.17 (m, 2H, 17', 21'), 2.37 (s, 3H, 49), 2.92 (dt, *J* = 12.0, 3.5 Hz, 2H, 17'', 21''), 3.25 (q, *J* = 6.5 Hz, 2H, 39), 3.38 (dt, *J* = 12.3, 6.2 Hz, 19H), 3.59 (s, 2H, 16), 3.82 (s, 3H, 69), 4.07 (tt, *J* = 11.6, 4.3 Hz, 1H, 19), 4.43 (t, *J* = 7.0 Hz, 2H, 13), 5.64 (s, 2H, 8), 6.08 (q, *J* = 6.6 Hz, 1H, 30), 6.46 (d, *J* = 3.1 Hz, 1H), 6.89 (d, *J* = 1.8 Hz, 1H, 24), 7.18 (dd, *J* = 8.4, 1.7 Hz, 1H), 7.36 (ddd, *J* = 19.6, 11.9, 4.6 Hz, 5H), 7.43 (t, *J* = 8.7 Hz, 1H, 35), 7.47 (d, *J* = 8.4 Hz, 1H), 7.52 (d, *J* = 3.2 Hz, 2H), 7.55 (s, 1H), 7.55 – 7.58 (m, 1H, 34), 7.75 (s, 1H, 22), 7.92 (s, 1H), 8.05 (s, 1H, 15), 8.48 (t, *J* = 5.6 Hz, 1H, 38). <sup>13</sup>C NMR (151 MHz, DMSO-*d*<sub>6</sub>) δ 15.64, 19.07, 31, 19.29, 49, 30.22, 40, 32.48, 18, 20, 33.01, 36.73, 39, 47.66, 13, 51.98, 17, 21, 52.91, 58.88, 65.39, 72.43, 30, 101.03, 109.56, 114.92, 24, 117.88, 117.90 (d, *J* = 23.1 Hz, 35), 119.45, 119.55, 121.44, 37, 121.56,

121.73, 121.81, 123.64, 123.95, 124.33, 125.03, 128.23, 129.20 (d,  $J = 3.3$  Hz), 130.62, 131.03, 131.31, 132.20, 132.87, 134.99, 135.92, 22, 136.01, 137.29, 138.64, 139.27, 143.89, 14, 149.91, 151.43, 157.29 (d,  $J = 247.5$  Hz, 36), 158.33.  $^{19}\text{F}$  NMR (471 MHz, DMSO- $d_6$ )  $\delta$  -113.18 (dd,  $J = 8.6, 5.1$  Hz).  $^{19}\text{F}$  NMR (CPD 471 MHz, DMSO- $d_6$ )  $\delta$  -113.18.

**N-[3-[4-[3-[4-[4-[6-amino-5-[(1R)-1-(2,6-dichloro-3-fluoro-phenyl)ethoxy]-3-pyridyl]pyrazol-1-yl]-1-piperidyl]propyl]triazol-1-yl]propyl]-5-[[6-chloro-5-(1-methylindol-5-yl)-1H-benzimidazol-2-yl]oxy]-2-methyl-benzamide, CCT392812**

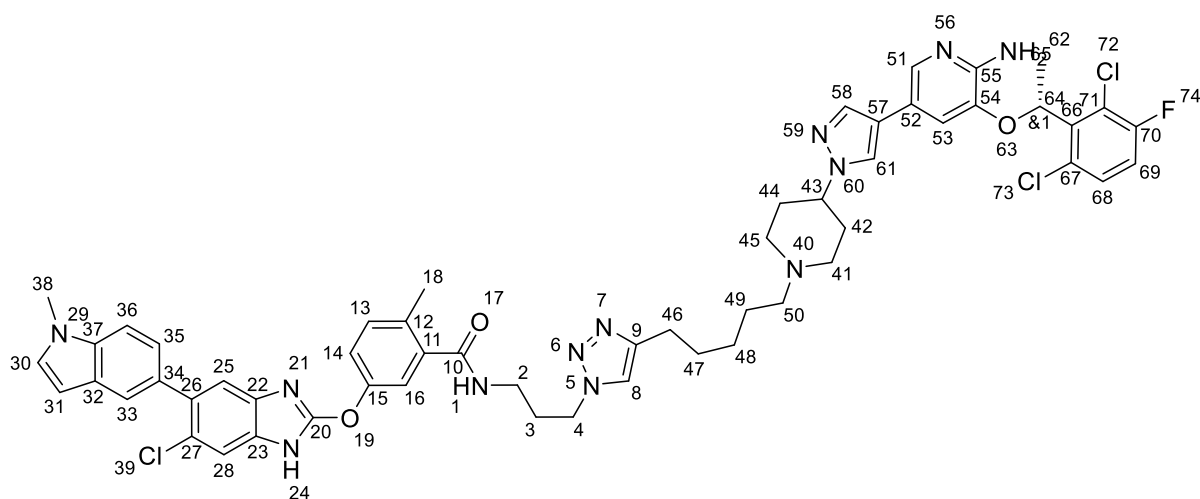


The general procedure for click coupling was carried out with the desired azide (N-(3-azidopropyl)-5-[[6-chloro-5-(1-methylindol-5-yl)-1H-benzimidazol-2-yl]oxy]-2-methyl-benzamide, 60 and alkyne (3-[(1R)-1-(2,6-dichloro-3-fluoro-phenyl)ethoxy]-5-[1-(1-pent-4-ynyl-4-piperidyl)pyrazol-4-yl]pyridin-2-amine, 74) to afford the title compound as an off white solid (39%)

Formula C<sub>53</sub>H<sub>52</sub>Cl<sub>3</sub>FN<sub>12</sub>O<sub>3</sub>. Observed m/z 1029.3404455. Calculated m/z 1029.3407714. Error (ppm) -0.32. Ion Species (M+H)<sup>+</sup>  $^1\text{H}$  NMR (600 MHz, DMSO- $d_6$ )  $\delta$  1.75 (q,  $J = 7.4$  Hz, 2H, 17), 1.80 (d,  $J = 6.6$  Hz, 3H, 63), 1.93 (dtd,  $J = 35.8, 12.3, 3.7$  Hz, 4H, 10'', 12''), 2.01 – 2.10 (m, 4H, 3, 9'', 13''), 2.34 (t,  $J = 7.3$  Hz, 2H, 18), 2.37 (s, 3H), 2.63 (t,  $J = 7.6$  Hz, 2H, 16), 2.93 (dt,  $J = 12.1, 3.7$  Hz, 2H, 9', 13'), 3.24 (q,  $J = 6.5$  Hz, 2H, 2), 3.82 (s, 3H, 10', 12', 47), 4.08 (tt,  $J = 11.3, 4.3$  Hz, 1H, 11), 4.39 (t,  $J = 7.0$  Hz, 2H, 4), 5.64 (s, 2H, 60), 6.08 (q,  $J = 6.6$  Hz, 1H, 62), 6.46 (d,  $J = 3.0$  Hz, 1H), 6.90 (d,  $J = 1.8$  Hz, 1H, 51), 7.18 (dd,  $J = 8.4, 1.7$  Hz, 1H), 7.33 (d,  $J = 6.7$  Hz, 1H), 7.34 –

7.37 (m, 2H), 7.39 (dd,  $J = 8.3, 2.6$  Hz, 1H), 7.43 (t,  $J = 8.7$  Hz, 1H, 67), 7.47 (d,  $J = 8.4$  Hz, 1H), 7.51 (s, 1H), 7.53 (s, 1H), 7.55 (d,  $J = 1.6$  Hz, 1H), 7.57 (dd,  $J = 9.0, 4.9$  Hz, 1H, 66), 7.75 (d,  $J = 1.8$  Hz, 1H, 49), 7.90 (s, 1H, 14), 7.95 (s, 1H), 8.46 (t,  $J = 5.6$  Hz, 1H, 1).  $^{13}\text{C}$  NMR (151 MHz,  $\text{DMSO-}d_6$ )  $\delta$  15.64, 19.07, 63, 19.27, 23.41, 16, 27.00, 17, 30.24, 3, 32.62, 10, 12, 33.01, 47, 36.79, 47.58, 4, 52.47, 9, 13, 57.41, 18, 59.15, 11, 65.39, 72.44, 62, 101.02, 109.56, 114.93, 51, 117.90, 117.91 (d,  $J = 23.1$  Hz, 67), 119.41, 119.56, 121.44, 121.57, 121.73, 121.78, 122.44, 123.64, 123.93, 124.97, 128.23, 129.22, 65, 130.62, 131.04, 66, 131.33, 132.19, 132.81, 134.94, 135.94, 136.01, 137.31, 138.63, 139.26, 147.12, 149.91, 151.47, 157.27 (d,  $J = 248.0$  Hz, 68), 158.43, 168.65.  $^{19}\text{F}$  NMR (471 MHz,  $\text{DMSO-}d_6$ )  $\delta$  -113.18 (dd,  $J = 8.4, 5.0$  Hz).  $^{19}\text{F}$  NMR (CPD 471 MHz,  $\text{DMSO-}d_6$ )  $\delta$  -113.18.

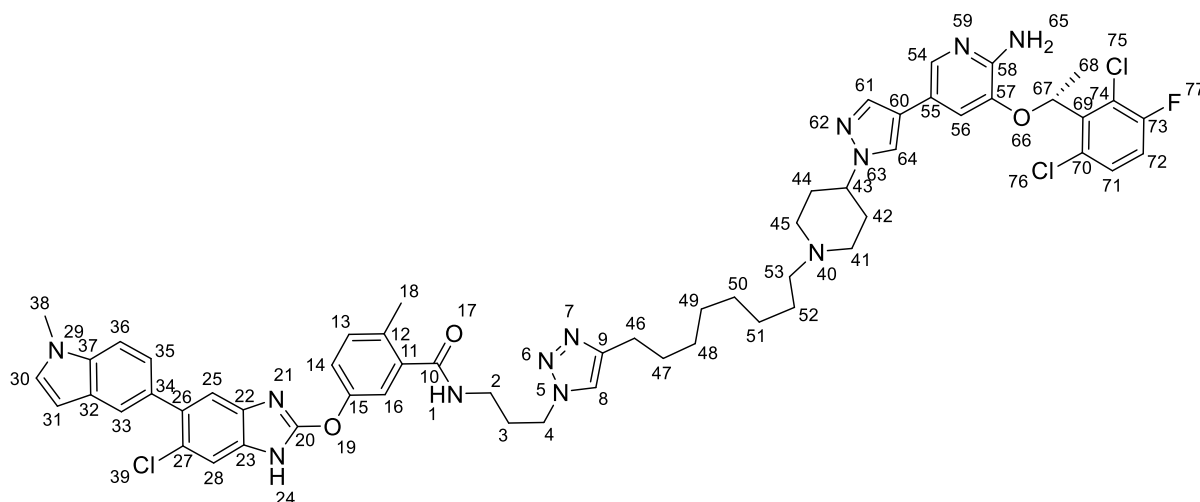
**N-[3-[4-[5-[4-[4-[6-amino-5-[(1R)-1-(2,6-dichloro-3-fluoro-phenyl)ethoxy]-3-pyridyl]pyrazol-1-yl]-1-piperidyl]pentyl]triazol-1-yl]propyl]-5-[[6-chloro-5-(1-methylindol-5-yl)-1H-benzimidazol-2-yl]oxy]-2-methyl-benzamide, CCT392813**



The general procedure for click coupling was carried out with the desired azide ((N-(3-azidopropyl)-5-[[6-chloro-5-(1-methylindol-5-yl)-1H-benzimidazol-2-yl]oxy]-2-methyl-benzamide, 60) and alkyne (3-[(1R)-1-(2,6-dichloro-3-fluoro-phenyl)ethoxy]-N-hept-6-ynyl-5-[1-(1-hept-6-ynyl-4-piperidyl)pyrazol-4-yl]pyridin-2-amine, 75/CCT390196) to afford the title compound as a light tan solid (35%)

Formula C<sub>55</sub>H<sub>56</sub>Cl<sub>3</sub>FN<sub>12</sub>O<sub>3</sub>. Observed m/z 1057.3676733. Calculated m/z 1057.3720715. Error (ppm) -4.16. <sup>1</sup>H NMR (600 MHz, DMSO-*d*<sub>6</sub>) δ 1.10 (t, *J* = 7.0 Hz, 1H), 1.35 (d, *J* = 10.1 Hz, 2H, 48), 1.63 (s, 2H, 47), 1.72 (s, 2H), 1.81 (d, *J* = 6.7 Hz, 3H, 65), 2.07 (s, 2H), 2.25 (s, 3H), 2.37 (s, 3H), 2.55 (s, 3H), 2.63 (d, *J* = 8.2 Hz, 2H, 46), 3.06 (s, 4H), 3.24 (d, *J* = 6.6 Hz, 2H, 2), 3.83 (d, *J* = 5.4 Hz, 3H), 4.39 (t, *J* = 7.2 Hz, 3H, 4), 5.70 (s, 2H, 62), 6.09 (q, *J* = 6.7 Hz, 1H, 64), 6.44 – 6.49 (m, 1H), 6.91 (d, *J* = 1.8 Hz, 1H, 53), 7.18 (dd, *J* = 21.2, 8.5 Hz, 1H), 7.29 – 7.41 (m, 5H), 7.44 (t, *J* = 8.7 Hz, 1H, 69), 7.48 (d, *J* = 8.8 Hz, 1H), 7.51 – 7.63 (m, 3H, 68), 7.78 (s, 1H, 51), 7.92 (d, *J* = 8.7 Hz, 2H, 8), 8.49 (s, 1H, 1), 10.08 (s, 1H), 12.62 (s, 1H). <sup>13</sup>C NMR (151 MHz, DMSO-*d*<sub>6</sub>) δ 19.09, 65, 19.29, 25.19, 46, 26.03, 48, 28.91, 47, 30.25, 3, 33.02, 36.75, 2, 40.90, 47.56, 4, 72.47, 101.02, 109.58, 114.96, 117.53, 117.85, 118.00, 118.34, 119.46, 119.81, 57, 121.52 (d, *J* = 19.1 Hz, 71), 121.79 (d, *J* = 16.8 Hz), 122.46, 8, 123.62, 125.09, 128.23, 129.20, 67, 129.22, 130.67, 131.06, 132.23, 132.89, 136.01, 137.28, 66, 138.64, 139.20, 54, 146.96, 150.05, 55, 151.39, 157.30 (d, *J* = 242.4 Hz, 70), 168.65. <sup>19</sup>F NMR (471 MHz, DMSO-*d*<sub>6</sub>) δ -113.13 (dd, *J* = 8.7, 5.1 Hz). <sup>19</sup>F NMR (CPD, 471 MHz, DMSO-*d*<sub>6</sub>) δ -113.13.

**N-[3-[4-[8-[4-[4-[6-amino-5-[(1R)-1-(2,6-dichloro-3-fluoro-phenyl)ethoxy]-3-pyridyl]pyrazol-1-yl]-1-piperidyl]octyl]triazol-1-yl]propyl]-5-[[6-chloro-5-(1-methylindol-5-yl)-1H-benzimidazol-2-yl]oxy]-2-methyl-benzamide, CCT392814**

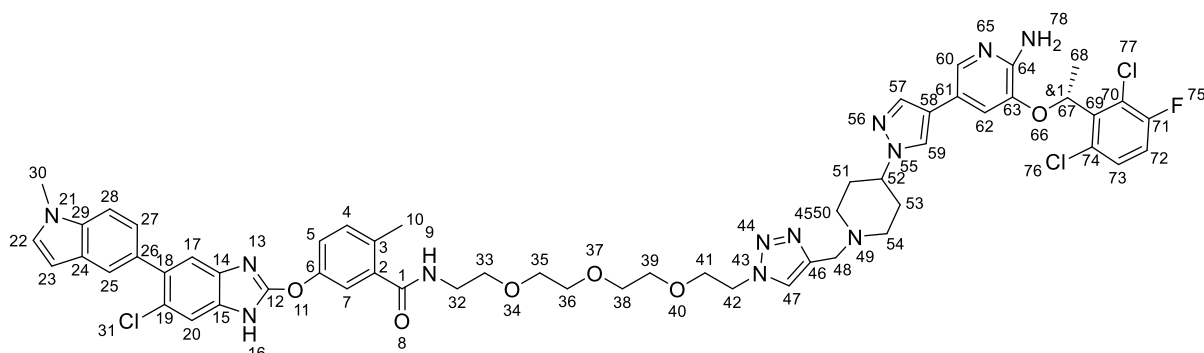


The general procedure for click coupling was carried out with the desired azide (N-(3-azidopropyl)-5-[[6-chloro-5-(1-methylindol-5-yl)-1H-benzimidazol-2-yl]oxy]-2-

methyl-benzamide, 60 and alkyne (5-[1-(1-dec-9-ynyl-4-piperidyl)pyrazol-4-yl]-3-[(1R)-1-(2,6-dichloro-3-fluoro-phenyl)ethoxy]pyridin-2-amine, 76) to afford the title compound as an off white solid (27%)

Formula C<sub>58</sub>H<sub>62</sub>Cl<sub>3</sub>FN<sub>12</sub>O<sub>3</sub>. Observed m/z 1099.4198440. Calculated m/z 1099.4190217. Error (ppm) 0.75. <sup>1</sup>H NMR (600 MHz, DMSO-*d*<sub>6</sub>) δ 1.27 (h, *J* = 8.8, 7.8 Hz, 8H), 1.41 (p, *J* = 7.1 Hz, 2H), 1.57 (p, *J* = 7.3 Hz, 2H), 1.80 (d, *J* = 6.6 Hz, 3H, 68), 1.84 – 2.01 (m, 6H, 41'', 42'', 44'', 45''), 2.01 – 2.09 (m, 2H, 3), 2.27 (t, *J* = 7.4 Hz, 2H), 2.36 (s, 3H, 18), 2.55 (s, 2H), 2.59 (t, *J* = 7.6 Hz, 2H), 2.91 (dd, *J* = 9.7, 5.6 Hz, 2H, 41', 45'), 3.23 (q, *J* = 6.5 Hz, 2H, 2), 3.39 (t, *J* = 6.6 Hz, 7H), 3.83 (s, 3H, 38), 4.06 (tt, *J* = 11.2, 4.3 Hz, 1H, 43), 4.38 (t, *J* = 7.0 Hz, 2H, 4), 5.64 (s, 2H, 65), 6.08 (q, *J* = 6.6 Hz, 1H, 67), 6.46 (d, *J* = 3.0 Hz, 1H), 6.90 (d, *J* = 1.8 Hz, 1H, 56), 7.16 – 7.21 (m, 1H), 7.34 (dd, *J* = 12.8, 4.4 Hz, 3H), 7.36 – 7.40 (m, 2H), 7.44 (t, *J* = 8.7 Hz, 1H, 72), 7.47 (d, *J* = 8.5 Hz, 1H), 7.51 (s, 1H), 7.52 (s, 1H), 7.54 (s, 1H), 7.57 (dd, *J* = 9.0, 4.9 Hz, 1H, 71), 7.75 (s, 1H, 54), 7.87 (s, 1H, 8), 7.95 (s, 1H), 8.45 (t, *J* = 5.6 Hz, 1H, 1). <sup>13</sup>C NMR (151 MHz, DMSO-*d*<sub>6</sub>) δ 19.07, 19.27, 25.48, 27.10, 27.44, 29.25, 29.38, 29.44, 30.24, 3, 32.61, 33.01, 36.77, 2, 47.55, 4, 52.51, 41, 45, 58.18, 59.19, 43, 72.43, 67, 101.02, 109.55, 114.92, 56, 117.90, 117.91 (d, *J* = 23.2 Hz, 72), 119.38, 119.56, 60, 121.51 (d, *J* = 19.9 Hz, 74), 121.73, 122.34, 123.65, 123.91, 128.23, 129.20, 70, 130.61, 131.01 (d, *J* = 6.6 Hz, 71), 131.37, 132.18, 132.75, 134.93, 135.93, 54, 136.00, 137.31, 69, 138.61, 139.26, 57, 147.29, 9, 149.90, 58, 151.51, 157.28 (d, *J* = 254.2 Hz, 73), 168.65. <sup>19</sup>F NMR (471 MHz, DMSO-*d*<sub>6</sub>) δ -113.19 (dd, *J* = 8.4, 5.1 Hz). <sup>19</sup>F NMR (CPD, 471 MHz, DMSO-*d*<sub>6</sub>) δ -113.19.

**N-[2-[2-[2-[2-[4-[[4-[4-[6-amino-5-[(1R)-1-(2,6-dichloro-3-fluoro-phenyl)ethoxy]-3-pyridyl]pyrazol-1-yl]-1-piperidyl]methyl]triazol-1-yl]ethoxy]ethoxy]ethoxy]ethyl]-5-[[6-chloro-5-(1-methylindol-5-yl)-1H-benzimidazol-2-yl]oxy]-2-methyl-benzamide, CCT392659**



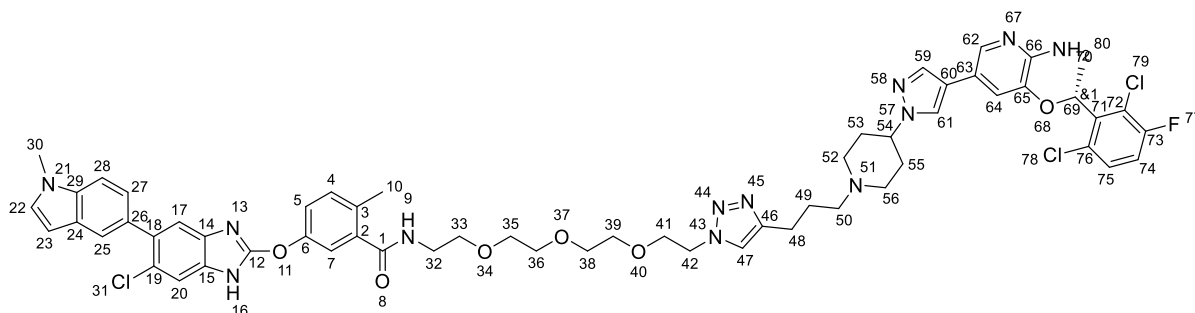
The general procedure for click coupling was carried out with the desired azide (N-[2-[2-[2-(2-azidoethoxy)ethoxy]ethoxy]ethyl]-5-[[6-chloro-5-(1-methylindol-5-yl)-1H-benzimidazol-2-yl]oxy]-2-methyl-benzamide, 57) and alkyne (3-[(1R)-1-(2,6-dichloro-3-fluoro-phenyl)ethoxy]-5-[1-(1-prop-2-ynyl-4-piperidyl)pyrazol-4-yl]pyridin-2-amine, 73) to afford the title compound as an off white solid (37%)

Formula C<sub>56</sub>H<sub>58</sub>Cl<sub>3</sub>FN<sub>12</sub>O<sub>6</sub> Observed m/z 1119.3715418 Calculated m/z 1119.3724655 Error (ppm) -0.83. <sup>1</sup>H NMR (600 MHz, DMSO-*d*<sub>6</sub>) δ 1.80 (d, *J* = 6.6 Hz, 3H, 68), 2.35 (s, 3H), 3.38 (t, *J* = 5.9 Hz, 2H, 32), 3.51 (dt, *J* = 21.2, 5.1 Hz, 12H, 33, 35, 36, 38, 39, 48), 3.81 (d, *J* = 8.8 Hz, 2H), 3.83 (s, 2H), 4.55 (s, 2H, 42), 5.73 (s, 2H, 78), 6.08 (q, *J* = 6.7 Hz, 1H, 67), 6.46 (s, 1H, 23), 6.90 (d, *J* = 1.9 Hz, 1H, 62), 7.19 (dd, *J* = 13.8, 6.4 Hz, 1H), 7.29 – 7.40 (m, 5H, 22), 7.43 (t, *J* = 8.7 Hz, 1H, 72), 7.48 (d, *J* = 9.0 Hz, 1H), 7.51 – 7.59 (m, 3H, 73), 7.76 (d, *J* = 1.8 Hz, 1H, 60), 7.92 (s, 1H), 8.14 (s, OH), 8.19 (s, 1H), 8.38 (d, *J* = 5.9 Hz, 1H, 9), 12.61 (s, 1H, 16). <sup>13</sup>C NMR (151 MHz, DMSO-*d*<sub>6</sub>) δ 19.08, 68, 19.23, 10, 33.02, 30, 42.58, 49.99, 69.12, 69.21, 69.98, 70.03, 70.11, 70.20, 33, 35, 36, 38, 39, 48, 72.48, 101.03, 109.58, 113.29, 115.01, 62, 117.61, 57, 117.93 (d, *J* = 23.3 Hz, 72), 130.65, 131.27 (d, *J* = 13.8 Hz), 132.22, 132.40, 132.90, 135.04, 135.44, 135.67, 136.02, 137.24, 138.68, 139.31, 140.84, 149.94, 151.37, 157.60 (d, *J* = 264.9 Hz, 71), 163.51, 168.59. <sup>19</sup>F NMR (471 MHz,



DMSO-*d*<sub>6</sub>)  $\delta$  -113.14 (dd,  $J$  = 8.4, 4.9 Hz). <sup>19</sup>F NMR (CPD 471 MHz, DMSO-*d*<sub>6</sub>)  $\delta$  -113.14.

**N-[2-[2-[2-[2-[4-[3-[4-[4-[6-amino-5-[(1R)-1-(2,6-dichloro-3-fluoro-phenyl)ethoxy]-3-pyridyl]pyrazol-1-yl]-1-piperidyl]propyl]triazol-1-yl]ethoxy]ethoxy]ethoxy]ethyl]-5-[[6-chloro-5-(1-methylindol-5-yl)-1H-benzimidazol-2-yl]oxy]-2-methyl-benzamide, CCT391400**

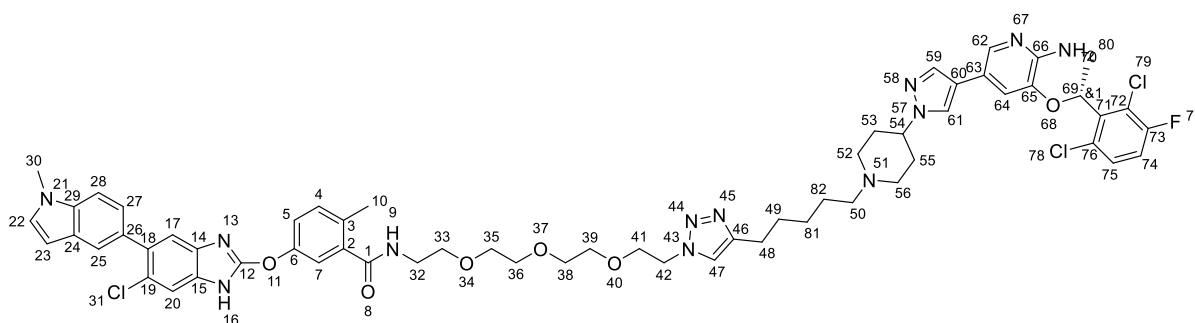


The general procedure for click coupling was carried out with the desired azide (N-[2-[2-[2-(2-azidoethoxy)ethoxy]ethoxy]ethyl]-5-[[6-chloro-5-(1-methylindol-5-yl)-1H-benzimidazol-2-yl]oxy]-2-methyl-benzamide, 57) and alkyne (3-[(1R)-1-(2,6-dichloro-3-fluoro-phenyl)ethoxy]-5-[1-(1-pent-4-ynyl-4-piperidyl)pyrazol-4-yl]pyridin-2-amine, 74) to afford the title compound as an off white solid (9%)

Formula C<sub>58</sub>H<sub>62</sub>Cl<sub>3</sub>FN<sub>12</sub>O<sub>6</sub>. Observed  $m/z$  1147.4070919. Calculated  $m/z$  1147.4037656. Error (ppm) 2.90. <sup>1</sup>H NMR (600 MHz, DMSO-*d*<sub>6</sub>)  $\delta$  1.81 (d,  $J$  = 6.6 Hz, 3H), 2.06 (s, 2H), 2.24 (s, 3H), 2.36 (s, 3H), 2.70 (s, 2H), 3.13 (s, 4H), 3.33 (s, 23H), 3.36 – 3.43 (m, 2H), 3.49 (s, 7H), 3.53 (s, 5H), 3.60 (s, 1H, 52', 56'), 3.78 (d,  $J$  = 5.4 Hz, 3H), 3.83 (d,  $J$  = 5.6 Hz, 3H), 4.38 – 4.54 (m, 3H), 5.71 (s, 2H, 80), 6.09 (q,  $J$  = 6.6 Hz, 1H, 69), 6.43 – 6.49 (m, 1H), 6.89 – 6.93 (m, 1H), 7.18 (dd,  $J$  = 20.2, 8.4 Hz, 1H), 7.30 – 7.36 (m, 2H), 7.38 (q,  $J$  = 7.4, 6.9 Hz, 2H), 7.44 (t,  $J$  = 8.7 Hz, 1H, 74), 7.48 (d,  $J$  = 8.1 Hz, 0H), 7.51 – 7.59 (m, 2H), 7.60 (s, 1H), 7.78 (s, 1H, 62), 7.89 (s, 1H), 7.93 (s, 1H), 8.39 (s, 1H, 9), 12.62 (s, 1H). <sup>13</sup>C NMR (151 MHz, DMSO-*d*<sub>6</sub>)  $\delta$  19.09, 19.23, 33.02, 69.22, 69.23, 70.00, 70.10, 70.20, 72.48, 101.03, 109.58, 114.99, 117.93 (d,  $J$  = 23.1 Hz), 118.33, 119.35, 121.52 (d,  $J$  = 19.2 Hz), 121.73, 122.95, 123.62, 125.10,

128.23, 129.21, 132.22, 132.90, 136.02, 137.27, 138.68, 150.03, 151.38, 158.11, 168.59. <sup>19</sup>F NMR (471 MHz, DMSO-*d*<sub>6</sub>) δ -114.28 – -112.61 (m).

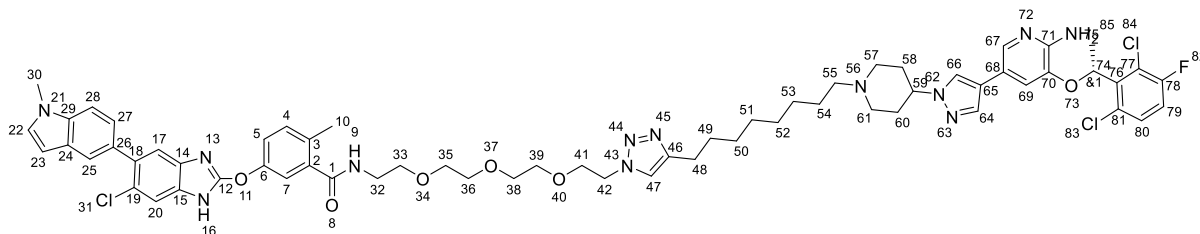
**pyridyl]pyrazol-1-yl]-1-piperidyl]pentyl]triazol-1-yl]ethoxy]ethoxy]ethoxy]ethyl]-5-[[6-chloro-5-(1-methylindol-5-yl)-1H-benzimidazol-2-yl]oxy]-2-methyl-benzamide, CCT391401**



The general procedure for click coupling was carried out with the desired azide (N-[2-[2-[2-(2-azidoethoxy)ethoxy]ethoxy]ethyl]-5-[[6-chloro-5-(1-methylindol-5-yl)-1H-benzimidazol-2-yl]oxy]-2-methyl-benzamide, 57) and alkyne (3-[(1R)-1-(2,6-dichloro-3-fluoro-phenyl)ethoxy]-N-hept-6-ynyl-5-[1-(1-hept-6-ynyl-4-piperidyl)pyrazol-4-yl]pyridin-2-amine, 75/CCT390196) to afford the title compound as an off white solid (9%)

Formula C<sub>60</sub>H<sub>66</sub>Cl<sub>3</sub>FN<sub>12</sub>O<sub>6</sub>. Observed m/z 1175.4355519. Calculated m/z 1175.4350657. Error (ppm) 0.41. <sup>1</sup>H NMR (600 MHz, DMSO-*d*<sub>6</sub>) δ 1.33 (p, *J* = 10.7, 9.3 Hz, 2H), 1.62 (t, *J* = 7.7 Hz, 2H), 1.80 (d, *J* = 6.6 Hz, 3H), 2.22 (s, 3H), 2.36 (s, 3H), 2.62 (t, *J* = 7.6 Hz, 2H), 3.05 (s, 3H), 3.38 (q, *J* = 5.8 Hz, 2H), 3.50 (dt, *J* = 24.6, 5.9 Hz, 10H), 3.77 (t, *J* = 5.3 Hz, 2H), 3.83 (s, 3H), 4.44 (t, *J* = 5.3 Hz, 2H), 5.68 (s, 2H, 80), 6.09 (q, *J* = 6.6 Hz, 1H, 69), 6.46 (s, 1H), 6.91 (d, *J* = 1.9 Hz, 1H), 7.18 (s, 1H), 7.29 – 7.40 (m, 4H), 7.44 (t, *J* = 8.7 Hz, 1H, 74), 7.46 – 7.60 (m, 4H), 7.77 (d, *J* = 1.8 Hz, 1H, 62), 7.81 (s, 1H), 7.93 (s, 1H), 8.38 (t, *J* = 5.7 Hz, 1H), 12.61 (s, 1H). <sup>13</sup>C NMR (151 MHz, DMSO-*d*<sub>6</sub>) δ 19.09, 19.23, 25.23, 33.02, 49.64, 69.22, 69.25, 70.00, 70.09, 70.20, 101.03, 109.58, 114.95, 117.84, 118.00, 119.35, 121.52 (d, *J* = 19.2 Hz), 121.72, 122.62, 123.62, 125.10, 128.24, 129.22, 130.65, 132.21, 132.90, 135.06, 136.03, 137.29, 138.68, 139.26, 148.48 (d, *J* = 469.3 Hz), 151.38, 168.58. <sup>19</sup>F NMR (471 MHz, DMSO-*d*<sub>6</sub>) δ -113.19.

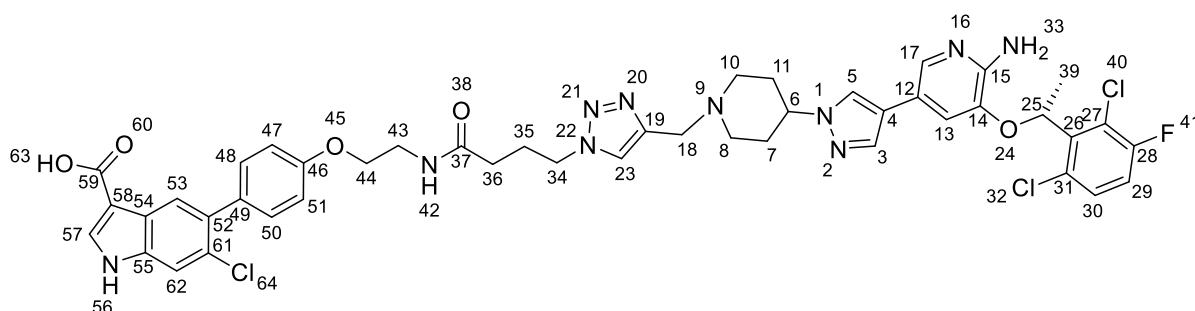
**N-[2-[2-[2-[2-[4-[8-[4-[4-[6-amino-5-[(1R)-1-(2,6-dichloro-3-fluoro-phenyl)ethoxy]-3-pyridyl]pyrazol-1-yl]-1-piperidyl]octyl]triazol-1-yl]ethoxy]ethoxy]ethoxy]ethyl]-5-[[6-chloro-5-(1-methylindol-5-yl)-1H-benzimidazol-2-yl]oxy]-2-methyl-benzamide, CCT390628**



The general procedure for click coupling was carried out with the desired azide (N-[2-[2-[2-(2-azidoethoxy)ethoxy]ethoxy]ethyl]-5-[[6-chloro-5-(1-methylindol-5-yl)-1H-benzimidazol-2-yl]oxy]-2-methyl-benzamide, 57) and alkyne (5-[1-(1-dec-9-ynyl)-4-piperidyl]pyrazol-4-yl]-3-[(1R)-1-(2,6-dichloro-3-fluoro-phenyl)ethoxy]pyridin-2-amine, 76) to afford the title compound as a brown solid (19%)

$^1\text{H}$  NMR (600 MHz, Chloroform-*d*)  $\delta$  1.22 – 1.31 (m, 12H), 1.57 (p,  $J$  = 7.5 Hz, 3H), 1.67 (q,  $J$  = 8.0, 7.1 Hz, 3H), 1.88 (d,  $J$  = 6.6 Hz, 4H), 2.33 (qd,  $J$  = 9.1, 4.6 Hz, 5H), 2.45 (s, 3H), 2.60 – 2.66 (m, 2H), 2.77 (t,  $J$  = 8.2 Hz, 3H), 3.40 (dt,  $J$  = 10.8, 4.7 Hz, 2H), 3.50 (dd,  $J$  = 5.9, 3.0 Hz, 2H), 3.54 (dd,  $J$  = 6.1, 3.2 Hz, 2H), 3.58 (dd,  $J$  = 5.7, 3.0 Hz, 2H), 3.60 – 3.70 (m, 6H), 3.75 (t,  $J$  = 5.1 Hz, 2H), 3.83 (s, 3H), 4.31 (p,  $J$  = 7.2, 6.7 Hz, 1H), 4.38 (t,  $J$  = 5.1 Hz, 2H), 5.61 (s, 2H), 6.09 (q,  $J$  = 6.7 Hz, 1H), 6.52 (d,  $J$  = 3.1 Hz, 1H), 6.89 (d,  $J$  = 1.8 Hz, 1H), 7.06 (dd,  $J$  = 8.9, 7.8 Hz, 1H), 7.10 (d,  $J$  = 3.1 Hz, 1H), 7.24 (d,  $J$  = 1.6 Hz, 2H), 7.31 (s, 0H), 7.31 – 7.34 (m, 0H), 7.44 (s, 1H), 7.50 (s, 1H), 7.52 (d,  $J$  = 4.7 Hz, 0H), 7.55 (s, 2H), 7.65 (dd,  $J$  = 6.3, 1.7 Hz, 2H), 8.51 (s, 2H).  $^{13}\text{C}$  NMR (151 MHz, Chloroform-*d*)  $\delta$  28.84, 28.89, 29.20, 29.71, 32.94, 39.64, 49.98, 57.17, 69.42, 69.80, 70.20, 70.27, 70.30, 70.51, 72.75, 101.24, 108.50, 115.45, 116.93 (d,  $J$  = 23.4 Hz), 118.45, 119.17, 119.89, 121.41, 122.02 (d,  $J$  = 7.0 Hz), 123.84, 126.26, 128.18, 128.94, 129.39, 131.59, 132.30, 132.66, 133.75, 135.75 (d,  $J$  = 42.6 Hz), 135.99, 136.50, 137.64, 140.19, 148.52 (d,  $J$  = 138.4 Hz), 150.99, 157.74, 167.69, 169.25.  $^{19}\text{F}$  NMR (471 MHz, Chloroform-*d*)  $\delta$  -111.80.  $^{19}\text{F}$  NMR (471 MHz, Chloroform-*d*)  $\delta$  -111.86, m

**5-[4-[2-[4-[4-[[4-[4-[6-amino-5-[(1R)-1-(2,6-dichloro-3-fluoro-phenyl)ethoxy]-3-pyridyl]pyrazol-1-yl]-1-piperidyl]methyl]triazol-1-yl]butanoylamino]ethoxy]phenyl]-6-chloro-1H-indole-3-carboxylic acid,**  
**CCT392658**

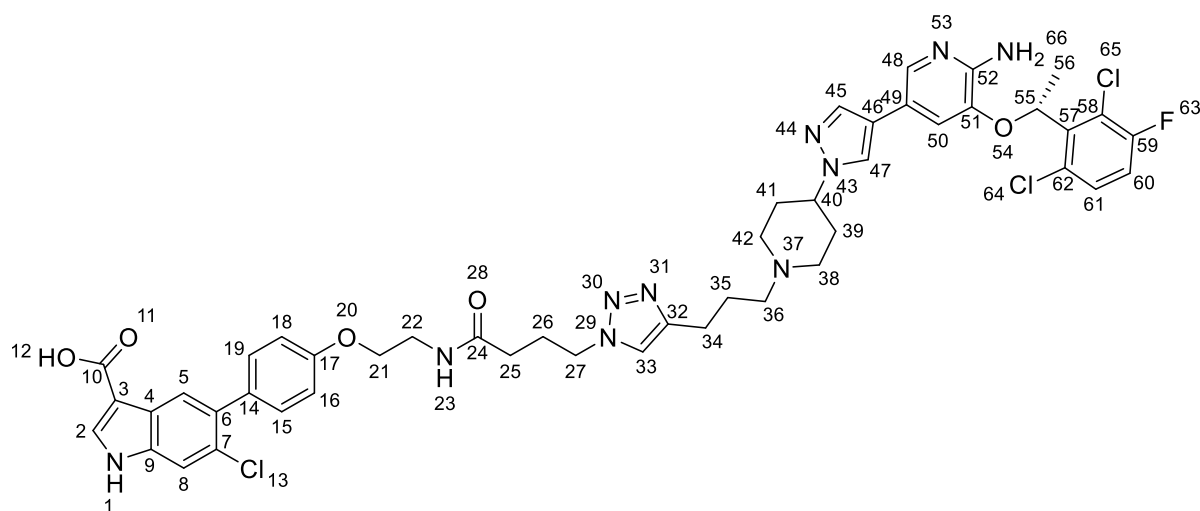


The general procedure for click coupling was carried out with the desired azide (N-(3-azidopropyl)-5-[[6-chloro-5-(1-methylindol-5-yl)-1H-benzimidazol-2-yl]oxy]-2-methyl-benzamide, 60) and alkyne (3-[(1R)-1-(2,6-dichloro-3-fluoro-phenyl)ethoxy]-5-[1-(1-prop-2-ynyl-4-piperidyl)pyrazol-4-yl]pyridin-2-amine, 73) to afford the title compound as an off white solid (66%)

Formula C<sub>45</sub>H<sub>44</sub>Cl<sub>3</sub>FN<sub>10</sub>O<sub>5</sub>. Observed m/z 929.2649020. Calculated m/z 929.2618524. Error (ppm) 3.28. <sup>1</sup>H NMR (600 MHz, DMSO-*d*<sub>6</sub>) δ 1.79 (d, *J* = 6.7 Hz, 3H, 39), 1.84 – 2.00 (m, 3H, 7'', 11''), 2.01 – 2.10 (m, 2H, 35), 2.10 – 2.17 (m, 3H, 8'', 8''', 10', 10'', 36), 2.88 – 2.96 (m, 2H, 8', 10'), 3.46 (q, *J* = 5.6 Hz, 2H, 43), 3.58 (s, 2H, 18), 4.05 (t, *J* = 5.6 Hz, 1H, 44), 4.06 – 4.10 (m, 11H, 6), 4.35 (t, *J* = 6.9 Hz, 2H, 34), 5.65 (s, 2H, 33), 6.07 (q, *J* = 6.7 Hz, 1H, 25), 6.88 (s, 1H, 13), 6.99 – 7.04 (m, 2H, 47, 51), 7.31 – 7.36 (m, 2H, 48, 50), 7.42 (t, *J* = 8.6 Hz, 1H, 29), 7.51 (s, 1H, 3), 7.55 (dd, *J* = 9.0, 4.9 Hz, 1H, 30), 7.61 (s, 1H, 62), 7.75 (s, 1H, 17), 7.91 (s, 1H, 5), 7.93 (s, 1H, 53), 7.99 (s, 1H, 23), 8.06 (d, *J* = 2.3 Hz, 1H, 57), 8.16 (t, *J* = 5.6 Hz, 1H, 42), 11.96 (s, 1H, 56). <sup>13</sup>C NMR (151 MHz, DMSO-*d*<sub>6</sub>) δ 18.61, 39, 25.86, 35, 31.89, 36, 32.00, 7, 11, 38.29, 43, 48.89, 34, 51.51, 8, 10, 52.41, 18, 58.41, 6, 66.37, 44, 71.98, 25, 107.69, 58, 112.88, 62, 114.06, 47, 51, 114.44, 13, 117.45 (d, *J* = 23.0 Hz, 29), 119.12, 4, 121.05 (d, *J* = 19.4 Hz, 27), 122.73, 53, 123.51, 5, 123.72, 23, 125.30, 54, 125.81, 61, 128.75 (d, *J* = 3.3 Hz, 31), 130.56, 30, 130.80, 48, 50, 132.54, 49,

132.76 , 52, 133.80 , 57, 134.54 , 3, 135.36 , 17, 135.95 , 55, 136.83 , 26, 138.91 , 14, 143.44 , 19, 149.47 , 15, 156.84 (d,  $J = 247.1$  Hz, 28), 157.62 , 46, 165.69 , 59, 171.43 , 37.

**5-[4-[2-[4-[4-[3-[4-[4-[6-amino-5-[(1R)-1-(2,6-dichloro-3-fluoro-phenyl)ethoxy]-3-pyridyl]pyrazol-1-yl]-1-piperidyl]propyl]triazol-1-yl]butanoylamino]ethoxy]phenyl]-6-chloro-1H-indole-3-carboxylic acid, CCT392656**

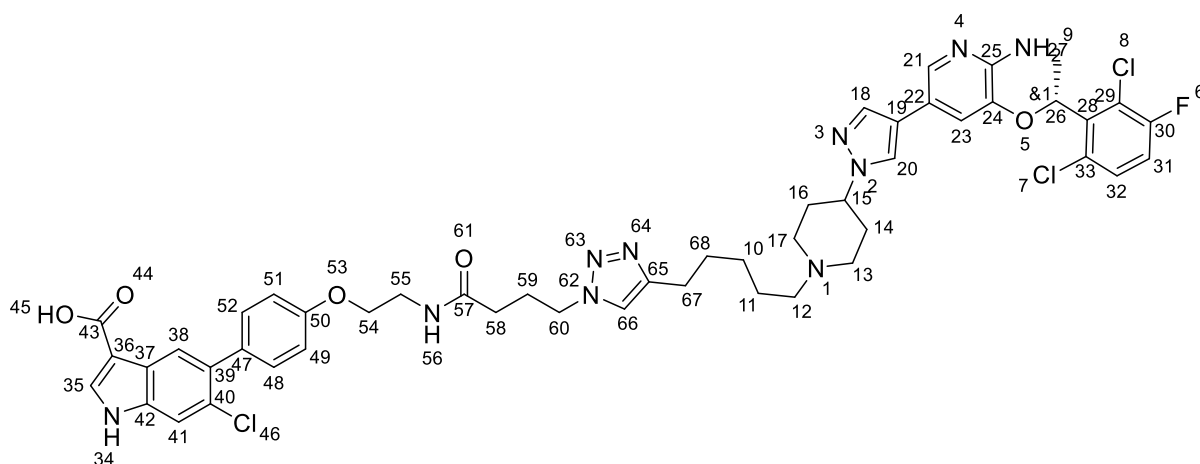


The general procedure for click coupling was carried out with the desired azide (N-(3-azidopropyl)-5-[[6-chloro-5-(1-methylindol-5-yl)-1H-benzimidazol-2-yl]oxy]-2-methyl-benzamide, 60) and alkyne (3-[(1R)-1-(2,6-dichloro-3-fluoro-phenyl)ethoxy]-5-[1-(1-pent-4-ynyl-4-piperidyl)pyrazol-4-yl]pyridin-2-amine, 74) to afford the desired compound (59%) as an off white solid

Formula C<sub>47</sub>H<sub>48</sub>Cl<sub>3</sub>FN<sub>10</sub>O<sub>5</sub>. Observed m/z 957.2930111. Calculated m/z 957.2931525. Error (ppm) -0.15. <sup>1</sup>H NMR (600 MHz, DMSO-d<sub>6</sub>) δ 1.74 – 1.78 (m, 1H, 35), 1.80 (d,  $J = 6.6$  Hz, 3H, 56), 1.87 – 2.00 (m, 4H, 39', 41'), 2.00 – 2.08 (m, 4H, 26, 38'', 42''), 2.13 (t,  $J = 7.4$  Hz, 2H, 25), 2.35 (t,  $J = 7.3$  Hz, 2H, 36), 2.62 (t,  $J = 7.6$  Hz, 2H, 34), 2.91 – 2.96 (m, 2H, 38', 42'), 3.46 (q,  $J = 5.6$  Hz, 2H, 22), 4.06 (d,  $J = 5.6$  Hz, 2H, 21), 4.06 – 4.11 (m, 1H, 40), 4.32 (t,  $J = 7.0$  Hz, 2H, 27), 5.65 (s, 2H, 66), 6.08 (q,  $J = 6.6$  Hz, 1H, 55), 6.90 (d,  $J = 1.3$  Hz, 1H, 50), 6.99 – 7.05 (m, 2H, 16, 18), 7.32 – 7.37 (m, 2H, 15, 19), 7.44 (t,  $J = 8.7$  Hz, 1H, 60), 7.53 (s, 1H, 45), 7.57 (dd,  $J =$

9.0, 4.9 Hz, 1H, 61), 7.62 (s, 1H, 8), 7.76 (s, 1H, 48), 7.84 (s, 1H, 33), 7.94 (s, 1H, 5), 7.95 (s, 1H, 47), 8.06 (s, 1H, 2), 8.16 (t, J = 5.6 Hz, 1H, 23), 11.96 (s, 1H, 1).  
<sup>13</sup>C NMR (151 MHz, DMSO-d<sub>6</sub>) δ 18.60 , 56, 22.96 , 34, 25.87 , 26, 26.50 , 35, 31.87 , 25, 32.11 , 39, 41, 38.27 , 22, 48.74 , 27, 51.97 , 38, 42, 54.92, 56.93 , 36, 58.64 , 40, 66.36 , 21, 71.98 , 55, 107.72 , 3, 112.86 , 8, 114.05 , 16, 18, 114.45 , 50, 117.44 (d, J = 23.1 Hz, 60), 119.11 , 46, 121.04 (d, J = 19.2 Hz, 58), 121.78 , 33, 122.73 , 5, 123.47 , 47, 125.29 , 4, 125.77 , 7, 128.73 , 62, 130.56 , 61, 130.78 , 15, 19, 132.53 , 14, 132.72 , 6, 133.74 , 2, 134.49 , 45, 135.42 , 48, 135.93 , 9, 136.84 , 57, 138.85 , 51, 146.70 , 32, 149.45 , 52, 156.82 (d, J = 247.0 Hz, 59), 157.61 , 17, 165.69 , 10, 171.41 , 24.

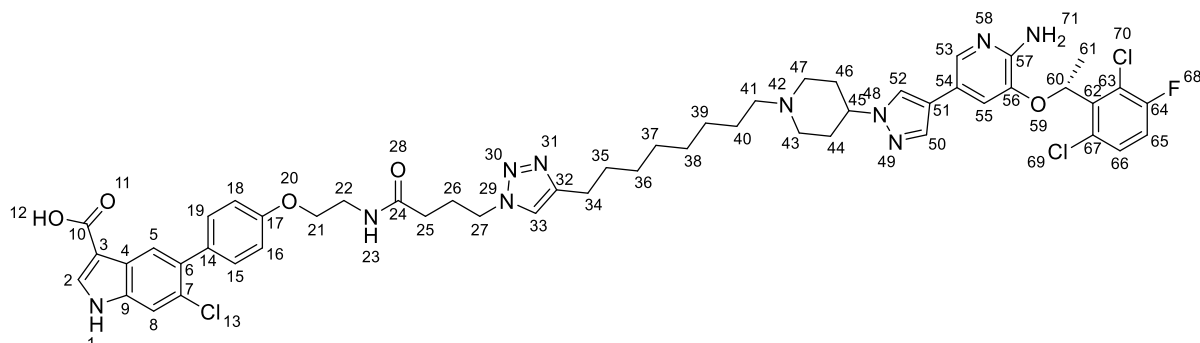
**5-[4-[2-[4-[4-[5-[4-[4-[6-amino-5-[(1R)-1-(2,6-dichloro-3-fluoro-phenyl)ethoxy]-3-pyridyl]pyrazol-1-yl]-1-piperidyl]pentyl]triazol-1-yl]butanoylamino]ethoxy]phenyl]-6-chloro-1H-indole-3-carboxylic acid,**  
**CCT392655**



The general procedure for click coupling was carried out with the desired azide (N-(3-azidopropyl)-5-[[6-chloro-5-(1-methylindol-5-yl)-1H-benzimidazol-2-yl]oxy]-2-methyl-benzamide, 60) and alkyne (3-[(1R)-1-(2,6-dichloro-3-fluoro-phenyl)ethoxy]-N-hept-6-ynyl-5-[1-(1-hept-6-ynyl-4-piperidyl)pyrazol-4-yl]pyridin-2-amine, 75/CCT390196) to afford the desired compound (40%) as an off white solid

Formula C<sub>49</sub>H<sub>52</sub>Cl<sub>3</sub>FN<sub>10</sub>O<sub>5</sub>. Observed m/z 985.3245637. Calculated m/z 985.3244526. Error (ppm) 0.11. <sup>1</sup>H NMR (600 MHz, DMSO-*d*<sub>6</sub>) δ 1.29 (h, *J* = 7.4, 6.7 Hz, 2H, 10), 1.44 (p, *J* = 7.5 Hz, 2H, 11), 1.59 (s, 1H, 68), 1.79 (d, *J* = 6.6 Hz, 3H, 27), 1.89 (qd, *J* = 11.8, 3.5 Hz, 2H, 14', 16'), 1.93 – 2.00 (m, 4H, 13'', 14'', 16'', 17''), 2.02 (dq, *J* = 11.5, 5.4, 3.9 Hz, 3H), 2.12 (t, *J* = 7.3 Hz, 2H, 58), 2.24 – 2.30 (m, 2H, 12), 2.54 (s, 17H), 2.59 (t, *J* = 7.6 Hz, 2H, 67), 2.91 (d, *J* = 10.8 Hz, 2H, 13', 17'), 3.45 (q, *J* = 5.6 Hz, 2H, 55), 4.04 (t, *J* = 5.6 Hz, 2H, 54), 4.07 (t, *J* = 6.0 Hz, 1H, 15), 4.30 (t, *J* = 6.9 Hz, 2H, 60), 5.64 (s, 2H, 9), 6.08 (q, *J* = 6.6 Hz, 1H, 26), 6.89 (s, 1H, 23), 7.01 (d, *J* = 8.3 Hz, 2H, 49, 51), 7.34 (d, *J* = 8.2 Hz, 2H, 48, 52), 7.43 (t, *J* = 8.7 Hz, 1H, 31), 7.52 (s, 1H, 18), 7.56 (dd, *J* = 9.0, 4.8 Hz, 1H, 32), 7.61 (s, 1H, 41), 7.76 (s, 1H, 21), 7.81 (s, 1H, 66), 7.94 (d, *J* = 6.7 Hz, 2H, 20, 38), 8.05 (s, 1H, 35), 8.15 (t, *J* = 5.6 Hz, 1H, 56), 11.96 (s, 1H, 34). <sup>13</sup>C NMR (151 MHz, DMSO-*d*<sub>6</sub>) δ 18.60 , 27, 25.04 , 67, 25.88 , 59, 26.33 , 11, 26.57 , 10, 28.93 , 68, 31.87 , 58, 32.10 , 14, 16, 38.26 , 55, 48.72 , 60, 52.00 , 13, 17, 57.56 , 12, 58.69 , 15, 66.36 , 54, 71.98 , 26, 107.83 , 36, 112.85 , 41, 114.04 , 49, 51, 114.43 , 23, 117.44 (d, *J* = 23.3 Hz, 31), 119.11 , 19, 121.04 (d, *J* = 19.1 Hz, 29), 121.70 , 66, 122.75 , 38, 123.47 , 20, 125.31 , 37, 125.75 , 40, 128.74 (d, *J* = 3.3 Hz, 33), 130.56 , 32, 130.77 , 48, 52, 132.54 , 47, 132.68 , 39, 133.69 , 35, 134.48 , 18, 135.41 , 21, 135.94 , 42, 136.84 , 28, 138.79 , 24, 146.85 , 65, 149.46 , 25, 156.82 (d, *J* = 247.1 Hz), 157.60 , 43, 157.67 , 50, 171.40 , 57. <sup>19</sup>F NMR (471 MHz, Chloroform-*d*) δ -70.19.

**5-[4-[2-[4-[4-[8-[4-[4-[6-amino-5-[(1R)-1-(2,6-dichloro-3-fluoro-phenyl)ethoxy]-3-pyridyl]pyrazol-1-yl]-1-piperidyl]octyl]triazol-1-yl]butanoylamino]ethoxy]phenyl]-6-chloro-1H-indole-3-carboxylic acid, CCT392657**



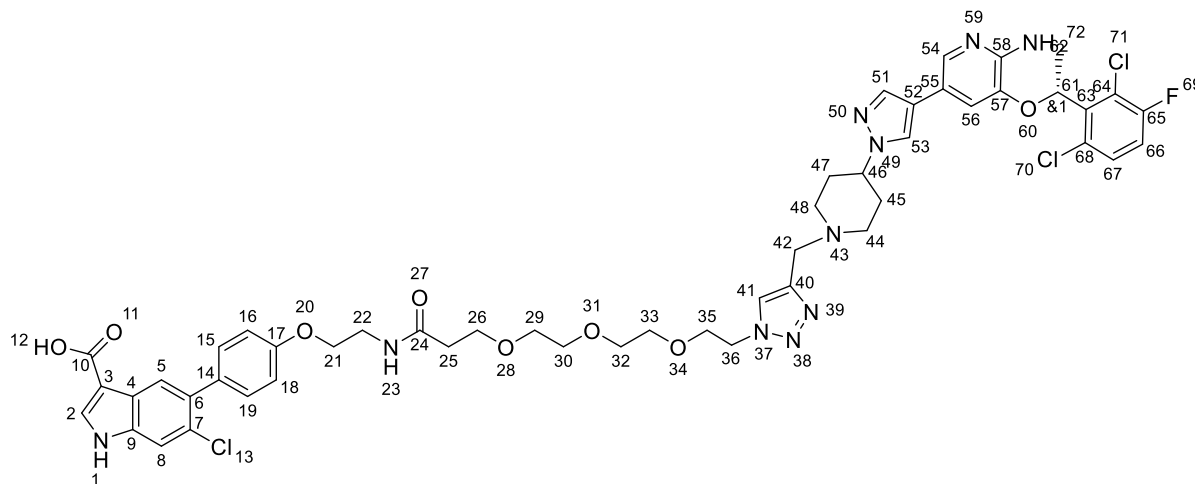
The general procedure for click coupling was carried out with the desired azide (N-(3-azidopropyl)-5-[[6-chloro-5-(1-methylindol-5-yl)-1H-benzimidazol-2-yl]oxy]-2-methyl-benzamide, 60) and alkyne (5-[1-(1-dec-9-ynyl-4-piperidyl)pyrazol-4-yl]-3-[(1R)-1-(2,6-dichloro-3-fluoro-phenyl)ethoxy]pyridin-2-amine, 76) to afford the title compound (14%)

Formula C<sub>52</sub>H<sub>58</sub>Cl<sub>3</sub>FN<sub>10</sub>O<sub>5</sub>. Observed m/z 1027.3723346. Calculated m/z 1027.3714028. Error (ppm) 0.91. <sup>1</sup>H NMR (600 MHz, DMSO-*d*<sub>6</sub>) δ 1.27 (dt, *J* = 15.9, 11.4 Hz, 10H), 1.41 (s, 2H), 1.52 – 1.61 (m, 2H), 1.80 (d, *J* = 6.6 Hz, 3H), 1.90 (t, *J* = 11.3 Hz, 1H), 1.94 – 2.00 (m, 2H), 2.03 (p, *J* = 7.1 Hz, 2H, 26), 2.12 (t, *J* = 7.3 Hz, 2H, 25), 2.27 (s, 2H), 2.59 (d, *J* = 7.6 Hz, 2H), 2.92 (d, *J* = 10.7 Hz, 2H), 3.46 (q, *J* = 5.6 Hz, 2H, 22), 4.05 (q, *J* = 8.0, 5.6 Hz, 3H, 21), 4.31 (t, *J* = 6.9 Hz, 2H), 5.65 (s, 2H, 71), 6.08 (q, *J* = 6.6 Hz, 1H, 60), 6.90 (s, 1H, 55), 7.02 (d, *J* = 8.1 Hz, 2H, 16, 18), 7.34 (d, *J* = 8.1 Hz, 2H, 15, 19), 7.44 (t, *J* = 8.7 Hz, 1H, 65), 7.53 (s, 1H), 7.57 (dd, *J* = 9.0, 4.9 Hz, 1H, 66), 7.62 (s, 1H, 8), 7.81 (s, 1H), 7.96 (s, 2H), 8.05 (s, 1H, 2), 8.15 (t, *J* = 5.6 Hz, 1H, 23), 11.96 (s, 1H, 1). <sup>13</sup>C NMR (151 MHz, DMSO-*d*<sub>6</sub>) δ 19.08, 25.52, 26.33, 26, 27.07, 27.44, 29.06, 29.25, 29.38, 29.46, 32.33, 25, 32.60, 38.73, 22, 42.58, 49.07, 49.18, 52.47, 58.13, 59.18, 66.82, 72.49, 113.35, 8, 114.50, 16, 18, 114.89, 117.92 (d, *J* = 23.2 Hz, 65), 121.51 (d, *J* = 19.3 Hz), 122.16, 124.06, 126.22, 129.21 (d, *J* = 3.4 Hz),



131.02 , 66, 131.23 , 15, 19, 133.04 , 14, 134.15 , 2, 134.96, 137.30, 147.37, 157.30  
(d,  $J = 248.7$  Hz, 64), 158.06 , 17, 171.86.

**5-[4-[2-[3-[2-[2-[2-[4-[4-[6-amino-5-[(1R)-1-(2,6-dichloro-3-fluoro-phenyl)ethoxy]-3-pyridyl]pyrazol-1-yl]-1-piperidyl]methyl]triazol-1-yl]ethoxy]ethoxy]ethoxy]propanoylamino]ethoxy]phenyl]-6-chloro-1H-indole-3-carboxylic acid, CCT391404**

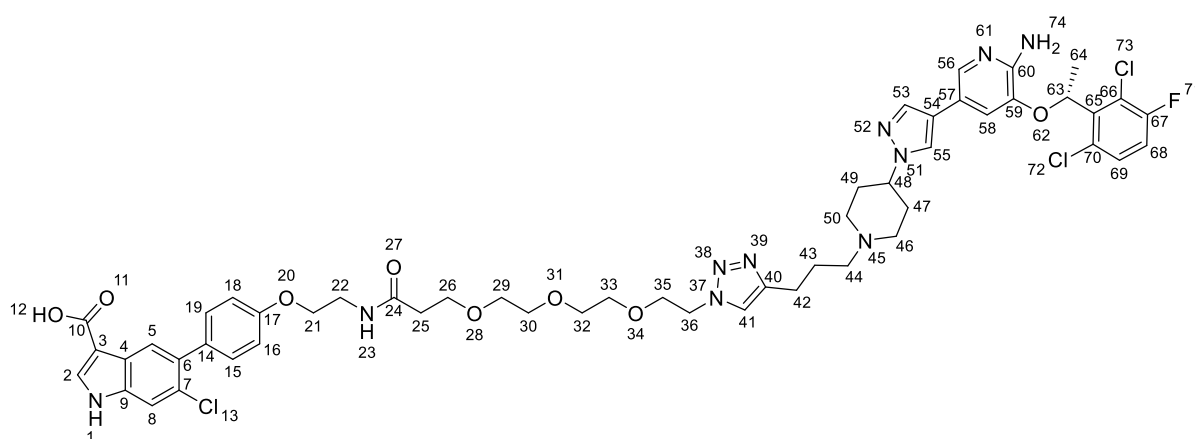


The general procedure for click coupling was carried out with the desired azide (N-[2-[2-[2-(2-azidoethoxy)ethoxy]ethoxy]ethyl]-5-[[6-chloro-5-(1-methylindol-5-yl)-1H-benzimidazol-2-yl]oxy]-2-methyl-benzamide 57) and alkyne (3-[(1R)-1-(2,6-dichloro-3-fluoro-phenyl)ethoxy]-5-[1-(1-prop-2-ynyl-4-piperidyl)pyrazol-4-yl]pyridin-2-amine, 73) to afford the desired compound (23%) as an off white solid.

Formula C<sub>57</sub>H<sub>68</sub>Cl<sub>3</sub>FN<sub>10</sub>O<sub>8</sub>. Observed m/z 1145.4320404. Calculated m/z 1145.4343970. Error (ppm) -2.06. Ion Species (M+H)<sup>+</sup> <sup>1</sup>H NMR (600 MHz, DMSO-*d*<sub>6</sub>)  $\delta$  1.80 (d,  $J = 6.6$  Hz, 3H, 62), 1.84 – 2.00 (m, 4H, 45', 45'', 47'), 2.12 (dt,  $J = 12.1, 6.4$  Hz, 2H, 44, 48), 2.36 (t,  $J = 6.4$  Hz, 2H, 25), 2.89 – 2.95 (m, 2H, 44, 48), 3.45 (tq,  $J = 5.5, 2.8, 2.4$  Hz, 7H), 3.50 (dd,  $J = 5.9, 3.4$  Hz, 2H), 3.58 (s, 2H, 26', 26'', 42), 3.61 (t,  $J = 6.4$  Hz, 2H, 26', 26''), 3.81 (t,  $J = 5.3$  Hz, 2H, 35), 4.03 (t,  $J = 5.6$  Hz, 2H, 21), 4.05 – 4.10 (m, 1H, 46), 4.50 (q,  $J = 5.1$  Hz, 2H, 36), 5.64 (s, 2H, 72), 5.76 (s, 0H), 6.08 (q,  $J = 6.7$  Hz, 1H, 61), 6.89 (d,  $J = 1.8$  Hz, 1H, 56), 6.99 – 7.03 (m, 2H, 16, 18), 7.32 – 7.36

(m, 2H, 15, 19), 7.43 (t,  $J = 8.7$  Hz, 1H, 66), 7.52 (s, 1H, 51), 7.56 (dd,  $J = 9.0, 4.9$  Hz, 1H, 67), 7.62 (s, 1H, 8), 7.74 (d,  $J = 1.8$  Hz, 1H, 54), 7.92 (s, 1H), 7.93 (s, 1H), 7.96 (s, 1H, 41), 8.07 (d,  $J = 2.9$  Hz, 1H, 2), 8.14 (t,  $J = 5.6$  Hz, 1H, 23), 11.94 (s, 1H).  $^{13}\text{C}$  NMR (151 MHz,  $\text{DMSO-}d_6$ )  $\delta$  19.07, 32.45, 45, 47, 36.49, 38.73, 42.58, 49.74, 36, 51.97, 44, 48, 52.85, 66.87, 21, 67.23, 26, 69.17, 35, 70.05 (d,  $J = 14.4$  Hz), 70.12, 72.42, 61, 113.33, 8, 114.49, 16, 18, 114.92, 56, 117.84 (d,  $J = 6.9$  Hz, 66), 119.54, 123.15, 123.96, 124.56, 125.72, 126.28, 131.24, 133.11 (d,  $J = 41.6$  Hz), 134.99, 135.90, 54, 143.82, 40, 149.90, 58, 158.08, 17, 170.93.  $^{19}\text{F}$  NMR (471 MHz,  $\text{DMSO-}d_6$ )  $\delta$  -113.18 (t,  $J = 8.5, 5.1$  Hz).  $^{19}\text{F}$  NMR (CPD 471 MHz,  $\text{DMSO-}d_6$ )  $\delta$  -113.18.

**5-[4-[2-[3-[2-[2-[2-[4-[3-[4-[4-[6-amino-5-[(1R)-1-(2,6-dichloro-3-fluorophenyl)ethoxy]-3-pyridyl]pyrazol-1-yl]-1-piperidyl]propyl]triazol-1-yl]ethoxy]ethoxy]ethoxy]propanoylamino]ethoxy]phenyl]-6-chloro-1H-indole-3-carboxylic acid, CCT391403**

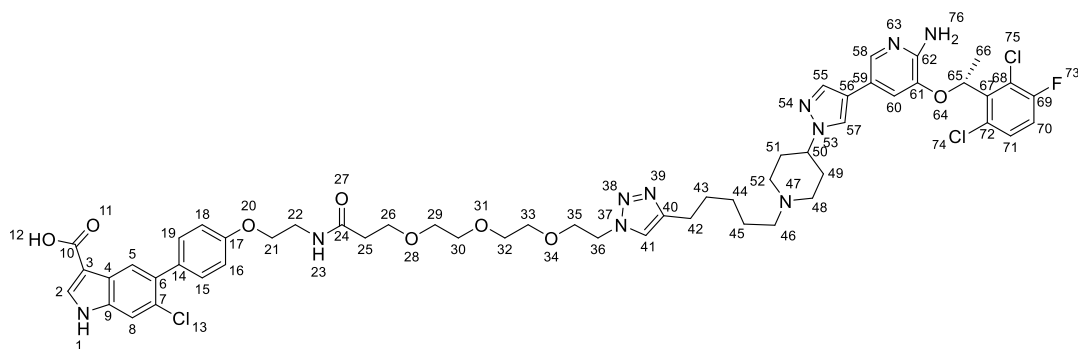


The general procedure for click coupling was carried out with the desired azide (N-[2-[2-[2-(2-azidoethoxy)ethoxy]ethoxy]ethyl]-5-[[6-chloro-5-(1-methylindol-5-yl)-1H-benzimidazol-2-yl]oxy]-2-methyl-benzamide 57) and alkyne (3-[(1R)-1-(2,6-dichloro-3-fluoro-phenyl)ethoxy]-5-[1-(1-pent-4-ynyl-4-piperidyl)pyrazol-4-yl]pyridin-2-amine, 74) to afford the desired compound (39%) as an off white solid.

Formula  $\text{C}_{52}\text{H}_{58}\text{Cl}_3\text{FN}_{10}\text{O}_8$ . Observed  $m/z$  1075.3536425. Calculated  $m/z$  1075.3561467. Error (ppm) -2.33.  $^1\text{H}$  NMR (600 MHz,  $\text{DMSO-}d_6$ )  $\delta$  1.75 (q,  $J = 7.4$  Hz, 2H, 43), 1.79 (t,  $J = 6.7$  Hz, 3H, 64), 1.87 – 2.01 (m, 4H, 47', 47'', 49', 49''), 2.07 (dd,  $J = 12.8, 9.9$  Hz, 2H, 46'', 50''), 2.33 – 2.39 (m, 4H, 25, 44), 2.62 (t,  $J = 7.4$  Hz, 2H,

42), 2.91 – 2.98 (m, 2H, 46', 50'), 3.41 – 3.50 (m, 10H, 22, 29, 30, 32, 33), 3.61 (t,  $J = 6.4$  Hz, 2H, 26), 3.78 (t,  $J = 5.3$  Hz, 2H, 35), 4.02 (t,  $J = 5.6$  Hz, 2H, 21), 4.08 (tt,  $J = 11.2, 4.3$  Hz, 1H, 48), 4.45 (t,  $J = 5.2$  Hz, 2H, 36), 5.64 (s, 2H, 74), 6.07 (q,  $J = 6.7$  Hz, 1H, 63), 6.89 (d,  $J = 1.8$  Hz, 1H, 58), 6.98 – 7.03 (m, 2H, 16, 18), 7.31 – 7.37 (m, 2H, 15, 19), 7.43 (t,  $J = 8.7$  Hz, 1H, 68), 7.52 (s, 1H, 53), 7.55 (dd,  $J = 8.7, 4.9$  Hz, 1H, 69), 7.61 (s, 1H, 8), 7.75 (d,  $J = 1.8$  Hz, 1H, 56), 7.81 (s, 1H, 41), 7.93 (s, 1H, 5), 7.95 (s, 1H, 55), 8.06 (d,  $J = 2.4$  Hz, 1H, 2), 8.14 (t,  $J = 5.6$  Hz, 1H, 23), 11.94 (s, 1H, 1).  $^{13}\text{C}$  NMR (151 MHz, DMSO- $d_6$ )  $\delta$  18.60, 64, 22.90, 42, 26.41, 43, 32.01, 47, 49, 36.02, 25, 38.27, 22, 49.20, 36, 51.91, 46, 50, 56.85, 44, 58.53, 48, 66.41, 21, 66.78, 26, 68.78, 35, 69.44 – 69.70 (m, 29, 30, 32, 33), 71.97, 63, 107.65, 3, 112.86, 8, 114.02, 16, 18, 114.46, 58, 117.42, 57, 117.44 (d,  $J = 23.2$  Hz, 68), 119.10, 54, 121.04 (d,  $J = 19.2$  Hz, 66), 122.20, 41, 122.70, 5, 123.49, 55, 125.28, 4, 125.80, 7, 128.74 (d,  $J = 3.4$  Hz, 70), 130.57, 69, 130.78, 15, 19, 132.51, 14, 132.76, 6, 133.77, 2, 134.51, 53, 135.45, 56, 135.92, 9, 136.84, 65, 138.80, 59, 146.50, 40, 149.44, 60, 156.82 (d,  $J = 247.3$  Hz, 67), 157.61, 17, 165.65, 10, 170.44, 24.

**5-[4-[2-[3-[2-[2-[2-[4-[5-[4-[4-[6-amino-5-[(1R)-1-(2,6-dichloro-3-fluorophenyl)ethoxy]-3-pyridyl]pyrazol-1-yl]-1-piperidyl]pentyl]triazol-1-yl]ethoxy]ethoxy]ethoxy]propanoylamino]ethoxy]phenyl]-6-chloro-1H-indole-3-carboxylic acid, CCT391402**

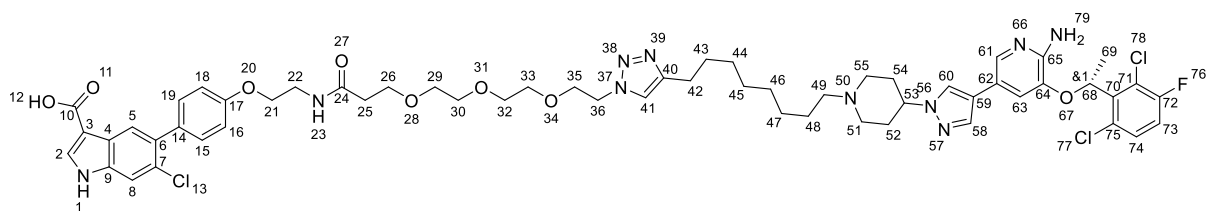


The general procedure for click coupling was carried out with the desired azide (N-[2-[2-[2-(2-azidoethoxy)ethoxy]ethoxy]ethyl]-5-[[6-chloro-5-(1-methylindol-5-yl)-1H-benzimidazol-2-yl]oxy]-2-methyl-benzamide 57) and alkyne (3-[(1R)-1-(2,6-dichloro-3-fluoro-phenyl)ethoxy]-N-hept-6-ynyl-5-[1-(1-hept-6-ynyl)-4-

piperidyl)pyrazol-4-yl]pyridin-2-amine, 75/CCT390196) to afford the desired compound (40%) as an off white solid

Formula C<sub>54</sub>H<sub>62</sub>Cl<sub>3</sub>FN<sub>10</sub>O<sub>8</sub> Observed m/z 1103.3852647 Calculated m/z 1103.3874468 Error (ppm) -1.98. <sup>1</sup>H NMR (600 MHz, DMSO-*d*<sub>6</sub>) δ 1.26 – 1.35 (m, 2H, 44), 1.46 (p, *J* = 7.6 Hz, 2H, 45), 1.59 (p, *J* = 7.6 Hz, 2H, 43), 1.79 (d, *J* = 6.7 Hz, 3H, 66), 1.86 – 2.00 (m, 4H, 49, 51), 2.02 – 2.11 (m, 2H, 48, 52), 2.27 – 2.33 (m, 2H, 46), 2.36 (t, *J* = 6.4 Hz, 2H, 25), 2.59 (t, *J* = 7.6 Hz, 2H, 42), 2.94 (dd, *J* = 12.0, 4.7 Hz, 2H, 48, 52), 3.42 – 3.50 (m, 10H, 22, 29, 30, 32, 33), 3.61 (t, *J* = 6.4 Hz, 2H, 26), 3.77 (t, *J* = 5.3 Hz, 2H, 35), 4.03 (t, *J* = 5.6 Hz, 2H, 21), 4.05 – 4.12 (m, 1H, 50), 4.44 (t, *J* = 5.3 Hz, 2H, 36), 5.64 (s, 2H, 76), 6.08 (q, *J* = 6.7 Hz, 1H, 65), 6.89 (d, *J* = 1.8 Hz, 1H, 60), 6.98 – 7.03 (m, 2H, 16, 18), 7.31 – 7.37 (m, 2H, 15, 19), 7.43 (t, *J* = 8.8 Hz, 1H, 70), 7.52 (s, 1H, 55), 7.56 (t, *J* = 8.8 Hz, 1H, 71), 7.61 (s, 1H, 8), 7.75 (d, *J* = 1.8 Hz, 1H, 58), 7.78 (s, 1H, 41), 7.93 (s, 1H, 5), 7.94 (s, 1H, 57), 8.06 (d, *J* = 2.3 Hz, 1H, 2), 8.14 (t, *J* = 5.6 Hz, 1H, 23), 11.95 (s, 1H, 1). <sup>13</sup>C NMR (151 MHz, DMSO-*d*<sub>6</sub>) δ 18.60 , 66, 24.98 , 42, 26.14 , 45, 26.51 , 44, 28.93 , 43, 31.91 , 49, 51, 36.02 , 25, 38.27 , 22, 49.18 , 36, 51.88 , 48, 52, 57.44 , 46, 58.48 , 50, 66.41 , 21, 66.78 , 26, 68.78 , 35, 69.49 – 69.72 (m, 29, 30, 32, 33), 71.97, 107.70 , 3, 112.85 , 8, 114.02 , 16, 18, 114.45 , 60, 117.41 , 59, 117.44 (d, *J* = 23.2 Hz, 70), 119.11 , 56, 121.04 (d, *J* = 19.5 Hz, 68), 122.09 , 41, 122.71 , 5, 123.48 , 57, 125.29 , 4, 125.78 , 7, 128.74 (d, *J* = 3.4 Hz, 72), 130.55 , 71, 130.78 , 15, 19, 132.52 , 14, 132.74 , 6, 133.75 , 2, 134.51 , 55, 135.45 , 58, 135.93 , 9, 136.84 , 67, 138.80 , 61, 146.69 , 40, 149.44 , 62, 156.83 (d, *J* = 247.7 Hz, 69), 157.61 , 17, 165.68 , 10, 170.43 , 24.

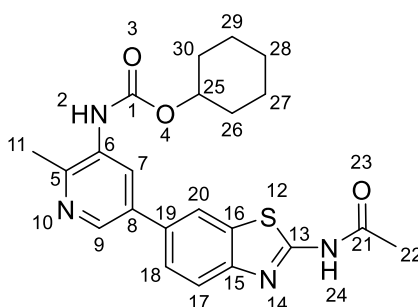
**5-[4-[2-[3-[2-[2-[2-[4-[8-[4-[4-[6-amino-5-[(1R)-1-(2,6-dichloro-3-fluorophenyl)ethoxy]-3-pyridyl]pyrazol-1-yl]-1-piperidyl]octyl]triazol-1-yl]ethoxy]ethoxy]ethoxy]propanoylamino]ethoxy]phenyl]-6-chloro-1H-indole-3-carboxylic acid, CCT391405**



The general procedure for click coupling was carried out with the desired azide (N-[2-[2-[2-(2-azidoethoxy)ethoxy]ethoxy]ethyl]-5-[[6-chloro-5-(1-methylindol-5-yl)-1H-benzimidazol-2-yl]oxy]-2-methyl-benzamide 57) and alkyne (5-[1-(1-dec-9-ynyl)-4-piperidyl]pyrazol-4-yl]-3-[(1R)-1-(2,6-dichloro-3-fluoro-phenyl)ethoxy]pyridin-2-amine, 76) to afford the title compound (14%)

Formula C<sub>57</sub>H<sub>68</sub>Cl<sub>3</sub>FN<sub>10</sub>O<sub>8</sub>. Observed m/z 1145.4343634. Calculated m/z 1145.4343970. Error (ppm) -0.03. <sup>1</sup>H NMR (600 MHz, DMSO-*d*<sub>6</sub>) δ 1.30 (p, *J* = 6.1, 4.8 Hz, 9H), 1.52 – 1.77 (m, 6H), 1.85 (d, *J* = 6.6 Hz, 2H), 2.27 (d, *J* = 23.3 Hz, 4H), 2.37 (t, *J* = 6.4 Hz, 2H), 2.57 – 2.64 (m, 2H), 3.00 – 3.13 (m, 3H), 3.46 (h, *J* = 2.9 Hz, 8H), 3.50 (dd, *J* = 6.0, 3.4 Hz, 2H), 3.62 (t, *J* = 6.4 Hz, 2H), 3.78 (t, *J* = 5.2 Hz, 2H), 4.04 (t, *J* = 5.6 Hz, 2H), 4.45 (q, *J* = 4.7, 4.1 Hz, 3H), 6.22 (t, *J* = 6.5 Hz, 1H), 6.99 – 7.04 (m, 2H), 7.07 (s, 1H), 7.33 – 7.36 (m, 2H), 7.38 (d, *J* = 8.6 Hz, 0H), 7.47 (d, *J* = 8.7 Hz, 0H), 7.61 (s, 1H), 7.63 (s, 1H), 7.67 (d, *J* = 5.2 Hz, 1H), 7.78 – 7.83 (m, 2H), 7.93 (s, 1H), 7.97 (d, *J* = 18.7 Hz, 0H), 8.03 (d, *J* = 4.5 Hz, 1H), 8.08 (d, *J* = 2.9 Hz, 1H), 8.17 (d, *J* = 6.2 Hz, 1H), 11.92 – 12.01 (m, 1H), 12.10 (s, 1H). <sup>13</sup>C NMR (151 MHz, DMSO-*d*<sub>6</sub>) δ 25.44, 26.52, 28.90, 28.97, 29.46, 36.49, 38.73, 49.64, 66.87, 67.24, 69.24, 70.00, 70.08, 70.12, 108.00, 113.35, 114.50, 117.64, 121.61, 122.55, 123.14, 125.72, 126.26, 131.24, 132.98, 133.23, 134.26, 136.39, 147.16, 158.07, 166.05, 170.91. <sup>19</sup>F NMR (471 MHz, DMSO-*d*<sub>6</sub>) δ -112.8, m. <sup>19</sup>F NMR (471 MHz, DMSO-*d*<sub>6</sub>) δ -112.85.

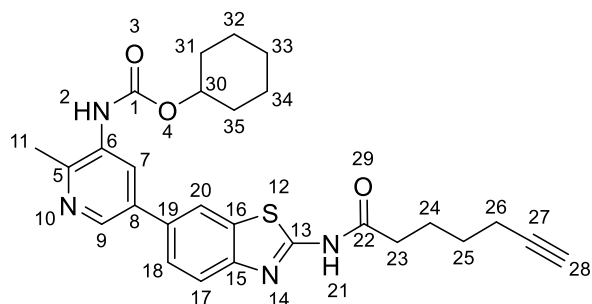
**cyclohexyl** **N-[5-(2-acetamido-1,3-benzothiazol-6-yl)-2-methyl-3-pyridyl]carbamate**



cyclohexyl N-[5-(2-amino-1,3-benzothiazol-6-yl)-2-methyl-3-pyridyl]carbamate ( 10.00 mg, 0.0261 mmol) was taken up in DMA ( 0.26 mL, 0.1000 M ) giving a brown solution, which was cooled to 0C. After 5 mins N,N-Diisopropylethylamine ( 9.15 uL, 0.0523 mmol) was added, followed by acetyl chloride ( 1.86 uL, 0.0261 mmol, 1 equiv). The brown solution was stirred at 0C for 30 mins, then rt for 3h. The solution was cooled to 0C then acetyl chloride ( 1.86 uL, 0.0261 mmol) and N,N-Diisopropylethylamine ( 9.15 uL, 0.0523 mmol) were added and the solution stirred at rt overnight. The solution was cooled to 0C then acetyl chloride ( 1.86 uL, 0.0261 mmol) and N,N-Diisopropylethylamine ( 9.15 uL, 0.0523 mmol) were added again and the solution stirred for another 3h at rt then at 40C overnight, then to 60C for 3 days. 0.5 mL water and then the solution concentrated then taken up in 0.8 mL DMSO and directly purified by reverse-phase chromatography (Biotage reverse-phase 12 g Ultra C-18 column; 10-60-80-100% MeOH in H<sub>2</sub>O (containing 0.1% formic acid)). Relevant fractions evaporated then dissolved 500ul of 1:1 DMSO:acetonitrile and purified via HPLC 40:60 to 0:100 H<sub>2</sub>O:MeOH (both modified with 0.1% formic acid). Relevant fractions concentrated *in vacuo* to afford the title compound (3.7 mg, 32%, 0.0083 mmol) as an off white solid.

Ret time = 2.66 mins. Formula C<sub>22</sub>H<sub>24</sub>N<sub>4</sub>O<sub>3</sub>S. Observed m/z 425.1636472. Calculated m/z 425.1641878. Error (ppm) -1.27. <sup>1</sup>H NMR (600 MHz, DMSO-*d*<sub>6</sub>) δ 1.20 – 1.27 (m, 1H, 28), 1.30 – 1.38 (m, 2H, 27', 27'', 29', 29''), 1.39 – 1.47 (m, 2H, 26', 26'', 30', 30''), 1.49 – 1.56 (m, 1H), 1.69 – 1.75 (m, 2H, 27', 27'', 29', 29''), 1.88 – 1.95 (m, 2H, 26', 26'', 30', 30''), 2.22 (s, 3H, 22), 2.46 (s, 3H, 11), 4.60 – 4.70 (m, 1H, 25), 5.75 (s, 1H), 7.72 (dd, *J* = 8.4, 1.9 Hz, 1H, 18), 7.82 (d, *J* = 8.4 Hz, 1H, 17), 8.10 (d, *J* = 2.2 Hz, 1H, 7), 8.31 (d, *J* = 1.9 Hz, 1H, 20), 8.59 (d, *J* = 2.2 Hz, 1H, 9), 9.11 (s, 1H, 2), 12.40 (s, 1H). <sup>13</sup>C NMR (151 MHz, DMSO-*d*<sub>6</sub>) δ 20.74 , 11, 22.80 , 22, 23.46 , 27, 29, 24.92 , 28, 31.64 , 26, 30, 72.88 , 25, 119.74 , 20, 120.94 , 17, 124.96 , 18, 129.02 , 7, 132.23 , 19, 132.57, 132.89 , 6, 133.30 , 8, 142.63 , 9, 148.40 , 15, 150.30 , 5, 153.98 , 1, 158.65 , 13, 169.53 , 21.

**cyclohexyl N-[5-[2-(hept-6-ynoylamino)-1,3-benzothiazol-6-yl]-2-methyl-3-pyridyl]carbamate**

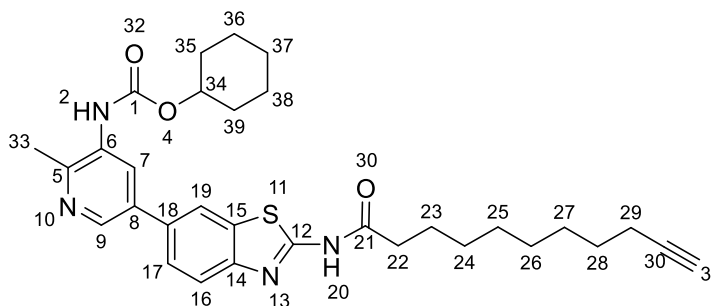


HATU ( 59.65 mg, 0.1569 mmol), 6-Heptynoic acid ( 19.85 uL, 0.1569 mmol) and N,N-Diisopropylethylamine ( 68.31 uL, 0.3922 mmol) were taken up in DMF ( 0.65 mL, 0.2000 M ) and the yellow solution stirred at rt for 10 mins. cyclohexyl N-[5-(2-amino-1,3-benzothiazol-6-yl)-2-methyl-3-pyridyl]carbamate ( 50.00 mg, 0.1307 mmol) was added giving a brown suspension which was stirred at 35C overnight. Then 6-Heptynoic acid ( 9.92 uL, 0.0784 mmol), N,N-Diisopropylethylamine ( 34.15 uL, 0.1961 mmol) and HATU ( 29.82 mg, 0.0784 mmol) were added, and the black solution stirred at 35C over the weekend. The black solution was partitioned between 15 mL of 1:1 water:brine and 15 mL EtOA. The aq phase was extracted 3 x 15 mL EtOAc and combined organics dried over MgSO<sub>4</sub>, vacuum filtered and concentrated in vacuo. Purified via column chromatography (Biotage sfar duo 10g 1 - 6 MeOH in DCM). Relevant fractions evaporated and dissolved in DMSO (1 mL) and directly purified by reverse-phase chromatography (Biotage reverse-phase 12 g Ultra C-18 column; 10-70-80-100% MeOH in H<sub>2</sub>O (containing 0.1% formic acid)), then concentrated *in vacuo* to afford the title compound (42 mg, 62%, 0.0813 mmol) as a white solid.

Ret time = 3.21 mins. Formula C<sub>27</sub>H<sub>30</sub>N<sub>4</sub>O<sub>3</sub>S. Observed m/z 491.2110. Calculated m/z 491.2117. Error (ppm) -1.4. <sup>1</sup>H NMR (600 MHz, DMSO) δ 1.23 (dddd, J = 13.7, 10.6, 7.3, 3.7 Hz, 1H, 33), 1.29 – 1.55 (m, 7H, 25, 31', 31'', 32'', 34'', 35', 35''), 1.68 – 1.74 (m, 4H, 24, 32', 34'), 1.92 (dq, J = 12.7, 4.0 Hz, 2H, 31', 31'', 35', 35''), 2.20 (td, J = 7.1, 2.7 Hz, 2H, 26), 2.46 (s, 3H, 11), 2.53 (t, J = 7.4 Hz, 2H, 23), 2.78 (t, J = 2.7 Hz, 1H, 28), 4.06 (s, 1H), 4.65 (tt, J = 9.4, 3.9 Hz, 1H, 30), 7.72 (dd, J = 8.4, 1.9 Hz, 1H, 18), 7.81 (d, J = 8.4 Hz, 1H, 17), 8.10 (d, J = 2.3 Hz, 1H, 7), 8.20 (d, J = 1.5 Hz, 0H),

8.31 (d,  $J = 1.8$  Hz, 1H, 20), 8.44 (s, 0H), 8.59 (d,  $J = 2.2$  Hz, 1H, 9), 9.11 (s, 1H, 2), 12.40 (s, 1H, 21).  $^{13}\text{C}$  NMR (151 MHz, DMSO)  $\delta$  17.48, 26, 20.75, 11, 23.47, 32, 34, 23.68, 24, 24.93, 27.43, 25, 31.65, 34.57, 71.41, 28, 72.89, 30, 84.24, 27, 119.74, 20, 120.91, 17, 124.95, 18, 129.01, 7, 132.22, 16, 132.59, 19, 132.90, 6, 133.30, 8, 142.63, 9, 148.42, 15, 150.30, 5, 153.99, 1, 158.61, 13, 172.22, 22.

**Cyclohexyl N-[2-methyl-5-[2-(undec-10-ynoylamino)-1,3-benzothiazol-6-yl]-3-pyridyl]carbamate**



10-

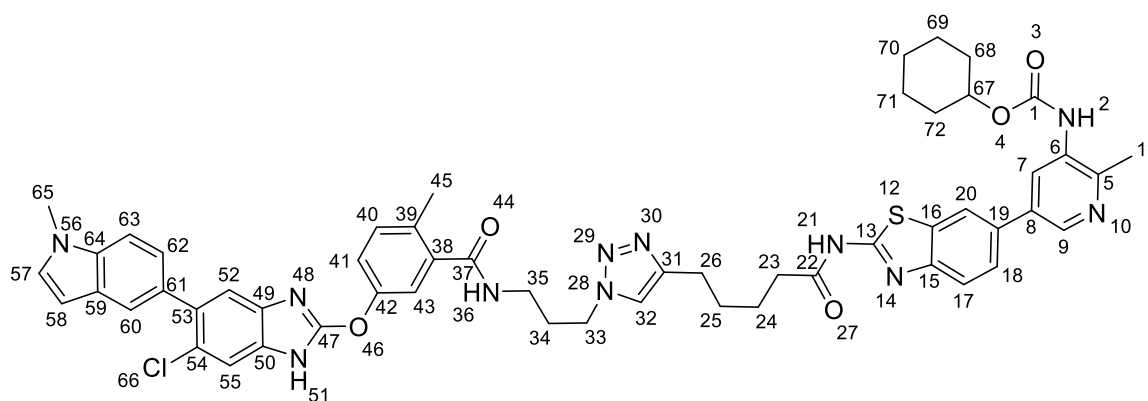
Undecynoic acid ( 35.74 mg, 0.1961 mmol) was taken up in DMF ( 0.52 mL, 0.2500 M ) giving a colourless solution. HATU ( 74.56 mg, 0.1961 mmol) and N,N-Diisopropylethylamine ( 68.31  $\mu\text{L}$ , 0.3922 mmol) were added and the yellow solution stirred at rt for 10 mins. cyclohexyl N-[5-(2-amino-1,3-benzothiazol-6-yl)-2-methyl-3-pyridyl]carbamate ( 50.00 mg, 0.1307 mmol) was added giving a brown suspension which was stirred at rt overnight. Then 10-Undecynoic acid ( 11.91 mg, 0.0654 mmol) , HATU ( 24.85 mg, 0.0654 mmol) and N,N-Diisopropylethylamine ( 22.77  $\mu\text{L}$ , 0.1307 mmol) were added and the reaction mixture stirred at rt for 3 days. The black solution was partitioned between 20 mL (1:1 brine: water) and 15 mL EtOAc. The aq phase was extracted 3 x 15 mL EtOAc and combined organics dried over  $\text{MgSO}_4$ , vacuum filtered and concentrated in vacuo. Purified via column chromatography (Biotage sfar duo 10g 0 - 5 MeOH in DCM). Relevant fractions concentrated *in vacuo* to give the title compound (69 mg, 92%, 0.1199 mmol) as a white solid Ret time = 3.269 mins. Observed  $m/z$  547.2747849. Calculated  $m/z$  547.2737383. Ion Species (M+H)<sup>+</sup>. Formula  $\text{C}_{31}\text{H}_{38}\text{N}_4\text{O}_3\text{S}$ . Error (ppm) 1.91.  $^1\text{H}$  NMR (600 MHz,  $\text{DMSO}-d_6$ )  $\delta$  1.21 – 1.40 (m, 14H, 24, 25, 26, 27, 28, 36, 38), 1.44 (tt,  $J = 11.8, 5.7$  Hz, 3H, 35'', 37, 39''), 1.50 – 1.57 (m, 1H, 37), 1.63 (p,  $J = 7.2$  Hz, 2H,



23), 1.73 (dt,  $J = 9.3, 4.4$  Hz, 2H, 36, 38), 1.89 – 1.96 (m, 2H, 35', 39'), 2.14 (td,  $J = 7.0, 2.6$  Hz, 2H, 29), 2.46 (s, 3H, 33), 2.48 – 2.50 (m, 1H, 22), 2.72 (t,  $J = 2.7$  Hz, 1H, 31), 4.65 (tt,  $J = 9.1, 4.0$  Hz, 1H, 34), 7.71 – 7.75 (m, 1H, 17), 7.81 (d,  $J = 8.4$  Hz, 1H, 16), 8.09 – 8.13 (m, 1H, 7), 8.32 (d,  $J = 1.9$  Hz, 1H, 19), 8.59 (d,  $J = 2.1$  Hz, 1H, 9), 9.11 (s, 1H, 2), 12.37 (s, 1H, 20).  $^{13}\text{C}$  NMR (151 MHz,  $\text{DMSO-}d_6$ )  $\delta$  17.65, 29, 20.72, 33, 23.45, 36, 38, 24.48, 23, 24.90, 37, 27.92, 28.09, 28.31, 28.48, 28.61, 31.63, 35, 39, 35.10, 22, 71.10, 31, 72.85, 34, 84.54, 30, 119.71, 19, 120.87, 16, 124.92, 17, 128.97, 7, 132.17, 15, 132.56, 18, 132.88, 6, 133.27, 8, 142.58, 9, 148.40, 14, 150.25, 5, 153.96, 1, 158.60, 12, 172.40, 21.

**cyclohexyl N-[5-[2-[5-[1-[3-[[5-[[6-chloro-5-(1-methylindol-5-yl)-1H-benzimidazol-2-yl]oxy]-2-methyl-benzoyl]amino]propyl]triazol-4-yl]pentanoylamino]-1,3-benzothiazol-6-yl]-2-methyl-3-pyridyl]carbamate, CCT393763**

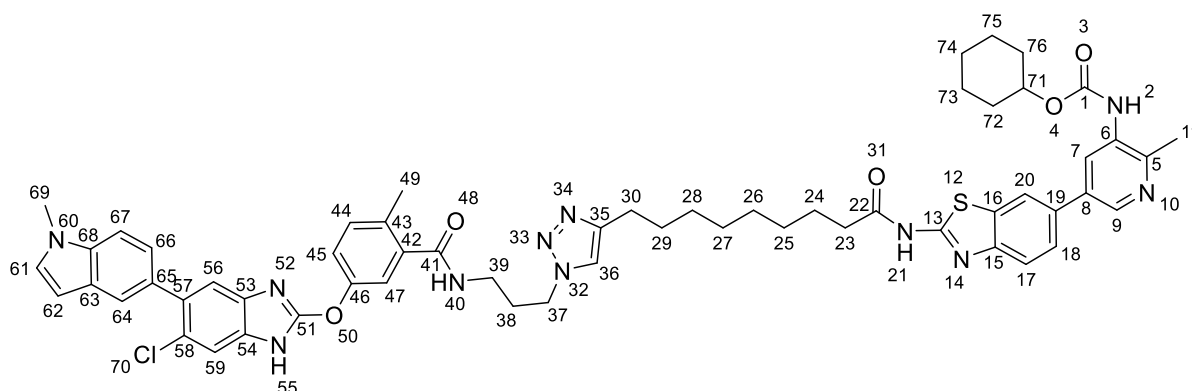
The general procedure for click coupling was carried out with the desired azide (N-(3-azidopropyl)-5-[[6-chloro-5-(1-methylindol-5-yl)-1H-benzimidazol-2-yl]oxy]-2-methyl-benzamide, 60) and alkyne (cyclohexyl N-[5-[2-(hept-6-ynoylamino)-1,3-benzothiazol-6-yl]-2-methyl-3-pyridyl]carbamate) to give the title compound (42%) as an off white solid.



Ret time = 3.20 mins. Formula  $\text{C}_{54}\text{H}_{54}\text{ClN}_{11}\text{O}_5\text{S}$ , Observed  $m/z$  1004.3774931. Calculated  $m/z$  1004.3791388., Error (ppm) -1.64.  $^1\text{H}$  NMR (600 MHz,  $\text{DMSO}$ )  $\delta$  1.23 (d,  $J = 3.5$  Hz, 4H), 1.34 (dt,  $J = 13.9, 10.6$  Hz, 2H, 69', 71'), 1.38 – 1.47 (m, 2H, 68'',

72"), 1.52 (dt,  $J = 16.0, 5.7$  Hz, 1H, 70), 1.67 (tdd,  $J = 21.8, 8.7, 4.0$  Hz, 6H, 24, 25, 69", 71"), 1.91 (dd,  $J = 12.6, 5.0$  Hz, 2H), 2.05 (p,  $J = 6.9$  Hz, 2H, 34), 2.35 (s, 3H, 45), 2.46 (s, 3H, 11), 2.54 (t,  $J = 7.1$  Hz, 2H, 23), 2.64 (t,  $J = 7.2$  Hz, 2H, 26), 3.23 (q,  $J = 6.5$  Hz, 2H, 35), 3.81 (s, 3H, 65), 4.37 (t,  $J = 7.0$  Hz, 2H, 33), 4.60 – 4.69 (m, 1H, 67), 6.45 (d,  $J = 3.0$  Hz, 1H, 58), 7.17 (d,  $J = 8.4$  Hz, 1H, 62), 7.30 – 7.40 (m, 6H, 40, 41, 43, 52, 57), 7.46 (d,  $J = 8.4$  Hz, 1H, 63), 7.51 (s, 1H, 55, 60), 7.54 (s, 1H, 60), 7.71 (d,  $J = 8.3$  Hz, 1H, 17), 7.80 (d,  $J = 8.4$  Hz, 1H, 18), 7.90 (s, 1H, 32), 8.10 (s, 1H, 7), 8.27 – 8.32 (m, 1H, 20), 8.45 (q,  $J = 5.2$  Hz, 1H, 36), 8.58 (d,  $J = 2.2$  Hz, 1H, 9), 9.11 (s, 1H, 2).  $^{13}\text{C}$  NMR (151 MHz, DMSO)  $\delta$  18.83, 45, 20.75, 11, 23.47, 69, 71, 24.14, 24.78, 26, 24.93, 70, 28.49, 29.04 (d,  $J = 3.2$  Hz), 29.81, 34, 31.65, 68, 72, 32.57, 65, 34.89, 23, 36.33, 35, 47.13, 33, 72.90, 67, 100.59, 58, 109.12, 63, 118.98, 52, 119.73, 20, 120.91, 18, 121.29, 60, 121.35, 41, 121.99, 32, 123.19, 62, 124.60, 54, 124.95, 17, 127.79, 129.01, 7, 130.18, 57, 130.86, 59, 131.76, 40, 132.21, 39, 132.43, 8, 132.60, 132.91, 6, 133.31, 19, 134.56, 53, 135.57, 64, 138.19, 38, 142.63, 9, 146.54, 31, 148.42, 15, 150.33, 5, 150.97, 42, 154.01, 1, 157.86, 158.62, 168.22, 37, 172.34, 22.

**cyclohexyl N-[5-[2-[9-[1-[3-[[5-[[6-chloro-5-(1-methylindol-5-yl)-1H-benzimidazol-2-yl]oxy]-2-methyl-benzoyl]amino]propyl]triazol-4-yl]nonanoylamino]-1,3-benzothiazol-6-yl]-2-methyl-3-pyridyl]carbamate, CCT393214**

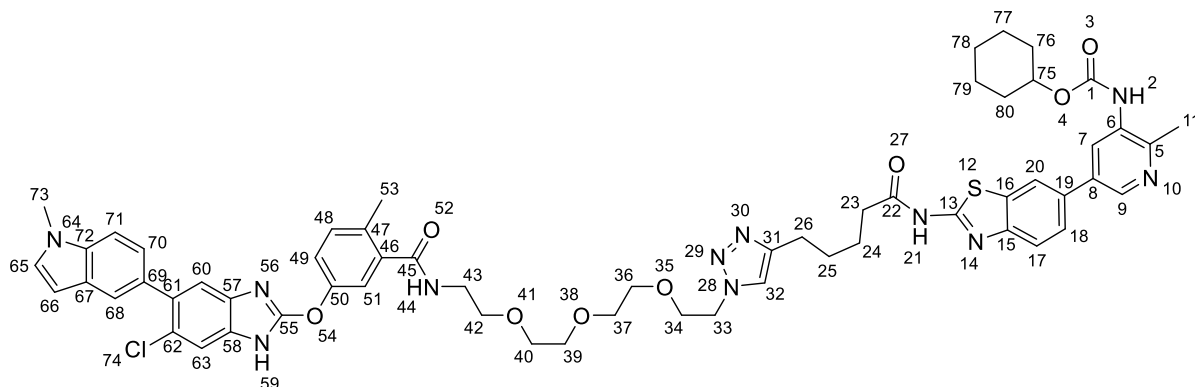


The general procedure for click coupling was carried out with the desired azide (N-(3-azidopropyl)-5-[[6-chloro-5-(1-methylindol-5-yl)-1H-benzimidazol-2-yl]oxy]-2-

methyl-benzamide, 60) and alkyne (Cyclohexyl N-[2-methyl-5-[2-(undec-10-ynoylamino)-1,3-benzothiazol-6-yl]-3-pyridyl]carbamate) to give the title compound (61%) as an off white solid.

Ret time = 3.41 mins. Formula C<sub>58</sub>H<sub>62</sub>ClN<sub>11</sub>O<sub>5</sub>S. Observed m/z 1060.4428299. Calculated m/z 1060.4417391. Error (ppm) 1.03. <sup>1</sup>H NMR (600 MHz, DMSO-*d*<sub>6</sub>) δ 1.19 – 1.26 (m, 2H, 74), 1.31 – 1.47 (m, 4H, 25, 26, 27, 28, 72', 72'', 73', 73'', 75', 75'', 76', 76''), 1.49 – 1.54 (m, 1H), 1.60 (dq, *J* = 28.8, 7.0 Hz, 3H, 24, 29), 1.72 (tt, *J* = 8.2, 4.3 Hz, 2H, 73', 73'', 75', 75''), 1.92 (dt, *J* = 13.0, 4.1 Hz, 2H, 72', 72'', 76', 76''), 2.04 (p, *J* = 6.9 Hz, 2H, 38), 2.36 (s, 3H, 49), 2.46 (s, 3H, 11), 2.48 (d, *J* = 7.5 Hz, 1H, 23), 2.58 (t, *J* = 7.6 Hz, 2H, 30), 3.22 (q, *J* = 6.5 Hz, 2H, 39), 3.82 (s, 3H, 69), 4.37 (t, *J* = 7.0 Hz, 2H, 37), 4.65 (tt, *J* = 9.4, 3.9 Hz, 1H, 71), 5.75 (s, 0H), 6.45 (d, *J* = 3.0 Hz, 1H, 62), 7.18 (dd, *J* = 8.4, 1.7 Hz, 1H, 66), 7.31 – 7.37 (m, 4H, 44, 47, 56, 61), 7.38 (dd, *J* = 8.3, 2.6 Hz, 1H, 45), 7.46 (d, *J* = 8.5 Hz, 1H, 67), 7.51 (s, 1H, 59), 7.54 (d, *J* = 1.7 Hz, 1H, 64), 7.71 (dd, *J* = 8.4, 1.9 Hz, 1H, 18), 7.80 (d, *J* = 8.4 Hz, 1H, 17), 7.86 (s, 1H, 36), 8.10 (d, *J* = 2.2 Hz, 1H, 7), 8.31 (d, *J* = 1.8 Hz, 1H, 20), 8.44 (t, *J* = 5.6 Hz, 1H, 40), 8.59 (d, *J* = 2.2 Hz, 1H, 9), 9.11 (s, 1H, 2), 12.43 (s, 2H, 21). <sup>13</sup>C NMR (151 MHz, DMSO-*d*<sub>6</sub>) δ 18.80 , 49, 20.73 , 11, 23.45 , 73, 75, 24.50, 24.90 , 30, 25.02, 28.52, 28.58, 28.62, 28.65, 28.97, 29.77 , 38, 31.63 , 72, 76, 32.54 , 69, 35.12, 36.31 , 39, 47.08 , 37, 72.85 , 71, 100.55 , 62, 109.09 , 67, 118.95, 119.70 , 20, 120.87 , 17, 121.26 , 64, 121.32 , 45, 121.84 , 36, 123.16 , 66, 124.58 , 58, 124.92 , 18, 127.76 , 63, 128.93 , 7, 130.15 , 61, 130.82, 131.72 , 44, 132.17, 132.39 , 19, 132.57, 132.88 , 6, 133.27 , 8, 134.54, 135.54 , 68, 138.17 , 42, 142.60 , 9, 146.82 , 35, 148.40 , 15, 150.26 , 5, 150.94 , 46, 153.97 , 1, 157.80, 158.61, 168.16 , 41, 172.42 , 22.

**cyclohexyl N-[5-[2-[5-[1-[2-[2-[2-[2-[[5-[[6-chloro-5-(1-methylindol-5-yl)-1H-benzimidazol-2-yl]oxy]-2-methyl-benzoyl]amino]ethoxy]ethoxy]ethoxy]ethyl]triazol-4-yl]pentanoylamino]-1,3-benzothiazol-6-yl]-2-methyl-3-pyridyl]carbamate, CCT393764**



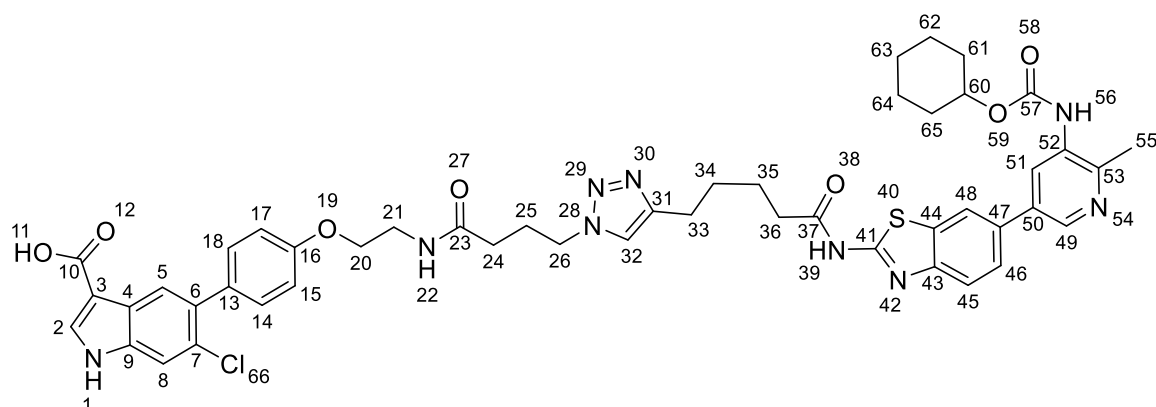
The general procedure for click coupling was carried out with the desired azide (N-[2-[2-[2-(2-azidoethoxy)ethoxy]ethoxy]ethyl]-5-[[6-chloro-5-(1-methylindol-5-yl)-1H-benzimidazol-2-yl]oxy]-2-methyl-benzamide 57) and alkyne (cyclohexyl N-[5-[2-(hept-6-ynoylamino)-1,3-benzothiazol-6-yl]-2-methyl-3-pyridyl]carbamate) to give the title compound (22%) as an off white solid.

Ret time = 3.18 mins. Formula C<sub>59</sub>H<sub>64</sub>ClN<sub>11</sub>O<sub>8</sub>S. Observed m/z 1122.4404811. Calculated m/z 1122.4421330. Error (ppm) -1.47. <sup>1</sup>H NMR (600 MHz, DMSO-*d*<sub>6</sub>) δ 0.87 (m, 1H, 78), 1.16 – 1.55 (m, 7H, 25, 76'', 77', 78, 79', 80''), 1.58 – 1.75 (m, 4H, 24, 77'', 79''), 1.88 – 1.94 (m, 2H, 76', 80'), 2.34 (s, 3H, 53), 2.45 (s, 3H, 11), 2.51 – 2.56 (m, 2H, 23), 2.63 (t, *J* = 7.2 Hz, 2H, 26), 3.35 – 3.39 (m, 2H, 43), 3.41 – 3.52 (m, 10H), 3.75 (t, *J* = 5.2 Hz, 2H, 34), 3.81 (s, 3H, 73), 4.43 (t, *J* = 5.3 Hz, 2H, 33), 4.64 (tt, *J* = 9.4, 3.9 Hz, 1H, 75), 6.45 (p, *J* = 4.0, 3.1 Hz, 1H, 66), 7.18 (t, *J* = 8.3 Hz, 1H, 70), 7.28 – 7.38 (m, 5H, 48, 49, 51, 60, 65), 7.43 – 7.57 (m, 3H, 63, 68, 71), 7.71 (dd, *J* = 8.4, 1.9 Hz, 1H, 18), 7.79 – 7.82 (m, 2H, 17, 32), 8.05 – 8.13 (m, 1H, 7), 8.30 (d, *J* = 1.8 Hz, 1H, 20), 8.35 (t, *J* = 5.7 Hz, 1H, 44), 8.59 (s, 1H, 9), 9.11 (s, 1H, 2). <sup>13</sup>C NMR (151 MHz, DMSO-*d*<sub>6</sub>) δ 18.76, 53, 20.75, 11, 23.46, 77, 79, 24.12, 25, 24.74, 26, 24.92, 78, 28.50, 24, 31.64, 76, 80, 32.56, 73, 34.87, 23, 38.86, 43, 49.20, 33, 68.77, 68.77, 34, 69.53, 69.55, 69.63, 69.73, 72.88, 75, 100.57, 66, 109.12, 71, 118.89, 119.72, 20, 120.90, 17, 121.24, 51, 121.27, 122.20, 32, 123.16, 124.65,



18.77 , 24, 20.75 , 61, 23.48 , 69, 71, 24.53 , 76, 24.94 , 82, 25.01 , 70, 28.55 , 77, 28.60 , 78, 28.65 , 79, 28.69 , 80, 29.03 , 81, 31.66 , 68, 72, 32.57 , 44, 35.15 , 74, 38.88 , 2, 49.19 , 12, 68.78, 68.80 , 11, 69.56 , 3, 69.65, 69.76, 72.91 , 67, 100.59 , 37, 109.13 , 42, 118.89 , 31, 119.74 , 50, 120.91 , 47, 121.24 , 34, 39, 121.29 , 20, 122.09 , 84, 123.19 , 41, 124.66 , 33, 124.96 , 48, 127.80 , 38, 129.03 , 60, 130.19 , 36, 130.84 , 40, 131.76, 132.21 , 18, 132.47 , 55, 132.60, 132.92 , 59, 133.32 , 49, 134.62 , 32, 135.58 , 43, 138.23 , 17, 142.63 , 56, 146.77 , 83, 148.44 , 46, 150.20 , 58, 150.93 , 21, 154.02 , 64, 157.74, 158.65, 168.15 , 16, 172.46 , 73.

**6-chloro-5-[4-[2-[4-[4-[5-[[6-[5-(cyclohexoxycarbonylamino)-6-methyl-3-pyridyl]-1,3-benzothiazol-2-yl]amino]-5-oxo-pentyl]triazol-1-yl]butanoylamino]ethoxy]phenyl]-1H-indole-3-carboxylic acid, CCT393761**

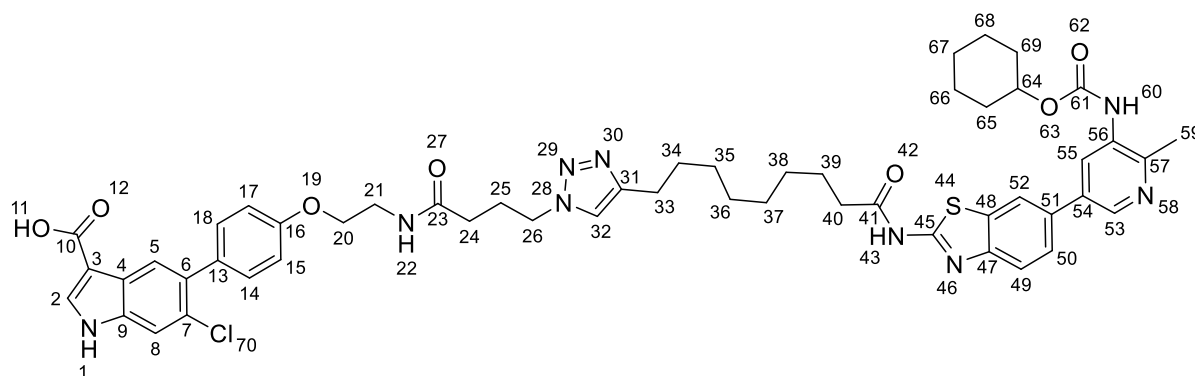


The general procedure for click coupling was carried out with the desired azide (N-(3-azidopropyl)-5-[[6-chloro-5-(1-methylindol-5-yl)-1H-benzimidazol-2-yl]oxy]-2-methyl-benzamide, 60) and alkyne (cyclohexyl N-[5-[2-(hept-6-ynoylamino)-1,3-benzothiazol-6-yl]-2-methyl-3-pyridyl]carbamate) to give the title compound (52%) as an off white solid.

Ret time = 3.12 mins. Formula C<sub>48</sub>H<sub>50</sub>ClN<sub>9</sub>O<sub>7</sub>S. Observed m/z 932.3320. Calculated m/z 932.3311. Error (ppm) -1.0. <sup>1</sup>H NMR (600 MHz, DMSO) δ 1.19 – 1.27 (m, 1H, 63), 1.29 – 1.39 (m, 2H, 62', 64'), 1.39 – 1.47 (m, 2H, 61, 65), 1.49 – 1.55 (m, 1H, 63),

1.59 – 1.75 (m, 6H, 34, 35, 62", 64"), 1.87 – 1.95 (m, 2H, 61, 65), 1.99 – 2.08 (m, 2H, 25), 2.12 (t,  $J = 7.4$  Hz, 2H, 24), 2.45 (s, 3H, 55), 2.52 – 2.56 (m, 2H, 36), 2.64 (t,  $J = 7.2$  Hz, 2H, 33), 3.45 (q,  $J = 5.8$  Hz, 2H, 21), 4.03 (t,  $J = 5.7$  Hz, 2H, 20), 4.31 (t,  $J = 6.9$  Hz, 2H, 26), 4.64 (tt,  $J = 9.1, 3.9$  Hz, 1H, 60), 6.96 – 7.03 (m, 2H, 15, 17), 7.31 – 7.36 (m, 2H, 14, 18), 7.61 (s, 1H, 8), 7.71 (dd,  $J = 8.4, 1.9$  Hz, 1H, 46), 7.80 (d,  $J = 8.4$  Hz, 1H, 45), 7.84 (s, 1H, 32), 7.92 (s, 1H, 5), 8.06 (d,  $J = 2.3$  Hz, 1H, 2), 8.10 (s, 1H, 51), 8.14 (t,  $J = 5.6$  Hz, 1H, 22), 8.31 (d,  $J = 1.8$  Hz, 1H, 48), 8.59 (s, 1H, 49), 9.11 (s, 1H, 56), 11.93 (s, 1H, 1), 12.40 (s, 1H, 12).  $^{13}\text{C}$  NMR (151 MHz, DMSO)  $\delta$  21.19 , 55, 23.91 , 62, 64, 24.58, 25.23 , 33, 25.36 , 63, 26.32 , 25, 28.93, 32.09 , 61, 65, 32.34 , 24, 35.33 , 36, 38.73 , 21, 49.23 , 26, 66.80 , 20, 73.34 , 60, 108.09 , 3, 113.33 , 8, 114.50 , 15, 17, 120.18 , 48, 121.36 , 45, 122.25 , 32, 123.17 , 5, 125.40 , 46, 125.74 , 4, 126.27 , 7, 129.47 , 51, 131.24 , 14, 18, 132.65 , 50, 132.98 , 13, 133.04 , 44, 133.22 , 6, 133.37 , 52, 133.77 , 47, 134.25 , 2, 136.38 , 9, 143.06 , 49, 147.03 , 31, 148.86 , 43, 150.75 , 53, 154.45 , 57, 158.06 , 16, 159.06 , 41, 166.10 , 10, 171.91 , 23, 172.78 , 37.

**6-chloro-5-[4-[2-[4-[4-[9-[[6-[5-(cyclohexoxycarbonylamino)-6-methyl-3-pyridyl]-1,3-benzothiazol-2-yl]amino]-9-oxo-nonyl]triazol-1-yl]butanoylamino]ethoxy]phenyl]-1H-indole-3-carboxylic acid, CCT393215**

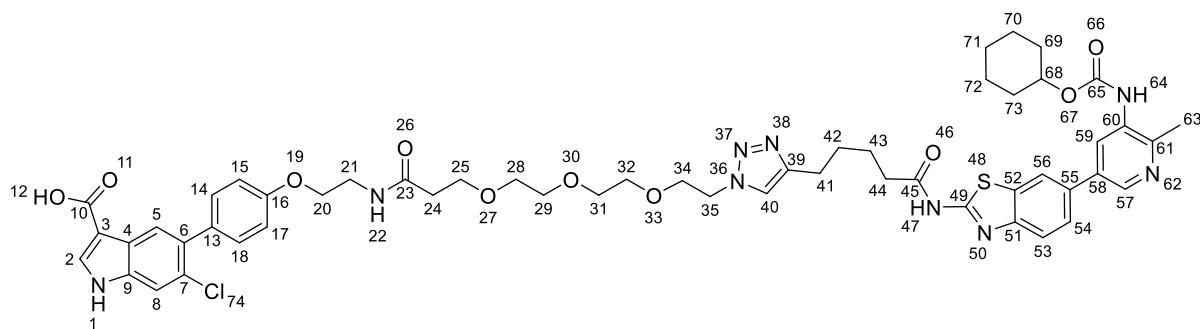


The general procedure for click coupling was carried out with the desired azide (N-(3-azidopropyl)-5-[[6-chloro-5-(1-methylindol-5-yl)-1H-benzimidazol-2-yl]oxy]-2-methyl-benzamide, 60) and alkyne (Cyclohexyl N-[2-methyl-5-[2-(undec-10-

ynoylamino)-1,3-benzothiazol-6-yl]-3-pyridyl]carbamate) to give the title compound (74%) as an off white solid.

Ret time = 3.09 mins. Formula C52H58ClN9O7S. Observed m/z 988.3971936. Calculated m/z 988.3941202. Error (ppm) 3.11. <sup>1</sup>H NMR (600 MHz, DMSO-*d*<sub>6</sub>) δ 1.20 – 1.64 (m, 7H, 34, 35, 36, 37, 38, 39, 65, 66, 68, 69), 1.69 – 1.74 (m, 2H, 66, 68), 1.92 (dq, *J* = 12.4, 3.8 Hz, 2H, 65, 69), 2.02 (p, *J* = 7.2 Hz, 2H, 25), 2.12 (t, *J* = 7.4 Hz, 2H, 24), 2.46 (s, 3H, 59), 2.47 – 2.49 (m, 2H, 40), 2.57 (t, *J* = 7.6 Hz, 2H, 33, 67), 3.17 (s, 1H), 3.45 (q, *J* = 5.7 Hz, 5H, 21), 4.04 (t, *J* = 5.7 Hz, 2H, 20), 4.30 (t, *J* = 7.0 Hz, 2H, 26), 4.65 (tt, *J* = 9.4, 3.9 Hz, 1H, 64), 6.98 – 7.04 (m, 2H, 15, 17), 7.31 – 7.36 (m, 2H, 14, 18), 7.61 (s, 1H, 8), 7.72 (dd, *J* = 8.4, 1.9 Hz, 1H, 50), 7.79 – 7.82 (m, 2H, 32, 49), 7.93 (s, 1H, 5), 8.06 (d, *J* = 1.7 Hz, 1H, 2), 8.10 (d, *J* = 2.2 Hz, 1H, 55), 8.14 (t, *J* = 5.6 Hz, 1H, 22), 8.24 (s, OH), 8.31 (d, *J* = 1.8 Hz, 1H, 52), 8.59 (d, *J* = 2.2 Hz, 1H, 53), 9.11 (s, 1H, 60), 11.93 (s, 1H, 1), 12.37 (s, 1H, 11). <sup>13</sup>C NMR (151 MHz, DMSO-*d*<sub>6</sub>) δ 20.73 , 59, 23.45 , 66, 68, 24.49 , 39, 24.90 , 67, 25.04 , 33, 25.86 , 25, 28.52 , 37, 38, 28.60 , 36, 28.64 , 35, 28.98 , 34, 31.63 , 65, 69, 31.87 , 24, 35.12 , 40, 38.26 , 21, 48.71 , 26, 66.35 , 20, 72.85 , 64, 107.66 , 3, 112.84 , 8, 114.03 , 15, 17, 119.71 , 52, 120.87 , 49, 121.64 , 32, 122.70 , 5, 124.92 , 50, 125.27 , 4, 125.77 , 7, 128.97 , 55, 130.77 , 14, 18, 132.17, 132.52 , 13, 132.56, 132.73 , 6, 132.88 , 56, 133.27 , 54, 133.74 , 2, 135.91 , 9, 142.60 , 53, 146.87 , 31, 148.40 , 47, 150.26 , 57, 153.96, 157.60 , 16, 158.60, 171.40 , 23, 172.42 , 41.

**6-chloro-5-[4-[2-[3-[2-[2-[2-[4-[5-[[6-[5-(cyclohexoxycarbonylamino)-6-methyl-3-pyridyl]-1,3-benzothiazol-2-yl]amino]-5-oxo-pentyl]triazol-1-yl]ethoxy]ethoxy]ethoxy]propanoylamino]ethoxy]phenyl]-1H-indole-3-carboxylic acid, CCT393762**

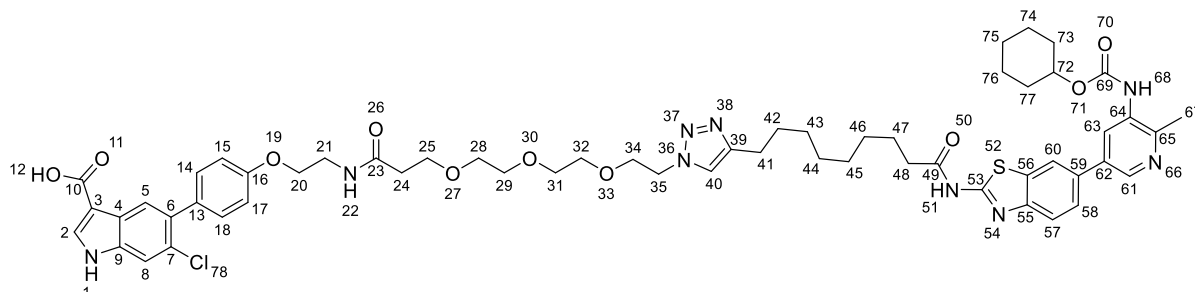




The general procedure for click coupling was carried out with the desired azide (N-[2-[2-[2-(2-azidoethoxy)ethoxy]ethoxy]ethyl]-5-[[6-chloro-5-(1-methylindol-5-yl)-1H-benzimidazol-2-yl]oxy]-2-methyl-benzamide 57) and alkyne (cyclohexyl N-[5-[2-(hept-6-ynoylamino)-1,3-benzothiazol-6-yl]-2-methyl-3-pyridyl]carbamate) to give the title compound (41%) as an off white solid.

Ret time = 3.15 mins. Formula C<sub>53</sub>H<sub>60</sub>ClN<sub>9</sub>O<sub>10</sub>S. Observed m/z 1050.3969. Calculated m/z 1050.3950. Error (ppm) 1.8. <sup>1</sup>H NMR (600 MHz, DMSO) δ 1.18 – 1.27 (m, 1H, 71), 1.30 – 1.38 (m, 2H, 70', 72'), 1.39 – 1.47 (m, 2H, 69, 73), 1.49 – 1.56 (m, 1H, 71), 1.60 – 1.75 (m, 6H, 42, 43, 70'', 72''), 1.88 – 1.94 (m, 2H, 69, 73), 2.35 (t, J = 6.4 Hz, 2H, 24), 2.45 (s, 3H, 63), 2.52 – 2.56 (m, 3H, 44), 2.64 (t, J = 7.2 Hz, 2H, 41), 3.40 – 3.50 (m, 12H, 21, 28, 29, 31, 32), 3.57 – 3.66 (m, 28H, 25), 3.77 (t, J = 5.3 Hz, 2H, 34), 4.02 (t, J = 5.6 Hz, 2H, 20), 4.44 (t, J = 5.3 Hz, 2H, 35), 4.59 – 4.70 (m, 1H, 68), 6.98 – 7.04 (m, 2H, 15, 17), 7.31 – 7.36 (m, 2H, 14, 18), 7.61 (s, 1H, 8), 7.71 (dd, J = 8.4, 1.9 Hz, 1H, 54), 7.80 (d, J = 7.2 Hz, 2H, 40, 53), 7.92 (s, 1H, 5), 8.06 (d, J = 2.5 Hz, 1H, 2), 8.09 – 8.11 (m, 1H, 59), 8.14 (t, J = 5.6 Hz, 1H, 22), 8.31 (d, J = 1.8 Hz, 1H, 56), 8.57 – 8.61 (m, 1H, 57), 9.11 (s, 1H, 64), 11.93 (d, J = 3.0 Hz, 1H, 1), 12.40 (s, 1H, 12). <sup>13</sup>C NMR (151 MHz, DMSO) δ 20.75 , 63, 23.48 , 70, 72, 24.14, 24.75 , 41, 24.93 , 71, 28.51, 31.65 , 69, 73, 34.89 , 44, 36.04 , 24, 38.30 , 21, 49.23 , 35, 66.42 , 20, 66.78 , 25, 68.78 , 34, 69.55, 69.57, 69.63, 69.66, 72.90 , 68, 107.63 , 3, 112.89 , 8, 114.05 , 15, 17, 119.74 , 56, 120.92 , 53, 122.22 , 40, 122.71 , 5, 124.96 , 54, 125.28 , 4, 125.83 , 7, 128.96 , 2, 130.80 , 14, 18, 132.21 , 58, 132.53 , 13, 132.60 , 52, 132.79 , 6, 132.91 , 60, 133.31 , 55, 133.81 , 59, 135.94 , 9, 142.62 , 57, 146.44 , 39, 148.42 , 51, 150.30 , 61, 154.00 , 65, 157.63 , 16, 158.61 , 49, 165.65 , 10, 170.50 , 23, 172.32 , 45.

**6-chloro-5-[4-[2-[3-[2-[2-[2-[4-[9-[[6-[5-(cyclohexoxycarbonylamino)-6-methyl-3-pyridyl]-1,3-benzothiazol-2-yl]amino]-9-oxo-nonyl]triazol-1-yl]ethoxy]ethoxy]ethoxy]propanoylamino]ethoxy]phenyl]-1H-indole-3-carboxylic acid, CCT393218**



The general procedure for click coupling was carried out with the desired azide (N-[2-[2-[2-(2-azidoethoxy)ethoxy]ethoxy]ethyl]-5-[[6-chloro-5-(1-methylindol-5-yl)-1H-benzimidazol-2-yl]oxy]-2-methyl-benzamide 57) and alkyne (Cyclohexyl N-[2-methyl-5-[2-(undec-10-ynoylamino)-1,3-benzothiazol-6-yl]-3-pyridyl]carbamate) to give the title compound (85%) as an off white solid.

Ret time = 3.07 mins. Formula C<sub>57</sub>H<sub>68</sub>ClN<sub>9</sub>O<sub>10</sub>. Observed m/z 1106.4549851. Calculated m/z 1106.4571144. Error (ppm) -1.92. <sup>1</sup>H NMR (600 MHz, DMSO-*d*<sub>6</sub>) δ 1.18 – 1.47 (m, 14H, 43, 44, 45, 46, 73, 74, 76, 77), 1.48 – 1.65 (m, 4H, 42, 47), 1.72 (dt, *J* = 14.0, 4.3 Hz, 2H, 74, 76), 1.87 – 1.96 (m, 2H, 73, 77), 2.35 (t, *J* = 6.4 Hz, 2H, 24), 2.46 (s, 3H, 67), 2.47 – 2.49 (m, 3H, 48), 2.57 (t, *J* = 7.6 Hz, 2H, 41), 3.40 – 3.50 (m, 10H, 21, 28, 29, 31, 32), 3.60 (t, *J* = 6.4 Hz, 2H, 25), 3.76 (t, *J* = 5.3 Hz, 2H, 34), 4.03 (t, *J* = 5.6 Hz, 2H, 20), 4.44 (t, *J* = 5.3 Hz, 2H, 35), 4.65 (tt, *J* = 9.4, 3.9 Hz, 1H, 72), 6.98 – 7.03 (m, 2H, 15, 17), 7.32 – 7.36 (m, 2H, 14, 18), 7.61 (s, 1H, 8), 7.72 (dd, *J* = 8.4, 1.9 Hz, 1H, 58), 7.77 (s, 1H, 40), 7.81 (d, *J* = 8.4 Hz, 1H, 57), 7.93 (s, 1H, 5), 8.07 (d, *J* = 2.9 Hz, 1H, 2), 8.10 (s, 1H, 63), 8.12 – 8.15 (m, 1H, 22), 8.31 (d, *J* = 1.8 Hz, 1H, 60), 8.59 (d, *J* = 2.2 Hz, 1H, 61), 9.11 (s, 1H, 68), 11.92 (d, *J* = 3.0 Hz, 1H, 1), 12.18 (s, 2H, 12), 12.36 (s, 1H, 51). <sup>13</sup>C NMR (151 MHz, DMSO-*d*<sub>6</sub>) δ 20.72, 67, 23.45, 74, 76, 24.49, 75, 24.90, 41, 24.99, 47, 28.52, 46, 28.57, 45, 28.62, 42, 28.66, 44, 29.00, 43, 31.63, 73, 77, 35.12, 48, 36.01, 24, 38.26, 21, 49.16, 35, 66.40, 20, 66.77, 25,

68.77 , 34, 69.53 , 31, 32, 69.61 , 29, 69.65 , 28, 72.86 , 72, 107.55 , 3, 112.85 , 8,  
114.02 , 15, 17, 119.71 , 60, 120.87, 122.06 , 40, 122.68 , 5, 124.92 , 58, 125.25 , 4,  
125.81 , 7, 128.95 , 63, 130.77 , 14, 18, 132.17, 132.50 , 13, 132.57, 132.77 , 6,  
132.88 , 64, 133.28, 133.79 , 2, 135.91 , 9, 142.59 , 61, 146.73 , 39, 148.40, 150.25 ,  
65, 153.96, 157.61 , 16, 158.60, 163.03 , 53, 165.58 , 10, 170.42 , 23, 172.41 , 49.

## Chapter 7 References

---

- (1) Ubersax, J. A.; Ferrell, J. E. Mechanisms of specificity in protein phosphorylation. *Nat Rev Mol Cell Bio* **2007**, *8* (7), 530-541. DOI: 10.1038/nrm2203.
- (2) Ma, B.; Marcotte, D.; Paramasivam, M.; Michelsen, K.; Wang, T.; Bertolotti-Ciarlet, A.; Jones, J. H.; Moree, B.; Butko, M.; Salafsky, J.; et al. ATP-Competitive MLKL Binders Have No Functional Impact on Necroptosis. *PLoS One* **2016**, *11* (11), 11-30. DOI: 10.1371/journal.pone.0165983.
- (3) Ardito, F.; Giuliani, M.; Perrone, D.; Troiano, G.; Lo Muzio, L. The crucial role of protein phosphorylation in cell signaling and its use as targeted therapy. *Int J Mol Med* **2017**, *40* (2), 271-280. DOI: 10.3892/ijmm.2017.3036. Mann, M.; Jensen, O. N. Proteomic analysis of post-translational modifications. *Nat Biotechnol* **2003**, *21* (3), 255-261. DOI: 10.1038/nbt0303-255.
- (4) Pike, A. C. W.; Rellos, P.; Niesen, F. H.; Turnbull, A.; Oliver, A. W.; Parker, S. A.; Turk, B. E.; Pearl, L. H.; Knapp, S. Activation segment dimerization: a mechanism for kinase autophosphorylation of non-consensus sites. *Embo J* **2008**, *27* (4), 704-714. DOI: 10.1038/emboj.2008.8.
- (5) Khoury, G. A.; Baliban, R. C.; Floudas, C. A. Proteome-wide post-translational modification statistics: frequency analysis and curation of the swiss-prot database. *Sci Rep-Uk* **2011**, *1*. DOI: ARTN 90  
10.1038/srep00090.
- (6) Schaffer, B. E.; Levin, R. S.; Hertz, N. T.; Maures, T. J.; Schoof, M. L.; Hollstein, P. E.; Benayoun, B. A.; Banko, M. R.; Shaw, R. J.; Shokat, K. M.; et al. Identification of AMPK Phosphorylation Sites Reveals a Network of Proteins Involved in Cell Invasion and Facilitates Large-Scale Substrate Prediction. *Cell Metab* **2015**, *22* (5), 907-921. DOI: 10.1016/j.cmet.2015.09.009.
- (7) Bhullar, K. S.; Lagaron, N. O.; McGowan, E. M.; Parmar, I.; Jha, A.; Hubbard, B. P.; Rupasinghe, H. P. V. Kinase-targeted cancer therapies: progress, challenges and future directions. *Mol Cancer* **2018**, *17*. DOI: ARTN 48  
10.1186/s12943-018-0804-2. Kannaiyan, R.; Mahadevan, D. A comprehensive review of protein kinase inhibitors for cancer therapy. *Expert Rev Anticanc* **2018**, *18* (12), 1249-1270. DOI: 10.1080/14737140.2018.1527688.

- (8) Roskoski, R. Properties of FDA-approved small molecule protein kinase inhibitors: A 2022 update. *Pharmacol Res* **2022**, *175*. DOI: ARTN 106037  
10.1016/j.phrs.2021.106037.
- (9) Goebel, G. L.; Qiu, X.; Wu, P. Kinase-targeting small-molecule inhibitors and emerging bifunctional molecules. *Trends Pharmacol Sci* **2022**. DOI: 10.1016/j.tips.2022.04.006.
- (10) Fabbro, D. 25 Years of Small Molecular Weight Kinase Inhibitors: Potentials and Limitations. *Mol Pharmacol* **2015**, *87* (5), 766-775. DOI: 10.1124/mol.114.095489. Fabbro, D.; Cowan-Jacob, S. W.; Moebitz, H. Ten things you should know about protein kinases: IUPHAR Review 14. *Brit J Pharmacol* **2015**, *172* (11), 2675-2700. DOI: 10.1111/bph.13096.
- (11) Bishop, A. C.; Chen, V. L. Brought to life: targeted activation of enzyme function with small molecules. *J Chem Biol* **2009**, *2* (1), 1-9. DOI: 10.1007/s12154-008-0012-4.
- (12) Hardy, J. A.; Wells, J. A. Searching for new allosteric sites in enzymes. *Curr Opin Struct Biol* **2004**, *14* (6), 706-715. DOI: 10.1016/j.sbi.2004.10.009.
- (13) Lindsley, J. E.; Rutter, J. Whence cometh the allosterome? *P Natl Acad Sci USA* **2006**, *103* (28), 10533-10535. DOI: 10.1073/pnas.0604452103.
- (14) Sadowsky, J. D.; Burlingame, M. A.; Wolan, D. W.; McClendon, C. L.; Jacobson, M. P.; Wells, J. A. Turning a protein kinase on or off from a single allosteric site via disulfide trapping. *P Natl Acad Sci USA* **2011**, *108* (15), 6056-6061. DOI: 10.1073/pnas.1102376108.
- (15) Lan, P.; Romero, F. A.; Wodka, D.; Kassick, A. J.; Dang, Q.; Gibson, T.; Cashion, D.; Zhou, G.; Chen, Y.; Zhang, X.; et al. Hit-to-Lead Optimization and Discovery of 5-((5-([1,1'-Biphenyl]-4-yl)-6-chloro-1H-benzo[d]imidazol-2-yl)oxy)-2-methylbenzoic Acid (MK-3903): A Novel Class of Benzimidazole-Based Activators of AMP-Activated Protein Kinase. *J Med Chem* **2017**, *60* (21), 9040-9052. DOI: 10.1021/acs.jmedchem.7b01344.
- (16) Barr, A. J. Protein tyrosine phosphatases as drug targets: strategies and challenges of inhibitor development. *Future Med Chem* **2010**, *2* (10), 1563-1576. DOI: 10.4155/Fmc.10.241. Bishop, A. C.; Davis, O. B. Target-specific inhibition and activation of sensitized protein tyrosine phosphatases with biarsenical probes. *Abstr Pap Am Chem S* **2012**, *243*.
- (17) Krzyzosiak, A.; Sigurdardottir, A.; Luh, L.; Carrara, M.; Das, I.; Schneider, K.; Bertolotti, A. Target-Based Discovery of an Inhibitor of the Regulatory Phosphatase PPP1R15B. *Cell* **2018**, *174* (5), 1216-+. DOI: 10.1016/j.cell.2018.06.030.
- (18) Sanchez, C. P.; Moliner Cubel, S.; Nyboer, B.; Jankowska-Dollken, M.; Schaeffer-Reiss, C.; Ayoub, D.; Planelles, G.; Lanzer, M. Phosphomimetic substitution at Ser-33 of the

chloroquine resistance transporter PfCRT reconstitutes drug responses in *Plasmodium falciparum*. *J Biol Chem* **2019**, *294* (34), 12766-12778. DOI: 10.1074/jbc.RA119.009464.

(19) Chen, Z.; Cole, P. A. Synthetic approaches to protein phosphorylation. *Curr Opin Chem Biol* **2015**, *28*, 115-122. DOI: 10.1016/j.cbpa.2015.07.001.

(20) Szczepanowska, J.; Ramachadran, U.; Herring, C. J.; Gruschus, J. M.; Qin, J.; Korn, E. D.; Brzeska, H. Effect of mutating the regulatory phosphoserine and conserved threonine on the activity of the expressed catalytic domain of *Acanthamoeba* myosin I heavy chain kinase. *P Natl Acad Sci USA* **1998**, *95* (8), 4146-4151. DOI: DOI 10.1073/pnas.95.8.4146.

Hao, M. M.; Lowy, A. M.; Kapoor, M.; Deffie, A.; Liu, G.; Lozano, G. Mutation of phosphoserine 389 affects p53 function in vivo. *J Biol Chem* **1996**, *271* (46), 29380-29385. DOI: DOI 10.1074/jbc.271.46.29380. Littlepage, L. E.; Wu, H.; Andresson, T.; Deanehan, J. K.; Amundadottir, L. T.; Ruderman, J. V. Identification of phosphorylated residues that affect the activity of the mitotic kinase Aurora-A. *P Natl Acad Sci USA* **2002**, *99* (24), 15440-15445. DOI: 10.1073/pnas.202606599.

(21) Spencer, D. M.; Wandless, T. J.; Schreiber, S. L.; Crabtree, G. R. Controlling signal transduction with synthetic ligands. *Science* **1993**, *262* (5136), 1019-1024. DOI: 10.1126/science.7694365.

(22) Zengerle, M.; Chan, K. H.; Ciulli, A. Selective Small Molecule Induced Degradation of the BET Bromodomain Protein BRD4. *Acs Chemical Biology* **2015**, *10* (8), 1770-1777. DOI: 10.1021/acscchembio.5b00216.

(23) Sakamoto, K. M.; Kim, K. B.; Kumagai, A.; Mercurio, F.; Crews, C. M.; Deshaies, R. J. Protacs: Chimeric molecules that target proteins to the Skp1-Cullin-F box complex for ubiquitination and degradation. *P Natl Acad Sci USA* **2001**, *98* (15), 8554-8559. DOI: DOI 10.1073/pnas.141230798.

(24) Schneekloth, A. R.; Pucheault, M.; Tae, H. S.; Crews, C. M. Targeted intracellular protein degradation induced by a small molecule: En route to chemical proteomics. *Bioorg Med Chem Lett* **2008**, *18* (22), 5904-5908. DOI: 10.1016/j.bmcl.2008.07.114.

(25) Qin, C.; Hu, Y.; Zhou, B.; Fernandez-Salas, E.; Yang, C. Y.; Liu, L.; McEachern, D.; Przybranowski, S.; Wang, M.; Stuckey, J.; et al. Discovery of QCA570 as an Exceptionally Potent and Efficacious Proteolysis Targeting Chimera (PROTAC) Degradator of the Bromodomain and Extra-Terminal (BET) Proteins Capable of Inducing Complete and Durable Tumor Regression. *Journal of Medicinal Chemistry* **2018**, *61* (15), 6685-6704. DOI: 10.1021/acs.jmedchem.8b00506.

(26) Salami, J.; Alabi, S.; Willard, R. R.; Vitale, N. J.; Wang, J.; Dong, H. Q.; Jin, M. Z.; McDonnell, D. P.; Crew, A. P.; Neklesa, T. K.; et al. Androgen receptor degradation by the proteolysis-targeting chimera ARCC-4 outperforms enzalutamide in cellular models of prostate cancer drug resistance. *Commun Biol* **2018**, *1*. DOI: ARTN 100

10.1038/s42003-018-0105-8.

(27) Crew, A. P.; Raina, K.; Dong, H. Q.; Qian, Y. M.; Wang, J.; Vigil, D.; Serebrenik, Y. V.; Hamman, B. D.; Morgan, A.; Ferraro, C.; et al. Identification and Characterization of Von Hippel-Lindau-Recruiting Proteolysis Targeting Chimeras (PROTACs) of TANK-Binding Kinase 1. *Journal of Medicinal Chemistry* **2018**, *61* (2), 583-598. DOI: 10.1021/acs.jmedchem.7b00635.

(28) Bekes, M.; Langley, D. R.; Crews, C. M. PROTAC targeted protein degraders: the past is prologue. *Nature Reviews Drug Discovery* **2022**, *21* (3), 181-200. DOI: 10.1038/s41573-021-00371-6.

(29) Henning, N. J.; Boike, L.; Spradlin, J. N.; Ward, C. C.; Liu, G.; Zhang, E.; Belcher, B. P.; Brittain, S. M.; Hesse, M. J.; Dovala, D.; et al. Deubiquitinase-targeting chimeras for targeted protein stabilization. *Nature Chemical Biology* **2022**, *18* (4), 412-+. DOI: 10.1038/s41589-022-00971-2.

(30) Li, Z. N. A.; Pinch, B. J.; Olson, C. M.; Donovan, K. A.; Nowak, R. P.; Mills, C. E.; Scott, D. A.; Doctor, Z. M.; Eleuteri, N. A.; Chung, M.; et al. Development and Characterization of a Wee1 Kinase Degradation. *Cell Chem Biol* **2020**, *27* (1), 57-+. DOI: 10.1016/j.chembiol.2019.10.013.

(31) Liu, X. G.; Ciulli, A. DUB be good to me. *Nature Chemical Biology* **2022**, *18* (4), 358-359. DOI: 10.1038/s41589-022-00978-9.

(32) Wang, W. W.; Chen, L. Y.; Wozniak, J. M.; Jadhav, A. M.; Anderson, H.; Malone, T. E.; Parker, C. G. Targeted Protein Acetylation in Cells Using Heterobifunctional Molecules. *J Am Chem Soc* **2021**, *143* (40), 16700-16708. DOI: 10.1021/jacs.1c07850.

(33) Donovan, K. A.; Ferguson, F. M.; Bushman, J. W.; Eleuteri, N. A.; Bhunia, D.; Ryu, S.; Tan, L.; Shi, K.; Yue, H.; Liu, X.; et al. Mapping the Degradable Kinome Provides a Resource for Expedited Degradation Development. *Cell* **2020**. DOI: 10.1016/j.cell.2020.10.038.

(34) Lai, A. C.; Toure, M.; Hellerschmied, D.; Salami, J.; Jaime-Figueroa, S.; Ko, E.; Hines, J.; Crews, C. M. Modular PROTAC Design for the Degradation of Oncogenic BCR-ABL. *Angew Chem Int Edit* **2016**, *55* (2), 807-810. DOI: 10.1002/anie.201507634.

(35) Schiemer, J.; Horst, R.; Meng, Y. L.; Montgomery, J. I.; Xu, Y. R.; Feng, X. D.; Borzilleri, K.; Uccello, D. P.; Leverett, C.; Brown, S.; et al. Snapshots and ensembles of BTK and cIAP1

protein degrader ternary complexes. *Nature Chemical Biology* **2021**, *17* (2), 152-160. DOI: 10.1038/s41589-020-00686-2.

(36) Yamazoe, S.; Tom, J.; Fu, Y.; Wu, W. Q.; Zeng, L.; Sun, C. L.; Liu, Q.; Lin, J.; Lin, K.; Fairbrother, W. J.; et al. Heterobifunctional Molecules Induce Dephosphorylation of Kinases-A Proof of Concept Study. *Journal of Medicinal Chemistry* **2020**, *63* (6), 2807-2813. DOI: 10.1021/acs.jmedchem.9b01167.

(37) Siriwardena, S. U.; Godage, D. N. P. M.; Shoba, V. M.; Lai, S.; Shi, M. C.; Wu, P.; Chaudhary, S. K.; Schreiber, S. L.; Choudhary, A. Phosphorylation-Inducing Chimeric Small Molecules. *J Am Chem Soc* **2020**, *142* (33), 14052-14057. DOI: 10.1021/jacs.0c05537.

(38) Shoba, V. M.; Godage, D. N. P. M.; Chaudhary, S. K.; Deb, A.; Siriwardena, S. U.; Choudhary, A. Synthetic Reprogramming of Kinases Expands Cellular Activities of Proteins. *Angew Chem Int Edit* **2022**, *61* (29). DOI: ARTN e202202770

10.1002/anie.202202770.

(39) Sun, Y. H.; Zhao, X. W.; Ding, N.; Gao, H. Y.; Wu, Y.; Yang, Y. Q.; Zhao, M.; Hwang, J.; Song, Y. Q.; Liu, W. L.; et al. PROTAC-induced BTK degradation as a novel therapy for mutated BTK C481S induced ibrutinib-resistant B-cell malignancies. *Cell Res* **2018**, *28* (7), 779-781. DOI: 10.1038/s41422-018-0055-1.

(40) Soares, P.; Gadd, M. S.; Frost, J.; Galdeano, C.; Ellis, L.; Epemolu, O.; Rocha, S.; Read, K. D.; Ciulli, A. Group-Based Optimization of Potent and Cell-Active Inhibitors of the von Hippel-Lindau (VHL) E3 Ubiquitin Ligase: Structure-Activity Relationships Leading to the Chemical Probe (2S,4R)-1-((S)-2-(1-Cyanocyclopropanecarboxamido)-3,3-dimethylbutanoyl)-4-hydroxy-N-(4-(4-methylthiazol-5-yl)benzopyrrolidine-2-carboxamide (VH298). *Journal of Medicinal Chemistry* **2018**, *61* (2), 599-618. DOI: 10.1021/acs.jmedchem.7b00675.

(41) Chan, K. H.; Zengerle, M.; Testa, A.; Ciulli, A. Impact of Target Warhead and Linkage Vector on Inducing Protein Degradation: Comparison of Bromodomain and Extra-Terminal (BET) Degraders Derived from Triazolodiazepine (JQ1) and Tetrahydroquinoline (I-BET726) BET Inhibitor Scaffolds. *Journal of Medicinal Chemistry* **2018**, *61* (2), 504-513. DOI: 10.1021/acs.jmedchem.6b01912.

(42) Cyrus, K.; Wehenkel, M.; Choi, E. Y.; Han, H. J.; Lee, H.; Swanson, H.; Kim, K. B. Impact of linker length on the activity of PROTACs. *Mol Biosyst* **2011**, *7* (2), 359-364. DOI: 10.1039/c0mb00074d.



- (43) Steinebach, C.; Sosic, I.; Lindner, S.; Bricelj, A.; Kohl, F.; Ng, Y. L. D.; Monschke, M.; Wagner, K. G.; Kronke, J.; Gutschow, M. A MedChem toolbox for cereblon-directed PROTACs. *Medchemcomm* **2019**, *10* (6), 1037-1041. DOI: 10.1039/c9md00185a.
- (44) Han, X.; Zhao, L. J.; Xiang, W. G.; Qin, C.; Miao, B. K. Y.; Xu, T. F.; Wang, M.; Yang, C. Y.; Chinnaswamy, K.; Stuckey, J.; et al. Discovery of Highly Potent and Efficient PROTAC Degraders of Androgen Receptor (AR) by Employing Weak Binding Affinity VHL E3 Ligase Ligands. *Journal of Medicinal Chemistry* **2019**, *62* (24), 11218-11231. DOI: 10.1021/acs.jmedchem.9b01393.
- (45) Garcia, D.; Shaw, R. J. AMPK: Mechanisms of Cellular Energy Sensing and Restoration of Metabolic Balance. *Mol Cell* **2017**, *66* (6), 789-800. DOI: 10.1016/j.molcel.2017.05.032.
- (46) Cool, B.; Zinker, B.; Chiou, W.; Kifle, L.; Cao, N.; Perham, M.; Dickinson, R.; Adler, A.; Gagne, G.; Iyengar, R.; et al. Identification and characterization of a small molecule AMPK activator that treats key components of type 2 diabetes and the metabolic syndrome. *Cell Metab* **2006**, *3* (6), 403-416. DOI: 10.1016/j.cmet.2006.05.005.
- (47) Cameron, K. O.; Kung, D. W.; Kalgutkar, A. S.; Kurumbail, R. G.; Miller, R.; Salatto, C. T.; Ward, J.; Withka, J. M.; Bhattacharya, S. K.; Boehm, M.; et al. Discovery and Preclinical Characterization of 6-Chloro-5-[4-(1-hydroxycyclobutyl)phenyl]-1H-indole-3-carboxylic Acid (PF-06409577), a Direct Activator of Adenosine Monophosphate-activated Protein Kinase (AMPK), for the Potential Treatment of Diabetic Nephropathy. *Journal of Medicinal Chemistry* **2016**, *59* (17), 8068-8081. DOI: 10.1021/acs.jmedchem.6b00866.
- (48) Petrie, E. J.; Sandow, J. J.; Jacobsen, A. V.; Smith, B. J.; Griffin, M. D. W.; Lucet, I. S.; Dai, W.; Young, S. N.; Tanzer, M. C.; Wardak, A.; et al. Conformational switching of the pseudokinase domain promotes human MLKL tetramerization and cell death by necroptosis. *Nat Commun* **2018**, *9* (1), 2422. DOI: 10.1038/s41467-018-04714-7.
- (49) Murphy, J. M.; Czabotar, P. E.; Hildebrand, J. M.; Lucet, I. S.; Zhang, J. G.; Alvarez-Diaz, S.; Lewis, R.; Lalaoui, N.; Metcalf, D.; Webb, A. I.; et al. The pseudokinase MLKL mediates necroptosis via a molecular switch mechanism. *Immunity* **2013**, *39* (3), 443-453. DOI: 10.1016/j.immuni.2013.06.018.
- (50) Hildebrand, J. M.; Tanzer, M. C.; Lucet, I. S.; Young, S. N.; Spall, S. K.; Sharma, P.; Pierotti, C.; Garnier, J. M.; Dobson, R. C.; Webb, A. I.; et al. Activation of the pseudokinase MLKL unleashes the four-helix bundle domain to induce membrane localization and necroptotic cell death. *Proc Natl Acad Sci U S A* **2014**, *111* (42), 15072-15077. DOI: 10.1073/pnas.1408987111.

(51) Kung, J. E.; Jura, N. Prospects for pharmacological targeting of pseudokinases. *Nat Rev Drug Discov* **2019**, *18* (7), 501-526. DOI: 10.1038/s41573-019-0018-3.

(52) Cai, Z. Y.; Jitkaew, S.; Zhao, J.; Chiang, H. C.; Choksi, S.; Liu, J.; Ward, Y.; Wu, L. G.; Liu, Z. G. Plasma membrane translocation of trimerized MLKL protein is required for TNF-induced necroptosis (vol 16, pg 55, 2014). *Nat Cell Biol* **2014**, *16* (2), 200-200. DOI: DOI 10.1038/ncb2908. Chen, X.; Li, W. J.; Ren, J. M.; Huang, D. L.; He, W. T.; Song, Y. L.; Yang, C.; Li, W. Y.; Zheng, X. R.; Chen, P. D.; et al. Translocation of mixed lineage kinase domain-like protein to plasma membrane leads to necrotic cell death. *Cell Res* **2014**, *24* (1), 105-121. DOI: 10.1038/cr.2013.171. Dondelinger, Y.; Declercq, W.; Montessuit, S.; Roelandt, R.; Goncalves, A.; Bruggeman, I.; Hulpiau, P.; Weber, K.; Sehon, C. A.; Marquis, R. W.; et al. MLKL Compromises Plasma Membrane Integrity by Binding to Phosphatidylinositol Phosphates. *Cell Rep* **2014**, *7* (4), 971-981. DOI: 10.1016/j.celrep.2014.04.026. Wang, H. Y.; Sun, L. M.; Su, L. J.; Rizo, J.; Liu, L.; Wang, L. F.; Wang, F. S.; Wang, X. D. Mixed Lineage Kinase Domain-like Protein MLKL Causes Necrotic Membrane Disruption upon Phosphorylation by RIP3. *Molecular Cell* **2014**, *54* (1), 133-146. DOI: 10.1016/j.molcel.2014.03.003.

(53) Moriwaki, K.; Bertin, J.; Gough, P. J.; Orłowski, G. M.; Chan, F. K. Differential roles of RIPK1 and RIPK3 in TNF-induced necroptosis and chemotherapeutic agent-induced cell death. *Cell Death & Disease* **2015**, *6*, e1636, Original Article. DOI: 10.1038/cddis.2015.16

<https://www.nature.com/articles/cddis201516#supplementary-information>.

(54) Nugues, A. L.; El Bouazzati, H.; Hetuin, D.; Berthon, C.; Loyens, A.; Bertrand, E.; Jouy, N.; Idziorek, T.; Quesnel, B. RIP3 is downregulated in human myeloid leukemia cells and modulates apoptosis and caspase-mediated p65/RelA cleavage. *Cell Death Dis* **2014**, *5*. DOI: ARTN e1384

10.1038/cddis.2014.347.

(55) Koo, G. B.; Morgan, M. J.; Lee, D. G.; Kim, W. J.; Yoon, J. H.; Koo, J. S.; Kim, S. I.; Kim, S. J.; Son, M. K.; Hong, S. S.; et al. Methylation-dependent loss of RIP3 expression in cancer represses programmed necrosis in response to chemotherapeutics. *Cell Res* **2015**, *25* (6), 707-725. DOI: 10.1038/cr.2015.56.

(56) Hanahan, D.; Weinberg, R. A. Hallmarks of Cancer: The Next Generation. *Cell* **2011**, *144* (5), 646-674. DOI: 10.1016/j.cell.2011.02.013.

(57) Su, Z.; Yang, Z.; Xie, L.; DeWitt, J. P.; Chen, Y. Cancer therapy in the necroptosis era. *Cell Death and Differentiation* **2016**, *23* (5), 748-756. DOI: 10.1038/cdd.2016.8.

- (58) Villen, J.; Gygi, S. P. The SCX/IMAC enrichment approach for global phosphorylation analysis by mass spectrometry. *Nat Protoc* **2008**, *3* (10), 1630-1638. DOI: 10.1038/nprot.2008.150.
- (59) Thompson, A.; Wolmer, N.; Koncarevic, S.; Selzer, S.; Bohm, G.; Legner, H.; Schmid, P.; Kienle, S.; Penning, P.; Hohle, C.; et al. TMTpro: Design, Synthesis, and Initial Evaluation of a Proline-Based Isobaric 16-Plex Tandem Mass Tag Reagent Set. *Anal Chem* **2019**, *91* (24), 15941-15950. DOI: 10.1021/acs.analchem.9b04474.
- (60) Li, J. M.; Van Vranken, J. G.; Vaites, L. P.; Schweppe, D. K.; Huttlin, E. L.; Etienne, C.; Nandhikonda, P.; Viner, R.; Robitaille, A. M.; Thompson, A. H.; et al. TMTpro reagents: a set of isobaric labeling mass tags enables simultaneous proteome-wide measurements across 16 samples. *Nat Methods* **2020**, *17* (4), 399-+. DOI: 10.1038/s41592-020-0781-4.
- (61) von Stechow, L.; Francavilla, C.; Olsen, J. V. Recent findings and technological advances in phosphoproteomics for cells and tissues. *Expert Rev Proteomic* **2015**, *12* (5), 469-487. DOI: 10.1586/14789450.2015.1078730.
- (62) Casement, R.; Bond, A.; Craigon, C.; Ciulli, A. Mechanistic and Structural Features of PROTAC Ternary Complexes. *Methods Mol Biol* **2021**, *2365*, 79-113. DOI: 10.1007/978-1-0716-1665-9\_5 From NLM Medline.
- (63) Hughes, S. J.; Ciulli, A. Molecular recognition of ternary complexes: a new dimension in the structure-guided design of chemical degraders. *Essays Biochem* **2017**, *61* (5), 505-516. DOI: 10.1042/Ebc20170041.
- (64) Roy, M. J.; Winkler, S.; Hughes, S. J.; Whitworth, C.; Galant, M.; Farnaby, W.; Rumpel, K.; Ciulli, A. SPR-Measured Dissociation Kinetics of PROTAC Ternary Complexes Influence Target Degradation Rate. *ACS Chem Biol* **2019**, *14* (3), 361-368. DOI: 10.1021/acscchembio.9b00092.
- (65) Bondeson, D. P.; Smith, B. E.; Burslem, G. M.; Buhimschi, A. D.; Hines, J.; Jaime-Figueroa, S.; Wang, J.; Hamman, B. D.; Ishchenko, A.; Crews, C. M. Lessons in PROTAC Design from Selective Degradation with a Promiscuous Warhead. *Cell Chem Biol* **2018**, *25* (1), 78-+. DOI: 10.1016/j.chembiol.2017.09.010.
- (66) Xiao, B.; Sanders, M. J.; Carmena, D.; Bright, N. J.; Haire, L. F.; Underwood, E.; Patel, B. R.; Heath, R. B.; Walker, P. A.; Hallen, S.; et al. Structural basis of AMPK regulation by small molecule activators. *Nat Commun* **2013**, *4*, 3017. DOI: 10.1038/ncomms4017.
- (67) Oladimeji, P. O.; Lin, W. W.; Brewer, C. T.; Chen, T. S. Glucose-dependent regulation of pregnane X receptor is modulated by AMP-activated protein kinase. *Sci Rep-Uk* **2017**, *7*. DOI: ARTN 46751

10.1038/srep46751.

(68) Yan, B.; Liu, L.; Huang, S.; Ren, Y.; Wang, H.; Yao, Z.; Li, L.; Chen, S.; Wang, X.; Zhang, Z. Discovery of a new class of highly potent necroptosis inhibitors targeting the mixed lineage kinase domain-like protein. *Chem Commun (Camb)* **2017**, *53* (26), 3637-3640. DOI: 10.1039/c7cc00667e.

(69) Pierotti, C. L.; Tanzer, M. C.; Jacobsen, A. V.; Hildebrand, J. M.; Garnier, J. M.; Sharma, P.; Lucet, I. S.; Cowan, A. D.; Kersten, W. J. A.; Luo, M. X.; et al. Potent Inhibition of Necroptosis by Simultaneously Targeting Multiple Effectors of the Pathway. *ACS Chem Biol* **2020**, *15* (10), 2702-2713. DOI: 10.1021/acscchembio.0c00482.

(70) Kufareva, I.; Abagyan, R. Type-II Kinase Inhibitor Docking, Screening, and Profiling Using Modified Structures of Active Kinase States. *Journal of Medicinal Chemistry* **2008**, *51* (24), 7921-7932. DOI: 10.1021/jm8010299.

(71) DiscoverX. *KINOMEscan® Assay Process & Data Quality Metrics*. 2019. <https://www.discoverx.com/technologies-platforms/competitive-binding-technology/kinomescan-technology-platform> (accessed 2019 19.09.2019).

(72) Hill, A. P.; Young, R. J. Getting physical in drug discovery: a contemporary perspective on solubility and hydrophobicity. *Drug Discov Today* **2010**, *15* (15-16), 648-655. DOI: 10.1016/j.drudis.2010.05.016.

(73) Reyner, E. L.; Sevidal, S.; West, M. A.; Clouser-Roche, A.; Freiwald, S.; Fenner, K.; Ullah, M.; Lee, C. A.; Smith, B. J. In Vitro Characterization of Axitinib Interactions with Human Efflux and Hepatic Uptake Transporters: Implications for Disposition and Drug Interactions. *Drug Metab Dispos* **2013**, *41* (8), 1575-1583. DOI: 10.1124/dmd.113.051193.

(74) Fink, C.; Sun, D. J.; Wagner, K.; Schneider, M.; Bauer, H.; Dolgos, H.; Mader, K.; Peters, S. A. Evaluating the Role of Solubility in Oral Absorption of Poorly Water-Soluble Drugs Using Physiologically-Based Pharmacokinetic Modeling. *Clin Pharmacol Ther* **2020**, *107* (3), 650-661. DOI: 10.1002/cpt.1672.

(75) Brase, S.; Gil, C.; Knepper, K.; Zimmermann, V. Organic azides: An exploding diversity of a unique class of compounds. *Angew Chem Int Edit* **2005**, *44* (33), 5188-5240. DOI: 10.1002/anie.200400657.

(76) Li, L.; Zhang, Z. Y. Development and Applications of the Copper-Catalyzed Azide-Alkyne Cycloaddition (CuAAC) as a Bioorthogonal Reaction. *Molecules* **2016**, *21* (10). DOI: ARTN 1393

10.3390/molecules21101393.

(77) Davis, M. I.; Hunt, J. P.; Herrgard, S.; Ciceri, P.; Wodicka, L. M.; Pallares, G.; Hocker, M.; Treiber, D. K.; Zarrinkar, P. P. Comprehensive analysis of kinase inhibitor selectivity. *Nat Biotechnol* **2011**, *29* (11), 1046-U1124. DOI: 10.1038/nbt.1990.

(78) Van den Eynden, J.; Umapathy, G.; Ashouri, A.; Cervantes-Madrid, D.; Szydzik, J.; Ruuth, K.; Koster, J.; Larsson, E.; Guan, J.; Palmer, R. H.; et al. Phosphoproteome and gene expression profiling of ALK inhibition in neuroblastoma cell lines reveals conserved oncogenic pathways. *Sci Signal* **2018**, *11* (557). DOI: ARTN eaar5680

10.1126/scisignal.aar5680.

(79) Walter, S. A.; Cutler, R. E.; Martinez, R.; Gishizky, M.; Hill, R. J. Stk10, a new member of the polo-like kinase family highly expressed in hematopoietic tissue. *J Biol Chem* **2003**, *278* (20), 18221-18228. DOI: 10.1074/jbc.M212556200.

(80) Arora, S.; Gonzales, I. M.; Hagelstrom, R. T.; Beaudry, C.; Choudhary, A.; Sima, C.; Tibes, R.; Mousses, S.; Azorsa, D. O. RNAi phenotype profiling of kinases identifies potential therapeutic targets in Ewing's sarcoma. *Mol Cancer* **2010**, *9*. DOI: Artn 218

10.1186/1476-4598-9-218. Zhang, L.; Lu, S. Y.; Guo, R.; Ma, J. X.; Tang, L. Y.; Wang, J. J.; Shen, C. L.; Lu, L. M.; Liu, J.; Wang, Z. G.; et al. STK10 knockout inhibits cell migration and promotes cell proliferation via modulating the activity of ERM and p38 MAPK in prostate cancer cells. *Exp Ther Med* **2021**, *22* (2), 851. DOI: 10.3892/etm.2021.10283.

(81) Serafim, R. A. M.; Sorrell, F. J.; Berger, B. T.; Collins, R. J.; Vasconcelos, S. N. S.; Massirer, K. B.; Knapp, S.; Bennett, J.; Fedorov, O.; Patel, H.; et al. Discovery of a Potent Dual SLK/STK10 Inhibitor Based on a Maleimide Scaffold. *J Med Chem* **2021**. DOI: 10.1021/acs.jmedchem.0c01579.

(82) Anastassiadis, T.; Deacon, S. W.; Devarajan, K.; Ma, H. C.; Peterson, J. R. Comprehensive assay of kinase catalytic activity reveals features of kinase inhibitor selectivity. *Nat Biotechnol* **2011**, *29* (11), 1039-U1117. DOI: 10.1038/nbt.2017.

(83) Berger, B.-T. Structural Mechanisms of Binding Kinetics. **2020**.

(84) Davies, M. *Crizotinib* *KINOME*. 2016. <https://lincs.hms.harvard.edu/db/datasets/20200/> (accessed 2020).

(85) Robers, M. B.; Wilkinson, J. M.; Vasta, J. D.; Berger, L. M.; Berger, B. T.; Knapp, S. Single tracer-based protocol for broad-spectrum kinase profiling in live cells with NanoBRET. *STAR Protoc* **2021**, *2* (4), 100822. DOI: 10.1016/j.xpro.2021.100822.

(86) Vasta, J. D.; Corona, C. R.; Wilkinson, J.; Zimprich, C. A.; Hartnett, J. R.; Ingold, M. R.; Zimmerman, K.; Machleidt, T.; Kirkland, T. A.; Huwiler, K. G.; et al. Quantitative, Wide-

Spectrum Kinase Profiling in Live Cells for Assessing the Effect of Cellular ATP on Target Engagement. *Cell Chem Biol* **2018**, *25* (2), 206-+. DOI: 10.1016/j.chembiol.2017.10.010.

(87) Klein, V. G.; Townsend, C. E.; Testa, A.; Zengerle, M.; Maniaci, C.; Hughes, S. J.; Chan, K. H.; Ciulli, A.; Lokey, R. S. Understanding and Improving the Membrane Permeability of VH032-Based PROTACs. *Acs Med Chem Lett* **2020**, *11* (9), 1732-1738. DOI: 10.1021/acsmchemlett.0c00265. <linker-dependent-folding-rationalizes-protac-cell-permeability.pdf>.

(88) Yegorova, S.; Chavarroche, A. E.; Rodriguez, M. C.; Minond, D.; Cudic, M. Development of an AlphaScreen assay for discovery of inhibitors of low-affinity glycan-lectin interactions. *Anal Biochem* **2013**, *439* (2), 123-131. DOI: 10.1016/j.ab.2013.04.028. Watson, V. G.; Drake, K. M.; Peng, Y.; Napper, A. D. Development of a High-Throughput Screening-Compatible Assay for the Discovery of Inhibitors of the AF4-AF9 Interaction Using AlphaScreen Technology. *Assay Drug Dev Techn* **2013**, *11* (4), 253-268. DOI: 10.1089/adt.2012.495.

(89) Simpson, D. S.; Gabrielyan, A.; Feltham, R. RIPK1 ubiquitination: Evidence, correlations and the undefined. *Semin Cell Dev Biol* **2021**, *109*, 76-85. DOI: 10.1016/j.semcdb.2020.08.008.

(90) Patel, S.; Webster, J. D.; Varfolomeev, E.; Kwon, Y. C.; Cheng, J. H.; Zhang, J.; Dugger, D. L.; Wickliffe, K. E.; Maltzman, A.; Sujatha-Bhaskar, S.; et al. RIP1 inhibition blocks inflammatory diseases but not tumor growth or metastases. *Cell Death Differ* **2020**, *27* (1), 161-175. DOI: 10.1038/s41418-019-0347-0. Speir, M.; Djajawi, T. M.; Conos, S. A.; Tye, H.; Lawlor, K. E. Targeting RIP Kinases in Chronic Inflammatory Disease. *Biomolecules* **2021**, *11* (5). DOI: 10.3390/biom11050646.

(91) Peltzer, N.; Darding, M.; Walczak, H. Holding RIPK1 on the Ubiquitin Leash in TNFR1 Signaling. *Trends Cell Biol* **2016**, *26* (6), 445-461. DOI: 10.1016/j.tcb.2016.01.006.

(92) Nailwal, H.; Chan, F. K. M. Necroptosis in anti-viral inflammation. *Cell Death and Differentiation* **2019**, *26* (1), 4-13. DOI: 10.1038/s41418-018-0172-x. Shubina, M.; Tummers, B.; Boyd, D. F.; Zhang, T.; Yin, C. R.; Gautam, A.; Guo, X. Z. J.; Rodriguez, D. A.; Kaiser, W. J.; Vogel, P.; et al. Necroptosis restricts influenza A virus as a stand-alone cell death mechanism. *J Exp Med* **2020**, *217* (11). DOI: ARTN e20191259  
10.1084/jem.20191259.

(93) Dondelinger, Y.; Delanghe, T.; Rojas-Rivera, D.; Priem, D.; Delvaeye, T.; Bruggeman, I.; Van Herreweghe, F.; Vandenabeele, P.; Bertrand, M. J. M. MK2 phosphorylation of RIPK1 regulates TNF-mediated cell death. *Nat Cell Biol* **2017**, *19* (10), 1237-1247. DOI: 10.1038/ncb3608.

- (94) McQuade, T.; Cho, Y.; Chan, F. K. M. Positive and negative phosphorylation regulates RIP1-and RIP3-induced programmed necrosis. *Biochemical Journal* **2013**, *456*, 409-415. DOI: 10.1042/Bj20130860.
- (95) Degterev, A.; Huang, Z. H.; Boyce, M.; Li, Y. Q.; Jagtap, P.; Mizushima, N.; Cuny, G. D.; Mitchison, T. J.; Moskowitz, M. A.; Yuan, J. Y. Chemical inhibitor of nonapoptotic cell death with therapeutic potential for ischemic brain injury (vol 1, pg 112, 2005). *Nature Chemical Biology* **2005**, *1* (4), 234-234. DOI: DOI 10.1038/nchembio0905-234a. Degterev, A.; Hitomi, J.; Germscheid, M.; Ch'en, I. L.; Korkina, O.; Teng, X.; Abbott, D.; Cuny, G. D.; Yuan, C.; Wagner, G.; et al. Identification of RIP1 kinase as a specific cellular target of necrostatins. *Nature Chemical Biology* **2008**, *4* (5), 313-321. DOI: 10.1038/nchembio.83.
- (96) Harris, P. A.; Faucher, N.; George, N.; Eidam, P. M.; King, B. W.; White, G. V.; Anderson, N. A.; Bandyopadhyay, D.; Beal, A. M.; Beneton, V.; et al. Discovery and Lead-Optimization of 4,5-Dihydropyrazoles as Mono-Kinase Selective, Orally Bioavailable and Efficacious Inhibitors of Receptor Interacting Protein 1 (RIP1) Kinase. *Journal of Medicinal Chemistry* **2019**, *62* (10), 5096-5110. DOI: 10.1021/acs.jmedchem.9b00318.
- (97) Harris, P. A.; Marinis, J. M.; Lich, J. D.; Berger, S. B.; Chirala, A.; Cox, J. A.; Eidam, P. M.; Finger, J. N.; Gough, P. J.; Jeong, J. U.; et al. Identification of a RIP1 Kinase Inhibitor Clinical Candidate (GSK3145095) for the Treatment of Pancreatic Cancer. *Acs Med Chem Lett* **2019**, *10* (6), 857-+. DOI: 10.1021/acsmedchemlett.9b00108.
- (98) Hou, J.; Ju, J.; Zhang, Z.; Zhao, C.; Li, Z.; Zheng, J.; Sheng, T.; Zhang, H.; Hu, L.; Yu, X.; et al. Discovery of potent necroptosis inhibitors targeting RIPK1 kinase activity for the treatment of inflammatory disorder and cancer metastasis. *Cell Death Dis* **2019**, *10* (7), 493. DOI: 10.1038/s41419-019-1735-6.
- (99) Martens, S.; Goossens, V.; Devisscher, L.; Hofmans, S.; Claeys, P.; Vuylsteke, M.; Takahashi, N.; Augustyns, K.; Vandenabeele, P. RIPK1-dependent cell death: a novel target of the Aurora kinase inhibitor Tozasertib (VX-680). *Cell Death Dis* **2018**, *9*. DOI: ARTN 211 10.1038/s41419-017-0245-7. Fauster, A.; Rebsamen, M.; Huber, K. V. M.; Bigenzahn, J. W.; Stukalov, A.; Lardeau, C. H.; Scorzoni, S.; Bruckner, M.; Gridling, M.; Parapatics, K.; et al. A cellular screen identifies ponatinib and pazopanib as inhibitors of necroptosis. *Cell Death Dis* **2015**, *6*. DOI: ARTN e1767 10.1038/cddis.2015.130. Najjar, M.; Suebsuwong, C.; Ray, S. S.; Thapa, R. J.; Maki, J. L.; Nogusa, S.; Shah, S.; Saleh, D.; Gough, P. J.; Bertin, J.; et al. Structure Guided Design of Potent and Selective Ponatinib-Based Hybrid Inhibitors for RIPK1. *Cell Rep* **2015**, *10* (11), 1850-1860. DOI: 10.1016/j.celrep.2015.02.052. Harris, P. A.; Bandyopadhyay, D.; Berger, S.

B.; Campobasso, N.; Capriotti, C. A.; Cox, J. A.; Dare, L.; Finger, J. N.; Hoffman, S. J.; Kahler, K. M.; et al. Discovery of Small Molecule RIP1 Kinase Inhibitors for the Treatment of Pathologies Associated with Necroptosis. *Acs Med Chem Lett* **2013**, *4* (12), 1238-1243. DOI: 10.1021/ml400382p.

(100) Dondelinger, Y.; Delanghe, T.; Priem, D.; Wynosky-Dolfi, M. A.; Sorobetea, D.; Rojas-Rivera, D.; Giansanti, P.; Roelandt, R.; Gropengiesser, J.; Ruckdeschel, K.; et al. Serine 25 phosphorylation inhibits RIPK1 kinase-dependent cell death in models of infection and inflammation. *Nature Communications* **2019**, *10*. DOI: ARTN 1729

10.1038/s41467-019-09690-0.